

UCSF

UC San Francisco Electronic Theses and Dissertations

Title

Structural Determinants for Reversible β -lactamase Inhibition

Permalink

<https://escholarship.org/uc/item/9g00g95n>

Author

DeFrees, Kyle

Publication Date

2019

Peer reviewed|Thesis/dissertation

Structural Determinants for Reversible β -lactamase Inhibition

by
Kyle DeFrees

DISSERTATION

Submitted in partial satisfaction of the requirements for degree of
DOCTOR OF PHILOSOPHY

in

Chemistry and Chemical Biology

in the

GRADUATE DIVISION

of the

UNIVERSITY OF CALIFORNIA, SAN FRANCISCO

Approved:

DocuSigned by:

Adam Renslo

Adam Renslo

FBDB6299FCD244B...

Chair

DocuSigned by:

Jason Gestwicki

Jason Gestwicki

DocuSigned by:

Michelle Arkin

Michelle Arkin

DocuSigned by:

Matthew Jacobson

Matthew Jacobson

F0D9291273674CD...

Committee Members

Copyright 2019

by

Kyle DeFrees

Acknowledgments

I would like to acknowledge everyone who has helped me throughout the years – science is community driven, and it truly takes a village. First, I would like to thank my thesis advisor, Adam Renslo, for providing the resources, guidance, and support that enabled me to develop as a scientist in his lab. I am forever grateful for the academic freedom provided; being allowed to fail, and the associated hard work to solve such problems, has allowed me to grow tremendously as a scientist and individual. I would also like to acknowledge the amazing members of the lab whom I have overlapped with over the past 5+ years. I learned a lot from this group of scientists, and the friendships formed truly made the time a wonderful experience. I also want to acknowledge my classmates whose brilliance, hard work, and friendship serves as a constant inspiration. I also want to thank my thesis committee – Michelle Arkin, Matt Jacobson, and Jason Gestwicki – for their valuable advice about research and career development. Lastly, special thanks to my parents for instilling the value of hard work and fostering a scientific household at an early age; the practical expectations of research and results has been more than valuable in my progression and scientific mindset, and for that I am forever grateful.

Special scientific thanks are due to the following individuals who contributed in various ways along the course of this project:

- Priya Jaishankar: for being an excellent teammate and scientist; for laying the groundwork of this project through previous work.

- Stacie Bulfer and Sam Pfaff: for teaching me everything I know about SPR.
- Ahmed Mohamed and Xochina El-Hilali: for work on the amide- π series.
- Maurice Horton: for being a great mentee, and work on the original aryl scaffold.
- Yu Chen: for being an outstanding collaborator; without the provided help this project and its various facets would not be possible.
- Derek Nichols: for previous biochemical and crystallographic work on CTX-M.
- Xiujun Zhang: for purified protein.
- Afroza Akhtar: for crystallography and fragment characterization.
- Michael Kemp: for docking and crystallography.

Contributions

Chapters 2 and 3 of this thesis are reprints of the material as it appears in:

DeFrees K., Kemp M.T., ElHilali-Pollard X., Zhang X., Mohamed A., Chen Y., Renslo A.R. “An empirical study of amide–heteroarene π -stacking interactions using reversible inhibitors of a bacterial serine hydrolase.” **Org. Chem. Front.** 2019, 6, 1749-1756.

*Torelli N.J., *Akhtar A., *DeFrees K., Jaishankar P., Pemberton O.A., Zhang X., Johnson C., Renslo A.R., Chen Y. “Active-Site Druggability of Carbapenemases and Broad-Spectrum Inhibitor Discovery.” **ACS Infect. Dis.** 2019, 5 (6), 1013-1021.

*Denotes equal contribution

Chapter 4 of this thesis was adapted from a manuscript in preparation:

DeFrees K., Akhtar A., Zhang X., Nichols D., Cambeis, E., Chen Y., Renslo A.R. “Targeting the Conserved Hydrophobic Shelf of Carbapenemase KPC-2.”

Abstract

Structural Determinants for Reversible β -lactamase Inhibition

Kyle DeFrees

Antibiotic resistance is one of the largest health concerns of the modern era, threatening decades of progress in antibacterial research and development. β -lactams, the first line of defense against most Gram positive and negative pathogens, are increasingly ineffective in clinical settings, driven in large part by the proliferation of β -lactamases, enzymes which degrade β -lactams. While these proteins have evolved over millions of years with hundreds of known variants, clinical selection has led to the proliferation of extended spectrum β -lactamases and carbapenems like CTX-M and KPC-2, respectively. Previous generation β -lactamase inhibitors such as clavulanic acid and sulbactam are ineffective against these enzymes, creating a pressing need for new inhibitor development.

While the recent discovery and approval of covalent-reversible avibactam and vaborbactam have shown great promise in bridging this gap, further clinical selection will likely drive new enzymes and mutations resistant to these agents, such as the spread of metallo-lactamases, or mutations within the KPC-2 family. Given the paucity of information around non-covalent β -lactamase inhibition, we sought to further characterize the specific interactions of a potent, non-covalent CTX-M inhibitor, revealing the importance of amide- π stacking against the β_3 backbone (**Chapter 2**). Building off of this work, we also discovered new non-covalent scaffolds for the inhibition of KPC-2 (**Chapters 3 and 4**). Our work revealed how the improved

hydrophobicity and conformational flexibility of carbapenemases such as KPC-2 can be exploited for building non-covalent affinity, supporting future efforts towards combating emerging resistance. These structure-guided efforts are also being supported by unbiased fragment screening (**Chapter 5**), which aims to bridge the inhibition gap between enzyme classes, with the overall goal of developing a non-covalent scaffold with broader β -lactamase activity.

Table of Contents

	Page
Chapter 1	1
β-lactamases and Non-covalent Inhibitor Discovery	
References:	19
Chapter 2	21
An Empirical Study of Amide–Heteroarene π-stacking Interactions Using Reversible Inhibitors of a Bacterial Serine Hydrolase	
References:	45
Chapter 3	111
Active-Site Druggability of Carbapenemases and Broad-Spectrum Inhibitor Discovery	
References:	135
Chapter 4	159
Targeting the Conserved Hydrophobic Shelf for Carbapenemase KPC-2	
References:	180
Chapter 5	327
Fragment Discovery for Diverse β-lactamases	
References:	341

List of Figures

	Page
Figure 1-1	2
Schematic of peptidoglycan formation.	
Figure 1-2	3
β -lactams mimic native substrate D-Ala-D-Ala.	
Figure 1-3	4
β -lactamases deactivate β -lactams via hydrolysis.	
Figure 1-4	6
All approved β -lactamase inhibitors are covalent substrates.	
Figure 1-5	8
Crystal structure of apo CTX-M-9.	
Figure 1-6	9
Fragment based lead discovery of compound 1.	
Figure 1-7	10
Compound 1 in complex with CTX-M-9 at 0.89 Å.	
Figure 1-8	12
Most tetrazole replacements were entirely inactive.	
Figure 1-9	12
Amide- π interactions of compound 1.	

Figure 1-10	14
The tetrazole of 1 stabilizes a low barrier hydrogen bond in CTX-M.	
Figure 1-11	16
Sulfonic acid analog of 1 in complex with KPC-2.	
Figure 1-12	17
Compound 1 complex with CTX-M-9 superimposed onto an apo KPC-2 structure.	
Figure 1-13	18
Synthesized analogs of the original aryl scaffold.	
Figure 2-1	24
Coordinate system employed in computational studies of amide– heteroarene interactions.	
Figure 2-2	24
A Rebek imide host bound through complementary hydrogen bonding to its cognate guest.	
Figure 2-3	25
Factor Xa inhibitor and its interaction with Gln192 in the complex crystal structure.	
Figure 2-4	27
Known CTX-M inhibitor 1 and new analogues 2–20 described herein.	
Figure 2-5	28
Structure of CTX-M inhibitors 2–20 bearing diverse heteroaryl substituents R.	
Figure 2-6	30
Complex structures of analogues 3, 14, and 20 bound to CTX-M-14.	

Figure 2-7.	32
Complex structures of analogues 14 and 20 bound to CTX-M-27.	
Figure 2-8	36
Computed dipole moments (μ) vs. $\Delta\Delta G_{Ki}$ and $\Delta\Delta G_{Kd}$ for 2–20.	
Figure 2-9	37
Relative orientation of Gly238 and heteroarene substituent R in analogues 3–5.	
Figure 2-10	37
Relative orientation of Gly238 and heteroarene substituent R for analogues 6–8.	
Figure 2-11	47
Compound 1 in complex with CTX-M-14 at 0.89Å.	
Figure 2-12	47
Comparison of calculated dipoles between solvents and models.	
Figure 2-13	48
Front and top view of compound 14 with CTX-M-14.	
Figure 3-1	119
Complex crystal structure of compounds 3 and 6 with CTX-M-14 and KPC-2.	
Figure 3-2	121
Complex crystal structure of compound 7 with KPC-2 and NDM-1.	
Figure 3-3	124
Complex crystal structure of compound 9 with KPC-2 and NDM-1.	

Figure 3-4	150
Complex crystal structure of compound 7s with KPC-2.	
Figure 3-5	150
Complex crystal structure of compound 8 with KPC-2 and NDM-1.	
Figure 4-1	161
Compound 1 complex with CTX-M-9 superimposed onto an apo KPC-2 structure.	
Figure 4-2	163
Crystal structures reveal binding mode of indane 2 to CTX-M-9 and KPC-2.	
Figure 4-3	166
Crystal structure of indoline 7 with KPC-2; docking pose of indoline 9 with KPC-2.	
Figure 4-4	168
Crystal structure reveals the binding mode of indoline 16 to KPC-2.	
Figure 4-5	176
Compound 2 complex with CTX-M-9 superimposed onto the compound 16 complex with KPC-2.	
Figure 4-6	181
Selected docking poses of compounds 7 and 11 with KPC-2.	
Figure 4-7	181
Compound 16 complex with KPC-2 superimposed onto a structure of apo OXA-48.	
Figure 5-1	330
Compound 1 binding to CTX-M-14.	

Figure 5-2	331
Captopril binding to NDM-1.	
Figure 5-3	331
Compound 2 binding to OXA-48.	
Figure 5-4	332
Histogram analysis of both fragment libraries.	
Figure 5-5	334
Primary screening scatterplots for CTX-M-14, NDM-1, and OXA-48.	

List of Tables

	Page
Table 1-1	15
KPC-2 activity is unaffected by tetrazole replacement.	
Table 2-1	33
K _i and K _d values for heterocycles 2–20 with CTX-M-14 and CTX-M-27.	
Table 2-2	62
X-ray data collection and refinement statistics.	
Table 3-1	116
Inhibition by hydrolyzed β -lactam products.	
Table 3-2	118
Inhibition by tetrazole-based compounds.	
Table 3-3	123
Inhibition by analogs of compound 8.	
Table 3-4	148
Crystallographic data collection and refinement statistics.	
Table 4-1	162
Biochemical activities of indanes 2-6.	
Table 4-2	165
Biochemical activities of analogs 7-12.	

Table 4-3	167
Biochemical activities of analogs 13-17.	
Table 4-4	170
Biochemical activities of indoline analogs 18-28.	
Table 4-5	172
Biochemical activities of analogs 29-36.	
Table 4-6	173
Biochemical activities of analogs 37-45.	
Table 4-7	175
Biochemical activities of analogs 46-52.	
Table 4-8	182
NDM-1 activities of indoline analogs 16, 18-28.	
Table 4-9	183
NDM-1 activities of amido-tetrazole analogs 29-34, 44, and 46-52.	
Table 4-10	184
OXA-48 activities of various amido-tetrazole analogs.	
Table 5-1	335
Hit rate by enzyme and library.	
Table 5-2	336
Single point inhibition for selected hits.	

Chapter 1

β -lactamases and Non-covalent Inhibitor Discovery

β-lactams and β-lactamases:

β-lactam antibiotics have been a staple in the modern antibacterial arsenal since penicillin's mass production in 1940, treating otherwise incurable bacterial infections. β-lactams target penicillin-binding proteins (PBPs), the enzyme class responsible for assembling peptidoglycan. Traditional "Class A" PBPs are two domain enzymes; the N-terminal transglycosylase domain stitches together MurNAc and GlcNAc, whereas the C-terminal transpeptidase domain recognizes the D-Ala-D-Ala stem peptide and attaches it to a coupling partner (**Figure 1-1**).¹ The nucleophilic residue of the coupling partner varies per organism, but is often the amine of glycine (typically from a pentaglycine linker), lysine, or a diaminopimelate (DAP) group.¹ As PBPs are essential for bacterial growth and replication, isolated transglycosylase (Class B) and transpeptidase (Class C) domains also exist; these variants allow for precise localization and modification of the peptidoglycan to fit the organisms needs.¹

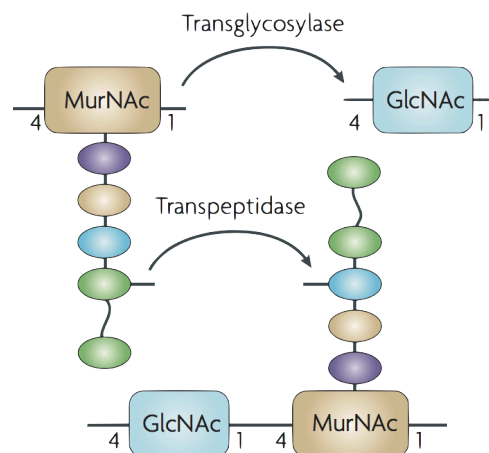


Figure 1-1. Schematic of peptidoglycan formation. Adapted from reference 2.

β -lactam antibiotics target the transpeptidase domain of Class A and C PBPs; the lactam-acid motif mimics the D-Ala-D-Ala substrate, and upon nucleophilic attack, results in a stable acyl intermediate, thus inhibiting the enzyme (**Figure 1-2**). This process is not bactericidal alone, but peptidoglycan is constantly being remodeled to accommodate growth and reproduction, so inhibition eventually results in a peptidoglycan-deficient organism (L-form), which is susceptible to oxidative stress or osmotic shock in certain environments.^{3, 4}

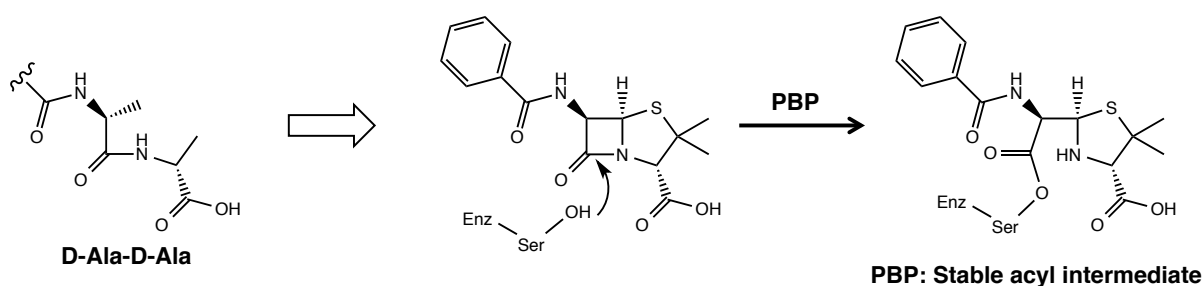


Figure 1-2. β -lactams mimic native substrate D-Ala-D-Ala.

Given the importance of the transpeptidase domain, bacteria have developed a number of mechanisms to overcome β -lactam antibiotics. The first, and perhaps most worrying, is modification of PBPs. Overproduction can often compensate for natively resistant organisms, but mutations yielding decreased affinity for β -lactams have also been observed.⁵⁻⁷ Some of these mutants are also capable of slowly hydrolyzing the stable acyl-PBP complex, resulting in deactivated antibiotic and unbound PBP.^{6, 7} Further modifications of the donor and acceptor stem peptides have also been observed; these modifications vary by organism, and are often associated with increased resistance to β -lactams, presumably by promoting the production and use of PBPs that carry intrinsic resistance due to the aforementioned modifications.⁵⁻⁷ Aside

from PBP modification, bacteria also possess strong homeostatic control as a part of nutrient acquisition and xenobiotic repulsion; porin and importer loss can therefore provide total resistance, though modulation is often detrimental to overall fitness.⁸ Active repulsion via ATP-binding cassette (ABC) exporters typically provide moderate resistance; β -lactams only need to reach the periplasm in Gram negatives however, so exporter overexpression is best suited for organisms with intrinsically impermeable outer membranes.⁸ Given these limitations, the most common resistance mechanism across all organisms is β -lactamase expression, an enzyme class that deactivates β -lactams. Like PBPs, these enzymes will recognize a lactam substrate and form an acyl intermediate, except β -lactamases have an activated tetrahedral intermediate that is primed for subsequent hydrolysis, thus destroying the antibiotic (**Figure 1-3**). β -lactamase production is capable of providing complete resistance without any fitness detriment, and thus is the preferred resistance mechanism among most Gram positive and negative bacteria.

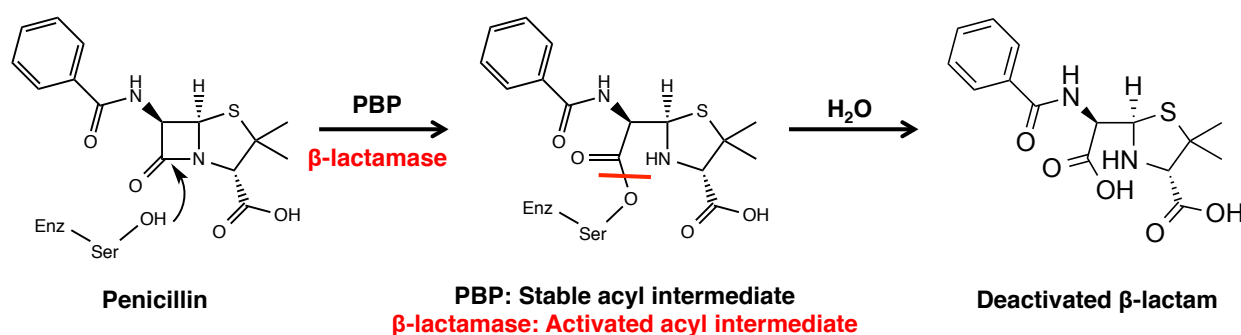


Figure 1-3. β -lactamases deactivate β -lactams via hydrolysis. Hydrolysis occurs via ordered, nucleophilic water.

β -lactamase evolution has taken place over millions of years; there are over 1400 known β -lactamases, with more being discovered every year.⁹⁻¹¹ Broadly, these

enzymes can be classified by structural homology into four distinct classes: A-D.⁹⁻¹¹ Class A β -lactamases are canonical serine hydrolases that evolved from PBPs with discreet structural modifications, such as the introduction of a loop to block stem peptide binding. Typical members include variants like CTX-M, KPC, TEM, and SHV; there are many known point mutants for these enzymes. Class B enzymes are di-Zn hydrolases, and are entirely structurally unrelated to PBPs and the other β -lactamase classes. While the evolutionary history for these enzymes remains murky, it is thought that many evolved from tRNAses, some of which already poses weak β -lactamase activity.¹² Typical members of this class include IMP, VIM, and NDM. Class C enzymes also evolved from PBPs, but have a mutated acid-binding motif, and are typically under chromosomal control (most β -lactamases are now on mobile plasmids, but originated as chromosomal proteins, such as the Class A KPC from *Klebsiella*). Typical members of this family include AmpC, CMY, and ACT. Class D enzymes are also related to PBPs, but these have an open stem-peptide binding channel and use a carboxylated lysine as a general base. This class is comprised of the OXA enzymes, which have many known point mutants.

Given the importance of β -lactamases towards clinical resistance, significant effort has been made to inhibit these enzymes, and thus restore β -lactam activity. The first approved β -lactamase inhibitor is a β -lactam itself, clavulanic acid, which presents a secondary electrophile upon lactam scission. While limited in substrate scope (**Figure 1-4**), this compound inhibited the clinically relevant β -lactamases of the time, SHV and TEM. Shortly thereafter another β -lactam based inhibitor was approved for use, sulbactam, which improved the spectrum of inhibition within Class A enzymes. While

these two inhibitors are still used in combination therapies today, the clinical expression of β -lactamases has expanded over the resulting decades, creating an antibiotic resistance crisis.¹¹ Recent developments in the field, which occurred during the duration of this research, resulted in two additional β -lactamase inhibitors, avibactam and vaborbactam. Avibactam, approved in 2015, is a cyclic-N-sulfated urea (**Figure 1-4**) that acts as a covalent reversible inhibitor; this inhibitor type has an improved spectrum of inhibition, hitting almost all Class A and C enzymes, and some Class D enzymes. Vaborbactam, which is a cyclic boronic acid, was approved in 2017; this covalent molecule has a similar spectrum of inhibition to avibactam (**Figure 1-4**).

















	Clavulanic Acid	Sulbactam	Avibactam	Vaborbactam
Class A - Serine hydrolases - e.g. CTX-M, KPC, TEM				
Class B - di-Zn hydrolases - e.g. IMP, VIM, NDM				
Class C - Serine hydrolases - Typically chromosomal - e.g. AmpC, CMY, ACT				
Class D - Serine hydrolases - Uses carboxylated lysine - e.g. OXA				

Figure 1-4. All approved β -lactamase inhibitors are covalent substrates. Avibactam (2015) and vaborbactam (2017) have greatly improved inhibition profiles.

While these two classes have revolutionized clinical outcomes with their improved spectrum of inhibition, many future challenges remain. To start, neither scaffold has Class B activity, particularly against NDM or VIM enzymes, which are increasingly prevalent in clinical isolates. While a variant of vaborbactam might have useful activity against some Class B enzymes,¹³ all of the approved β -lactamase inhibitors are covalent, and primarily rely on K_{inact} for potent inhibition. K_{iapp} is modest, typically in the μM range,^{14, 15} and the covalent mechanisms employed are incompatible with Class B enzymes, as the nucleophile is an ordered, bridging water. Both compound classes also struggle with Class D inhibition, particularly with K_{iapp} – some OXA variants are completely resistant to both scaffolds.^{15, 16} Avibactam also has a scaffold-specific liability, as the N-sulfate required for activity is hydrolytically labile. Some β -lactamases such as KPC have been observed to catalyze this desulfation, inactivating avibactam.^{14, 17} Importantly, this behavior has not been evolutionarily selected for, suggesting a potential mechanism for future avibactam-type resistance. Avibactam and vaborbactam are also covalent reversible, so they are susceptible to improved deacylation rates. Evolutionary selection has guided β -lactamases towards being “good enough,” but further pressure may result in more efficient enzymes that are better at hydrolyzing both β -lactam substrates and future covalent inhibitors.

Taken together, there is an outstanding need for improved K_{i} across enzyme classes, but a lack of concerted knowledge about implementation. Many companies and researchers have tried to build non-covalent scaffolds over the preceding decades, but as evidenced by the approved inhibitors, were not successful. The challenges presented by β -lactamases are primarily two-fold: 1) the active site is particularly solvent

exposed (**Figure 1-5**); substrate β -lactams are polar, and recognition is primarily via H-bonds, and 2) broader spectrum enzymes (i.e. can hydrolyze a larger diversity of β -lactams) are more conformationally dynamic, sometimes at the expense of key residues used for building non-covalent affinity.^{18, 19} While challenging to address, it is important to note that there is a high degree of structural conservation, with similar substrate envelopes across diverse enzymes. Notably, hydrolyzed substrates are weak non-covalent inhibitors themselves, with K_i in the μM range for many enzymes (see **Chapter 3** for more discussion). Given the substrate homology, it therefore appears feasible to build non-covalent affinity across multiple distinct enzymes. To that end, this project aimed to better understand the molecular requirements for reversible inhibition, and to discover novel chemical matter with improved K_i against multiple enzyme classes.

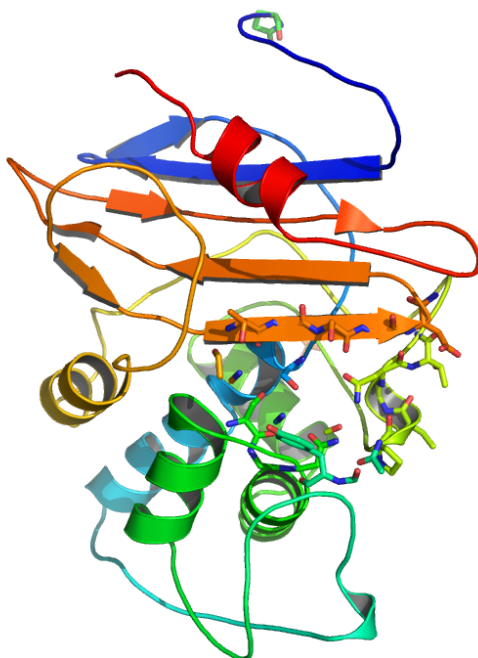


Figure 1-5. Apo CTX-M-9. Active site residues shown as sticks (PDB: 2P74).

Non-covalent Inhibitor Discovery:

Our lab, in collaboration with Prof. Yu Chen at University of South Florida, previously sought to generate the first non-covalent inhibitors of a model Class A enzyme, CTX-M. CTX-M is an extended spectrum β -lactamase whose substrate scope includes penicillins and later generation cephalosporins, and as such, was a prime target for discovery due to a versatile substrate envelope and clinical significance. Inhibitor discovery for this enzyme first began as a Docking fragment screen,²⁰ resulting in high mM fragments with similar chemotypes, such as a tetrazole, which binds the acid-binding motif, as well as a fluoro-aryl, which appeared to pack against the β 3 strand (**Figure 1-6**). These efforts were supported by crystallography, and through a series of SAR-by-purchase resulted in low mM fragments presenting both aryl and tetrazole motifs. Further structure-based optimization resulted in a 21 μ M aryl-F compound, as well as a 1.3 μ M benzimidazole. Combining the two motifs as a CF_3 -benzimidazole resulted in **1**, a 90 nM inhibitor of CTX-M-9.²¹

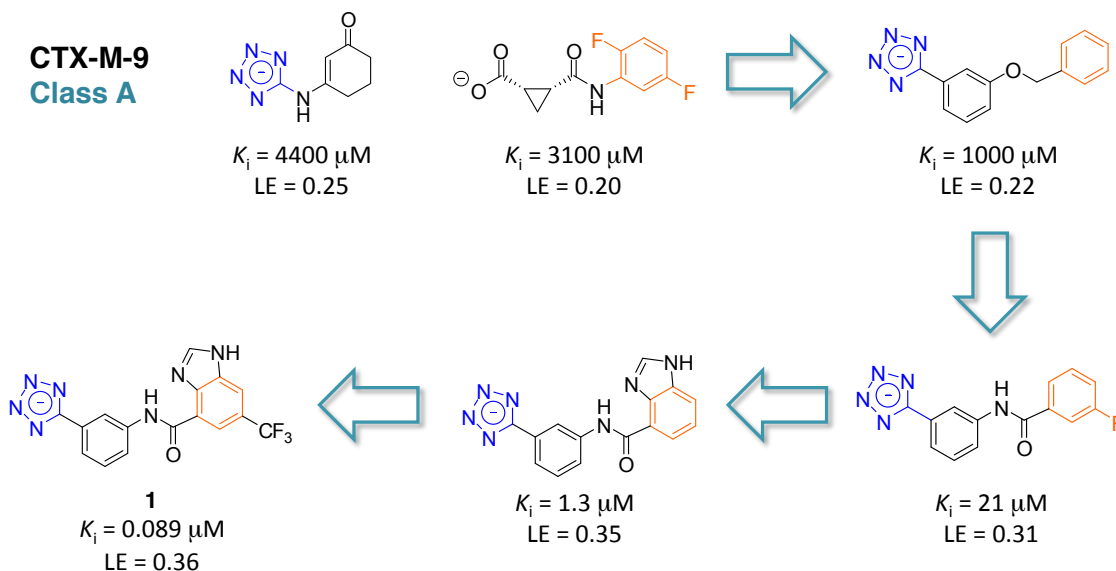


Figure 1-6. Fragment based lead discovery of compound 1. K_i calculated from a biochemical IC_{50} (nitrocefim substrate) using $K_i = \text{IC}_{50}/(1 + [\text{S}]/K_m)$.

High-resolution crystallography of **1** with CTX-M-9 (0.89 Å) supported the previous analog structures (**Figure 1-7**); the tetrazole sits nicely in the Thr235/Ser237/Ser130 acid-binding motif, and the amide carbonyl hydrogen bonds with Asn132 and Asn104. The CF₃-benzimidazole packs against the β₃ strand and hydrogen bonds with Asp240 – the H seems to be localized on the benzimidazole – whereas the CF₃ anchors in the hydrophobic Pro167 sub pocket. Compound **1** also restored cefotaxime activity in CTX-M expressing clinical isolates,²² representing the first utility of a potent, non-covalent inhibitor of a β-lactamase. Overall, this fragment based approach resulted in a > 10,000 fold increase in affinity with only ~ 40 compounds synthesized, suggesting that this process could be expanded to other target enzymes in the future.

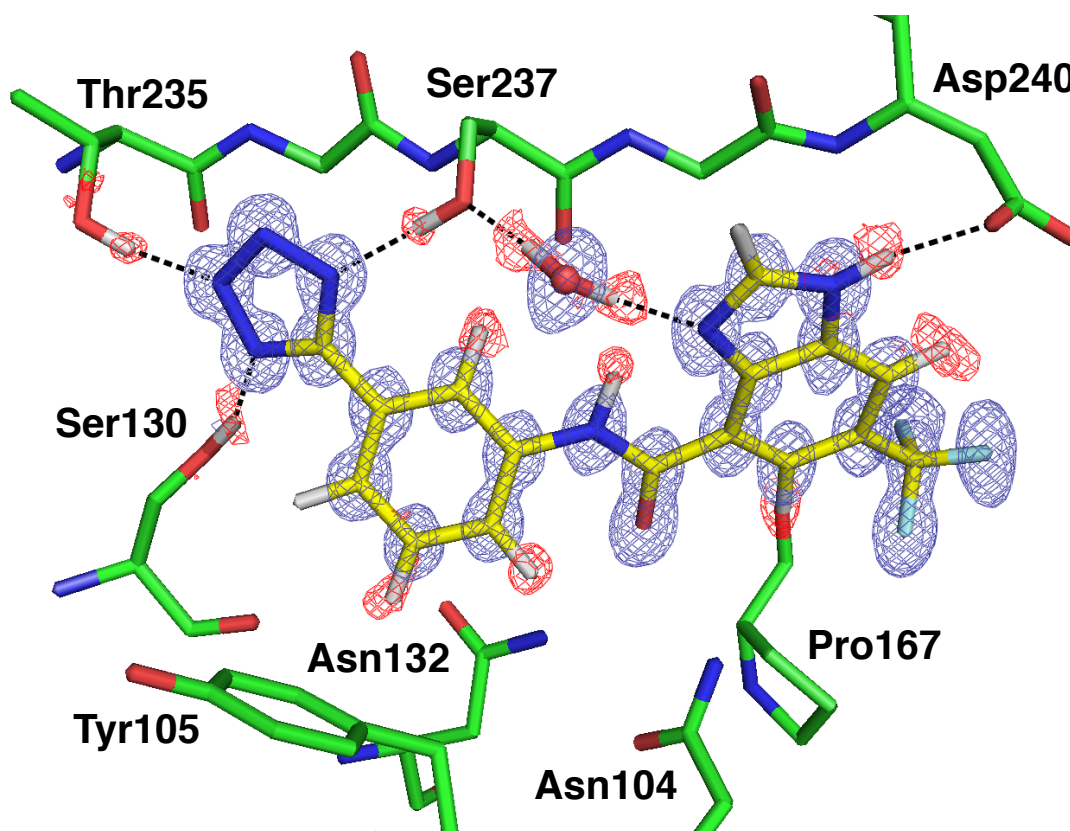


Figure 1-7. Compound 1 in complex with CTX-M-9 at 0.89 Å. $2F_o-F_c$ (blue) and F_o-F_c (red) contoured to 1.5σ and 2.5σ , respectively (PDB: 4UA7). Black dashes denote hydrogen bonds.

Exploring Molecular Interactions with CTX-M:

Given the lab's previous success with compound **1**, the focus of this project was to understand the nuances of CTX-M inhibition and apply it towards inhibition of other β -lactamases. The structure-based design process resulting in compound **1** incorporated a tetrazole to engage the acid-binding motif, and only tested three anionic isosteres in the aryl-CF₃ progenitor series (**Figure 1-8**). We sought to explore whether the tetrazole was required for potent inhibition, and attempted replacement with non-anionic azoles, H-bond donor/acceptor groups, and acids. Surprisingly, none of these analogs were very active, and even the free acid, of which a tetrazole is a bioisostere, was nearly inactive. These results suggested that the charge and π character of the tetrazole was important; neither acid nor azole was sufficient alone. It was observed that the tetrazole forms a π stacking interaction with the amide of the β 3 strand Gly236; this is actually one of two such stacking interactions by **1**, as the benzimidazole also packs against the amide of the β 3 strand Gly238 (**Figure 1-9**). These interactions appeared to be very important for the observed CTX-M affinity, and resulted in the probing of heteroarene amide- π interactions, as discussed more thoroughly in **Chapter 2**.

While the tetrazole was the best heterocycle tested in our amide- π study, the activity of **1** may also be bolstered by an observed low-barrier hydrogen bond (LBHB), which is a special type of short, strong hydrogen bond where the pKa of the donor and acceptor atoms are equal, resulting in a bond where the hydrogen is equally shared and more covalent in character.²³ These bonds are much stronger than normal hydrogen bonds, with an estimated ΔH of formation of 15-20 kcal/mol.²³ Compound **1** is important for the observed bond; the tetrazole hydrogen bonds to Ser130, which hydrogen bonds to Lys73, which has the observed LBHB with Ser70 (**Figure 1-10**).²⁴ The aryl ring is also likely important, as the hydration state changes from the apo structure, with waters 1 and 4 supporting H-bonding partner Ser70. Importantly, the observed hydrogen density is equidistant from both atoms, with a total bond length of 2.53 Å, in line with predicted LBHBs.²³ While there is a fair amount of debate about the role of LBHBs in protein structure and function, recent NMR work supports our crystallographic observations, suggesting that it is a true LBHB. It therefore seems likely that the observed LBHB is stabilizing the bound form of **1**.

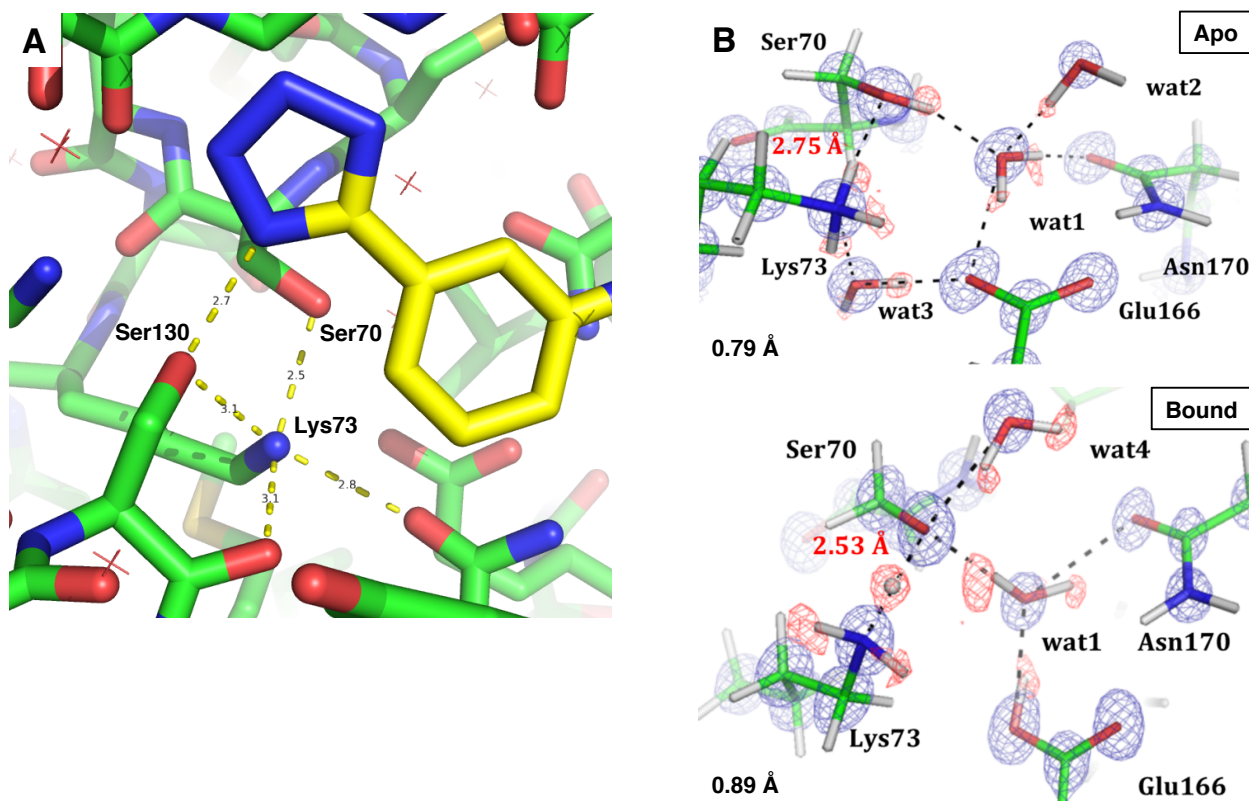


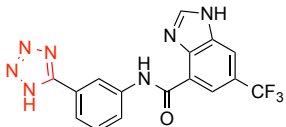
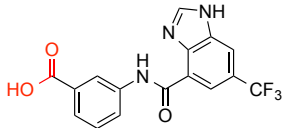
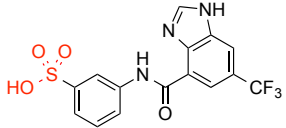
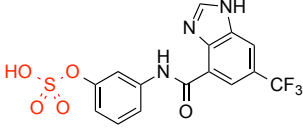
Figure 1-10. The tetrazole of 1 stabilizes a low barrier hydrogen bond in CTX-M. (A) The tetrazole engages in a hydrogen-bonding network involving Lys73 and Ser70. (B) Apo (top) and 1 (bottom) bound CTX-M at 0.79 Å and 0.89 Å, respectively. $2F_o - F_c$ maps (blue) are contoured at 1.5σ . The positive $F_o - F_c$ peaks (red, 2σ) indicate the positions of hydrogen atoms. Note the differences in hydration and the Lys73—Ser70 LBHB. Adapted from reference 24.

Translation to KPC-2 Inhibition:

The previous work revealed the importance of the tetrazole and amide- π interactions towards potent, non-covalent CTX-M inhibition. When tested against other similar enzymes, like the Class A TEM-1 or SHV-2, compound **1** quickly lost activity (**Table 1-1**). The previous acid analogs also showed a similar trend, with no detectable TEM-1 activity, and a similar (though not as severe) drop in SHV-2 activity, with a noticeable penalty for tetrazole replacement. Surprisingly, the Class A carbapenemase KPC-2 showed the least preference for acid-type, with no drop in activity on tetrazole

replacement. Curious, we were able to obtain a structure of the sulfonic acid analog bound to KPC-2 (**Figure 1-11**), which revealed an unexpected binding orientation – the sulfonic acid pointed into the acid binding motif, but the CF₃-benzimidazole sat near the Tyr105 hydrophobic shelf. This positioning is clearly suboptimal, and mirrored additional KPC-2 structures obtained for other analogs within the original aryl series (not shown).

Table 1-1. KPC-2 activity is unaffected by tetrazole replacement.

	CTX-M-14 K _i (μM)	TEM-1 K _i (μM)	SHV-2 K _i (μM)	KPC-2 K _i (μM)
	0.089	> 1700	27	182
	1500	> 2000	200	232
	889	> 2000	149	184
	450	> 7000	180	160

K_i calculated from a biochemical IC₅₀ (nitrocefin substrate) using $K_i = IC_{50}/(1 + [S]/K_m)$.

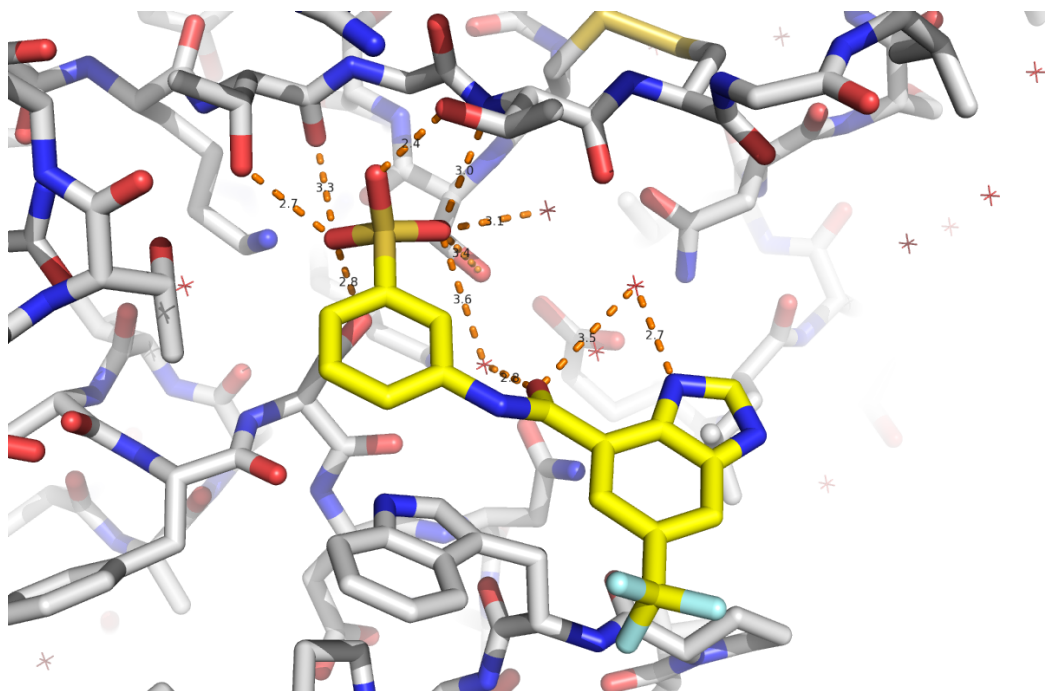


Figure 1-11. Sulfonic acid analog of 1 in complex with KPC-2. Orange dashes denote hydrogen bonds. Note the suboptimal CF₃-benzimidazole orientation.

KPC-2 is of particular interest due to its ability to hydrolyze nearly all β -lactams, especially carbapenems, one the most efficacious β -lactam classes for serious Gram-negative infections. Given the clinical significance, we wanted to transition CTX-M specific scaffold **1** into a potent KPC-2 inhibitor. Looking at the superimposition of KPC-2 onto the CTX-M complex of **1** (**Figure 1-12**), there are several key enzyme differences. For one, while the acid-binding motif is still intact, there is a S237T mutation, and further down the β 3 strand, a twist enforced by a structural disulfide. We hypothesized that steric occlusion caused by this twist gave the unfavorable binding pose observed for the sulfonic acid analog. At the “bottom” of the active site, we lose a hydrogen bond with the amide via a N104P mutation, but the hydrophobic sub-pocket is retained with P167L. Given these changes, we felt that it was possible to retain favorable interactions while avoiding steric clash with the β 3 strand, so we synthesized

~ 80 analogs roughly falling into four categories (**Figure 1-13**): 1) aryl replacements, with an emphasis on smaller heterocycles near the amide linkage, 2) different aryl meta substitutions – a ring twist would putatively accommodate the β 3 strand, 3) sulfonamide analogs, in order to provide *sp*³ flexibility and optimal Asn interactions, and 4) truncated fusions, to reduce total interactions near the β 3 twist. Unfortunately, all of these analogs failed to significantly improve KPC-2 activity, and led us to believe that the aryl tetrazole scaffold was not well suited for inhibiting other β -lactamases. These observations directly lead to the scaffold discovery and optimization efforts of **Chapters 3** and **4**, which are focused primarily on KPC-2, as well as the fragment discovery efforts of **Chapter 5**, which aim to discover broad-spectrum scaffolds against diverse β -lactamases.

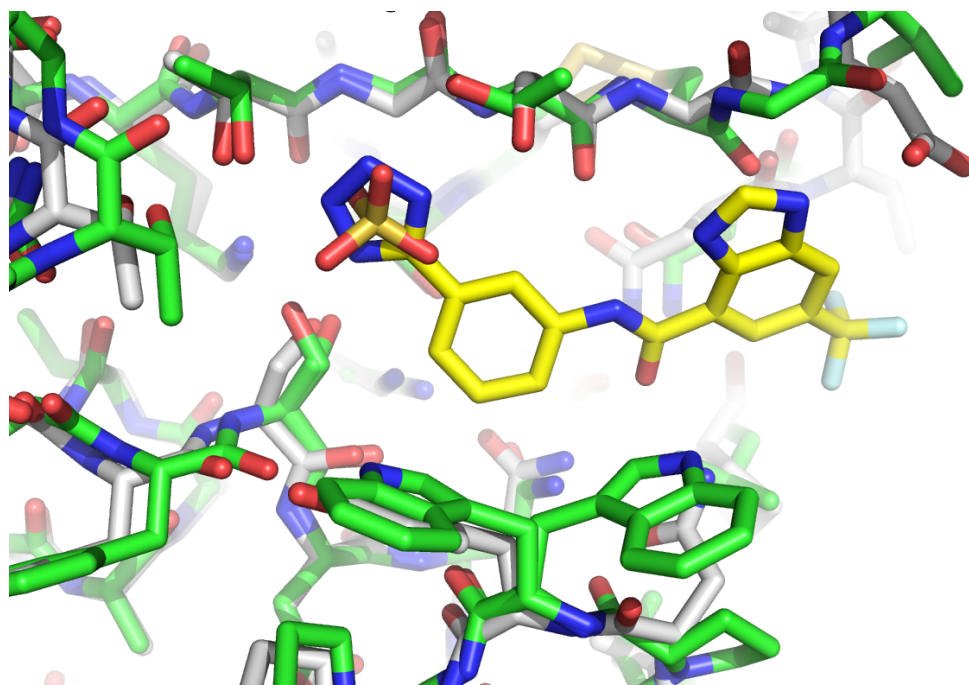


Figure 1-12. Compound 1 complex with CTX-M-9 superimposed onto an apo KPC-2 structure. CTX-M (white and yellow, PDB code 4UA7); apo KPC-2 (green, PDB code 5UL8). Apo KPC-2 structure has a bound sulfate in the acid-binding motif.

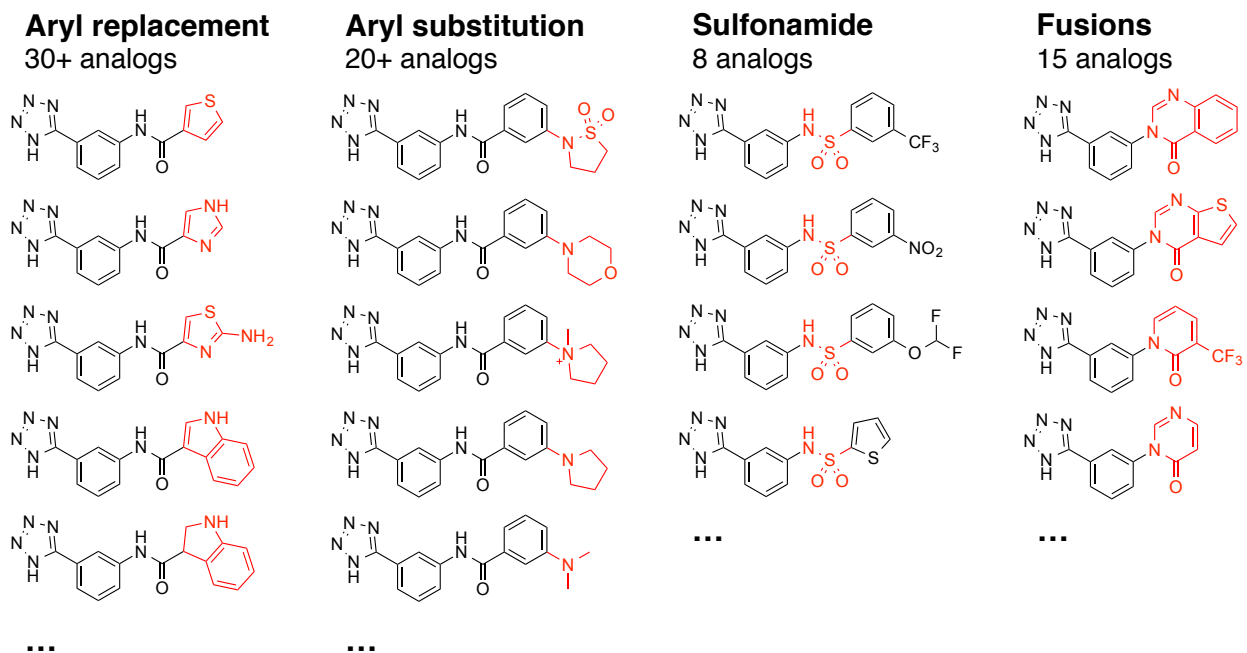


Figure 1-13. Synthesized analogs of the original aryl scaffold. ~ 80 total analogs were synthesized to improve KPC-2 activity; none were successful in improving K_i .

References:

1. P. Macheboeuf, C. Contreras-Martel, V. Job, O. Dideberg, and A. Dessen, *FEMS Microbiol. Rev.*, 2006, 30, 673-691.
2. M. Thanbichler, L. Shapiro. *Nat. Rev. Microbiol.* 2008, 6, 28-40.
3. Y. Kawai, K. Mickiewicz, J. Errington. *Cell*, 2018, 172 (5), 1038-1049.
4. Y. Kawai, R. Mercier, L. J. Wu, P. Dominguez-Cuevas, T. Oshima, J. Errington. *Current Biology*, 2015, 25, 1613-1618.
5. C. Fuda, M. Suvorov, S. B. Vakulenko, and S. Mobashery. *JBC*, 2004, 279 (39), 40802-40806.
6. S. Sun, M. Selmer, and D. I. Andersson. *PLOS One*, 2014, 9 (5), e97202.
7. C. Urbach, J. Fastrez, and P. Soumillion. *JBC*, 2008, 283, 32516-32526.
8. H. Nikaido. *Microbiol. and Mol. Biol. Rev.*, 2003, 67 (4), 593-656.
9. S. M. Drawz, R. A. Bonomo. *Clin. Microbiol. Rev.*, 2010, 23 (1), 160-201.
10. K. Bush. *Antimicrob. Agents Chemother.*, 2018, 62 (10), e01076-18.
11. K. Bush, P. A. Bradford. *Nat. Rev. Microbiol.*, 2019, 17, 295-306.
12. R. G. Alderson, D. Barker, J. B. O. Mitchell. *J. Mol. Evol.*, 2014, 79(3-4), 117-129.
13. S. T. Cahill, R. Cain, D. Y. Wang, C. T. Lohans, D. W. Wareham, H. P. Oswin, J. Mohammed, J. Spencer, C. W. G. Fishwick, M. A. McDonough, C. J. Schofield, and J. Brem. *Antimicrob. Agents Chemother.*, 2017, 61 (4), e02260-16.
14. C. L. Tooke, P. Hinchliffe, P. A. Lang, A. J. Mulholland, J. Brem, C. J. Schofield, and J. Spencer. *Antimicrob. Agents Chemother.*, 2019, 63 (10), e00564-19.
15. K. M. Papp-Wallace, N. Q. Nguyen, M. R. Jacobs, C. R. Bethel, M. D. Barnes, V. Kumar, S. Bajaksouzian, S. D. Rudin, P. N. Rather, S. Bhavsar, T. Ravikumar, P.

- K. Deshpande, V. Patil, R. Yeole, S. S. Bhagwat, M. V. Patel, F. van den Akker, and R. A. Bonomo. *J. Med. Chem.*, 2018, 61, 4067-4086.
16. R. Tsivkovski and O. Lomovskaya. *Antimicrob. Agents Chemother.* 2019, just accepted, DOI: 10.1128/AAC.01935-19.
 17. D. E. Ehmann, H. Jahic, P. L. Ross, R. Gu, J. Hu, T. F. Durand-Reville, S. Lahiri, J. Thresher, S. Livchak, N. Gao, T. Palmer, G. K. Walkup, and S. L. Fisher. *J. Biol. Chem.* 2013, 288 (39), 27960-27971.
 18. J. Delmas, Y. Chen, F. Prati, F. Robin, B. K. Shoichet, R. Bonnet. *J. Mol. Biol.* 2008, 375, 192-201.
 19. K. M. Papp-Wallace, M. L. Winkler, M. A. Taracila, R. A. Bonomo. *Antimicrob. Agents Chemother.*, 2015, 59 (7), 3710-3717.
 20. Y. Chen and B. Shoichet. *Nat. Chem. Biol.*, 2009, 5 (5), 358-364.
 21. D. A. Nichols, P. Jaishankar, W. Larson, E. Smith, G. Liu, R. Beyrouthy, R. Bonnet, A. R. Renslo, and Y. Chen. *J. Med. Chem.*, 2012, 55, 2163-2172.
 22. O. A. Pemberton, X. Zhang, D. A. Nichols, K. DeFrees, P. Jaishankar, R. Bonnet, J. Adams, L. N. Shaw, A. R. Renslo, and Y. Chen. *Antimicrob. Agents Chemother.*, 2018, 62 (8), e02563-17.
 23. W. W. Cleland, P. A. Frey, and J. A. Gerlt. *J. Biol. Chem.*, 1998, 273 (40), 25529-25532.
 24. D. A. Nichols, J. C. Hargis, R. Sanishvili, P. Jaishankar, K. DeFrees, E. W. Smith, K. W. Wang, F. Prati, A. R. Renslo, H. L. Woodcock, and Y. Chen. *JACS.* 2015, 137, 8076-8095.

Chapter 2

An Empirical Study of Amide–Heteroarene π -stacking Interactions Using Reversible Inhibitors of a Bacterial Serine Hydrolase

Kyle DeFrees, M. Trent Kemp, Xochina ElHilali-Pollard, Xiujun Zhang, Ahmed
Mohamed, Yu Chen, and Adam R. Renslo

Abstract:

Compared to aryl–aryl π -stacking interactions, the analogous stacking of heteroarenes on amide π systems is less well understood and vastly underutilized in structure-based drug design. Recent theoretical studies have delineated the important geometric coordinates of the interaction, some of which have been confirmed with synthetic model systems based on Rebek imides. Unfortunately, a broadly useful and tractable protein–ligand model system of this interaction has remained elusive. Here we employed a known inhibitor scaffold to study π -stacking of diverse heteroarene substituents on the amide face of Gly238 in the cephalosporinases CTX-M-14 and CTX-M-27. Biochemical inhibition constants (K_i) and biophysical binding constants (K_d) were determined for nineteen new analogues against both enzymes, while multiple high-resolution co-crystal structures revealed remarkably consistent placement of the probe heteroarene on Gly238. The data presented support the predicted importance of opposing dipoles in amide–heteroarene interactions and should be useful for evaluating other theoretical predictions concerning these interactions.

Introduction:

Mining of large crystallographic data sets has revealed the importance of non-canonical intermolecular interactions in protein structure and also in protein–ligand binding.¹⁻⁴ One of these is the ability of protein backbone amides to participate in stacking interactions with their π surfaces. First noted in the stacking of aromatic side chains on backbone amides,¹ the importance of the interaction in protein–ligand binding is becoming increasingly apparent. An important example is found in the S1 pocket of the serine protease factor Xa (fXa), which is lined by an amide backbone π surface that can engage heterocycles in the P1 side chain of fXa inhibitors.^{5, 6} In a recent computational study, Sherrill and co-workers concluded that the well-known affinity of chloroarene P1 moieties for the S1 pocket is better understood in terms of π stacking with the backbone amides than by a Cl– π interaction with Tyr228.

Recent computational studies by Imai,⁷ Diederich,⁸ and Wheeler⁹ have sought to define the optimal geometries and distances for amide–heteroarene interaction, using formamide⁷ or N-methylacetamide^{8, 9} (NMAC) as a model amide (**Figure 2-1**). In general these studies have suggested a preference for offset stacking in which the dipole moments or local electric field of the amide and heteroarene are roughly opposed (i.e. $\alpha \sim 180^\circ$, **Figure 2-1**). Wheeler showed, however, that intermolecular N–H₃C interactions could override the preference for opposed dipoles in some cases. Wheeler’s model⁹ therefore introduces additional molecular descriptors to better capture these local effects and has most recently¹⁰ been extended to stacking on the π surface of Arg–Asp salt bridges.

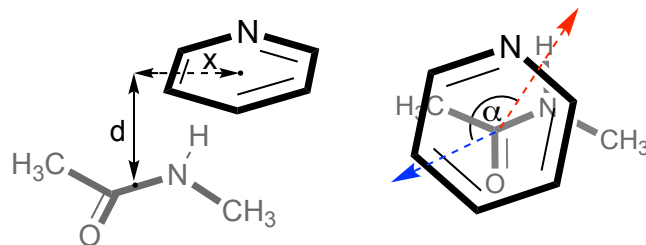


Figure 2-1. Coordinate system employed in computational studies of amide–heteroarene interactions. Dipole moment vectors for the pyridyl ring (red arrow) and amide (blue arrow) are shown, using the physics convention with arrowhead electropositive.

Rebek introduced the use of cleft-like imides derived from Kemp's triacid¹¹ to model a variety of molecular phenomena, from the stacking and H-bonding of adenine bases to abiotic self-replicating systems.^{12, 13} Recently, Diederich¹⁴ described an elegant application of this platform to interrogate amide–heteroarene π -stacking interactions. This system comprises a Rebek imide host and cognate 2,6-di(isobutyramido)pyridine guest that associate in non-polar solvents with their respective para substituents held in close proximity for interaction (**Figure 2-2**). Using double-mutant analyses to isolate incremental Gibbs free energies ($\Delta\Delta G$) for the interacting distal substituents, this study confirmed the favourable effects of N-methyl carboxamide stacking on several different heteroarenes and confirmed N-Me amides as preferred stacking partners compared to phenyl, ethyl, or thiomethyl groups.

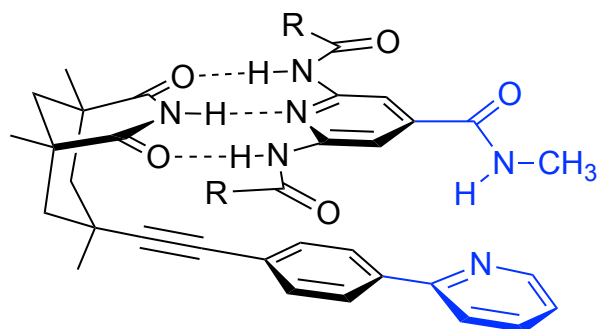


Figure 2-2. A Rebek imide host bound through complementary hydrogen bonding to its cognate guest, placing pendant substituents (blue) in close proximity.

Factor Xa and its known ligands (**Figure 2-3**) would appear to be excellent models to study amide–heteroarene interactions in a more pharmacologically relevant context. A strong cation– π interaction in the S4 pocket along with a Cl– π interaction in S1 places an oxazole ring ~ 3.8 Å from the amide surface of Gln192, well placed for an amide–heteroarene interaction. However, a liability of this scaffold is the fact that the heteroarene ring being probed also serves as a linker to the P1 side chain. As noted by Diederich,⁶ replacement of 2,4-oxazole with related heteroarenes such as isoxazole or 2,5-oxazole significantly alters the angular relationship between the tricyclic core and the terminal chlorothiophene, an effect that is likely to overwhelm and confound any attempt to isolate and study the amide–heteroarene interaction within this system.

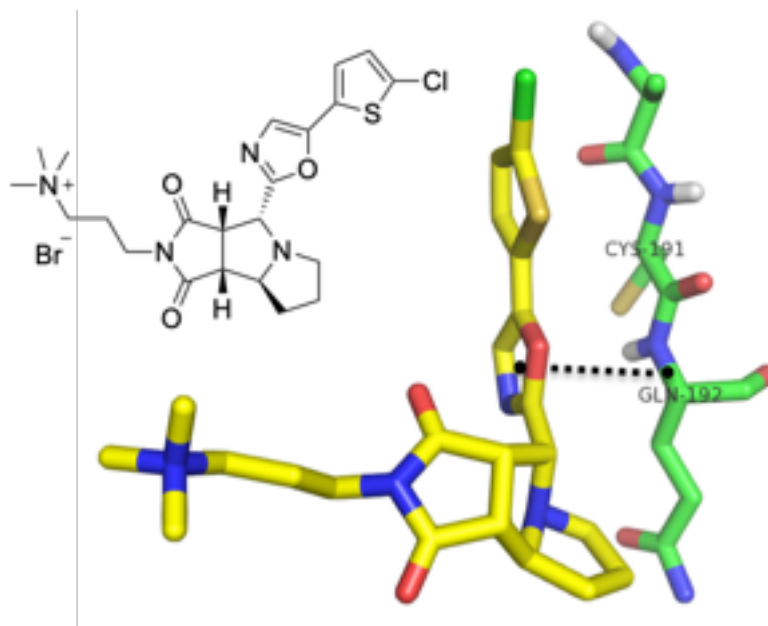


Figure 2-3. Factor Xa inhibitor (left) and its interaction with Gln192 in the complex crystal structure (PDB: 2Y5G).

A more recent study by the same group¹⁵ employed reversible-covalent inhibitors of the cysteine protease cathepsin L in which the terminus of the P3 side chain was

altered with diverse heteroarenes expected to interact with an amide π surface lining the S3 pocket. With a terminal heteroarene, this system avoids the problem of variable angles of departing bonds in different heteroarenes. However, study of the cathepsin inhibitors revealed a different complication – the targeted amides of Gly67 and Gly68 in the S3 pockets are arranged with opposite dipole orientations. Thus, while the expected preference of heteroarenes over simple arenes was confirmed, flexibility in the ligand's P3 side chain allowed interaction with the amide π surface of either Gly67 or Gly68, rendering the effects of relative dipole–dipole angles impossible to discern.

Here we propose the serine hydrolase CTX-M, an extended-spectrum β -lactamase, as an improved model system for study of amide–heteroarene π -stacking under physiological conditions. The utility of this system hinges on a non-covalent, reversible inhibitor scaffold previously described by our laboratories,^{16, 17} and exemplified by **1** (**Figure 2-4**). Extensive crystallographic characterization of **1** and its congeners has revealed a highly conserved binding mode enforced by multiple polar and hydrophobic interactions in the active site of CTX-M enzymes. These interactions include H-bonding and stacking of the tetrazole ring with the β -3 strand, H-bonding with Asn132 and Asn104, and a hydrophobic interaction between the trifluoromethyl group and Pro167 (ESI, **Figure 2-11**). Most relevant to the current study is Gly238 of the β -3 strand, which presents a π surface ideally positioned for stacking with probe heterocycles (i.e., R) in analogues such as **2–20** (**Figure 2-4**).

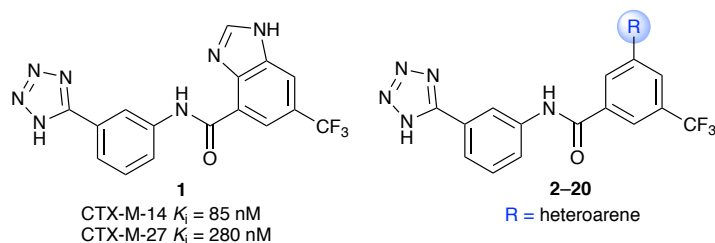


Figure 2-4. Known CTX-M inhibitor 1 and new analogues 2–20 described herein.

Herein we describe the synthesis of **2–20** and the determination of K_i and K_D values for all analogues against CTX-M-14 and CTX-M-27. High-resolution complex crystal structures of select analogues confirmed the expected binding mode, which places the heteroarene substituent $\sim 3.7\text{--}3.9$ Å from Gly238. The activity and binding data are interpreted in terms of suggested^{8, 9} ‘rules-of-thumb’ governing the interaction. We find these rules to be useful for predicting affinities in congeneric series, but caution that more rigorous computational analysis will be required to understand the subtleties of this interaction.

Results and Discussion:

The heteroarenes employed in analogues **2–20** were selected to encompass the majority of ring systems examined in earlier computational studies, and included regioisomeric pyridine, pyrimidine, furan, and thiophene analogues, as well as nitrogen heterocycles of increasing N-atom count (**Figure 2-5**). The phenyl analogue **2** was prepared as a control and comparator. The synthesis of **2–20** involved the late-stage coupling of the relevant benzoic acid intermediates with commercial 3-(1*H*-tetrazol-5-yl)aniline using HATU. Benzoic acids for **2–13** and **15** were synthesized via Suzuki coupling of heterocyclic boronic acids or bromides with tert-butyl 3-bromo-5-

(trifluoromethyl) benzoate or 3-bromo-5-(trifluoromethyl)benzoic acid, followed by cleavage of the t-butyl ester (when required). Benzoic acid intermediates for the preparation of analogues **14** and **16** were prepared via Ullman/Goldberg coupling, while compound **17** was obtained by reaction of tert-butyl 3-bromo-5-(trifluoromethyl)benzoate with imidazole in the presence of CuI and Pd(OAc)₂.¹⁸ Benzoic acid intermediates used for the preparation of compounds **18–20** were obtained via cycloaddition or cyclization reactions of the corresponding azide, amine, or nitrile, respectively. All final analogues were purified by HPLC before evaluation. Full synthetic details and characterization of all analogues are provided in the ESI.

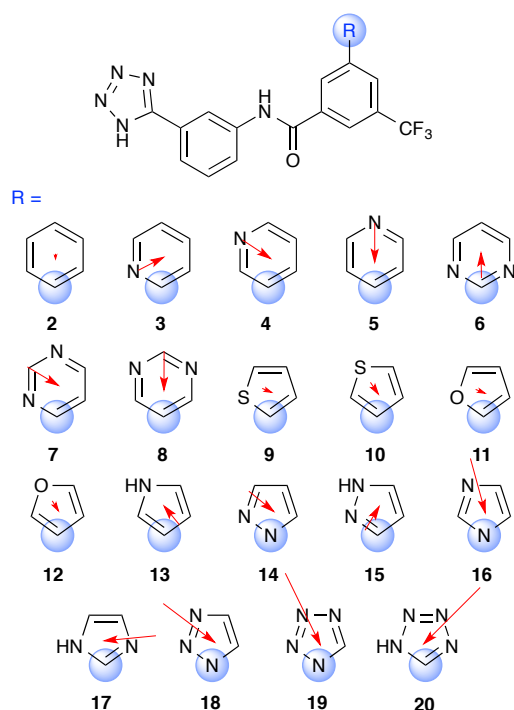


Figure 2-5. Structure of CTX-M inhibitors 2–20 bearing diverse heteroaryl substituents R. Blue spheres denote atom of attachment. Red arrows depict direction and magnitude of calculated dipole moments of corresponding methyl-substituted heteroarenes using B3LYP/6-31G** with PBF solvation (10.64ε).

To determine whether the pendant heteroarenes in **2–20** are properly positioned to stack on Gly238 in the β -3 strand, the structures of representative analogues were

solved in complex with both CTX-M-14 and CTX-M-27. These CTX-M isoforms differ only by the presence of Asp (CTX-M-14) or Gly (CTX-M-27) at position 240 of the β -3 strand, directly adjacent to the site of amide–heteroarene interaction with Gly238 (there is no residue 239 in the CTX-M sequence due to numbering conventions in Class A β -lactamases). Ligands **3**, **14**, and **20** were solved in complex with CTX-M-14 to resolutions of 1.4 Å, 1.4 Å, and 1.25 Å, respectively. These structures revealed a highly conserved binding orientation that is exactly analogous to that of **1**, with the pendant heteroarene involved in an apparent stacking interaction with Gly238, as posited (**Figure 2-6** and ESI **Figure 2-12**). In all three structures, the side chain of Asp240 swings away from the terminal heteroarene ring towards solvent to accommodate the stacking interaction.

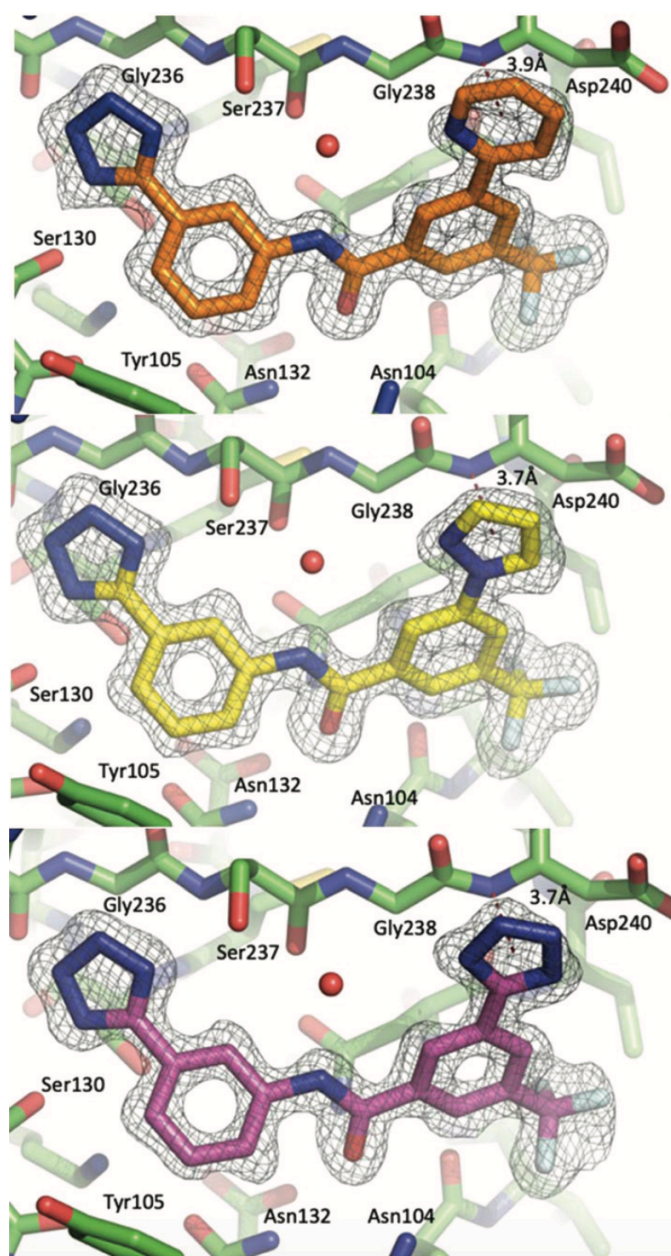


Figure 2-6. Complex structures of analogues 3 (PDB: 600K; top), 14 (PDB: 600J; middle) and 20 (PDB: 600F; bottom) bound to CTX-M-14 at 1.4 Å, 1.4 Å, and 1.25 Å resolution. Unbiased F_o-F_c densities are shown at 3σ . Stacking distances are indicated, as measured from centroid of the heteroarene to the amide nitrogen atom.

It is notable that compound **20** binds in the canonical fashion when one considers that an unfavourable charge–charge interaction might have been expected between the tetrazol-5-yl ring and Asp240. Consistent with this, analogue **20** was both the weakest inhibitor of CTX-M-14, and the most potent inhibitor of CTX-M-27, Gly240 replacing

Asp240 in the latter enzyme, thereby removing the putative charge–charge interaction (**Table 2-1**). Thus, a likely unfavourable interaction with Gly240 in CTX-M-14 is insufficient to produce a distinct binding mode for **20**, thus suggesting that the remaining analogues in the series bind similarly.

High resolution (1.5 Å and 1.25 Å) structures were also solved of compounds **14** and **20** in complex with CTX-M-27 and revealed the expected binding mode and engagement of Gly238 (**Figure 2-7**). Amide–heteroarene stacking distances in the five new complex structures were measured from the centre of electron density of the heteroarene ring to the midpoint of the amide nitrogen atom and varied between 3.7–3.9 Å, values that are consistent with those expected for an amide–heteroarene π -stacking interaction.

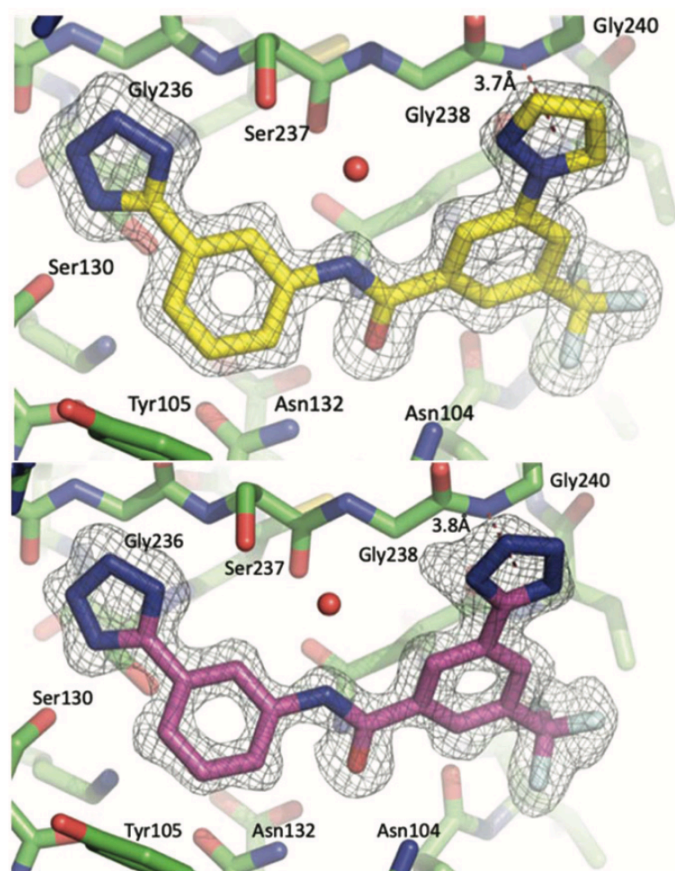


Figure 2-7. Complex structures of analogues 14 (PDB: 6OOH; top) and 20 (PDB: 6OOE; bottom) bound to CTX-M-27 at 1.5 Å and 1.25 Å. Unbiased F_o-F_c densities are shown at 3σ . Stacking distances are indicated, as measured from centroid of the heteroarene to the amide nitrogen atom.

Compounds **2–20** were tested in 11-point dose response, in technical triplicate, for inhibition of both CTX-M-14 and CTX-M-27 using a nitrocefin substrate assay (**Table 2-1**). The inhibition curves for all replicates are provided as ESI and speak to the precision of the measured K_i values. Consistent with the movement of Asp240 noted in the X-ray structures, analogues **2–20** returned K_i values that were *ca.* 5–10-fold weaker for CTX-M-14 than for CTX-M-27, the latter requiring no analogous movement of residue 240 to accommodate ligand binding (**Figure 2-6 and 2-7**). Similar isoform potency shifts across the analogue series provides additional evidence for a conserved binding mode.

Table 2-1. K_i and K_d values for heterocycles 2–20 with CTX-M-14 and CTX-M-27.

Cmpd	CTX-M-14			CTX-M-27			
	R=	K_i^a (μM)	K_d^b (μM)	K_i^a (μM)	K_d^c (μM)	$\Delta\Delta G_{K_i}^d$ (kcal mol $^{-1}$)	$\Delta\Delta G_{K_d}^e$ (kcal mol $^{-1}$)
2	Phenyl	79.6 \pm 9.2	N.D. ^f	10.4 \pm 0.4	40.3 \pm 2.7 ^g	—	—
3	Pyrid-2-yl	27.7 \pm 0.9	8.14 \pm 0.08	3.92 \pm 0.48	1.79 \pm 0.05	0.578	1.844
4	Pyrid-3-yl	29.3 \pm 1.9	43.5 \pm 0.9	2.65 \pm 0.31	3.85 \pm 0.05	0.810	1.390
5	Pyrid-4-yl	18.5 \pm 1.3	30.3 \pm 0.6	3.06 \pm 0.24	5.90 \pm 0.13	0.724	1.138
6	Pyrimidin-2-yl	15.3 \pm 2.1	4.07 \pm 0.04	2.26 \pm 0.28	0.834 \pm 0.024	0.904	2.296
7	Pyrimidin-4-yl	18.9 \pm 2.1	8.34 \pm 0.08	3.72 \pm 0.23	2.91 \pm 0.05	0.609	1.556
8	Pyrimidin-5-yl	53.8 \pm 4.8	42.1 \pm 0.9	4.00 \pm 0.36	4.41 \pm 0.04	0.566	1.310
9	Thiophen-2-yl	27.3 \pm 1.8	50.2 \pm 0.6	5.50 \pm 0.27	13.8 \pm 1.2 ^g	0.377	0.635
10	Thiophen-3-yl	31.1 \pm 2.2	51.0 \pm 1.2	5.21 \pm 0.28	11.4 \pm 0.7 ^g	0.409	0.748
11	Furan-2-yl	17.2 \pm 0.3	15.7 \pm 0.3	3.86 \pm 0.37	2.50 \pm 0.07	0.587	1.646
12	Furan-3-yl	17.4 \pm 0.4	26.1 \pm 1.2	3.02 \pm 0.45	3.28 \pm 0.07	0.732	1.485
13	1 <i>H</i> -Pyrrol-3-yl	10.6 \pm 0.8	17.6 \pm 0.7	2.07 \pm 0.24	2.28 \pm 0.06	0.956	1.701
14	1 <i>H</i> -Pyrazol-1-yl	22.5 \pm 2.7	19.4 \pm 0.3	2.81 \pm 0.33	2.19 \pm 0.06	0.775	1.725
15	1 <i>H</i> -Pyrazol-3-yl	12.6 \pm 0.5	16.8 \pm 0.5	1.69 \pm 0.14	1.95 \pm 0.07	1.076	1.793
16	1 <i>H</i> -Imidazol-1-yl	30.5 \pm 1.6	29.5 \pm 0.6	3.63 \pm 0.30	6.21 \pm 0.07	0.623	1.107
17	1 <i>H</i> -Imidazol-2-yl	16.9 \pm 0.7	8.63 \pm 0.17	4.04 \pm 0.34	1.33 \pm 0.03	0.560	2.020
18	1,2,3-Triazol-1-yl	32.7 \pm 0.7	32.3 \pm 0.9	3.65 \pm 0.47	4.16 \pm 0.10	0.620	1.345
19	Tetrazol-1-yl	29.7 \pm 0.7	29.8 \pm 1.2	5.30 \pm 0.23	7.24 \pm 0.06	0.399	1.017
20	Tetrazol-5-yl	82.0 \pm 11.6	11.9 \pm 0.1	1.49 \pm 0.25	0.292 \pm 0.004	1.151	2.918

^a Mean \pm SEM of three replicates. Calculated from IC_{50} using $K_i = IC_{50}/(1 + [S]/K_m)$. K_m values were measured for each replicate. ^b Mean \pm SEM of four replicates. SPR generated K_d values were measured at binding equilibrium. ^c Mean \pm SEM of two replicates. SPR generated K_d values were measured at binding equilibrium. ^d Calculated from $\Delta\Delta G = -RT\ln(K_{i,N}/K_{i,2})$ at 298 K, where N represents the compound to which reference compound **2** is being compared. Positive values indicate improved affinity. ^e Same as d, except K_d values were used relative to compound **2**. Positive values indicate improved affinity. ^f Not determined due to solubility limits. ^g Mean \pm SEM of four replicates.

Compared to phenyl congener **2**, the heteroarene-bearing compounds **3–20** exhibited K_i values that were improved by \sim 3–6-fold (analogue **20** being an exception, for the reasons noted above). This was the expected result, and is consistent with the predictions of the computational studies that enhanced dipole–dipole and local electrostatic interaction favour heteroarenes as stacking partners over simple arenes. The magnitude of the potency shift was modest but statistically significant given the high precision of the K_i determinations. The compressed range of K_i values would be consistent with the expected weak nature of the amide–heteroarene interaction, and might further imply relatively small differences in desolvation energies across the congeneric series. If correct, this would be notable, given that previous model systems

have exploited more hydrophobic binding pockets, in part to mitigate confounding desolvation effects.

To probe the binding affinities of **2–20** for CTX-M, we determined K_d values against both proteins by surface plasmon resonance (SPR) spectroscopy, employing the same avi-tagged proteins used for the K_i determinations. Standard error in the mean values (SEM) revealed the high precision of the K_d determinations, similar to the K_i data. We found the K_d values in absolute terms to be remarkably close to the biochemical K_i values for the majority of analogues, whereas some compounds like **3**, **6**, **7**, **9** and **10** showed modest ~2–3-fold differences between K_d and K_i . In fact, only compound **20** exhibited K_d values that were more than 3-fold different from K_i against both proteins. Limited solubility of phenyl comparator **2** did not allow a K_d determination vs. CTX-M-14, while the K_d value of **2** vs. CTX-M-27 was ~ 4-fold weaker than the respective K_i . Overall, the biochemical and biophysical evaluation of **2–20** vs. CTX-M-14 and CTX-M-27 provided a robust data set for analyses of amide–heteroarene interactions. We used the CTX-M-27 K_i and K_d values to calculate $\Delta\Delta G_{K_i}$ and $\Delta\Delta G_{K_d}$ values for analogues **3–20** in reference to comparator **2** (**Table 2-1**).

Taken together, the earlier computational studies of Diederich and Wheeler predict that stronger amide–heteroarene π -stacking interactions should be expected when one or more of the following conditions are met:

- (1) An antiparallel orientation of amide and heteroarene dipole moment vectors.
- (2) A greater magnitude of the dipole moment(s).
- (3) The heteroarene is more electron-deficient.
- (4) Heteroarene ring nitrogens can participate in N \cdots H–C interactions with the

proximal amide function.

We considered whether these simple ‘rules-of-thumb’, as might be applied by a practiced medicinal chemist, could be used to predict rank-order differences in the measured K_i and K_d values for **2–20**. In performing this analysis, we assume that differences in $\Delta\Delta G$ values arise from the relative strength of the corresponding amide–heteroarene interaction, and ignore differences in desolvation penalties between analogues (though admittedly these may be important in certain cases). To eliminate the confounding effects of Asp240 and its interaction with the various heteroarenes, we limit the analysis to the data generated for CTX-M-27.

In computational studies of amide–heteroarene stacking the dipole interaction angle α (**Figure 2-1**) is varied systematically so as to identify the optimal value. In the present case, the binding mode of **2–20** in CTX-M places strict geometric constraints on the orientation of Gly238 and the interacting heteroarene, producing relative sub-optimal α values in many cases. Unsurprisingly then, calculated dipole magnitude alone was a poor predictor of experimental $\Delta\Delta G_{K_i}$ and $\Delta\Delta G_{K_d}$ values (**Figure 2-8**). Discerning the effects of α on $\Delta\Delta G$ instead requires consideration of computed dipole magnitude *and direction* in the context of the established crystallographic binding mode.

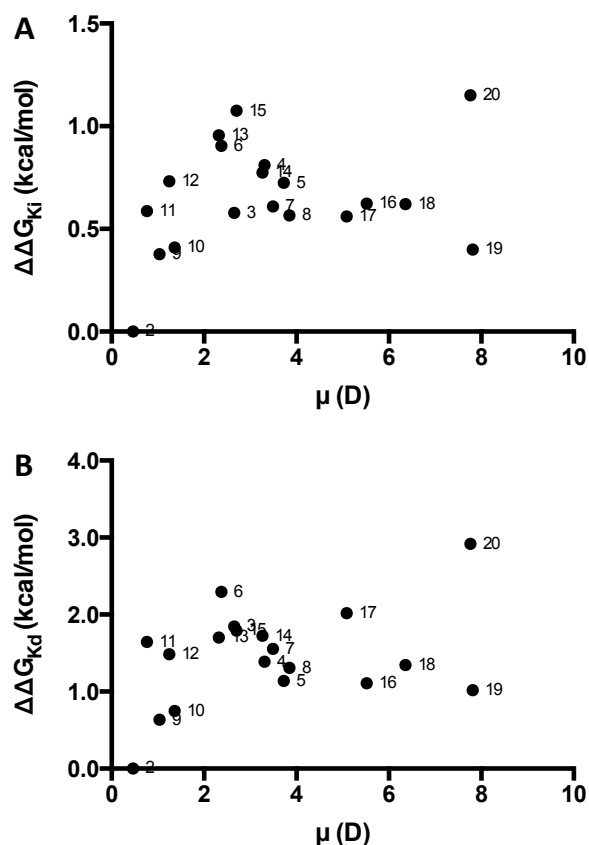


Figure 2-8. Computed dipole moments (μ) vs. (A) $\Delta\Delta G_{K_i}$ and (B) $\Delta\Delta G_{K_d}$ for 2–20. Dipole moments calculated from the corresponding methyl derivatives using B3LYP/6-31G** with PBF solvation (10.64 ϵ).

First, we considered regioisomeric series of pyridine (3–5) and pyrimidine (5–8) congeners, which are presented below in their predicted orientation relative to amide Gly238 when bound in CTX-M (Figure 2-9 and 2-10). Among these six analogues, the 2-pyridyl (3) and 2-pyrimidyl (6) heteroarenes are arranged with opposed dipole moments relative to the Gly238 amide, while 4–5 and 7–8 have less favourable dipole–dipole orientations. In fact, the expected α values for 3 and 6 when bound to CTX-M are quite close to the optimal values of 105° (for 3) and 176° (for 6) reported by Wheeler for these heteroarenes in isolation.⁹ It is therefore significant that compounds 3 and 6 exhibited the best K_d values within each regioisomeric analogue set. The K_i values for

3–8 were more compressed and while the same rank-order trend holds for pyrimidines **6–8**, the K_i values of **3–5** are very similar or within experimental error. Nevertheless, it was striking that rank-order binding affinities (K_d) of analogues **3–8** could be correctly predicted solely on the basis of the amide–heteroarene interaction.

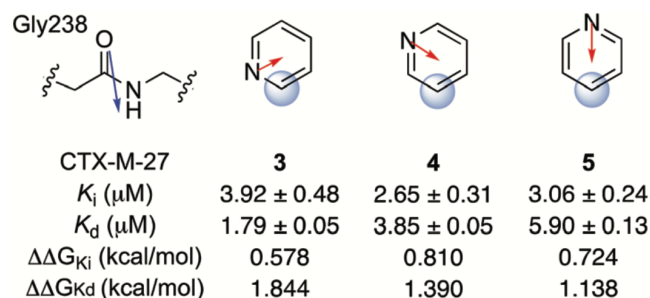


Figure 2-9. Relative orientation of Gly238 and heteroarene substituent R in analogues 3–5. Calculated dipole moments are shown in red; amide dipole in blue as reported by Diederich.¹⁵

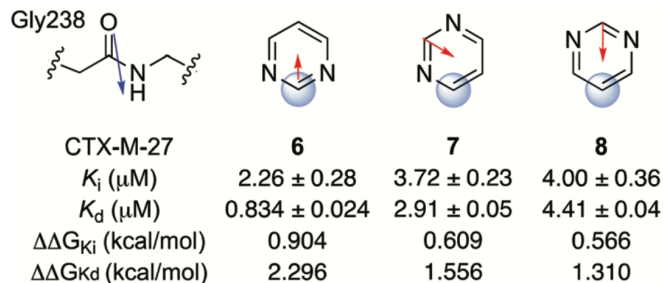


Figure 2-10. Relative orientation of Gly238 and heteroarene substituent R for analogues 6–8.

The predicted⁸ beneficial effect of additional ring nitrogen atoms was also reflected in the superior K_d values of pyrimidines **6–8** as compared to their corresponding pyridine regioisomers **3–5**. The 3–5-fold differences in K_d across the two series are admittedly modest and one might be wary of overinterpreting these differences. On the other hand, a medicinal chemist applying a qualitative dipole–dipole analysis prospectively would have judged correctly which analogues to prioritize for synthesis

and evaluation, and so such rules-of-thumb appear useful as applied to a rigid ligand scaffold and well behaved ligand–protein binding interaction such as that explored here.

In contrast to **6–8**, the regioisomeric forms of the thiophene (**9–10**) and furan (**11–12**) analogues exhibited practically identical K_i and K_d values (**Table 2-1**). This finding is consistent with the similar magnitude and direction of dipole moments for these regioisomers (**Figure 2-5**). Also the K_i and K_d values of **11–12** were superior to **9–10** across all four data sets, consistent with a stronger amide-stacking interaction for the more electron-deficient furans as compared to thiophenes. The data for the remaining heterocyclic analogues **13–20** were not interpretable in terms of the rules of thumb applied. The presence of N–H donors in many of these analogues (**13**, **15**, and **17**) likely make polar interactions and desolvation penalties more significant, and these effects may overwhelm the more subtle contributions of dipole–dipole and local electrostatic interactions. A more rigorous analysis involving computed descriptions of local electrostatics and surface polarizability will likely be required to understand and make accurate predictions across a broader range of heterocycle–amide interactions present in **13–20**. The exceptional binding affinity of tetrazole analogue **20** is however consistent with the predictions of Wheeler⁹ regarding tetrazole–amide interaction.

Finally, it is worth noting that analogues bearing axially unsymmetrical heteroarenes will have two distinct rotameric states capable of stacking on Gly238. The present crystal structures of **3** and **14** are of insufficient resolution to identify a preferred rotamer, but such analysis may be possible in the future, given that sub-Å resolution structures of **1** have been solved in which unambiguous heteroatom assignments are possible (ESI, **Figure 2-11**).¹⁹ The identification of a preferred rotameric state in this

way would enable a more refined understanding of how α values and other factors impact binding affinity in this model system.

Conclusions:

Herein we present a new model system to study amide–heteroarene π -stacking in a pharmacologically relevant context. The bacterial hydrolase CTX-M-27 and inhibitor scaffold represented by **2–20** offer several advantages over previously employed model systems. These include: (1) a reversible and non-covalent ligand scaffold into which diverse heteroarenes can be incorporated in a terminal position, (2) a highly predictable and conserved binding mode that places the probe heterocycle unambiguously in contact with Gly238, and (3) a protein system that is highly amenable to X-ray crystallographic studies at high and ultra-high resolutions. The activity and binding data described herein appear to significantly report on the relative strength of amide–heteroarene stacking interactions between analogues, providing the first example where easily applied rules-of-thumb were used successfully to explain experimental binding affinity data, at least for congeneric series of analogues. In closing, we note that computational studies of the heteroarene-amide interaction present in this new model system should be facilitated by the geometric constraints imposed by the binding mode of **2–20** in CTX-M. It is our hope that a combination of theoretical and empirical study of this model system will produce new insights into the factors governing this intermolecular interaction.

Experimental:

Synthesis and characterization

The syntheses and characterization of new compounds **2–20** are described in the ESI. All compounds tested were judged to be of >95% purity as assessed by a Waters Micromass ZQ 4000 equipped with Waters 2795 Separation Module, Waters 2996 Photodiode Array Detector (254 nm), and Waters 2424 ELS detector. Separations were carried out with an XBridge BEH C18, 3.5 μm , 4.6 \times 20 mm column, at ambient temperature (unregulated) using a mobile phase of water–methanol containing a constant 0.05% formic acid.

Protein expression and purification

All enzymes from this study were expressed using the BL21 (DE3) cell line. Cells were grown on LB agar plates supplemented with 50 $\mu\text{g mL}^{-1}$ kanamycin from cell stocks stored at $-80\text{ }^{\circ}\text{C}$. Single colonies were used to inoculate 50 mL of LB broth with 50 mg mL^{-1} kanamycin and grown at $37\text{ }^{\circ}\text{C}$ overnight. From the overnight culture, 10 mL of cells were used to inoculate 1 L of 2 \times YT broth for untagged and avitagged CTX-M-14 and CTX-M-27. The cells were grown at $37\text{ }^{\circ}\text{C}$ until an OD₆₀₀ of 0.5 to 0.8 was reached at 600 nm. Overexpression of protein was induced with the addition of 0.5 mM isopropyl β -D-1-thiogalactopyranoside (IPTG) at $20\text{ }^{\circ}\text{C}$ for 24 hours, and the cells were harvested with centrifugation at 5000 RPM for 15 minutes at $4\text{ }^{\circ}\text{C}$.

For the untagged CTX-M-14 and CTX-M-27 cell pellets were resuspended in 50 mM MES pH 8.0 with 2 mM EDTA, while AviTag CTX-M-14 and CTX-M-27 were resuspended in 20 mM Tris pH 8.0, 300 mM NaCl, 10% glycerol with 10 mM imidazole. Cells were lysed with sonication and cellular components separated via

ultracentrifugation at 45000 RPM for 1 hour. Untagged enzymes were loaded onto a CM sepharose column and eluted with an increasing NaCl gradient. The AviTag CTX-M was loaded onto a HisTrap affinity column and eluted with an increasing imidazole gradient. All enzymes were additionally purified using a size exclusion HiLoad 16/60 Superdex 75 column. Final protein purity was evaluated with SDS-Page to be at or greater than 95%.

β -lactamase inhibition assays

The hydrolytic activity of CTX-M-14 and CTX-M-27 was determined using the β -lactamase substrate nitrocefin in a reaction buffer containing 100 mM Tris pH 7.0, 20 mM NaCl, 0.02% Triton X-100, and 5% DMSO. Nitrocefin hydrolysis was monitored via absorbance (486 nm) using a FlexStation 3 microplate reader at 37 °C. The nitrocefin concentration was 50 μ M for all inhibition assays. Compounds were tested for IC_{50} in 11-point dose response up to 2.5 mM and 500 μ M for CTX-M-14 and CTX-M-27, respectively (as solubility allowed). The protein was added last to initiate the reaction; the final protein concentration was 0.1 nM for both enzymes. All compounds were tested as technical triplicates with three independent replicates. IC_{50} values were converted to K_i using $K_i = IC_{50}/(1 + [S]/K_m)$. The K_m of nitrocefin was measured for each replicate: 50–64 μ M for CTX-M-14, and 14–22 μ M for CTX-M-27 (data in ESI). Nitrocefin was purchased from Sigma-Aldrich.

SPR binding assays

Compound K_d values were measured on a Biacore 4000 at 25 °C. Avi-CTX-M-14 and Avi-CTX-M-27 were immobilized on a Series S CM5 chip with EDC/NHS coupled

Neutravidin using 10 mM HEPES pH 7.5, 150 mM NaCl, 0.05% Tween 20, and 250 μ M TCEP-HCl. Protein immobilization levels varied between 3340–6166 RU and 4104–6634 RU for CTX-M-14 and CTX-M-27, respectively. Running buffer consisted of 10 mM HEPES pH 7.5, 150 mM NaCl, 0.05% Tween 20, 250 μ M TCEP-HCl, and 5% DMSO. Compounds were flowed for 90 s on and 120 s off, with a 50% DMSO needle wash between injections. Compounds were tested in 10-point dose response with two internal blanks up to 500 μ M and 50 μ M for CTX-M-14 and CTX-M-27, respectively (as solubility allowed). Sensogram data was reference subtracted, solvent corrected, and blank subtracted; K_d values were measured at equilibrium binding between 65–85 s. All compounds were tested in quadruplicate for CTX-M-14 and in duplicate for CTX-M-27. Representative sensograms and K_d fits can be viewed in the ESI.

Crystallization and structure determination

All enzyme crystals were grown using the hanging drop approach, where both CTX-M-14 and CTX-M-27 protein stocks used were at 20 mg mL⁻¹. Equal parts well solution of 1 M potassium phosphate pH 7.9 were mixed with protein and incubated at 20 °C. Complex structures were generated by soaking 5–10 mM ligand concentrations with protein crystals for 6–12 hours in 1 M potassium phosphate pH 7.9 or 1.44 M sodium citrate prior to cryoprotecting with 30% (wt/vol) sucrose supplemented crystal mother liquor. Crystal diffraction data sets were collected at the beamlines 22-ID, 22-BM, and 19-BM at Argonne National Lab Advanced Photon Source (APS). The data sets were indexed, integrated and scaled using the program HKL2000. Initial models were obtained via molecular replacement with the program Phaser in the Phenix suite. Refinement was carried out using phenix.refine, and ligand restraint files were

generated with the program elBOW. The mF_o-DF_c and $2mF_o-DF_c$ maps were generated with the program phenix.mtz2map program for all structures. PDB codes for deposited structures are provided below.

CTX-M-14 with compound **3**: 6OOK

CTX-M-14 with compound **14**: 6OOJ

CTX-M-27 with compound **14**: 6OOH

CTX-M-14 with compound **20**: 6OOF

CTX-M-27 with compound **20**: 6OOE

Dipole calculations

Dipole moments were calculated with Jaguar in Maestro using the corresponding methyl derivatives, as done by Diederich in previous studies. Structures were first optimized using B3LYP/6-31G**, then dipoles were calculated using B3LYP/6-31G** with PBF solvation (10.64ϵ). This dielectric was chosen as a surrogate for the local binding environment in CTX-M, which is moderately solvent exposed. Dipoles were also calculated for water (80.37ϵ) and CHCl_3 (4.806ϵ), which had little effect on the magnitude and no effect on the relative rank order of dipole strength (ESI, **Figure 2-12**). Model type also held no effect; M06-2X/6-31G** and B3LYP-D3/6-31G** with PBF solvation (10.64ϵ) was the same as B3LYP/6-31G**, and gas phase B3LYP/6-31G** was the same as LMP2/6-31G** (ESI, **Figure 2-12**). These results suggest that the reported dipole magnitude and rank order are accurate.

Acknowledgements:

This work was funded in part by the National Institutes of Health (NIH) grant AI103158. We thank Dr Wilian Cortopassi Coelho (Jacobson Laboratory, UCSF) for guidance in performing the dipole calculations.

References:

1. G. Duan, V. H. Smith and D. F. Weaver, *J. Phys. Chem. A*, 2000, 104, 4521-4532.
2. E. A. Meyer, R. K. Castellano and F. Diederich, *Angew. Chem., Int. Ed. Engl.*, 2003, 42, 1210–1250.
3. C. Bissantz, B. Kuhn and M. Stahl, *J. Med. Chem.*, 2010, 53, 5061–5084.
4. L. M. Salonen, M. Ellermann and F. Diederich, *Angew. Chem., Int. Ed.*, 2011, 50, 4808–4842.
5. L. M. Salonen, C. Bucher, D. W. Banner, W. Haap, J.-L. Mary, J. Benz, O. Kuster, P. Seiler, W. B. Schweizer and F. Diederich, *Angew. Chem., Int. Ed.*, 2009, 48, 811–814.
6. L. M. Salonen, M. C. Holland, P. S. Kaib, W. Haap, J. Benz, J. L. Mary, O. Kuster, W. B. Schweizer, D. W. Banner and F. Diederich, *Chemistry*, 2012, 18, 213–222.
7. Y. N. Imai, Y. Inoue, I. Nakanishi and K. Kitaura, *J. Comput. Chem.*, 2009, 30, 2267–2276.
8. M. Harder, B. Kuhn and F. Diederich, *ChemMedChem*, 2013, 8, 397–404.
9. A. N. Bootsma and S. E. Wheeler, *ChemMedChem*, 2018, 13, 835–841.
10. A. N. Bootsma and S. E. Wheeler, *J. Chem. Inf. Model.*, 2019, 59, 149–158.
11. D. S. Kemp and K. S. Petrakis, *J. Org. Chem.*, 1981, 46, 5140–5143.
12. J. Rebek, *Acc. Chem. Res.*, 1990, 23, 399–404.
13. E. A. Wintner, M. M. Conn and J. Rebek, *J. Am. Chem. Soc.*, 1994, 116, 8877-8884.

14. M. Harder, M. A. Carnero Corrales, N. Trapp, B. Kuhn and F. Diederich, *Chem. Eur. J.*, 2015, 21, 8455–8463.
15. M. Giroud, J. Ivkovic, M. Martignoni, M. Fleuti, N. Trapp, W. Haap, A. Kuglstatler, J. Benz, B. Kuhn, T. Schirmeister and F. Diederich, *ChemMedChem*, 2017, 12, 257–270.
16. D. A. Nichols, P. Jaishankar, W. Larson, E. Smith, G. Liu, R. Beyrouthy, R. Bonnet, A. R. Renslo and Y. Chen, *J. Med. Chem.*, 2012, 55, 2163–2172.
17. O. A. Pemberton, X. Zhang, D. A. Nichols, K. DeFrees, P. Jaishankar, R. Bonnet, J. Adams, L. N. Shaw, A. R. Renslo and Y. Chen, *Antimicrob. Agents Chemother.*, 2018, 62, e02563-17.
18. F. Bellina, S. Cauteruccio and R. Rossi, *J. Org. Chem.*, 2007, 72, 8543–8546.
19. D. A. Nichols, J. C. Hargis, R. Sanishvili, P. Jaishankar, K. DeFrees, E. W. Smith, K. K. Wang, F. Prati, A. R. Renslo, H. L. Woodcock and Y. Chen, *J. Am. Chem. Soc.*, 2015, 137, 8086–8095.

Electronic Supporting Information

Supplementary Figures

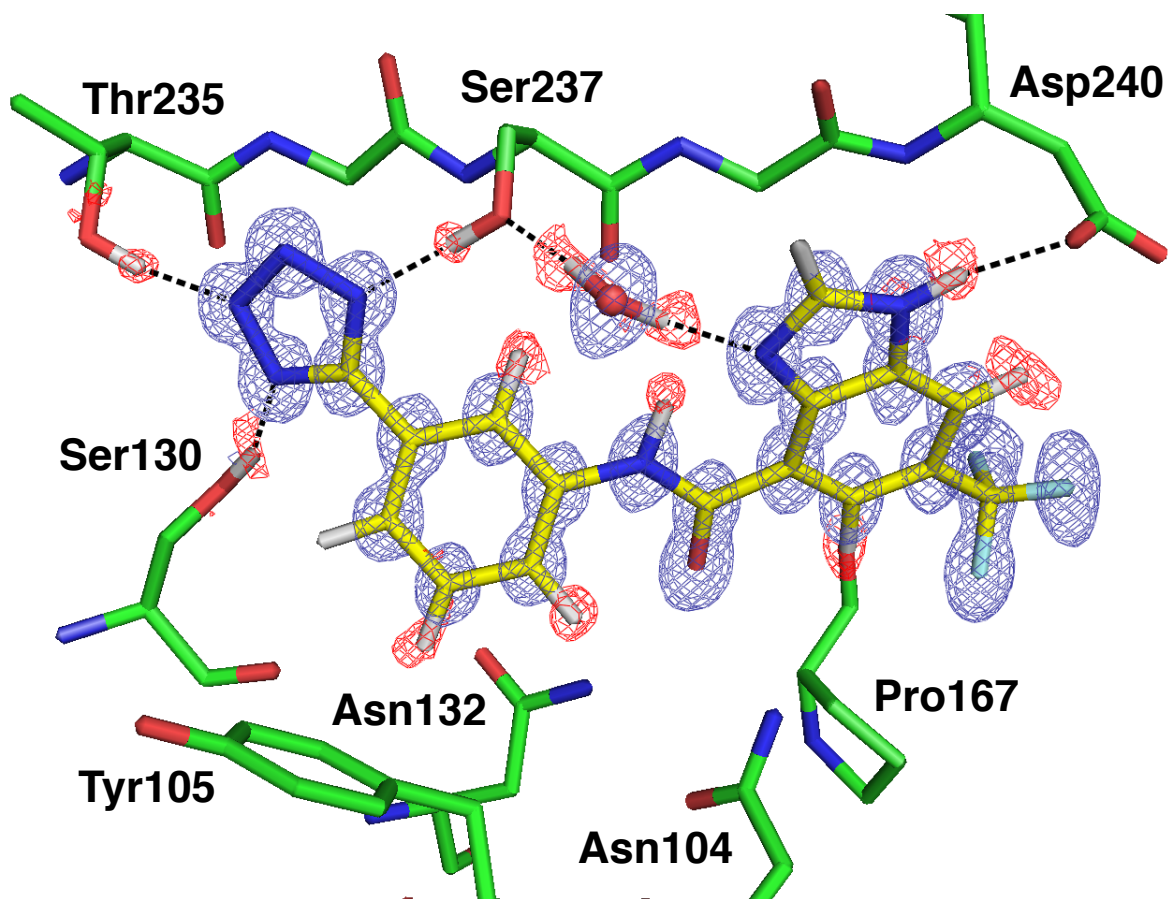


Figure 2-11. Compound 1 in complex with CTX-M-14 at 0.89Å. $2F_o-F_c$ (blue): 1.5σ ; F_o-F_c (red): 2.5σ (H-omit). Compound previously reported in references 16 and 17 in the main text; PDB: 4UA7.

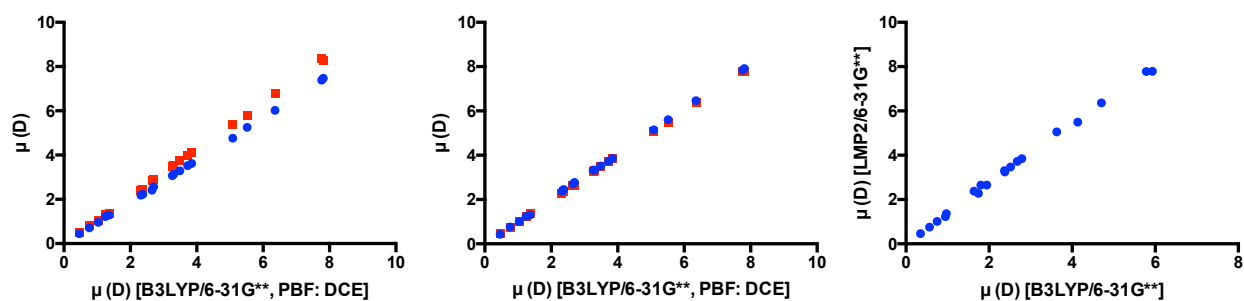


Figure 2-12. Comparison of calculated dipoles between solvents and models. A) B3LYP/6-31G**, PBF: DCE (10.65ϵ) vs. PBF: H₂O (blue, 80.37ϵ) and PBF: CHCl₃ (red, 4.806ϵ). B) B3LYP/6-31G**, PBF: DCE vs. M06-2X/6-31G**, PBF: DCE (blue) and

B3LYP-D3/6-31G**, PBF: DCE (red). C) B3LYP/6-31G**, gas phase vs. LMP2/6-31G**, gas phase.

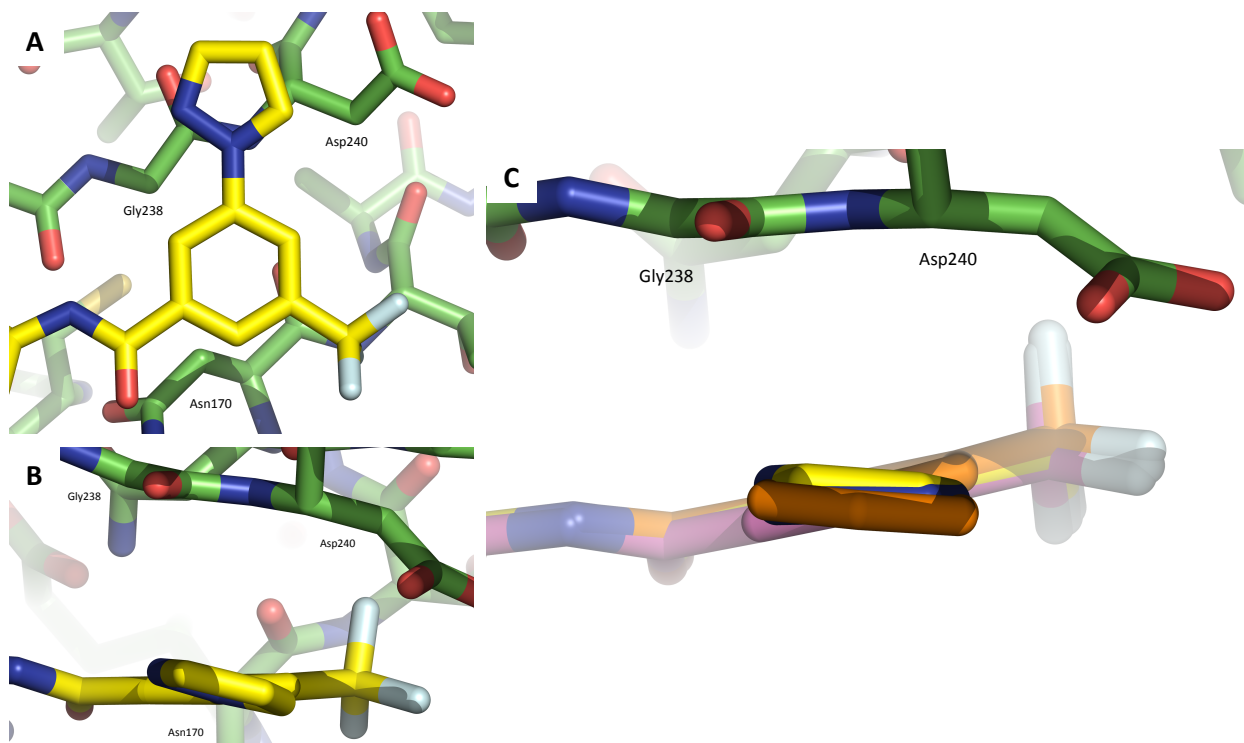
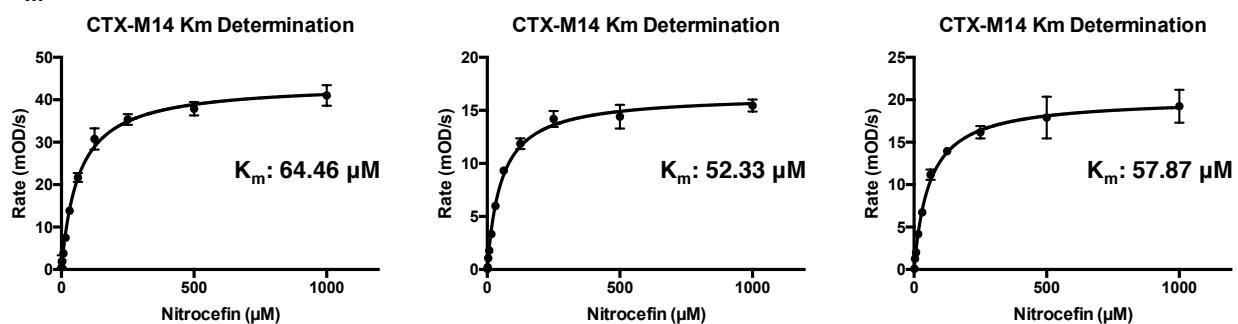


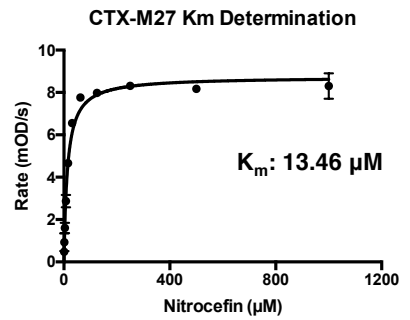
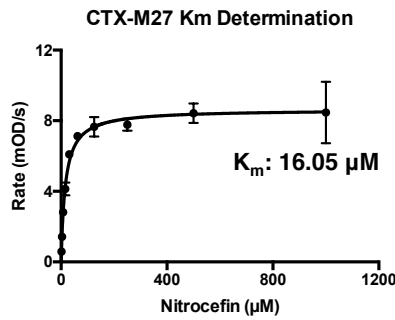
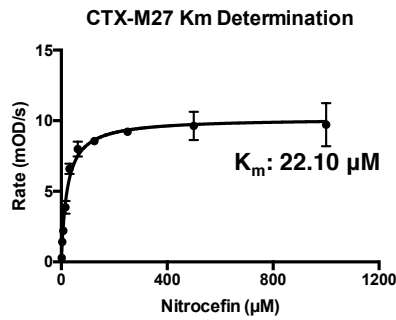
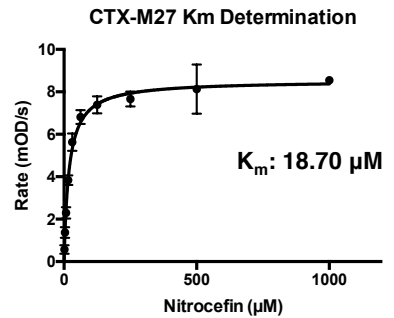
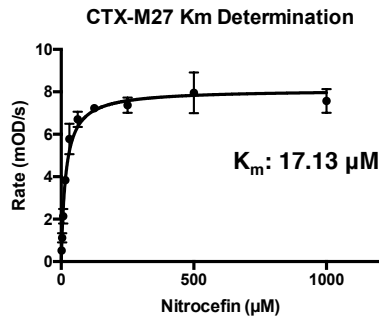
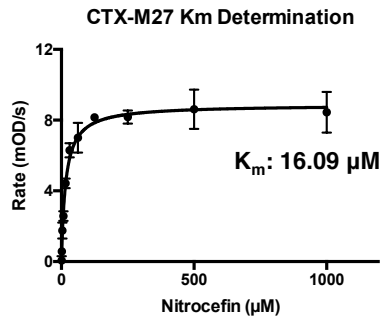
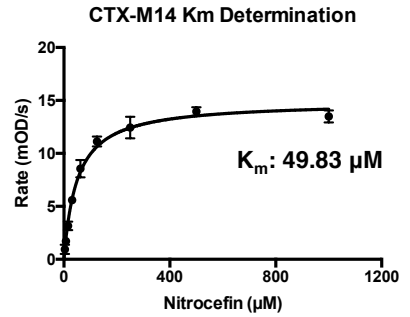
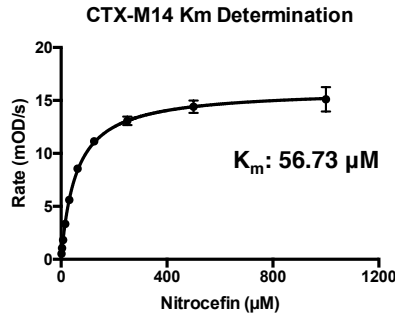
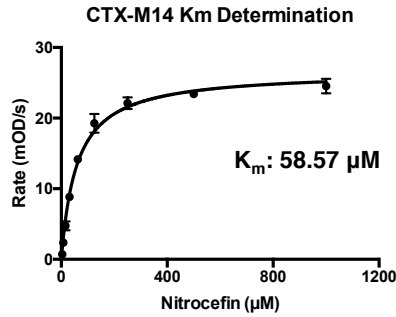
Figure 2-13. Front (A) and top (B) view of compound 14 with CTX-M-14. C) Superimposed top view of 3, 14, and 20 with CTX-M-14.

Biochemical Data

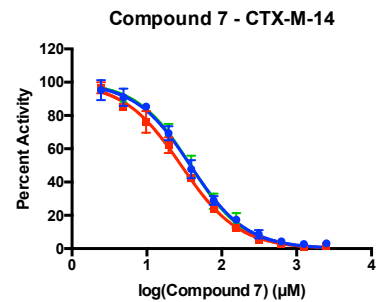
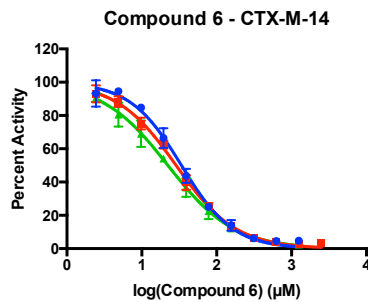
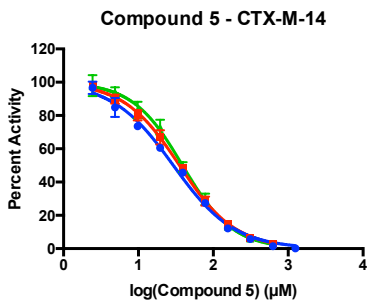
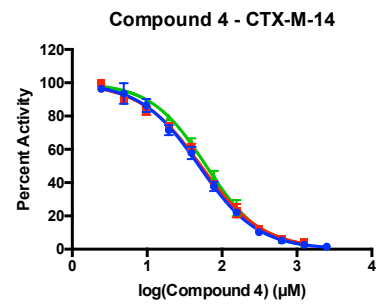
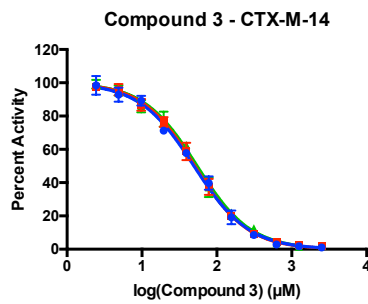
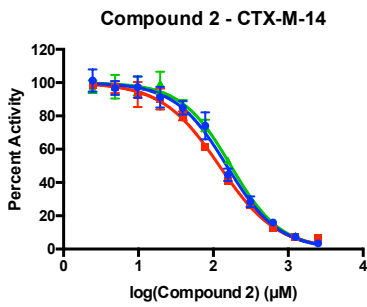
Each curve is a replicate generated from a technical triplicate. Compounds were tested up to 2.5 mM or 500 uM for CTX-M-14 and CTX-M-27, respectively (as solubility allowed).

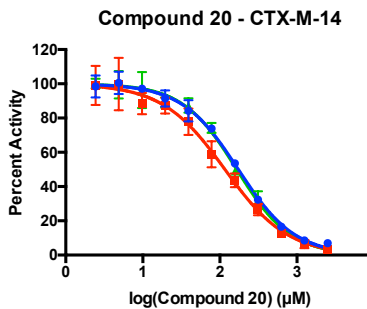
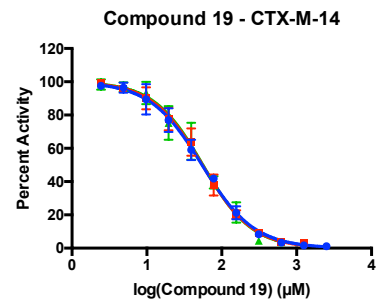
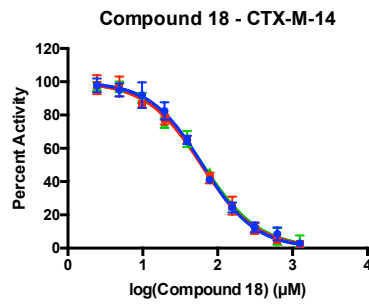
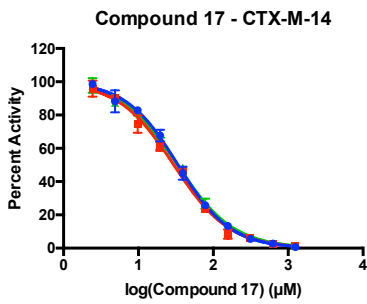
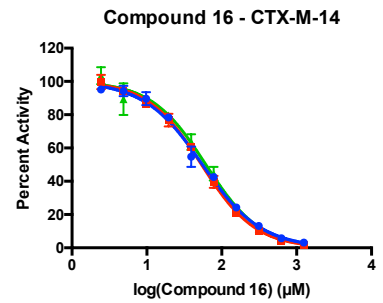
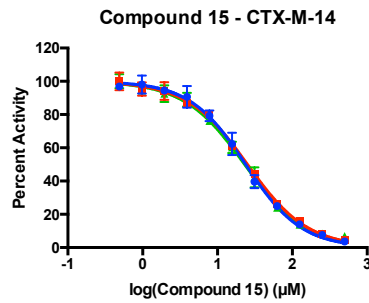
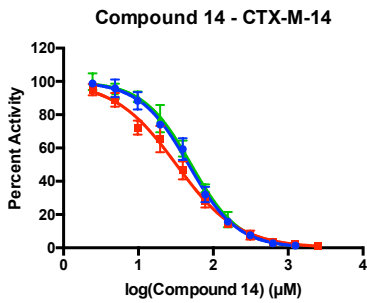
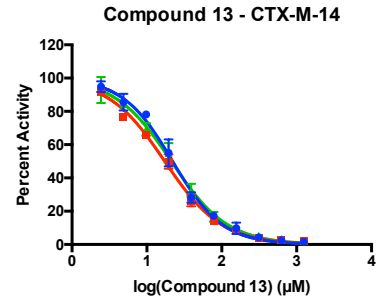
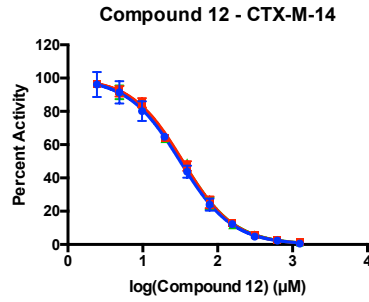
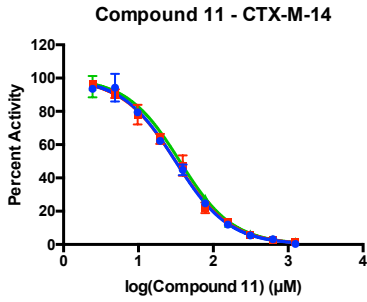
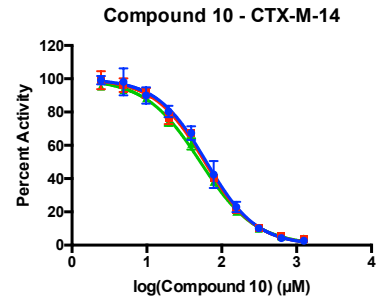
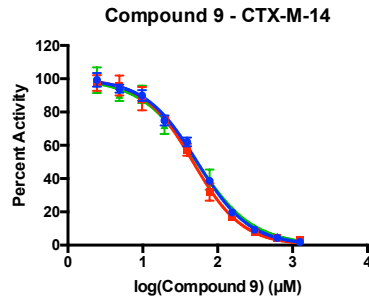
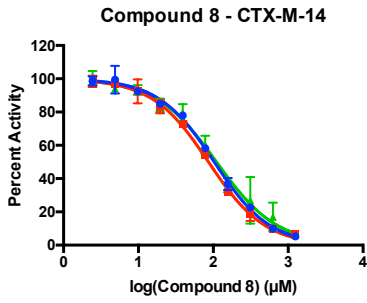
K_m Measurements:



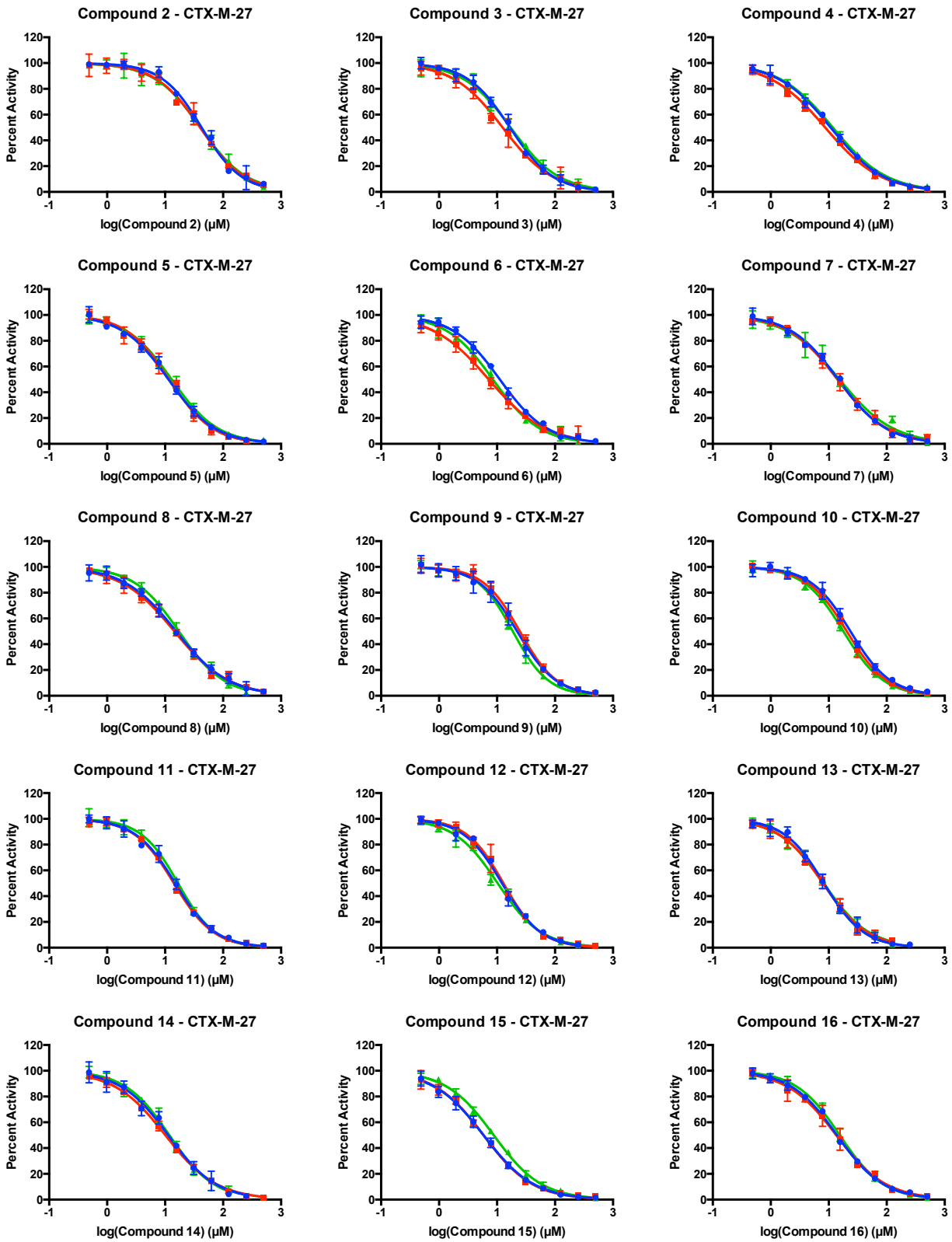


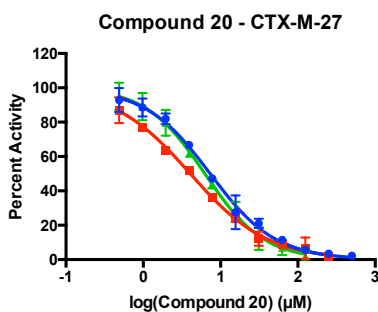
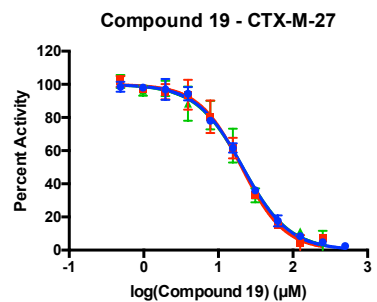
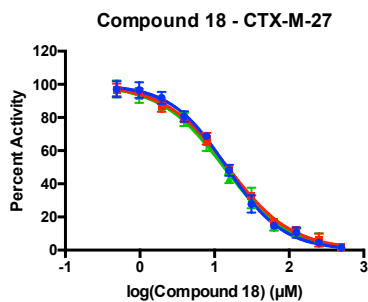
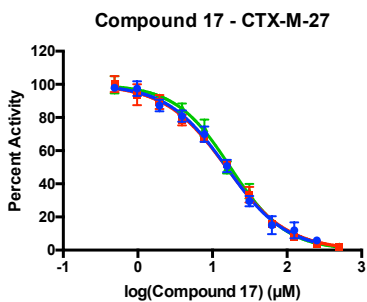
K_m Measurements:





CTX-M-27 Biochemical Data:

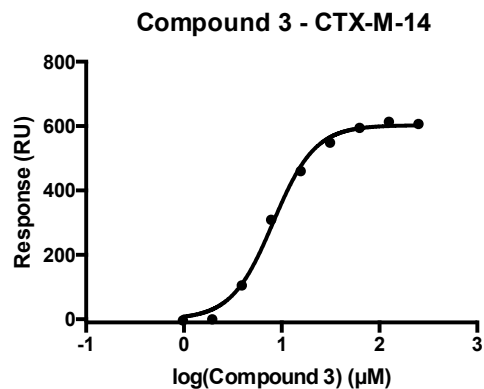
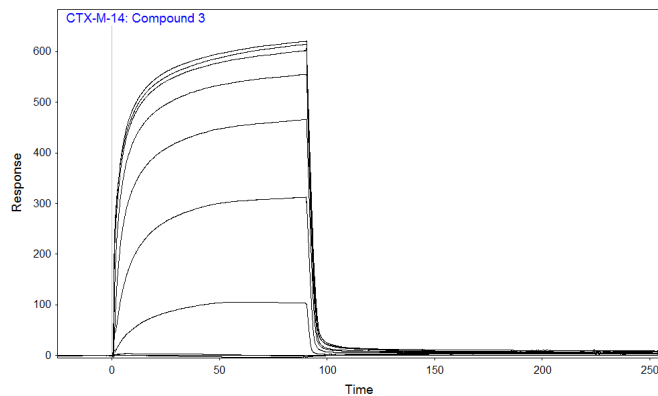


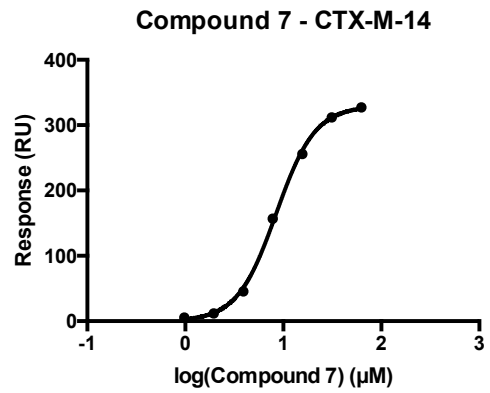
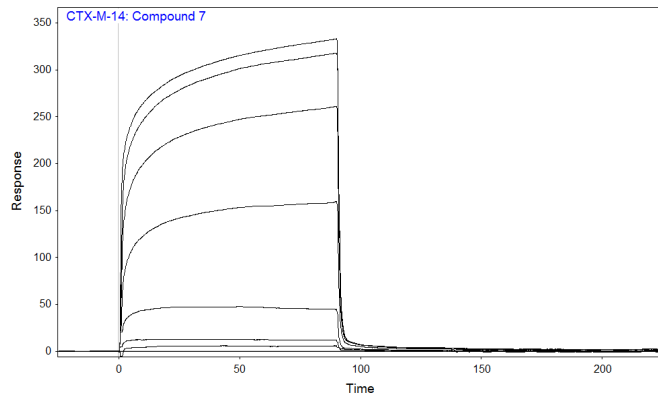
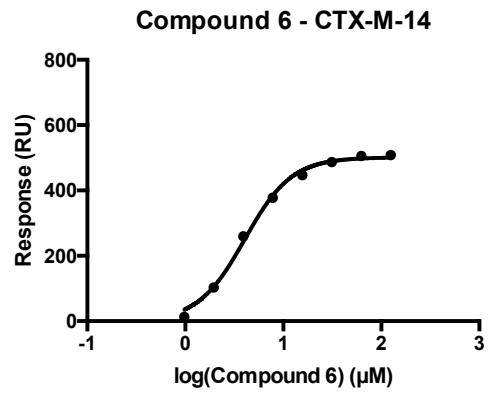
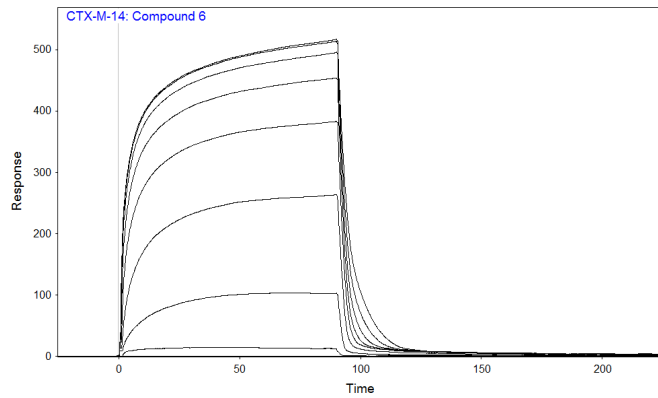
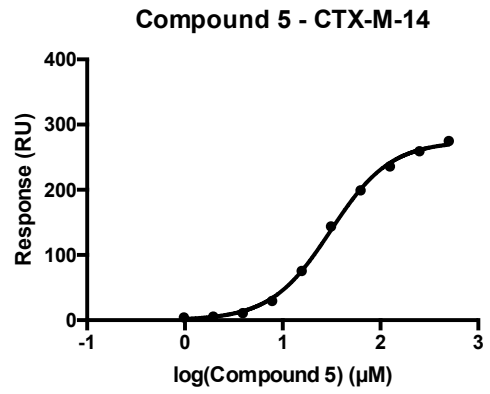
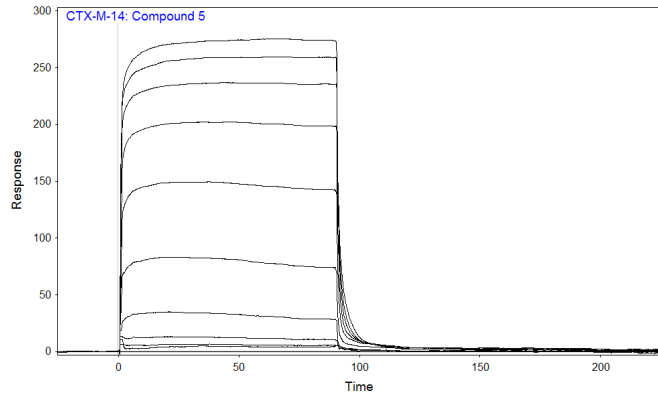
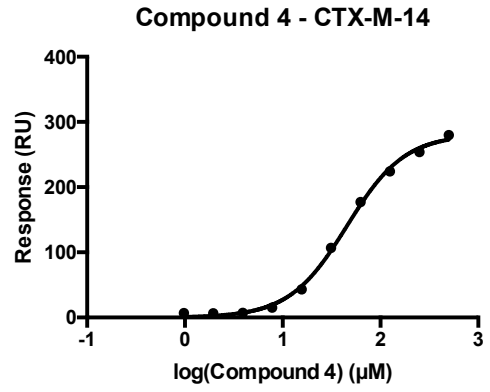
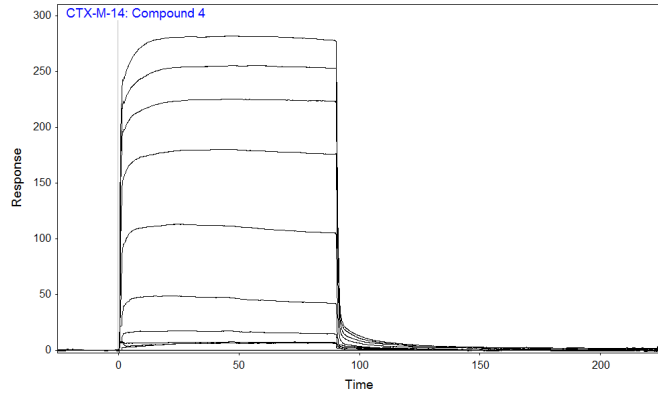


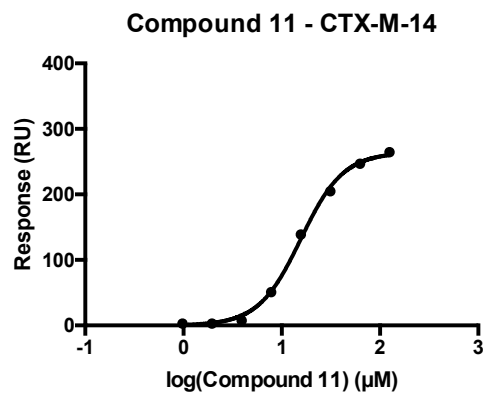
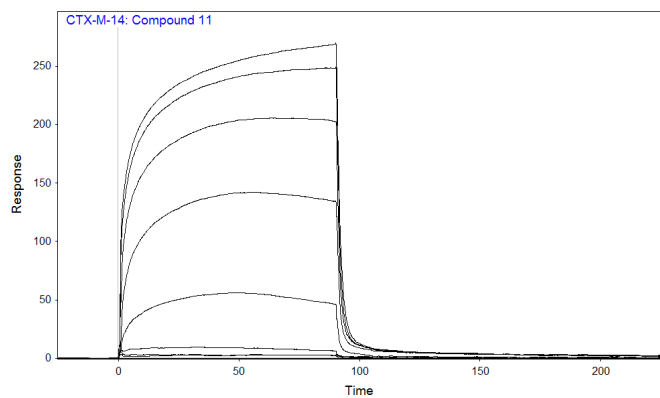
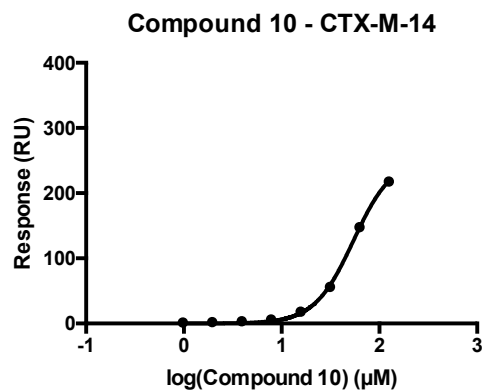
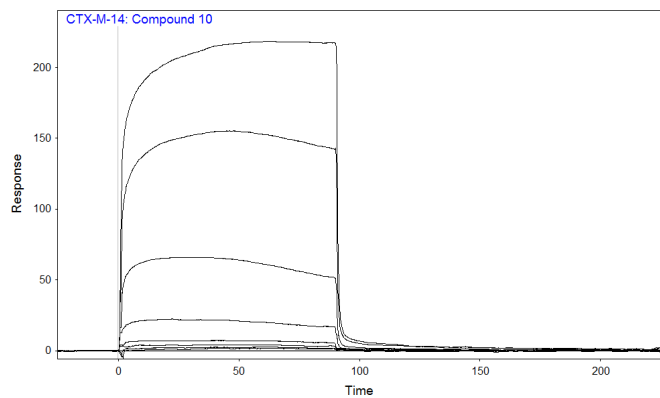
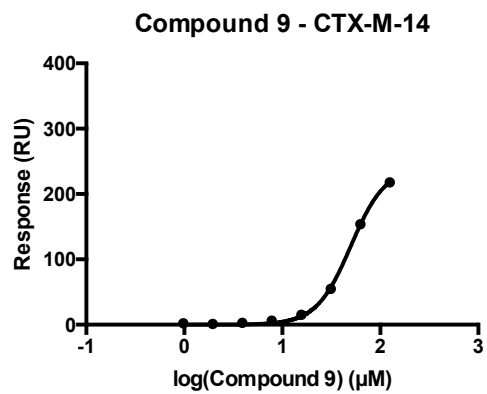
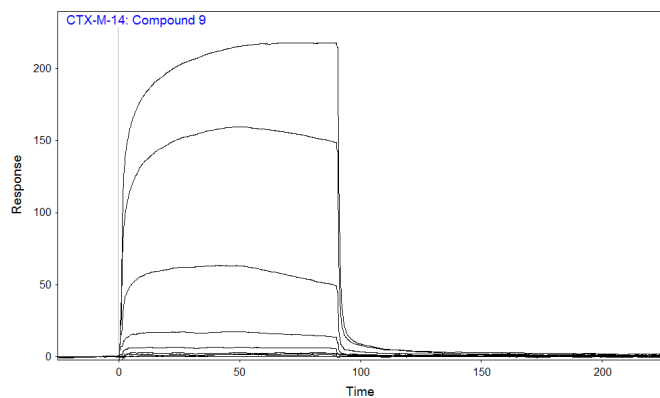
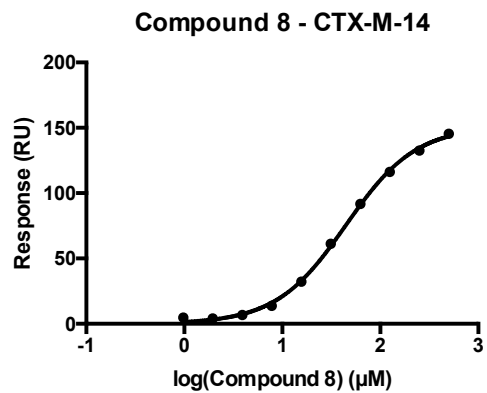
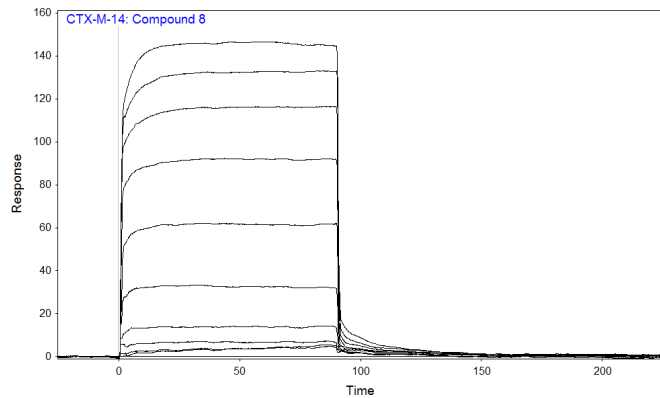
SPR Data

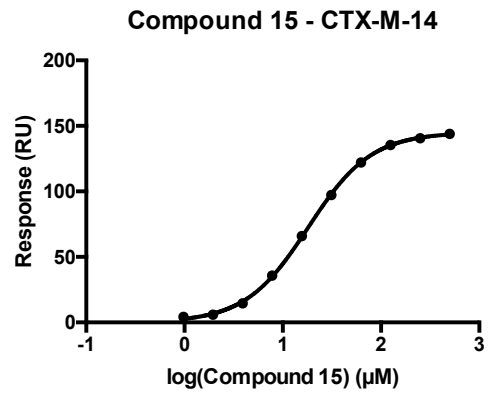
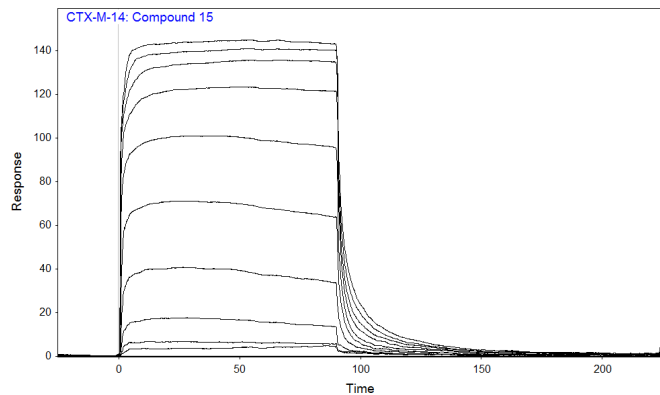
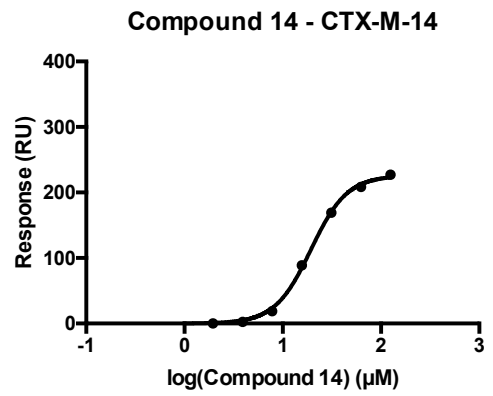
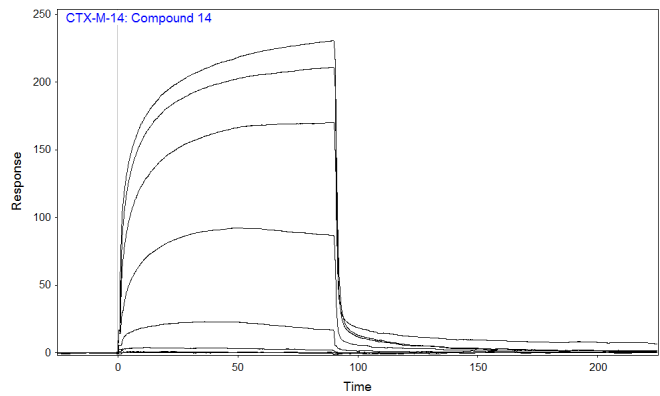
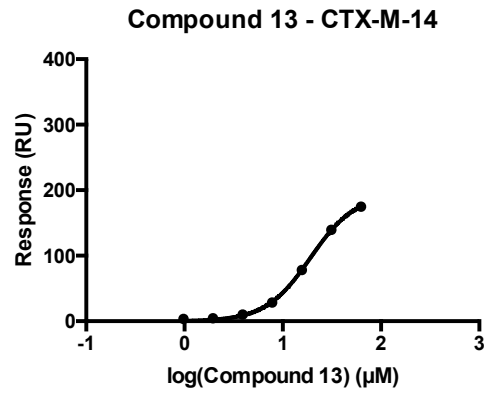
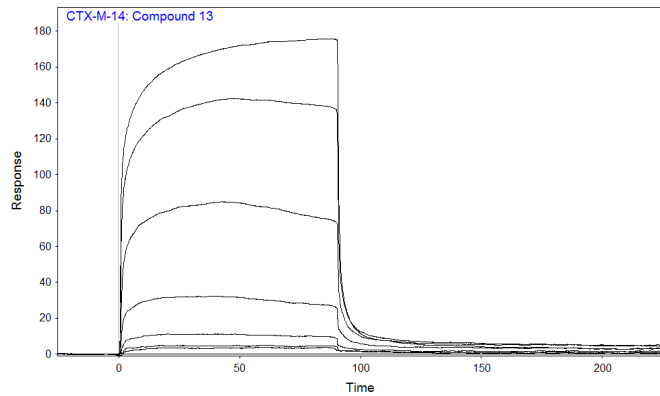
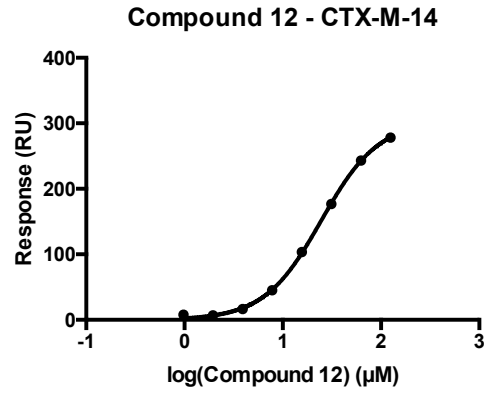
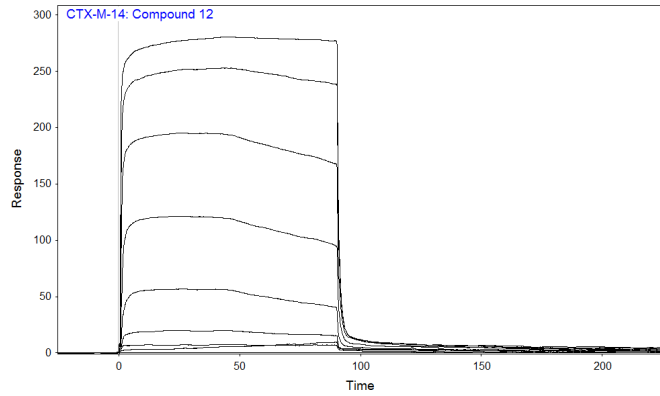
Compounds were tested in 10-point dose response with two internal blanks up to 500 μM and 50 μM for CTX-M-14 and CTX-M-27, respectively (as solubility allowed). All compounds were tested in quadruplicate for CTX-M-14 and in duplicate for CTX-M-27. K_d was measured at equilibrium binding between 65-85s.

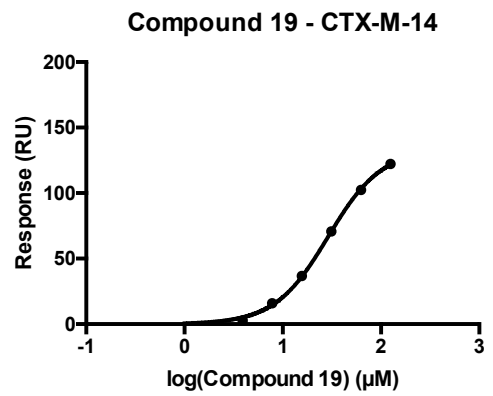
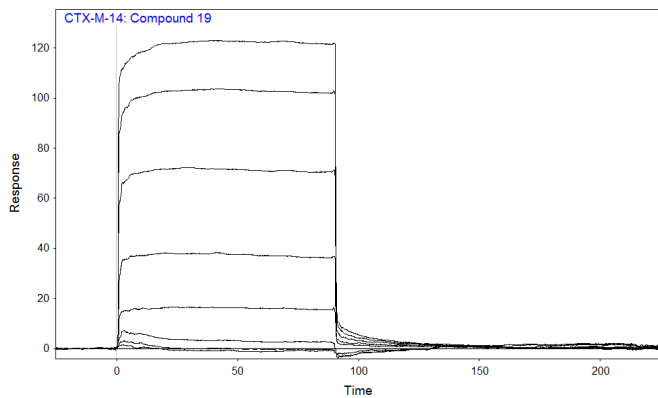
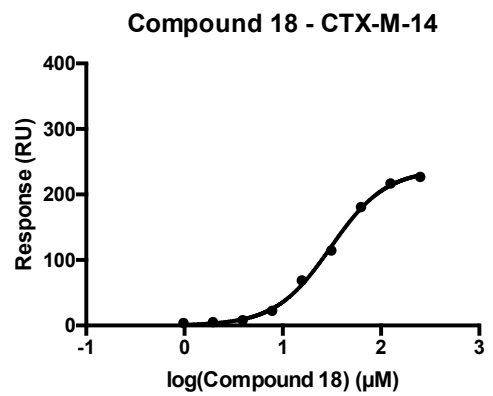
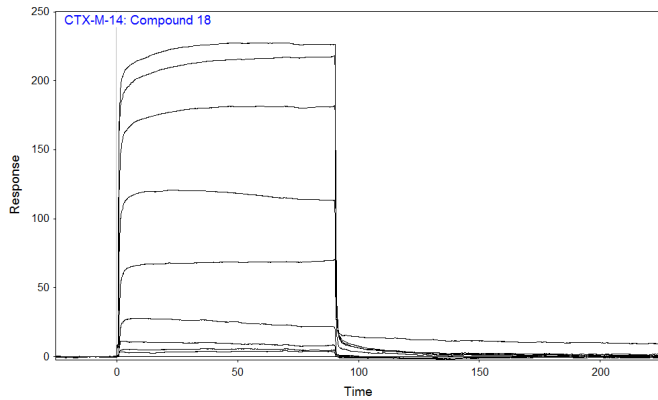
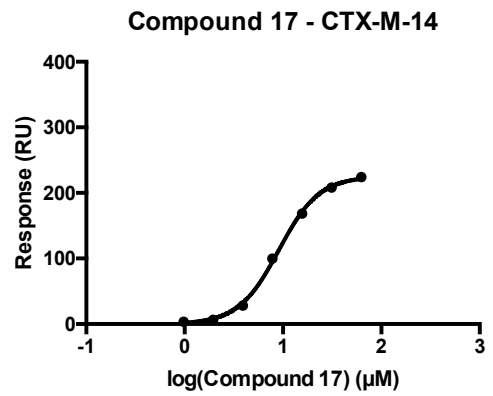
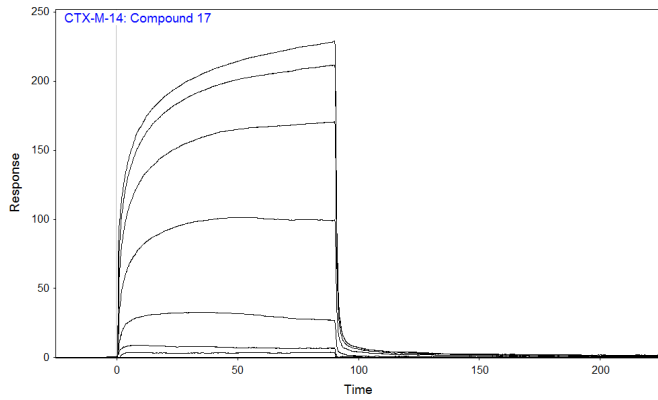
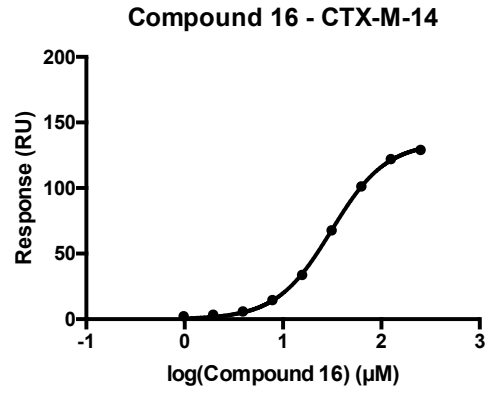
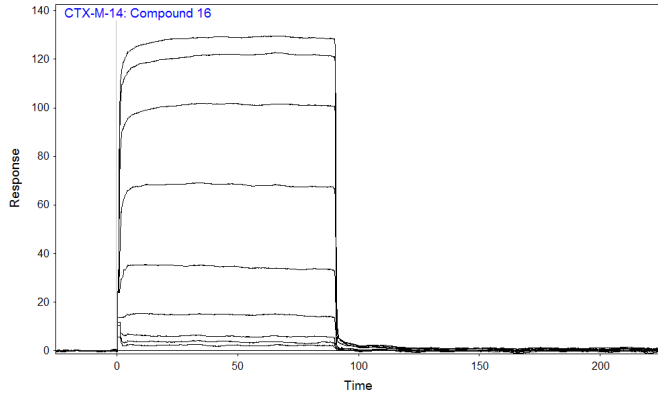
Representative sensograms for CTX-M-14:

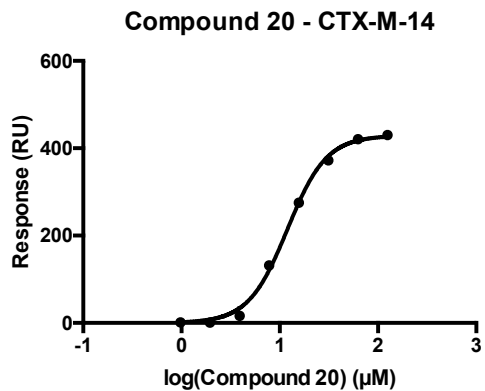
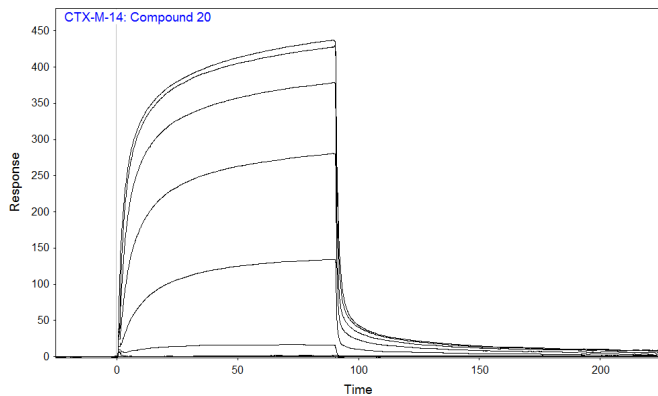




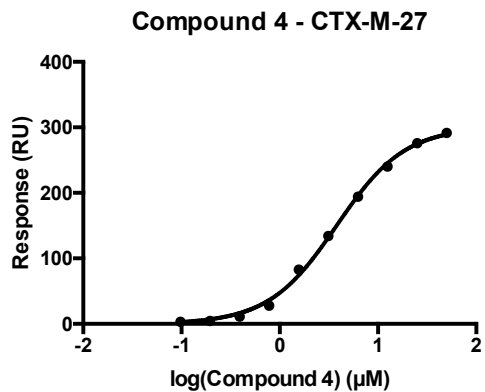
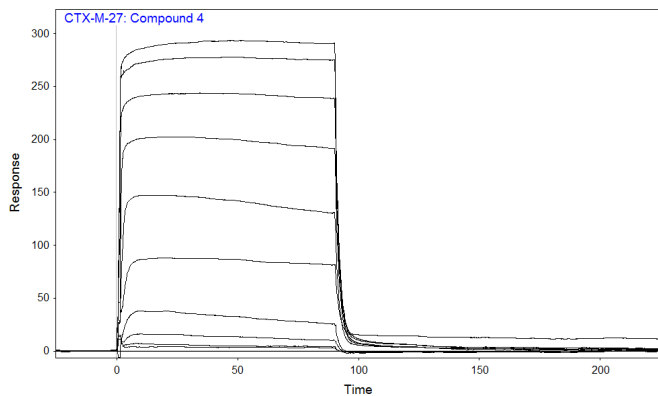
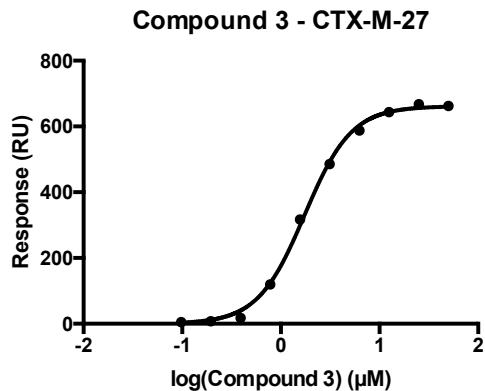
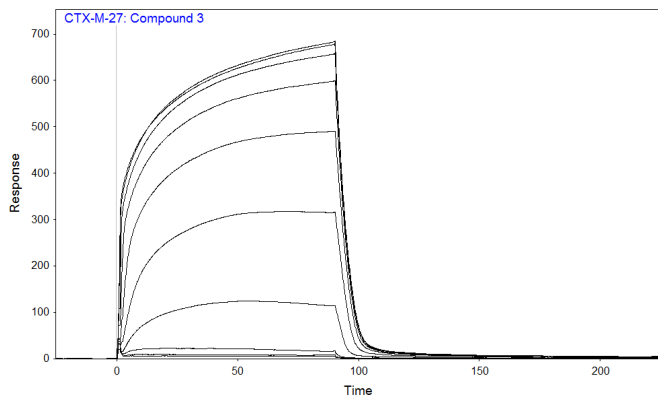
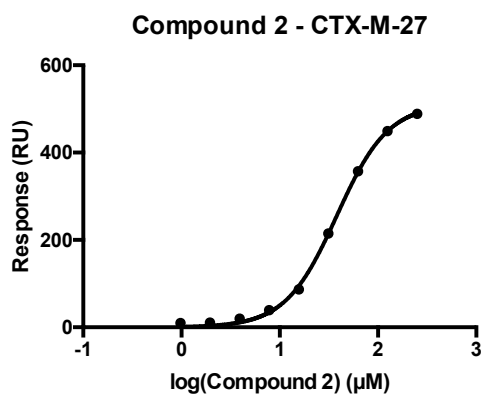
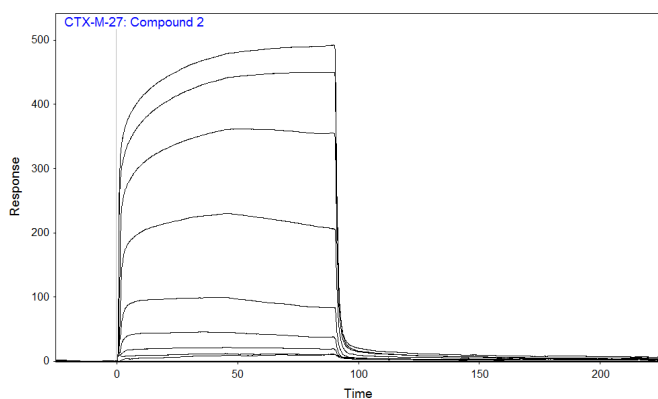


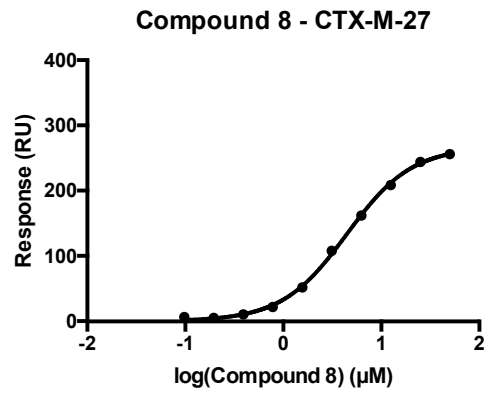
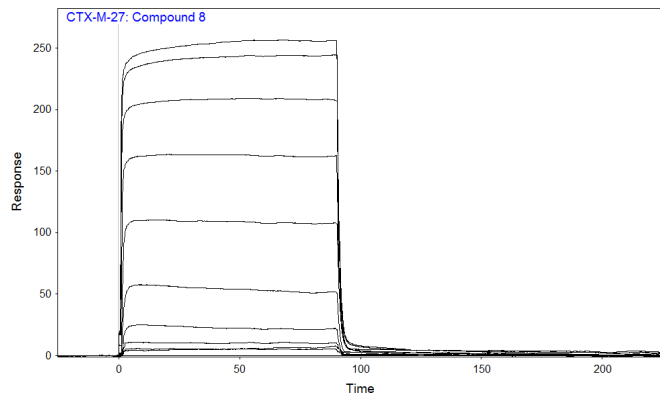
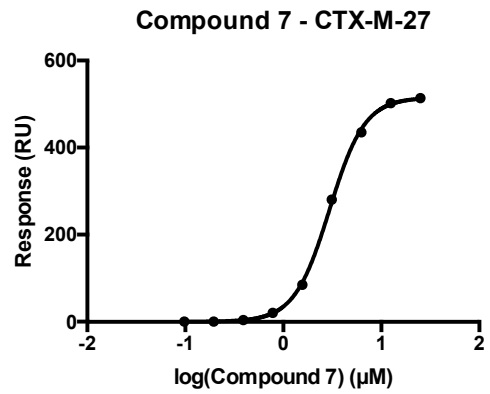
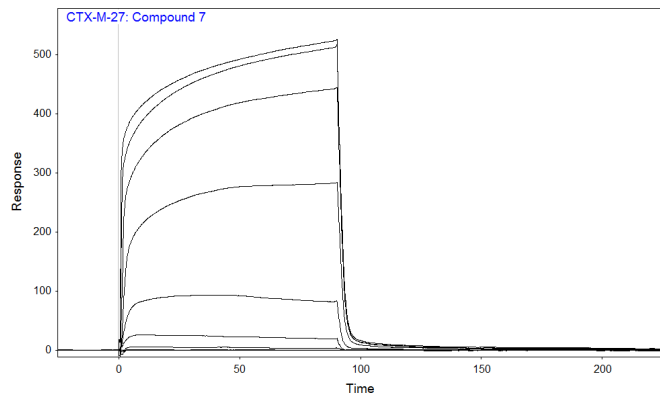
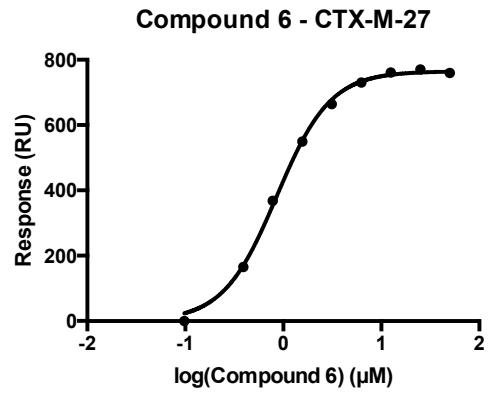
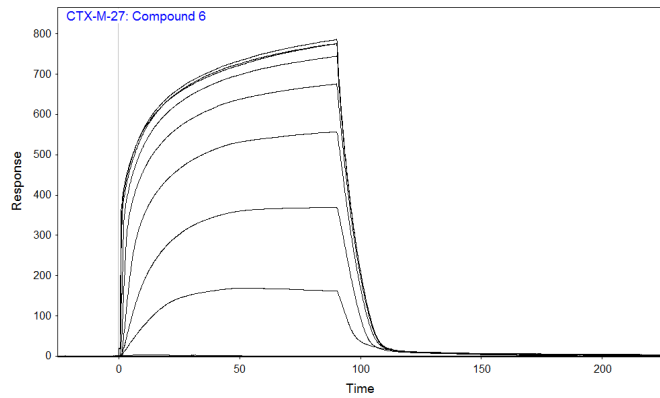
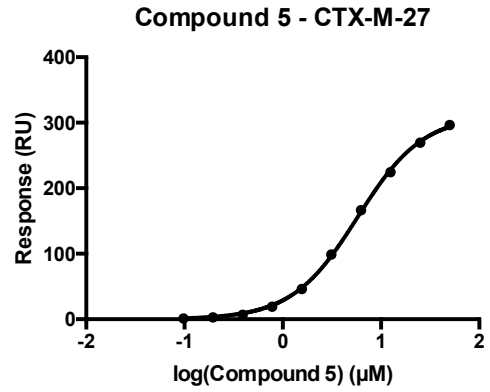
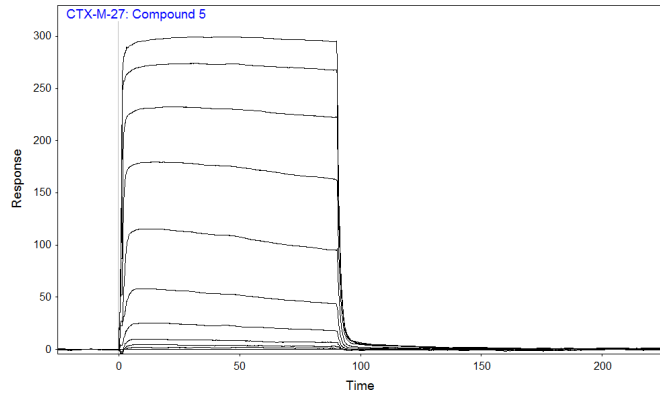


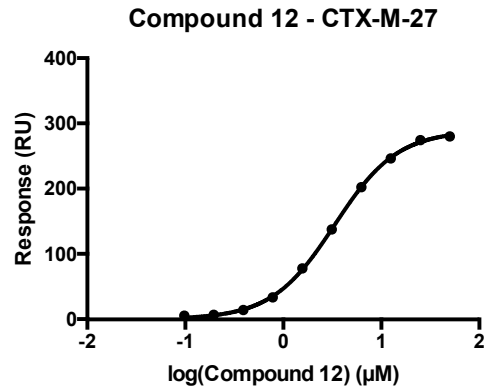
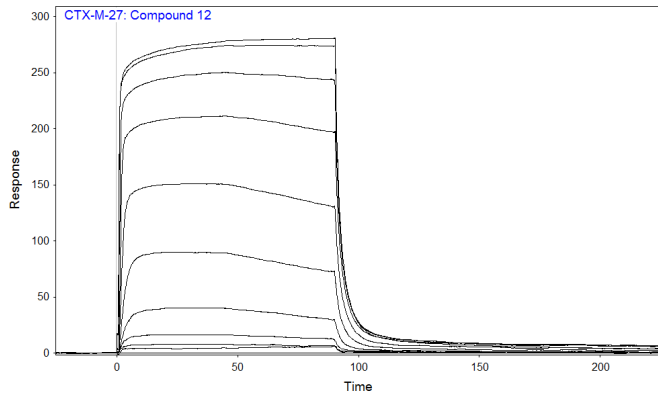
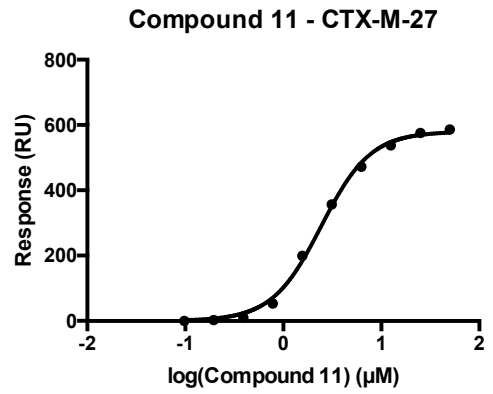
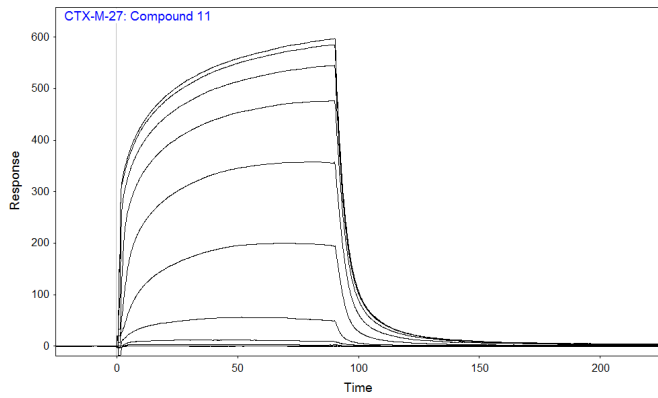
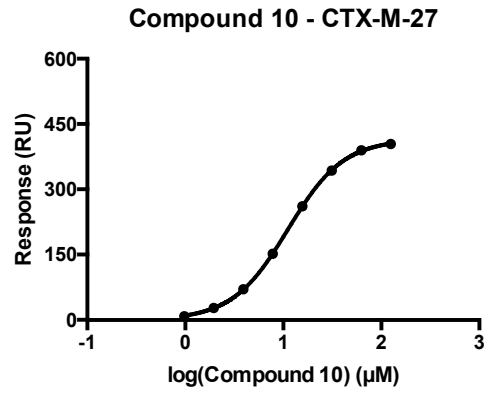
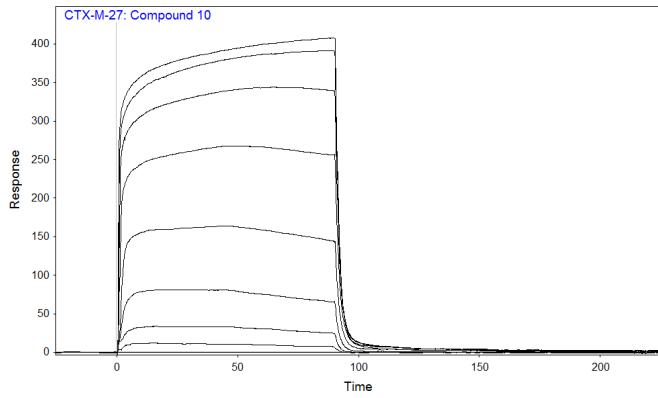
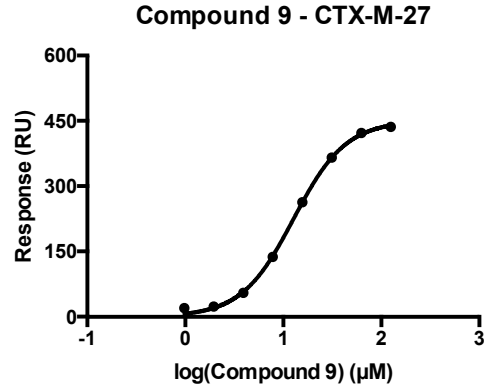
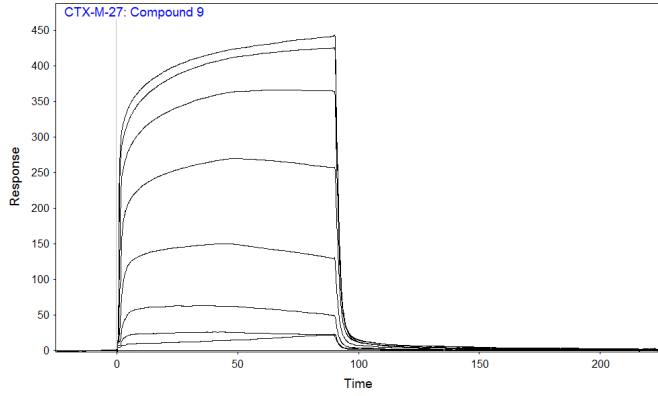


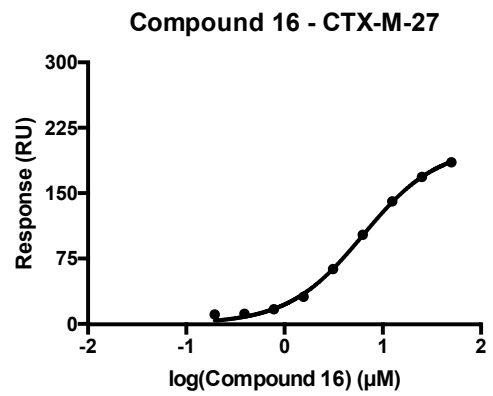
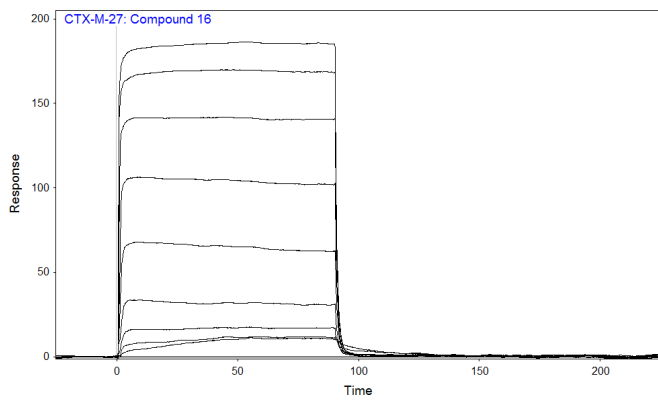
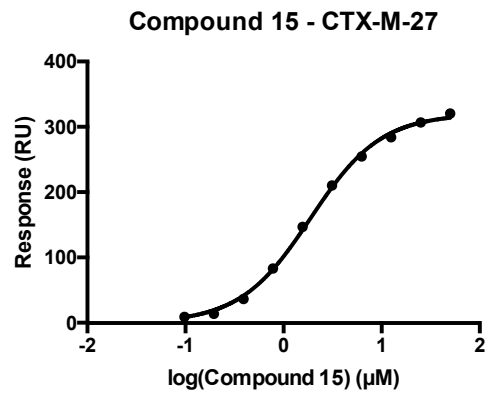
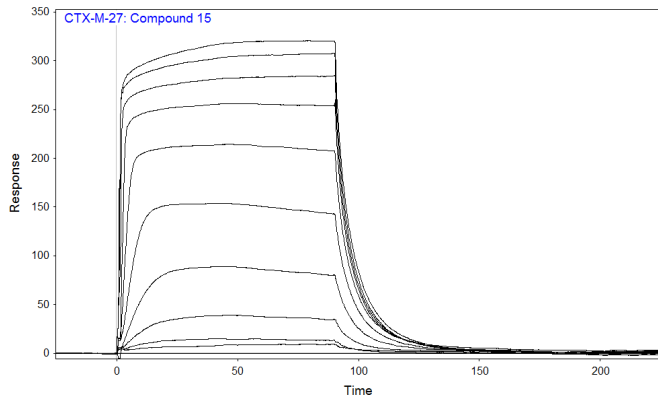
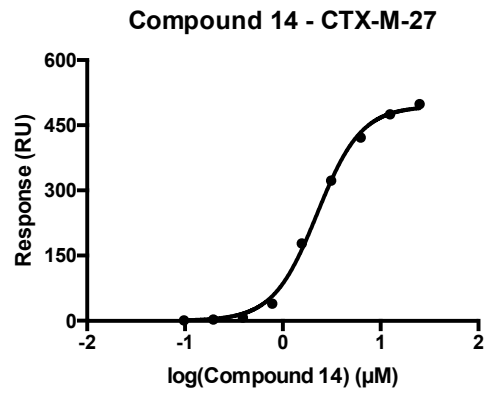
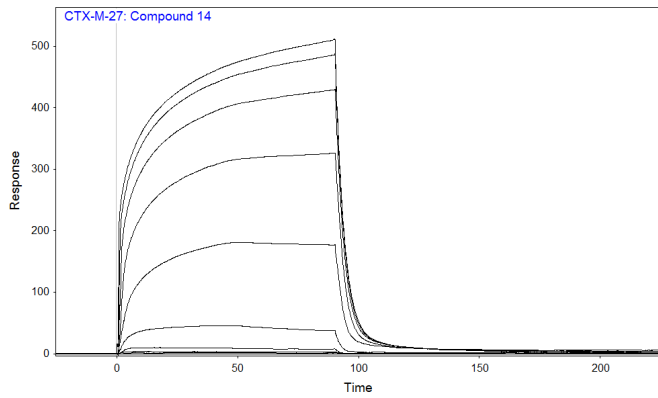
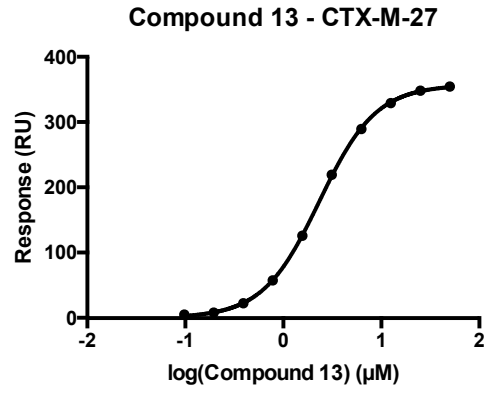
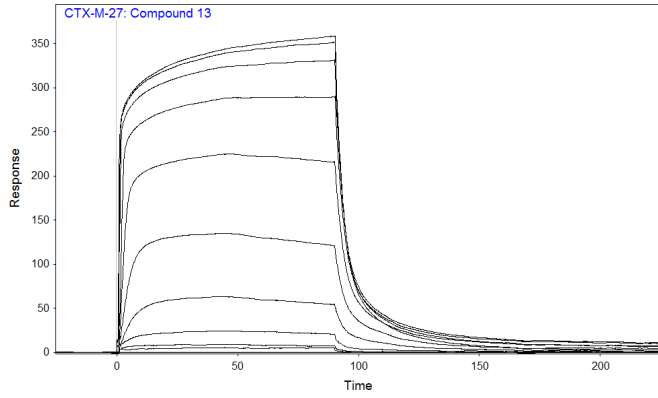


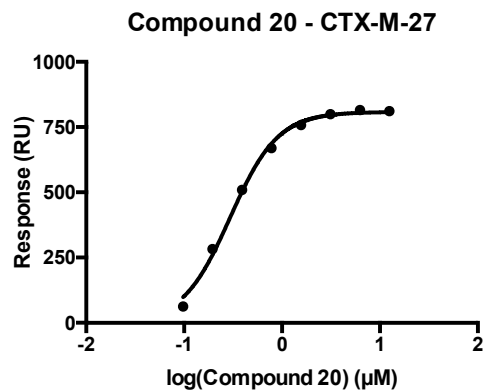
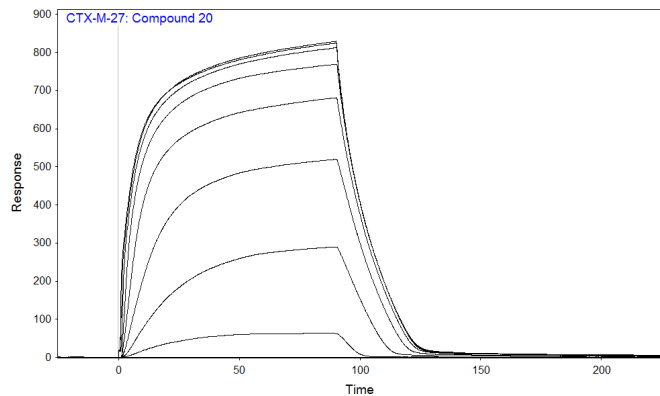
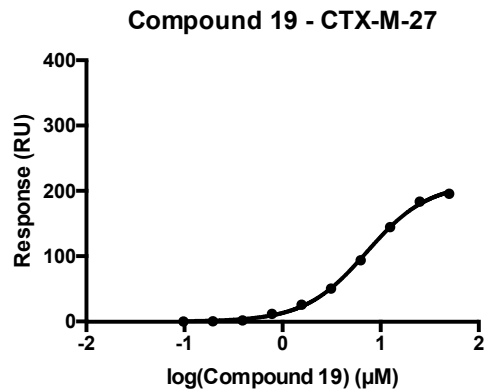
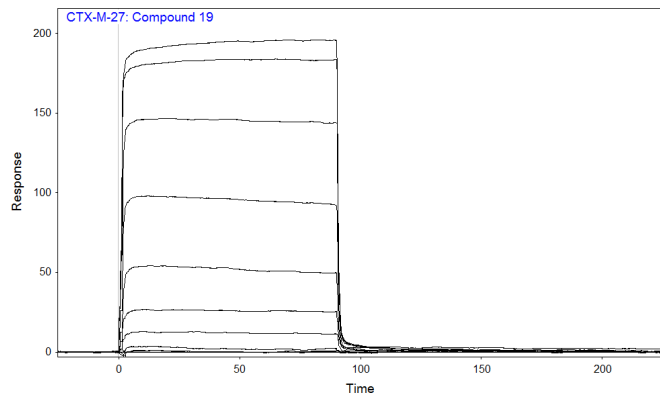
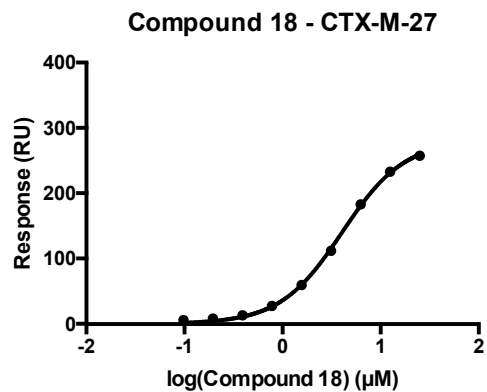
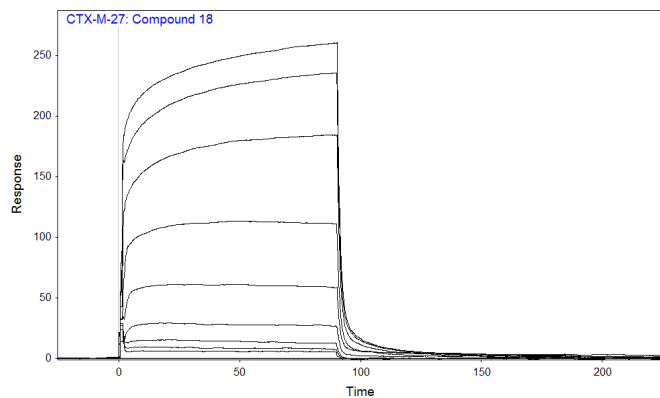
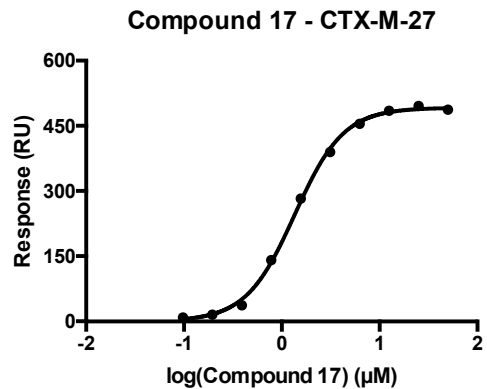
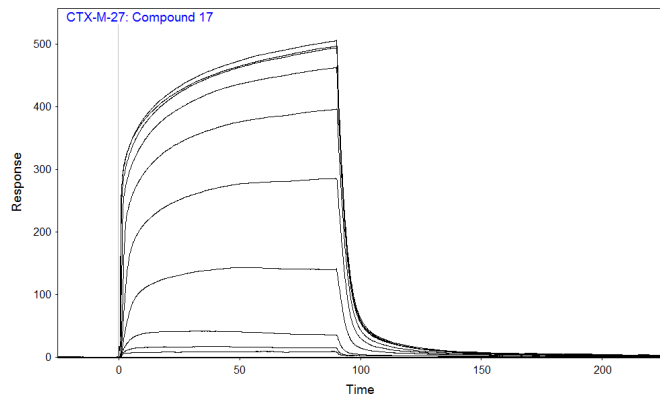
Representative sensograms for CTX-M-27:











Crystallographic Data

Table 2-2. X-ray data collection and refinement statistics.

Data Collection					
Structure (PDB ID)	<u>6OOF</u>	<u>6OOE</u>	<u>6OOJ</u>	<u>6OOH</u>	<u>6OOK</u>
Space Group	P 1 21 1	P 1 21 1	P 1 21 1	P 1 21 1	P 1 21 1
Cell Dimensions					
<i>a</i> , <i>b</i> , <i>c</i> (Å)	45.161	45.323	45.096	45.129	45.003
	107.211	107.482	106.929	107.157	106.725
	47.884	48.057	47.83	47.92	47.736
α , β , γ (°)	90	90	90	90	90
	101.656	101.715	101.611	101.906	101.73
	90	90	90	90	90
Resolution (Å)	35.3 - 1.236	30 - 1.26	25.71 - 1.4	29.92 - 1.499	25.27 - 1.4
No. Reflections	111033	107 923	86936	70775	82095
R_{merge} (%)	10.3	10.6	5.0	6.6	2.7
<i>I</i> / σI	22.36(2.15)	25.16(2.69)	26.52(3.9)	16.81(2.8)	44.04(8.02)
Completeness (%)	87.8	89.2	99.9	99.4	94.8
Redundancy	4.2(3.9)	5.7(5.8)	3.7(2.9)	3.2(2.8)	3.6(2.9)
Refinement					
Resolution (Å)	35.3 - 1.236	30 - 1.26	25.71 - 1.4	29.92 - 1.499	25.27 - 1.4
$R_{\text{work}}/R_{\text{free}}$ (%)	17.20/20.13	14.5/16.95	14.53/16.29	14.43/17.14	12.03/15.39
No. Heavy Atoms					
Protein	4988	4206	4121	4131	4136
Ligand/Ion	116	116	145	145	125
Water	691	729	738	787	697
B-Factors (Å²)					
Protein	14.00	12.10	15.84	15.14	15.72
Ligand/Ion	16.12	14.73	18.57	18.37	29.83
Water	26.43	25.92	29.59	27.74	29.02
Ramachandran Plot					
Most Favored Region(%)	97.3	97.7	97.7	97.9	97.9
Additionally Allowed (%)	2.32	1.93	1.93	1.73	1.74
Generously Allowed (%)	0.39	0.39	0.39	0.39	0.39
* Values in parentheses represent highest resolution shells					

Dipole Calculations

Dipoles were calculated with a methyl at the point of attachment; structures were optimized with B3LYP/6-31G** prior to dipole calculation.

B3LYP/6-31G; PBF: DCE (10.65 ε)**

Compound	Gas Phase Energy	Solution Phase Energy	Solvation Energy (kcal/mol)	HOMO	LUMO	QM Dipole (D)	QM Dipole X (D)	QM Dipole Y (D)	QM Dipole Z (D)
2	-271.578488	-271.58247	-2.499131	-0.240232	-0.002133	0.463176	-0.285068	-0.36506	0
3	-287.616296	-287.624158	-4.932937	-0.25393	-0.026293	2.651741	2.623243	-0.387716	0
4	-287.613682	-287.621816	-5.104312	-0.253439	-0.024655	3.309159	1.229136	3.072419	0
5	-287.614708	-287.623465	-5.495336	-0.262352	-0.024947	3.727299	-1.913623	-3.198563	0
6	-303.655234	-303.666316	-6.954164	-0.257676	-0.04309	2.377625	1.099734	2.108005	0
7	-303.655009	-303.666395	-7.145241	-0.262914	-0.043459	3.493428	1.07138	3.325084	0
8	-303.651512	-303.662934	-7.167572	-0.262527	-0.045594	3.844931	-1.995047	3.286835	0
9	-592.330722	-592.335014	-2.693378	-0.227616	-0.010871	1.034642	0.665349	-0.792335	-0.000768
10	-592.329452	-592.333807	-2.732275	-0.230464	-0.012426	1.363993	-0.104598	-1.359976	0.000603
11	-269.353086	-269.357967	-3.062408	-0.217858	0.016877	0.763495	0.425025	-0.634254	0.00001
12	-269.347484	-269.352356	-3.057625	-0.221196	0.014465	1.244542	-0.097378	-1.240726	0.000847
13	-249.495923	-249.504932	-5.653324	-0.20191	0.04379	2.321089	-0.426593	2.28155	0.001166
14	-265.522355	-265.532677	-6.4773	-0.244642	0.015965	3.266098	1.68403	-2.798471	-0.000869
15	-265.529696	-265.542853	-8.256297	-0.246401	0.017209	2.701276	2.409078	1.22198	0.000098
16	-265.535403	-265.549161	-8.632925	-0.228099	0.025706	5.520107	-1.256347	-5.375237	0.000983
17	-265.548463	-265.563967	-9.728804	-0.221107	0.031191	5.083593	-4.764769	1.771959	0.007474
18	-281.544963	-281.560477	-9.735667	-0.264789	-0.01048	6.360991	2.105532	-6.002412	0.000069
19	-297.573052	-297.591624	-11.654125	-0.304945	-0.026451	7.815559	0.845976	7.769638	0
20	-297.583578	-297.6046	-13.191199	-0.300764	-0.023761	7.766349	7.333139	2.557586	0

B3LYP/6-31G; PBF: H2O (80.37 ε)**

Compound	Gas Phase Energy	Solution Phase Energy	Solvation Energy (kcal/mol)	HOMO	LUMO	QM Dipole (D)	QM Dipole X (D)	QM Dipole Y (D)	QM Dipole Z (D)
2	-271.578452	-271.581714	-2.046934	-0.239484	-0.00143	0.44862	-0.278004	-0.3521	0
3	-287.616222	-287.622584	-3.991815	-0.253299	-0.025335	2.414631	2.385242	-0.375586	0
4	-287.613617	-287.620324	-4.208525	-0.252981	-0.023801	3.133705	1.137203	2.920082	0
5	-287.614634	-287.621834	-4.518118	-0.261632	-0.023975	3.516843	-1.807647	-3.016719	0
6	-303.655093	-303.664322	-5.791053	-0.255578	-0.042322	2.231569	1.033354	1.977898	0
7	-303.654888	-303.66437	-5.949808	-0.260599	-0.042648	3.289413	0.981849	3.13946	0
8	-303.651395	-303.66086	-5.939002	-0.260244	-0.044793	3.621407	-1.879782	3.095321	0
9	-592.330647	-592.334221	-2.242323	-0.226654	-0.009866	0.963784	0.588012	-0.763624	-0.000018
10	-592.329344	-592.33299	-2.288027	-0.229424	-0.011389	1.291218	-0.092571	-1.287895	-0.000954
11	-269.353019	-269.357124	-2.575602	-0.217087	0.017587	0.715456	0.400727	-0.592702	-0.000246
12	-269.34739	-269.352191	-3.01288	-0.220349	0.014368	1.218788	-0.088761	-1.215551	0.000546
13	-249.495807	-249.503211	-4.646594	-0.200576	0.044627	2.186178	-0.391365	2.150862	0.001224
14	-265.522241	-265.530827	-5.387862	-0.24328	0.017347	3.06943	1.536605	-2.657112	-0.000978
15	-265.529418	-265.540434	-6.912604	-0.244663	0.018496	2.559449	2.267994	1.186162	0.000329
16	-265.535249	-265.546636	-7.145288	-0.226629	0.026859	5.250173	-1.205787	-5.109833	0.000633
17	-265.548258	-265.560962	-7.971984	-0.219736	0.031883	4.76464	-4.462819	1.668834	0.005931
18	-281.544782	-281.557569	-8.023798	-0.263267	-0.008382	6.019743	-1.947741	5.695929	0
19	-297.572866	-297.588371	-9.729789	-0.301057	-0.024633	7.474376	0.847945	7.426122	0
20	-297.5832	-297.600634	-10.939654	-0.299287	-0.022213	7.383831	6.948783	2.497072	0

B3LYP/6-31G; PBF: CHCl₃ (4.806 ε)**

Compound	Gas Phase Energy	Solution Phase Energy	Solvation Energy (kcal/mol)	HOMO	LUMO	QM Dipole (D)	QM Dipole X (D)	QM Dipole Y (D)	QM Dipole Z (D)
2	-271.578452	-271.578534	-0.051712	-0.240829	-0.002739	0.48856	-0.300036	-0.385577	0
3	-287.616222	-287.621639	-3.399163	-0.255681	-0.028817	2.842759	2.809459	-0.433384	0
4	-287.613617	-287.619234	-3.524996	-0.254987	-0.027062	3.534241	1.29068	3.290138	0
5	-287.614634	-287.620832	-3.889164	-0.264011	-0.027126	3.974551	-2.03931	-3.41149	0
6	-303.655093	-303.663985	-5.579627	-0.264041	-0.047122	2.44517	1.136897	2.164791	0
7	-303.654888	-303.6647	-6.156897	-0.269557	-0.047199	3.755247	1.174285	3.566922	0
8	-303.651395	-303.661228	-6.170466	-0.268779	-0.049059	4.092602	-2.135383	3.491351	0
9	-592.330647	-592.331157	-0.320023	-0.228298	-0.011627	1.044568	0.645105	-0.82156	0.000932
10	-592.329344	-592.329858	-0.322362	-0.231187	-0.013194	1.379518	-0.09718	-1.376091	0.000775
11	-269.353019	-269.352458	0.352449	-0.218771	0.015738	0.802421	0.467163	-0.65241	-0.000225
12	-269.34739	-269.346688	0.440413	-0.222276	0.013178	1.296883	-0.091947	-1.293619	0.000312
13	-249.495807	-249.501927	-3.840296	-0.20204	0.043967	2.403203	-0.434937	2.363516	0.002206
14	-265.522241	-265.53082	-5.383658	-0.247448	0.012345	3.484909	1.927776	-2.903146	-0.003404
15	-265.529418	-265.541846	-7.798577	-0.248477	0.014121	2.880142	2.612758	1.211904	-0.001133
16	-265.535249	-265.547646	-7.779101	-0.230055	0.023664	5.787087	-1.285639	-5.642474	-0.0005
17	-265.548258	-265.563499	-9.564275	-0.222501	0.02984	5.398173	-5.038694	1.936953	0.006607
18	-281.544782	-281.559717	-9.371439	-0.270039	-0.016725	6.79725	-2.322442	6.388182	0
19	-297.572866	-297.591159	-11.479392	-0.314829	-0.033862	8.279873	0.906028	8.230153	0
20	-297.5832	-297.606237	-14.455879	-0.306172	-0.02977	8.366223	7.912965	2.716371	0

M06-2X/6-31G; PBF: DCE (10.65 ε)**

Compound	Gas Phase Energy	Solution Phase Energy	Solvation Energy (kcal/mol)	HOMO	LUMO	QM Dipole (D)	QM Dipole X (D)	QM Dipole Y (D)	QM Dipole Z (D)
2	-271.442768	-271.447608	-3.036903	-0.292104	0.032375	0.432983	-0.270257	-0.338284	0
3	-287.479704	-287.488451	-5.488838	-0.305341	0.010172	2.693945	2.669744	-0.36029	0
4	-287.477151	-287.486049	-5.58377	-0.304821	0.01217	3.325684	1.266235	3.075195	0
5	-287.478142	-287.487715	-6.007428	-0.314898	0.01127	3.731682	-1.914788	-3.202973	0
6	-303.518445	-303.53042	-7.514676	-0.323877	-0.004964	2.452971	1.138653	2.17268	0
7	-303.518217	-303.530406	-7.648937	-0.328906	-0.005923	3.513279	1.11233	3.332544	0
8	-303.514755	-303.52687	-7.602285	-0.326966	-0.00753	3.852266	-1.998159	3.293526	0
9	-592.199498	-592.204572	-3.184479	-0.297941	0.025431	1.006035	0.654288	-0.764208	-0.000739
10	-592.198112	-592.203298	-3.254658	-0.282648	0.024006	1.307978	-0.098133	-1.304291	0.000691
11	-269.231198	-269.236944	-3.605648	-0.269791	0.058325	0.764255	0.447519	-0.619527	-0.000053
12	-269.2255	-269.23125	-3.607936	-0.273627	0.056013	1.236591	-0.08754	-1.233488	0.000887
13	-249.377746	-249.387944	-6.399138	-0.253976	0.085194	2.3648	-0.424663	2.326358	0.001263
14	-265.402102	-265.413447	-7.119553	-0.298399	0.059076	3.327758	1.717168	-2.850492	-0.000942
15	-265.408965	-265.423429	-9.076523	-0.300771	0.05996	2.770402	2.474451	1.245879	0.000179
16	-265.41715	-265.432012	-9.326421	-0.281143	0.069265	5.606389	-1.283138	-5.457578	0.000982
17	-265.430052	-265.44682	-10.521879	-0.273885	0.074125	5.149403	-4.821765	1.807453	0.007536
18	-281.422654	-281.438995	-10.25389	-0.318599	0.03554	6.463688	-2.120071	6.106108	0
19	-297.449575	-297.468754	-12.035135	-0.370799	0.022432	7.914928	0.869632	7.867009	0
20	-297.459801	-297.481551	-13.648337	-0.357342	0.025114	7.833508	7.413467	2.530681	0

B3LYP-D3/6-31G; PBF: DCE (10.65 ε)**

Compound	Gas Phase Energy	Solution Phase Energy	Solvation Energy (kcal/mol)	HOMO	LUMO	QM Dipole (D)	QM Dipole X (D)	QM Dipole Y (D)	QM Dipole Z (D)
2	-271.586283	-271.590317	-2.531579	-0.240484	-0.002368	0.460872	-0.28335	-0.363478	0
3	-287.623258	-287.631235	-5.005546	-0.254	-0.026448	2.653929	2.625399	-0.3881	0
4	-287.620856	-287.629059	-5.147537	-0.253428	-0.024674	3.301769	1.224918	3.066147	0
5	-287.621888	-287.630728	-5.547271	-0.262344	-0.024969	3.720652	-1.909846	-3.193077	0
6	-303.661245	-303.672505	-7.065548	-0.258114	-0.043193	2.378039	1.099844	2.108415	0
7	-303.661277	-303.672723	-7.182538	-0.262396	-0.043493	3.47384	1.062114	3.307488	0
8	-303.657945	-303.669523	-7.26515	-0.262922	-0.045637	3.845258	-1.995072	3.287202	0
9	-592.336615	-592.34097	-2.732324	-0.227609	-0.010826	1.009217	0.638246	-0.781768	-0.000738
10	-592.335265	-592.339726	-2.799249	-0.230406	-0.012386	1.364935	-0.105954	-1.360816	0.000601
11	-269.358227	-269.363164	-3.097821	-0.217786	0.016959	0.750408	0.414392	-0.625612	-0.000029
12	-269.352698	-269.357654	-3.109574	-0.221117	0.01455	1.227594	-0.098625	-1.223626	0.000815
13	-249.50171	-249.51078	-5.69162	-0.201869	0.043741	2.279418	-0.414338	2.241443	0.001174
14	-265.527471	-265.537828	-6.499675	-0.244664	0.016147	3.249848	1.667978	-2.78915	-0.00086
15	-265.534464	-265.547799	-8.367494	-0.246286	0.017235	2.65305	2.361626	1.208883	0.000157
16	-265.540644	-265.554512	-8.702104	-0.228082	0.02573	5.498556	-1.254802	-5.353465	0.000953
17	-265.553358	-265.568995	-9.812129	-0.221088	0.031158	5.05346	-4.737936	1.757659	0.007338
18	-281.549329	-281.565063	-9.872712	-0.264785	-0.010604	6.364264	-2.109336	6.004544	0
19	-297.576723	-297.595385	-11.71033	-0.304661	-0.026359	7.787776	0.847453	7.74153	0
20	-297.586912	-297.608356	-13.456348	-0.300768	-0.023764	7.777045	7.344791	2.556654	0

B3LYP/6-31G; gas phase**

Compound	Gas Phase Energy	Solution Phase Energy	Solvation Energy (kcal/mol)	HOMO	LUMO	QM Dipole (D)	QM Dipole X (D)	QM Dipole Y (D)	QM Dipole Z (D)
2	-271.578452	-271.590317	-2.531579	-0.235541	0.002387	0.350155	-0.216006	-0.27559	0
3	-287.616222	-287.631235	-5.005546	-0.247809	-0.020994	1.803148	1.779325	-0.292143	0
4	-287.613617	-287.629059	-5.147537	-0.248305	-0.01909	2.369615	0.837358	2.216733	0
5	-287.614634	-287.630728	-5.547271	-0.249441	-0.019466	2.678329	-1.376729	-2.297404	0
6	-303.655093	-303.672505	-7.065548	-0.24486	-0.038586	1.636696	0.765002	1.446909	0
7	-303.654888	-303.672723	-7.182538	-0.249001	-0.038582	2.516365	0.699957	2.417055	0
8	-303.651395	-303.669523	-7.26515	-0.248332	-0.040486	2.78933	-1.449873	2.382904	0
9	-592.330647	-592.34097	-2.732324	-0.222568	-0.005639	0.74899	0.421677	-0.619011	-0.000133
10	-592.329344	-592.339726	-2.799249	-0.225458	-0.00733	0.970368	-0.084307	-0.966698	-0.000455
11	-269.353019	-269.363164	-3.097821	-0.213146	0.021886	0.566741	0.305094	-0.477612	-0.000307
12	-269.34739	-269.357654	-3.109574	-0.217191	0.018931	0.94826	-0.079153	-0.944951	0.000181
13	-249.495807	-249.51078	-5.69162	-0.195236	0.04802	1.744903	-0.29823	1.719228	0.001119
14	-265.522241	-265.537828	-6.499675	-0.236191	0.023951	2.379334	1.07995	-2.120126	-0.000401
15	-265.529418	-265.547799	-8.367494	-0.236305	0.023972	1.942908	1.694168	0.951151	0.000847
16	-265.535249	-265.554512	-8.702104	-0.220244	0.031237	4.134794	-0.965472	-4.020495	0.00027
17	-265.548258	-265.568995	-9.812129	-0.214502	0.034837	3.62858	-3.40388	1.257053	0.0031
18	-281.544782	-281.565063	-9.872712	-0.256426	-0.000158	4.703161	-1.40877	4.487214	0
19	-297.572866	-297.595385	-11.71033	-0.282679	-0.01712	5.932309	0.747572	5.885017	0
20	-297.5832	-297.608356	-13.456348	-0.283974	-0.015807	5.78498	5.413476	2.039676	0

LMP2/6-31G**; gas phase

Compound	Gas Phase Energy	Solution Phase Energy	Solvation Energy (kcal/mol)	HOMO	LUMO	QM Dipole (D)	QM Dipole X (D)	QM Dipole Y (D)	QM Dipole Z (D)
2	-270.660593	-271.590317	-2.531579	-0.316801	0.143843	0.460872	-0.28335	-0.363478	0
3	-286.67968	-287.631235	-5.005546	-0.331147	0.122068	2.653929	2.625399	-0.3881	0
4	-286.678839	-287.629059	-5.147537	-0.330547	0.125119	3.301769	1.224918	3.066147	0
5	-286.679482	-287.630728	-5.547271	-0.340129	0.124353	3.720652	-1.909846	-3.193077	0
6	-302.704589	-303.672505	-7.065548	-0.360591	0.108706	2.378039	1.099844	2.108415	0
7	-302.702124	-303.672723	-7.182538	-0.366447	0.107929	3.47384	1.062114	3.307488	0
8	-302.70012	-303.669523	-7.26515	-0.35725	0.1059	3.845258	-1.995072	3.287202	0
9	-591.120704	-592.34097	-2.732324	-0.311406	0.132776	1.009217	0.638246	-0.781768	-0.000738
10	-591.119356	-592.339726	-2.799249	-0.315113	0.129543	1.364935	-0.105954	-1.360816	0.000601
11	-268.511014	-269.363164	-3.097821	-0.301147	0.170253	0.750408	0.414392	-0.625612	-0.000029
12	-268.505703	-269.357654	-3.109574	-0.30605	0.166146	1.227594	-0.098625	-1.223626	0.000815
13	-248.684136	-249.51078	-5.69162	-0.281473	0.195672	2.279418	-0.414338	2.241443	0.001174
14	-264.696015	-265.537828	-6.499675	-0.332034	0.173594	3.249848	1.667978	-2.78915	-0.00086
15	-264.702661	-265.547799	-8.367494	-0.333524	0.172465	2.65305	2.361626	1.208883	0.000157
16	-264.708941	-265.554512	-8.702104	-0.308957	0.183902	5.498556	-1.254802	-5.353465	0.000953
17	-264.721616	-265.568995	-9.812129	-0.303034	0.187446	5.05346	-4.737936	1.757659	0.007338
18	-280.703001	-281.565063	-9.872712	-0.350306	0.152408	6.364264	-2.109336	6.004544	0
19	-296.715009	-297.595385	-11.71033	-0.40561	0.14152	7.787776	0.847453	7.74153	0
20	-296.724616	-297.608356	-13.456348	-0.39568	0.142856	7.777045	7.344791	2.556654	0

Synthetic Procedures

General Procedures: Reactions were magnetically stirred. Air and/or moisture sensitive reactions were carried out under an argon atmosphere in oven-dried glassware using anhydrous solvents from commercial suppliers. Air and/or moisture sensitive reagents were transferred via syringe or cannula and were introduced into reaction vessels through rubber septa. All anhydrous solvents used were purchased from Sigma-Aldrich and used without further purification. Solvents to be employed in flash column chromatography and reaction work-up procedures were purchased from either Sigma-Aldrich or Fisher Scientific. All other reagents were obtained commercially and used without further purification, unless otherwise stated. Reactions were monitored using LCMS and thin layer chromatography (TLC) performed on 0.25-mm EMD pre-coated glass-backed silica gel 60 F-254 plates. Compounds were visualized under UV light or through staining with permanganate, bromocresol green, or magic, when appropriate. Reaction products and chromatography fractions were concentrated

by rotary evaporation at 30-35 °C at 20 Torr, then Hi-Vac at 0.5 Torr overnight, unless otherwise indicated.

Instrumentation: NMR spectra were recorded on a Bruker AvanceIII HD 400 MHz spectrometer (with 5 mm BBFO Z-gradient Smart Probe) calibrated to CH(D)Cl₃ as an internal reference (7.26 and 77.00 ppm for ¹H and ¹³C NMR spectra, respectively). Data for ¹H NMR spectra are reported in terms of chemical shift (δ, ppm), multiplicity, coupling constant (Hz), and integration. Data for ¹³C NMR spectra are reported in terms of chemical shift (δ, ppm), with multiplicity and coupling constants in the case of C–F coupling. The following abbreviations are used to denote the multiplicities: s = singlet; d = doublet; dd = doublet of doublets; dt = doublet of triplets; dq = doublet of quartets; ddd = doublet of doublet of doublets; t = triplet; td = triplet of doublets; tt = triplet of triplets; q = quartet; qd = quartet of doublets; quin = quintet; sex = sextet; m = multiplet. LCMS and compound purity were determined using a Waters Micromass ZQ 4000, equipped with a Waters 2795 Separation Module, Waters 2996 Photodiode Array Detector, and a Waters 2424 ELSD. Separations were carried out with an XBridge BEH C18, 5μm, 4.6 x 20 mm column, at ambient temperature (unregulated), using a mobile phase of water-methanol containing a constant 0.1% formic acid. HPLC was performed on a Waters 2535 Separation Module with a Waters 2998 Photodiode Array Detector. Separations were carried out with an XBridge BEH C18, 5μm, 19 x 50 mm column, at ambient temperature (unregulated), using a mobile phase of water-methanol containing a constant 0.05% formic acid. Column chromatography was carried out using a Biotage SP1 flash chromatography system with silica gel cartridges from Silicycle.

General Procedure A: A 20 mL vial is charged with the appropriate carboxylic acid (1.0 equiv.), commercially available 3-(1*H*-tetrazol-5-yl)aniline (1.1 equiv.), DMF, *N,N*-diisopropylethylamine (2.1 equiv.), and HATU (1.1 equiv.). The reaction mixture is stirred for 18h or until judged complete by LCMS. The crude reaction mixture is directly purified by reverse phase HPLC (water/MeOH/0.05% formic acid) to afford the desired product.

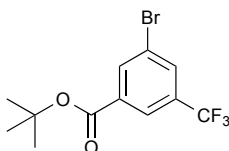
General Procedure B: A 20 mL vial is charged with the appropriate carboxylic acid (1.0 equiv.), DMF, and *N,N*-diisopropylethylamine (1.0 equiv.). HATU (1.05 equiv.) is then added, and the reaction mixture is allowed to stir for 20 minutes. Commercially available 3-(1*H*-tetrazol-5-yl)aniline (1.1 equiv.) and *N,N*-diisopropylethylamine (1.1 equiv.) are subsequently added, and the reaction is stirred at room temperature for 24 h or until judged complete by LCMS. The crude reaction mixture is directly purified by reverse phase HPLC (water/MeOH/0.05% formic acid) to afford the desired product.

General Procedure C: A 20 mL vial is charged with the appropriate t-butyl ester (1.0 equiv.), fitted with a septa, and purged with Ar. The vial is then charged with dry 4M HCl in dioxanes (4 mL), and the reaction is stirred at room temperature for 18-72h or until judged complete by LCMS. The reaction mixture is then concentrated and dried under hovac overnight, affording the desired semi-crude product.

General Procedure D: A 3 mL vial with cap is purged with Ar and charged with the appropriate halide (1.0 equiv), bis(pinacolato)diboron (1.1 equiv.), potassium acetate (2.0 equiv.), 1,1'-bis(diphenylphosphino)ferrocene-palladium(II)dichloride dichloromethane complex (0.02 equiv.), and dry tetrahydrofuran (1 mL). The reaction mixture is purged with Ar, sealed, and heated at 80 °C for 18h. The reaction mixture is then cooled to rt and charged with a solution of potassium carbonate (2.0 equiv.) in water (620 uL), the second halide (1.2 equiv.), and 1,1'-bis(diphenylphosphino)ferrocene-palladium(II)dichloride dichloromethane complex (0.02 equiv.). The reaction mixture is purged with Ar, sealed, and vigorously stirred at 80 °C for 18h. The crude reaction mixture is then transferred to a sep funnel with ~ 75 mL EtOAc and ~10 mL water. ~ 50 mL sat. NaHCO₃ is added, the layers separated, and the organic layer further washed with ~ 40 mL water and brine. The organic layer is dried over MgSO₄, concentrated, and purified on a silica column with EtOAc:hexanes to afford the desired product.

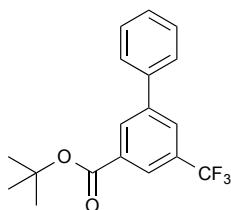
General Procedure E: S1 (1 equiv.) and an aqueous K₂CO₃ solution (1M, 1.25 equiv.) were added to 0.5 mL of 1,4 dioxane. Argon was bubbled through the resulting solution to remove oxygen before the boronic acid (1.2 equiv.) and 1,1'-bis(diphenylphosphino)ferrocene-palladium(II)dichloride dichloromethane complex (0.05 equiv.) were added. The reaction was then warmed to 80 °C and stirred until complete by LCMS (18–24h). The reaction mixture was allowed to cool to r.t., diluted with MeOH, and filtered through celite. The filtrate was concentrated and purified as noted.

General Procedure F: Aryl t-butyl ester (1 equiv.) was suspended in 1:1 TFA/CH₂Cl₂ and stirred until complete by either TLC or LCMS (3-18 h). Solvent was removed *in vacuo* and the resulting crude acid was used without further purification. The newly generated acid (1.0 equiv.), triethylamine (3.0 equiv.), and 3-(1*H*-tetrazol-5-yl)aniline (1.2 equiv.) were suspended in 0.5 mL DMF and placed under argon. HATU (1.5 equiv.) was added and the reaction was stirred until complete by LCMS (18-24h). The reaction was then diluted with DMF and purified by reverse phase HPLC (water/MeOH/0.05% formic acid) to afford the desired product.

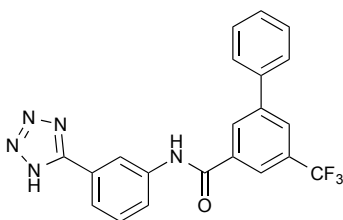


tert-butyl 3-bromo-5-(trifluoromethyl)benzoate (S1). Commercially available 3-bromo-5-trifluoromethylbenzoic acid (5.000 g, 18.6 mmol, 1.0 equiv) was dissolved in dry dichloromethane (50 ml). *N,N*-dimethylformamide (400 ul, 5.2 mmol, 0.3 equiv) was added; oxalyl chloride (2.000 ml, 23.3 mmol, 1.3 equiv.) was subsequently added dropwise. The reaction mixture was allowed to stir at rt for 4h. The solvent was then removed under reduced pressure, and the residue was azeotroped with toluene twice. The remaining residue was diluted with dry tetrahydrofuran (65 mL) and cooled to 0 °C. Lithium tert-butoxide (2.976 g, 37.2 mmol, 2.0 equiv) was added in bulk to the reaction mixture; the reaction mixture was allowed to slowly warm to rt over 18h. ~ 100 mL water was then added, and the reaction mixture was extracted with 2 x 100 mL EtOAc. The organics were washed with ~ 50 mL 0.1 N HCl, water, and brine, then dried over MgSO₄. Purified on a silica column with 0-5% EtOAc:hexanes. **S1** (4.589, 76%)

obtained as a colorless, crystalline solid. ^1H NMR (400 MHz, CDCl_3) δ = 8.30 (s, 1H), 8.18 (s, 1H), 7.93 (s, 1H), 1.63 (s, 9H); ^{13}C NMR (100 MHz, CDCl_3) δ = 163.01, 135.72, 134.67, 132.49 (q, J = 33.5 Hz), 132.00 (q, J = 3.7 Hz), 125.02 (q, J = 3.7 Hz), 122.71, 122.83 (q, J = 272.9 Hz), 82.78, 28.08; ^{19}F NMR (376 MHz, CDCl_3) δ = -62.89 (s, 3F); did not ionize by ESI.

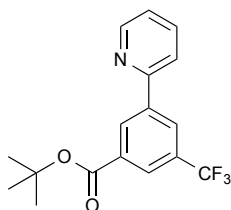


tert-butyl 5-(trifluoromethyl)-[1,1'-biphenyl]-3-carboxylate (S2). S1 was reacted with commercially available phenylboronic acid according to general procedure E. Crude product was filtered through a silica gel plug; the plug was washed with hexanes and the product eluted with ethyl acetate. S2 (46 mg, 65%) obtained as a colorless liquid. ^1H NMR (400 MHz, CDCl_3) δ = 8.42 (s, 1H), 8.24 (s, 1H), 8.01 (s, 1H), 7.64 - 7.67 (m, 2H), 7.50 - 7.54 (m, 2H), 7.43 - 7.47 (m, 1 H), 1.67 (s, 9H); did not ionize by ESI.

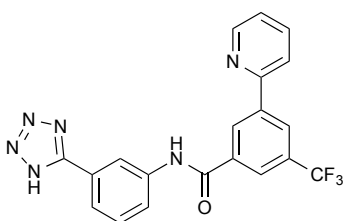


N-(3-(1H-tetrazol-5-yl)phenyl)-5-(trifluoromethyl)-[1,1'-biphenyl]-3-carboxamide (2). S2 (46.0 mg, 0.173 mmol, 1.0 equiv) was reacted according to general procedure F. 2 (28.8 mg, 50% over two steps) was obtained as a white solid. ^1H NMR (400 MHz, acetone- d_6) δ = 10.16 (br s, 1H), 8.69 (s, 1H), 8.61 (s, 1H), 8.35 (s, 1H), 8.19 (s, 1H), 8.07 (br d, J = 8.04 Hz, 1H), 7.93 (br d, J = 7.67 Hz, 1H), 7.86 (br d, J = 7.43 Hz, 2H),

7.54 - 7.65 (m, 3H), 7.46 - 7.53 (m, 1H); ^{13}C NMR (100 MHz, acetone- d_6) δ = 164.22, 156.83, 142.57, 139.97, 138.60, 136.75, 131.07 (q, J = 32.28 Hz), 129.79, 129.69, 129.19, 128.59, 127.29, 126.21 - 126.47 (m), 125.84, 123.18 - 123.40 (m), 122.60, 118.78; ^{19}F NMR (376 MHz, acetone- d_6) δ = -63.03 (s, 3F); HRMS (ESI) calculated for $\text{C}_{21}\text{H}_{13}\text{F}_3\text{N}_5\text{O}$ [$\text{M} - \text{H}$] $^-$ m/z 408.1078, found 408.1070.

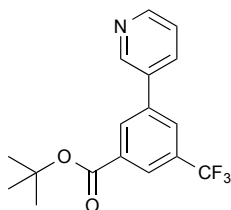


tert-butyl 3-(pyridin-2-yl)-5-(trifluoromethyl)benzoate (S3). **S1** (65.0 mg, 0.20 mmol, 1 equiv) was reacted with commercially available 2-bromopyridine according to general procedure D, except 5 mol% catalyst was used. Instead of a workup, the reaction mixture was allowed to cool to room temperature, diluted with MeOH, and filtered through celite. The filtrate was concentrated and purified via silica gel with EtOAc:hexanes. **S3** (18.0 mg, 26%) obtained as a clear liquid. ^1H NMR (400 MHz, CDCl_3) δ = 8.72 - 8.80 (m, 2H), 8.50 - 8.55 (m, 1H), 8.29 (s, 1H), 7.83 - 7.89 (m, 2H), 7.31 - 7.38 (m, 1H), 1.66 (s, 9H); LRMS (ESI) calculated for $\text{C}_{17}\text{H}_{17}\text{F}_3\text{NO}_2$ [$\text{M} + \text{H}$] $^+$ m/z 324.11, found 324.02.

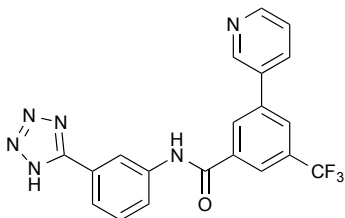


N-(3-(1H-tetrazol-5-yl)phenyl)-3-(pyridin-2-yl)-5-(trifluoromethyl)benzamide (3). **S3** (18.0 mg, 0.056 mmol, 1.0 equiv) was reacted according to general procedure F. **3**

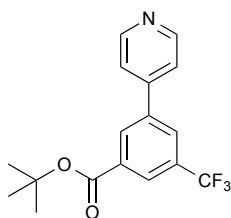
(16.4 mg, 78% over two steps) obtained as a white solid. ^1H NMR (400 MHz, acetone- d_6) δ = 10.31 (br s, 1H), 9.05 (s, 1H), 8.77 (dd, J = 4.75, 0.73 Hz, 1H), 8.75 (s, 1H), 8.71 (s, 1H), 8.44 (s, 1H), 8.26 (d, J = 7.91 Hz, 1H), 8.17 (br d, J = 8.16 Hz, 1H), 7.95 - 8.01 (m, 2H), 7.57 (t, J = 7.97 Hz, 1H), 7.46 (ddd, J = 7.52, 4.78, 0.73 Hz, 1H); ^{13}C NMR (100 MHz, acetone- d_6) δ = 164.09, 154.21, 149.91, 140.80, 139.95, 137.42, 136.69, 130.93 (d, J = 32.28 Hz), 129.62, 129.10, 126.11 (br d, J = 3.67 Hz), 124.78 (br d, J = 3.67 Hz), 123.59, 122.52, 122.07, 120.87, 118.94; ^{19}F NMR (376 MHz, acetone- d_6) δ = -63.12 (s, 3F); HRMS (ESI) calculated for $\text{C}_{20}\text{H}_{12}\text{F}_3\text{N}_6\text{O}$ [$\text{M} - \text{H}$] $^-$ m/z 409.1030, found 409.1022.



tert-butyl 3-(pyridin-3-yl)-5-(trifluoromethyl)benzoate (S4). **S1** was reacted with commercially available pyridin-3-ylboronic acid according to general procedure E. Crude product was purified via silica gel with EtOAc:hexanes. **S4** (26 mg, 40%) obtained as a colorless liquid. ^1H NMR (400 MHz, CDCl_3) δ = 8.89 - 8.94 (m, 1H), 8.70 (br d, J = 4.14 Hz, 1H), 8.40 (s, 1H), 8.28 (s, 1H), 7.99 (s, 1H), 7.93 - 7.97 (m, 1H), 7.46 (dd, J = 7.91, 4.87 Hz, 1H), 1.66 (s, 9H); ^{13}C NMR (100 MHz, CDCl_3) δ = 164.03, 149.56, 148.20, 139.04, 134.60, 133.86, 131.86 (q, J = 30.08 Hz), 131.26, 127.35 - 127.54 (m), 125.62 - 125.95 (m), 123.82, 82.49, 28.14; ^{19}F NMR (376 MHz, CDCl_3) δ = -62.68 (s, 3F); LRMS (ESI) calculated for $\text{C}_{17}\text{H}_{17}\text{F}_3\text{NO}_2$ [$\text{M} + \text{H}$] $^+$ m/z 324.11, found 324.02.

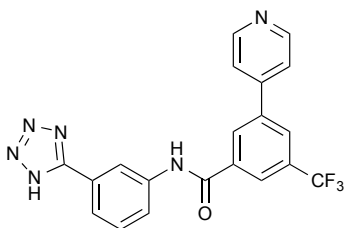


N-(3-(1*H*-tetrazol-5-yl)phenyl)-3-(pyridin-3-yl)-5-(trifluoromethyl)benzamide (4). S4 (34 mg, 0.105 mmol, 1.0 equiv) was reacted according to general procedure F. **4** (25 mg, 58% over two steps) obtained as a white solid. ¹H NMR (400 MHz, pyridine-*d*₅) δ = 11.72 (s, 1H), 9.27 (br s, 1H), 9.07 - 9.22 (m, 3H), 9.04 (br s, 1H), 8.76 (br d, *J* = 4.75 Hz, 1H), 8.70 (s, 2H), 8.64 (s, 1H), 8.21 (br dd, *J* = 6.15, 1.03 Hz, 2H), 8.12 (s, 1H), 7.85 (br dd, *J* = 7.85, 1.28 Hz, 1H), 7.33 (br dd, *J* = 7.85, 4.81 Hz, 1H); ¹³C NMR (100 MHz, pyridine-*d*₅) δ = 165.24, 149.76, 148.58, 140.59, 139.35, 137.59, 134.48, 134.16, 131.07 (d, *J* = 32.28 Hz), 130.48, 129.99, 127.61, 126.56 (br d, *J* = 3.67 Hz), 124.48 (br d, *J* = 4.40 Hz), 123.82, 123.13, 122.85, 119.87; ¹⁹F NMR (376 MHz, pyridine-*d*₅) δ = -62.03 (s, 3F); HRMS (ESI) calculated for C₂₀H₁₂F₃N₆O [M - H]⁻ *m/z* 409.1030, found 409.1023.

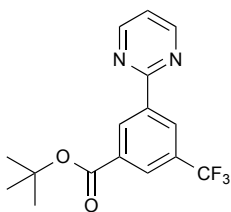


tert-butyl 3-(pyridin-4-yl)-5-(trifluoromethyl)benzoate (S5). S1 was reacted with commercially available pyridin-4-ylboronic acid according to general procedure E. Crude product was purified via HPLC using water/MeOH/0.05% formic acid. **S5** (34 mg, 54%) obtained as a white powder. ¹H NMR (400 MHz, CDCl₃) δ = 8.79 (br s, 2H), 8.45 (s, 1H), 8.31 (s, 1H), 8.04 (s, 1H), 7.59 (br s, 2H), 1.66 (s, 9H); ¹³C NMR (100 MHz, CDCl₃)

δ = 163.90, 150.61, 146.09, 139.42, 133.95, 131.92 (d, J = 33.01 Hz), 131.15, 127.35 (br d, J = 3.67 Hz), 126.61 (q, J = 3.67 Hz), 82.60, 28.14; ^{19}F NMR (376 MHz, CDCl_3) δ = -62.70 (s, 3F); LRMS (ESI) calculated for $\text{C}_{17}\text{H}_{17}\text{F}_3\text{NO}_2$ $[\text{M} + \text{H}]^+$ m/z 324.11, found 324.09.

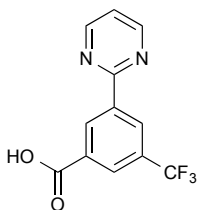


N-(3-(1H-tetrazol-5-yl)phenyl)-3-(pyridin-4-yl)-5-(trifluoromethyl)benzamide (5). S5 (19.4 mg, 0.060 mmol, 1.0 equiv) was reacted according to general procedure F. **5** (19 mg, 77% over two steps) obtained as a white solid. ^1H NMR (400 MHz, pyridine- d_5) δ = 11.74 (s, 1H), 9.26 (br d, J = 1.46 Hz, 1H), 8.77 - 8.83 (m, 2H), 8.70 (s, 3H), 8.66 (s, 1H), 8.17 - 8.23 (m, 2H), 8.15 (s, 1H), 7.56 - 7.61 (m, 1H), 7.46 - 7.52 (m, 2H); ^{13}C NMR (100 MHz, pyridine- d_5) δ = 165.10, 150.80, 145.43, 140.57, 139.53, 137.64, 131.12 (d, J = 33.01 Hz), 130.42, 130.03, 127.47, 126.53 (br d, J = 3.67 Hz), 125.17 - 125.70 (m), 123.16, 121.69, 119.87; ^{19}F NMR (376 MHz, pyridine- d_5) δ = -62.07 (s, 3F); HRMS (ESI) calculated for $\text{C}_{20}\text{H}_{12}\text{F}_3\text{N}_6\text{O}$ $[\text{M} - \text{H}]^-$ m/z 409.1030, found 409.1023.

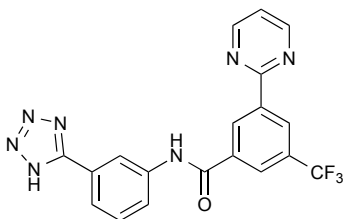


tert-butyl 3-(pyrimidin-2-yl)-5-(trifluoromethyl)benzoate (S6). S1 (100 mg, 0.308 mmol, 1.0 equiv) was reacted with commercially available 2-bromopyrimidine according

to general procedure D. **S6** (75.2 mg, 75%) obtained as a white solid. ^1H NMR (400 MHz, CDCl_3) δ = 9.23 (br s, 1H), 8.90 (br s, 1H), 8.86 (d, J = 4.9 Hz, 2H), 8.35 (s, 1H), 7.28 (t, J = 4.9 Hz, 1H), 1.69 - 1.63 (m, 9H); ^{13}C NMR (100 MHz, CDCl_3) δ = 164.23, 162.64, 157.44, 138.87, 133.48, 132.12, 131.33 (q, J = 33.0 Hz), 128.58 (q, J = 3.7 Hz), 128.13 (q, J = 4.2 Hz), 123.77 (q, J = 272.9 Hz), 120.03, 82.17, 28.14; ^{19}F NMR (376 MHz, CDCl_3) δ = -62.66 (s, 3F); LRMS (ESI) calculated for $\text{C}_{16}\text{H}_{16}\text{F}_3\text{N}_2\text{O}_2$ $[\text{M} + \text{H}]^+$ m/z 325.11, found 324.94.

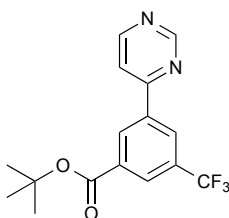


3-(pyrimidin-2-yl)-5-(trifluoromethyl)benzoic acid (S7). **S6** (75.2 mg, 0.232 mmol, 1.0 equiv) was reacted according to general procedure C (24h). Semi-crude **S7** (65.6 mg, 106%) obtained as a white solid. ^1H NMR (400 MHz, CD_3OD , drops CDCl_3) δ = 9.20 (br s, 1H), 8.90 (d, J = 4.9 Hz, 2H), 8.83 (br s, 1H), 8.34 (br s, 1H), 7.46 (t, J = 5.0 Hz, 1H); ^{13}C NMR (100 MHz, CD_3OD , drops CDCl_3) δ = 166.42, 161.55, 157.62, 138.31, 132.48, 132.26, 131.21 (q, J = 33.0 Hz), 128.38 (q, J = 3.7 Hz), 128.11 (q, J = 3.7 Hz), 120.49, 123.67 (q, J = 272.2 Hz); ^{19}F NMR (376 MHz, CD_3OD , drops CDCl_3) δ = -63.99 (s, 3F); LRMS (ESI) calculated for $\text{C}_{12}\text{H}_6\text{F}_3\text{N}_2\text{O}_2$ $[\text{M} - \text{H}]^-$ m/z 267.05, found 267.06.



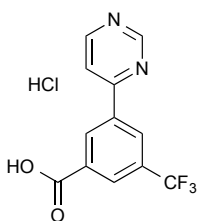
N-(3-(1*H*-tetrazol-5-yl)phenyl)-3-(pyrimidin-2-yl)-5-(trifluoromethyl)benzamide (6).

S7 (65.6 mg, 0.245 mmol, 1.0 equiv) was reacted with 3-(1*H*-tetrazol-5-yl)aniline in 3 mL DMF according to general procedure B. **6** (65.4 mg, 65%) obtained as a white solid. ¹H NMR (400 MHz, CD₃OD, drops CDCl₃) δ = 9.18 (br s, 1H), 8.84 (d, *J* = 4.9 Hz, 2H), 8.83 (br s, 1H), 8.35 (t, *J* = 1.7 Hz, 1H), 8.32 (br s, 1H), 7.91 (br dd, *J* = 1.2, 8.3 Hz, 1H), 7.74 (br d, *J* = 7.8 Hz, 1H), 7.50 (t, *J* = 7.9 Hz, 1H), 7.36 (t, *J* = 4.9 Hz, 1H); ¹³C NMR (100 MHz, CD₃OD, drops CDCl₃) δ = 166.65, 163.18, 158.59, 157.50, 140.31, 139.95, 137.21, 132.38 (q, *J* = 30.1 Hz), 131.34, 130.75, 128.59 (d, *J* = 3.7 Hz), 127.37 (q, *J* = 3.7 Hz), 126.03, 124.49, 124.01, 124.72 (q, *J* = 272.2 Hz), 121.38, 120.32; ¹⁹F NMR (376 MHz, CD₃OD, drops CDCl₃) δ = -63.57 (s, 3F); HRMS (ESI) calculated for C₁₉H₁₁F₃N₇O [M - H]⁻ m/z 410.0983, found 410.0974.

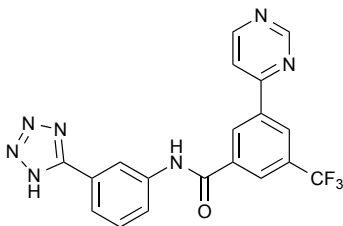


tert-butyl 3-(pyrimidin-4-yl)-5-(trifluoromethyl)benzoate (S8). **S1** (100 mg, 0.308 mmol, 1.0 equiv) was reacted with commercially available 4-chloropyrimidine hydrochloride according to general procedure D, except potassium carbonate (136 mg, 0.984 mmol, 3.2 equiv) and water (992 ul) were used in the second step. **S8** (84.5 mg, 85%) obtained as a white solid. ¹H NMR (400 MHz, CDCl₃) δ = 9.31 (br d, *J* = 1.4 Hz,

1H), 8.84 (d, $J = 5.4$ Hz, 1H), 8.80 (br s, 1H), 8.57 (br s, 1H), 8.33 (br s, 1H), 7.81 (dd, $J = 1.5, 5.4$ Hz, 1H), 1.63 (s, 9H); ^{13}C NMR (100 MHz, CDCl_3) $\delta = 163.71, 161.41, 159.24, 158.03, 137.67, 133.77, 131.82$ (q, $J = 33.0$ Hz), 130.86, 128.32 (q, $J = 3.9$ Hz), 127.56 (q, $J = 3.7$ Hz), 123.43 (q, $J = 272.9$ Hz), 117.03, 82.53, 28.03; ^{19}F NMR (376 MHz, CDCl_3) $\delta = -62.78$ (s, 3F); LRMS (ESI) calculated for $\text{C}_{16}\text{H}_{16}\text{F}_3\text{N}_2\text{O}_2$ $[\text{M} + \text{H}]^+$ m/z 325.11, found 325.01.

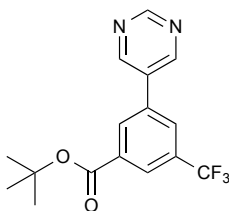


3-(pyrimidin-4-yl)-5-(trifluoromethyl)benzoic acid hydrochloride (S9). **S8** (84.5 mg, 0.261 mmol, 1.0 equiv) was reacted according to general procedure C (24h). Semi-crude **S9** (80.8 mg, 102%) obtained as a white solid. ^1H NMR (400 MHz, CD_3OD) $\delta = 9.60$ (br s, 1H), 9.20 (d, $J = 6.1$ Hz, 1H), 9.16 (br s, 1H), 8.86 (br s, 1H), 8.67 (dd, $J = 1.0, 6.1$ Hz, 1H), 8.50 (br s, 1H); ^{13}C NMR (100 MHz, CD_3OD) $\delta = 166.81, 165.56, 153.72, 152.18, 136.13, 133.41, 132.52, 131.91$ (q, $J = 33.0$ Hz), 129.89 (q, $J = 4.2$ Hz), 128.70 (q, $J = 3.9$ Hz), 123.43 (q, $J = 272.2$ Hz), 118.72; ^{19}F NMR (376 MHz, CD_3OD) $\delta = -64.35$ (s, 3F); LRMS (ESI) calculated for $\text{C}_{12}\text{H}_6\text{F}_3\text{N}_2\text{O}_2$ $[\text{M} - \text{H}]^-$ m/z 267.05, found 267.06.



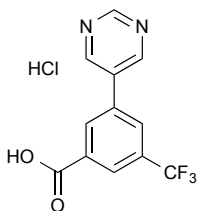
N-(3-(1*H*-tetrazol-5-yl)phenyl)-3-(pyrimidin-4-yl)-5-(trifluoromethyl)benzamide (7).

S9 (80.8 mg, 0.265 mmol, 1.0 equiv) was reacted with 3-(1*H*-tetrazol-5-yl)aniline in 3 mL DMF according to general procedure B, except 2 equiv *N,N*-diisopropylethylamine (93 μ L) was used in the first step. **7** (68.8 mg, 63%) obtained as a white solid. ^1H NMR (400 MHz, DMSO- d_6) δ = 10.84 (s, 1H), 9.36 (d, J = 1.0 Hz, 1H), 9.07 (br s, 1H), 9.00 (d, J = 5.4 Hz, 1H), 8.73 (s, 1H), 8.58 (s, 1H), 8.50 (s, 1H), 8.37 (dd, J = 1.2, 5.4 Hz, 1H), 8.03 (dd, J = 1.1, 8.2 Hz, 1H), 7.80 (d, J = 7.8 Hz, 1H), 7.63 (t, J = 8.0 Hz, 1H); ^{13}C NMR (100 MHz, DMSO- d_6) δ = 163.76, 160.33, 158.90, 158.70, 155.77, 139.63, 137.60, 136.49, 130.21, 129.90, 130.22 (q, J = 33.0 Hz), 126.70 (br q, J = 3.7 Hz), 126.40 (br q, J = 3.7 Hz), 124.93, 122.96, 122.48, 123.72 (q, J = 272.9 Hz), 118.91, 117.95; ^{19}F NMR (376 MHz, DMSO- d_6) δ = -61.16 (s, 3F); HRMS (ESI) calculated for $\text{C}_{19}\text{H}_{11}\text{F}_3\text{N}_7\text{O}$ [$\text{M} - \text{H}$] $^-$ m/z 410.0983, found 410.0975.

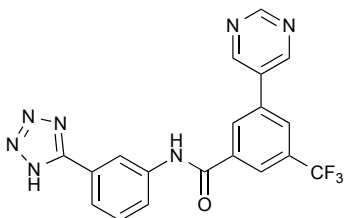


tert-butyl 3-(pyrimidin-5-yl)-5-(trifluoromethyl)benzoate (S10). **S1** (100 mg, 0.308 mmol, 1.0 equiv) was reacted with commercially available 5-bromopyrimidine according to general procedure D. **S10** (74.3 mg, 75%) obtained as a white solid. ^1H NMR (400 MHz, CDCl_3) δ = 9.26 (s, 1H), 9.00 (s, 2H), 8.37 (br s, 1H), 8.30 (br s, 1H), 7.96 (br s,

1H), 1.61 (s, 9H); ^{13}C NMR (100 MHz, CDCl_3) δ = 163.55, 158.37, 154.96, 135.53, 134.21, 132.40, 132.16 (q, J = 33.0 Hz), 131.06, 127.18 (q, J = 3.7 Hz), 126.53 (q, J = 4.2 Hz), 123.32 (q, J = 272.9 Hz), 82.67, 28.02; ^{19}F NMR (376 MHz, CDCl_3) δ = -62.77 (s, 3F); LRMS (ESI) calculated for $\text{C}_{16}\text{H}_{16}\text{F}_3\text{N}_2\text{O}_2$ $[\text{M} + \text{H}]^+$ m/z 325.11, found 325.09.

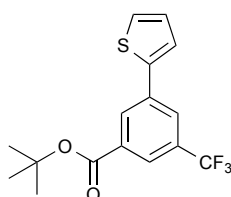


3-(pyrimidin-5-yl)-5-(trifluoromethyl)benzoic acid hydrochloride (S11). **S10** (74.3 mg, 0.229 mmol, 1.0 equiv) was reacted according to general procedure C (48h). Semi-crude **S11** (70.1 mg, 100%) obtained as a white solid. ^1H NMR (400 MHz, CD_3OD , drops CDCl_3) δ = 9.36 (s, 1H), 9.28 (s, 2H), 8.56 (s, 1H), 8.19 (s, 1H), 7.98 (s, 1H); ^{19}F NMR (376 MHz, CD_3OD , drops CDCl_3) δ = -63.56 (s, 3F); LRMS (ESI) calculated for $\text{C}_{12}\text{H}_6\text{F}_3\text{N}_2\text{O}_2$ $[\text{M} - \text{H}]^-$ m/z 267.05, found 266.99.



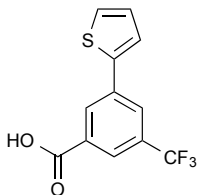
N-(3-(1H-tetrazol-5-yl)phenyl)-3-(pyrimidin-5-yl)-5-(trifluoromethyl)benzamide (8). **S11** (70.1 mg, 0.230 mmol, 1.0 equiv) was reacted with 3-(1H-tetrazol-5-yl)aniline in 2.5 mL DMF according to general procedure B, except 2 eq *N,N*-diisopropylethylamine (80.2 μL) was used in the first step. **8** (16.5 mg, 17%) obtained as a white solid. ^1H NMR (400 MHz, $\text{CD}_3\text{OD}/\text{CD}_3\text{CN}/\text{CDCl}_3$) δ = 10.60 (s, 1H), 10.55 (br s, 2H), 9.91 (br s, 1H),

9.88 - 9.84 (m, 1H), 9.75 (br s, 1H), 9.61 (br s, 1H), 9.29 (br d, $J = 8.3$ Hz, 1H), 9.17 (br d, $J = 7.8$ Hz, 1H), 8.99 - 8.92 (m, 1H); ^{13}C NMR (100 MHz, $\text{CD}_3\text{OD}/\text{CD}_3\text{CN}/\text{CDCl}_3$) $\delta = 166.15, 159.15, 157.98, 156.69, 140.71, 138.28, 137.25, 133.85, 133.01$ (q, $J = 33.0$ Hz), 131.22, 128.23 (br q, $J = 3.7$ Hz), 126.86, 126.21 (br q, $J = 4.4$ Hz), 124.51, 124.33, 120.54; ^{19}F NMR (376 MHz, $\text{CD}_3\text{OD}/\text{CD}_3\text{CN}/\text{CDCl}_3$) $\delta = -62.05$ (s, 3F); HRMS (ESI) calculated for $\text{C}_{19}\text{H}_{11}\text{F}_3\text{N}_7\text{O}$ [$\text{M} - \text{H}$] $^-$ m/z 410.0983, found 410.0976.

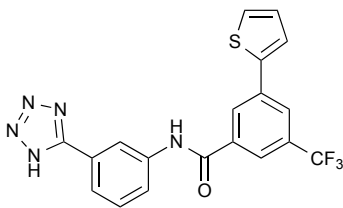


tert-butyl 3-(thiophen-2-yl)-5-(trifluoromethyl)benzoate (S12). A 3 mL vial with cap was purged with Ar and charged with **S1** (100 mg, 0.308 mmol, 1.0 equiv), thiophene-2-boronic acid (98 mg, 0.769 mmol, 2.5 equiv), cesium carbonate (251 mg, 0.769 mmol, 2.5 equiv), tetrakis(triphenylphosphine)palladium(0) (21 mg, 0.018 mmol, 0.06 equiv), and dry 1,2-dimethoxyethane (2.5 mL). The reaction mixture was purged again, sealed, and heated at 80 °C for 18h. The crude reaction mixture was transferred to a sep funnel with ~ 75 mL EtOAc and ~ 5 mL water. ~ 50 mL sat. NaHCO_3 was added, the layers separated, and the organic layer washed with ~ 50 mL water and brine. The EtOAc was dried over MgSO_4 and concentrated. Purified on a silica column with 0-15% EtOAc:hexanes. **S12** (70.7 mg, 70%) obtained as a glassy solid. ^1H NMR (400 MHz, CDCl_3) $\delta = 8.39$ (br s, 1H), 8.13 (br s, 1H), 7.97 (br s, 1H), 7.43 (dd, $J = 1.0, 3.7$ Hz, 1H), 7.38 (dd, $J = 1.2, 5.1$ Hz, 1H), 7.13 (dd, $J = 3.7, 5.1$ Hz, 1H), 1.66 (s, 9H); ^{13}C NMR (100 MHz, CDCl_3) $\delta = 164.09, 141.67, 135.55, 133.55, 131.51$ (q, $J = 33.0$ Hz), 129.71, 128.33, 126.35, 125.88 (q, $J = 3.7$ Hz), 124.68, 124.71 (q, $J = 3.7$ Hz), 123.61 (q, $J =$

272.9 Hz), 82.23, 28.08; ^{19}F NMR (376 MHz, CDCl_3) δ = -62.77 (s, 3F); did not ionize by ESI.

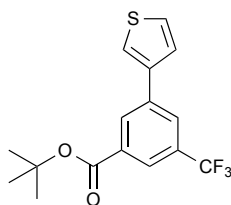


3-(thiophen-2-yl)-5-(trifluoromethyl)benzoic acid (S13). **S12** (70.7 mg, 0.215 mmol, 1.0 equiv) was reacted according to general procedure C (48h). Semi-crude **S13** (59.6 mg, 102%) obtained as a white solid. ^1H NMR (400 MHz, CD_3OD) δ = 8.36 (s, 1H), 8.09 (s, 1H), 7.99 (br s, 1H), 7.48 (dd, J = 1.2, 3.7 Hz, 1H), 7.45 (dd, J = 1.0, 5.1 Hz, 1H), 7.10 (dd, J = 3.7, 5.1 Hz, 1H); ^{13}C NMR (100 MHz, CD_3OD) δ = 166.29, 140.95, 135.90, 132.61, 131.32 (q, J = 33.0 Hz), 129.42, 128.23, 126.35, 125.29 (q, J = 3.7 Hz), 124.82, 124.23 (q, J = 3.7 Hz), 123.66 (q, J = 271.7 Hz); ^{19}F NMR (376 MHz, CD_3OD) δ = -64.35 (s, 3F); LRMS (ESI) calculated for $\text{C}_{12}\text{H}_6\text{F}_3\text{O}_2\text{S}$ [$\text{M} - \text{H}$] $^-$ m/z 271.01, found 270.93.

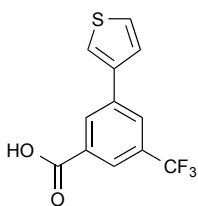


N-(3-(1H-tetrazol-5-yl)phenyl)-3-(thiophen-2-yl)-5-(trifluoromethyl)benzamide (9). **S13** (59.6 mg, 0.219 mmol, 1.0 equiv) was reacted with 3-(1H-tetrazol-5-yl)aniline in 2.5 mL DMF according to general procedure B. **9** (60.9 mg, 67%) obtained as a white solid. ^1H NMR (400 MHz, DMSO-d_6) δ = 10.77 (s, 1H), 8.57 (t, J = 1.7 Hz, 1H), 8.50 (s, 1H), 8.24 (s, 1H), 8.18 (s, 1H), 8.01 (dd, J = 1.2, 8.3 Hz, 1H), 7.83 (dd, J = 1.0, 3.7 Hz, 1H), 7.80 (d, J = 7.8 Hz, 1H), 7.71 (dd, J = 1.1, 5.0 Hz, 1H), 7.61 (t, J = 7.9 Hz, 1H), 7.23 (dd,

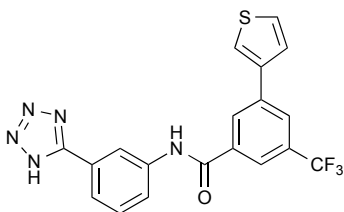
$J = 3.7, 4.9$ Hz, 1H); ^{13}C NMR (100 MHz, DMSO- d_6) $\delta = 163.83, 156.04, 140.62, 139.56, 136.45, 135.31, 130.25$ (d, $J = 32.3$ Hz), 129.73, 128.81, 128.34, 127.60, 126.11, 125.34, 124.40 (br d, $J = 4.4$ Hz), 122.95 (d, $J = 4.4$ Hz), 122.78, 122.40, 123.69 (d, $J = 272.9$ Hz), 118.91; ^{19}F NMR (376 MHz, DMSO- d_6) $\delta = -61.16$ (s, 3F); HRMS (ESI) calculated for $\text{C}_{19}\text{H}_{11}\text{F}_3\text{N}_5\text{OS}$ [$\text{M} - \text{H}$] $^-$ m/z 414.0642, found 414.0634.



tert-butyl 3-(thiophen-3-yl)-5-(trifluoromethyl)benzoate (S14). A 3 mL vial with cap was purged with Ar and charged with **S1** (100 mg, 0.308 mmol, 1.0 equiv), thiophene-3-boronic acid (98 mg, 0.769 mmol, 2.5 equiv), cesium carbonate (251 mg, 0.769 mmol, 2.5 equiv), tetrakis(triphenylphosphine)palladium(0) (21 mg, 0.018 mmol, 0.06 equiv), and dry 1,2-dimethoxyethane (2.5 mL). The reaction mixture was purged again, sealed, and heated at 80 °C for 18h. The crude reaction mixture was transferred to a sep funnel with ~ 75 mL EtOAc and ~ 5 mL water. ~ 50 mL sat. NaHCO_3 was added, the layers separated, and the organic layer washed with ~ 50 mL water and brine. The EtOAc was dried over MgSO_4 and concentrated under reduced pressure. Purified on a silica column with 0-15% EtOAc:hexanes. **S14** (90.1 mg, 89%) obtained as a glassy solid. ^1H NMR (400 MHz, CDCl_3) $\delta = 8.39$ (br s, 1H), 8.16 (br s, 1H), 7.98 (br s, 1H), 7.59 (dd, $J = 1.8, 2.6$ Hz, 1H), 7.45 (d, $J = 1.2$ Hz, 1H), 7.44 (s, 1H), 1.66 (s, 9H); ^{13}C NMR (100 MHz, CDCl_3) $\delta = 164.28, 139.96, 136.83, 133.40, 131.36$ (q, $J = 32.5$ Hz), 130.35, 127.03, 126.55 (q, $J = 3.7$ Hz), 125.96, 124.56 (q, $J = 3.7$ Hz), 123.73 (q, $J = 272.9$ Hz), 122.02, 82.11, 28.09; ^{19}F NMR (376 MHz, CDCl_3) $\delta = -62.67$ (s, 3F); did not ionize by ESI.

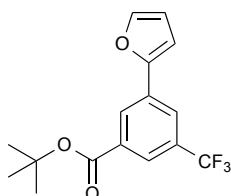


3-(thiophen-3-yl)-5-(trifluoromethyl)benzoic acid (S15). **S14** (90.1 mg, 0.274 mmol, 1.0 equiv) was reacted according to general procedure C (48h). Semi-crude **S15** (79.3 mg, 106%) obtained as a white solid. ^1H NMR (400 MHz, CD_3OD) δ = 8.41 (t, J = 1.3 Hz, 1H), 8.12 - 8.10 (m, 1H), 8.05 - 8.02 (m, 1H), 7.74 (dd, J = 1.5, 2.9 Hz, 1H), 7.50 - 7.48 (m, 1H), 7.46 - 7.43 (m, 1H); ^{13}C NMR (100 MHz, CD_3OD) δ = 168.34, 141.13, 138.91, 134.07, 132.87 (q, J = 33.0 Hz), 131.90, 128.59, 127.96 (q, J = 3.7 Hz), 127.14, 125.78 (q, J = 4.2 Hz), 123.89, 125.54 (q, J = 271.7 Hz); ^{19}F NMR (376 MHz, CD_3OD) δ = -64.16 (s, 3F); LRMS (ESI) calculated for $\text{C}_{12}\text{H}_6\text{F}_3\text{O}_2\text{S}$ $[\text{M} - \text{H}]^-$ m/z 271.01, found 270.93.

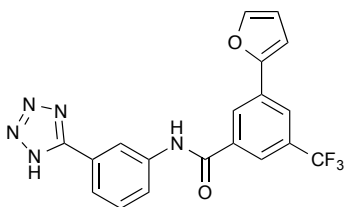


N-(3-(1H-tetrazol-5-yl)phenyl)-3-(thiophen-3-yl)-5-(trifluoromethyl)benzamide (10). **S15** (79.3 mg, 0.291 mmol, 1.0 equiv) was reacted with 3-(1H-tetrazol-5-yl)aniline in 2.5 mL DMF according to general procedure B. **10** (97.3 mg, 80%) obtained as a white solid. ^1H NMR (400 MHz, DMSO-d_6) δ = 10.74 (s, 1H), 8.61 (s, 1H), 8.58 (t, J = 1.7 Hz, 1H), 8.28 (s, 1H), 8.23 (dd, J = 1.3, 2.8 Hz, 1H), 8.21 (s, 1H), 8.04 - 8.00 (m, 1H), 7.83 - 7.78 (m, 2H), 7.76 - 7.72 (m, 1H), 7.62 (t, J = 8.0 Hz, 1H); ^{13}C NMR (100 MHz, DMSO-d_6) δ = 164.16, 155.92, 139.64, 139.15, 136.56, 136.23, 130.10 (q, J = 31.5 Hz),

129.77, 129.00, 127.73, 126.33, 125.36 (d, $J = 3.2$ Hz), 125.10, 123.49, 122.85, 122.71 (d, $J = 3.7$ Hz), 123.86 (d, $J = 272.9$ Hz), 122.37, 118.88; ^{19}F NMR (376 MHz, DMSO- d_6) $\delta = -60.21$ (s, 3F); HRMS (ESI) calculated for $\text{C}_{19}\text{H}_{11}\text{F}_3\text{N}_5\text{OS}$ $[\text{M} - \text{H}]^-$ m/z 414.0642, found 414.0635.

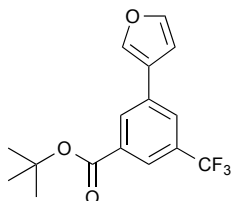


tert-butyl 3-(furan-2-yl)-5-(trifluoromethyl)benzoate (S16). **S1** was reacted with commercially available furan-2-ylboronic acid according to general procedure E. Crude product was filtered through a silica gel plug; the plug was washed with hexanes and the product was eluted with CH_2Cl_2 . **S16** (31 mg, 50%) obtained as a colorless liquid. ^1H NMR (400 MHz, CDCl_3) $\delta = 8.41 - 8.46$ (m, 1H), 8.29 (s, 1H), 8.02 (s, 1H), 7.65 (dd, $J = 5.66, 3.35$ Hz, 1H), 7.48 (dd, $J = 5.78, 3.23$ Hz, 1H), 1.67 (s, 9H); did not ionize by ESI.

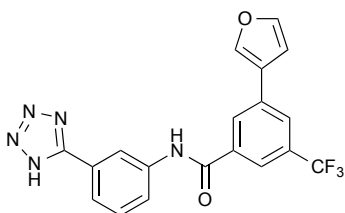


N-(3-(1H-tetrazol-5-yl)phenyl)-3-(furan-2-yl)-5-(trifluoromethyl)benzamide (11). **S16** (28.3 mg, 0.091 mmol, 1.0 equiv) was reacted according to general procedure F. **11** (21 mg, 58% over two steps) obtained as a white solid. ^1H NMR (400 MHz, pyridine- d_5) $\delta = 11.71$ (br s, 1H), 10.56 (br s, 2H), 9.24 (br s, 1H), 8.35 (br s, 1H), 8.08 - 8.21 (m, 3H), 7.66 (br s, 1H), 6.96 (br d, $J = 1.83$ Hz, 1H), 6.54 (br s, 1H); ^{13}C NMR (100 MHz, pyridine- d_5) $\delta = 166.77, 153.04, 145.23, 142.14, 138.84, 133.62, 132.38$ (br d, $J = 31.54$

Hz), 131.53, 128.61, 128.12, 124.25, 121.40, 113.94, 109.59; ^{19}F NMR (376 MHz, pyridine- d_5) δ = -62.3 (s, 3F); HRMS (ESI) calculated for $\text{C}_{19}\text{H}_{11}\text{F}_3\text{N}_5\text{O}_2$ [$\text{M} - \text{H}$] $^-$ m/z 398.0870, found 398.0865.

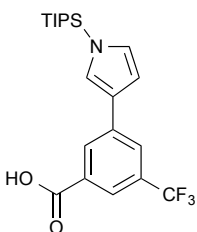


tert-butyl 3-(furan-3-yl)-5-(trifluoromethyl)benzoate (S17). **S1** was reacted with commercially available furan-3-ylboronic acid according to general procedure E. Crude product was purified via silica gel with hexanes: CH_2Cl_2 . **S17** (50.3 mg, 77%) obtained as a colorless liquid. ^1H NMR (400 MHz, CDCl_3) δ = 8.27 - 8.29 (m, 1H), 8.12 (s, 1H), 7.86 (d, J = 0.85 Hz, 2H), 7.54 (t, J = 1.70 Hz, 1H), 6.78 (dd, J = 1.70, 0.73 Hz, 1H), 1.65 (s, 9H); ^{13}C NMR (100 MHz, CDCl_3) δ = 164.31, 144.28, 139.47, 133.73, 133.43, 131.42 (q, J = 32.52 Hz), 129.78, 125.73 - 126.14 (m), 124.79, 124.49 (q, J = 3.67 Hz), 108.56, 82.19, 28.11; ^{19}F NMR (376 MHz, CDCl_3) δ = -62.79 (s, 3F); did not ionize by ESI.



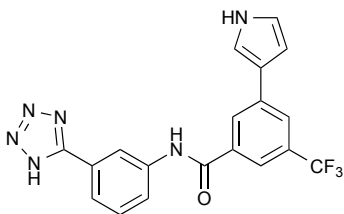
N-(3-(1H-tetrazol-5-yl)phenyl)-3-(furan-3-yl)-5-(trifluoromethyl)benzamide (12). **S17** (30.5 mg, 0.098 mmol, 1.0 equiv) was reacted according to general procedure F. **12** (39 mg, 50% over two steps) obtained as a white solid. ^1H NMR (400 MHz, pyridine- d_5) δ = 11.82 - 12.21 (m, 2H), 11.65 - 11.75 (m, 1H), 9.22 - 9.33 (m, 1H), 8.59 - 8.69 (m, 1H),

8.37 - 8.46 (m, 1H), 8.10 - 8.32 (m, 4H), 7.70 - 7.80 (m, 1H), 7.15 - 7.35 (m, 2H), 6.92 - 7.03 (m, 1H); ^{13}C NMR (100 MHz, pyridine- d_5) δ = 165.47, 144.69, 140.66, 137.37, 134.23, 131.04, 130.72, 130.02, 129.17, 128.91, 128.42, 127.11, 125.54 (br d, J = 3.67 Hz), 125.13 (br d, J = 3.67 Hz), 124.93, 119.86, 108.79; ^{19}F NMR (376 MHz, pyridine- d_5) δ = -62.17 (s, 3F); HRMS (ESI) calculated for $\text{C}_{19}\text{H}_{11}\text{F}_3\text{N}_5\text{O}_2$ [$\text{M} - \text{H}$] $^-$ m/z 398.0870, found 398.0863.



3-(trifluoromethyl)-5-(1-(triisopropylsilyl)-1H-pyrrol-3-yl)benzoic acid (S18).

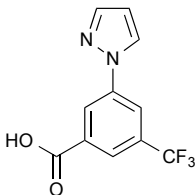
Commercially available 3-bromo-5-(trifluoromethyl)benzoic acid (54 mg, 0.20 mmol, 1 equiv) was reacted with commercially available (1-(triisopropylsilyl)-1H-pyrrol-3-yl)boronic acid according to general procedure E. Crude product was loaded onto a plug of C18-silica; the plug was washed with water and the product eluted with MeOH. Crude **S18** was used without further purification. LRMS (ESI) calculated for $\text{C}_{21}\text{H}_{27}\text{F}_3\text{NO}_2\text{Si}$ [$\text{M} - \text{H}$] $^-$ m/z 410.18, found 410.2.



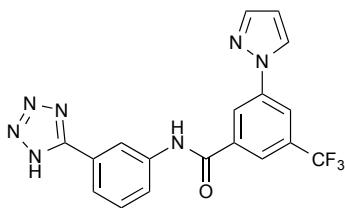
N-(3-(1H-tetrazol-5-yl)phenyl)-3-(1H-pyrrol-3-yl)-5-(trifluoromethyl)benzamide (13).

Crude **S18** was taken up in 1.0 mL of a 1M tetrabutylammonium fluoride solution in

THF. The reaction was stirred until complete by TLC (ca. 2 hr), then concentrated. The resulting crude 3-(1*H*-pyrrol-3-yl)-5-(trifluoromethyl)benzoic acid was reacted according to general procedure F. **13** (12 mg, 15% over three steps) obtained as a white solid. ¹H NMR (400 MHz, pyridine-*d*₅) δ = 12.17 - 12.39 (m, 1H), 11.57 - 11.72 (m, 1H), 9.23 (br s, 1H), 8.14 - 8.42 (m, 5H), 6.75 - 6.91 (m, 2H); ¹⁹F NMR (376 MHz, pyridine-*d*₅) δ = -62.11 (s, 3F); HRMS (ESI) calculated for C₁₉H₁₂F₃N₆O [M - H]⁻ m/z 397.1030, found 397.1023.

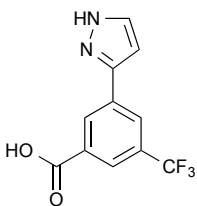


3-(1*H*-pyrazol-1-yl)-5-(trifluoromethyl)benzoic acid (S19). Commercially available 3-bromo-5-(trifluoromethyl)benzoic acid (54 mg, 0.20 mmol, 1 equiv), K₂CO₃ (155 mg, 1.1 mmol, 5.6 equiv), and *N,N*-dimethylglycine hydrochloride (45 mg, 0.3 mmol, 1.6 equiv) were suspended in 0.5 mL of dry DMSO. Argon was bubbled through the resulting solution to remove oxygen before copper(I) iodide (30 mg, 0.2 mmol, 0.8 equiv) and pyrazole (18 mg, 0.3 mmol, 1.3 equiv) were added to the reaction mixture. The reaction was then warmed to 100 °C and stirred for 18h. The reaction mixture was allowed to cool to room temperature, diluted with MeOH, and filtered through celite. Crude **S19** was used without further purification. LRMS (ESI) calculated for C₁₁H₆F₃N₂O₂ [M - H]⁻ m/z 255.05, found 254.97.

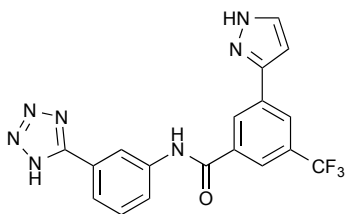


N-(3-(1*H*-tetrazol-5-yl)phenyl)-3-(1*H*-pyrazol-1-yl)-5-(trifluoromethyl)benzamide

(14). Crude **S19** was reacted according to general procedure F. **14** (17 mg, 21% over two steps) obtained as a white solid. ^1H NMR (400 MHz, pyridine- d_5) δ = 11.76 (br d, J = 13.15 Hz, 1H), 9.23 (br d, J = 12.90 Hz, 1H), 8.91 (br d, J = 13.27 Hz, 1H), 8.50 - 8.57 (m, 1H), 8.27 - 8.45 (m, 3H), 8.09 - 8.24 (m, 3H), 7.91 (br d, J = 13.76 Hz, 1H), 6.57 (br d, J = 12.66 Hz, 1H); ^{13}C NMR (100 MHz, pyridine- d_5) δ = 164.87, 142.05, 140.95, 140.51, 138.19, 131.34 (d, J = 33.01 Hz), 130.00, 127.86, 127.38, 123.20, 121.84 - 122.04 (m), 121.49, 119.91, 117.97 (d, J = 2.93 Hz), 108.81; ^{19}F NMR (376 MHz, pyridine- d_5) δ = -62.33 (s, 3F); HRMS (ESI) calculated for $\text{C}_{18}\text{H}_{11}\text{F}_3\text{N}_7\text{O}$ [$\text{M} - \text{H}$] $^-$ m/z 398.0983, found 398.0976.

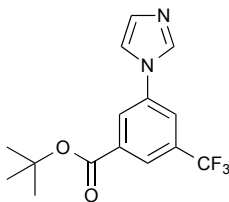


3-(1*H*-pyrazol-3-yl)-5-(trifluoromethyl)benzoic acid (S20). Commercially available 3-bromo-5-(trifluoromethyl)benzoic acid (54 mg, 0.20 mmol, 1 equiv) was reacted with commercially available (1*H*-pyrazol-3-yl)boronic acid according to general procedure E. Crude product was loaded onto a plug of C18-silica; the plug was washed with water and the product eluted with MeOH. Crude **S20** was used without further purification. LRMS (ESI) calculated for $\text{C}_{11}\text{H}_6\text{F}_3\text{N}_2\text{O}_2$ [$\text{M} - \text{H}$] $^-$ m/z 255.05, found 254.97.



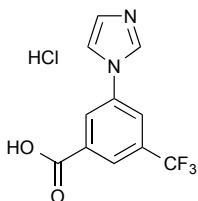
N-(3-(1*H*-tetrazol-5-yl)phenyl)-3-(1*H*-pyrazol-5-yl)-5-(trifluoromethyl)benzamide

(15). Crude **S20** was reacted according to general procedure F. **15** (1.4 mg, 1.8% over two steps) obtained as a white solid. ^1H NMR (400 MHz, acetone- d_6) δ = 8.63 (br d, J = 15.22 Hz, 2H), 8.33 (br s, 2H), 8.18 (s, 2H), 8.07 - 8.12 (m, 1H), 7.94 (br d, J = 7.79 Hz, 1H), 7.58 (t, J = 7.97 Hz, 1H); ^{19}F NMR (376 MHz, acetone- d_6) δ = -63.14 (s, 3F); HRMS (ESI) calculated for $\text{C}_{18}\text{H}_{11}\text{F}_3\text{N}_7\text{O}$ [$\text{M} - \text{H}$] m/z 398.0983, found 398.0977.

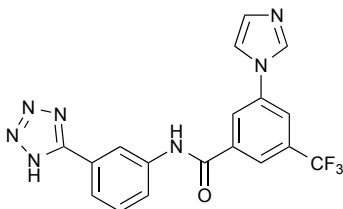


tert-butyl 3-(1*H*-imidazol-1-yl)-5-(trifluoromethyl)benzoate (S21). A 3 mL vial with cap was purged with Ar and charged with **S1** (100 mg, 0.308 mmol, 1.0 equiv), imidazole (27 mg, 0.400 mmol, 1.3 equiv), potassium carbonate (238 mg, 1.72 mmol, 5.6 equiv), copper(I) iodide (47 mg, 0.246 mmol, 0.8 equiv), and *N,N*-dimethylglycine hydrochloride (69 mg, 0.492 mmol, 1.6 equiv). The vial was purged with Ar; dry dimethyl sulfoxide (1.5 ml) was then added, and the vial was sealed and heated at 120 °C for 18h. The crude reaction mixture was transferred to a sep funnel with ~ 75 mL EtOAc and ~10 mL water. ~ 50 mL sat. NaHCO_3 was added, the layers separated, and the organic layer washed with ~ 40 mL water and brine. The organic layer was dried over MgSO_4 and concentrated under reduced pressure. Purified on a silica column with 0-

60% EtOAc:hexanes. **S21** (34.7 mg, 36%) obtained as a white solid. ^1H NMR (400 MHz, CDCl_3) δ = 8.20 (s, 1H), 8.19 (br d, J = 1.9 Hz, 1H), 7.94 (s, 1H), 7.79 (br s, 1H), 7.36 (t, J = 1.3 Hz, 1H), 7.26 (br s, 1H), 1.63 (s, 9H); ^{13}C NMR (100 MHz, CDCl_3) δ = 163.08, 137.94, 135.47, 135.02, 132.70 (q, J = 33.5 Hz), 131.30, 125.16, 124.85 (q, J = 3.7 Hz), 121.51 (q, J = 3.7 Hz), 122.97 (q, J = 272.9 Hz), 117.97, 83.02, 28.02; ^{19}F NMR (376 MHz, CDCl_3) δ = -62.84 (s, 3F); LRMS (ESI) calculated for $\text{C}_{15}\text{H}_{16}\text{F}_3\text{N}_2\text{O}_2$ $[\text{M} + \text{H}]^+$ m/z 313.11, found 313.01.

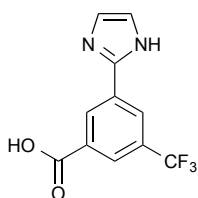


3-(1H-imidazol-1-yl)-5-(trifluoromethyl)benzoic acid hydrochloride (S22). **S21** (34.7 mg, 0.111 mmol, 1.0 equiv) was reacted according to general procedure C (24h). Semi-crude **S22** (33.8 mg, 104%) obtained as a white solid. ^1H NMR (400 MHz, CD_3OD) δ = 9.70 (s, 1H), 8.62 (s, 1H), 8.46 (s, 1H), 8.41 (s, 1H), 8.25 (s, 1H), 7.84 (br s, 1H); ^{13}C NMR (100 MHz, CD_3OD) δ = 164.90, 136.16, 135.26, 134.52, 132.63 (q, J = 34.2 Hz), 127.16 (q, J = 3.7 Hz), 127.04, 123.63 (q, J = 3.7 Hz), 122.98 (d, J = 272.2 Hz), 121.59, 120.90; ^{19}F NMR (376 MHz, CD_3OD) δ = -64.15 (s, 3F); LRMS (ESI) calculated for $\text{C}_{11}\text{H}_6\text{F}_3\text{N}_2\text{O}_2$ $[\text{M} - \text{H}]^-$ m/z 255.05, found 255.06.



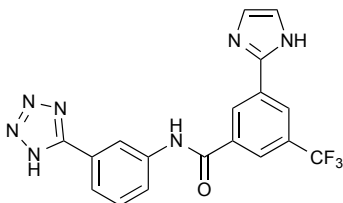
N-(3-(1*H*-tetrazol-5-yl)phenyl)-3-(1*H*-imidazol-1-yl)-5-(trifluoromethyl)benzamide

(16). **S22** (33.8 mg, 0.115 mmol, 1.0 equiv) was reacted with 3-(1*H*-tetrazol-5-yl)aniline in 2 mL DMF according to general procedure B, except 2 eq *N,N*-diisopropylethylamine (40 μ L) was used in the first step. **16** (30.2 mg, 66%) obtained as a white solid. ^1H NMR (400 MHz, DMSO- d_6) δ = 10.77 (s, 1H), 8.55 (s, 3H), 8.32 (s, 1H), 8.26 (s, 1H), 8.03 (s, 1H), 8.00 (dd, J = 1.2, 8.3 Hz, 1H), 7.80 (d, J = 7.8 Hz, 1H), 7.61 (t, J = 7.9 Hz, 1H), 7.20 (s, 1H); ^{13}C NMR (100 MHz, DMSO- d_6) δ = 163.91, 156.70, 139.94, 138.21, 137.84, 136.59 (br s), 131.36 (d, J = 32.3 Hz), 130.83, 130.31, 126.17, 123.83, 123.03, 122.96, 122.93 - 122.78 (m), 123.91 (d, J = 272.9 Hz), 120.46 - 120.30 (m), 119.25, 118.77; ^{19}F NMR (376 MHz, DMSO- d_6) δ = -61.02 (s, 3F); HRMS (ESI) calculated for $\text{C}_{18}\text{H}_{11}\text{F}_3\text{N}_7\text{O}$ [$\text{M} - \text{H}$] $^-$ m/z 398.0983, found 398.0976.



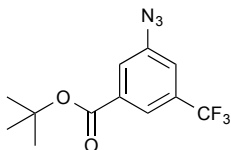
3-(1*H*-imidazol-2-yl)-5-(trifluoromethyl)benzoic acid (S23). A 3 mL vial with cap/septa was purged with Ar and charged with imidazole (22 mg, 0.323 mmol, 1.0 equiv), palladium(II) acetate (4 mg, 0.016 mmol, 0.05 equiv), copper(I) iodide (123 mg, 0.646 mmol, 2.0 equiv), and **S1** (210 mg, 0.646 mmol, 2.0 equiv). The vial was purged with Ar and charged with 1.62 mL degassed DMF (Ar bubbling for 30 min). The vial was

sealed and heated at 140 °C for 48h. After cooling to rt, the reaction mixture was filtered through a nylon 0.2 um syringe filter and purified by reverse phase HPLC (water/MeOH/0.05% formic acid) to afford the desired product. **S23** (15.9 mg, 19%) obtained as a light blue solid. ¹H NMR (400 MHz, CD₃OD, drops CDCl₃) δ = 8.80 (br s, 1H), 8.40 (br s, 1H), 8.27 (br s, 1H), 7.33 (br s, 2H); ¹⁹F NMR (376 MHz, CD₃OD, drops CDCl₃) δ = -64.29 (s, 3F); LRMS (ESI) calculated for C₁₁H₆F₃N₂O₂ [M - H]⁻ m/z 255.05, found 255.11.

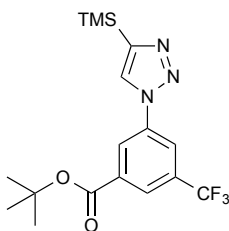


N-(3-(1H-tetrazol-5-yl)phenyl)-3-(1H-imidazol-2-yl)-5-(trifluoromethyl)benzamide

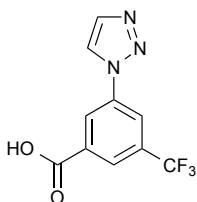
(17). **S23** (15.9 mg, 0.062 mmol, 1.0 equiv) was reacted with 3-(1H-tetrazol-5-yl)aniline in 2.5 mL DMF according to general procedure A, except 3 eq *N,N*-diisopropylethylamine (32 uL) was used. **17** (14.1 mg, 57%) obtained as a white solid. ¹H NMR (400 MHz, DMSO-d₆) δ = 10.73 (br s, 1H), 8.85 (br s, 1H), 8.48 (br s, 2H), 8.29 (s, 1H), 7.92 (br d, *J* = 7.8 Hz, 1H), 7.82 (br s, 1H), 7.48 (br s, 1H), 7.27 (br s, 2H); ¹⁹F NMR (376 MHz, DMSO-d₆) δ = -61.20 (s, 3F); HRMS (ESI) calculated for C₁₈H₁₁F₃N₇O [M - H]⁻ m/z 398.0983, found 398.0979.



tert-butyl 3-azido-5-(trifluoromethyl)benzoate (S24). A 3 mL vial with cap was purged with Ar and charged with **S1** (125 mg, 0.384 mmol, 1.0 equiv), sodium azide (50 mg, 0.769 mmol, 2.0 equiv), copper(I) iodide (7.3 mg, 0.038 mmol, 0.1 equiv), sodium ascorbate (3.8 mg, 0.019 mmol, 0.05 equiv), and *N,N'*-dimethylethylenediamine (6.2 ul, 0.058 mmol, 0.15 equiv). Ethanol (1.28 ml) and water (550 ul) were then added; the vial was purged with Ar, sealed, and heated at 80 °C for 3h. The crude reaction mixture was then transferred to a sep funnel with ~ 75 mL EtOAc and ~ 30 mL water. The aqueous layer was basified by the addition of ~ 20 mL sat. NaHCO₃; the layers were separated, and the organic layer was further extracted with ~ 50 mL water and brine. The organic layer was dried over MgSO₄ and concentrated to an oil. Purified on a silica column with 0-10% EtOAc:hexanes. Product containing fractions were combined and carefully rotovapped. (**Note:** Product is moderately volatile) **S24** (93.7 mg, 85%) obtained as a light yellow oil. ¹H NMR (400 MHz, CDCl₃) δ = 7.98 (s, 1H), 7.83 (br s, 1H), 7.38 (br s, 1H), 1.62 (s, 9H); ¹³C NMR (100 MHz, CDCl₃) δ = 163.44, 141.48, 134.72, 132.49 (q, *J* = 33.5 Hz), 122.83, 122.47 (q, *J* = 4.2 Hz), 119.51 (q, *J* = 3.7 Hz), 123.15 (q, *J* = 272.9 Hz), 82.62, 28.04; ¹⁹F NMR (376 MHz, CDCl₃) δ = -63.00 (s, 3F); did not ionize by ESI.

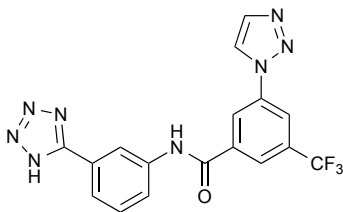


tert-butyl 3-(trifluoromethyl)-5-(4-(trimethylsilyl)-1H-1,2,3-triazol-1-yl)benzoate (S25). A 3 mL vial was charged with **S24** (93.7 mg, 0.326 mmol, 1.0 equiv), ethynyltrimethylsilane (1.153 mL, 8.16 mmol, 25.0 equiv), copper(I) iodide (186 mg, 0.979 mmol, 3.0 equiv), and *N,N*-diisopropylethylamine (511 μ L, 2.94 mmol, 9.0 equiv). 1.76 mL dry THF was then added, and the vial was sealed and heated at 80 °C overnight. The crude reaction mixture was filtered, and the filtrand was washed with ~ 50 mL cold THF. The filtrate was concentrated under reduced pressure, affording crude **S25** (168.4 mg, 134%) as a light brown solid. LRMS (ESI) calculated for $C_{17}H_{22}F_3N_3O_2Si$ $[M + H]^+$ m/z 386.14, found 386.01.

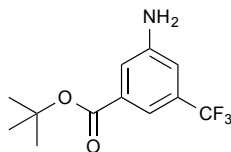


3-(1H-1,2,3-triazol-1-yl)-5-(trifluoromethyl)benzoic acid (S26). Crude **S25** (168.4 mg) was reacted according to general procedure C (32h), except after the *t*-butyl was removed by LCMS, 4 mL water was added, and the reaction mixture was heated at 40 °C for an additional 16h. The reaction mixture was then transferred to a sep funnel with ~ 75 mL EtOAc and ~ 30 mL water. The aqueous layer was basified by the addition of ~ 30 mL sat. $NaHCO_3$; the layers were separated, and the aqueous layer was acidified to pH 1 with concentrated HCl. The aqueous layer was further extracted with 3 x 50 mL

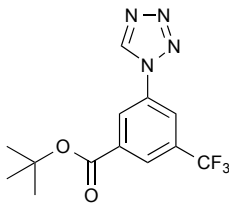
EtOAc. The new organic layers were combined, dried over MgSO₄, and concentrated. Semi-crude **S26** (36.8 mg, 44% over two steps) obtained as a white solid. ¹H NMR (400 MHz, CD₃OD, drops CDCl₃) δ = 8.73 (s, 1H), 8.70 (s, 1H), 8.42 (s, 1H), 8.33 (s, 1H), 7.93 (s, 1H); ¹³C NMR (100 MHz, CD₃OD, drops CDCl₃) δ = 166.89, 139.35, 137.41, 133.91 (q, *J* = 33.7 Hz), 127.38 (q, *J* = 3.7 Hz), 125.87, 124.68, 124.19, 122.31 (q, *J* = 3.7 Hz), 124.69 (q, *J* = 272.2 Hz); ¹⁹F NMR (376 MHz, CD₃OD, drops CDCl₃) δ = -64.16 (s, 3F); LRMS (ESI) calculated for C₁₀H₅F₃N₃O₂ [M - H]⁻ m/z 256.04, found 256.05.



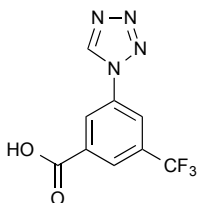
N-(3-(1H-tetrazol-5-yl)phenyl)-3-(1H-1,2,3-triazol-1-yl)-5-(trifluoromethyl)benzamide (18). **S26** (36.8 mg, 0.143 mmol, 1.0 equiv) was reacted with 3-(1H-tetrazol-5-yl)aniline in 2.5 mL DMF according to general procedure B. **18** (28.0 mg, 49%) obtained as a white solid. ¹H NMR (400 MHz, DMSO-d₆, drops EtOAc) δ = 10.85 (s, 1H), 9.12 (s, 1H), 8.88 (s, 1H), 8.53 (s, 2H), 8.45 (s, 1H), 8.08 (s, 1H), 7.97 (br d, *J* = 7.5 Hz, 1H), 7.81 (br s, 1H), 7.56 (br t, *J* = 6.6 Hz, 1H); ¹³C NMR (100 MHz, DMSO-d₆, drops EtOAc) δ = 163.03, 156.04, 139.26, 137.48, 137.39, 134.92, 130.81 (q, *J* = 33.8 Hz), 129.55, 127.54 (br), 124.10 (br d, *J* = 2.9 Hz), 123.92, 123.28, 122.42 (br d, *J* = 2.9 Hz), 123.34 (d, *J* = 272.9 Hz), 121.76, 119.63 (br d, *J* = 2.2 Hz), 118.71 (br); ¹⁹F NMR (376 MHz, DMSO-d₆, drops EtOAc) δ = -61.14 (s, 3F); HRMS (ESI) calculated for C₁₇H₁₀F₃N₈O [M - H]⁻ m/z 399.0935, found 399.0928.



tert-butyl 3-amino-5-(trifluoromethyl)benzoate (S27). **S1** (250 mg, 0.769 mmol, 1.0 equiv), copper(I) iodide (29 mg, 0.154 mmol, 0.2 equiv), potassium carbonate (319 mg, 2.31 mmol, 3.0 equiv), and trans-4-hydroxy-L-proline (40 mg, 0.308 mmol, 0.4 equiv) were added to a teflon screw capped vial. dimethyl sulfoxide (3 mL) and 30.0% ammonium hydroxide (1.500 ml, 13.5 mmol, 17.6 equiv) were added, and the reaction mixture was sealed and heated at 70 °C for 18h (**Note:** The solution began to degass upon addition of NH₄OH – seal the vessel quickly). The reaction mixture was transferred to a sep funnel with ~ 75 mL water and ~ 40 mL EtOAc. The layers were separated, and the aqueous layer was further extracted with 2 x 40 mL EtOAc. The organic layers were combined, dried over MgSO₄, and concentrated to give colorless oil. Purified on a silica column with 0-15% EtOAc:hexanes. **S27** (46.5 mg, 23%) obtained as a colorless oil. ¹H NMR (400 MHz, CDCl₃) δ = 7.58 (s, 1H), 7.44 (s, 1H), 7.02 (s, 1H), 1.59 (s, 9H); ¹³C NMR (100 MHz, CDCl₃) δ = 164.68, 146.90, 133.83, 131.69 (q, *J* = 32.3 Hz), 123.78 (q, *J* = 272.2 Hz), 118.53, 115.87 (q, *J* = 4.4 Hz), 114.68 (q, *J* = 4.2 Hz), 81.69, 28.07; ¹⁹F NMR (376 MHz, CDCl₃) δ = -62.97 (s, 3F); LRMS (ESI) calculated for C₁₂H₁₅F₃NO₂ [M + H]⁺ m/z 262.10, found 261.97.

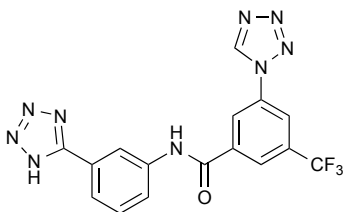


tert-butyl 3-(1H-tetrazol-1-yl)-5-(trifluoromethyl)benzoate (S28). A 3 mL vial was charged with **S27** (46.5 mg, 0.178 mmol, 1.0 equiv). The vial was backfilled with Ar and charged with triethyl orthoformate (148 ul, 0.890 mmol, 5.0 equiv), sodium azide (58 mg, 0.890 mmol, 5.0 equiv), and glacial acetic acid (1 mL). The reaction mixture was sealed and heated at 100 °C for 3h, then transferred to a sep funnel with ~ 75 mL water and ~ 40 mL EtOAc. The layers were separated, and the aqueous layer was further extracted with 2 x 40 mL EtOAc. The organic layers were combined, dried over MgSO₄, and concentrated to give colorless oil. Purified on silica gel with 0-15% EtOAc:hexanes. **S28** (33.4 mg, 60%) obtained as a white solid. ¹H NMR (400 MHz, CDCl₃) δ = 9.22 (s, 1H), 8.49 (br s, 1H), 8.37 (s, 1H), 8.23 (s, 1H), 1.64 (s, 9H); ¹³C NMR (100 MHz, CDCl₃) δ = 162.49, 140.57, 135.48, 134.38, 133.21 (q, *J* = 34.0 Hz), 127.35 (q, *J* = 3.7 Hz), 124.74, 121.66 (q, *J* = 3.7 Hz), 122.66 (q, *J* = 273.4 Hz), 83.61, 28.01; ¹⁹F NMR (376 MHz, CDCl₃) δ = -62.92 (s, 3F); LRMS (ESI) calculated for C₁₃H₁₄F₃N₄O₂ [M + H]⁺ *m/z* 315.10, found 315.06.



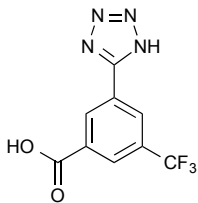
3-(1H-tetrazol-1-yl)-5-(trifluoromethyl)benzoic acid (S29). **S28** (33.4 mg, 0.106 mmol, 1.0 equiv) was reacted according to general procedure C (48h). Semi-crude **S29**

(30.0 mg, 109%) obtained as an off-white solid. ^1H NMR (400 MHz, CD_3OD) δ = 9.98 (s, 1H), 8.74 (s, 1H), 8.48 (s, 1H), 8.40 (s, 1H); ^{13}C NMR (100 MHz, CD_3OD) δ = 166.54, 143.46, 136.67, 135.85, 133.96 (q, J = 34.2 Hz), 128.10 (q, J = 3.7 Hz), 126.66, 123.14 (q, J = 3.2 Hz), 124.59 (q, J = 272.2 Hz); ^{19}F NMR (376 MHz, CD_3OD) δ = -64.39 (s, 3F); LRMS (ESI) calculated for $\text{C}_9\text{H}_4\text{F}_3\text{N}_4\text{O}_2$ $[\text{M} - \text{H}]^-$ m/z 257.04, found 257.04.

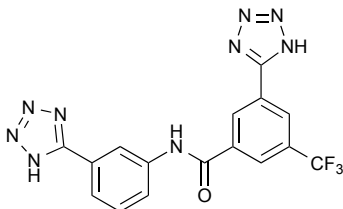


N-(3-(1*H*-tetrazol-5-yl)phenyl)-3-(1*H*-tetrazol-1-yl)-5-(trifluoromethyl)benzamide

(19). S29 (30.0 mg, 0.116 mmol, 1.0 equiv) was reacted with 3-(1*H*-tetrazol-5-yl)aniline in 2 mL DMF according to general procedure B. **21** (22.1 mg, 47%) obtained as a white solid. ^1H NMR (400 MHz, CD_3OD , drops CD_3CN) δ = 9.52 (s, 1H), 8.53 (s, 1H), 8.34 (s, 1H), 8.29 (s, 1H), 8.23 (s, 1H), 7.75 (dd, J = 1.2, 8.0 Hz, 1H), 7.65 (d, J = 7.8 Hz, 1H), 7.43 (t, J = 8.0 Hz, 1H); ^{13}C NMR (100 MHz, CD_3OD , drops CD_3CN) δ = 164.82, 157.96, 143.39, 140.43, 139.27, 136.29, 133.36 (q, J = 33.7 Hz), 131.17, 127.04, 126.57 (q, J = 3.4 Hz), 125.43, 124.35, 124.24, 124.52 (d, J = 272.2 Hz), 122.40 (q, J = 3.7 Hz), 120.32; ^{19}F NMR (CD_3OD , drops CD_3CN) δ = -62.20 (s, 3F); HRMS (ESI) calculated for $\text{C}_{16}\text{H}_9\text{F}_3\text{N}_9\text{O}$ $[\text{M} - \text{H}]^-$ m/z 400.0888, found 400.0881.



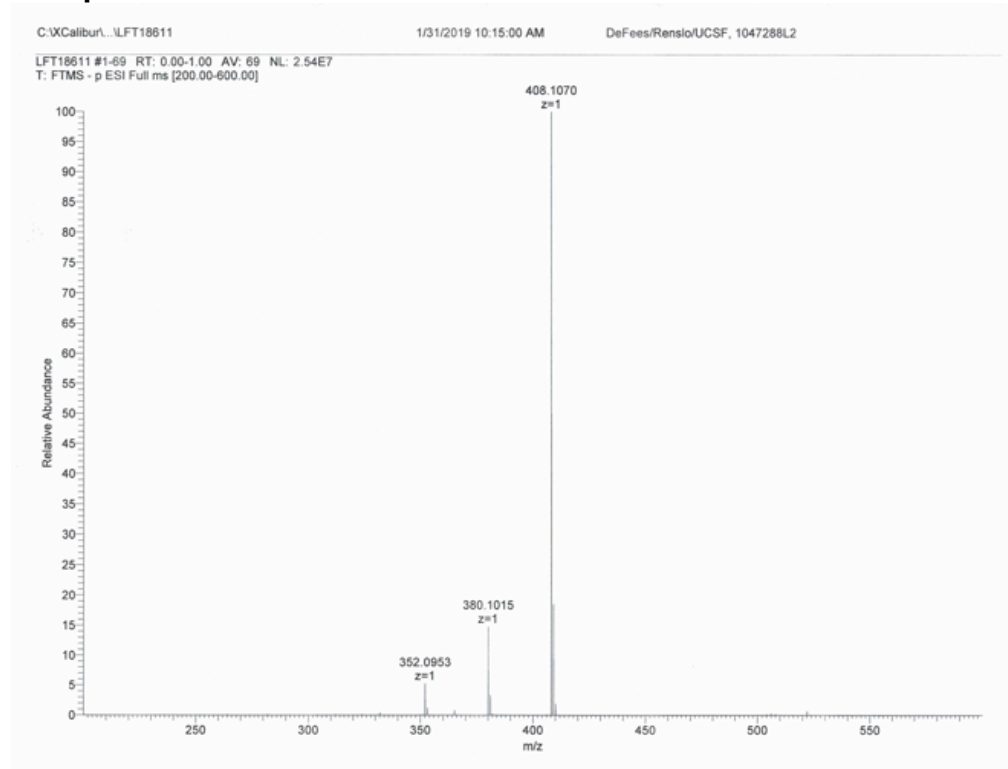
3-(1H-tetrazol-5-yl)-5-(trifluoromethyl)benzoic acid (S30). A 15 mL sealed tube was backfilled with argon and charged with commercially available 3-cyano-5-(trifluoromethyl)benzoic acid (100 mg, 0.465 mmol, 1.0 equiv), sodium azide (91 mg, 1.40 mmol, 3.0 equiv), and ammonium chloride (81 mg, 1.63 mmol, 3.5 equiv). 4 mL DMF was then used to wash the walls/seal area; the tube was flushed with Ar, sealed, and stirred at 100 °C for 18h. The crude reaction mixture was transferred to a sep funnel with ~ 75 mL H₂O and EtOAc, and the aqueous layer was adjusted to pH 1 with conc. HCl. The layers were separated, and the aqueous layer was further extracted with 2 x 30 mL EtOAc. The organics were combined, dried over MgSO₄, and concentrated, giving brown oil. Dried on hivac overnight. The remaining residue was rotovaped with 2 x 10 mL portions of toluene and dried under hivac again, yielding semi-crude **S30** (129.7 mg, 108%) as a brown solid. ¹H NMR (400 MHz, CD₃OD) δ = 8.80 (s, 1H), 8.46 (s, 1H), 8.30 (s, 1H); ¹³C NMR (100 MHz, CD₃OD) δ = 167.01, 158.00, 134.66, 133.11 (q, *J* = 33.0 Hz), 132.41, 129.29 (br d, *J* = 3.7 Hz), 128.49 (br d, *J* = 3.7 Hz), 128.33, 124.83 (q, *J* = 272.2 Hz); ¹⁹F NMR (376 MHz, CD₃OD) δ = -64.41 (s, 3F); LRMS (ESI) calculated for C₉H₄F₃N₄O₂ [M - H]⁻ *m/z* 257.04, found 257.04.



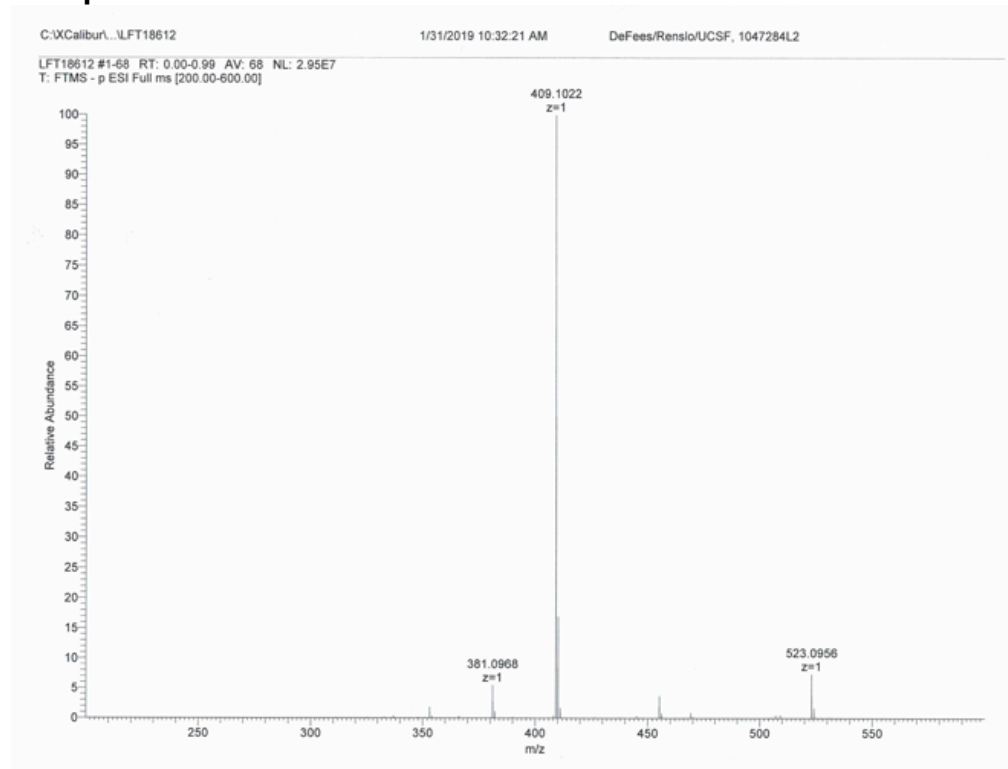
N-(3-(1*H*-tetrazol-5-yl)phenyl)-3-(1*H*-tetrazol-5-yl)-5-(trifluoromethyl)benzamide

(20). **S30** (130 mg, 0.502 mmol, 1.0 equiv) was reacted with 3-(1*H*-tetrazol-5-yl)aniline in 3 mL DMF according to general procedure A. **22** (122.7 mg, 61%) obtained as a light tan solid. ^1H NMR (400 MHz, CD_3OD) δ = 8.82 (s, 1H), 8.45 (br s, 1H), 8.44 (t, J = 1.8 Hz, 1H), 8.35 (s, 1H), 7.82 (dt, J = 8.2, 1.0 Hz, 1H), 7.72 - 7.67 (m, 1H), 7.48 (t, J = 7.9 Hz, 1H); ^{13}C NMR (100 MHz, CD_3OD) δ = 166.17, 158.70, 157.72, 140.86, 138.41, 133.14 (q, J = 33.0 Hz), 131.12, 131.01, 128.91, 127.75 - 127.47 (m), 126.25, 124.87, 124.34, 125.02 (d, J = 272.2 Hz), 120.71; ^{19}F NMR (376 MHz, CD_3OD) δ = -64.25 (s, 3F); HRMS (ESI) calculated for $\text{C}_{16}\text{H}_9\text{F}_3\text{N}_9\text{O}$ $[\text{M} - \text{H}]^-$ m/z 400.0888, found 400.0882.

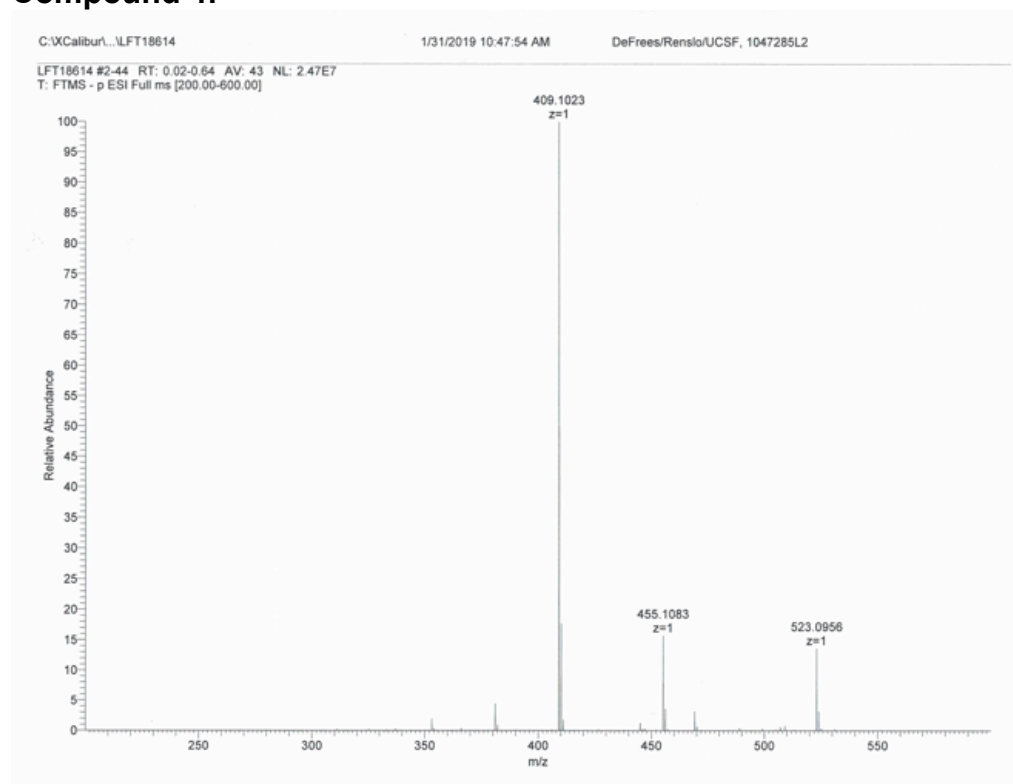
HRMS Spectra Compound 2:



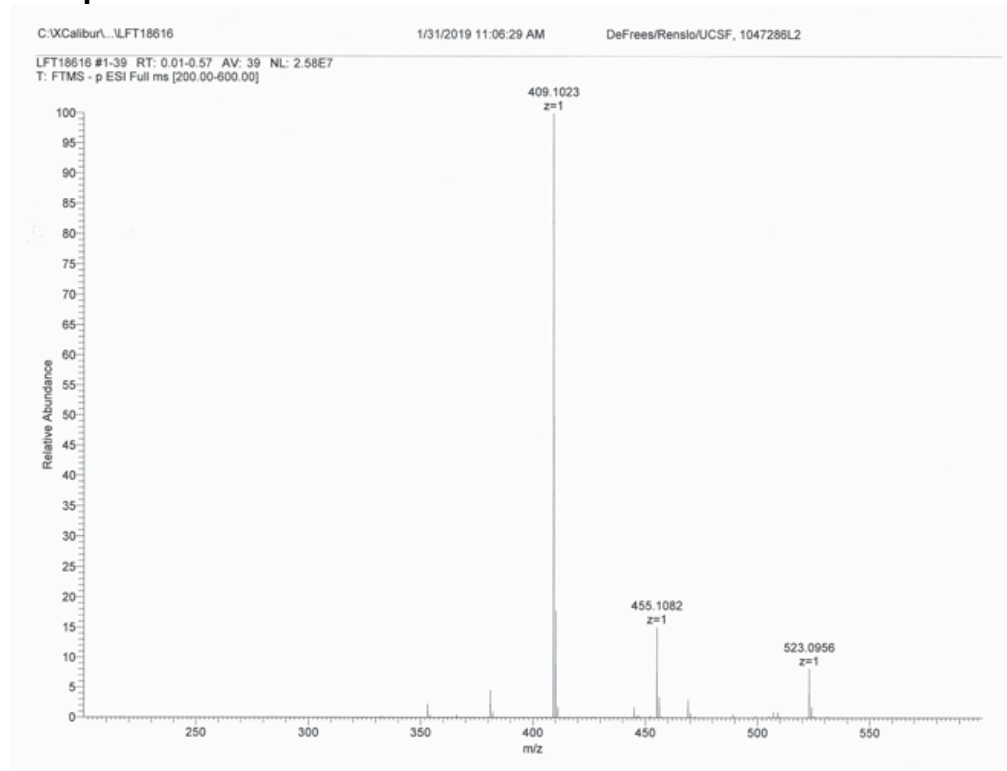
Compound 3:



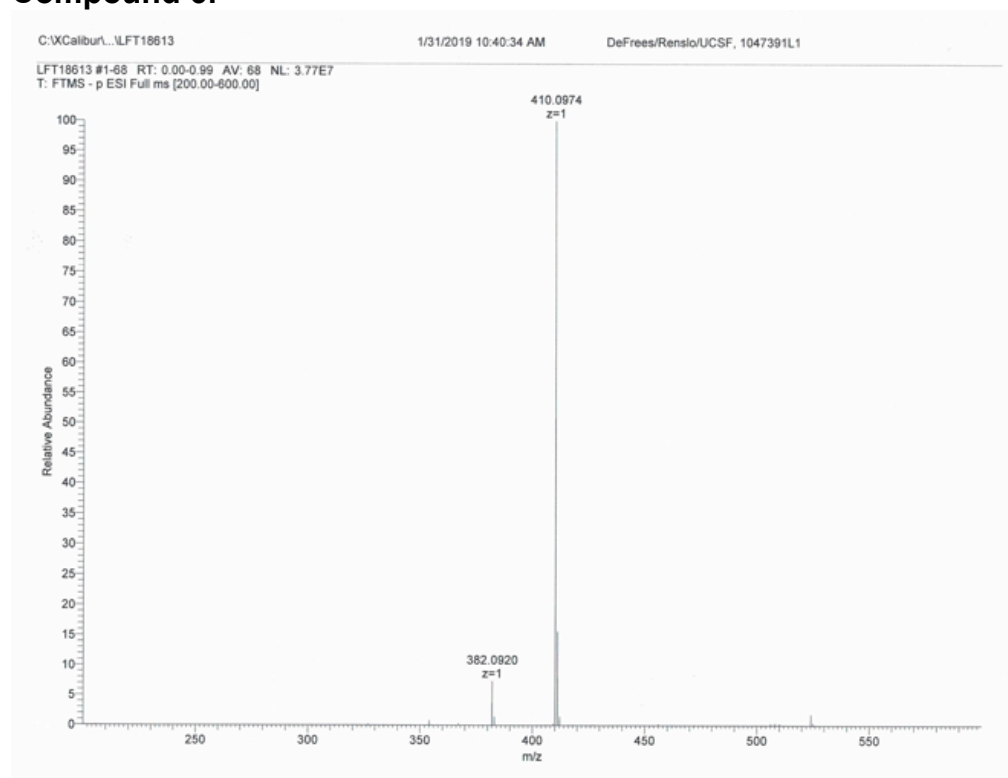
Compound 4:



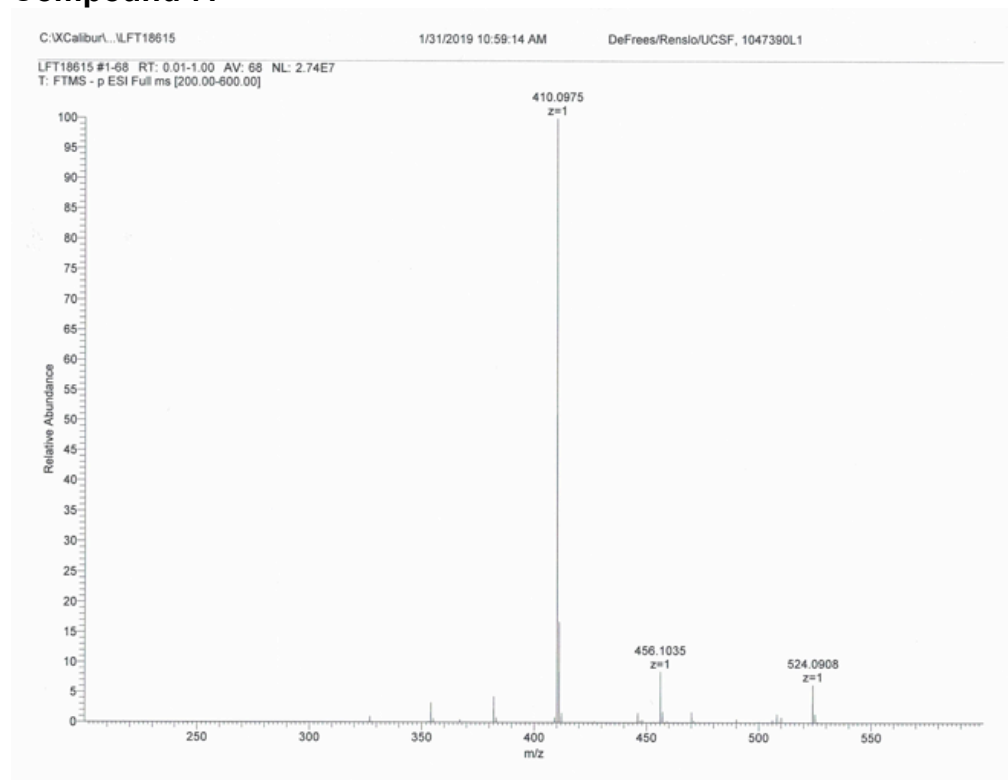
Compound 5:



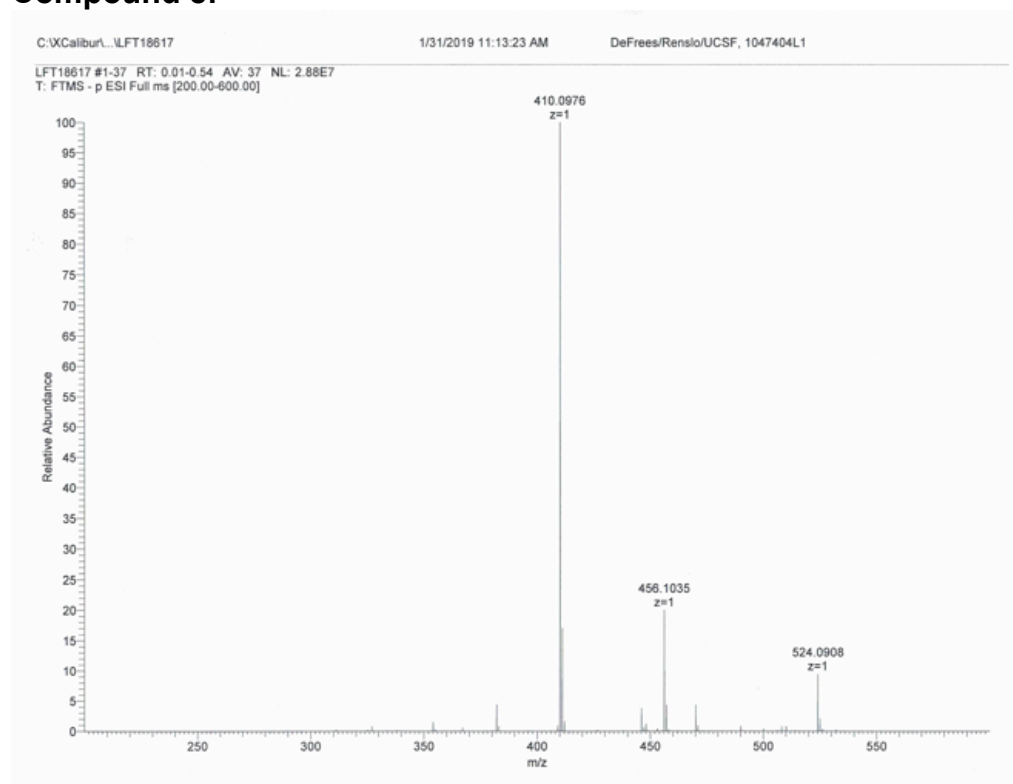
Compound 6:



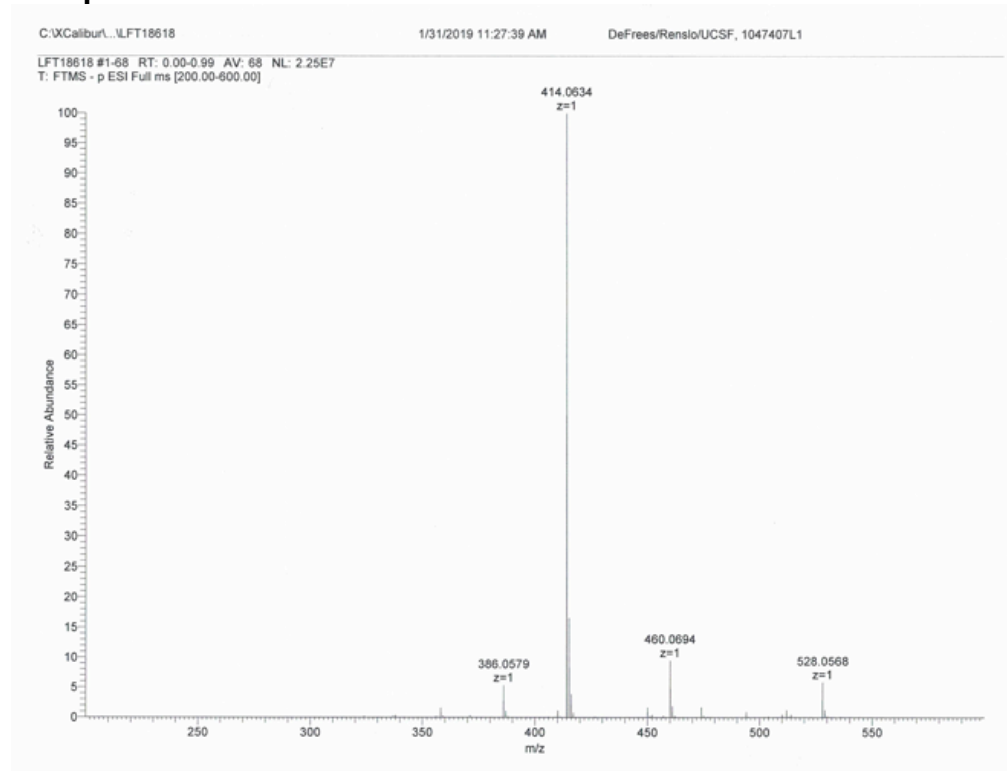
Compound 7:



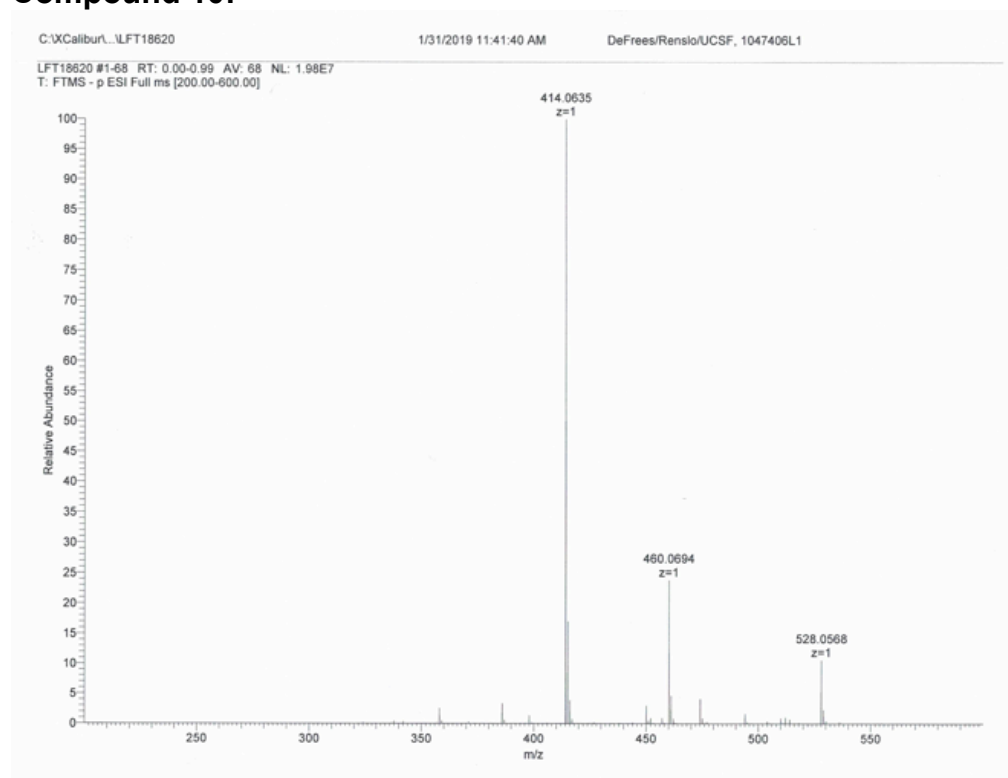
Compound 8:



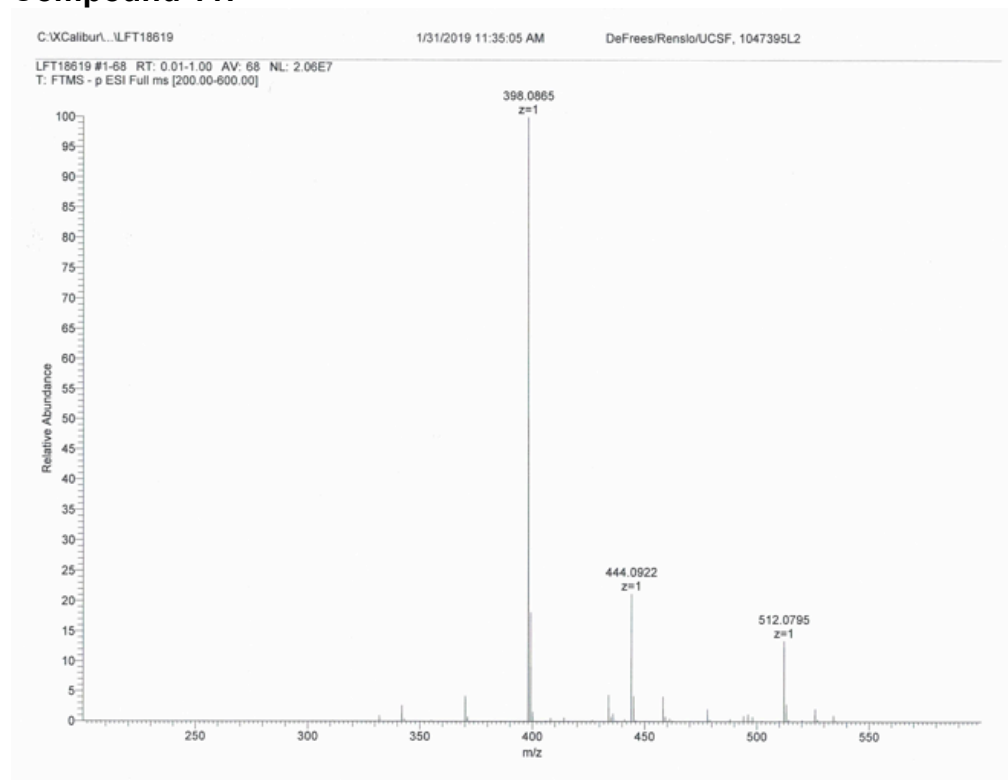
Compound 9:



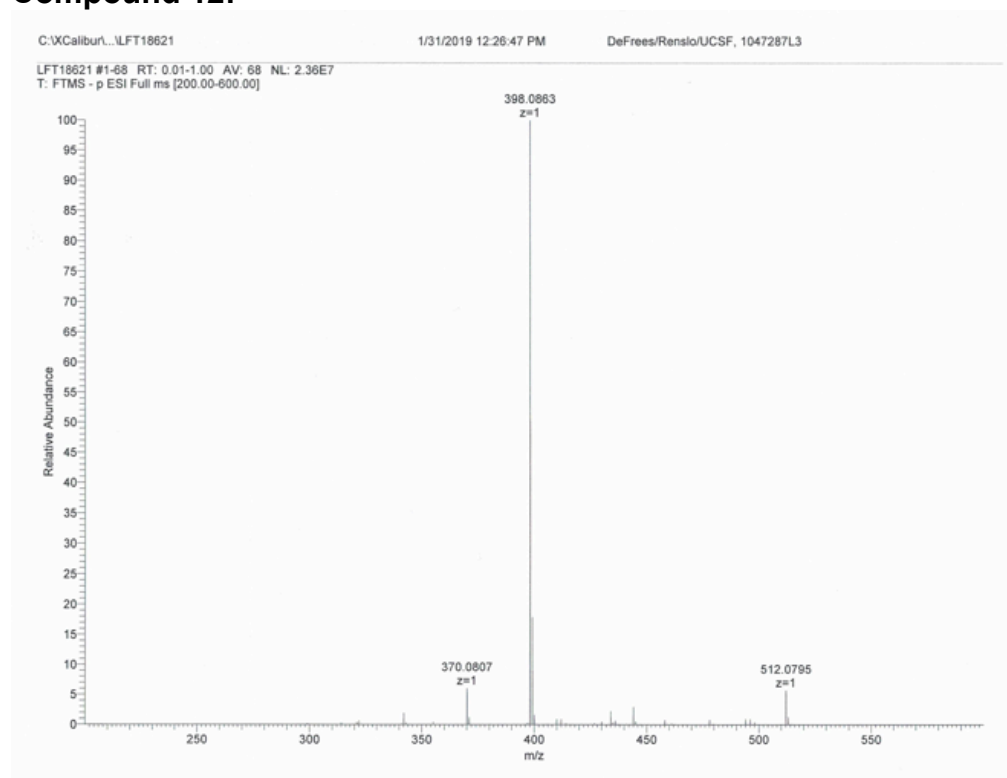
Compound 10:



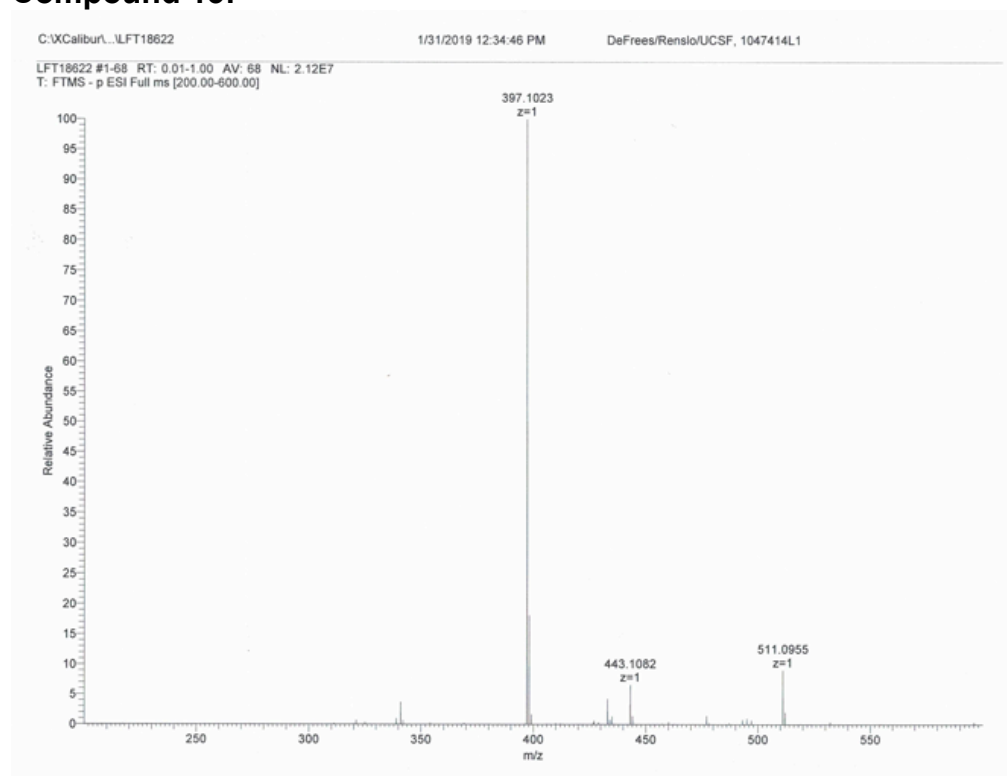
Compound 11:



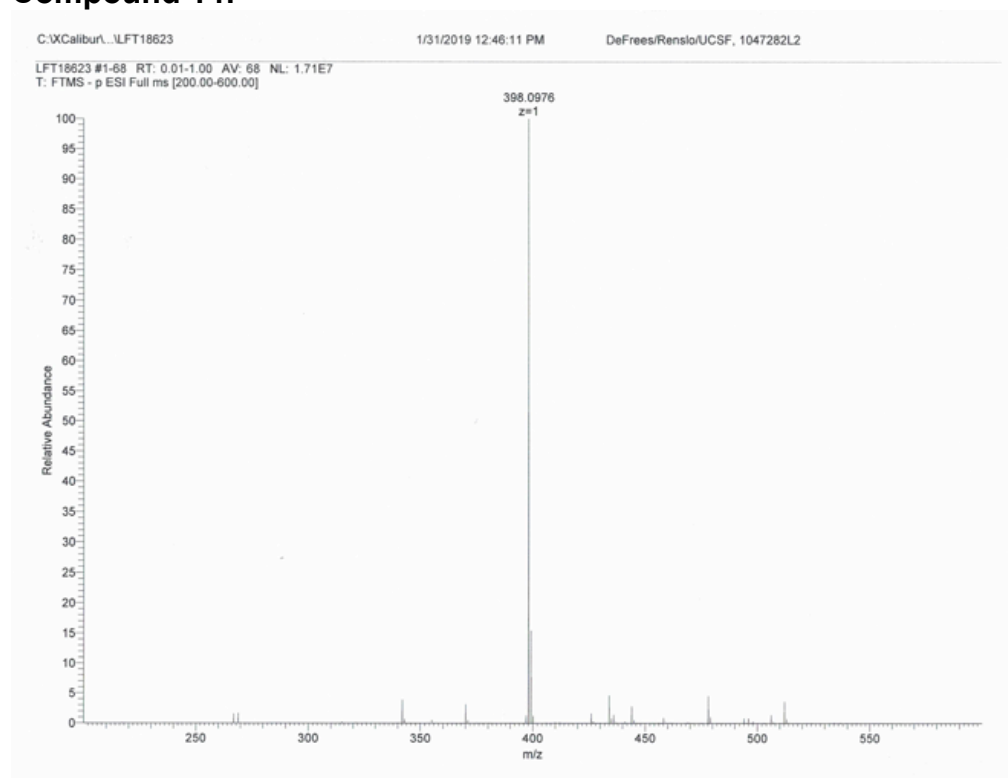
Compound 12:



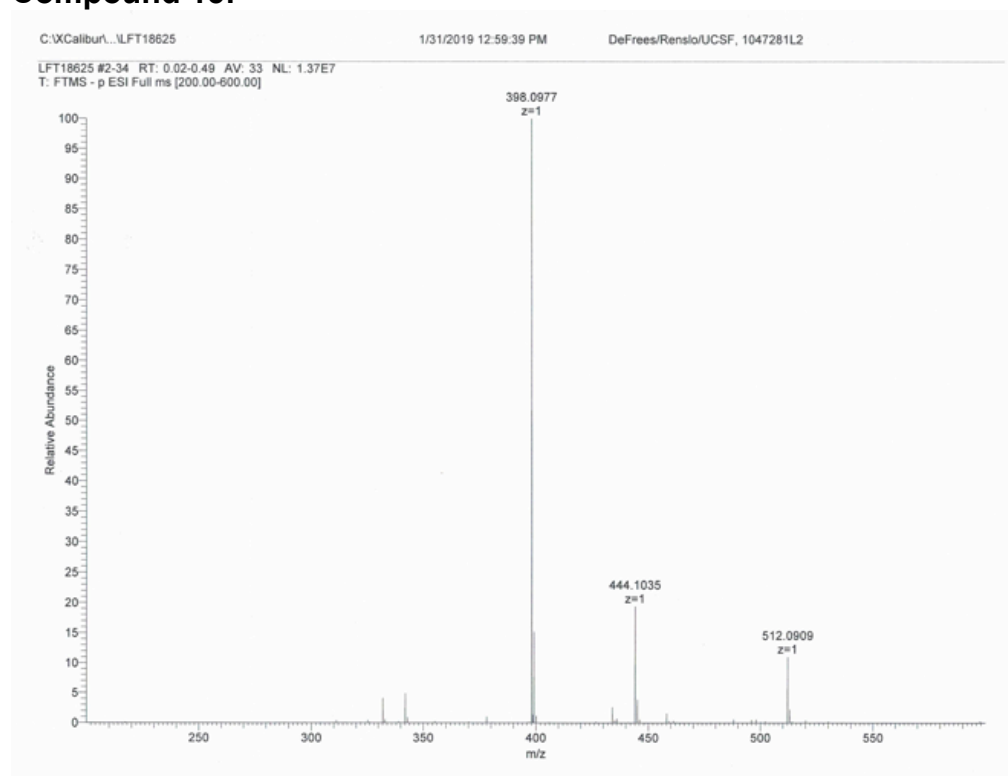
Compound 13:



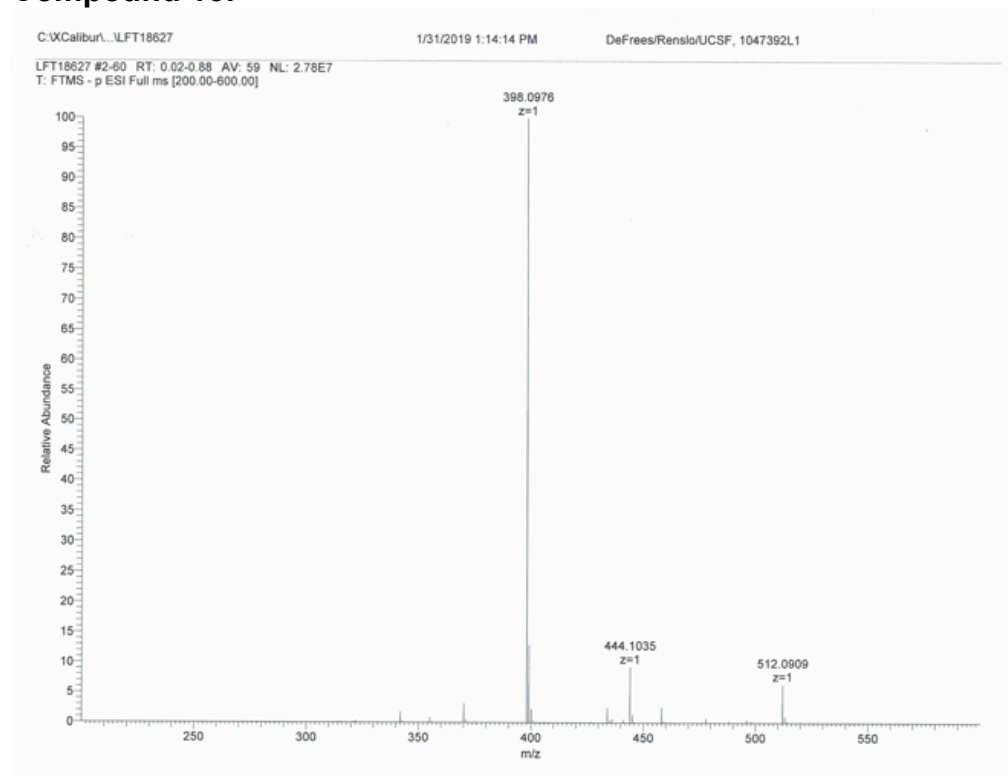
Compound 14:



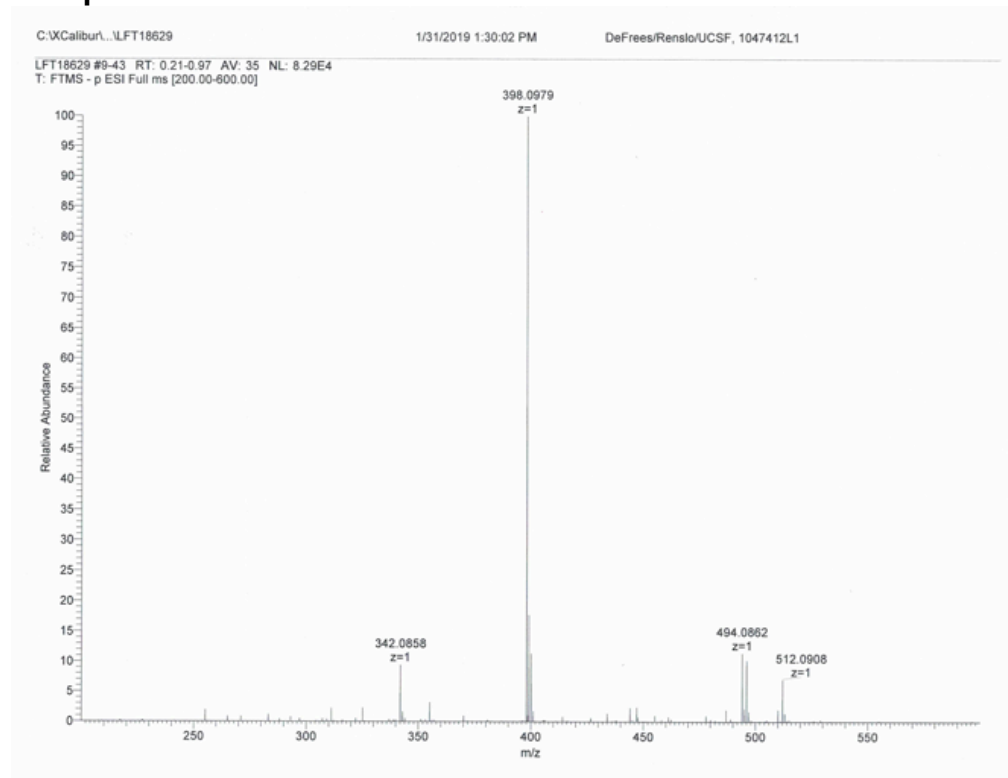
Compound 15:



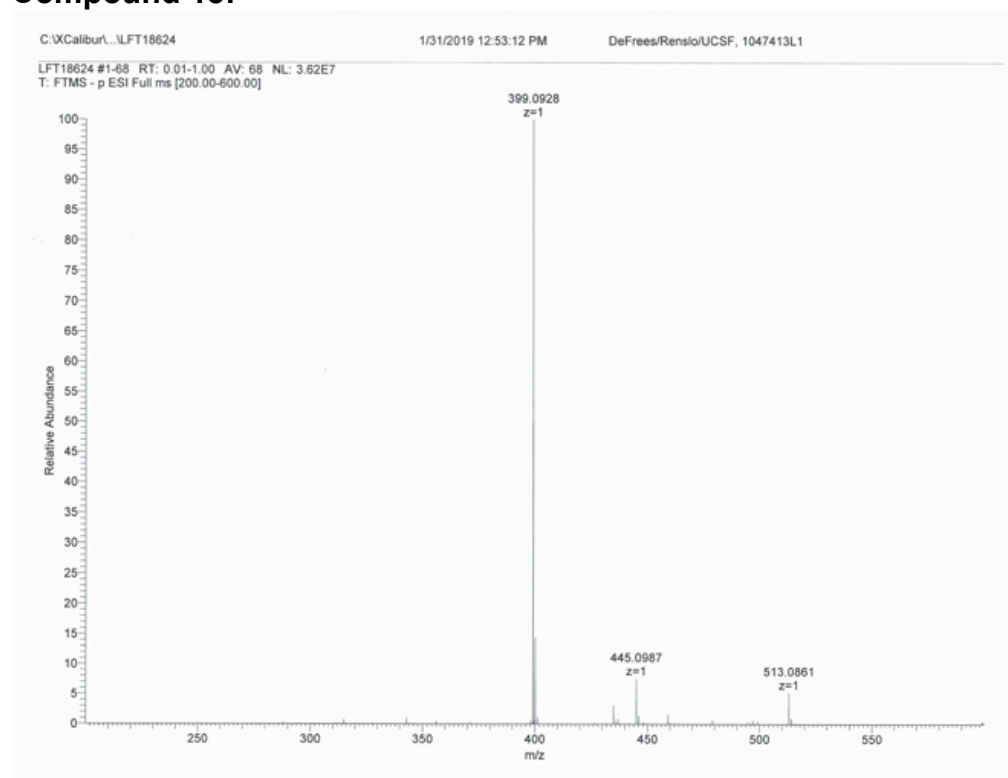
Compound 16:



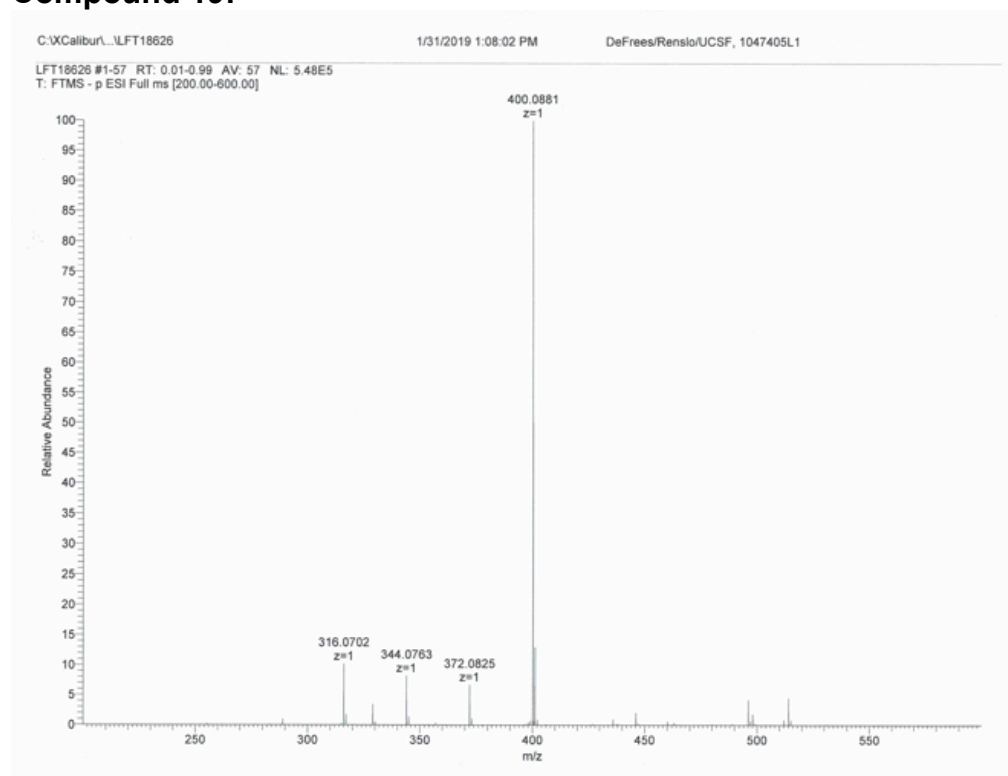
Compound 17:



Compound 18:



Compound 19:



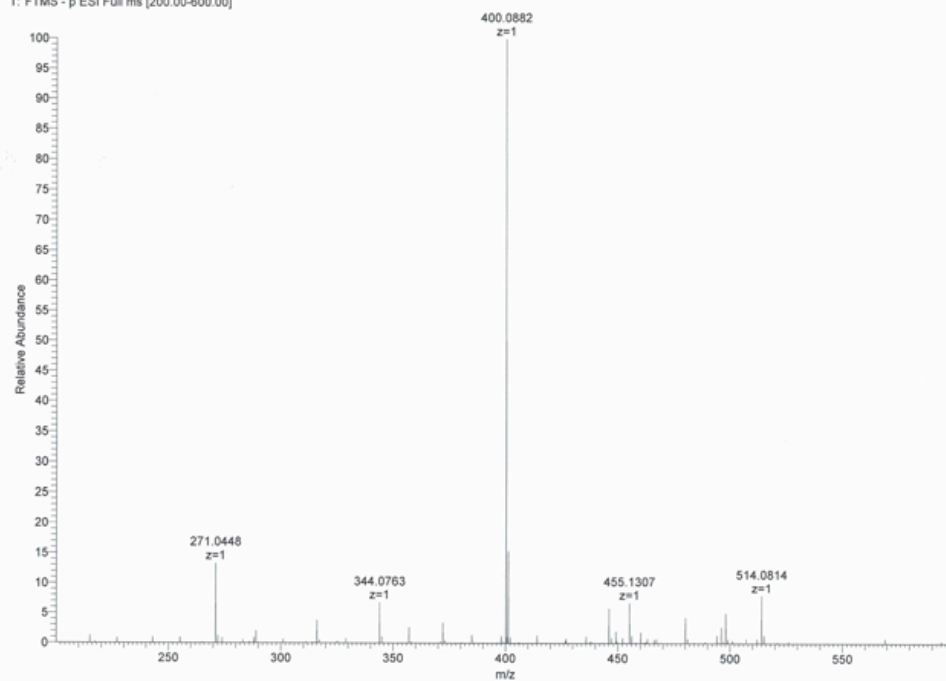
Compound 20:

C:\Calibur\...LFT18628

1/31/2019 1:22:56 PM

DeFrees/Renslo/UCSF, 1047393L1

LFT18628 #1-55 RT: 0.01-1.00 AV: 55 NL: 2.18E5
T: FTMS - p ESI Full ms [200.00-600.00]



Chapter 3

Active-Site Druggability of Carbapenemases and Broad-Spectrum Inhibitor Discovery

*Nicholas J. Torelli, *Afroza Akhtar, *Kyle DeFrees, Priyadarshini Jaishankar, Orville A. Pemberton, Xiujun Zhang, Cody Johnson, Adam R. Renslo, and Yu Chen

**Denotes equal contribution*

Abstract:

Serine and metallo-carbapenemases are a serious health concern due to their capability to hydrolyze nearly all β -lactam antibiotics. However, the molecular basis for their unique broad-spectrum substrate profile is poorly understood, particularly for serine carbapenemases, such as KPC-2. Using substrates and newly identified small molecules, we compared the ligand binding properties of KPC-2 with the noncarbapenemase CTX-M-14, both of which are Class A β -lactamases with highly similar active sites. Notably, compared to CTX-M-14, KPC-2 was more potently inhibited by hydrolyzed β -lactam products (product inhibition), as well as by a series of novel tetrazole-based inhibitors selected from molecular docking against CTX-M-14. Together with complex crystal structures, these data suggest that the KPC-2 active site has an enhanced ability to form favorable interactions with substrates and small molecule ligands due to its increased hydrophobicity and flexibility. Such properties are even more pronounced in metallo-carbapenemases, such as NDM-1, which was also inhibited by some of the novel tetrazole compounds, including one displaying comparable low μ M affinities against both KPC-2 and NDM-1. Our results suggest that carbapenemase activity confers an evolutionary advantage on producers via a broad β -lactam substrate scope but also a mechanistic Achilles' heel that can be exploited for new inhibitor discovery. The complex structures demonstrate, for the first time, how noncovalent inhibitors can be engineered to simultaneously target both serine and metallo-carbapenemases. Despite the relatively modest activity of the current compounds, these studies also demonstrate that hydrolyzed products and tetrazole-

based chemotypes can provide valuable starting points for broad-spectrum inhibitor discovery against carbapenemases.

Introduction:

β -lactam compounds, such as penicillins, are the most widely used antibiotics due to their effective inhibition of transpeptidases during bacterial cell wall synthesis.¹⁻³ β -lactamases catalyze β -lactam hydrolysis and are the primary mediators of bacterial resistance to these antibiotics in Gram negative bacteria.^{4, 5} There are four β -lactamase families; classes A, C, and D use a catalytic serine to form an acyl-enzyme complex during catalysis, whereas Class B are metalloenzymes that rely on Zn(II) ions to mediate the hydrolysis reaction without a covalent intermediate.^{6, 7}

Although extended-spectrum β -lactam antibiotics (e.g., ceftazidime) and carbapenems (e.g., imipenem) initially resisted hydrolysis by β -lactamases, new β -lactamase activity has evolved against these antibiotics.⁸⁻¹⁰ Most notably, the past decade has seen the rise of carbapenemases able to deactivate carbapenems, often regarded as antibiotics of a last resort.¹¹⁻¹⁵ Even more alarming is that many of these enzymes also function as extended-spectrum β -lactamases (ESBLs) and hydrolyze nearly all other β -lactam antibiotics. Among them, KPC-2¹⁶⁻¹⁹ (Class A) and NDM-1^{20, 21} (Class B) enzymes cause the most serious health concerns.

Despite the biomedical importance of KPC-2, the molecular basis of its carbapenemase activity is not well understood, particularly with regard to its ability to bind to a wide range of β -lactam substrates. The KPC-2 active site is highly similar to other Class A enzymes, such as CTX-M-14, a common ESBL that lacks carbapenemase activity.²²⁻²⁴ We have recently determined two complex structures of KPC-2 bound by hydrolyzed β -lactam products, the first such complexes obtained with a wild-type (WT) serine β -lactamase.²³ Previous studies have suggested that the newly

generated carboxylate group in the product may cause unfavorable steric and electrostatic interactions in the active site, leading to the release of the product.²⁵ The KPC-2 product complexes illustrate the differences between KPC-2 and noncarbapenemases, such as CTX-M-14, including a more open and hydrophobic active site in KPC-2. Such features are also observed in NDM-1, which harbors a relatively flat substrate binding pocket with a large number of hydrophobic residues.^{26, 27}

In this study, we investigate how these unique binding site features manifest themselves in carbapenemases' interactions with small molecules, especially how these properties may translate into their broad substrate profile and the prospects for inhibitor discovery. Although the use of a β -lactamase inhibitor in conjunction with a β -lactam antibiotic is a well-established strategy to counter resistance, including the recent success of broad spectrum cyclic boronate compounds,²⁸⁻³¹ developing cross-class β -lactamase inhibitors active against both serine and metallo-carbapenemases remains extremely challenging because of their fundamentally different catalytic mechanisms and three-dimensional structures.^{28, 32, 33} Our results, particularly crystal structures of novel compounds bound noncovalently by KPC-2 and NDM-1, provide valuable insights for drug discovery efforts against these clinically important enzymes.

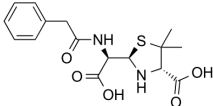
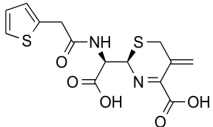
Results and Discussion:

Product inhibition of noncarbapenemase vs carbapenemase

Our recent determination of two KPC-2 product complex crystal structures, together with previous NDM-1 product complexes,^{26, 34, 35} suggest that hydrolyzed β -lactam products can potentially serve as inhibitors of carbapenemases. In comparison,

previous attempts to obtain product complexes with other WT serine β -lactamase crystals were unsuccessful, partially for reasons described above. To quantify the difference in interactions with the product, we tested two hydrolyzed products, penicillin **1** (penicillin G) and cephalosporin **2** (cephalothin), against the noncarbapenemase CTX-M-14, as well as the carbapenemases KPC-2 and NDM-1 (**Table 3-1**). Interestingly, both products inhibited KPC-2 much more potently than CTX-M-14, despite the highly similar active sites of the two Class A β -lactamases. Hydrolyzed penicillin G did not show any inhibition of CTX-M-14 at the highest concentration tested in our assays (10 mM), although previous studies showed that hydrolyzed penicillins inhibited other narrow-spectrum β -lactamases with a $K_i \sim 40$ mM.³⁶ In comparison, the hydrolyzed penicillin G was found to be a high- μ M inhibitor of both KPC-2 and NDM-1. Even more impressively, hydrolyzed cephalothin inhibited KPC-2 and NDM-1 with apparent K_i values of 1.96 and 63.5 μ M, respectively, while showing only mM affinity for CTX-M-14. These results demonstrate that the hydrolyzed β -lactams studied interact more favorably with carbapenemases as compared to otherwise similar noncarbapenemases.

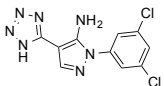
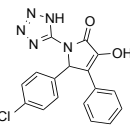
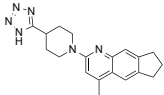
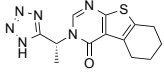
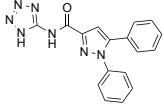
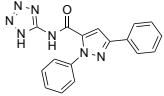
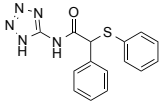
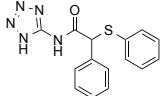
Table 3-1. Inhibition by Hydrolyzed β -Lactam Products

	Structure	CTX-M-14 (μ M)	KPC-2 (μ M)	NDM-1 (μ M)
1		No inhibition	637 \pm 59	400 \pm 73
2		3320 \pm 300	1.96 \pm 0.46	63.5 \pm 10.0

Binding of novel small molecule ligands by CTX-M-14 and KPC-2

We have previously used a structure-based fragment-screening approach to identify the first nM non-covalent serine β -lactamase inhibitors using a tetrazole-based scaffold, targeting CTX-M.^{37, 38} We found that the tetrazole ring displays high shape and electrostatic complementarity with an active site pocket that binds to the substrate C3(4)-carboxylate group in CTX-M. On the basis of the conservation of this site in Class A β -lactamases, we hypothesized that tetrazole-bearing compounds may inhibit KPC-2 as well. We virtually screened a series of tetrazole-containing fragments and lead-sized compounds against CTX-M-14, followed by biochemical evaluation against CTX-M-14, KPC-2, and NDM-1. Among the active inhibitors identified, every one demonstrated enhanced activity against KPC-2 compared to CTX-M-14, by approximately 5-fold or more (**Table 3-2**).

Table 3-2. Inhibition by Tetrazole-Based Compounds^a

Structure	CTX-M14 (μM)	KPC-2 (μM)	NDM-1 (μM)
	4200 \pm 300	386 \pm 33	No inhibition
	No inhibition	123 \pm 37	No inhibition
	1780 \pm 320	288 \pm 27	No inhibition
	2540 \pm 410	195 \pm 44	No inhibition
	1850 \pm 640	239 \pm 23	56 \pm 8
	637 \pm 123	44 \pm 6	62 \pm 9
	No inhibition	231 \pm 6	376 \pm 22
	No inhibition	315 \pm 19	290 \pm 13

^a All compounds were obtained from commercial sources, except **7s*** and **8***, which were synthesized. Compounds **8** and **8*** are racemates.

To illustrate the structural basis of this difference, we determined the crystal structures of two compounds in complex with CTX-M-14 and KPC-2, which, for the first time, demonstrated that the tetrazole moiety can indeed bind to the C3(4)-carboxylate binding site in other Class A β -lactamases besides CTX-M (**Figure 3-1**). Compound **3** showed a nearly identical binding mode for both proteins (**Figure 3-1A, B**). The tetrazole moiety is nestled in a conserved subpocket consisting of three polar residues

and a Gly. It stacks on top of the relatively flat peptide backbone surrounding Gly236 and forms three hydrogen bonds with Ser130, Thr235, and Ser/Thr237 in CTX-M-14/KPC-2. Compound **3** also establishes a hydrogen bond with Asn132 in both proteins. However, the distal dichlorobenzene ring engages in more nonpolar interactions with Pro104, Trp105, and Leu167 in KPC-2, in comparison to Asn104 and Tyr105 in CTX-M-14.

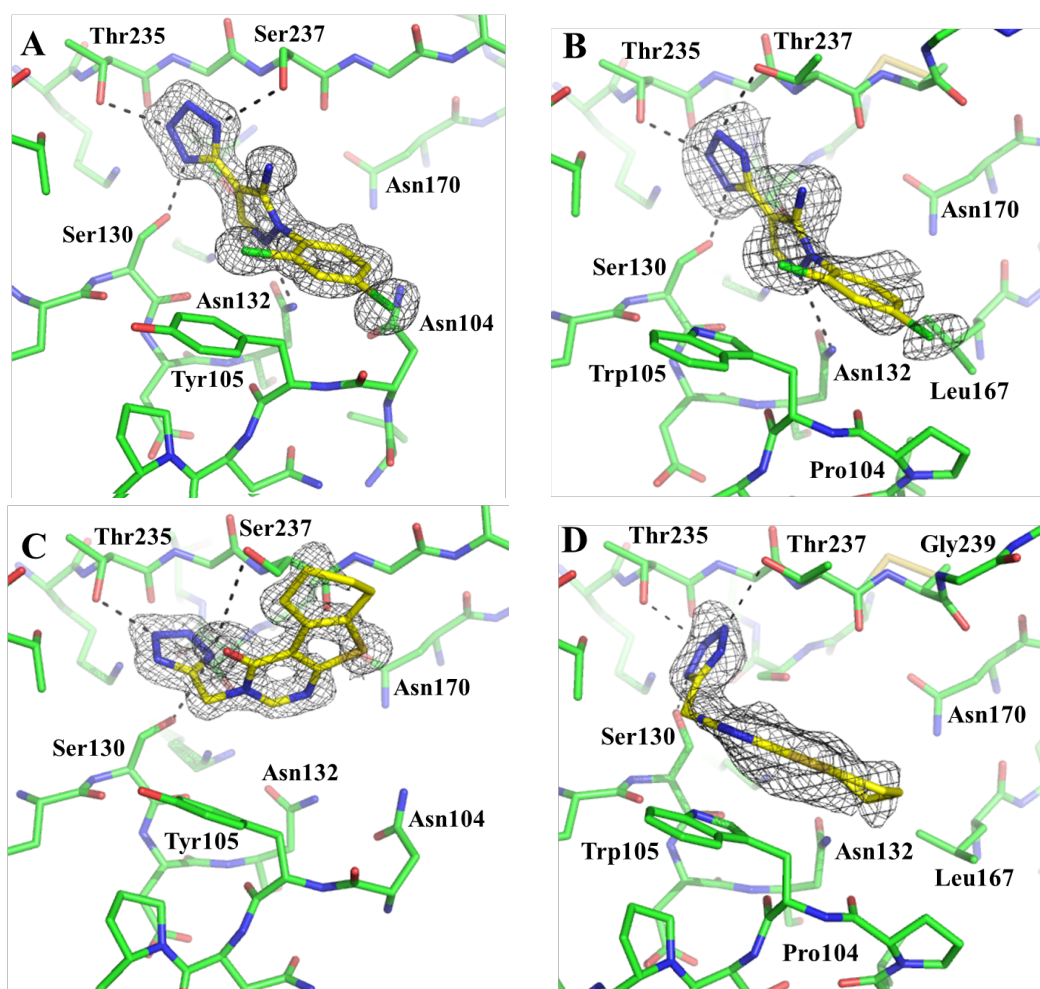


Figure 3-1. Complex crystal structure of compounds **3 and **6** with CTX-M-14 and KPC-2.** (A) Compound **3** with CTX-M-14. (B) Compound **3** with KPC-2. (C) Compound **6** with CTX-M-14. (D) Compound **6** with KPC-2. The simulated annealing composite $F_o - F_c$ omit map (gray) are contoured at 2.5σ and 2σ for the CTX-M-14 (1.4 Å resolutions) and KPC-2 structures (1.7–2.2 Å resolutions), respectively. Black-dashed lines depict hydrogen bonds.

Compound **6** adopted slightly different poses in the two Class A β -lactamases (**Figure 3-1C, D**). In CTX-M-14, the tricyclic ring system flips up to interact with Ser237 and the protein backbone between Ser237 and Gly238 at the end of the β 3 strand; in KPC-2, it stacks on top of Trp105 while forming additional nonpolar interactions with Leu167. The more extensive nonpolar interactions of both **3** and **6** in KPC-2 explain the approximately 10 fold higher binding affinity.

Dual inhibition of serine and metallo-carbapenemases

The majority of the newly identified tetrazole compounds did not inhibit NDM-1. This result is unsurprising, considering that Class A and B β -lactamases have drastically different catalytic mechanisms and three-dimensional structures, and that the compounds were originally selected for CTX-M-14. However, two compounds, **7** and **8**, were active against both KPC-2 and NDM-1, despite exhibiting little to no activity against CTX-M-14 (**Table 3-2**). In particular, compound **7** showed K_i values of 239 μ M for KPC-2 and 56 μ M for NDM-1. Unexpectedly, the X-ray complex crystal structures of **7** clearly revealed the bound ligand to be a regioisomer of the purported structure (**7s**) provided by the commercial compound supplier (**Figure 3-2**). In KPC-2, the tetrazole moiety binds in the same pocket as the other complex structures. The carbonyl group is positioned in the oxyanion hole, formed by the backbone groups of Ser70 and Thr237, and establishes a hydrogen bond with Thr237N. The two benzene rings have nonpolar contacts with Pro104, Leu167, and Asn170. In NDM-1, the tetrazole group forms hydrogen bonds with Lys211N ζ and Asn220N and also interacts with one of the zinc

ions. This is the same subpocket bound by the substrate C3(4)-carboxylate group in previous NDM-1 product complex structures.^{26, 34, 35} Meanwhile, the amide linker points its oxygen toward the zinc ion, with a distance of 2.5 Å, suggesting weak interactions. In addition, the distal ring system forms extensive nonpolar interactions with Leu65, Met67, Val73, and Trp93.

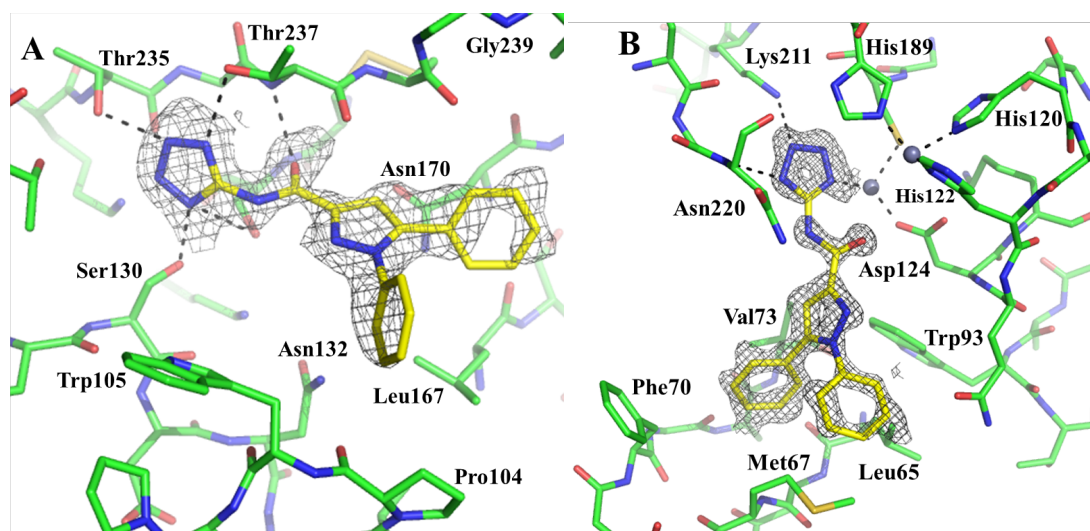


Figure 3-2. Complex crystal structure of compound 7 with KPC-2 (A) and NDM-1 (B). The simulated annealing composite $F_o - F_c$ omit map (gray) contoured at 2.0σ for KPC-2 (1.86 Å resolution) and 2.5σ for NDM-1 (1.15 Å resolution). Black-dashed lines depict hydrogen bonds or coordination with metal ions.

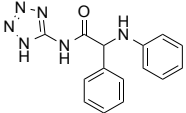
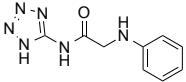
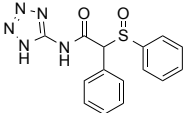
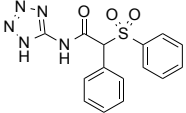
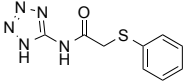
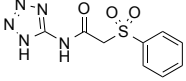
We subsequently synthesized compound **7s**, and the regioisomeric form purported to comprise the original commercial sample. Compared with **7**, analog **7s** displayed similar activity for NDM-1 but better affinity for KPC-2, resulting in comparable K_i 's for both proteins (44 and 62 μM for KPC-2 and NDM-1, respectively) and similar ligand efficiency values (0.24 and 0.23 kcal/mol per heavy atom (relative binding free energy/HA)). The crystal structure of **7s** with KPC-2 clearly shows that the amide carbonyl group is positioned outside the oxyanion hole, different from **7** (ESI, **Figure 3-**

4). The densities for the two benzene rings are significantly weaker, likely due to potential alternative conformations. Overall, one of the rings is oriented downward to interact with Pro104, Trp105, and Leu167; whereas the other one points upward to form contacts with the Thr237 side chain. It appears that the aryl rings of both **7** and **7s** can establish a large number of nonpolar interactions with the protein, yet **7s** is 5-fold more potent than **7**. We hypothesize this could be due to the displacement of the structural water in the oxyanion hole by **7**, which can be energetically costly due to the three favorable hydrogen bond interactions the water forms with Ser70 and Thr237. In comparison, compound **7** establishes only one hydrogen bond with Thr237N through its carbonyl oxygen, while slightly displacing the carbonyl group of Thr237 due to some unfavorable interactions involving the bridging five-membered ring (**Figure 3-2**).

Compound **8** also showed comparable activities for both serine and metallo- β -lactamases (**Table 3-2**). To further probe the shared binding hot spots of serine and metallo-carbapenemases, we synthesized a small series of compound **8** analogs, including deconstructed fragments (**10**, **13**, and **14**) that may serve as a better starting point for future lead optimization (**Table 3-3**). The results further demonstrate that the amido-tetrazole scaffold could provide a novel chemotype active against two structurally different, yet functionally related enzymes. As expected, the majority of these compounds did not display better activities than compound **8**. Interestingly, compound **13** exhibited higher activity against NDM-1 than **8**, even though it lacks one of the aryl side chains. This observation suggests that the backbone of **8** is suboptimal in its ability to enable both aryl groups to interact with protein. In addition, some of the new analogs,

particularly **11–13**, are less potent against **KPC-2** than **NDM-1**, underscoring the structural differences between these two enzymes.

Table 3-3. Inhibition by Analogs of Compound 8^a

	Structure	CTX-M-14 (μM)	KPC-2 (μM)	NDM-1 (μM)
9		No inhibition	479 \pm 41	477 \pm 40
10		No inhibition	1070 \pm 160	2140 \pm 70
11		No inhibition	1570 \pm 70	203.5 \pm 29
12		No inhibition	2000 \pm 50	310 \pm 19
13		No inhibition	No inhibition	91.5 \pm 3.53
14		No inhibition	2370 \pm 650	353 \pm 3.53

^a Compounds **9**, **11**, and **12** are racemates.

Complex crystal structures were determined for **9**, a close analog of **8**, with KPC-2 and NDM-1, showing how this inhibitor is accommodated in the active sites of the two proteins (**Figure 3-3**). Although **9** was synthesized as a racemate, the R stereoisomer appears to fit the electron density the best in both KPC-2 and NDM-1. Despite the significant structural difference between these enzymes, side chains in **9** are seen to

interact favorably with residues of both proteins. The amido-tetrazole moiety is anchored similarly to that of compound **7** in both KPC-2 and NDM-1, although the amide linker is placed outside the oxyanion hole of KPC-2, resembling compound **7s**. The electron densities for the side chains are relatively weak. There appears to be alternative conformations due to the rotation of the amide linker, although it is not possible to model them accurately at the current resolutions. Overall the α -phenyl side chain forms nonpolar contacts with Leu167/Asn170 in KPC-2 and Leu65/Trp93 in NDM-1. The aniline side chain establishes less contact with both proteins; it is within van der Waals contact distance with selected atoms of Thr237/Gly239 of KPC-2, and Val73/Asn220 of NDM-1. We have also determined several other crystal structures, including **8** (ESI, **Figure 3-5**), **10**, **12**, and **13**. The amido-tetrazole groups of these structures adopted similar binding modes to **9**, but the densities for the side chains were also relatively weak for most of these compounds, again suggesting that the aryl rings cannot form optimal protein contacts when displayed from this scaffold backbone.

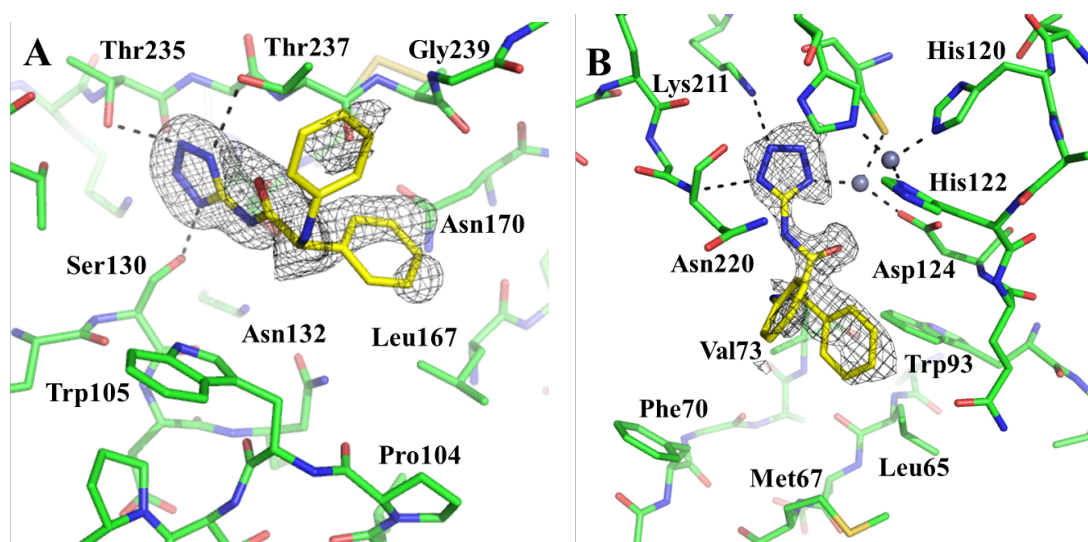


Figure 3-3. Complex crystal structure of compound 9 with KPC-2 and NDM-1. (A) KPC-2, (B) NDM-1. The simulated annealing composite $F_o - F_c$ omit map (gray)

contoured at 2.5σ (1.42 Å resolution) for KPC-2 and 2σ (1.65 Å resolution) for NDM-1. Black dashed lines depict hydrogen bonds or coordination with metal ions.

Active site druggability in carbapenemase function and inhibition

Carbapenemases, such as KPC-2 and NDM-1, can hydrolyze nearly all β -lactam compounds. Our results, particularly those comparing KPC-2 and CTX-M-14, suggest that carbapenemases' broad substrate spectrum correlates with their active sites' enhanced druggability, i.e., ability to interact favorably with small molecules. The active sites of CTX-M-14 and KPC-2 are similar, with nearly identical main chain configurations, except at the end of the β 3 strand (G238/D240 in CTX-M-14 and C238/G239/V240 in KPC-2; note, that residue 239 is missing in CTX-M-14 due to numbering conventions) caused by the Cys69-Cys238 disulfide bond in KPC-2. The most significant side chain differences between the active sites of CTX-M-14 and KPC-2 include N104P, Y105W, and P167L substitutions. These substitutions increase the hydrophobicity of the active site, while also making the binding pocket slightly more open, particularly surrounding Pro104 in KPC-2. Similarly, in NDM-1, there are a large number of hydrophobic residues, and the active site is relatively flat compared with serine β -lactamases.^{26, 27} In addition, in previous structures, Trp105 has demonstrated considerable side chain flexibility in KPC-2 compared with the equivalent Tyr105 of CTX-M-14, possibly allowing KPC-2 to adapt to different ligands.²³ This plasticity is even more evident in NDM-1 with the movement of the Met67-Phe70 loop.^{21, 26, 34, 35} The increased hydrophobicity, flexibility, and openness of the active sites enables the carbapenemases to accommodate a wide range of β -lactams potentially also with enhanced binding affinities. Whereas this broad-spectrum substrate profile confers

evolutionary advantage in bacterial resistance, the enhanced active site druggability makes carbapenemases susceptible to novel inhibitor binding, exposing a key weakness of these enzymes.

Tetrazole-based inhibitors have previously been identified against either serine^{38, 39} or metallo- β -lactamases,^{40, 41} highlighting the utility of the tetrazole moiety as an anchor for inhibitor binding in these enzymes. In particular, the placement of the tetrazole moiety in our NDM-1 complex structures, determined at pH 3.85, is nearly identical to that in a previous complex structure of a different tetrazole inhibitor and the *Bacteroides fragilis* metallo- β -lactamase (PDB, 1A8T),³⁶ determined at pH 6.6. These observations suggest that the low pH used for our NDM-1 complex crystals did not affect the binding of the titratable tetrazole group to the protein, most likely because the pKa of the tetrazole group is perturbed by the interactions with the positively charged Zn ions and Lys211. Furthermore, to our knowledge, these inhibitors represent the first tetrazole-based dual-activity compounds active against both serine and metallo- β -lactamases. They are also the only cross-class inhibitors showing the same mode of action against these enzymes. Previous inhibitors, including the cyclobutanone analogs of β -lactam antibiotics,^{42, 43} cyclic boronates,^{31, 44} alkylboronates,⁴⁵ and the recently discovered bisphosphonate compounds,⁴⁶ appear to serve as noncovalent inhibitors for the metallo enzymes but deactivate serine β -lactamases mostly through a covalent mechanism. In addition, despite the success of cyclic boronate inhibitors, cross-class inhibitor development has remained challenging, with most inhibitor discovery efforts focusing on either serine⁴⁷⁻⁵⁵ or metallo β -lactamases.⁵⁶⁻⁶⁴

Our biochemical and structural data demonstrate the functional similarities between these two groups of enzymes, and indicate that other tetrazole-based compounds can potentially be developed as high affinity dual-activity inhibitors. Admittedly, the potencies of the unoptimized compounds described herein are relatively modest and are not presented as drug leads per se. Nevertheless, specific analogs, such as **7s**, exhibit reasonable ligand efficiency values (~ 0.24 kcal/mol per HA) against both KPC-2 and NDM-1, and thus represent useful starting points for cross-class inhibitor discovery. Moreover, the complex crystal structures presented herein demonstrate how an amido-tetrazole can occupy the substrate C3(4)-carboxylate binding subsite in both KPC-2 and NDM-1 and furthermore reveal additional binding hot spots in the active site. This structural information should be broadly useful to studies of lead discovery and optimization for these important drug targets.

The inhibition of KPC-2 and NDM-1 by hydrolyzed β -lactam products, especially hydrolyzed cephalosporins, suggests the possibility of using these scaffolds in designing carbapenemase inhibitors. Our recent structure of CTX-M-14 with a penilloate product, where the newly generated carboxylate group is eliminated through a decarboxylation process, also demonstrates the broad potential of these compounds as β -lactamase inhibitors, similar to previous studies on *Bacillus cereus* β -lactamase.^{36,65} Inhibition by a product fragment of tazobactam was observed for GES-2 Class A carbapenemase as well, although its distinct structure and binding mode represents a special case.⁶⁶ Interestingly, hydrolyzed piperacillin products have also been shown to inhibit *Pseudomonas aeruginosa* PBP3, a member of the penicillin-binding protein (PBP) family, highlighting the potential value of β -lactam products in novel antibiotic

discovery, and the active site features shared between PBPs and serine β -lactamases.⁶⁷

Conclusion:

The biochemical and structural data in this study have illustrated unique ligand binding properties of carbapenemases that can be exploited in novel antibiotic development. Increased druggability may be characteristic of the active site not only for carbapenemases but also for other enzymes with broad-spectrum substrate profiles. In addition to hydrolyzed β -lactam products, the amido-tetrazole scaffold described here provides new chemotypes for further inhibitor discovery, targeting both serine and metallo-carbapenemases, in efforts to counter antibiotic resistance, particularly in bacteria coproducing both of these enzymes.

Material and Methods:

Construct design

CTX-M-14 and KPC-2 were cloned as previously described.^{23, 37} The NDM-1 gene sequence (residues 42–270) was cloned into the pET-GST expression vector with an N-terminal 6X His-tag and thrombin cleavage site. The NDM-1 construct was transformed into NEB 5-alpha competent *E. coli* and plated onto an LB agar plate containing 50 μ g/mL kanamycin. Single colonies were grown overnight at 37 °C in LB media containing 50 μ g/mL kanamycin. A mini-prep kit was used to isolate plasmid DNA, and the nucleotide sequence of the NDM-1 construct was verified.

Protein expression and purification

BL21(DE3) competent *E. coli* cells were transformed and used for protein expression for CTX-M-14, KPC-2, and NDM-1. CTX-M-14 and KPC-2 were expressed and purified as previously described.^{23, 37} For NDM-1, BL21(DE3) cells were inoculated into 50 mL of LB media containing 50 µg/mL of kanamycin and grown overnight at 37 °C. For large scale production, 1 L of 2xYT media containing 50 µg/mL of kanamycin was inoculated with 10 mL of the overnight starter culture and grown at 37 °C with shaking until the OD600 reached 0.6–0.8. To initiate protein expression, isopropyl β-D-1-thiogalactopyranoside (IPTG) was added to 0.5 mM, and protein expression was continued at 20 °C for 22 h. The cell pellet was prepared by centrifugation at 4000g for 20 min at 4 °C. The cell pellet was resuspended in 35 mL of buffer A (20 mM HEPES pH 8.0, 500 mM NaCl, 10% (v/v) glycerol, 20 mM imidazole, 50 µM ZnSO₄) with a protease inhibitor cocktail tablet (Roche). Cells were lysed through sonication, and the cell lysate was centrifuged at 45000 rpm for 1 h. The supernatant was filtered and loaded onto a His-trap nickel affinity column (GE healthcare Life Sciences, USA) previously equilibrated with buffer A. After the sample was loaded, the column was washed with five column volumes of the same buffer, and a linear gradient of increasing imidazole was used to elute the protein. Fractions containing NDM-1, based on SDS-PAGE, were pooled, and exchanged with buffer containing 20 mM Tris-HCl pH 8.0, 150 mM NaCl, 10% (v/v) glycerol. The 6X His-tag was cleaved at 20 °C using thrombin at an 1:100 ratio (thrombin:NDM-1). After overnight cleavage, samples were again run through a His-trap nickel affinity column, and the flow through containing untagged NDM-1 was collected. The samples were then concentrated and prepared for a final gel

filtration column run. Before loading the sample, a Superdex 75 16/60 gel filtration column (GE healthcare Life Sciences, USA) was equilibrated with 20 mM HEPES pH 8.0, 100 mM NaCl, and 100 μ M ZnSO₄. The concentration of the protein was measured through absorbance at 280 nm using an extinction coefficient of 27 960 M⁻¹ cm⁻¹. SDS-PAGE analysis indicated that the protein was more than 95% pure. Protein fractions were pooled together and concentrated to 20 mg/mL. Protein samples were aliquoted, flash frozen with liquid nitrogen, and stored at -80 °C.

Virtual screening

A database of commercially available tetrazole-containing compounds was downloaded from ZINC68 and docked to the active site of an in-house structure of CTX-M-14 using DOCK 3.669,⁷⁰ and procedures described previously.³⁸ The 1000 top ranking compounds were manually examined. Those showing the best complementarity with the protein and chemical diversity were selected and purchased.

Hydrolyzed products

Hydrolyzed penicillin G (**1**) was purchased from Sigma-Aldrich. Hydrolyzed cephalothin (**2**) was prepared as follows. Commercially available cephalothin (37.1 mg, 0.094 mmol, 1.0 equiv.) was dissolved in water (47 μ L) in a 1.5 mL epi tube, followed by dropwise addition of an aqueous 1 M sodium hydroxide solution (94 μ L, 0.094 mmol, 1.0 equiv.). The tube was lightly vortexed for 2 min, allowed to sit for 15 min, and then cooled to 0 °C with an ice bucket. A cooled 1 M solution of HCl (188 μ L, 0.188, 2.0 equiv.) was then added dropwise, and the resulting precipitate was filtered and washed

with 2 mL of 1 M HCl and 2 mL of cold water. The resulting tan powder was dried under hivaac, affording **2** (8.5 mg, 26%) as a light tan solid. LCMS of the solid indicated a single, broad peak. LRMS (ESI) (m/z): [M + H]⁺ calculated for C₁₄H₁₅N₂O₅S₂, 355.04; found, 355.03.

Novel inhibitors

Commercially available tetrazole compounds were purchased and purified before testing, except for **5** and **6**, due to the low quantity. Compound synthesis is described in the ESI.

β-lactamase inhibition assays

The hydrolytic activity of CTX-M-14 and KPC-2 was determined using the β-lactamase substrate nitrocefin in a reaction buffer containing 100 mM Tris pH 7.0 and 0.01% (v/v) Triton X-100. Nitrocefin hydrolysis was monitored using a Biotek Synergy Mx monochromator-based multimode microplate reader at a 486 nm wavelength. For CTX-M-14 and KPC-2 inhibition assays, the nitrocefin concentration used was 40 and 10 μM, respectively. The K_m of nitrocefin for CTX-M-14 is 22 μM, and for KPC-2, it is 10 μM. For NDM-1, nitrocefin was used as a substrate in a reaction buffer consisting of 50 mM HEPES pH 7.2, 50 μM ZnSO₄, 0.01% (v/v) Triton X-100, and 1 μg/mL bovine serum albumin (BSA). The K_m of nitrocefin for NDM-1 is 3 μM, and the nitrocefin concentration used in the reaction was 10 μM. Compounds were used for IC₅₀ measurements up to 10 mM based on their solubility in DMSO. The final protein concentration used in the reaction for CTX-M-14, KPC-2, and NDM-1 was 0.3, 1, and 2

nM, respectively. The protein was added last to initiate the reaction. The experiments were performed in triplicates, and the results were averaged.

Crystallization and structure determination

CTX-M-14 was crystallized as previously described.³⁷ Briefly; a 10 mg/ mL solution of CTX-M-14 was used to grow crystals in 1.0 M potassium phosphate dibasic pH 8.3. CTX-M-14 complex crystals were prepared via being soaked in 1.44 M sodium citrate and 5–10 mM inhibitors for 1–24 h based on crystal stability. KPC-2 was crystallized as previously described.²³ Briefly, 10–20 mg/mL of KPC-2 was used to grow crystals in 2 M $(\text{NH}_4)_2\text{SO}_4$ and 5% (v/v) ethanol. KPC-2 complex crystals were prepared via being soaked in 1.44 M sodium citrate and 10 mM inhibitors for 40 min. A 10 mg/mL solution of NDM-1 was used to grow crystals in 0.05 M potassium phosphate monobasic, 0.01 M calcium chloride, and 25% (w/v) PEG8000. Complex NDM-1 crystals were prepared via being soaked in 0.05 M sodium acetate pH 3.85, 25% (w/v) PEG8000, and 10 mM inhibitors. Diffraction data were collected at the beamlines 22-ID-D and 23-ID-D of the Advanced Photon Source (APS), Argonne National Laboratory (ANL), and beamline 8.3.1 at the Advanced Light Source (ALS), Lawrence Berkeley National Laboratory (LBNL). Data indexing, integration, and scaling were performed using HKL-2000,⁷¹ iMOSFLM,⁷² and SCALA⁷³ of the CCP4 suite.⁷⁴ Phasing was performed using molecular replacement (PDB accession code, 1YLT for CTX-M-14; 3C5A for KPC-2; and 4TZF for NDM-1) with the program phaser⁷⁵ of the PHENIX suite.⁷⁶ Structure refinement was performed using phenix.refine⁷⁷ of the PHENIX suite, and model building was performed using WinCoot.⁷⁸ The eLBOW program⁷⁹ of the PHENIX suite was used to generate

ligand restraints. The quality of the model was assessed by MolProbity.⁸⁰ The composite omit map program⁸¹ of the PHENIX suite was used to generate composite simulated annealing mF_o-DF_c omit maps. Protein structure figures were generated using PyMOL (Schrödinger, LLC).

Associated Content:

Supporting information

The electronic supporting information is provided at the end of this chapter.

Accession codes

The atomic coordinates and structure factors have been deposited in the Protein Data Bank (PDB) under accession codes: 6M7I (KPC-2, compound **3**), 6MNP (KPC-2, compound **6**), 6MLL (KPC-2, compound **7**), 6MEY (KPC-2, compound **9**), 6MD8 (CTX-M-14, compound **3**), 6MIA (CTX-M-14, compound **6**), 6MDU (NDM-1, compound **7**), and 6EFJ (NDM-1, compound **9**).

Author Information:

Corresponding Authors

*E-mail: adam.renslo@ucsf.edu.

*E-mail: ychen1@health.usf.edu.

ORCID

Adam R. Renslo: 0000-0002-1240-2846

Yu Chen: 0000-0002-5115-3600

Author Contributions

N.J.T., A.A., and K.D. contributed equally to this work.

Notes

The authors declare the following competing financial interest(s): N.J.T., K.D., P.J., O.A.P., X.Z., A.R.R., and Y.C. are listed as inventors on a patent application describing compounds studied herein.

Acknowledgements:

Support for this work was given by the National Institutes of Health (NIH) grant AI103158. We thank Michael Sacco for reading the manuscript, and the staff scientists of beamlines on SER CAT and SBC core at APS for assistance with X-ray diffraction data collection.

References:

1. Chen, Y., Zhang, W., Shi, Q., Heseck, D., Lee, M., Mobashery, S., and Shoichet, B. K. (2009) Crystal structures of penicillin-binding protein 6 from *Escherichia coli*. *J. Am. Chem. Soc.* 131 (40), 14345–54.
2. Tipper, D. J., and Strominger, J. L. (1965) Mechanism of action of penicillins: a proposal based on their structural similarity to acyl-D-alanyl-D-alanine. *Proc. Natl. Acad. Sci. U. S. A.* 54 (4), 1133–41.
3. Silvaggi, N. R., Anderson, J. W., Brinsmade, S. R., Pratt, R. F., and Kelly, J. A. (2003) The crystal structure of phosphonate-inhibited D-Ala-D-Ala peptidase reveals an analogue of a tetrahedral transition state. *Biochemistry* 42 (5), 1199–208.
4. Frere, J. M. (1995) Beta-lactamases and bacterial resistance to antibiotics. *Mol. Microbiol.* 16 (3), 385–95.
5. Taubes, G. (2008) The bacteria fight back. *Science* 321 (5887), 356–61.
6. Bush, K., Jacoby, G. A., and Medeiros, A. A. (1995) A functional classification scheme for beta-lactamases and its correlation with molecular structure. *Antimicrob. Agents Chemother.* 39 (6), 1211–33.
7. Livermore, D. M. (1995) beta-Lactamases in laboratory and clinical resistance. *Clin. Microbiol. Rev.* 8 (4), 557–84.
8. Bradford, P. A. (2001) Extended-spectrum beta-lactamases in the 21st century: characterization, epidemiology, and detection of this important resistance threat. *Clin Microbiol Rev.* 14 (4), 933–51.

9. Babic, M., Hujer, A. M., and Bonomo, R. A. (2006) What's new in antibiotic resistance? Focus on beta-lactamases. *Drug Resist. Updates* 9 (3), 142–56.
10. Perez, F., Endimiani, A., Hujer, K. M., and Bonomo, R. A. (2007) The continuing challenge of ESBLs. *Curr. Opin. Pharmacol.* 7 (5), 459–69.
11. Patel, G., and Bonomo, R. A. (2011) Status report on carbapenemases: challenges and prospects. *Expert Rev. Anti-Infect. Ther.* 9 (5), 555–70.
12. Frase, H., Shi, Q., Testero, S. A., Mobashery, S., and Vakulenko, S. B. (2009) Mechanistic basis for the emergence of catalytic competence against carbapenem antibiotics by the GES family of beta-lactamases. *J. Biol. Chem.* 284 (43), 29509–13.
13. Schneider, K. D., Karpen, M. E., Bonomo, R. A., Leonard, D. A., and Powers, R. A. (2009) The 1.4 Å crystal structure of the class D beta-lactamase OXA-1 complexed with doripenem. *Biochemistry* 48 (50), 11840–7.
14. Bush, K. (2010) Alarming beta-lactamase-mediated resistance in multidrug-resistant Enterobacteriaceae. *Curr. Opin. Microbiol.* 13 (5), 558–64.
15. Smith, C. A., Frase, H., Toth, M., Kumarasiri, M., Wiafe, K., Munoz, J., Mobashery, S., and Vakulenko, S. B. (2012) Structural basis for progression toward the carbapenemase activity in the GES family of beta-lactamases. *J. Am. Chem. Soc.* 134 (48), 19512–5.
16. Ke, W., Bethel, C. R., Thomson, J. M., Bonomo, R. A., and van den Akker, F. (2007) Crystal structure of KPC-2: insights into carbapenemase activity in class A beta-lactamases. *Biochemistry* 46 (19), 5732–40.

17. Bratu, S., Mooty, M., Nichani, S., Landman, D., Gullans, C., Pettinato, B., Karumudi, U., Tolaney, P., and Quale, J. (2005) Emergence of KPC-possessing *Klebsiella pneumoniae* in Brooklyn, New York: epidemiology and recommendations for detection. *Antimicrob. Agents Chemother.* 49 (7), 3018–20.
18. Naas, T., Nordmann, P., Vedel, G., and Poyart, C. (2005) Plasmid-mediated carbapenem-hydrolyzing beta-lactamase KPC in a *Klebsiella pneumoniae* isolate from France. *Antimicrob. Agents Chemother.* 49 (10), 4423–4.
19. Mehta, S. C., Rice, K., and Palzkill, T. (2015) Natural Variants of the KPC-2 Carbapenemase have Evolved Increased Catalytic Efficiency for Ceftazidime Hydrolysis at the Cost of Enzyme Stability. *PLoS Pathog.* 11 (6), No. e1004949.
20. Kumarasamy, K. K., Toleman, M. A., Walsh, T. R., Bagaria, J., Butt, F., Balakrishnan, R., Chaudhary, U., Doumith, M., Giske, C. G., Irfan, S., Krishnan, P., Kumar, A. V., Maharjan, S., Mushtaq, S., Noorie, T., Paterson, D. L., Pearson, A., Perry, C., Pike, R., Rao, B., Ray, U., Sarma, J. B., Sharma, M., Sheridan, E., Thirunarayan, M. A., Turton, J., Upadhyay, S., Warner, M., Welfare, W., Livermore, D. M., and Woodford, N. (2010) Emergence of a new antibiotic resistance mechanism in India, Pakistan, and the UK: a molecular, biological, and epidemiological study. *Lancet Infect. Dis.* 10 (9), 597–602.
21. King, D., and Strynadka, N. (2011) Crystal structure of New Delhi metallo-beta-lactamase reveals molecular basis for antibiotic resistance. *Protein Sci.* 20 (9), 1484–91.

22. Chen, Y., Delmas, J., Sirot, J., Shoichet, B., and Bonnet, R. (2005) Atomic resolution structures of CTX-M beta-lactamases: extended spectrum activities from increased mobility and decreased stability. *J. Mol. Biol.* 348 (2), 349–62.
23. Pemberton, O. A., Zhang, X., and Chen, Y. (2017) Molecular Basis of Substrate Recognition and Product Release by the *Klebsiella pneumoniae* Carbapenemase (KPC-2). *J. Med. Chem.* 60 (8), 3525– 3530.
24. Adamski, C. J., Cardenas, A. M., Brown, N. G., Horton, L. B., Sankaran, B., Prasad, B. V., Gilbert, H. F., and Palzkill, T. (2015) Molecular basis for the catalytic specificity of the CTX-M extended- spectrum beta-lactamases. *Biochemistry* 54 (2), 447–57.
25. Beadle, B. M., Trehan, I., Focia, P. J., and Shoichet, B. K. (2002) Structural milestones in the reaction pathway of an amide hydrolase: substrate, acyl, and product complexes of cephalothin with AmpC beta-lactamase. *Structure* 10 (3), 413–24.
26. King, D. T., Worrall, L. J., Gruninger, R., and Strynadka, N. C. (2012) New Delhi metallo-beta-lactamase: structural insights into beta-lactam recognition and inhibition. *J. Am. Chem. Soc.* 134 (28), 11362–5.
27. Zhang, H., and Hao, Q. (2011) Crystal structure of NDM-1 reveals a common beta-lactam hydrolysis mechanism. *FASEB J.* 25 (8), 2574–82.
28. Drawz, S. M., and Bonomo, R. A. (2010) Three decades of beta-lactamase inhibitors. *Clin Microbiol Rev.* 23 (1), 160–201.
29. Papp-Wallace, K. M., and Bonomo, R. A. (2016) New beta-lactamase Inhibitors in the Clinic. *Infect Dis Clin North Am.* 30 (2), 441–64.

30. Toussaint, K. A., and Gallagher, J. C. (2015) beta-lactam/beta-lactamase inhibitor combinations: from then to now. *Ann. Pharmacother.* 49 (1), 86–98.
31. Cahill, S. T., Cain, R., Wang, D. Y., Lohans, C. T., Wareham, D. W., Oswin, H. P., Mohammed, J., Spencer, J., Fishwick, C. W., McDonough, M. A., Schofield, C. J., and Brem, J. (2017) Cyclic Boronates Inhibit All Classes of beta-Lactamases. *Antimicrob. Agents Chemother.* 61 (4), e02260-16
32. King, D. T., and Strynadka, N. C. (2013) Targeting metallo-beta-lactamase enzymes in antibiotic resistance. *Future Med. Chem.* 5 (11), 1243–63.
33. Nichols, D. A., Renslo, A. R., and Chen, Y. (2014) Fragment-based inhibitor discovery against beta-lactamase. *Future Med. Chem.* 6 (4), 413–27.
34. Feng, H., Ding, J., Zhu, D., Liu, X., Xu, X., Zhang, Y., Zang, S., Wang, D. C., and Liu, W. (2014) Structural and mechanistic insights into NDM-1 catalyzed hydrolysis of cephalosporins. *J. Am. Chem. Soc.* 136 (42), 14694–7.
35. Feng, H., Liu, X., Wang, S., Fleming, J., Wang, D. C., and Liu, W. (2017) The mechanism of NDM-1-catalyzed carbapenem hydrolysis is distinct from that of penicillin or cephalosporin hydrolysis. *Nat. Commun.* 8 (1), 2242.
36. Kiener, P. A., and Waley, S. G. (1978) Reversible Inhibitors of Penicillinases. *Biochem. J.* 169, 197–204.
37. Nichols, D. A., Jaishankar, P., Larson, W., Smith, E., Liu, G., Beyrouthy, R., Bonnet, R., Renslo, A. R., and Chen, Y. (2012) Structure-Based Design of Potent and Ligand-Efficient Inhibitors of CTX-M Class A beta-Lactamase. *J. Med. Chem.* 55 (5), 2163–72.

38. Chen, Y., and Shoichet, B. K. (2009) Molecular docking and ligand specificity in fragment-based inhibitor discovery. *Nat. Chem. Biol.* 5 (5), 358–64.
39. Teotico, D. G., Babaoglu, K., Rocklin, G. J., Ferreira, R. S., Giannetti, A. M., and Shoichet, B. K. (2009) Docking for fragment inhibitors of AmpC beta-lactamase. *Proc. Natl. Acad. Sci. U. S. A.* 106 (18), 7455–60.
40. Skagseth, S., Akhter, S., Paulsen, M. H., Muhammad, Z., Lauksund, S., Samuelsen, O., Leiros, H. S., and Bayer, A. (2017) Metallo-beta-lactamase inhibitors by bioisosteric replacement: Preparation, activity and binding. *Eur. J. Med. Chem.* 135, 159–173.
41. Toney, J. H., Fitzgerald, P. M., Grover-Sharma, N., Olson, S. H., May, W. J., Sundelof, J. G., Vanderwall, D. E., Cleary, K. A., Grant, S. K., Wu, J. K., Kozarich, J. W., Pompliano, D. L., and Hammond, G. G. (1998) Antibiotic sensitization using biphenyl tetrazoles as potent inhibitors of *Bacteroides fragilis* metallo-beta-lactamase. *Chem. Biol.* 5 (4), 185–196.
42. Johnson, J. W., Gretes, M., Goodfellow, V. J., Marrone, L., Heynen, M. L., Strynadka, N. C., and Dmitrienko, G. I. (2010) Cyclobutanone analogues of beta-lactams revisited: insights into conformational requirements for inhibition of serine- and metallo- beta-lactamases. *J. Am. Chem. Soc.* 132 (8), 2558–60.
43. Devi, P., and Rutledge, P. J. (2017) Cyclobutanone Analogues of beta-Lactam Antibiotics: beta-Lactamase Inhibitors with Untapped Potential? *ChemBioChem* 18 (4), 338–351.
44. Brem, J., Cain, R., Cahill, S., McDonough, M. A., Clifton, I. J., Jimenez-Castellanos, J. C., Avison, M. B., Spencer, J., Fishwick, C. W., and Schofield, C.

- J. (2016) Structural basis of metallo-beta-lactamase, serine-beta-lactamase and penicillin-binding protein inhibition by cyclic boronates. *Nat. Commun.* 7, 12406.
45. Santucci, M., Spyraakis, F., Cross, S., Quotadamo, A., Farina, D., Tondi, D., De Luca, F., Docquier, J. D., Prieto, A. I., Ibacache, C., Blazquez, J., Venturelli, A., Cruciani, G., and Costi, M. P. (2017) Computational and biological profile of boronic acids for the detection of bacterial serine- and metallo-beta-lactamases. *Sci. Rep.* 7 (1), 17716.
46. Zhang, C., Pu, Y.-c., Yu, Z.-J., Wu, C.-y., Brem, J., McDonough, M. A., Schofield, C. J., Li, G.-B., and Wu, Y. (2018) Rh(iii)-Catalyzed directed C-H carbenoid coupling reveals aromatic bisphosphonates inhibiting metallo- and Serine- β -lactamases. *Org. Chem. Front.* 5 (8), 1288–1292.
47. Papp-Wallace, K. M., Nguyen, N. Q., Jacobs, M. R., Bethel, C. R., Barnes, M. D., Kumar, V., Bajaksouzian, S., Rudin, S. D., Rather, P. N., Bhavsar, S., Ravikumar, T., Deshpande, P. K., Patil, V., Yeole, R., Bhagwat, S. S., Patel, M. V., van den Akker, F., and Bonomo, R. A. (2018) Strategic Approaches to Overcome Resistance against Gram- Negative Pathogens Using beta-Lactamase Inhibitors and beta-Lactam Enhancers: Activity of Three Novel Diazabicyclooctanes WCK 5153, Zidebactam (WCK 5107), and WCK 4234. *J. Med. Chem.* 61 (9), 4067–4086.
48. Akhter, S., Lund, B. A., Ismael, A., Langer, M., Isaksson, J., Christopeit, T., Leiros, H. S., and Bayer, A. (2018) A focused fragment library targeting the antibiotic resistance enzyme - Oxacillinase-48: Synthesis, structural evaluation and inhibitor design. *Eur. J. Med. Chem.* 145, 634–648.

49. Caselli, E., Romagnoli, C., Powers, R. A., Taracila, M. A., Bouza, A. A., Swanson, H. C., Smolen, K. A., Fini, F., Wallar, B. J., Bonomo, R. A., and Prati, F. (2018) Inhibition of Acinetobacter-Derived Cephalosporinase: Exploring the Carboxylate Recognition Site Using Novel beta-Lactamase Inhibitors. *ACS Infect. Dis.* 4 (3), 337–348.
50. Bouza, A. A., Swanson, H. C., Smolen, K. A., VanDine, A. L., Taracila, M. A., Romagnoli, C., Caselli, E., Prati, F., Bonomo, R. A., Powers, R. A., and Wallar, B. J. (2018) Structure-Based Analysis of Boronic Acids as Inhibitors of Acinetobacter-Derived Cephalosporinase-7, a Unique Class C beta-Lactamase. *ACS Infect. Dis.* 4 (3), 325–336.
51. Werner, J. P., Mitchell, J. M., Taracila, M. A., Bonomo, R. A., and Powers, R. A. (2017) Exploring the potential of boronic acids as inhibitors of OXA-24/40 beta-lactamase. *Protein Sci.* 26 (3), 515– 526.
52. Nguyen, N. Q., Krishnan, N. P., Rojas, L. J., Prati, F., Caselli, E., Romagnoli, C., Bonomo, R. A., and van den Akker, F. (2016) Crystal Structures of KPC-2 and SHV-1 beta-Lactamases in Complex with the Boronic Acid Transition State Analog S02030. *Antimicrob. Agents Chemother.* 60 (3), 1760–6.
52. Rojas, L. J., Taracila, M. A., Papp-Wallace, K. M., Bethel, C. R., Caselli, E., Romagnoli, C., Winkler, M. L., Spellberg, B., Prati, F., and Bonomo, R. A. (2016) Boronic Acid Transition State Inhibitors Active against KPC and Other Class A beta-Lactamases: Structure-Activity Relationships as a Guide to Inhibitor Design. *Antimicrob. Agents Chemother.* 60 (3), 1751–9.

54. Spyarakis, F., Bellio, P., Quotadamo, A., Linciano, P., Benedetti, P., D'Arrigo, G., Baroni, M., Cendron, L., Celenza, G., and Tondi, D. (2019) First virtual screening and experimental validation of inhibitors targeting GES-5 carbapenemase. *J. Comput.-Aided Mol. Des.* 33, 295.
55. Tilvawala, R., Cammarata, M., Adediran, S. A., Brodbelt, J. S., and Pratt, R. F. (2015) A New Covalent Inhibitor of Class C beta-Lactamases Reveals Extended Active Site Specificity. *Biochemistry* 54 (50), 7375–84.
56. King, A. M., Reid-Yu, S. A., Wang, W., King, D. T., De Pascale, G., Strynadka, N. C., Walsh, T. R., Coombes, B. K., and Wright, G. D. (2014) Aspergillomarasmine A overcomes metallo-beta-lactamase antibiotic resistance. *Nature* 510 (7506), 503–6.
57. Brem, J., van Berkel, S. S., Aik, W., Rydzik, A. M., Avison, M. B., Pettinati, I., Umland, K. D., Kawamura, A., Spencer, J., Claridge, T. D., McDonough, M. A., and Schofield, C. J. (2014) Rhodanine hydrolysis leads to potent thioenolate mediated metallo-beta-lactamase inhibition. *Nat. Chem.* 6 (12), 1084–90.
58. Hinchliffe, P., Tanner, C. A., Krismanich, A. P., Labbe, G., Goodfellow, V. J., Marrone, L., Desoky, A. Y., Calvopina, K., Whittle, E. E., Zeng, F., Avison, M. B., Bols, N. C., Siemann, S., Spencer, J., and Dmitrienko, G. I. (2018) Structural and Kinetic Studies of the Potent Inhibition of Metallo-beta-lactamases by 6-Phosphonomethylpyridine-2-carboxylates. *Biochemistry* 57 (12), 1880–1892.
59. Hinchliffe, P., Gonzalez, M. M., Mojica, M. F., Gonzalez, J. M., Castillo, V., Saiz, C., Kosmopoulou, M., Tooke, C. L., Llarrull, L. I., Mahler, G., Bonomo, R. A., Vila, A. J., and Spencer, J. (2016) Cross- class metallo-beta-lactamase inhibition by

- bisthiazolidines reveals multiple binding modes. *Proc. Natl. Acad. Sci. U. S. A.* 113 (26), E3745–54.
60. Gonzalez, M. M., Kosmopoulou, M., Mojica, M. F., Castillo, V., Hinchliffe, P., Pettinati, I., Brem, J., Schofield, C. J., Mahler, G., Bonomo, R. A., Llarrull, L. I., Spencer, J., and Vila, A. J. (2015) Bisthiazolidines: A Substrate-Mimicking Scaffold as an Inhibitor of the NDM-1 Carbapenemase. *ACS Infect. Dis.* 1 (11), 544–54.
61. Chen, P., Horton, L. B., Mikulski, R. L., Deng, L., Sundriyal, S., Palzkill, T., and Song, Y. (2012) 2-Substituted 4,5-dihydrothiazole-4- carboxylic acids are novel inhibitors of metallo-beta-lactamases. *Bioorg. Med. Chem. Lett.* 22 (19), 6229–32.
62. Cain, R., Brem, J., Zollman, D., McDonough, M. A., Johnson, R. M., Spencer, J., Makena, A., Abboud, M. I., Cahill, S., Lee, S. Y., McHugh, P. J., Schofield, C. J., and Fishwick, C. W. G. (2018) In Silico Fragment-Based Design Identifies Subfamily B1 Metallo-beta-lactamase Inhibitors. *J. Med. Chem.* 61 (3), 1255–1260.
63. Li, G. B., Brem, J., Lesniak, R., Abboud, M. I., Lohans, C. T., Clifton, I. J., Yang, S. Y., Jimenez-Castellanos, J. C., Avison, M. B., Spencer, J., McDonough, M. A., and Schofield, C. J. (2017) Crystallographic analyses of isoquinoline complexes reveal a new mode of metallo-beta-lactamase inhibition. *Chem. Commun.* 53 (43), 5806–5809.

64. Linciano, P., Cendron, L., Gianquinto, E., Spyraakis, F., and Tondi, D. (2019) Ten Years with New Delhi Metallo-beta-lactamase-1 (NDM-1): From Structural Insights to Inhibitor Design. *ACS Infect. Dis.* 5, 9.
65. Lewandowski, E. M., Skiba, J., Torelli, N. J., Rajnisz, A., Solecka, J., Kowalski, K., and Chen, Y. (2015) Antibacterial properties and atomic resolution X-ray complex crystal structure of a ruthenocene conjugated beta-lactam antibiotic. *Chem. Commun.* 51 (28), 6186–9.
66. Frase, H., Smith, C. A., Toth, M., Champion, M. M., Mobashery, S., and Vakulenko, S. B. (2011) Identification of products of inhibition of GES-2 beta-lactamase by tazobactam by x-ray crystallography and spectrometry. *J. Biol. Chem.* 286 (16), 14396–409.
67. van Berkel, S. S., Nettleship, J. E., Leung, I. K., Brem, J., Choi, H., Stuart, D. I., Claridge, T. D., McDonough, M. A., Owens, R. J., Ren, J., and Schofield, C. J. (2013) Binding of (5S)-penicilloic acid to penicillin binding protein 3. *ACS Chem. Biol.* 8 (10), 2112–6.
68. Irwin, J. J., and Shoichet, B. K. (2005) ZINC—a free database of commercially available compounds for virtual screening. *J. Chem. Inf. Model.* 45 (1), 177–82.
69. Meng, E., Shoichet, B. K., and Kuntz, I. D. (1992) Automated docking with grid-based energy evaluation. *J. Comput. Chem.* 13 (13), 505–524.
70. Lorber, D. M., and Shoichet, B. K. (2005) Hierarchical docking of databases of multiple ligand conformations. *Curr. Top. Med. Chem.* 5 (8), 739–49.

71. Otwinowski, Z., and Minor, W. (1997) [20] Processing of X-ray diffraction data collected in oscillation mode. *In Methods in Enzymology*, Vol. 276, pp 307–326, Academic Press.
72. Battye, T. G., Kontogiannis, L., Johnson, O., Powell, H. R., and Leslie, A. G. (2011) iMOSFLM: a new graphical interface for diffraction-image processing with MOSFLM. *Acta Crystallogr. Sect. D: Biol. Crystallogr.* 67 (Pt4), 271–81.
73. Evans, P. (2006) Scaling and assessment of data quality. *Acta Crystallogr., Sect. D: Biol. Crystallogr.* 62 (Pt1), 72–82.
74. Winn, M. D., Ballard, C. C., Cowtan, K. D., Dodson, E. J., Emsley, P., Evans, P. R., Keegan, R. M., Krissinel, E. B., Leslie, A. G., McCoy, A., McNicholas, S. J., Murshudov, G. N., Pannu, N. S., Potterton, E. A., Powell, H. R., Read, R. J., Vagin, A., and Wilson, K. S. (2011) Overview of the CCP4 suite and current developments. *Acta Crystallogr., Sect. D: Biol. Crystallogr.* 67 (Pt4), 235–42.
75. McCoy, A. J., Grosse-Kunstleve, R. W., Adams, P. D., Winn, M. D., Storoni, L. C., and Read, R. J. (2007) Phaser crystallographic software. *J. Appl. Crystallogr.* 40 (Pt4), 658–674.
76. Adams, P. D., Afonine, P. V., Bunkoczi, G., Chen, V. B., Davis, I. W., Echols, N., Headd, J. J., Hung, L. W., Kapral, G. J., Grosse-Kunstleve, R. W., McCoy, A. J., Moriarty, N. W., Oeffner, R., Read, R. J., Richardson, D. C., Richardson, J. S., Terwilliger, T. C., and Zwart, P. H. (2010) PHENIX: a comprehensive Python-based system for macromolecular structure solution. *Acta Crystallogr., Sect. D: Biol. Crystallogr.* 66 (Pt2), 213–21.

77. Afonine, P. V., Grosse-Kunstleve, R. W., Echols, N., Headd, J. J., Moriarty, N. W., Mustyakimov, M., Terwilliger, T. C., Urzhumtsev, A., Zwart, P. H., and Adams, P. D. (2012) Towards automated crystallographic structure refinement with phenix.refine. *Acta Crystallogr., Sect. D: Biol. Crystallogr.* 68 (Pt4), 352–67.
78. Emsley, P., Lohkamp, B., Scott, W. G., and Cowtan, K. (2010) Features and development of Coot. *Acta Crystallogr., Sect. D: Biol. Crystallogr.* 66 (Pt4), 486–501.
79. Moriarty, N. W., Grosse-Kunstleve, R. W., and Adams, P. D. (2009) electronic Ligand Builder and Optimization Workbench (eLBOW): a tool for ligand coordinate and restraint generation. *Acta Crystallogr., Sect. D: Biol. Crystallogr.* 65 (Pt10), 1074–80.
80. Davis, I. W., Leaver-Fay, A., Chen, V. B., Block, J. N., Kapral, G. J., Wang, X., Murray, L. W., Arendall, W. B., 3rd, Snoeyink, J., Richardson, J. S., and Richardson, D. C. (2007) MolProbity: all-atom contacts and structure validation for proteins and nucleic acids. *Nucleic Acids Res.* 35, W375–W383.
81. Terwilliger, T. C., Grosse-Kunstleve, R. W., Afonine, P. V., Moriarty, N. W., Adams, P. D., Read, R. J., Zwart, P. H., and Hung, L. W. (2008) Iterative-build OMIT maps: map improvement by iterative model building and refinement without model bias. *Acta Crystallogr., Sect. D: Biol. Crystallogr.* 64 (Pt5), 515–24.

Electronic Supporting Information:

Crystallographic Data

Table 3-4. Crystallographic data collection and refinement statistics.

	KPC-2 compound 3	KPC-2 compound 6	CTX-M-14 compound 3	CTX-M-14 compound 6
Data collection				
Space group	<i>P22₁2₁</i>	<i>P22₁2₁</i>	<i>P2₁</i>	<i>P2₁</i>
Cell dimensions				
<i>a</i> , <i>b</i> , <i>c</i> (Å)	56.743, 59.244, 76.277	56.347 59.768, 77.094	45.202, 106.878, 47.781	45.34, 107.185, 47.881
α , β , γ (°)	90.00, 90.00, 90.00	90.00, 90.00, 90.00	90.00, 101.89, 90.00	90.00, 101.335, 90.00
Resolution (Å)	27.92 - 1.70 (1.76 - 1.70)	47.24 - 2.20 (2.28 - 2.20)	23.38 - 1.40 (1.45 - 1.40)	21.76 - 1.40 (1.45 - 1.40)
<i>R</i> _{merge}	0.039	0.101	0.031	0.028
<i>I</i> / σ (<i>I</i>)	51.53 (4.56)	12.11 (2.53)	48.91 (26.70)	49.92 (30.62)
Completeness (%)	99.75 (98.66)	98.20 (93.31)	98.83 (96.75)	98.76 (99.40)
Refinement				
Resolution (Å)	27.92 - 1.70	47.24 - 2.20	23.38 - 1.40	21.76 - 1.40
No. reflections/free	28848 (2799)	13501 (1257)	86581 (8466)	86966 (8769)
<i>R</i> _{work} / <i>R</i> _{free}	0.1802/0.2120	0.2259/0.2780	0.1478/0.1696	0.1494/0.1784
No. of atoms				
Protein	2020	1986	4060	4022
Ligand	76	66	65	120
Water	152	20	726	722
<i>B</i> -factors (Å ²)				
Protein	26.75	45.59	9.15	9.93
Ligand	36.80	59.42	10.46	21.66
Water	36.96	40.03	21.27	22.85
R.m.s. deviations				
Bond lengths (Å)	0.007	0.003	0.006	0.006
Bond angles (°)	1.20	0.65	1.25	1.23

	KPC-2 compound 7	KPC-2 compound 9	NDM-1 compound 7	NDM-1 compound 9
Data collection				
Space group	<i>P22₁2₁</i>	<i>P22₁2₁</i>	<i>P2₁</i>	<i>P2₁</i>
Cell dimensions				
<i>a, b, c</i> (Å)	57.112 58.445, 74.563	56.05, 59.86, 77.041	41.68, 58.87, 42.03	41.98, 58.77, 41.98
α, β, γ (°)	90.00, 90.00, 90.00	90.00, 90.00, 90.00	90.00, 98.17, 90.00	90.00, 97.48, 90.00
Resolution (Å)	31.43 - 1.86 (1.92 - 1.86)	32.39 - 1.42 (1.471 - 1.42)	33.98 - 1.15 (1.21 - 1.15)	33.97-1.65 (1.774-1.65)
<i>R</i> _{merge}	0.080	0.040	0.061	0.101
<i>I</i> / $\sigma(I)$	18.06 (2.66)	40.54 (2.11)	7.4 (2.0)	9.2 (3.6)
Completeness (%)	99.57 (97.79)	99.69 (98.45)	97.6(96.7)	90.96 (81.21)
Refinement				
Resolution (Å)	31.43 - 1.86	32.39 - 1.42	27.86 - 1.15	33.97-1.65
No. reflections/free	21576 (2077)	49527 (4834)	69465 (6837)	22259 (1989)
<i>R</i> _{work} / <i>R</i> _{free}	0.2277/ 0.2770	0.1590/0.1883	0.1669/ 0.1937	0.1904/0.2313
No. of atoms				
Protein	2004	1991	1731	1710
Ligand	31	66	27	24
Water	92	110	300	130
<i>B</i> -factors (Å ²)				
Protein	26.14	29.31	12.39	15.81
Ligand	28.54	49.39	12.49	23.88
Water	26.97	40.58	29.38	20.80
R.m.s. deviations				
Bond lengths (Å)	0.003	0.006	0.005	0.006
Bond angles (°)	0.57	1.21	1.18	1.14

* Data was collected from a single crystal for each structure. Values in parenthesis are for the highest-resolution shell.

Supplementary Figures

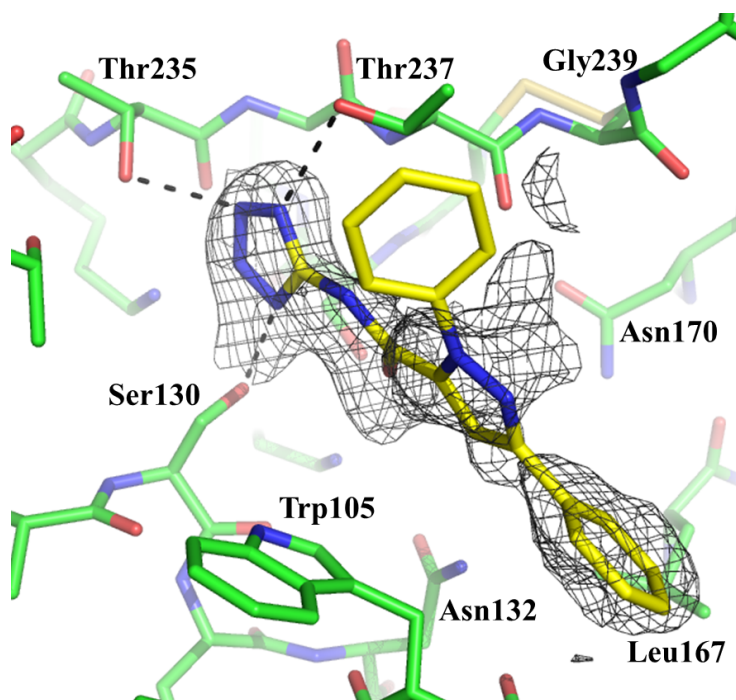


Figure 3-4. Complex crystal structure of compound 7s with KPC-2. The simulated annealing composite $F_o - F_c$ omit map (gray) contoured at 1.5σ for compound 7s with KPC-2. Black dashed lines depict hydrogen bonds.

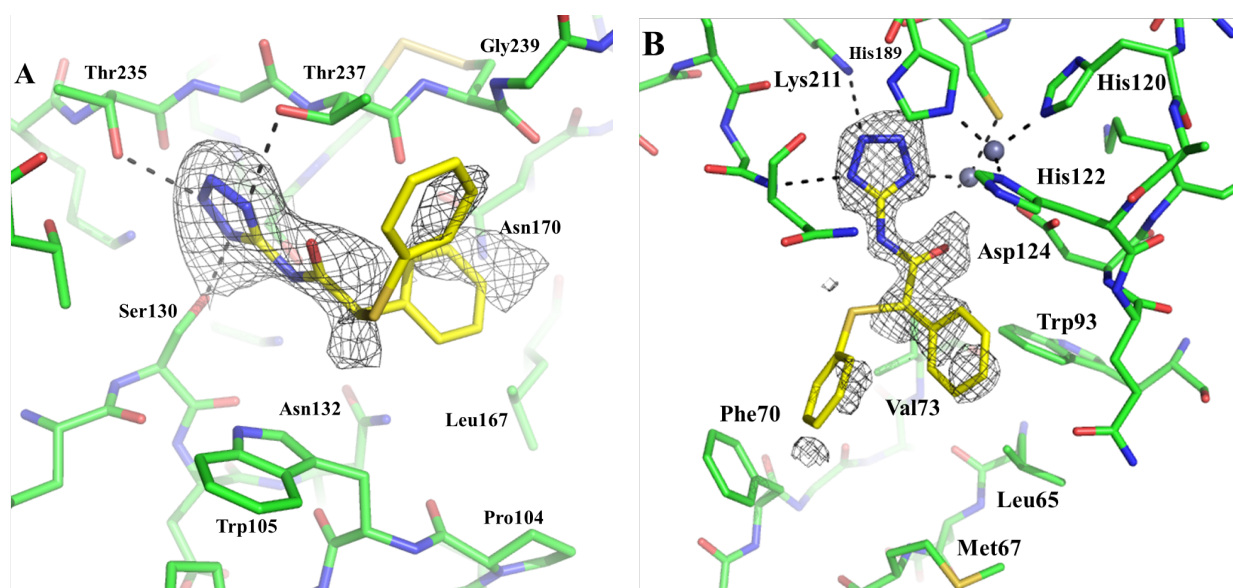


Figure 3-5. Complex crystal structure of compound 8 with KPC-2 and NDM-1. The simulated annealing composite $F_o - F_c$ omit map (gray) contoured at 2.0σ for both KPC-2 (A) and NDM-1 (B). Black dashed lines depict hydrogen bonds or coordination with metal ions.

Synthetic Procedures

General Procedures: Reactions were magnetically stirred unless otherwise indicated. Air and/or moisture sensitive reactions were carried out under an argon atmosphere in oven-dried glassware using anhydrous solvents from commercial suppliers. Air and/or moisture sensitive reagents were transferred via syringe or cannula and were introduced into reaction vessels through rubber septa. All anhydrous solvents used were purchased from Sigma-Aldrich and used without further purification. Solvents to be employed in flash column chromatography and reaction work-up procedures were purchased from either Sigma-Aldrich or Fisher Scientific. All other reagents were obtained commercially and used without further purification, unless otherwise stated. Reactions were monitored using LCMS and thin layer chromatography (TLC) performed on 0.25-mm EMD pre-coated glass-backed silica gel 60 F-254 plates. Compounds were visualized under UV light or through staining with permanganate. Reaction product solutions and chromatography fractions were concentrated by rotary evaporation at 30 °C at 20 Torr, then Hi-Vac at 0.5 Torr overnight, unless otherwise indicated.

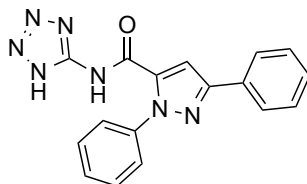
Instrumentation: NMR spectra were recorded on a Bruker AvanceIII HD 400 MHz spectrometer (with 5 mm BBFO Z-gradient Smart Probe) calibrated to CH(D)Cl₃ as an internal reference (7.26 and 77.00 ppm for ¹H and ¹³C NMR spectra, respectively). Data for ¹H NMR spectra are reported in terms of chemical shift (δ, ppm), multiplicity, coupling constant (Hz), and integration. Data for ¹³C NMR spectra are reported in terms of chemical shift (δ, ppm). The following abbreviations are used to denote the multiplicities: s = singlet; d = doublet; dd = doublet of doublets; dt = doublet of triplets;

dq = doublet of quartets; ddd = doublet of doublet of doublets; t = triplet; td = triplet of doublets; tt = triplet of triplets; q = quartet; qd = quartet of doublets; quin = quintet; sex = sextet; m = multiplet. LCMS and compound purity were determined using a Waters Micromass ZQ 4000, equipped with a Waters 2795 Separation Module, Waters 2996 Photodiode Array Detector, and a Waters 2424 ELSD. Separations were carried out with an XBridge BEH C18, 5 μ m, 4.6 x 20 mm column, at ambient temperature (unregulated) using a mobile phase of water-methanol containing a constant 0.1% formic acid. HPLC was performed on a Waters 2535 Separation Module with a Waters 2998 Photodiode Array Detector. Separations were carried out with an XBridge BEH C18, 5 μ m, 19 x 50 mm column, at ambient temperature (unregulated) using a mobile phase of water-methanol containing a constant 0.05% formic acid.

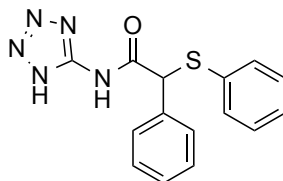
General Procedure A: A vial is charged with the appropriate carboxylic acid (1.0 equiv), DMF, and *N,N'*-diisopropylethylamine (1.0 equiv). HATU (1.05 equiv) is then added, and the reaction mixture is allowed to stir for 10 minutes. 5-aminotetrazole monohydrate (1.1 equiv) and *N,N'*-diisopropylethylamine (1.1 equiv) are subsequently added, and the reaction is stirred at room temperature for 24 h or until judged complete by LCMS. The crude reaction mixture is directly purified by reverse phase HPLC (water/MeOH/0.05% formic acid) to afford the desired product.

General Procedure B: An oven-dried flask is charged with the appropriate carboxylic acid (1.0 equiv), CH₂Cl₂ (305 equiv), and DMF (20 drops). Oxalyl chloride (1.1 equiv) is subsequently added dropwise, and the reaction is stirred at room temperature for 3 h.

Separately, 5-aminotetrazole monohydrate (2.0 equiv) is suspended in CH₂Cl₂ (305 equiv) and *N,N'*-diisopropylethylamine (3.0 equiv) in an oven-dried flask. The aforementioned oxalyl chloride solution is then added dropwise to this solution, followed by a 2.0 mL CH₂Cl₂ rinse of the parent flask. The reaction suspension is stirred at room temperature for 24 h or until judged complete by LCMS. The reaction mixture is concentrated under reduced pressure, taken up in DMF, and purified by reverse phase HPLC (water/MeOH/0.05% formic acid) to afford the desired product.

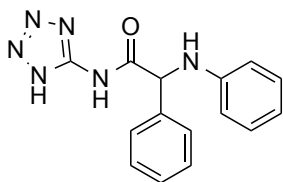


1,3-Diphenyl-N-(1*H*-tetrazol-5-yl)-1*H*-pyrazole-5-carboxamide (7s*). Commercially available 2,5-diphenyl-2*H*-pyrazole-3-carboxylic acid (50 mg, 0.189 mmol, 1.0 equiv) was reacted with 5-aminotetrazole monohydrate in DMF (1.0 mL) according to general procedure A to afford **7s*** (25.0 mg, 40%) as a white solid. ¹H NMR (400 MHz, DMSO-d₆) δ = 12.27 (br s, 1H), 7.72 - 7.11 (m, 11H); ¹³C NMR (100 MHz, DMSO-d₆) δ = 160.45, 145.25, 145.17, 139.57, 129.70, 129.47, 129.31, 129.21, 129.17, 126.08, 109.26; LRMS (ESI) calculated for C₁₇H₁₄N₇O [M + H]⁺ m/z 332.11, found 332.08.

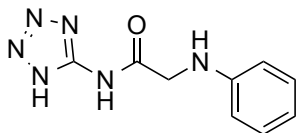


2-Phenyl-2-(phenylthio)-N-(1*H*-tetrazol-5-yl)acetamide (8*). Commercially available 2-phenyl-2-(phenylsulfanyl)acetic acid (100 mg, 0.409 mmol, 1.0 equiv) was reacted

with 5-aminotetrazole monohydrate according to general procedure B to afford **8*** (70 mg, 55%) as a white solid. ^1H NMR (400 MHz, DMSO- d_6) δ = 8.20 (s, 0.2H), 7.56 (br d, J = 6.8 Hz, 2H), 7.47 - 7.19 (m, 8H), 5.50 (s, 1H); ^{13}C NMR (100 MHz, DMSO- d_6) δ = 168.61, 151.34, 136.35, 134.18, 131.19, 129.69, 129.17, 128.86, 128.01, 55.58; LRMS (ESI) calculated for $\text{C}_{15}\text{H}_{14}\text{N}_5\text{OS}$ $[\text{M} + \text{H}]^+$ m/z 312.08, found 312.02.

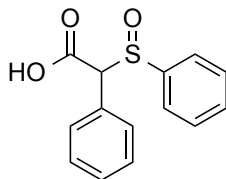


2-Phenyl-2-(phenylamino)-N-(1H-tetrazol-5-yl)acetamide (9). Commercially available anilino(phenyl)acetic acid (50 mg, 0.220 mmol, 1.0 eq) was reacted with 5-aminotetrazole monohydrate in DMF (2.5 mL) according to general procedure A to afford **9** (12.6 mg, 20%) as a white solid. ^1H NMR (400 MHz, CD_3OD) δ = 7.59 (br s, 2H), 7.49 - 7.28 (m, 3H), 7.13 (br t, J = 7.3 Hz, 2H), 6.82 - 6.63 (m, 3H), 5.22 (br s, 1H); ^{13}C NMR (100 MHz, CD_3OD) δ = 171.73, 161.72, 146.78, 137.62, 128.73, 128.56, 128.18, 127.39, 118.00, 113.44, 62.46; LRMS (ESI) calculated for $\text{C}_{15}\text{H}_{15}\text{N}_6\text{O}$ $[\text{M} + \text{H}]^+$ m/z 295.12, found 294.88.

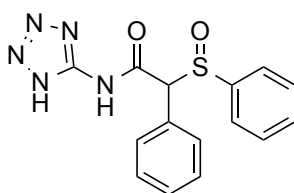


2-(Phenylamino)-N-(1H-tetrazol-5-yl)acetamide (10). Commercially available phenyl glycine (50 mg, 0.331 mmol, 1.0 equiv) was reacted with 5-aminotetrazole monohydrate in DMF (2.5 mL) according to general procedure A to afford **10** (7.1 mg, 10%). ^1H NMR (400 MHz, CD_3OD , drops DMSO- d_6) δ = 8.27 (s, 0.2H), 7.18 (br t, J = 7.5 Hz, 2H), 6.76

- 6.65 (m, 3H), 4.06 (s, 2H); LRMS (ESI) calculated for C₉H₁₁N₆O [M + H]⁺ m/z 219.09, found 218.97.

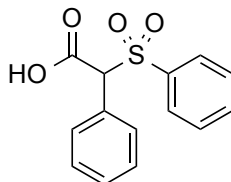


2-Phenyl-2-(phenylsulfinyl)acetic acid (S1). Commercially available 2-phenyl-2-(phenylsulfonyl)acetic acid (150 mg, 0.614 mmol, 1.0 equiv) was dissolved in MeOH (4.0 mL) in a glass vial. A solution of potassium monopersulfate (217 mg, 1.3 mmol, 2.1 equiv) in H₂O (1.0 mL) was then added dropwise, followed by a H₂O (0.5 mL) rinse of the vessel. The reaction suspension was stirred at room temperature for 2 h, and then concentrated under reduced pressure. The residue was suspended with ~ 3 mL cold water, filtered, washed with cold H₂O and hexanes, and dried under vacuum overnight. Semi-crude **S1** (155.2 mg) was used without further purification. LRMS (ESI) calculated for C₁₄H₁₃O₃S [M + H]⁺ m/z 261.05, found 260.87.

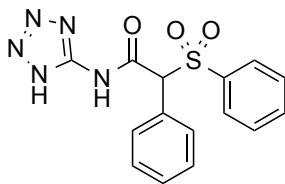


2-Phenyl-2-(phenylsulfinyl)-N-(1H-tetrazol-5-yl)acetamide (11). **S1** (97 mg, 0.374 mmol, 1.0 equiv) was reacted with 5-aminotetrazole monohydrate in DMF (2.5 mL) according to general procedure A to afford **11** (8.5 mg, 7%) as a white solid. **Note:** While the diastereomers are separable by HPLC, they interconvert on a day's timescale; the diastereomeric mixture was tested in the biochemical assay. ¹H NMR

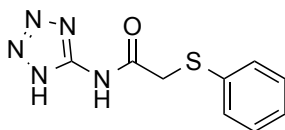
(400 MHz, CD₃OD, drops DMSO-d₆) δ = 8.45 (br s, 1H), 7.79 - 7.67 (m, 0.5H), 7.66 - 7.05 (m, 9.5H), 5.06 (br s, 0.5H), 4.99 (br s, 0.5H); LRMS (ESI) calculated for C₁₅H₁₄N₅O₂S [M + H]⁺ m/z 328.08, found 327.83.



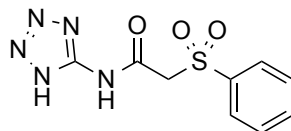
2-Phenyl-2-(phenylsulfonyl)acetic acid (S2). Commercially available 2-phenyl-2-(phenylsulfonyl)acetic acid (150 mg, 0.614 mmol, 1.0 equiv) was dissolved in MeOH (5.0 mL) in a glass vial. A solution of potassium monopersulfate (867 mg, 5.16 mmol, 8.4 equiv) in H₂O (4.0 mL) was then added dropwise at room temperature. The reaction suspension was stirred for 72 h, and then concentrated under reduced pressure. The slurry was suspended with ~ 10 mL cold water, filtered, washed with 3 x 10 mL cold H₂O and 10 mL hexanes, and dried under vacuum overnight. Semi-crude **S2** (146.1 mg) was used without further purification. **Note:** This intermediate was prone to spontaneous decarboxylation while in solution; appeared to be bench stable when dry. ¹H NMR (400 MHz, CD₃OD) δ = 7.72 - 7.64 (m, 3H), 7.54 - 7.47 (m, 2H), 7.43 - 7.36 (m, 3H), 7.34 - 7.28 (m, 2H), 5.39 (s, 1H); ¹³C NMR (100 MHz, CD₃OD) δ = 166.28, 137.06, 133.91, 130.21, 129.37, 129.15, 128.65, 128.43, 128.07, 74.39.



2-Phenyl-2-(phenylsulfonyl)-N-(1H-tetrazol-5-yl)acetamide (12). **S2** (30 mg, 0.109 mmol, 1.0 equiv) was reacted with 5-aminotetrazole monohydrate according to general procedure B, but with 5 mL CH₂Cl₂ (718 equiv) in each vessel. **12** (19.4 mg, 52%) obtained as a white solid. ¹H NMR (400 MHz, CD₃OD) δ = 8.33 (s, 0.4H), 7.71 - 7.64 (m, 3H), 7.54 - 7.45 (m, 4H), 7.39 (t, *J* = 7.3 Hz, 1H), 7.35 - 7.27 (m, 2H); ¹³C NMR (100 MHz, CD₃OD) δ = 162.63, 154.56, 136.78, 134.10, 130.29, 129.44, 129.31, 128.54, 128.39, 128.08, 100.00; LRMS (ESI) calculated for C₁₅H₁₄N₅O₃S [M + H]⁺ *m/z* 344.07, found 343.86.



2-(Phenylthio)-N-(1H-tetrazol-5-yl)acetamide (13). Commercially available 2-(phenylthio)acetic acid (100 mg, 0.499 mmol, 1.0 eq) was reacted with 5-aminotetrazole monohydrate in DMF (2.5 mL) according to general procedure A to afford **13** (18.0 mg, 13%). ¹H NMR (400 MHz, DMSO-*d*₆) δ = 8.16 (s, 0.3H), 7.41 (d, *J* = 7.5 Hz, 2H), 7.33 (br t, *J* = 7.5 Hz, 2H), 7.21 (t, *J* = 7.3 Hz, 1H), 3.95 (s, 2H); ¹³C NMR (100 MHz, DMSO-*d*₆) δ = 167.69, 163.61, 135.92, 129.53, 128.69, 126.65, 36.82; LRMS (ESI) calculated for C₉H₁₀N₅OS [M + H]⁺ *m/z* 236.05, found 235.82.



2-(Phenylsulfonyl)-N-(1*H*-tetrazol-5-yl)acetamide (14). Commercially available 2-(phenylsulfonyl)acetic acid (40 mg, 0.200 mmol, 1.0 equiv) was reacted with 5-aminotetrazole monohydrate according to general procedure B, but with 5 mL CH₂Cl₂ (390 equiv) in each vessel. **14** (12.2 mg, 23%) obtained as a white solid. ¹H NMR (400 MHz, DMSO-d₆) δ = 8.15 (s, 0.5H), 7.92 (d, *J* = 7.5 Hz, 2H), 7.76 (t, *J* = 7.3 Hz, 1H), 7.66 (t, *J* = 7.7 Hz, 2H), 4.58 (s, 2H); ¹³C NMR (100 MHz, DMSO-d₆) δ = 163.59, 160.11, 139.71, 134.57, 129.75, 128.53, 61.37; LRMS (ESI) calculated for C₉H₁₀N₅O₃S [M + H]⁺ m/z 268.04, found 267.78.

Chapter 4

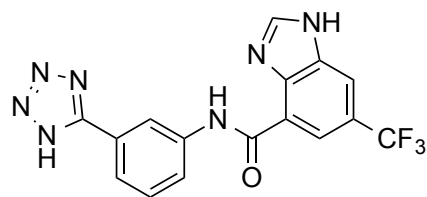
Targeting the Conserved Hydrophobic Shelf for Carbapenemase KPC-2

Kyle DeFrees, Afroza Akhtar, Xiujun Zhang, Derek Nichols, Erica Cambeis,

Yu Chen, and Adam R. Renslo

Identification of New Inhibitor Chemotypes:

We have previously used structure-based fragment screening to identify the first nM non-covalent serine β -lactamase inhibitors, resulting in compound **1**, an 85 nM inhibitor of CTX-M.¹ We found that the tetrazole of **1** displays high shape and electrostatic complementarity with the active site pocket that binds to the β -lactam C3(4)-carboxylate group. Given this sites conservation across Class A β -lactamases, we hypothesized that permutations of the tetrazole scaffold may be well suited to inhibit the carbapenemase KPC-2. As seen in the superimposition of KPC-2 with the CTX-M complex of **1** (**Figure 4-1**), KPC-2 harbors several important structural differences. While the C3(4)-carboxylate binding site is well conserved with a S237T mutation, G238C and a structural disulfide results in a twisted β 3 strand, putting G239 in direct steric clash with the benzimidazole of **1**. While the hydrophobic sub pocket near the CF₃ is conserved with P167L, a key hydrogen bond to the amide is lost with a N104P mutation. Notably, the Tyr105 hydrophobic shelf, which remains untargeted by the original scaffold, is maintained as Trp105 in KPC-2. Based off of these similarities, we hypothesized that analogs targeting this conserved shelf may be able to inhibit both CTX-M and KPC-2.



1

CTX-M-14 $K_i = 85$ nM

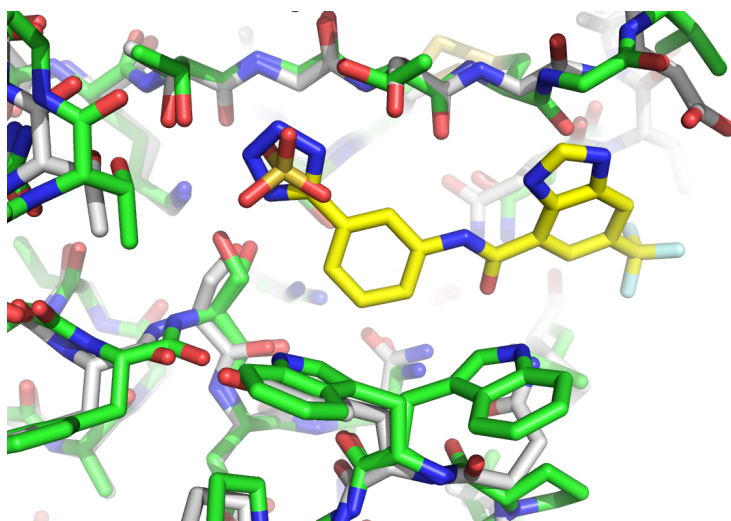
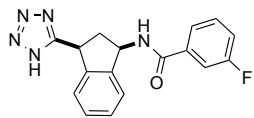
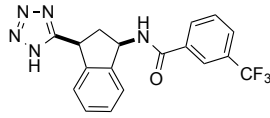
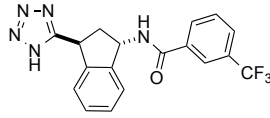
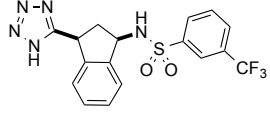
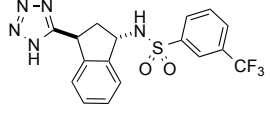


Figure 4-1. Compound 1 complex with CTX-M-9 superimposed onto an apo KPC-2 structure. CTX-M: white and yellow, PDB code 4UA7; KPC-2: green, PDB code 5UL8.

In order to better meet the steric requirements of the twisted β 3 strand, we synthesized a panel of indane-type analogs with a simple aryl component (**Table 4-1**). Using a nitrocefin biochemical assay, we found that 3-fluoro-aryl *syn* diastereomer **2** displayed modest CTX-M activity, but no detectable KPC-2 activity. Gratifyingly, *syn* CF_3 analog **3** improved CTX-M activity 5-fold, in line with the original SAR for CTX-M, and displayed detectable KPC-2 activity. As expected, *anti* diastereomer **4** displayed no observable activity for either enzyme. Crystallography with the more soluble **2** revealed the expected binding mode with CTX-M (**Figure 4-2A**); the indane is well positioned over the Tyr105 surface, with the aryl-amide portion binding in the same orientation as the original scaffold. Surprisingly, soaks of **2** with KPC-2 revealed an suboptimal binding orientation with the unexpected enantiomer of the *syn* diastereomer (**Figure 4-2B**);

instead of binding down the pocket, the indane scaffold sat over the Trp105 shelf and out into solvent. While this result could be attributed to the weak affinity of **2** towards KPC-2, we thought steric clash with G239 was driving the suboptimal binding mode, and sought to allow more aryl flexibility by synthesizing the sp³ sulfonamides **5** and **6**. *Syn* **5** did not improve KPC-2 activity over amide **3**, and *anti* **6** retained similar activity to **5**, suggesting that the indane scaffold was binding in an unproductive manner across all analogs.

Table 4-1. Biochemical activities of indanes 2-6.^a

		CTX-M-14 K_i^b (μ M)	KPC-2 K_i^b (μ M)
2		176	> 800
3		37	386
4		> 1500	> 800
5		> 1500	~ 270 ^c
6		> 1500	~ 460 ^c

^a Relative stereochemistry indicated as the *syn* or *anti* diastereomers. ^b Calculated from IC₅₀ using $K_i = IC_{50}/(1 + [S]/K_m)$. K_m values were measured the day of the experiment. IC₅₀ values were fit from a technical triplicate with a SE < 1.1 μ M. ^c Compound also displayed partial inhibition, see ESI for curves.

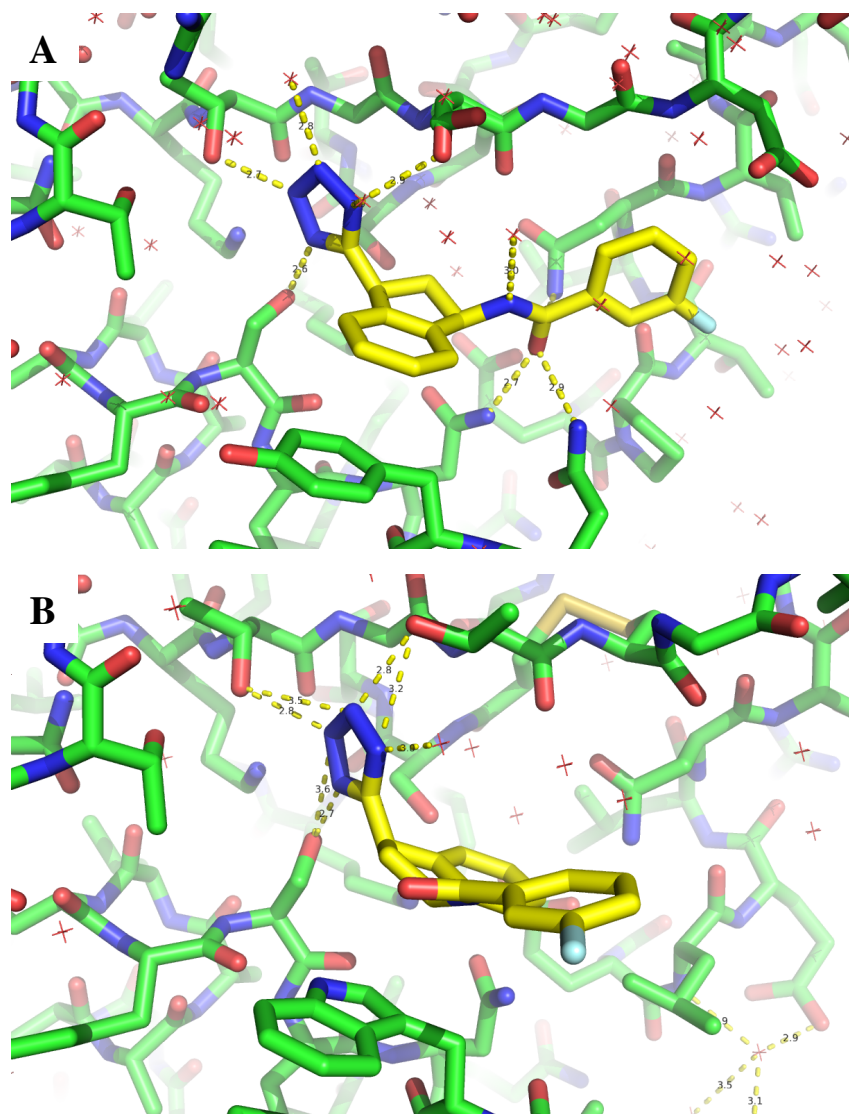
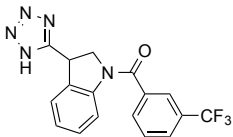
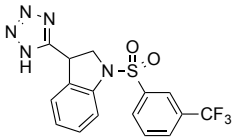
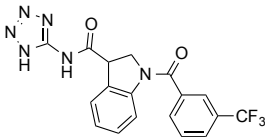
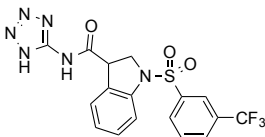
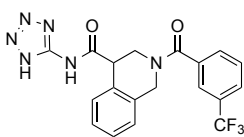
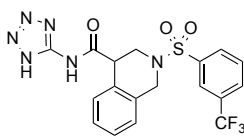


Figure 4-2. Crystal structures reveal binding mode of indane 2 to CTX-M-9 and KPC-2. (A) CTX-M-9. (B) KPC-2. Water molecules are shown as red hashes. Yellow dashes represent putative hydrogen bonds.

Given these results, it appeared larger changes were required for optimal KPC-2 inhibition. We hypothesized that pulling the amide in by one atom, to form an indoline, would help alleviate potential steric clashes with the β_3 twist. Docking of indoline 7 appeared to give putative binding modes where the indoline stacked against the G239 twist (ESI, Figure 4-6), so analogs 7 and 8 were synthesized. These analogs showed no detectable CTX-M activity, and like the indane, had minimal differences between

amide **7** and sulfonamide **8** (**Table 4-2**). Crystallography of **7** with KPC-2 revealed a similar binding mode to **2** (**Figure 4-3A**); the aryl-CF₃ stacked over Trp105 and out of the active site. When compared to the indane bound CTX-M (**Figure 4-2A**), the tetrazole of **7** appeared to bind at a slight angle, which may be a result of the preferred threonine conformation in KPC-2. With this angle in mind, we also docked amide-spaced tetrazole **9** (**Figure 4-3B**), which packed nicely against the β 3 twist, with additional H-bonding to Asp132 and hydrophobic interactions with Leu167. Biochemical testing of **9** and sulfonamide **10** revealed similar inhibition patterns however, with no detectable CTX-M activity, and no major differences in KPC-2 activity (**Table 4-2**). Docking with the more flexible tetrahydroisoquinoline **11** was uninspiring (**ESI, Figure 4-6**), and while amide **11** and sulfonamide **12** showed the best KPC-2 activity, the lack of difference between the *sp*² amide and *sp*³ sulfonamide suggested unproductive binding modes.

Table 4-2. Biochemical activities of analogs 7-12.^a

		CTX-M-14 K_i^b (μM)	KPC-2 K_i^b (μM)
7		> 1500	912
8		> 1500	530 ^b
9		> 1500	710
10		~ 1500	~ 350
11		1300	348
12		> 1500	249

^a All compounds are racemates. ^b Calculated from IC_{50} using $K_i = \text{IC}_{50}/(1 + [\text{S}]/K_m)$. K_m values were measured the day of the experiment. IC_{50} values were fit from a technical triplicate with a SE < 1.1 μM . ^c Compound also displayed partial inhibition, see ESI for curves.

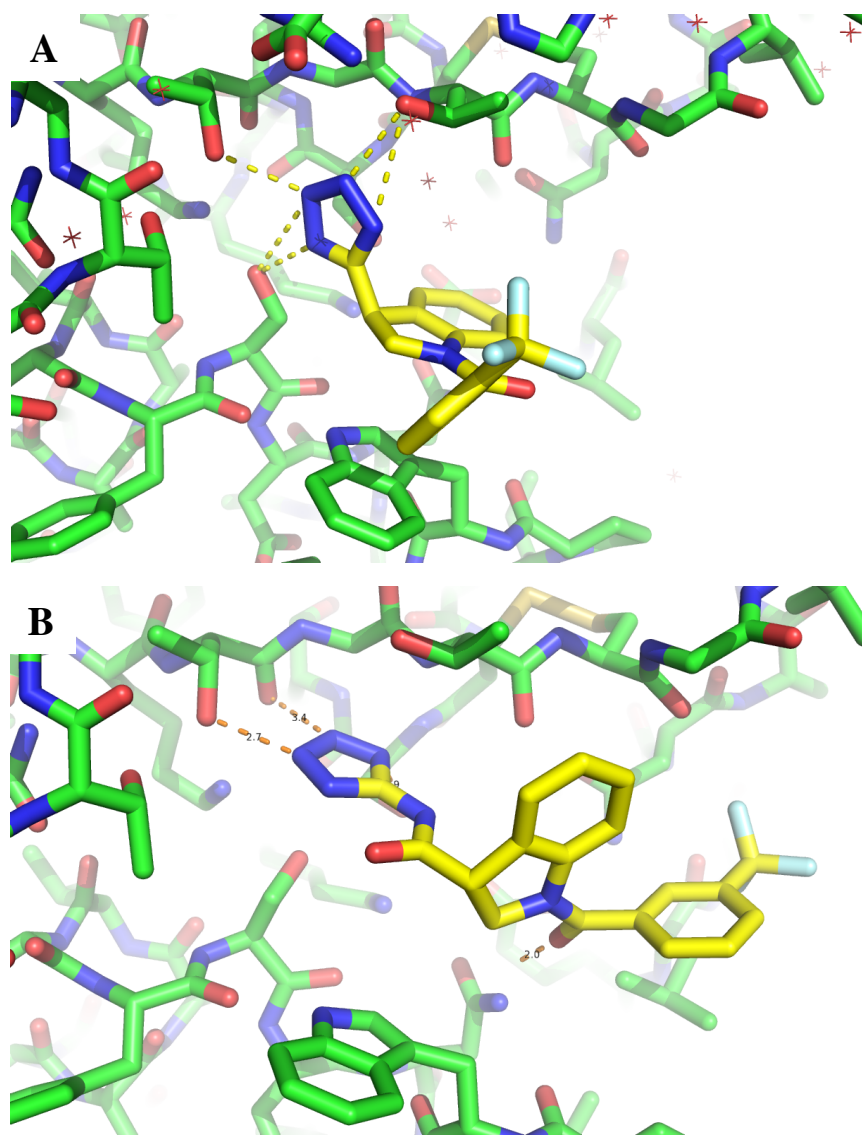
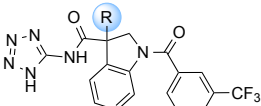


Figure 4-3. Crystal structure of indoline 7 with KPC-2; docking pose of indoline 9 with KPC-2. (A) Compound **7** bound to KPC-2. (B) Selected docking pose of compound **9** with KPC-2. Water molecules are shown as red dashes. Yellow dashed lines represent putative hydrogen bonds.

Attempts to gain structural insight into these analogs were unsuccessful, but the putative docking pose of **9** suggested an opportunity to build interactions towards the conserved hydrophobic shelf, so a few α -modified amido-tetrazole indolines were synthesized (**Table 4-3**). While smaller modifications like methyl **13** or phenyl **14** were not expected to fully reach the shelf, benzyl **15** began to pick up moderate KPC-2

activity. Surprisingly, NHBoc **16**, which was originally intended as a synthetic intermediate for further derivatization, showed the best activity with a 51 μM K_i against KPC-2, while amine **17** had no detectable activity. While our hypothesis was based on the putative pose of **9**, we were able to get a structure of **16** in complex with KPC-2, which revealed an unexpected binding mode (**Figure 4-4**). Instead of stacking over the Trp105 hydrophobic shelf, the NHBoc bound down the channel, pointing a carbonyl towards the oxyanion hole with a hydrogen bond to ordered water, and the tert-butyl packed over Leu167. The aryl- CF_3 surprisingly displaced the Trp105 shelf, packing over Pro107 and forcing the Trp into an alternate conformation where it engaged in a hydrophobic and π -offset interaction with the indoline core.

Table 4-3. Biochemical activities of analogs 13-17.^a

		CTX-M-14 K_i^b (μM)	KPC-2 K_i^b (μM)
9	H	> 1500	710
13	Me	> 850	~ 750
14	Ph	> 1500	634
15	Bn	> 1500	166
16	NHBoc	> 750	51
17	NH_2	> 1500	> 800

^a All compounds are racemates. ^b Calculated from IC_{50} using $K_i = IC_{50}/(1 + [S]/K_m)$. K_m values were measured the day of the experiment. IC_{50} values were fit from a technical triplicate with a SE < 1.1 μ M.

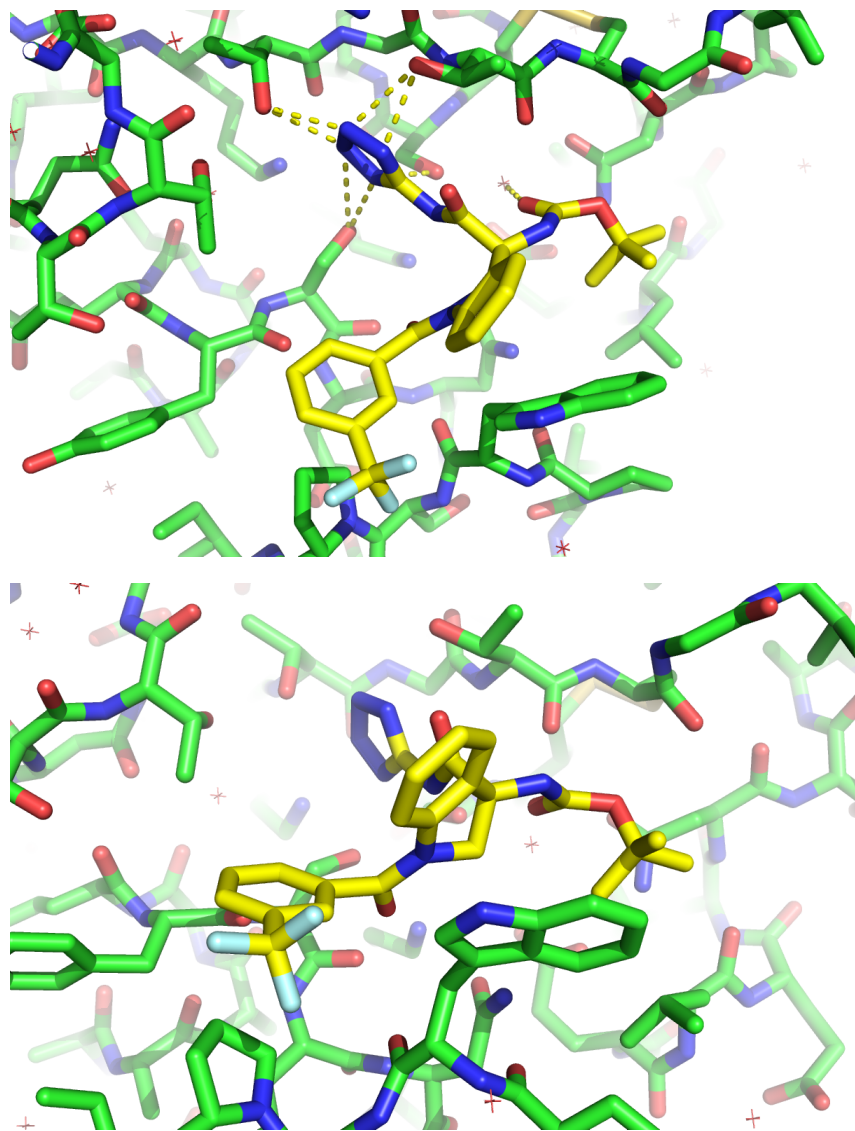
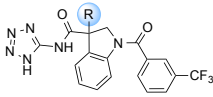
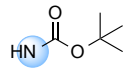
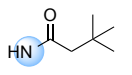
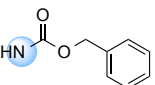
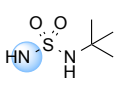
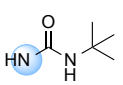
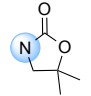
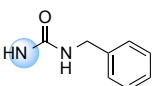
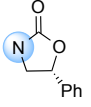
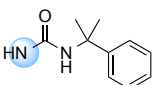
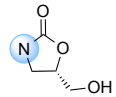
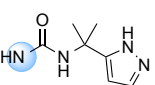
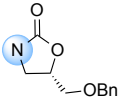


Figure 4-4. Crystal structure reveals the binding mode of indoline 16 to KPC-2. Top and side views. Water molecules are shown as red hashes. Yellow dashed lines represent putative hydrogen bonds.

Exploring KPC-2 Specific Interactions:

Given the activity and binding mode of **16**, we sought to further probe the role of the NHBoc by making a small series of derivatives (**Table 4-4**). Changing from the tightly packed t-butyl of **16** to the more open benzyl of **18** resulted in a 3-fold reduction in activity. Surprisingly, changing from a t-butyl carbamate to the t-butyl-urea of **19** or benzyl-urea of **20** was not well tolerated, and building further down the channel with cumyl **21** or gemdimethyl pyrazole **22** were not sufficient to compensate for the disfavored urea. The analogous carbamates of **21** and **22** could not be synthesized due to synthetic instability, with the carbamate preferring to engage in elimination. Changing to the butyric amide **23** was better tolerated with a 3-fold loss in activity, which was similar to the t-butyl sulfamate **24**. Given the bias towards carbamates, a few oxazolidinones were also synthesized to see if conformational restriction would offer any additional benefit. Unfortunately, gem-dimethyl oxazolidinone **25** was not tolerated, and phenyl analog **26** had a 4-fold reduction in activity, with analogs **27** and **28** showing no detectable activity. These results suggest that the carbamate is uniquely suited for binding at the G239 twist; modification disturbs the t-butyl anchoring on Leu167, which in turn destabilizes the Trp105 stack.

Table 4-4. Biochemical activities of indoline analogs 18-28.^a

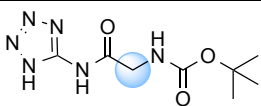



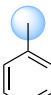
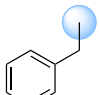

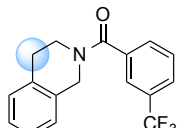
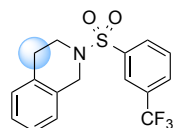
		CTX-M-14 K_i^b (μM)	KPC-2 K_i^b (μM)			CTX-M-14 K_i^b (μM)	KPC-2 K_i^b (μM)
16		> 750	51	23		> 300	136
18		> 1500	174	24		> 450	161
19		> 600	> 400	25		> 600	> 400
20		> 600	> 400	26		> 600	188
21		> 600	> 400	27		> 600	> 400
22		> 600	> 400	28		> 750	> 400

^a All compounds are racemates at the indoline stereocenter. ^b Calculated from IC_{50} using $K_i = \text{IC}_{50}/(1 + [\text{S}]/K_m)$. K_m values were measured the day of the experiment. IC_{50} values were fit from a technical triplicate with a SE < 1.1 μM .

Since initial attempts to replace or modify the t-butyl carbamate were not successful, we instead sought to explore the aryl- CF_3 and indoline core. Complete replacements via hydrophobic amino acid and amino acid-like amido-tetrazoles **29-34** were not tolerated (Table 4-5), and modification to the analogous tetrahydroisoquinolines **35** and **36** were also not tolerated, suggesting that the indoline core has important specific interactions. A series of truncations were devised to look at the contributions of individual components (Table 4-6). Notably, removing the sp^2 amide of **16** to give benzylic **37**

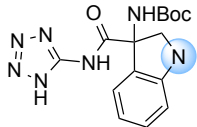
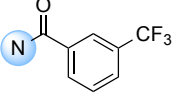
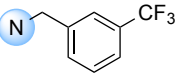
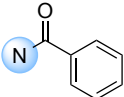
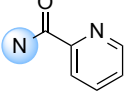
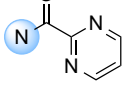
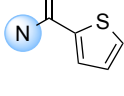
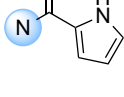
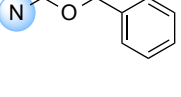
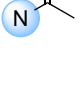
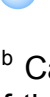
accounts for a > 10 fold decrease in activity (tested to solubility limits). Removing the CF₃ (**38**) accounts for a 4-fold decrease in activity, where introducing a pyridine (**39**) or pyrimidine (**40**), which should improve rotation around the amide, resulted in a further 3-fold loss in activity (12-fold from parent). Analogs with a 2-thiophene (**41**) or 2-pyrrole (**42**) were equivalent to the phenyl **38**, along with benzyl carbamate **43**. Further truncations to the acetyl (**44**) or amine (**45**) gave a 12-fold loss in activity, roughly equivalent to the pyridine or pyrimidine analogs. Taken together, these results suggest that significant interaction energy is coming from the stabilization of the *sp*² amide interacting with the offset Trp105 shelf (**Figure 4-4**), with the aryl-CF₃ serving as a hydrophobic “lever arm” to stabilize the overall bound complex.

Table 4-5. Biochemical activities of analogs 29-36.^a

		CTX-M-14 K_i^b (μM)	KPC-2 K_i^b (μM)
29		> 1500	> 800
30		> 1500	> 800
31		> 1500	> 800
32		> 1500	> 800
33		> 750	> 400
34		> 1500	> 800
35		> 1500	713
36		> 1500	> 800

^a All compounds are racemates (as applicable). ^b Calculated from IC_{50} using $K_i = IC_{50}/(1 + [S]/K_m)$. K_m values were measured the day of the experiment. IC_{50} values were fit from a technical triplicate with a SE < 1.1 μM .

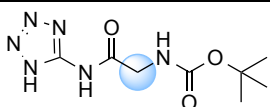
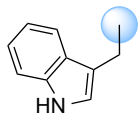
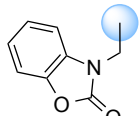
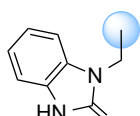
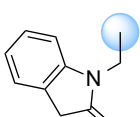
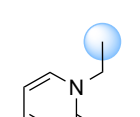
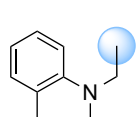
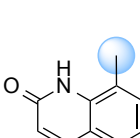
Table 4-6. Biochemical activities of analogs 37-45.^a

		CTX-M-14 K_i^b (μM)	KPC-2 K_i^b (μM)
16		> 750	51
37		> 1500	> 500
38		> 1500	200
39		> 1500	600
40		> 1500	561
41		> 1500	180
42		> 750	150
43		> 1500	253
44		> 1500	626
45		> 750	~ 600

^a All compounds are racemates. ^b Calculated from IC_{50} using $K_i = IC_{50}/(1 + [S]/K_m)$. K_m values were measured the day of the experiment. IC_{50} values were fit from a technical triplicate with a SE < 1.1 μM .

While Trp105 displacement onto Pro104 has been observed in various KPC-2 crystal structures, the binding mode observed for **16** is extremely KPC-2 specific; such conformers are not observed in CTX-M since Tyr105 cannot displace onto Asp104. Additionally, the ligand efficiency for the aryl-CF₃ indoline core is quite poor, so small amino acid-like compounds were synthesized to recapitulate Tyr105 interactions, while also providing improved side chain flexibility (**Table 4-7**). Tryptophan derivative **46** had no detectable KPC-2 activity, but hydroxybenzoxazole **47** was equivalent to the previous indoline truncations. Introducing a hydrogen bond donor in hydroxybenzimidazole **48** gave a K_i equivalent to the des-CF₃ analog **38**. Moving from hydroxybenzimidazole to oxindole **49** gave further improvement (124 μ M), with **49** being only 2.5-fold worse than parent indoline **16**. The smaller hydroxypyridine **50** had no detectable activity, whereas quinolone **51** and directly linked quinolone **52** had fringe activity. Given these results, it seems the carbonyl and hydrogen bond donating abilities of **48** and **49** are both preferred over either interaction alone (**46** and **47**). This smaller scaffold, though still relatively weak, has improved ligand efficiency over indoline **16**, and represents a tractable starting point for further inhibitor discovery.

Table 4-7. Biochemical activities of analogs 46-52.^a

		CTX-M-14 K_i^b (μM)	KPC-2 K_i^b (μM)
46		> 1500	> 800
47		> 1500	~ 650
48		> 1500	236
49		> 1500	124
50		> 1500	> 800
51		> 1500	~ 600
52		> 1500	~ 700

^a All compounds are racemates. ^b Calculated from IC_{50} using $K_i = IC_{50}/(1 + [S]/K_m)$. K_m values were measured the day of the experiment. IC_{50} values were fit from a technical triplicate with a SE < 1.1 μM .

Prospects for Broad-Spectrum Inhibitor Discovery:

While the pursuit of KPC-2 activity resulted in the loss of detectable CTX-M activity, both starting indane **2** and indoline **16** occupy similar envelope space (**Figure 4-5**), with the primary point of envelope divergence being the displacement of the hydrophobic

shelf in KPC-2. The more flexible oxindole **49** should better accommodate the rigid shelf requirements of CTX-M, but likely shows no detectable CTX-M activity due to the suboptimal t-butyl carbamate. Our previous work with aryl scaffold **1** showed the importance of the aryl-CF₃ and the benzimidazole packing interactions against the β 3 strand; further derivatization of the flexible carbamate in line with original SAR should allow for improved CTX-M activity. Furthermore, the small panel of heterocycles tested in **Table 4-7** was by no means exhaustive; depending on the binding mode of **49** with KPC-2, additional interactions may be gained through further heterocycle optimization.

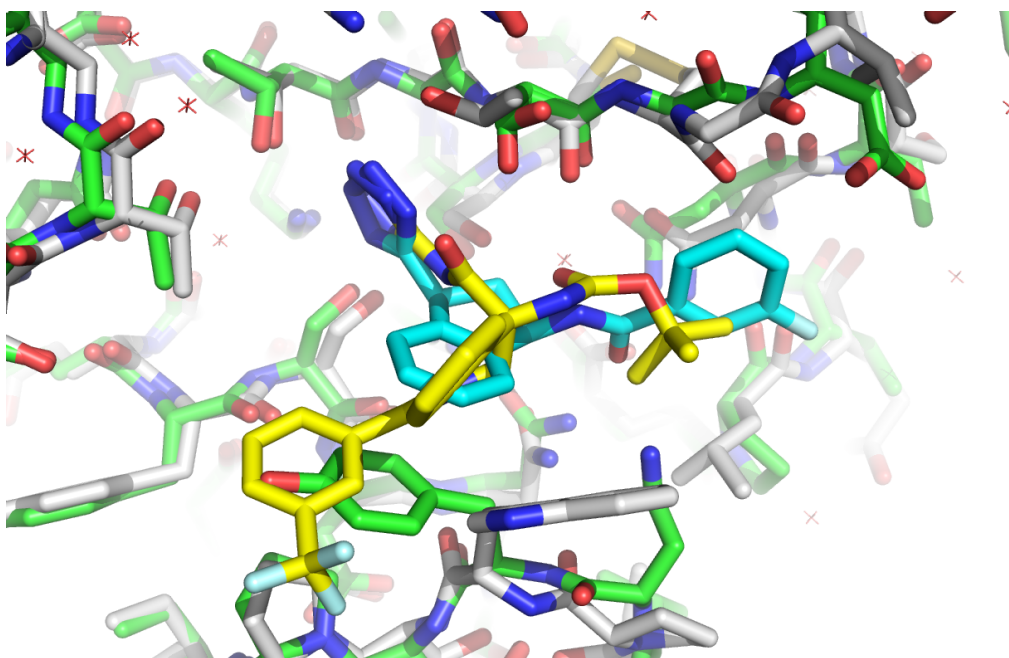


Figure 4-5. Compound 2 complex with CTX-M-9 superimposed onto the compound 16 complex with KPC-2. CTX-M-9: teal and green; KPC-2: yellow and white.

Though structurally divergent from the Class A CTX-M and KPC-2, we also tested our compounds against the metallo- β -lactamase NDM-1 (ESI, **Tables 4-8** and **4-9**). The larger indoline analogs in **Table 4-4** showed no detectable NDM-1 inhibition, at times

even showing paradoxical activation. While the size and shape of these molecules were likely to preclude binding, previous work by our labs has highlighted the potential for amido-tetrazoles to act as inhibitors of NDM-1,² primarily through hydrophobicity and chelation-driven interactions. The smaller amino acid-like analogs in **Table 4-5** and **Table 4-7** showed some traces of activity, but the NDM-1 active site seems to prefer aryl hydrophobicity to aliphatic or polar interactions. While cross-class inhibition appears tenable, further work on the amido-tetrazole scaffold would be required for improved NDM-1 inhibition.

We also tested our compounds against the distinct Class D serine- β -lactamase OXA-48 (ESI, **Table 4-10**). OXA-48 has a number of key differences from KPC-2 (ESI, **Figure 4-7**); the acid-binding motif loses a Thr for a Phe, and the resulting β 3 strand, though twisted, is very different from the Gly238 orientation in KPC-2. Perhaps most importantly, the hydrophobic shelf is also perturbed, with an Ile stacking over the targeted Trp. Unsurprisingly, none of our compounds showed detectable activity against OXA-48. It should be noted that many of the currently approved BLIs, such as avibactam, struggle with K_{iapp} against OXA enzymes;^{3, 4} building activity against this enzyme class would require significant work, as the SAR around non-covalent affinity is largely unknown.

Conclusion:

The biochemical and structural data herein have illustrated how the unique ligand binding properties of KPC-2 can be exploited to build non-covalent affinity, and how such data could be used to link potent, non-covalent ESBL scaffolds to carbapenemase

activity. The amido-tetrazole scaffolds described here provide further chemotypes for new inhibitor discovery, laying the groundwork for future work targeting both serine and metallo-carbapenemases. The discovery of such multi-mode inhibitors is an important area in the fight against future antibiotic resistance.

Materials and Methods:

Synthesis and Characterization

The syntheses and characterization of new compounds **2–52** are described in the ESI. All compounds tested were judged to be of > 95% purity as assessed by NMR and a Waters Micromass ZQ 4000 equipped with Waters 2795 Separation Module, Waters 2996 Photodiode Array Detector (254 nm), and Waters 2424 ELS detector. Separations were carried out with an XBridge BEH C18, 3.5 μ m, 4.6 \times 20 mm column, at ambient temperature (unregulated) using a mobile phase of water–methanol containing a constant 0.05% formic acid.

β -lactamase Inhibition Assays

The hydrolytic activity of CTX-M-14 and KPC-2 was determined using the β -lactamase substrate nitrocefin in a reaction buffer containing 100 mM Tris pH 7.0, 20 mM NaCl, 0.02% Triton X-100, and 5% DMSO; NDM-1 used a reaction buffer containing 100 mM HEPES pH 7.5, 150 mM NaCl, 50 μ M ZnCl₂, 0.01% Triton X-100, and 5% DMSO; OXA-48 used a reaction buffer containing 100 mM Tris-H₂SO₄ pH 7.0, 50 mM NaHCO₃, 0.01% Triton X-100, and 5% DMSO. Nitrocefin hydrolysis was monitored via absorbance (486 nm) using a FlexStation 3 microplate reader at 37 °C.

The nitrocefin concentration was 50 μM for all inhibition assays. Compounds were tested for IC_{50} in an 11-point dose response up to 2.5 mM as solubility allowed. For CTX-M-14 the protein was added last to initiate the reaction; the final protein concentration was 0.1 nM. For KPC-2, NDM-1, and OXA-48 the protein was added to compound and allowed to incubate for 30 m at 37 °C before addition of nitrocefin; the final protein concentration was 0.3 nM, 3 nM, and 0.1 nM, respectively. All compounds were tested as technical triplicates. IC_{50} values were converted to K_i using $K_i = \text{IC}_{50}/(1 + [\text{S}]/K_m)$. The K_m of nitrocefin was measured each day of testing: 40 - 107 μM for CTX-M-14, 8 - 27 μM for KPC-2, 4 – 6 μM for NDM-1, and 185 – 214 μM for OXA-48. All data is presented in the ESI. Nitrocefin was purchased from Sigma-Aldrich.

References:

1. D. A. Nichols, P. Jaishankar, W. Larson, E. Smith, G. Liu, R. Beyrouthy, R. Bonnet, A. R. Renslo, and Y. Chen. *J. Med. Chem.*, 2012, 55, 2163-2172.
2. N. J. Torelli, A. Akhtar, K. DeFrees, P. Jaishankar, O. A. Pemberton, X. Zhang, C. Johnson, A. R. Renslo, Y. Chen. *ACS Infect. Dis.*, 2019, 5 (6), 1013-1021.
3. K. M. Papp-Wallace, N. Q. Nguyen, M. R. Jacobs, C. R. Bethel, M. D. Barnes, V. Kumar, S. Bajaksouzian, S. D. Rudin, P. N. Rather, S. Bhavsar, T. Ravikumar, P. K. Deshpande, V. Patil, R. Yeole, S. S. Bhagwat, M. V. Patel, F. van den Akker, and R. A. Bonomo. *J. Med. Chem.*, 2018, 61, 4067-4086.
4. R. Tsivkovski and O. Lomovskaya. *Antimicrob. Agents Chemother.* 2019, just accepted, DOI: 10.1128/AAC.01935-19.

Electronic Supporting Information:

Supplementary Figures

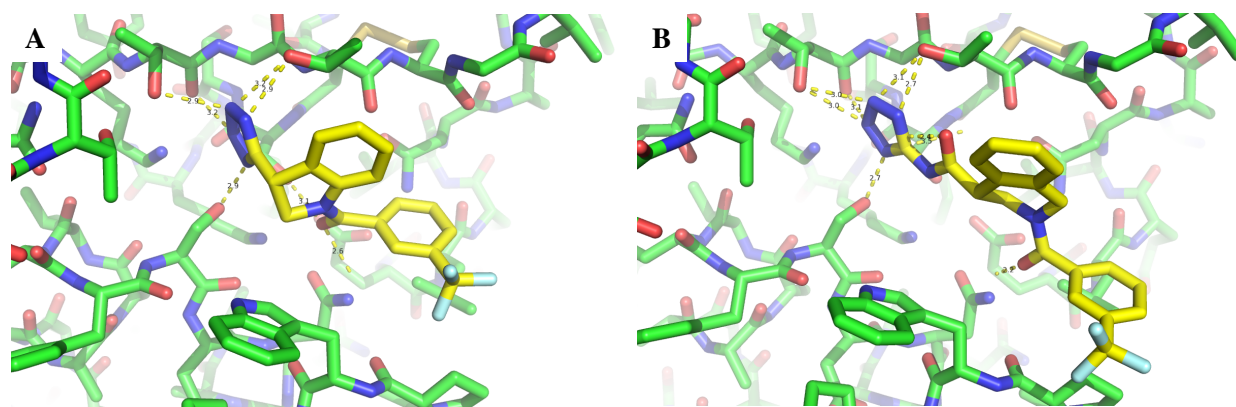


Figure 4-6. Selected docking poses of compounds 7 (A) and 11 (B) with KPC-2. Putative hydrogen bonds denoted by yellow dashes. Both enantiomers were docked.

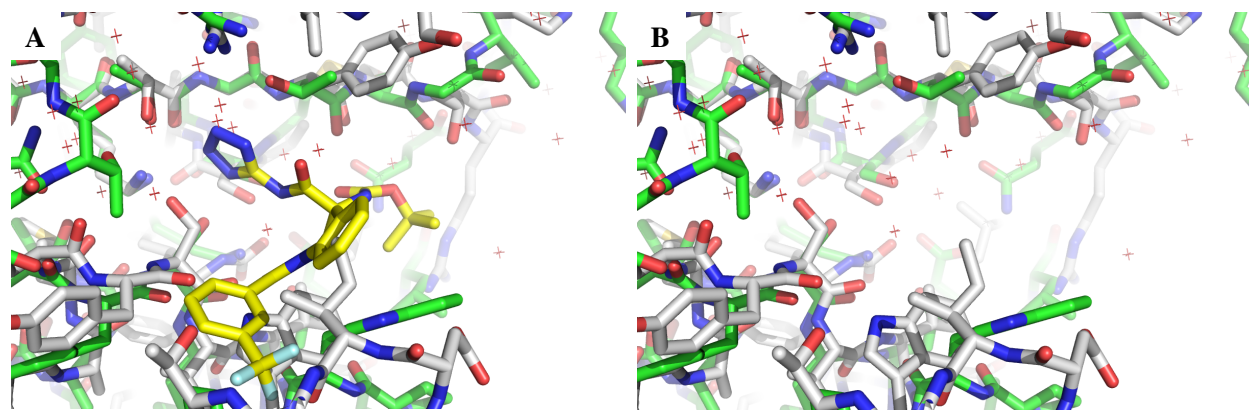
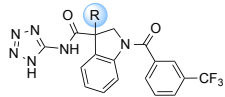
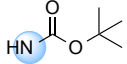
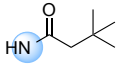
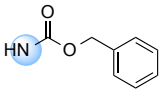
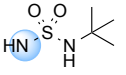
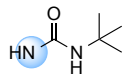
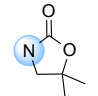
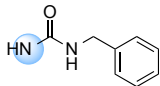
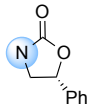
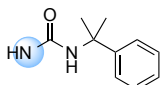
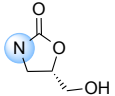
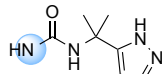
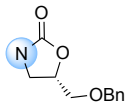


Figure 4-7. Compound 16 complex with KPC-2 superimposed onto a structure of apo OXA-48. With (A) and without (B) 16. KPC-2: yellow and green; OXA-48: white (PDB code 4S2P). Red hashes denote water.

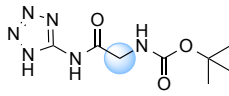

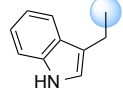

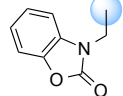

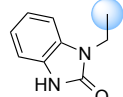

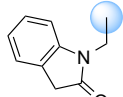
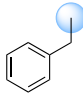
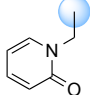

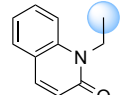
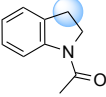
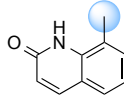
Supplementary Tables

Table 4-8. NDM-1 activities of indoline analogs 16, 18-28.^a

		NDM-1 K_i^b (μM)			NDM-1 K_i^b (μM)
16		> 250 ^c	23		> 250
18		> 250 ^c	24		> 250 ^c
19		> 250	25		> 250 ^c
20		> 250 ^c	26		> 250 ^c
21		> 250 ^c	27		~ 260
22		> 250	28		> 250 ^c

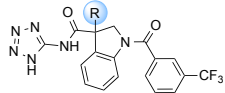
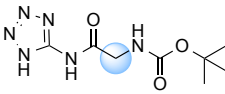
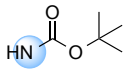
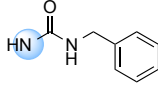
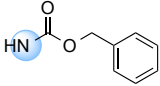
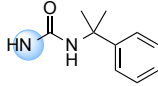

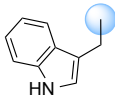

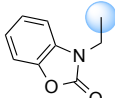

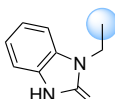
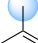
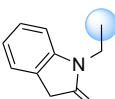
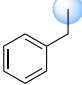
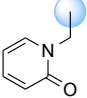
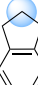
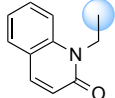
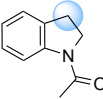
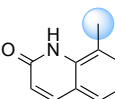
^a All compounds are racemates at the indoline stereocenter. ^b Calculated from IC_{50} using $K_i = IC_{50}/(1 + [S]/K_m)$. K_m values were measured the day of the experiment. IC_{50} values were fit from a technical triplicate. ^c Displayed paradoxical activation – see curves below.

Table 4-9. NDM-1 activities of amido-tetrazole analogs 29-34, 44, and 46-52.^a

		NDM-1 K_i^b (μM)			NDM-1 K_i^b (μM)
29		> 250	46		$\sim 60^c$
30		> 250	47		> 250
31		186	48		> 250
32		> 250	49		> 250
33		> 250	50		> 250
34		$\sim 54^c$	51		$\sim 127^c$
44		> 250	52		$\sim 66^c$

^a All compounds are racemates (when applicable). ^b Calculated from IC_{50} using $K_i = \text{IC}_{50}/(1 + [\text{S}]/K_m)$. K_m values were measured the day of the experiment. IC_{50} values were fit from a technical triplicate. ^c Displayed paradoxical activation – see curves below.

Table 4-10. OXA-48 activities of various amido-tetrazole analogs.^a

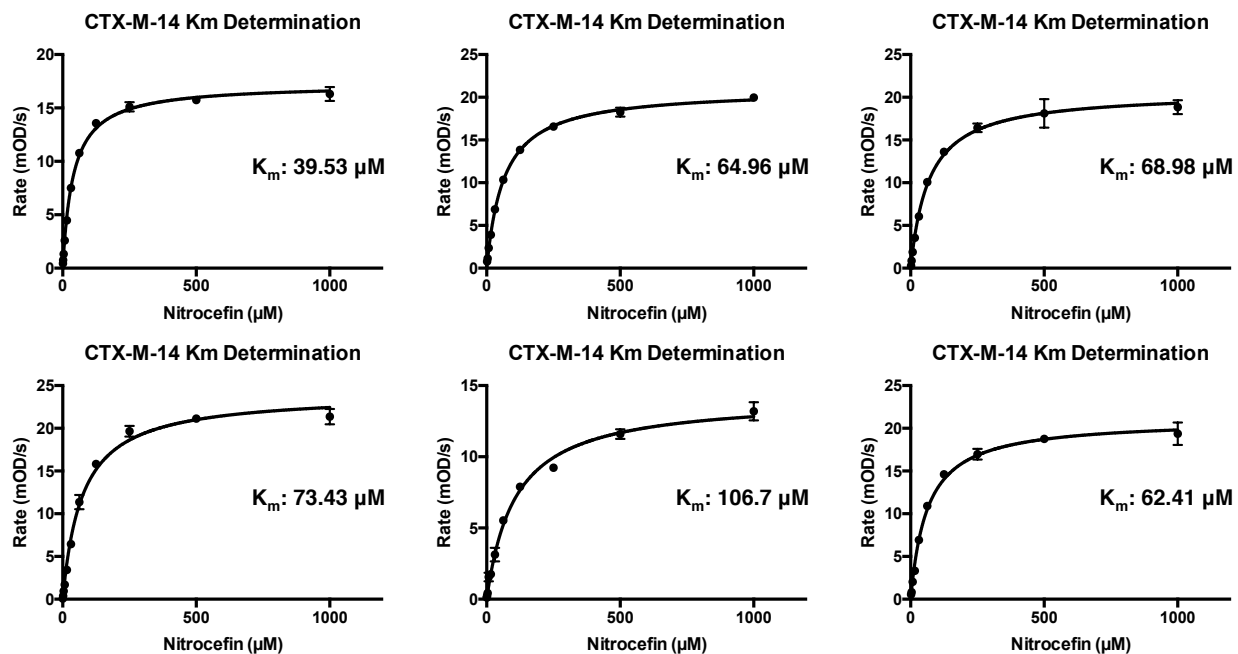
		OXA-48 K_i^b (μM)			OXA-48 K_i^b (μM)
16		> 850	20		~ 1100
18		> 1000	21		> 850
29		> 2000	46		> 2000
30		> 2000	47		> 2000
31		> 2000	48		> 2000
32		> 2000	49		> 2000
33		> 2000	50		> 2000
34		> 2000	51		> 2000
44		> 2000	52		> 2000

^a All compounds are racemates (when applicable). ^b Calculated from IC_{50} using $K_i = \text{IC}_{50}/(1 + [\text{S}]/K_m)$. K_m values were measured the day of the experiment. IC_{50} values were fit from a technical triplicate.

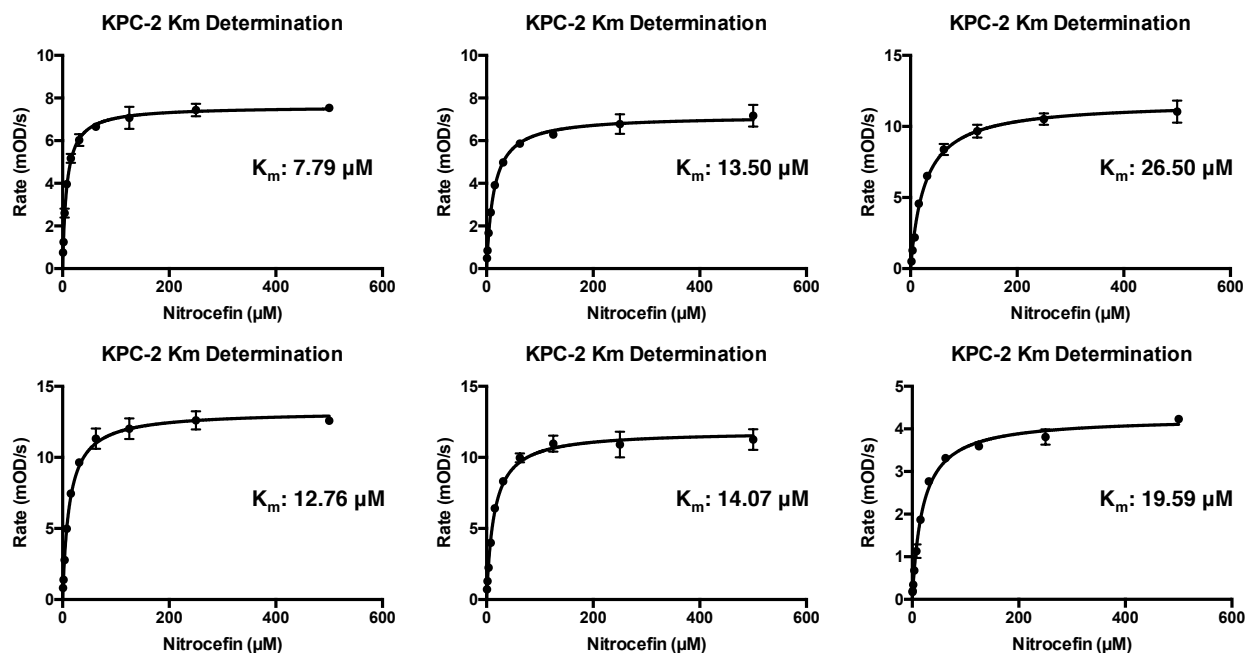
Biochemical Data

Each curve is generated from a technical triplicate. Top compound concentrations ranged from 500 μM to 2.5 mM, as solubility allowed.

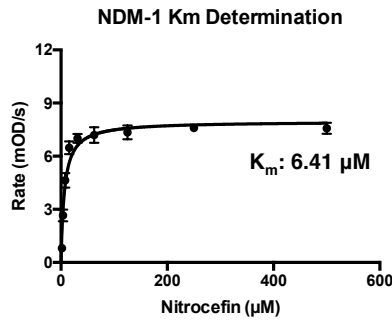
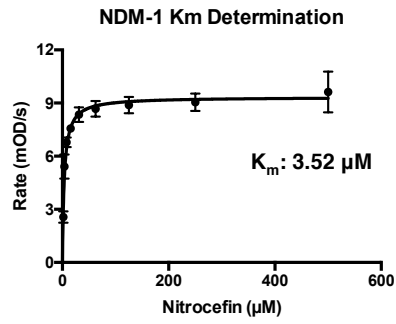
K_m Measurements – CTX-M-14:



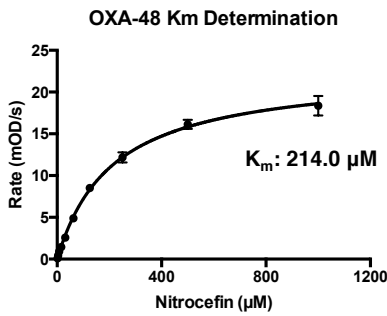
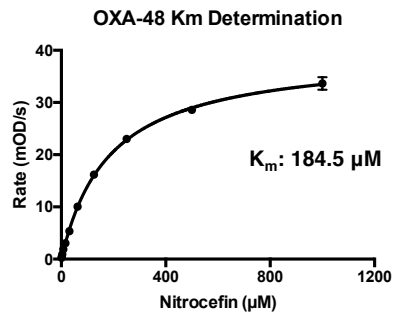
K_m Measurements – KPC-2:



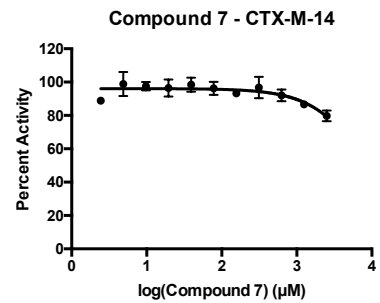
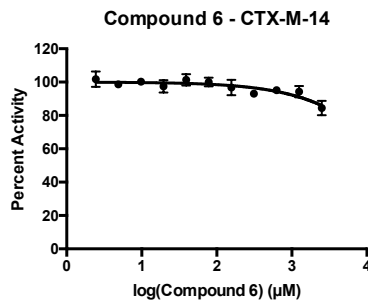
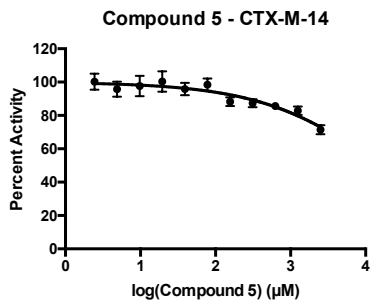
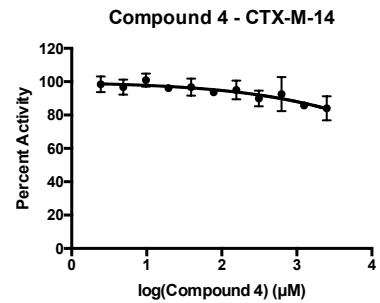
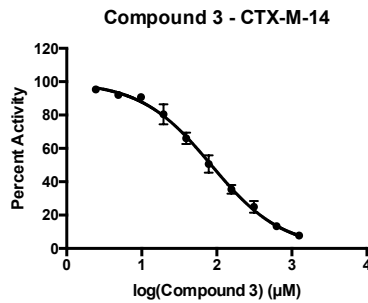
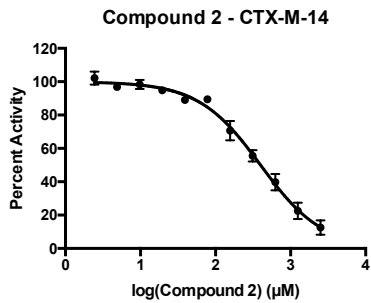
K_m Measurements – NDM-1:

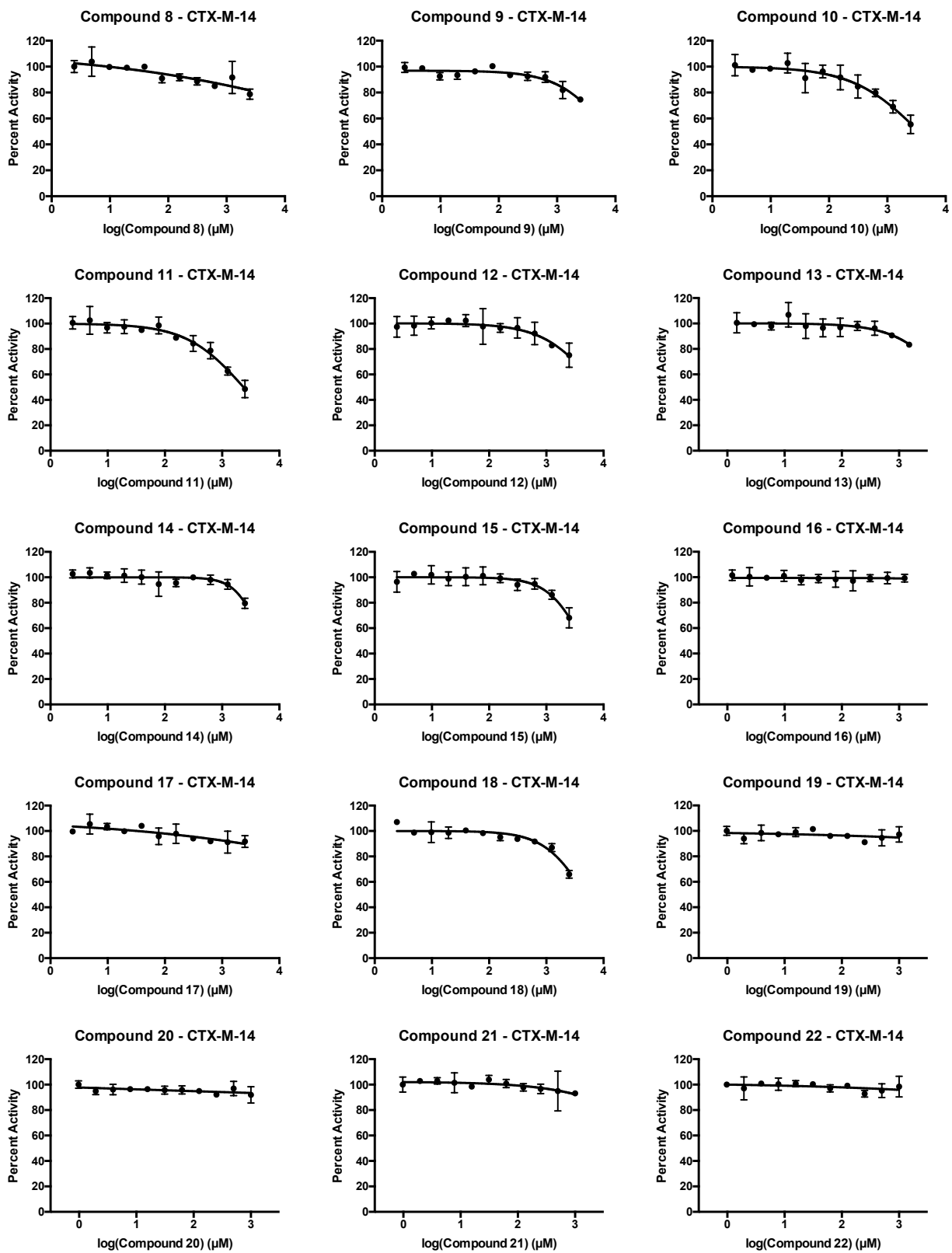


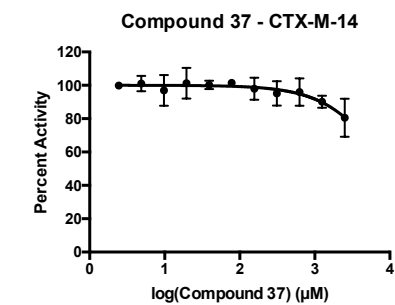
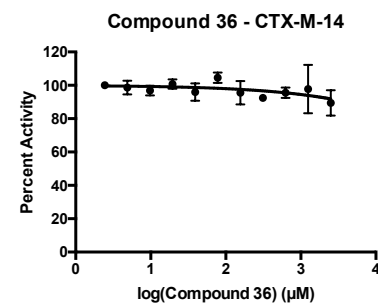
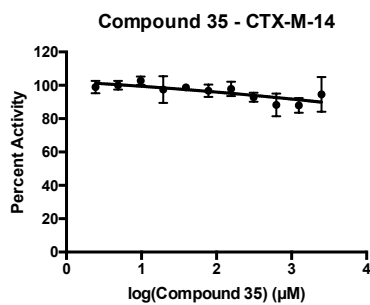
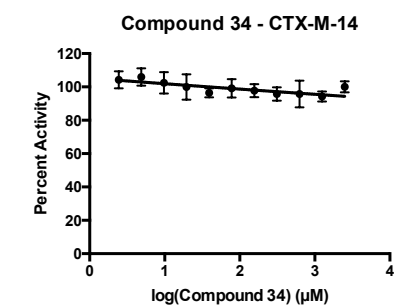
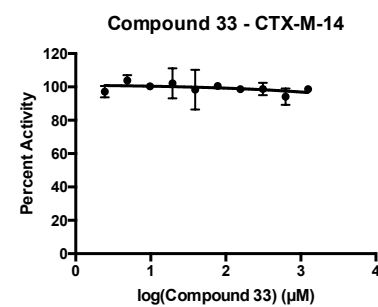
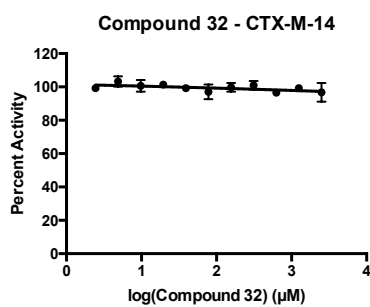
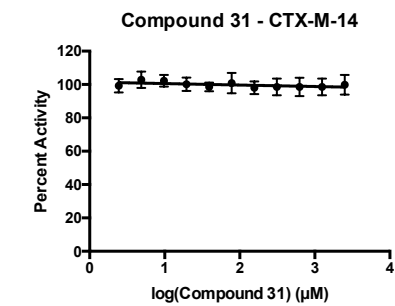
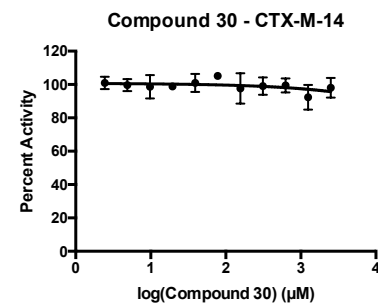
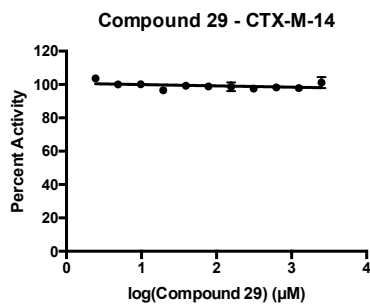
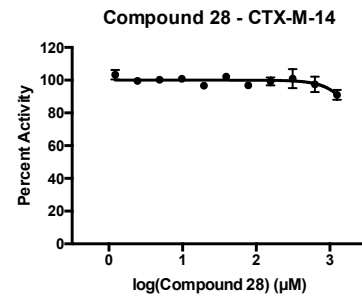
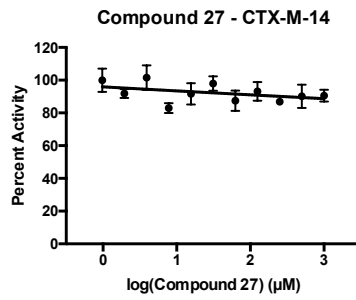
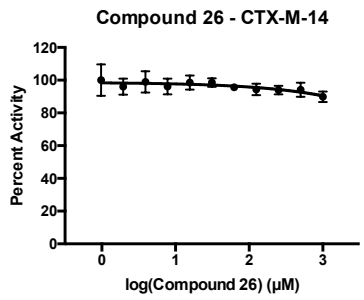
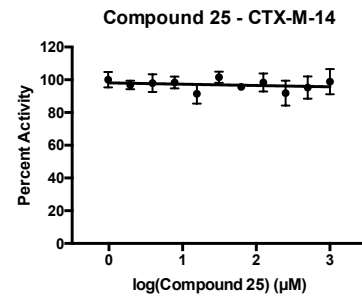
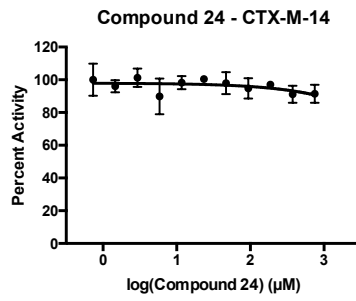
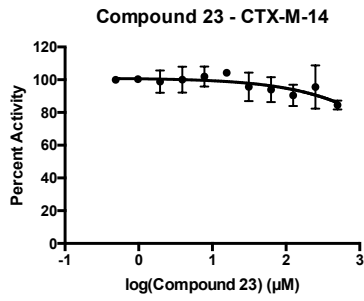
K_m Measurements – OXA-48:

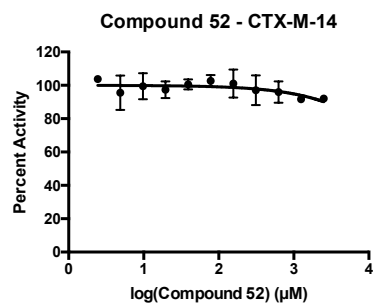
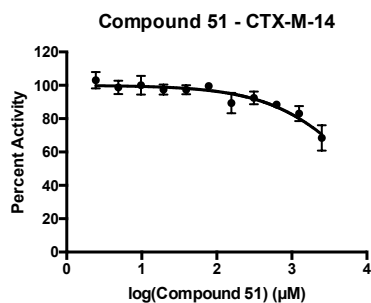
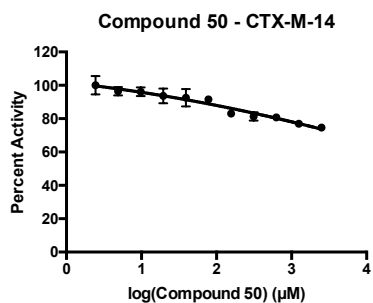
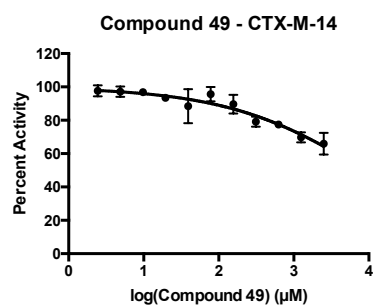
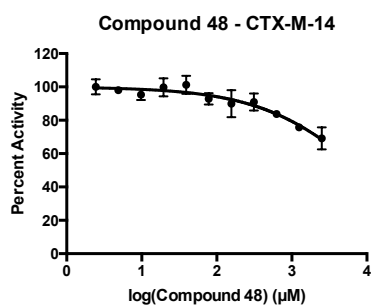
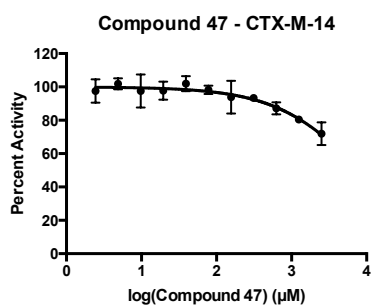
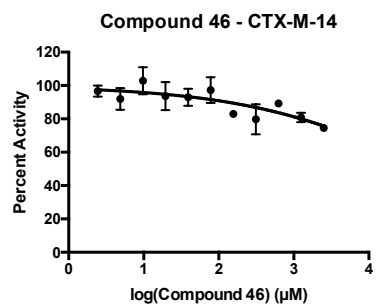
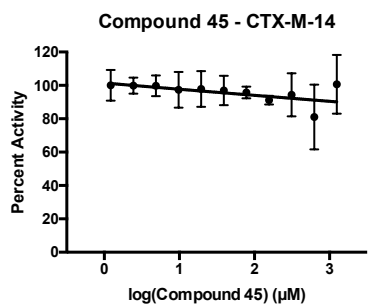
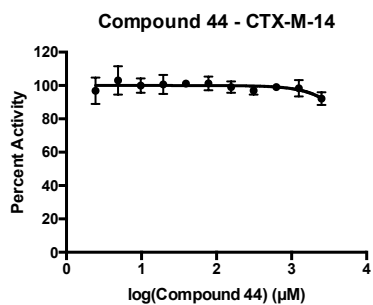
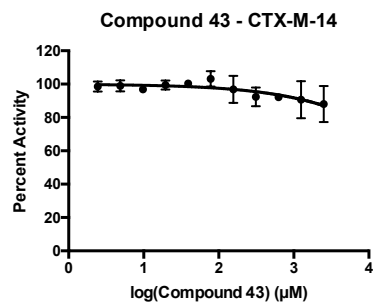
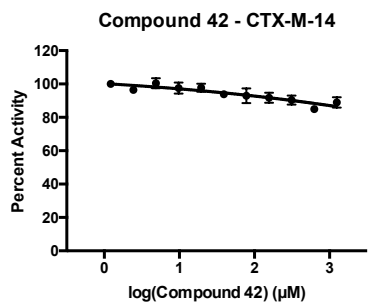
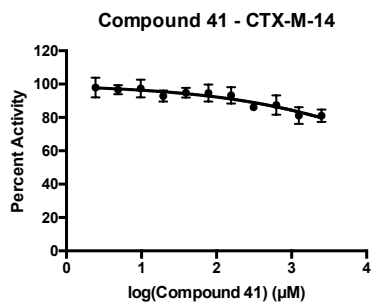
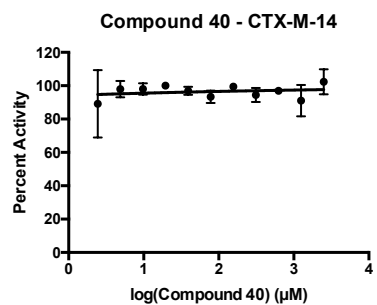
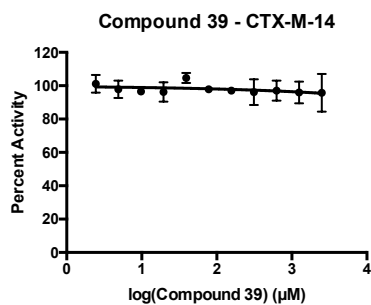
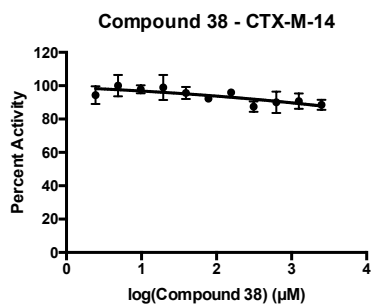


CTX-M-14 Biochemical Data:

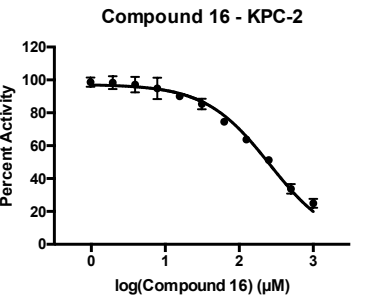
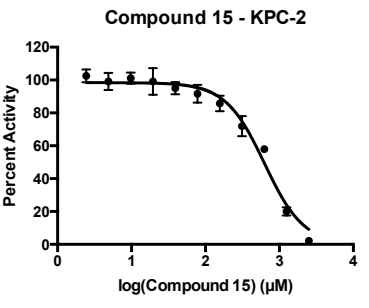
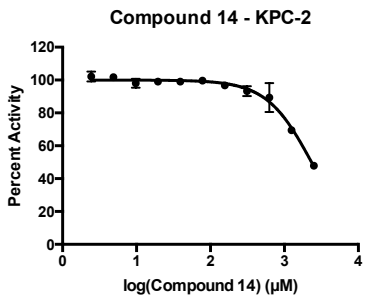
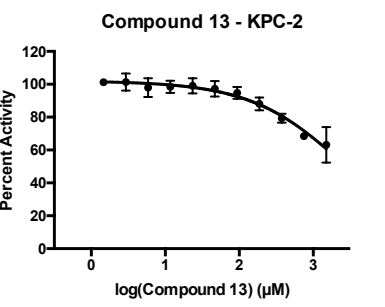
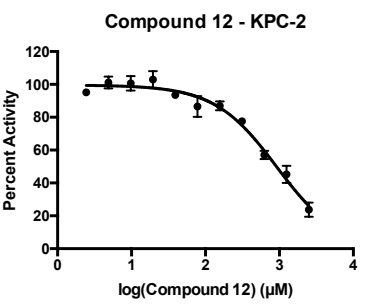
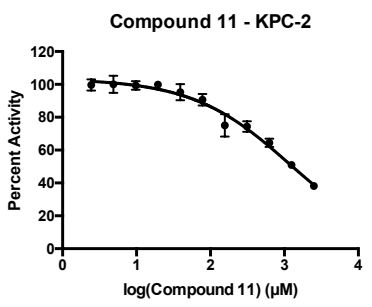
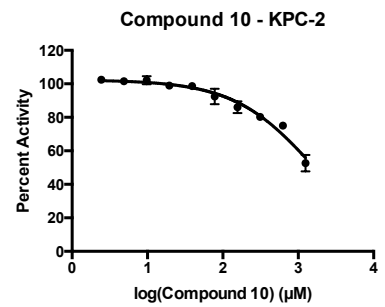
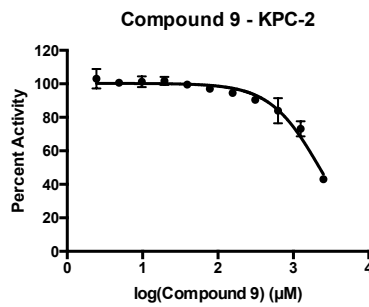
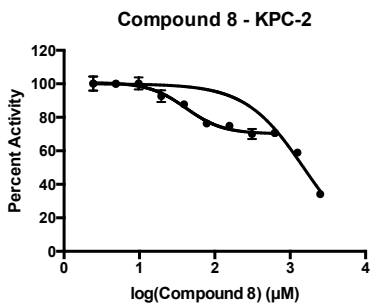
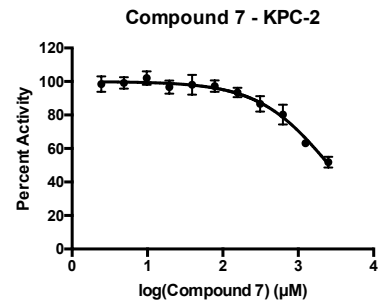
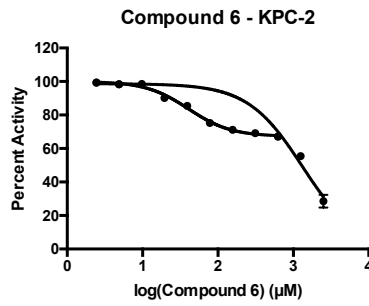
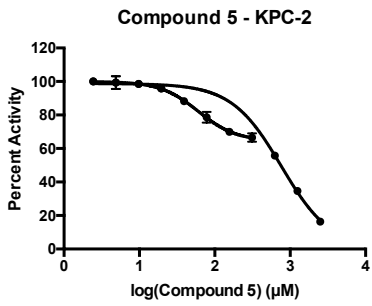
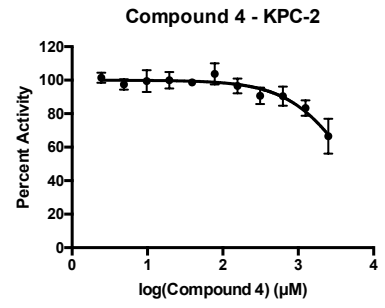
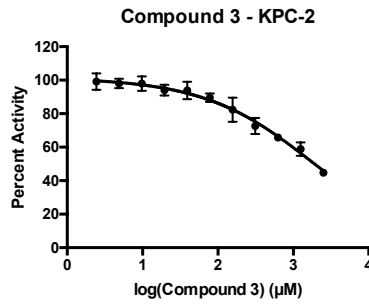
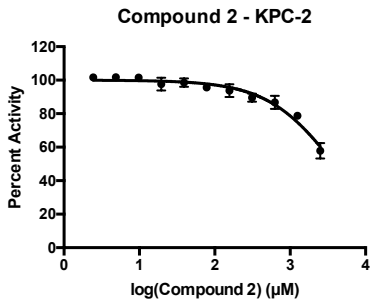


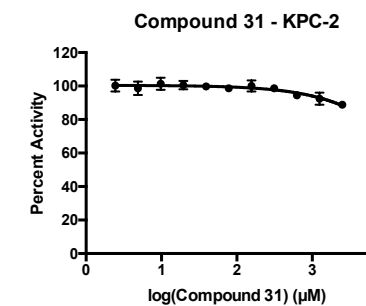
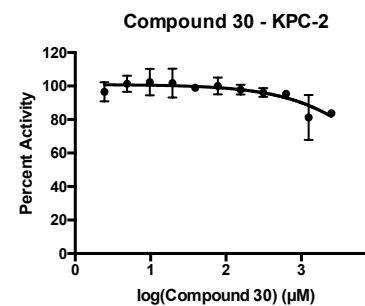
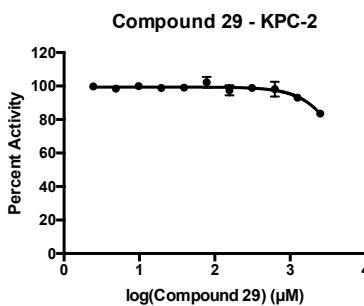
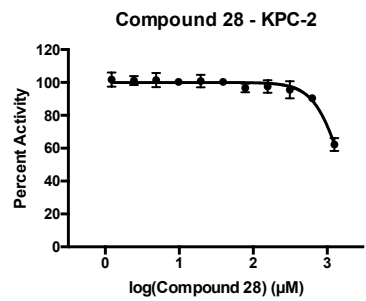
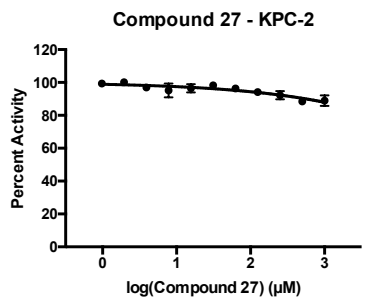
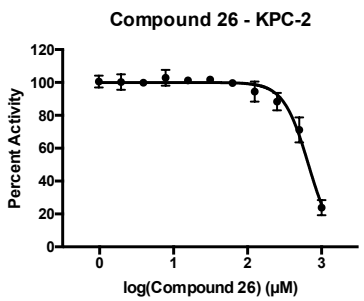
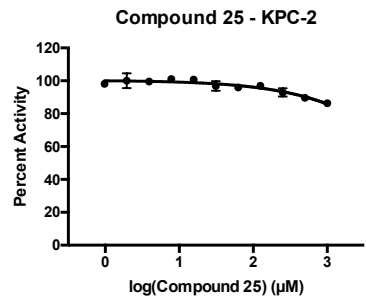
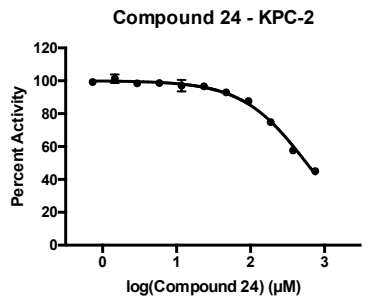
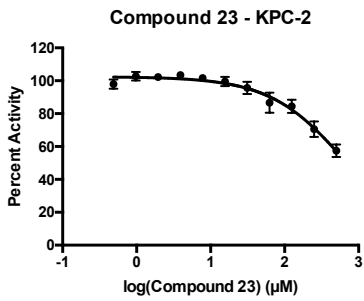
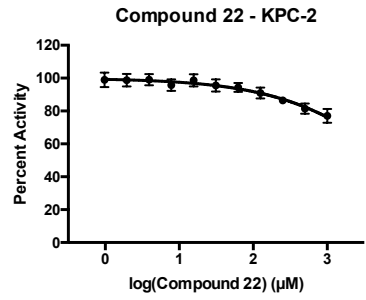
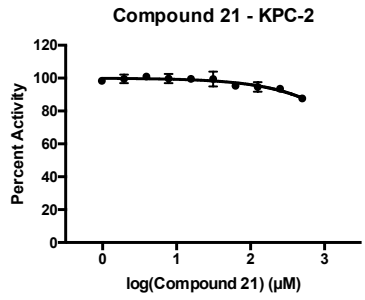
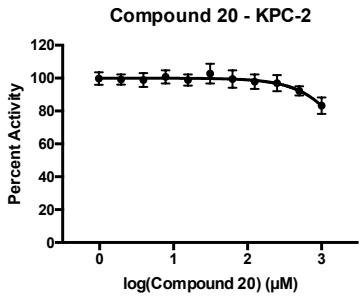
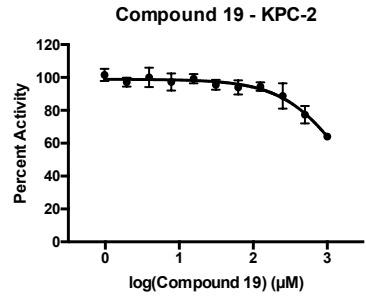
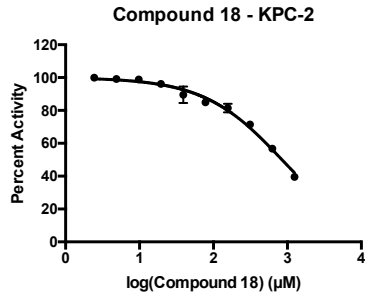
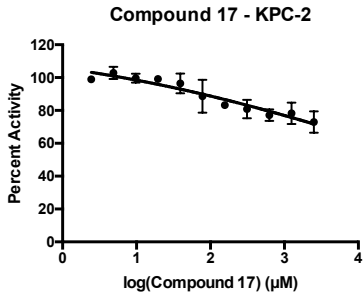


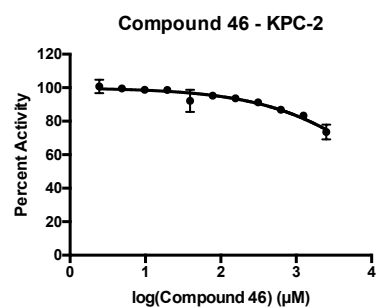
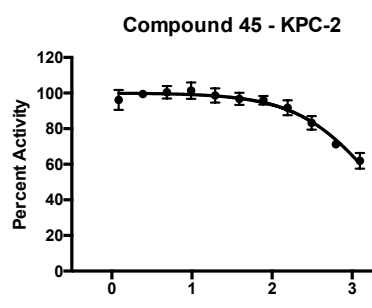
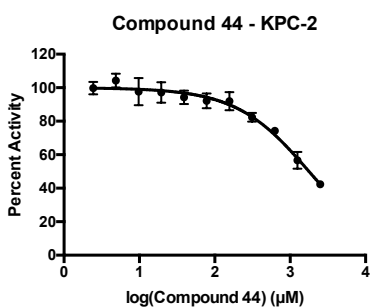
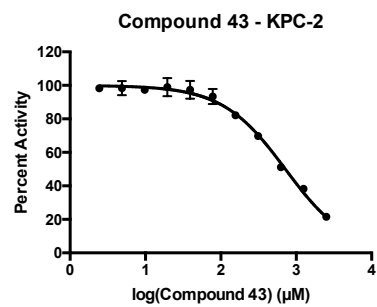
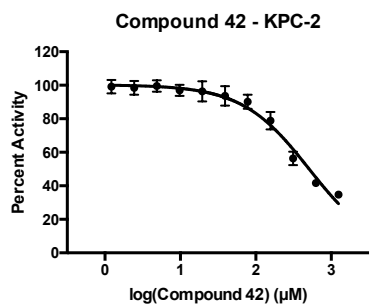
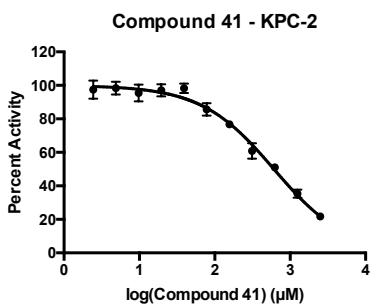
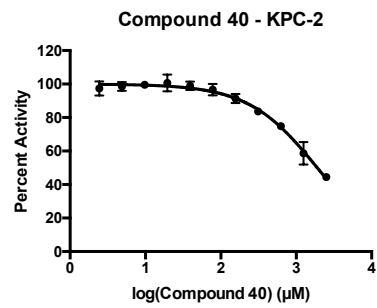
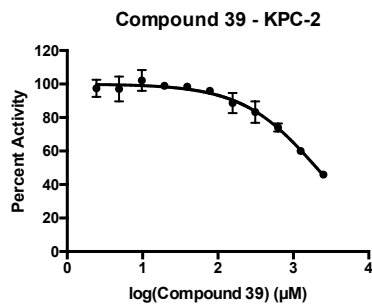
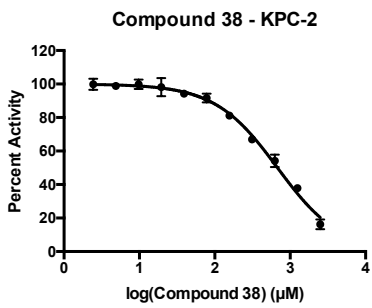
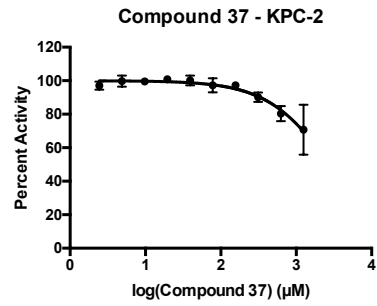
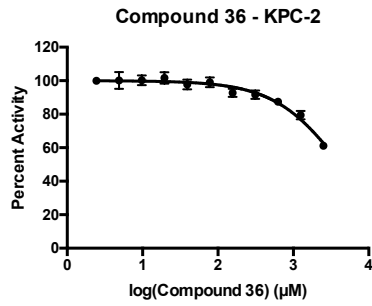
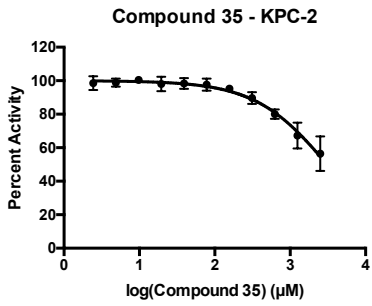
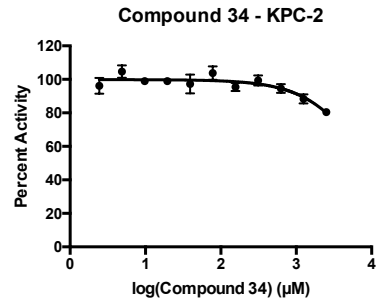
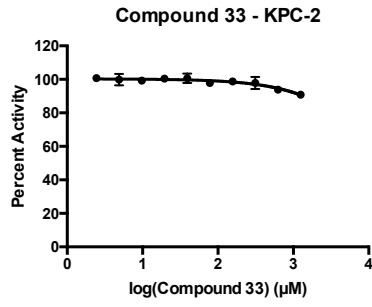
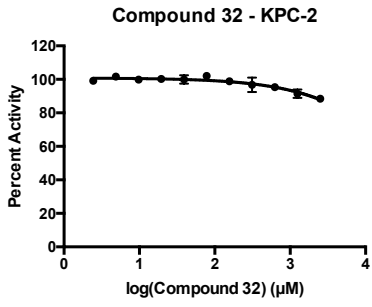


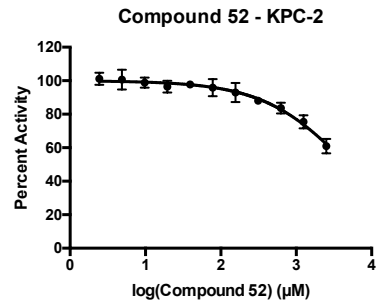
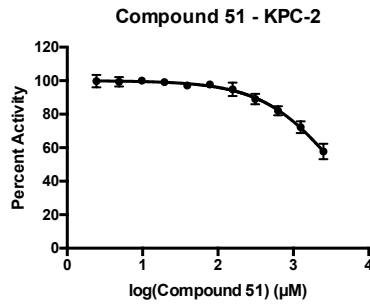
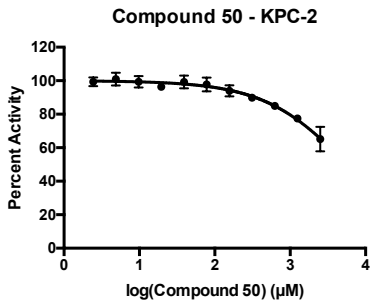
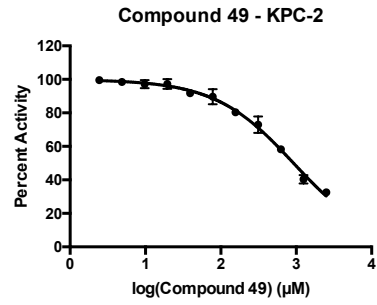
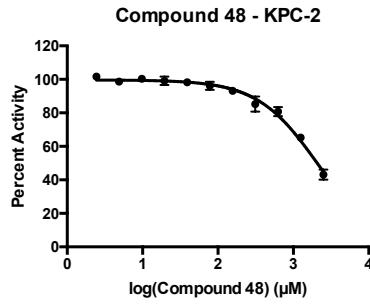
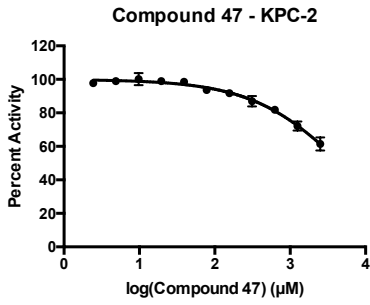


KPC-2 Biochemical Data:

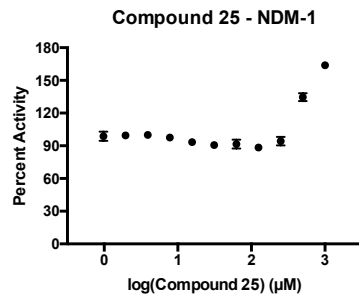
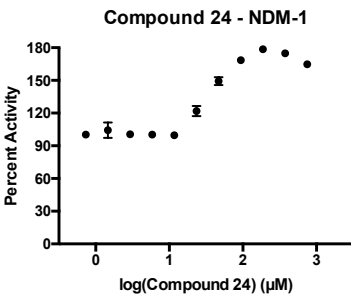
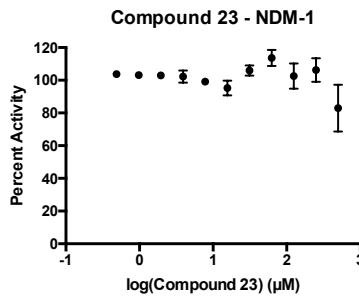
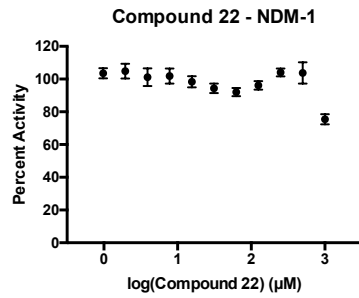
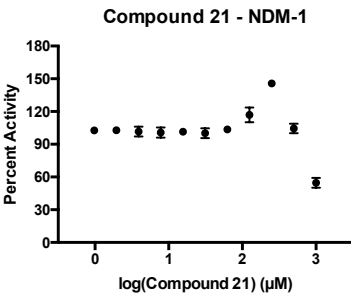
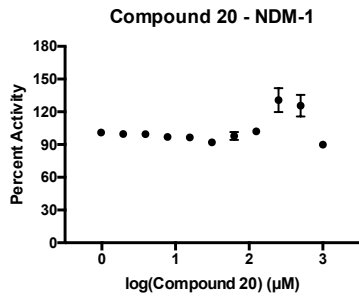
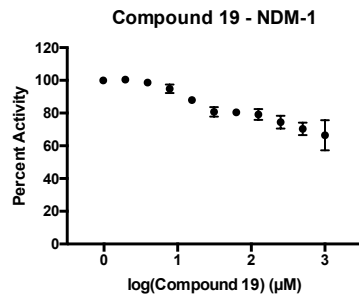
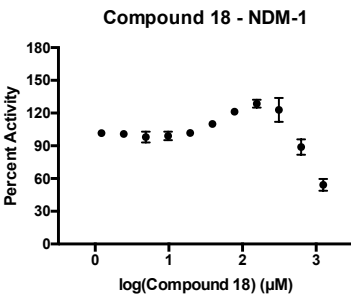
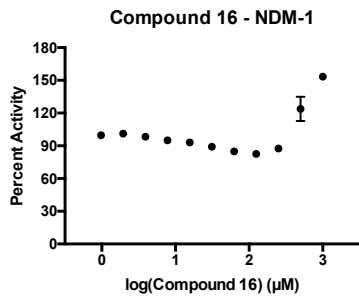


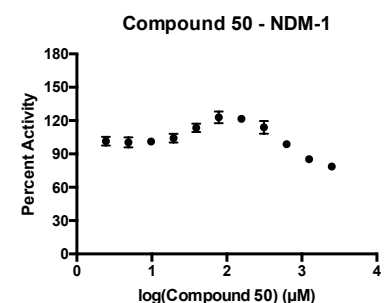
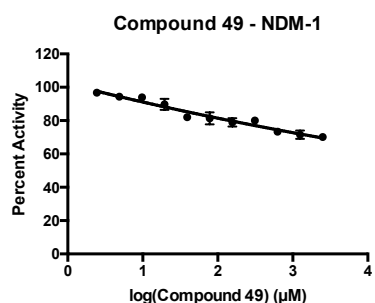
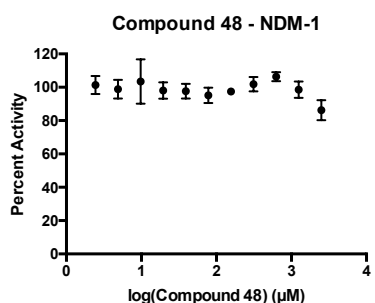
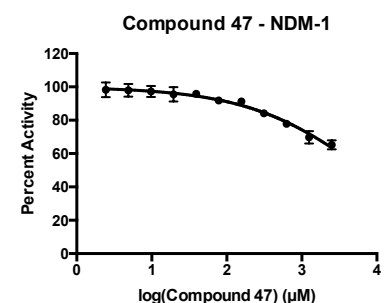
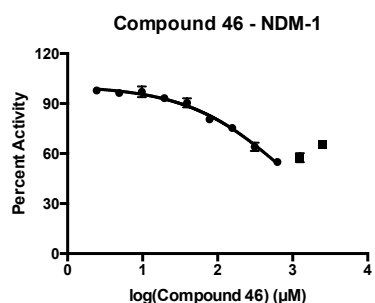
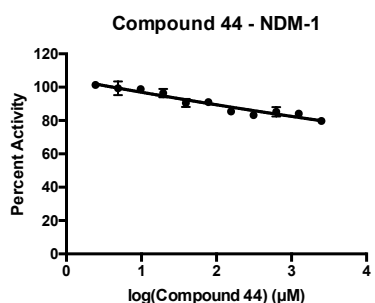
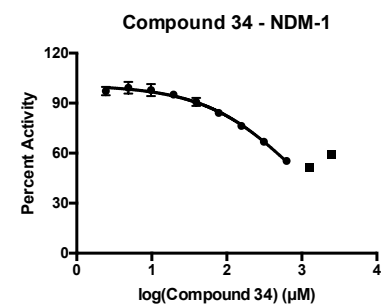
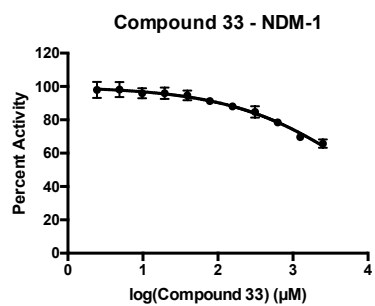
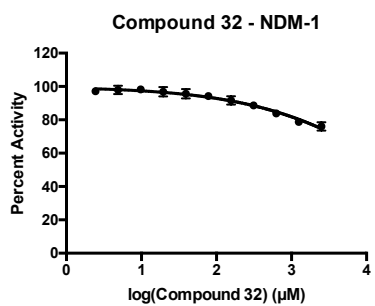
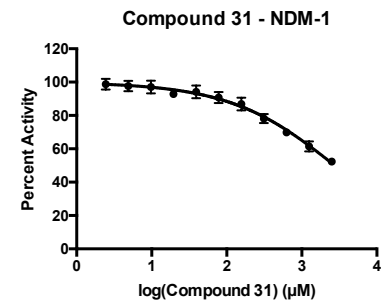
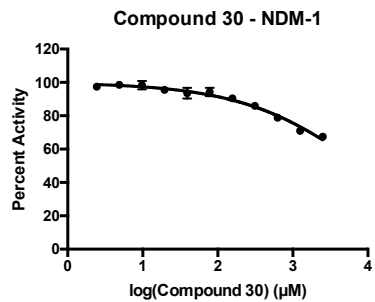
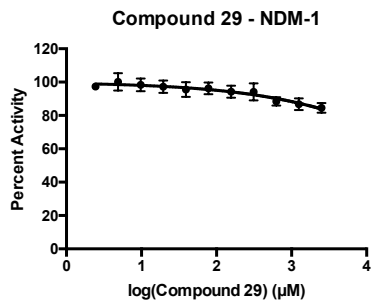
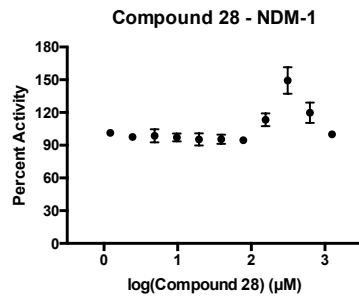
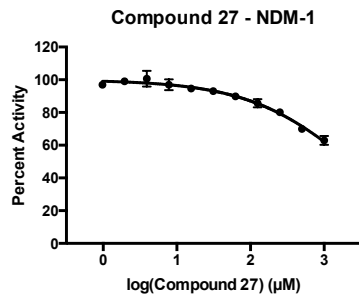
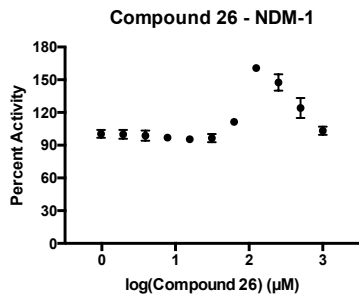


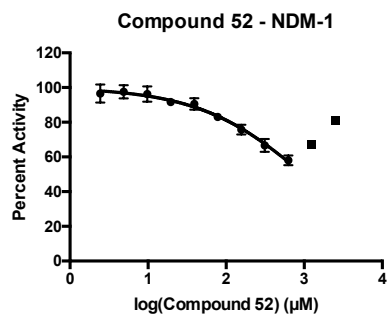
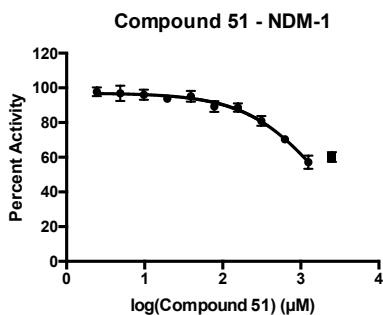




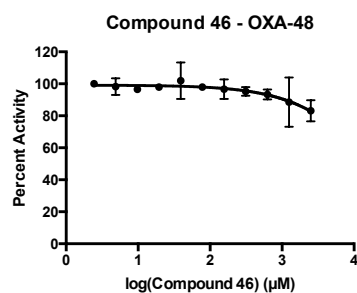
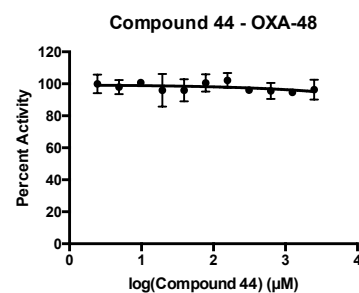
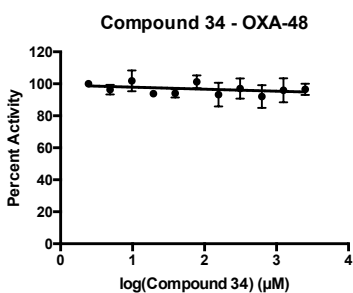
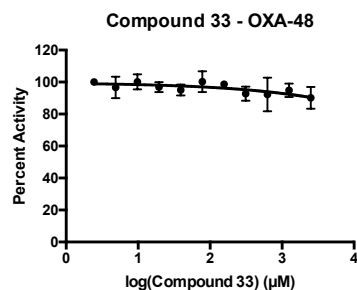
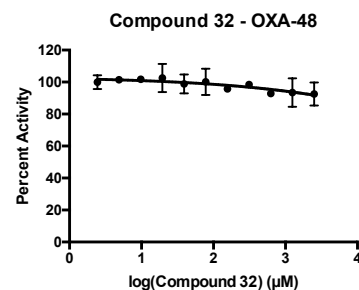
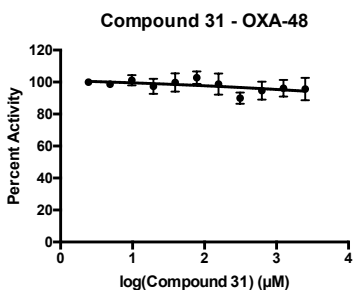
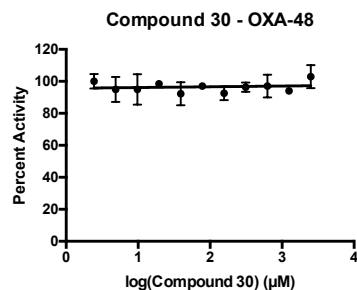
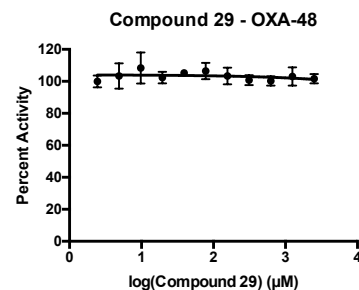
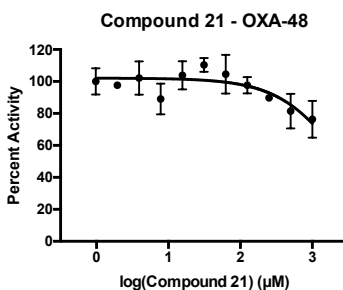
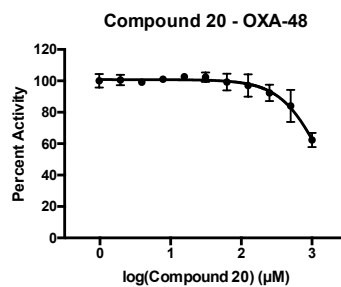
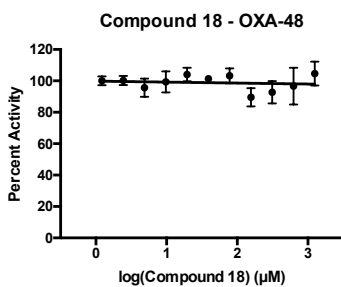
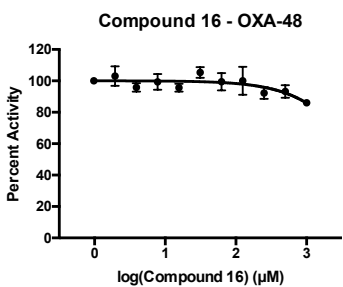
NDM-1 Biochemical Data:

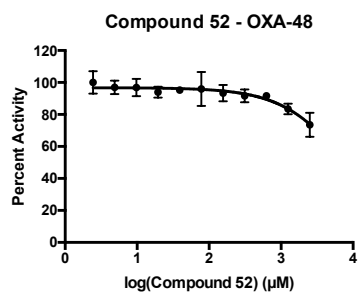
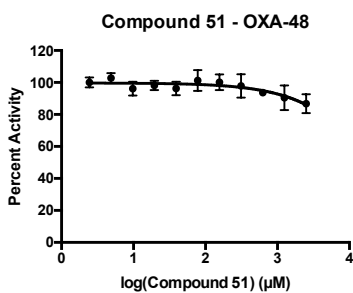
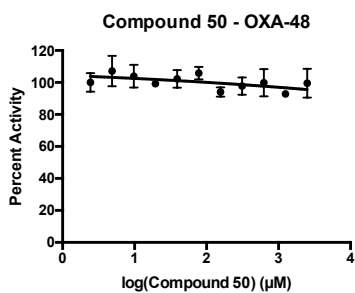
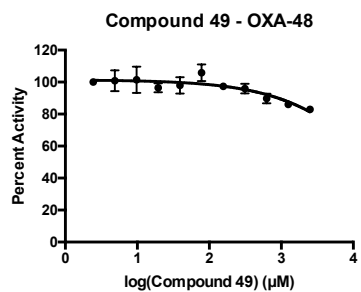
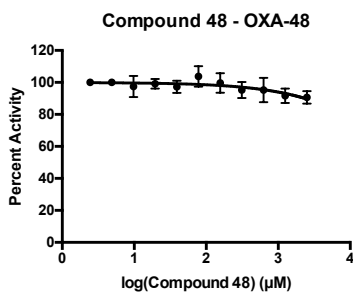
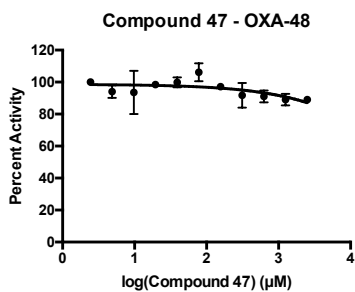






OXA-48 Biochemical Data:





Synthetic Procedures

General Procedures: Reactions were magnetically stirred. Air and/or moisture sensitive reactions were carried out under an argon atmosphere in oven-dried glassware using anhydrous solvents from commercial suppliers. Air and/or moisture sensitive reagents were transferred via syringe or cannula and were introduced into reaction vessels through rubber septa. All anhydrous solvents used were purchased from Sigma-Aldrich and used without further purification. Solvents to be employed in flash column chromatography and reaction work-up procedures were purchased from either Sigma-Aldrich or Fisher Scientific. All other reagents were obtained commercially and used without further purification, unless otherwise stated. Reactions were monitored using LCMS and thin layer chromatography (TLC) performed on 0.25-mm EMD pre-coated glass-backed silica gel 60 F-254 plates. Compounds were visualized under UV light or through staining with permanganate, ninhydrin, bromocresol green, or magic, when appropriate. Reaction products and chromatography fractions were

concentrated by rotary evaporation at 25-35 °C at 20 Torr, then hovac at 0.5 Torr overnight, unless otherwise indicated.

Instrumentation: NMR spectra were recorded on a Bruker AvanceIII HD 400 MHz spectrometer (with 5 mm BBFO Z-gradient Smart Probe) calibrated to CH(D)Cl₃ as an internal reference (7.26 and 77.00 ppm for ¹H and ¹³C NMR spectra, respectively). Data for ¹H NMR spectra are reported in terms of chemical shift (δ, ppm), multiplicity, coupling constant (Hz), and integration. Data for ¹³C NMR spectra are reported in terms of chemical shift (δ, ppm), with multiplicity and coupling constants in the case of C–F coupling. The following abbreviations are used to denote the multiplicities: s = singlet; d = doublet; dd = doublet of doublets; dt = doublet of triplets; dq = doublet of quartets; ddd = doublet of doublet of doublets; t = triplet; td = triplet of doublets; tt = triplet of triplets; q = quartet; qd = quartet of doublets; quin = quintet; sex = sextet; m = multiplet. LCMS and compound purity were determined using a Waters Micromass ZQ 4000, equipped with a Waters 2795 Separation Module, Waters 2996 Photodiode Array Detector, and a Waters 2424 ELSD. Separations were carried out with an XBridge BEH C18, 5μm, 4.6 x 20 mm column, at ambient temperature (unregulated), using a mobile phase of water-methanol containing a constant 0.1% formic acid. HPLC was performed on a Waters 2535 Separation Module with a Waters 2998 Photodiode Array Detector. Separations were carried out with an XBridge BEH C18, 5μm, 19 x 50 mm column, at ambient temperature (unregulated), using a mobile phase of water-methanol containing a constant 0.05% formic acid. Column chromatography was carried out using a Biotage SP1 flash chromatography system with silica gel cartridges from Silicycle.

General Procedure A: A round bottom is charged with the appropriate amine (1.0 equiv.), solvent, and *N,N*-diisopropylethylamine (3.1 equiv.). The acyl- or sulfonyl chloride (1.1 equiv.) is then added dropwise, and the reaction mixture is stirred for 14h or until judged complete by LCMS. The crude reaction mixture is then transferred to a sep funnel with ~ 75 mL EtOAc and ~ 10 mL water. ~ 50 mL sat. NaHCO₃ is added, the layers separated, and the organic layer further washed with ~ 40 mL water and brine. The organic layer is dried over MgSO₄, concentrated, and purified on a silica column with EtOAc:hexanes to afford the desired product.

General Procedure B: The appropriate methyl ester (1.0 equiv.) is suspended or dissolved in methanol, after which a 1M aqueous solution of lithium hydroxide is slowly added dropwise. The reaction mixture is stirred for 14h or until judged complete by LCMS; additional lithium hydroxide is added portion-wise as necessary. Once complete, the reaction mixture is transferred to a sep funnel with water, the aqueous pH adjusted to 1 with conc. HCl, and the aqueous layer extracted with three portions of EtOAc. The organics are combined, dried over MgSO₄, and concentrated under reduced pressure. Semi-crude product is taken forward as-is.

General Procedure C: An oven-dried flask is charged with the appropriate carboxylic acid (1.0 equiv.), dichloromethane, and DMF (drops). Oxalyl chloride (1.1 equiv.) is subsequently added dropwise, and the reaction is stirred at room temperature for 3 h. Separately, 5-aminotetrazole monohydrate (2.0 equiv) is suspended in dichloromethane

and *N,N'*-diisopropylethylamine (3.0 equiv.) in an oven-dried flask. The aforementioned oxalyl chloride solution is then added dropwise to this solution, followed by a dichloromethane rinse of the parent flask. The reaction suspension is stirred at room temperature for 24 h or until judged complete by LCMS, then concentrated under reduced pressure, taken up in DMF, and purified by reverse phase HPLC (water/MeOH/0.05% formic acid) to afford the desired product.

General Procedure D: A 20 mL vial is charged with the appropriate carboxylic acid (1.0 equiv.), DMF, and *N,N*-diisopropylethylamine (1.0 equiv.). HATU (1.05 equiv) is then added, and the reaction mixture is allowed to stir for 10m-1h. Commercially available amine (1.1 equiv.) and *N,N*-diisopropylethylamine (1.1 equiv.) are subsequently added, and the reaction is stirred at room temperature for 18h or until judged complete by LCMS. The crude reaction mixture is directly purified by reverse phase HPLC (water/MeOH/0.05% formic acid) to afford the desired product.

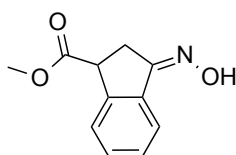
General Procedure E: A 20 mL vial is charged with the appropriate Boc protected amine (1.0 equiv.), fitted with a septa, and purged with Ar. The vial is then charged with dry 4M HCl in dioxanes, and the reaction is stirred at room temperature for 18-72h or until judged complete by LCMS. The reaction mixture is then concentrated and dried under hivac overnight, affording the desired semi-crude product as the HCl salt.

General Procedure F: A dried round bottom is charged with the appropriate methyl ester (1.0 equiv.) and dry tetrahydrofuran. After cooling to -78 °C, 1M LHMDs in

tetrahydrofuran is added dropwise (1.0 equiv). Separately, 2,4,6-triisopropylbenzene sulfonyl azide (1.3 equiv.) is dissolved in dry tetrahydrofuran, then cooled to -78 °C. After 45m-1h of enolization, the azide solution is cannulated over at -78 °C. Once addition is complete, the reaction is allowed to stir for 2 minutes, at which point glacial acetic acid is added (4.6 equiv.) – the reaction mixture is then immediately warmed to r.t. and allowed to stir overnight. The crude reaction mixture is then transferred to a sep. funnel with EtOAc and washed with sat. NaHCO₃ and brine. The organic layer is dried over MgSO₄, concentrated, and purified on a silica column with EtOAc:hexanes to afford the desired product.

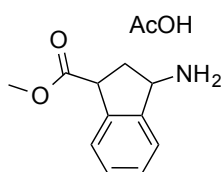
General Procedure G: A 3-mL vial is charged with amine (1.0 equiv.), dry dichloromethane (1.5 mL), and *N,N*-diisopropylethylamine (1.0 equiv.). The reaction vial is cooled to 0 °C and 4-nitrophenylchloroformate (1.1 equiv.) is added (**Note:** works best as bulk-solid addition); stirred at 0 °C for 30m. A solution of partner amine (1.1 equiv.) in dry dichloromethane (1 mL) is then added to the reaction, followed by *N,N*-diisopropylethylamine (1.2 equiv.). The reaction is allowed to slowly warm to r.t. overnight, after which it is transferred to a sep. funnel with ~ 75 mL dichloromethane and washed with 3 x 50 mL 1M Na₂CO₃ (or until yellow coloration ceases). The organic layer is washed with an additional 40 mL 0.1N HCl and brine, dried over MgSO₄, concentrated, and purified on a silica column with EtOAc:hexanes to afford the desired product.

General Procedure H: A 20 mL vial is charged with the appropriate carboxylic acid (1.0 equiv), DMF, commercially available 5-aminotetrazole monohydrate (1.1 equiv), and *N,N*-diisopropylethylamine (2.1 equiv). HATU (1.1 equiv) is then added, and the reaction mixture is stirred for 18h or until judged complete by LCMS. The crude reaction mixture is directly purified by reverse phase HPLC (water/MeOH/0.05% formic acid) to afford the desired product.

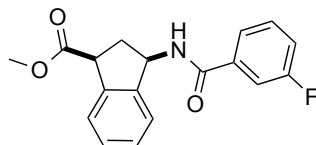


methyl 3-(hydroxyimino)-2,3-dihydro-1H-indene-1-carboxylate (S1). Commercially available 3-oxo-1-indancarboxylic acid (5.000 g, 28.4 mmol, 1.0 equiv.) was dissolved in dry methanol (50 mL). Sulfuric acid (62 μ L, 1.1 mmol, 0.04 equiv.) was then added, and the reaction mixture was refluxed at 100 $^{\circ}$ C for 13h. The crude reaction mixture was then concentrated to dryness and transferred to a sep funnel with \sim 75 mL EtOAc. The organic layer was washed with \sim 50 mL sat. NaHCO_3 , water, and brine; the combined aqueous layers were washed with an additional \sim 50 mL EtOAc. The organics were combined, dried over MgSO_4 , and concentrated to dryness, yielding a yellow-orange oil. The oil was dissolved in ethanol (40 mL); hydroxylamine hydrochloride (2.367 g, 34.1 mmol, 1.2 equiv.) and sodium acetate (4.657 g, 56.8 mmol, 2.0 equiv.) were subsequently added, followed by water (40 mL) and ethanol (40 mL) (rinsed walls). Stirred for 4h. The reaction mixture was concentrated to remove the ethanol and transferred to a sep funnel with \sim 150 mL EtOAc. The organic layer was washed with 2 x 50 mL water and 50 mL brine; dried over MgSO_4 and concentrated to dryness. **S1**

(5.56 g, 96%) obtained as fluffy tan solid. ^1H NMR (400 MHz, CDCl_3) δ = 8.88 (br s, 1H), 7.71 (d, J = 7.1 Hz, 1H), 7.58 - 7.52 (m, 1H), 7.44 - 7.33 (m, 2H), 4.23 (dd, J = 3.9, 8.8 Hz, 1H), 3.78 (s, 3H), 3.44 (dd, J = 4.1, 19.0 Hz, 1H), 3.27 - 3.18 (m, 1H); ^{13}C NMR (100 MHz, CDCl_3) δ = 172.72, 161.49, 144.62, 135.75, 130.74, 128.53, 125.77, 121.70, 52.52, 46.17, 29.65; LRMS (ESI) calculated for $\text{C}_{11}\text{H}_{12}\text{NO}_3$ $[\text{M} + \text{H}]^+$ m/z 206.08, found 206.03.

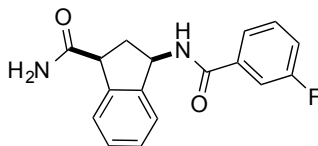


methyl 3-amino-2,3-dihydro-1H-indene-1-carboxylate acetate (S2). **S1** (5.547 g, 27.0 mmol, 1.0 equiv.) was dissolved in 200 mL 20% acetic acid in ethanol (slow to dissolve). The mixture was hydrogenated for 42h using an “H-Cube” flow hydrogenator with a 10% Pd/C cartridge; 1 mL/min, 30 bar H_2 , 45 °C, loop configuration. The reaction mixture was then concentrated to dryness and dried under hivac for 3d. Crude acetate **S2** (9.780 g, 144%) obtained as a thick, colorless oil (**Note:** free base is unstable; will spontaneously polymerize at 0 °C). ^1H NMR (400 MHz, CD_3OD) δ = 7.59 - 7.47 (m, 2H), 7.44 - 7.38 (m, 2H), 4.77 (dd, J = 5.1, 7.8 Hz, 1H), 4.20 (dd, J = 5.6, 8.0 Hz, 1H), 3.80 (s, 3H), 2.80 (td, J = 8.0, 14.1 Hz, 1H), 2.46 - 2.38 (m, 1H), 1.93 (s, 3H); ^{13}C NMR (100 MHz, CD_3OD) δ = 178.74, 175.54, 142.58, 140.69, 131.12, 129.97, 126.62, 126.13, 55.76, 53.28, 49.44, 35.27, 23.19; LRMS (ESI) calculated for $\text{C}_{11}\text{H}_{14}\text{NO}_2$ $[\text{M} + \text{H}]^+$ m/z 192.10, found 192.07.



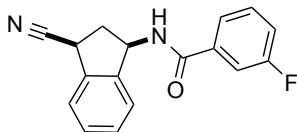
methyl (syn)-3-(3-fluorobenzamido)-2,3-dihydro-1H-indene-1-carboxylate (S3).

Crude **S2** (500 mg, 1.64 mmol, 1.0 equiv.) was suspended in dry dichloromethane (10 mL). 3-fluorobenzoyl chloride (300 μ L, 2.46 mmol, 1.5 equiv.), *N,N*-diisopropylethylamine (630 μ L, 3.61 mmol, 2.2 equiv.), and *N,N*-dimethylaminopyridine (1 flake) were then added, and the reaction was stirred for 14h. The crude reaction mixture was transferred to a sep funnel with additional dichloromethane and washed with ~ 50 mL NH_4Cl , sat. NaHCO_3 , and brine. The organic layer was dried over MgSO_4 , concentrated under reduced pressure, and purified on a silica column with 20% EtOAc:hexanes. Syn and anti diastereomers were separable; syn **S3** obtained as a tan solid (170 mg, 33%). ^1H NMR (400 MHz, CDCl_3) δ = 7.55 - 7.49 (m, 2H), 7.46 - 7.30 (m, 5H), 7.21 (ddt, J = 1.1, 2.6, 8.3 Hz, 1H), 6.33 (br d, J = 8.4 Hz, 1H), 5.89 (q, J = 7.7 Hz, 1H), 4.22 (dd, J = 3.8, 8.6 Hz, 1H), 3.73 (s, 3H), 3.05 (ddd, J = 4.0, 7.8, 13.6 Hz, 1H), 2.21 (ddd, J = 6.4, 8.7, 13.7 Hz, 1H); ^{13}C NMR (100 MHz, CDCl_3) δ = 173.39, 165.88, 162.75 (d, J = 248.0 Hz), 143.04, 140.33, 136.57 (d, J = 6.9 Hz), 130.26 (d, J = 7.6 Hz), 128.73, 128.56, 125.36, 124.54, 122.35 (d, J = 3.1 Hz), 118.62 (d, J = 21.4 Hz), 114.43 (d, J = 22.9 Hz), 54.57, 52.32, 48.34, 37.30.



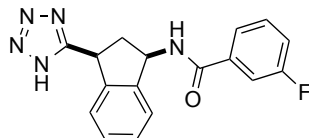
(syn)-3-(3-fluorobenzamido)-2,3-dihydro-1H-indene-1-carboxamide (S4). Syn **S3** (72 mg, 0.23 mmol, 1.0 equiv.) was taken in 3:2:1 tetrahydrofuran:methanol:water (2

mL). Solid lithium hydroxide was added (21 mg, 0.89 mmol, 4.0 equiv.), and the reaction was stirred for 1.5h. The solvent was then removed under reduced pressure, diluted with water, transferred to a sep funnel, and washed with 2 x ~ 50 mL EtOAc. The aqueous layer was adjusted to pH 1 and extracted with 3 x ~ 50 mL EtOAc; the extraction was dried over MgSO₄ and concentrated to give a white solid. The intermediate acid was taken up in acetone (2 mL); di-tert-butyl dicarbonate (65.3 mg, 0.299 mmol, 1.3 equiv.), pyridine (3 uL, 0.38 mmol, 1.65 equiv.), and ammonium bicarbonate (23.6 mg, 0.299 mmol, 1.3 equiv.) were then added. The reaction was stirred for 12h at which point it was poured into 5% HCl and extracted with 3 x ~ 50 mL EtOAc. Dried over MgSO₄ and concentrated, yielding semi-crude syn **S4** as a white solid (28 mg, 41%). ¹H NMR (400 MHz, CDCl₃) δ = 7.59 - 7.40 (m, 4H), 7.39 - 7.23 (m, 3H), 7.21 - 7.07 (m, 1H), 5.74 (dt, *J* = 2.3, 8.3 Hz, 1H), 4.13 - 4.08 (m, 1H), 2.71 (td, *J* = 8.1, 14.2 Hz, 1H), 2.33 (td, *J* = 2.6, 14.1 Hz, 1H).

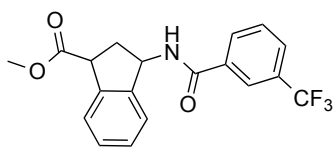


N-((syn)-3-cyano-2,3-dihydro-1H-inden-1-yl)-3-fluorobenzamide (S5). Syn **S4** (45 mg, 0.15 mmol, 1.0 equiv.) was taken up in 1,4-dioxane (600 uL) and pyridine (24 uL, 0.30 mmol, 2.0 equiv.); trifluoroacetic anhydride (23 uL, 0.166 mmol, 1.1 equiv.) was then added dropwise. The reaction mixture was stirred for 4h, after which it was diluted with ~ 30 mL dichloromethane and washed with 2 x ~ 30 mL water. Dried over Na₂SO₄ and concentrated under reduced pressure; purified on a silica column with 20% EtOAc:hexanes. Syn **S5** obtained as a white solid (28 mg, 67%). ¹H NMR (400 MHz, CDCl₃) δ = 7.58 - 7.47 (m, 3H), 7.45 - 7.37 (m, 4H), 7.23 (dt, *J* = 1.6, 8.3 Hz, 1H), 6.66 -

6.60 (m, 1H), 5.71 (q, $J = 7.8$ Hz, 1H), 4.15 - 4.07 (m, 1H), 3.13 (td, $J = 7.7, 13.0$ Hz, 1H), 2.28 (td, $J = 8.1, 13.2$ Hz, 1H).

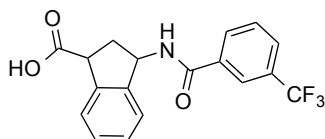


***N*-((*syn*)-3-(1*H*-tetrazol-5-yl)-2,3-dihydro-1*H*-inden-1-yl)-3-fluorobenzamide (2).** A vial was charged with *syn* **S5** (28 mg, 0.1 mmol, 1.0 equiv.), sodium azide (13 mg, 0.2 mmol, 2.0 equiv.), zinc bromide (11.3 mg, 0.05 mmol, 0.5 equiv.), isopropanol (150 μ L), and water (300 μ L). The vial was sealed and heated at 80 $^{\circ}$ C for 16h. The crude reaction mixture was transferred to a sep funnel with excess water, acidified with 3N HCl, and extracted with 3 x \sim 30 mL EtOAc. The combined organics were dried over MgSO_4 and concentrated; purified by reverse phase HPLC (water/MeOH/0.05% formic acid) to afford *syn* **2** (28 mg, 87%) as a white solid. ^1H NMR (400 MHz, CD_3OD) $\delta =$ 7.75 - 7.70 (m, 1H), 7.66 - 7.61 (m, 1H), 7.54 - 7.47 (m, 1H), 7.42 - 7.38 (m, 1H), 7.36 - 7.25 (m, 3H), 7.12 (d, $J = 7.3$ Hz, 1H), 5.79 (t, $J = 7.8$ Hz, 1H), 4.81 (br d, $J = 2.6$ Hz, 1H), 3.16 - 3.07 (m, 1H), 2.45 - 2.36 (m, 1H); LRMS (ESI) calculated for $\text{C}_{17}\text{H}_{13}\text{FN}_5$ [$\text{M} - \text{H}$] $^-$ m/z 322.11, found 322.05.

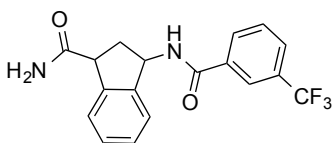


methyl 3-(3-(trifluoromethyl)benzamido)-2,3-dihydro-1*H*-indene-1-carboxylate (S6). **S2** (1.051 g, 4.18 mmol, 1.0 equiv.) was reacted with commercially available 3-(trifluoromethyl)benzoyl chloride in dry tetrahydrofuran (40 mL) and acetonitrile (20 mL) according to general procedure A. **S6** (715.6 mg, 47%) obtained as a white solid (nearly

all anti-diastereomer). ^1H NMR (400 MHz, CDCl_3) δ = 8.15 (s, 1H), 7.99 (d, J = 8.0 Hz, 1H), 7.74 (br dd, J = 0.7, 7.8 Hz, 2H), 7.62 - 7.53 (m, 2H), 7.44 - 7.39 (m, 1H), 7.34 - 7.28 (m, 2H), 5.80 (dt, J = 1.9, 8.4 Hz, 1H), 4.14 (dd, J = 2.1, 8.2 Hz, 1H), 3.79 (s, 3H), 2.74 (td, J = 8.0, 14.1 Hz, 1H), 2.38 (td, J = 2.1, 14.1 Hz, 1H); ^{13}C NMR (100 MHz, CDCl_3) δ = 175.79, 164.54, 143.79, 140.29, 135.21, 131.06 (q, J = 32.3 Hz), 130.01, 129.06, 128.90, 128.79, 127.91 (q, J = 3.7 Hz), 125.85, 124.87, 124.34 (q, J = 3.9 Hz), 123.75 (d, J = 272.2 Hz), 53.67, 52.71, 48.81, 35.79; ^{19}F NMR (376 MHz, CDCl_3) δ = -62.77 (s, 3F); LRMS (ESI) calculated for $\text{C}_{19}\text{H}_{16}\text{F}_3\text{NNaO}_3$ [$\text{M} + \text{Na}$] $^+$ m/z 386.10, found 385.91.

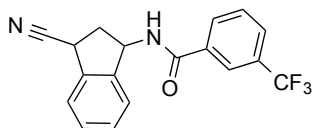


3-(3-(trifluoromethyl)benzamido)-2,3-dihydro-1H-indene-1-carboxylic acid (S7). **S6** (698.1 mg, 1.92 mmol, 1.0 equiv.) was reacted in methanol (25 mL) with 1M lithium hydroxide (15 mL, 15 mmol, 7.81 equiv.) according to general procedure B. Semi-crude **S7** (667.9 mg, 100%) obtained as a white solid (mixture of diastereomers). LRMS (ESI) calculated for $\text{C}_{18}\text{H}_{13}\text{F}_3\text{NO}_3$ [$\text{M} - \text{H}$] $^-$ m/z 348.09, found 348.01.



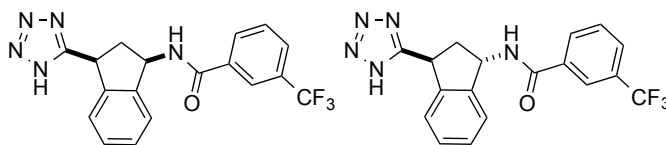
3-(3-(trifluoromethyl)benzamido)-2,3-dihydro-1H-indene-1-carboxamide (S8). Semi-crude **S7** (200.0 mg, 0.573 mmol, 1.0 equiv.) was taken up in DMF (5 mL) and *N,N*-diisopropylethylamine (100 μL , 0.573 mmol, 1.0 equiv.). HATU (283 mg, 0.744 mmol, 1.3 equiv.) was then added; after 10m ammonium chloride (153 mg, 2.86 mmol,

5.0 equiv) was added, followed by *N,N*-diisopropylethylamine (600 μ L, 3.44 mmol, 6.0 equiv.). After stirring for 14h, the reaction mixture was transferred to a sep funnel with \sim 125 mL EtOAc; the organic layer was washed with \sim 3 x 50 mL brine, dried over MgSO_4 , and concentrated under reduced pressure. Purified on a silica column with 50-100% EtOAc:hexanes. Wet **S8** (262.4 mg, 132%, wet with EtOAc) obtained as a white semi-solid (mixture of diastereomers). ^1H NMR (400 MHz, CD_3OD) δ = 8.18 (s, 1H), 8.13 - 8.07 (m, 1H), 7.82 (d, J = 7.8 Hz, 1H), 7.68 - 7.62 (m, 1H), 7.42 - 7.34 (m, 2H), 7.32 - 7.24 (m, 2H), 5.94 (t, J = 7.4 Hz, 0.5H), 5.68 (dd, J = 5.4, 7.8 Hz, 0.5H), 4.20 (dd, J = 3.7, 8.5 Hz, 0.5H), 4.06 (dd, J = 5.5, 7.9 Hz, 0.5H), 2.87 - 2.69 (m, 1H), 2.34 - 2.22 (m, 1H); ^{13}C NMR (100 MHz, CD_3OD) δ = 179.19, 167.28, 145.15, 145.11, 143.35, 143.14, 136.78, 136.61, 132.32 - 132.12 (m), 131.99 - 131.78 (m), 130.79, 130.68, 129.66, 129.49, 129.42 - 129.18 (m), 125.77 (t, J = 1.8 Hz), 125.57, 125.53 - 125.32 (m), 125.46 (q, J = 271.4 Hz), 125.44 (q, J = 271.4 Hz), 56.17, 55.29, 50.66, 50.55, 38.99, 38.22; ^{19}F NMR (376 MHz, CD_3OD) δ = -64.10 (s, 3F), -64.13 (s, 1F); LRMS (ESI) calculated for $\text{C}_{18}\text{H}_{16}\text{F}_3\text{N}_2\text{O}_2$ [$\text{M} + \text{H}$] $^+$ m/z 349.12, found 350.06.



***N*-(3-cyano-2,3-dihydro-1*H*-inden-1-yl)-3-(trifluoromethyl)benzamide (S9).** Wet **S7** (262.4 mg, 0.753 mmol, 1.0 equiv.) was suspended with dry 1,4-dioxane (10 mL); pyridine (182 μ L, 2.26 mmol, 3.0 equiv.) was then added, followed by dropwise addition of trifluoroacetic anhydride (314 μ L, 2.26 mmol, 3.0 equiv.). After stirring for 14h, the crude reaction mixture was transferred to a sep funnel with \sim 120 mL EtOAc and \sim 20 mL water. The organic layer was washed with 0.1 N HCl, water, and brine. Dried over

MgSO₄, concentrated, and purified on a silica column with EtOAc:hexanes. **S9** obtained as a white solid (169.0 mg, 68%) (mixture of diastereomers). ¹H NMR (400 MHz, DMSO-d₆) δ = 9.21 (d, *J* = 8.3 Hz, 0.6H), 9.13 (d, *J* = 7.8 Hz, 0.4H), 8.31 - 8.17 (m, 2H), 7.97 - 7.88 (m, 1H), 7.80 - 7.69 (m, 1H), 7.53 - 7.29 (m, 4H), 5.75 - 5.61 (m, 1H), 4.71 (dd, *J* = 5.6, 8.5 Hz, 0.4H), 4.52 (dd, *J* = 8.4, 9.4 Hz, 0.6H), 3.00 (td, *J* = 7.8, 12.2 Hz, 0.6H), 2.74 (ddd, *J* = 5.6, 7.8, 13.4 Hz, 0.4H), 2.54 - 2.44 (m, 0.4H), 2.28 (td, *J* = 9.8, 12.2 Hz, 0.6H); ¹³C NMR (100 MHz, DMSO-d₆) δ = 164.79, 164.65, 143.12, 142.96, 137.73, 137.19, 134.89, 134.84, 131.63, 129.71, 129.66, 128.69 (dd, *J* = 16.1, 38.9 Hz), 128.14 - 127.86 (m), 125.19, 124.48, 124.37, 123.98 (q, *J* = 272.0 Hz), 125.50 - 122.48 (m), 121.43, 121.20, 53.11, 52.71, 37.45, 37.11, 32.11, 31.22; ¹⁹F NMR (376 MHz, DMSO-d₆) δ = -61.11 (s, 1.9F), -61.13 (s, 3F); LRMS (ESI) calculated for C₁₈H₁₄F₃N₂O [M + H]⁺ m/z 331.11, found 330.99.



***N*-((*syn*)-3-(1*H*-tetrazol-5-yl)-2,3-dihydro-1*H*-inden-1-yl)-3-**

(trifluoromethyl)benzamide (3), *N*-((*anti*)-3-(1*H*-tetrazol-5-yl)-2,3-dihydro-1*H*-inden-

1-yl)-3-(trifluoromethyl)benzamide (4). A sealed tube was charged with **S9** (153.6 mg,

0.465 mmol, 1.0 equiv.), sodium azide (90.7 mg, 1.40 mmol, 3.0 equiv.), ammonium

chloride (79.6 mg, 1.49 mmol, 3.2 equiv.), and DMF (9 mL). The tube was sealed and

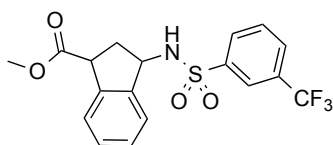
heated at 120 °C behind a blast shield for 14h. The crude reaction mixture was directly

purified by reverse phase HPLC (water/MeOH/0.05% formic acid) to afford *syn* **3** (43.1

mg, 25%) and *anti* **4** (77.3 mg, 45%) as white solids. **3**: ¹H NMR (400 MHz, CD₃OD,

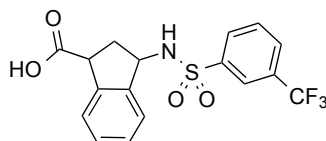
drops CDCl₃) δ = 8.15 (s, 1H), 8.05 (br d, *J* = 7.8 Hz, 1H), 7.74 (br d, *J* = 7.5 Hz, 1H),

7.61 - 7.54 (m, 1H), 7.47 - 7.40 (m, 1H), 7.33 - 7.23 (m, 2H), 7.16 (br d, $J = 6.6$ Hz, 1H), 5.87 (br dd, $J = 5.4, 7.3$ Hz, 1H), 5.06 (br t, $J = 7.2$ Hz, 1H), 2.88 - 2.78 (m, 1H), 2.63 (ddd, $J = 5.1, 8.3, 13.6$ Hz, 1H); ^{13}C NMR (100 MHz, CD_3OD , drops CDCl_3) $\delta = 167.58, 164.36, 143.29, 142.49, 135.53, 131.34, 129.68, 129.42, 129.02, 128.63$ (br d, $J = 2.9$ Hz), 125.58, 125.31, 125.01 (br s), 124.38 (q, $J = 271.4$ Hz), 54.76, 39.64, 39.23; ^{19}F NMR (376 MHz, CD_3OD , drops CDCl_3) $\delta = -63.26$ (s, 3F); LRMS (ESI) calculated for $\text{C}_{18}\text{H}_{13}\text{F}_3\text{N}_5\text{O}$ $[\text{M} - \text{H}]^-$ m/z 372.11, found 372.02. **4**: ^1H NMR (400 MHz, CD_3OD , drops CDCl_3) $\delta = 8.22$ (s, 1H), 8.13 (br d, $J = 7.8$ Hz, 1H), 7.76 (br d, $J = 7.5$ Hz, 1H), 7.61 (br t, $J = 7.8$ Hz, 1H), 7.41 (br d, $J = 7.3$ Hz, 1H), 7.31 - 7.19 (m, 2H), 7.06 (br d, $J = 7.1$ Hz, 1H), 5.82 (br t, $J = 6.9$ Hz, 1H), 4.78 (br t, $J = 7.4$ Hz, 1H), 3.11 (td, $J = 7.8, 13.4$ Hz, 1H), 2.40 (td, $J = 6.8, 13.3$ Hz, 1H); ^{13}C NMR (100 MHz, CD_3OD , drops CDCl_3) $\delta = 166.56, 160.44, 142.75, 141.51, 134.91, 130.94$ (q, $J = 32.3$ Hz), 130.53, 129.20, 128.57, 128.31, 128.20 - 127.92 (m), 124.58, 124.54 - 124.40 (m), 124.36, 123.81 (q, $J = 272.2$ Hz), 53.66, 39.00, 38.27; ^{19}F NMR (376 MHz, CD_3OD , drops CDCl_3) $\delta = -63.35$ (s, 3F); LRMS (ESI) calculated for $\text{C}_{18}\text{H}_{13}\text{F}_3\text{N}_5\text{O}$ $[\text{M} - \text{H}]^-$ m/z 372.11, found 372.02.

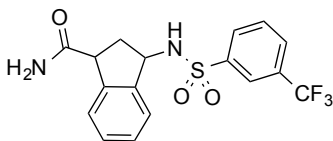


methyl 3-((3-(trifluoromethyl)phenyl)sulfonamido)-2,3-dihydro-1H-indene-1-carboxylate (S10). **S2** (1.027 g, 4.09 mmol, 1.0 equiv.) was reacted with commercially available 3-(trifluoromethyl)benzenesulfonyl chloride in dry tetrahydrofuran (40 mL) and acetonitrile (20 mL) according to general procedure A. **S10** (502.8 mg, 31%) obtained as a white solid (mixture of diastereomers). ^1H NMR (400 MHz, CDCl_3) $\delta = 8.25 - 8.09$ (m, 2H), 8.02 (d, $J = 8.0$ Hz, 0.5H), 7.90 - 7.82 (m, 1H), 7.70 (td, $J = 7.6, 15.5$ Hz, 1H),

7.63 - 7.57 (m, 0.5H), 7.44 (s, 0.3H), 7.40 (s, 0.3H), 7.37 - 7.31 (m, 1H), 7.30 - 7.20 (m, 2H), 7.18 - 7.13 (m, 0.5H), 5.12 (t, $J = 7.2$ Hz, 0.5H), 4.97 (s, 0.3H), 4.94 (s, 0.3H), 4.96 - 4.92 (m, 0.5H), 4.09 (dd, $J = 3.4, 8.5$ Hz, 0.5H), 3.94 (dd, $J = 3.2, 7.8$ Hz, 0.5H), 3.73 (s, 1.5H), 3.67 (s, 1.5H), 2.67 (ddd, $J = 3.5, 7.5, 13.5$ Hz, 0.5H), 2.42 (td, $J = 7.9, 14.1$ Hz, 0.5H), 2.07 - 1.96 (m, 1H); ^{13}C NMR (100 MHz, CDCl_3) $\delta = 174.91, 173.22, 146.69, 146.03, 142.90, 142.54, 141.72, 139.90, 130.26, 130.18, 129.99, 129.89, 129.51, 129.30, 129.07, 128.90, 128.70, 128.50, 127.98, 127.94, 125.48, 125.22, 124.79, 124.54, 124.18 - 124.03$ (m), 123.20, 123.16, 58.02, 57.72, 52.64, 52.28, 48.22, 47.89, 37.61, 35.92; ^{19}F NMR (376 MHz, CDCl_3) $\delta = -62.79$ (s, 1.5F), -62.81 (s, 1.5F); LRMS (ESI) calculated for $\text{C}_{18}\text{H}_{15}\text{F}_3\text{NO}_4\text{S}$ $[\text{M} - \text{H}]^-$ m/z 398.07, found 397.99.

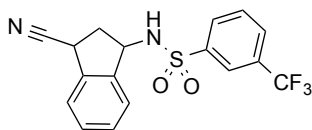


3-((3-(trifluoromethyl)phenyl)sulfonamido)-2,3-dihydro-1H-indene-1-carboxylic acid (S11). **S10** (484.7 mg, 1.21 mmol, 1.0 equiv.) was reacted in methanol (15 mL) with 1M lithium hydroxide (10 mL, 10 mmol, 8.24 equiv.) according to general procedure B. Semi-crude **S11** (473.5 mg, 101%) obtained as a white solid (mixture of diastereomers). LRMS (ESI) calculated for $\text{C}_{17}\text{H}_{13}\text{F}_3\text{NO}_4\text{S}$ $[\text{M} - \text{H}]^-$ m/z 384.05, found 384.10.



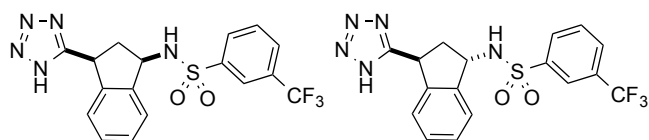
3-((3-(trifluoromethyl)phenyl)sulfonamido)-2,3-dihydro-1H-indene-1-carboxamide (S12). Semi-crude **S11** (214.5 mg, 0.557 mmol, 1.0 equiv.) was taken up in DMF (5 mL)

and *N,N*-diisopropylethylamine (97 μ L, 0.557 mmol, 1.0 equiv.). HATU (275 mg, 0.724 mmol, 1.3 equiv.) was then added; after 10m ammonium chloride (149 mg, 2.78 mmol, 5.0 equiv) was added, followed by *N,N*-diisopropylethylamine (582 μ L, 3.34 mmol, 6.0 equiv.). After stirring for 14h, the reaction mixture was transferred to a sep funnel with ~ 125 mL EtOAc; the organic layer was washed with ~ 3 x 50 mL brine, dried over MgSO₄, and concentrated under reduced pressure. Purified on a silica column with 30% EtOAc:hexanes. **S12** (130.4 mg, 61%) obtained as a yellow semi-solid (mixture of diastereomers). ¹H NMR (400 MHz, CD₃OD) δ = 8.28 - 8.23 (m, 2H), 8.02 (br d, *J* = 7.5 Hz, 1H), 7.90 - 7.83 (m, 1H), 7.37 - 7.21 (m, 3H), 7.21 - 7.18 (m, 0.5H), 7.12 (d, *J* = 7.5 Hz, 0.5H), 5.19 (t, *J* = 7.2 Hz, 0.5H), 4.93 (t, *J* = 7.1 Hz, 0.5H), 4.07 (dd, *J* = 3.5, 8.4 Hz, 0.5H), 3.88 (t, *J* = 7.4 Hz, 0.5H), 2.48 (ddd, *J* = 3.7, 7.8, 13.1 Hz, 0.5H), 2.39 (td, *J* = 7.7, 13.0 Hz, 0.5H), 2.07 - 1.96 (m, 0.5H), 1.96 - 1.87 (m, 0.5H); ¹³C NMR (100 MHz, CD₃OD) δ = 178.90, 178.44, 145.00, 144.97, 144.19, 143.99, 142.77, 142.43, 132.72 (q, *J* = 33.0 Hz), 131.80 (d, *J* = 2.9 Hz), 130.32 (t, *J* = 3.3 Hz), 129.71 (d, *J* = 2.2 Hz), 129.18, 129.05, 125.76, 125.66 (d, *J* = 3.7 Hz), 125.38, 124.89 (q, *J* = 4.2 Hz), 125.02 (q, *J* = 273.0 Hz), 59.53, 58.95, 50.22, 49.89, 39.32, 38.28; ¹⁹F NMR (376 MHz, CD₃OD) δ = -64.24 (s, 3F), -64.25 (s, 3F); LRMS (ESI) calculated for C₁₇H₁₆F₃N₂O₃S [M + H]⁺ *m/z* 385.08, found 385.01.



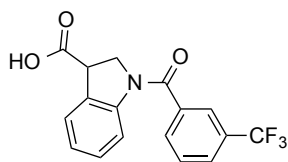
***N*-(3-cyano-2,3-dihydro-1*H*-inden-1-yl)-3-(trifluoromethyl)benzamide (S13).** **S12** (130.4 mg, 0.339 mmol, 1.0 equiv.) was suspended with dry 1,4-dioxane (8 mL); pyridine (82 μ L, 1.02 mmol, 3.0 equiv.) was then added, followed by dropwise addition

of trifluoroacetic anhydride (141 μ L, 1.02 mmol, 3.0 equiv.). After stirring for 14h, the crude reaction mixture was transferred to a sep funnel with \sim 120 mL EtOAc and \sim 20 mL water. The organic layer was washed with \sim 50 mL 0.1 N HCl, water, and brine. Dried over MgSO_4 , concentrated, and purified on a silica column with EtOAc:hexanes. **S13** (92.7 mg, 75%) obtained as an off-white solid (mixture of diastereomers). ^1H NMR (400 MHz, DMSO-d_6) δ = 8.64 (d, J = 8.5 Hz, 0.5H), 8.55 (d, J = 8.3 Hz, 0.5H), 8.25 - 8.17 (m, 1.5H), 8.15 - 8.06 (m, 1.5H), 7.95 - 7.87 (m, 1H), 7.45 - 7.32 (m, 2.5H), 7.32 - 7.26 (m, 0.5H), 7.16 - 7.11 (m, 0.5H), 7.03 (d, J = 7.5 Hz, 0.5H), 4.98 (dt, J = 5.5, 7.9 Hz, 0.5H), 4.91 - 4.82 (m, 0.5H), 4.55 (dd, J = 5.8, 8.5 Hz, 0.5H), 4.30 (dd, J = 8.3, 9.3 Hz, 0.5H), 2.58 - 2.51 (m, 0.5H), 2.41 (ddd, J = 5.8, 7.5, 13.4 Hz, 0.5H), 2.15 (ddd, J = 5.1, 8.4, 13.5 Hz, 0.5H), 1.87 (td, J = 9.6, 12.0 Hz, 0.5H); ^{13}C NMR (100 MHz, DMSO-d_6) δ = 143.37, 142.21, 142.18, 137.67, 137.10, 131.63, 131.55, 131.00, 130.47 (d, J = 35.9 Hz), 130.05 - 129.75 (m), 129.67, 129.32, 129.29, 129.10, 125.42, 125.08, 124.73, 124.51, 123.65 - 123.40 (m), 123.93 (q, J = 272.9 Hz), 121.52, 121.29, 57.14, 56.75, 38.67, 37.94, 32.25, 31.52; ^{19}F NMR (376 MHz, DMSO-d_6) δ = -61.38 (s, 3F), -61.41 (s, 3F); LRMS (ESI) calculated for $\text{C}_{17}\text{H}_{12}\text{F}_3\text{N}_2\text{O}_2\text{S}$ [$\text{M} - \text{H}$] $^-$ m/z 365.06, found 365.03.



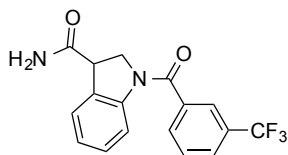
***N*-((*syn*)-3-(1*H*-tetrazol-5-yl)-2,3-dihydro-1*H*-inden-1-yl)-3-(trifluoromethyl)benzenesulfonamide (5), *N*-((*anti*)-3-(1*H*-tetrazol-5-yl)-2,3-dihydro-1*H*-inden-1-yl)-3-(trifluoromethyl)benzenesulfonamide (6).** A sealed tube was charged with **S13** (72.0 mg, 0.197 mmol, 1.0 equiv.), sodium azide (38.3 mg, 0.590 mmol, 3.0 equiv.), ammonium chloride (33.6 mg, 0.629 mmol, 3.2 equiv.), and DMF (5

mL). The tube was sealed and heated at 120 °C behind a blast shield for 14h. The crude reaction mixture was directly purified by reverse phase HPLC (water/MeOH/0.05% formic acid) to afford syn **5** (20.3 mg, 25%) and anti **6** (30.4 mg, 38%) as white solids. **5**: ^1H NMR (400 MHz, CD_3OD) δ = 8.25 - 8.17 (m, 2H), 7.96 (d, J = 7.8 Hz, 1H), 7.84 - 7.78 (m, 1H), 7.25 - 7.14 (m, 2H), 7.11 - 7.03 (m, 2H), 5.17 (dd, J = 5.4, 7.1 Hz, 1H), 4.91 - 4.86 (m, 1H), 2.56 (ddd, J = 6.1, 7.2, 13.2 Hz, 1H), 2.34 (ddd, J = 5.1, 8.3, 13.4 Hz, 1H); ^{13}C NMR (100 MHz, CD_3OD) δ = 167.08, 143.50, 142.37, 141.84, 131.23 (q, J = 33.8 Hz), 130.31, 130.25, 128.77 (d, J = 3.7 Hz), 128.59, 127.73, 124.59, 124.45, 123.52 - 123.29 (m), 123.53 (d, J = 272.2 Hz), 57.52, 39.87, 38.45; ^{19}F NMR (376 MHz, CD_3OD) δ = -64.28 (s, 3F); LRMS (ESI) calculated for $\text{C}_{17}\text{H}_{13}\text{F}_3\text{N}_5\text{O}_2\text{S}$ $[\text{M} - \text{H}]^-$ m/z 408.07, found 408.04. **6**: ^1H NMR (400 MHz, CD_3OD) δ = 8.24 - 8.18 (m, 2H), 7.92 (br d, J = 7.8 Hz, 1H), 7.81 - 7.73 (m, 1H), 7.24 - 7.13 (m, 3H), 6.93 (br d, J = 6.8 Hz, 1H), 4.97 (t, J = 8.0 Hz, 1H), 4.58 (br t, J = 8.5 Hz, 1H), 2.65 (td, J = 7.3, 12.7 Hz, 1H), 2.01 (td, J = 9.4, 12.4 Hz, 1H); ^{13}C NMR (100 MHz, CD_3OD) δ = 163.15, 143.49, 142.07, 141.01, 131.26 (d, J = 33.0 Hz), 130.32, 128.88 (q, J = 3.7 Hz), 128.24, 127.64, 123.99, 123.89, 123.42 (q, J = 3.7 Hz), 123.51 (d, J = 272.2 Hz), 57.01, 40.37, 37.66; ^{19}F NMR (376 MHz, CD_3OD) δ = -64.28 (s, 3F); LRMS (ESI) calculated for $\text{C}_{17}\text{H}_{13}\text{F}_3\text{N}_5\text{O}_2\text{S}$ $[\text{M} - \text{H}]^-$ m/z 408.07, found 408.04.



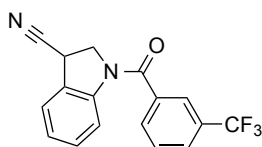
1-(3-(trifluoromethyl)benzoyl)indoline-3-carboxylic acid (S14). Commercially available indoline-3-carboxylic acid (100 mg, 0.613 mmol, 1.0 equiv.) was suspended

with dry dichloromethane (15 mL). *N,N*-diisopropylethylamine (267 μ L, 1.53 mmol, 2.5 equiv.) was then added, and the resulting solution was cooled to 0 °C. 3-(trifluoromethyl)benzoyl chloride (111 μ L, 0.735 mmol, 1.2 equiv.) was then added dropwise at 0 °C. The reaction mixture was allowed to warm to r.t. overnight. The solvent was then removed under reduced pressure and the reaction mixture redissolved in DMF; directly purified by reverse phase HPLC (water/MeOH/0.05% formic acid) to afford **S14** (129.7 mg, 63%) as a white solid. ^1H NMR (400 MHz, CD_3OD) δ = 8.11 (br s, 1H), 7.87 (br s, 1H), 7.80 (br d, J = 7.5 Hz, 2H), 7.69 - 7.61 (m, 1H), 7.45 (d, J = 7.5 Hz, 1H), 7.22 (br s, 1H), 7.07 (br s, 1H), 4.33 (br s, 1H), 4.21 - 4.04 (m, 2H); ^{13}C NMR (100 MHz, CD_3OD) δ = 174.46 (br s), 169.27 (br s), 143.60 - 143.03 (m), 139.01 (br s), 132.29 (q, J = 33.0 Hz), 131.94 (br s), 130.95, 129.66 (br s), 128.34 (br s), 126.58 (br s), 126.08 (br s), 125.29 (br s), 125.34 (q, J = 272.2 Hz), 119.03, 54.45 (br s), 46.84 (br s); ^{19}F NMR (376 MHz, CD_3OD) δ = -64.08 (s, 3F); LRMS (ESI) calculated for $\text{C}_{17}\text{H}_{11}\text{F}_3\text{NO}_3$ $[\text{M} - \text{H}]^-$ m/z 334.07, found 334.03.



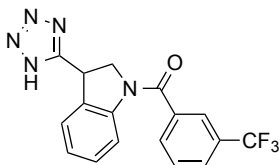
1-(3-(trifluoromethyl)benzoyl)indoline-3-carboxamide (S15). **S14** (129.7 mg, 0.387 mmol, 1.0 equiv.) was dissolved with dry acetone (3.5 mL); ammonium bicarbonate (40 mg, 0.503, 1.3 equiv.), pyridine (4 μ L, 0.05 mmol, 0.13 equiv.), and di-*tert*-butyl dicarbonate (110 mg, 0.503 mmol, 1.3 equiv.) were then added. The reaction was stirred for 14h, at which point the acetone was removed under reduced pressure. The resulting residue was transferred to a sep funnel with ~ 75 mL EtOAc; washed with

dilute citric acid, water, and brine. Dried over MgSO₄, concentrated, and purified on a silica column with 0-4% dichloromethane:MeOH. **S15** (90.9 mg, 70%) obtained as a white solid. ¹H NMR (400 MHz, CDCl₃, drops CD₃OD) δ = 8.12 (br s, 1H), 7.82 (br s, 1H), 7.73 (br d, *J* = 5.1 Hz, 2H), 7.63 - 7.54 (m, 1H), 7.31 (br d, *J* = 7.3 Hz, 1H), 7.25 (br s, 1H), 7.07 (br s, 1H), 4.35 (br s, 1H), 4.09 (br s, 1H), 3.73 (br s, 1H); ¹³C NMR (100 MHz, CDCl₃, drops CD₃OD) δ = 174.22 (br s), 167.81 (br s), 142.40 (br s), 137.32 (br s), 131.44 (q, *J* = 33.7 Hz), 130.64 (br s), 129.64, 129.05 (br s), 127.52 (br s), 125.49 - 124.01 (m), 53.95 (br s), 46.78 (br s); ¹⁹F NMR (376 MHz, CDCl₃, drops CD₃OD) δ = -59.08 (s, 3F); LRMS (ESI) calculated for C₁₇H₁₄F₃N₂O₂ [M + H]⁺ *m/z* 335.10, found 335.01.



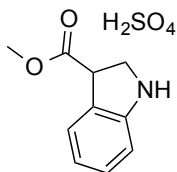
1-(3-(trifluoromethyl)benzoyl)indoline-3-carbonitrile (S16). **S15** (90.9 mg, 0.272 mmol, 1.0 equiv.) was dissolved with dry 1,4-dioxane (7 mL); pyridine (66 μ L, 0.816 mmol, 3.0 equiv.) was then added, and the reaction mixture was cooled to 0 °C. trifluoroacetic anhydride (114 μ L, 0.816 mmol, 3.0 equiv.) was then added dropwise, and the reaction mixture was allowed to slowly warm to r.t. After stirring for 14h, the crude reaction mixture was transferred to a sep funnel with ~ 120 mL EtOAc and ~ 20 mL water. The organic layer was washed with ~ 50 mL 0.1 N HCl, water, and brine. Dried over MgSO₄, concentrated, and purified on a silica column with EtOAc:hexanes. **S16** (87.3 mg, 102%, wet with EtOAc) obtained as a white solid. ¹H NMR (400 MHz, CD₃OD, drops CDCl₃) δ = 7.88 - 7.77 (m, 4H), 7.71 - 7.64 (m, 1H), 7.44 (d, *J* = 7.5 Hz,

1H), 7.28 (br s, 1H), 7.21 - 7.14 (m, 1H), 4.60 (dd, $J = 7.4, 9.1$ Hz, 1H), 4.42 (br t, $J = 10.0$ Hz, 1H), 4.31 - 4.22 (m, 1H); ^{13}C NMR (100 MHz, CD_3OD , drops CDCl_3) $\delta = 168.19, 142.23$ (br s), 137.22 (br s), 131.96 (q, $J = 32.8$ Hz), 131.25 (br s), 130.34, 130.25, 128.32 (br s), 127.54 (br s), 126.06 (br s), 125.63 (br s), 124.87 (br s), 124.33 (q, $J = 273.0$ Hz), 119.28, 54.63 - 54.00 (m), 31.35 (br s); ^{19}F NMR (376 MHz, CD_3OD , drops CDCl_3) $\delta = -63.62$ (s, 3F); LRMS (ESI) calculated for $\text{C}_{17}\text{H}_{10}\text{F}_3\text{N}_2\text{O}$ $[\text{M} - \text{H}]^-$ m/z 315.08, found 314.96.

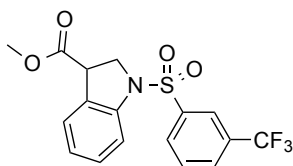


(3-(1H-tetrazol-5-yl)indolin-1-yl)(3-(trifluoromethyl)phenyl)methanone (7). A sealed tube was charged with **S16** (89.3 mg, 0.282 mmol, 1.0 equiv.), sodium azide (55 mg, 0.847 mmol, 3.0 equiv.), ammonium chloride (48 mg, 0.904 mmol, 3.2 equiv.), and DMF (4 mL). The tube was sealed and heated at 140 °C behind a blast shield for 14h. The crude reaction mixture was directly purified by reverse phase HPLC (water/MeOH/0.05% formic acid) to afford **7** (56.5 mg, 56%) as a white solid. ^1H NMR (400 MHz, DMSO-d_6) $\delta = 8.15$ (br s, 1H), 8.04 - 7.95 (m, 2H), 7.92 (br d, $J = 7.8$ Hz, 1H), 7.81 - 7.73 (m, 1H), 7.29 (br s, 2H), 7.11 (br s, 1H), 5.12 (br dd, $J = 6.8, 9.3$ Hz, 1H), 4.57 - 4.48 (m, 1H), 4.37 (br dd, $J = 6.7, 10.3$ Hz, 1H); ^{13}C NMR (100 MHz, DMSO-d_6) $\delta = 166.45, 157.59, 142.00$ (br s), 137.56 (br s), 131.68 (br s), 131.15 (br s), 129.90, 129.40 (q, $J = 32.0$ Hz), 128.42, 127.00 (br s), 125.37 - 125.09 (m), 124.54 (br s), 123.91 (br s), 123.86 (q, $J = 272.4$ Hz), 117.11 (br s), 55.09 - 54.49 (m), 36.25 - 35.49

(m); ^{19}F NMR (376 MHz, DMSO- d_6) δ = -61.18 (s, 3F); LRMS (ESI) calculated for $\text{C}_{17}\text{H}_{11}\text{F}_3\text{N}_5\text{O}$ $[\text{M} - \text{H}]^-$ m/z 358.09, found 358.12.

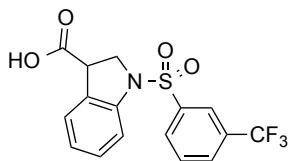


methyl indoline-3-carboxylate sulfate (S17). Commercially available indoline-3-carboxylic acid (100 mg, 0.613 mmol, 1.0 equiv.) was dissolved in dry methanol (25 mL). Sulfuric acid (37 μL , 0.674 mmol, 1.1 equiv.) was then added, and the reaction mixture was refluxed for 18h. The solvent was then removed under reduced pressure, and the residue dried under hivaac overnight. Wet **S17** (208.5 mg, 124%) obtained as a thick, brown oil. (**Note:** the free base is not stable; will spontaneously oxidize) ^1H NMR (400 MHz, CD_3OD) δ = 7.65 - 7.61 (m, 1H), 7.55 - 7.48 (m, 3H), 4.60 (dd, J = 5.2, 8.9 Hz, 1H), 4.25 - 4.19 (m, 1H), 4.07 (dd, J = 8.8, 12.2 Hz, 1H), 3.61 (s, 3H); ^{13}C NMR (100 MHz, CD_3OD) δ = 171.85, 137.11, 134.44, 131.53, 131.11, 127.67, 120.94, 55.30, 53.56, 48.08; LRMS (ESI) calculated for $\text{C}_{10}\text{H}_{12}\text{NO}_2$ $[\text{M} + \text{H}]^+$ m/z 178.09, found 177.94.

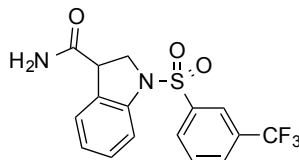


methyl 1-((3-(trifluoromethyl)phenyl)sulfonyl)indoline-3-carboxylate (S18). **S17** (208.5 mg, 0.757 mmol, 1.0 equiv.) was reacted with commercially available 3-(trifluoromethyl)benzene sulfonyl chloride (1.5 equiv.) in dry DMF (5 mL) according to general procedure A, except 5.0 equiv. of *N,N*-diisopropylethylamine was used. **S18** (108.0 mg, 37%) obtained as a tan oil. ^1H NMR (400 MHz, CDCl_3) δ = 8.07 (s, 1H), 8.00

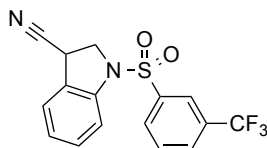
(d, $J = 8.0$ Hz, 1H), 7.81 (dd, $J = 0.7, 8.5$ Hz, 1H), 7.68 - 7.57 (m, 2H), 7.35 - 7.26 (m, 2H), 7.05 (dt, $J = 1.1, 7.6$ Hz, 1H), 4.40 (dd, $J = 5.8, 11.2$ Hz, 1H), 4.20 - 4.12 (m, 1H), 4.07 - 4.01 (m, 1H), 3.63 (s, 3H); ^{13}C NMR (100 MHz, CDCl_3) $\delta = 170.59, 140.97, 137.97, 131.56$ (q, $J = 33.7$ Hz), 130.38 (d, $J = 1.5$ Hz), 129.99 - 129.70 (m), 129.33, 128.60, 125.89, 124.45 - 124.27 (m), 125.72 (d, $J = 273.0$ Hz), 121.65, 114.90, 52.55, 51.71, 44.90; ^{19}F NMR (376 MHz, CDCl_3) $\delta = -62.94$ (s, 3F); LRMS (ESI) calculated for $\text{C}_{17}\text{H}_{14}\text{F}_3\text{NNaO}_4\text{S}$ [$\text{M} + \text{Na}$] $^+$ m/z 408.05, found 408.04.



1-((3-(trifluoromethyl)phenyl)sulfonyl)indoline-3-carboxylic acid (S19). **S18** (108.0 mg, 0.280 mmol, 1.0 equiv.) was reacted in methanol (4 mL) with 1M lithium hydroxide (3 mL, 3 mmol, 10.7 equiv.) according to general procedure B. Semi-crude **S19** (101.2 mg, 97%) obtained as a tan powder. ^1H NMR (400 MHz, CD_3OD , drops CDCl_3) $\delta = 8.03$ - 7.96 (m, 2H), 7.84 (d, $J = 7.8$ Hz, 1H), 7.68 - 7.57 (m, 2H), 7.36 (d, $J = 7.5$ Hz, 1H), 7.27 (t, $J = 7.7$ Hz, 1H), 7.04 (dt, $J = 1.0, 7.5$ Hz, 1H), 4.36 (dd, $J = 5.8, 11.2$ Hz, 1H), 4.16 - 4.08 (m, 1H), 4.04 - 3.97 (m, 1H); ^{13}C NMR (100 MHz, CD_3OD , drops CDCl_3) $\delta = 173.20, 141.90, 138.75, 132.36$ (q, $J = 33.7$ Hz), 131.52, 131.11, 130.91 (q, $J = 3.2$ Hz), 130.59, 129.90, 126.92, 125.38, 125.10 (q, $J = 3.9$ Hz), 124.14 (q, $J = 272.2$ Hz), 115.74, 52.93, 45.94; ^{19}F NMR (376 MHz, CD_3OD , drops CDCl_3) $\delta = -63.89$ (s, 3F); LRMS (ESI) calculated for $\text{C}_{16}\text{H}_{11}\text{F}_3\text{NO}_4\text{S}$ [$\text{M} - \text{H}$] $^-$ m/z 370.04, found 370.04.

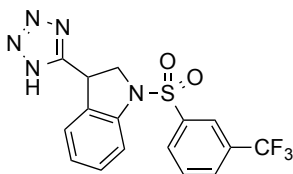


1-((3-(trifluoromethyl)phenyl)sulfonyl)indoline-3-carboxamide (S20). Semi-crude **S19** (101.2 mg, 0.273 mmol, 1.0 equiv.) was dissolved with dry acetone (3.5 mL); ammonium bicarbonate (28 mg, 0.354, 1.3 equiv.), pyridine (4 μ L, 0.05 mmol, 0.18 equiv.), and di-tert-butyl dicarbonate (77 mg, 0.354 mmol, 1.3 equiv.) were then added. The reaction was stirred for 14h, at which point the acetone was removed under reduced pressure. The resulting residue was transferred to a sep funnel with \sim 75 mL EtOAc; washed with dilute citric acid, water, and brine. Dried over MgSO_4 , concentrated, and run on a silica column with 0-5% dichloromethane:MeOH. Attempts to fully clean up the product were unsuccessful; crude **S20** (49.3 mg, est. 80% purity) obtained as an off-white solid. LRMS (ESI) calculated for $\text{C}_{16}\text{H}_{14}\text{F}_3\text{N}_2\text{O}_3\text{S}$ $[\text{M} + \text{H}]^+$ m/z 371.07, found 370.95.



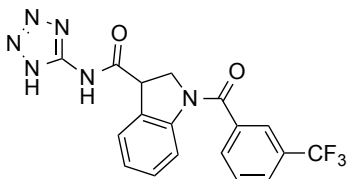
1-((3-(trifluoromethyl)phenyl)sulfonyl)indoline-3-carbonitrile (S21). Crude **S20** (101 mg, 0.272 mmol, 1.0 equiv.) was suspended with dry 1,4-dioxane (8 mL); pyridine (66 μ L, 0.817 mmol, 3.0 equiv.) was then added, followed by dropwise addition of trifluoroacetic anhydride (114 μ L, 0.817 mmol, 3.0 equiv.). After stirring for 14h, the crude reaction mixture was transferred to a sep funnel with \sim 120 mL EtOAc and \sim 20 mL water. The organic layer was washed with \sim 50 mL 0.1 N HCl, water, and brine. Dried over MgSO_4 , concentrated, and purified on a silica column with 0-25%

EtOAc:hexanes. **S21** (37.0 mg, 39% over two steps) obtained as a white solid. ^1H NMR (400 MHz, CD_3OD) δ = 8.07 (d, J = 8.0 Hz, 1H), 8.00 (s, 1H), 7.97 - 7.93 (m, 1H), 7.76 - 7.68 (m, 2H), 7.45 - 7.39 (m, 1H), 7.35 (d, J = 7.8 Hz, 1H), 7.18 (dt, J = 1.0, 7.5 Hz, 1H), 4.40 - 4.35 (m, 1H), 4.35 - 4.28 (m, 1H), 4.23 - 4.16 (m, 1H); ^{13}C NMR (100 MHz, CD_3OD) δ = 142.31, 138.84, 132.73 (q, J = 33.8 Hz), 132.00, 131.91, 131.65 (q, J = 3.4 Hz), 131.22, 128.71, 126.72, 126.66, 125.15 (q, J = 3.9 Hz), 124.51 (q, J = 272.2 Hz), 119.42, 117.38, 54.37, 31.55; ^{19}F NMR (376 MHz, CD_3OD) δ = -64.51 (s, 3F); LRMS (ESI) calculated for $\text{C}_{16}\text{H}_{10}\text{F}_3\text{N}_2\text{O}_2\text{S}$ [$\text{M} - \text{H}$] $^+$ m/z 351.04, found 350.29.

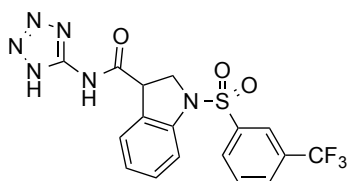


3-(1H-tetrazol-5-yl)-1-((3-(trifluoromethyl)phenyl)sulfonyl)indoline (8). A sealed tube was charged with **S21** (37.0 mg, 0.105 mmol, 1.0 equiv.), sodium azide (20.5 mg, 0.315 mmol, 3.0 equiv.), ammonium chloride (18 mg, 0.336 mmol, 3.2 equiv.), and DMF (4 mL). The tube was sealed and heated at 120 °C behind a blast shield for 14h. The crude reaction mixture was directly purified by reverse phase HPLC (water/MeOH/0.05% formic acid) to afford **8** (25.1 mg, 61%) as a white solid. ^1H NMR (400 MHz, DMSO-d_6) δ = 8.16 (br d, J = 7.8 Hz, 1H), 8.08 (br d, J = 8.0 Hz, 1H), 8.04 (s, 1H), 7.82 (t, J = 7.8 Hz, 1H), 7.59 (d, J = 8.0 Hz, 1H), 7.34 (t, J = 7.7 Hz, 1H), 7.20 (br d, J = 7.3 Hz, 1H), 7.11 - 7.04 (m, 1H), 4.96 (br dd, J = 6.8, 9.3 Hz, 1H), 4.52 (t, J = 10.3 Hz, 1H), 4.34 (dd, J = 6.6, 11.0 Hz, 1H); ^{13}C NMR (100 MHz, DMSO-d_6) δ = 161.69, 140.45, 136.99, 131.41 - 131.09 (m), 130.90, 130.75 (d, J = 2.9 Hz), 130.08 (d, J = 33.0 Hz), 129.22, 125.94, 124.68, 123.65 (d, J = 3.7 Hz), 123.15 (d, J = 272.9 Hz), 114.46,

54.22, 35.30; ^{19}F NMR (376 MHz, DMSO- d_6) δ = -61.50 (s, 3F); LRMS (ESI) calculated for $\text{C}_{16}\text{H}_{11}\text{F}_3\text{N}_5\text{O}_2\text{S}$ [$\text{M} - \text{H}$] $^-$ m/z 394.06, found 393.83.

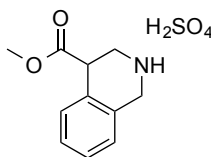


***N*-(1*H*-tetrazol-5-yl)-1-(3-(trifluoromethyl)benzoyl)indoline-3-carboxamide (9). S14** (342.3 mg, 1.02 mmol, 1.0 equiv.) was reacted with 5-aminotetrazole monohydrate in 50 mL dichloromethane according to general procedure C. **9** (91.2 mg, 22%) obtained as a white solid. **Note:** Unstable long-term at r.t. or in solution; store cold. ^1H NMR (400 MHz, DMSO- d_6) δ = 12.13 (br s, 1H), 8.34 - 7.66 (br m, 5H), 7.61 - 6.98 (br m, 3H), 4.68 - 4.12 (br m, 3H); ^{13}C NMR (100 MHz, DMSO- d_6) δ = 170.40, 166.83, 163.62, 152.17 (br s), 142.82 (br s), 138.21, 131.55 (br s), 130.44 (br s), 129.85 (br d, J = 35.2 Hz), 128.98 (br s), 127.46 (br s), 125.71 (br s), 125.53 (br s), 124.83 (br s), 124.25 (br s), 117.76 (br s), 53.45 (br s), 46.49 (br s); ^{19}F NMR (376 MHz, DMSO- d_6) δ = -61.16 (s, 3F); LRMS (ESI) calculated for $\text{C}_{18}\text{H}_{12}\text{F}_3\text{N}_6\text{O}_2$ [$\text{M} - \text{H}$] $^-$ m/z 401.10, found 400.99.

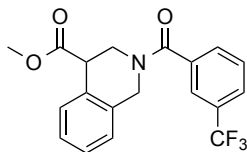


***N*-(1*H*-tetrazol-5-yl)-1-((3-(trifluoromethyl)phenyl)sulfonyl)indoline-3-carboxamide (10).** Semi-crude **S19** (130 mg, 0.350 mmol, 1.0 equiv.) was reacted with 5-aminotetrazole monohydrate in 3.5 mL DMF according to general procedure D (20m activation). **10** (20.8 mg, 14%) obtained as a white solid. **Note:** Unstable long-term at r.t. or in solution; store cold. ^1H NMR (400 MHz, DMSO- d_6) δ = 12.48 - 11.87 (br s, 1H),

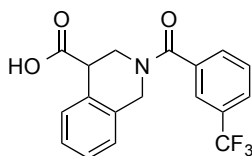
8.19 (br d, $J = 7.8$ Hz, 1H), 8.10 (br d, $J = 7.5$ Hz, 1H), 8.04 (s, 1H), 7.86 (br t, $J = 7.8$ Hz, 1H), 7.54 (br d, $J = 8.0$ Hz, 1H), 7.38 - 7.27 (m, 2H), 7.10 - 7.02 (m, 1H), 4.40 - 4.27 (m, 2H), 4.27 - 4.17 (m, 1H); ^{13}C NMR (100 MHz, DMSO- d_6) $\delta = 169.20, 163.04, 140.72, 137.04, 131.34, 131.19, 130.71$ (br d, $J = 3.6$ Hz), 130.14 (d, $J = 5.3$ Hz), $129.13, 125.57, 124.26, 123.74 - 123.38$ (m), 123.17 (d, $J = 273.1$ Hz), $113.98, 52.22, 45.40$; ^{19}F NMR (376 MHz, DMSO- d_6) $\delta = -61.46$ (s, 3F); LRMS (ESI) calculated for $\text{C}_{17}\text{H}_{12}\text{F}_3\text{N}_6\text{O}_3\text{S}$ $[\text{M} - \text{H}]^-$ m/z 437.06, found 437.12.



methyl 1,2,3,4-tetrahydroisoquinoline-4-carboxylate sulfate (S22). Commercially available 1,2,3,4-tetrahydroisoquinoline-4-carboxylic acid (200 mg, 1.13 mmol, 1.0 equiv.) was dissolved in dry methanol (25 mL). Sulfuric acid (69 μL , 1.24 mmol, 1.1 equiv.) was then added, and the reaction mixture was refluxed for 18h. The solvent was then removed under reduced pressure, and the residue dried under hivac overnight. Wet **S22** (429.5 mg, 132%) obtained as a thick, tan oil. ^1H NMR (400 MHz, CD_3OD) $\delta = 7.48 - 7.42$ (m, 1H), $7.33 - 7.27$ (m, 2H), $7.26 - 7.20$ (m, 1H), 4.39 (s, 2H), 4.20 (t, $J = 4.4$ Hz, 1H), 3.88 (dd, $J = 3.7, 13.1$ Hz, 1H), 3.72 (s, 3H), 3.53 (dd, $J = 5.2, 13.0$ Hz, 1H); ^{13}C NMR (100 MHz, CD_3OD) $\delta = 173.23, 130.51, 129.46, 129.34, 129.31, 129.16, 128.03, 55.09, 45.29, 43.88, 41.33$; LRMS (ESI) calculated for $\text{C}_{11}\text{H}_{14}\text{NO}_2$ $[\text{M} + \text{H}]^+$ m/z 192.10, found 191.91.

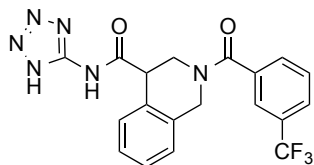


methyl 2-(3-(trifluoromethyl)benzoyl)-1,2,3,4-tetrahydroisoquinoline-4-carboxylate (S23). **S22** (215.2 mg, 0.744 mmol, 1.1 equiv.) was reacted with commercially available 3-(trifluoromethyl)benzoyl chloride in dry DMF (5 mL) according to general procedure A, with slight modification: prior to base addition, the reaction vessel was cooled to 0 °C; 5.0 equiv of *N,N*-diisopropylethylamine was used, and allowed to stir at 0 °C for 5m; after acyl chloride addition, the reaction mixture was allowed to slowly warm to r.t. **S23** (188.9 mg, 77%) obtained as a colorless oil. **Note:** Diastereomers from the atropisomers of the secondary amide observable by NMR. ¹H NMR (400 MHz, CDCl₃) δ = 7.73 - 7.65 (m, 2H), 7.61 (br d, *J* = 6.8 Hz, 1H), 7.57 - 7.50 (m, 1H), 7.22 (br s, 3H), 6.94 (br s, 1H), 5.13 (br s, 1H), 4.62 (br s, 2H), 4.10 (br s, 1H), 3.96 (br s, 1H), 3.84 - 3.54 (m, 3H); ¹³C NMR (100 MHz, CDCl₃) δ = 171.83 (br s), 169.27 (br s), 136.53 (br s), 132.27 (br s), 130.74 (q, *J* = 33.0 Hz), 130.21, 128.91 (d, *J* = 2.2 Hz), 127.71 (br s), 126.80 (br s), 126.32 (br s), 123.90 (q, *J* = 3.9 Hz), 123.51 (q, *J* = 272.9 Hz), 52.14, 49.26 (br s), 46.18 (br s), 44.20 (br s), 42.31 (br s); ¹⁹F NMR (376 MHz, CDCl₃) δ = -62.71 (s, 3F); LRMS (ESI) calculated for C₁₉H₁₇F₃NO₃ [M + H]⁺ *m/z* 364.12, found 363.96.



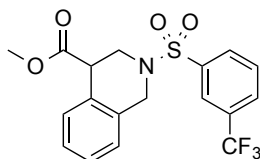
2-(3-(trifluoromethyl)benzoyl)-1,2,3,4-tetrahydroisoquinoline-4-carboxylic acid (S24). **S23** (98.5 mg, 0.271 mmol, 1.0 equiv.) was reacted in methanol (4 mL) with 1M

lithium hydroxide (4 mL, 4 mmol, 14.8 equiv.) according to general procedure B, except the reaction was cooled to 0 °C prior to hydroxide addition, and allowed to slowly warm to r.t. Semi-crude **S24** (89.6 mg, 95%) obtained as a colorless oil. **Note:** Diastereomers from the atropisomers of the secondary amide observable by NMR. ¹H NMR (400 MHz, CD₃OD, CDCl₃) δ = 7.84 - 7.60 (m, 4H), 7.34 - 7.18 (m, 3H), 6.98 (br s, 1H), 5.19 (br d, *J* = 17.3 Hz, 0.4H), 4.92 (br s, 0.6H), 4.76 (br d, *J* = 9.7 Hz, 0.4H), 4.58 (br s, 0.6H), 4.13 (br s, 0.4H), 3.98 (br s, 0.4H), 3.80 (br s, 0.6H), 3.76 - 3.56 (m, 0.6H); ¹³C NMR (100 MHz, CD₃OD, CDCl₃) δ = 173.00, 172.53, 169.79 (br s), 165.90, 135.88 (br s), 132.04, 131.43, 130.76 (br d, *J* = 30.8 Hz), 129.89 - 129.25 (m), 128.56 - 127.95 (m), 126.65, 125.91 - 125.25 (m), 125.15 (br d, *J* = 3.7 Hz), 123.23 - 122.59 (m), 123.01 (d, *J* = 273.0 Hz), 48.46 (br s), 45.68 (br s), 43.44, 41.51 (br s); ¹⁹F NMR (376 MHz, CD₃OD, CDCl₃) δ = -63.98 (br s, 3F), -64.04 (br s, 1.7F); LRMS (ESI) calculated for C₁₈H₁₃F₃NO₃ [M - H]⁻ m/z 348.09, found 348.23.



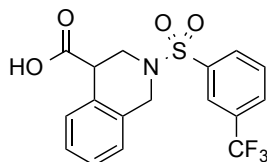
***N*-(1*H*-tetrazol-5-yl)-2-(3-(trifluoromethyl)benzoyl)-1,2,3,4-tetrahydroisoquinoline-4-carboxamide (11).** Semi-crude **S24** (89.6 mg, 0.257 mmol, 1.0 equiv.) was reacted with 5-aminotetrazole monohydrate (1.5 equiv.) in 4 mL DMF according to general procedure D (10m activation), except 3.0 equiv. *N,N*-diisopropylethylamine was added initially, with no second addition. **11** (29.0 mg, 27%) obtained as a white solid. **Note:** Diastereomers from the atropisomers of the secondary amide observable by NMR. ¹H NMR (400 MHz, DMF-d₇) δ = 7.83 (br s, 4H), 7.67 - 7.06 (br m, 4H), 5.22 (br s, 1H), 4.77 (br s, 1H), 4.59

- 4.33 (br m, 1H), 4.15 (br s, 1H), 3.97 (br s, 1H); ^{19}F NMR (376 MHz, DMF-d7) $\delta = -62.96$ (s, 3F), -63.04 (s, 3F); LRMS (ESI) calculated for $\text{C}_{19}\text{H}_{14}\text{F}_3\text{N}_6\text{O}_2$ $[\text{M} - \text{H}]^-$ m/z 415.11, found 415.26.

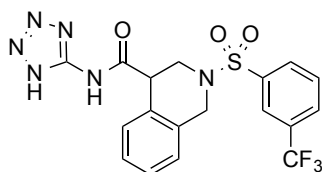


methyl 2-(3-(trifluoromethyl)benzoyl)-1,2,3,4-tetrahydroisoquinoline-4-carboxylate

(S25). **S22** (212.4 mg, 0.734 mmol, 1.1 equiv.) was reacted with commercially available 3-(trifluoromethyl)benzenesulfonyl chloride in dry DMF (5 mL) according to general procedure A, with slight modification: prior to base addition, the reaction vessel was cooled to 0 °C; 5.0 equiv of *N,N*-diisopropylethylamine was added and allowed to stir at 0 °C for 5m; after acyl chloride addition, the reaction mixture was allowed to slowly warm to r.t. **S25** (206.6 mg, 78%) obtained as a colorless oil. ^1H NMR (400 MHz, CDCl_3) $\delta = 8.09$ (s, 1H), 8.03 (d, $J = 8.0$ Hz, 1H), 7.84 (d, $J = 7.8$ Hz, 1H), 7.72 - 7.65 (m, 1H), 7.24 - 7.15 (m, 3H), 7.09 - 7.04 (m, 1H), 4.41 (d, $J = 15.1$ Hz, 1H), 4.23 (d, $J = 15.1$ Hz, 1H), 3.97 (dd, $J = 5.2, 12.1$ Hz, 1H), 3.92 - 3.88 (m, 1H), 3.69 (s, 3H), 3.41 (dd, $J = 4.6, 11.9$ Hz, 1H); ^{13}C NMR (100 MHz, CDCl_3) $\delta = 171.45, 137.92, 131.58$ (q, $J = 33.7$ Hz), 131.15, 130.71, 129.95, 129.90, 129.47 (q, $J = 3.4$ Hz), 129.22, 127.57, 127.01, 126.33, 124.35 (q, $J = 4.2$ Hz), 123.00 (q, $J = 273.0$ Hz), 52.30, 47.13, 45.42, 44.24; ^{19}F NMR (376 MHz, CDCl_3) $\delta = -62.75$ (s, 3F); LRMS (ESI) calculated for $\text{C}_{18}\text{H}_{17}\text{F}_3\text{NO}_4\text{S}$ $[\text{M} + \text{H}]^+$ m/z 400.08, found 399.98.

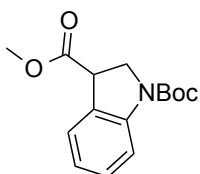


2-((3-(trifluoromethyl)phenyl)sulfonyl)-1,2,3,4-tetrahydroisoquinoline-4-carboxylic acid (S26). **S25** (108.5 mg, 0.272 mmol, 1.0 equiv.) was reacted in methanol (4 mL) with 1M lithium hydroxide (4 mL, 4 mmol, 14.7 equiv.) according to general procedure B, except the reaction was cooled to 0 °C prior to hydroxide addition, and allowed to slowly warm to r.t. Semi-crude **S26** (91.2 mg, 87%) obtained as a white solid. ^1H NMR (400 MHz, CD_3OD , CDCl_3) δ = 8.10 - 8.05 (m, 2H), 7.91 (d, J = 7.8 Hz, 1H), 7.80 - 7.72 (m, 1H), 7.25 - 7.14 (m, 3H), 7.11 - 7.06 (m, 1H), 4.41 (d, J = 15.3 Hz, 1H), 4.16 (d, J = 15.3 Hz, 1H), 4.00 (dd, J = 5.0, 12.1 Hz, 1H), 3.86 (t, J = 4.9 Hz, 1H), 3.37 (dd, J = 4.9, 12.2 Hz, 1H); ^{13}C NMR (100 MHz, CD_3OD , CDCl_3) δ = 174.94, 139.27, 132.76, 132.83 (q, J = 33.0 Hz), 132.35, 131.90, 131.69, 130.96 (q, J = 3.4 Hz), 130.74, 128.68, 128.18, 127.58, 125.56 (q, J = 4.2 Hz), 124.65 (q, J = 272.2 Hz), 48.64, 47.15, 45.62; ^{19}F NMR (376 MHz, CD_3OD , CDCl_3) δ = -63.81 (s, 3F); LRMS (ESI) calculated for $\text{C}_{17}\text{H}_{13}\text{F}_3\text{NO}_4\text{S}$ [$\text{M} - \text{H}$] $^-$ m/z 384.05, found 384.02.



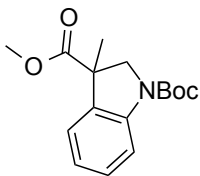
***N*-(1*H*-tetrazol-5-yl)-2-((3-(trifluoromethyl)phenyl)sulfonyl)-1,2,3,4-tetrahydroisoquinoline-4-carboxamide (12).** Semi-crude **S26** (91.2 mg, 0.237 mmol, 1.0 equiv.) was reacted with 5-aminotetrazole monohydrate (1.5 equiv.) in 4 mL DMF according to general procedure D (10m activation), except 3.0 equiv. *N,N*-

diisopropylethylamine was added initially, with no second addition. **12** (16.3 mg, 15%) obtained as a white solid. ^1H NMR (400 MHz, DMF-d7) δ = 8.52 - 7.69 (m, 4H), 7.28 (br s, 4H), 4.78 - 4.19 (m, 3H), 4.11 (br s, 1H), 3.64 (br s, 1H); ^{19}F NMR (376 MHz, DMF-d7) δ = -62.64 (s, 3F); LRMS (ESI) calculated for $\text{C}_{18}\text{H}_{14}\text{F}_3\text{N}_6\text{O}_3\text{S}$ $[\text{M} - \text{H}]^-$ m/z 451.08, found 450.90.



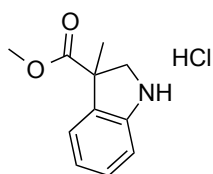
1-(tert-butyl) 3-methyl indoline-1,3-dicarboxylate (S27). Commercially available methyl indole-3-carboxylate (6.500 g, 37.1 mmol, 1.0 equiv.) and sodium hydride (60% in mineral oil) (2.226 g, 55.7 mmol, 1.5 equiv.) were placed in a 200 mL round bottom flask and cooled to 0 °C with an ice bath. Dry tetrahydrofuran (55 mL) was slowly added under Ar with stirring. After 30 minutes of cooling, di-tert-butyl dicarbonate (12.147 g, 55.7 mmol, 1.5 equiv.) was added in two portions at 0 °C, solidifying the solution. Additional dry tetrahydrofuran (100 mL) was subsequently added; stirred at r.t for 1.5h, then heated to 65 °C for 14h. The reaction mixture was quenched with a *slow* addition of ~ 20 mL sat. NH_4Cl -- the crude reaction slurry was transferred to a sep. funnel with ~ 500 mL ether, and the organic layer was washed with 3 x 500 mL water. The ether layer was dried over MgSO_4 , filtered, and concentrated; dried under hivac overnight. The resulting tan powder was dissolved in methanol (750 mL) and EtOAc (250 mL) and hydrogenated for 14d using an "H-Cube" flow hydrogenator with a 10% Pd/C cartridge; 1 mL/min, 60 bar H_2 , 50 °C, loop configuration. (**Note:** During this period the cartridge was replaced three times. Slurry hydrogenation sans EtOAc is likely a better option.)

After completion of the hydrogenation, the system was purged with methanol and the combined mixture concentrated under reduced pressure. Purified directly on a silica column with 0-3% dichloromethane:methanol. **S27** (7.590 g, 74%) obtained as colorless oil. (**Note:** will slowly oxidize back to indole, store cold) ^1H NMR (400 MHz, CDCl_3) δ = 7.89 (br s, 1H), 7.36 (d, J = 7.5 Hz, 1H), 7.24 (t, J = 7.8 Hz, 1H), 6.97 (t, J = 7.4 Hz, 1H), 4.39 (br dd, J = 5.8, 11.0 Hz, 1H), 4.26 - 4.19 (m, 1H), 4.19 - 4.06 (m, 1H), 3.79 (s, 3H), 1.58 (br s, 9H); ^{13}C NMR (100 MHz, CDCl_3) δ = 171.90, 152.06 (br), 142.00 (br), 128.95, 127.44 (br), 125.08 (br), 122.25, 114.92, 80.93 (br), 52.57, 49.77, 44.70 (br), 28.40; LRMS (ESI) calculated for $\text{C}_{15}\text{H}_{19}\text{NNaO}_4$ [$\text{M} + \text{Na}$] $^+$ m/z 300.12, found 299.98.

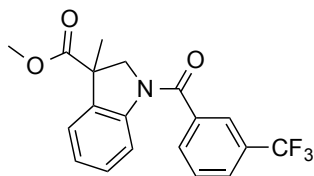


1-(tert-butyl) 3-methyl indoline-1,3-dicarboxylate (S28). **S27** (202.7 mg, 0.731 mmol, 1.0 equiv.) was dissolved in dry tetrahydrofuran (15 mL) and cooled to $-78\text{ }^\circ\text{C}$. n-butyl lithium (434 μL , 0.694 mmol, 0.95 equiv.) (1.6M in hexanes) was then added dropwise to the solution -- stirred for 60 min at $-78\text{ }^\circ\text{C}$. Separately, iodomethane was passed over a plug of activated alumina under Ar; iodomethane (137 μL , 2.19 mmol, 3.0 equiv.) was then added dropwise at $-78\text{ }^\circ\text{C}$. Allowed to slowly warm to r.t. over 14h. Quenched with 2 mL sat NH_4Cl and transferred to a sep. funnel; diluted with sat. NH_4Cl and extracted with 3 x ~ 30mL EtOAc. Organics were combined, washed with ~ 50 mL sat. NaHCO_3 and brine, dried over MgSO_4 , and concentrated. Purified on a silica column with 0-5% EtOAc:hexanes. **S28** (65.1 mg, 31%) obtained as a light tan oil. **Note:** Atropisomers of the secondary carbamate observable by NMR; caused extensive peak broadening. ^1H

NMR (400 MHz, CDCl₃) δ = 7.87 (br s, 0.6H), 7.50 (br s, 0.4H), 7.31 (d, J = 7.5 Hz, 1H), 7.23 (t, J = 7.7 Hz, 1H), 6.98 (t, J = 7.5 Hz, 1H), 4.58 (br d, J = 11.4 Hz, 1H), 3.72 (br s, 4H), 1.60 (s, 3H), 1.58 (br s, 9H); ¹³C NMR (100 MHz, CDCl₃) δ = 174.34, 152.11 (br), 141.96 (br), 134.07 (br), 128.83, 123.95 (br), 122.38, 114.77, 80.86 (br), 57.91 (br), 52.65, 49.74 (br s), 28.38, 25.58 (br); LRMS (ESI) calculated for C₁₆H₂₁NNaO₄ [M + Na]⁺ m/z 314.14, found 313.94.

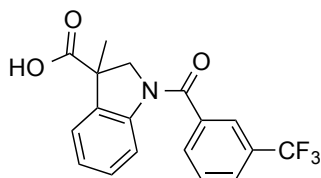


methyl 3-methylindoline-3-carboxylate hydrochloride (S29). **S28** (65.1 mg, 0.223 mmol, 1.0 equiv.) was reacted with 4M HCl in dioxanes (4 mL) according to general procedure E (20h). Semi-crude **S29** (62.4 mg, 123%) obtained as a colorless semi-solid. ¹H NMR (400 MHz, CD₃OD) δ = 7.65 - 7.60 (m, 1H), 7.60 - 7.52 (m, 3H), 4.47 (d, J = 11.9 Hz, 1H), 3.74 (s, 3H), 3.68 (d, J = 5.1 Hz, 1H), 1.74 (s, 3H); ¹³C NMR (100 MHz, CD₃OD) δ = 174.12, 139.70, 136.99, 131.88, 131.39, 126.67, 120.93, 56.13, 53.98, 53.84, 23.41; LRMS (ESI) calculated for C₁₁H₁₄NO₂ [M + H]⁺ m/z 192.10, found 191.89.

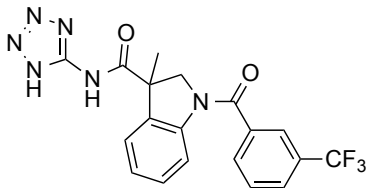


methyl 3-methyl-1-(3-(trifluoromethyl)benzoyl)indoline-3-carboxylate (S30). Semi-crude **S29** (62.4 mg, 0.274 mmol, 1.0 equiv.) was reacted with commercially available 3-(trifluoromethyl)benzoyl chloride in dry dichloromethane (5 mL) according to general

procedure A, with slight modification: prior to base addition, the reaction vessel was cooled to 0 °C; 2.5 equiv. of *N,N*-diisopropylethylamine was used, and allowed to stir at 0 °C for 5m; after acyl chloride addition, the reaction mixture was allowed to slowly warm to r.t. **S30** (70.3 mg, 71%) obtained as a colorless oil. ¹H NMR (400 MHz, CDCl₃) δ = 8.19 (br s, 1H), 7.87 (s, 1H), 7.82 - 7.73 (m, 2H), 7.65 - 7.58 (m, 1H), 7.40 (d, *J* = 7.8 Hz, 1H), 7.27 (br s, 1H), 7.12 (br s, 1H), 4.70 (br d, *J* = 9.7 Hz, 1H), 3.76 (br s, 1H), 3.72 (s, 3H), 1.62 (s, 3H); ¹³C NMR (100 MHz, CDCl₃) δ = 173.59, 167.09, 141.49 (br s), 137.25 (br s), 134.69 (br s), 131.19 (q, *J* = 33.0 Hz), 130.47 (br s), 129.27, 128.85 (br d, *J* = 2.9 Hz), 127.14 (br s), 124.87 - 124.56 (m), 124.45 - 123.81 (m), 123.59 (q, *J* = 272.4 Hz), 117.77 (br s), 60.44 (br s), 52.82, 50.53 (br s), 24.05; LRMS (ESI) calculated for C₁₉H₁₇F₃NO₃ [M + H]⁺ *m/z* 364.12, found 363.84.

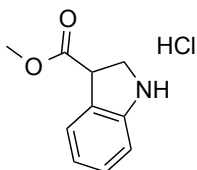


3-methyl-1-(3-(trifluoromethyl)benzoyl)indoline-3-carboxylic acid (S31). **S30** (67.0 mg, 0.193 mmol, 1.0 equiv.) was reacted in methanol (5 mL) with 1M lithium hydroxide (5 mL, 5 mmol, 26 equiv.) according to general procedure B, except the reaction was cooled to 0 °C prior to hydroxide addition, and allowed to slowly warm to r.t. Semi-crude **S31** (67.0 mg, 99%) obtained as a white solid. ¹H NMR (400 MHz, CD₃OD) δ = 8.15 (br s, 1H), 8.01 - 7.83 (m, 3H), 7.78 - 7.70 (m, 1H), 7.49 (br d, *J* = 7.5 Hz, 1H), 7.29 (br s, 1H), 7.16 (br s, 1H), 4.67 (br s, 1H), 3.82 (br d, *J* = 9.0 Hz, 1H), 1.59 (br s, 3H); LRMS (ESI) calculated for C₁₈H₁₃F₃NO₃ [M - H]⁻ *m/z* 348.09, found 347.96.

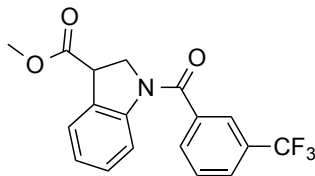


3-methyl-N-(1H-tetrazol-5-yl)-1-(3-(trifluoromethyl)benzoyl)indoline-3-carboxamide

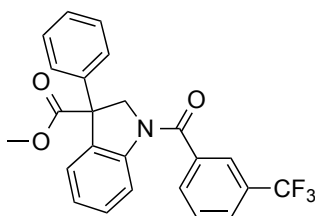
(13). Semi-crude **S31** (67.0 mg, 0.192 mmol, 1.0 equiv.) was reacted with 5-aminotetrazole monohydrate (1.1 equiv.) in 4 mL DMF according to general procedure D (10m activation). **13** (25.6 mg, 32%) obtained as a white solid. ^1H NMR (400 MHz, CD_3OD) δ = 8.14 (br s, 1H), 8.00 - 7.82 (m, 3H), 7.76 - 7.68 (m, 1H), 7.54 (br d, J = 6.8 Hz, 1H), 7.31 (br s, 1H), 7.18 (br s, 1H), 4.72 (br d, J = 8.3 Hz, 1H), 3.97 (br d, J = 10.0 Hz, 1H), 1.73 (br s, 3H); LRMS (ESI) calculated for $\text{C}_{19}\text{H}_{14}\text{F}_3\text{N}_6\text{O}_2$ $[\text{M} - \text{H}]^-$ m/z 415.11, found 415.04.



methyl indoline-3-carboxylate hydrochloride (S32). **S27** (782.4 mg, 2.82 mmol, 1.0 equiv.) was reacted with 4M HCl in dioxanes (10 mL) according to general procedure E (20h). Semi-crude **S32** (595.6 mg, 99%) obtained as a light pink foam. **Note:** Unstable; will spontaneously oxidize. Store cold. ^1H NMR (400 MHz, CD_3OD) δ = 7.66 - 7.60 (m, 1H), 7.56 - 7.45 (m, 3H), 4.60 (dd, J = 5.1, 8.8 Hz, 1H), 4.21 (dd, J = 5.4, 12.2 Hz, 1H), 4.06 (dd, J = 8.8, 12.2 Hz, 1H), 3.76 (s, 3H); ^{13}C NMR (100 MHz, CD_3OD) δ = 171.80, 137.08, 134.46, 131.51, 131.12, 127.71, 121.00, 53.65, 48.11; LRMS (ESI) calculated for $\text{C}_{10}\text{H}_{12}\text{NO}_2$ $[\text{M} + \text{H}]^+$ m/z 178.09, found 177.94.

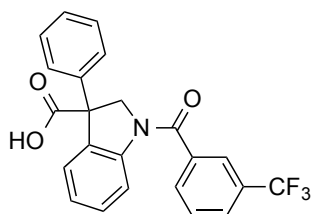


methyl 1-(3-(trifluoromethyl)benzoyl)indoline-3-carboxylate (S33). Semi-crude **S32** (595.6 mg, 2.79 mmol, 1.0 equiv.) was reacted with commercially available 3-(trifluoromethyl)benzoyl chloride in dry dichloromethane (25 mL) according to general procedure A, with slight modification: prior to base addition, the reaction vessel was cooled to 0 °C; 2.5 equiv. of *N,N*-diisopropylethylamine was used, and allowed to stir at 0 °C for 5m; after acyl chloride addition, the reaction mixture was allowed to slowly warm to r.t. **S33** (889.5 mg, 91%) obtained as a colorless oil. ¹H NMR (400 MHz, CDCl₃) δ = 8.18 (br s, 1H), 7.84 (s, 1H), 7.73 (br dd, *J* = 8.3, 11.2 Hz, 2H), 7.60 - 7.52 (m, 1H), 7.40 (d, *J* = 7.8 Hz, 1H), 7.20 (br s, 1H), 7.06 (br d, *J* = 6.3 Hz, 1H), 4.45 (br s, 1H), 4.23 - 4.15 (m, 1H), 4.08 (br s, 1H), 3.71 (s, 3H); ¹³C NMR (100 MHz, CDCl₃) δ = 170.99, 166.89 (br s), 141.84 (br s), 137.13 (br s), 130.87 (q, *J* = 33.0 Hz), 130.25 (br s), 129.11, 128.63 (br s), 126.89 (br s), 125.14 (br s), 124.37 (br s), 123.97 (br s), 123.45 (q, *J* = 272.9 Hz), 117.35 (br s), 60.05, 52.39, 45.02 (br s); ¹⁹F NMR (376 MHz, CDCl₃) δ = -62.78 (s, 3F); LRMS (ESI) calculated for C₁₈H₁₄F₃NNaO₃ [M + Na]⁺ *m/z* 372.08, found 371.94.



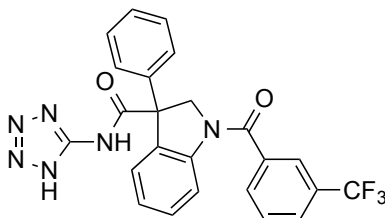
methyl 3-phenyl-1-(3-(trifluoromethyl)benzoyl)indoline-3-carboxylate (S34). **S33** (213.8 mg, 0.612 mmol, 1.0 equiv.) was dissolved in dry tetrahydrofuran (10 mL) and

cooled to -78 °C. LHMDS (581 uL, 0.581 mmol, 0.95 equiv.) (1M in tetrahydrofuran) was then added dropwise to the solution -- stirred at -78 °C. Separately, diphenyliodonium trifluoromethanesulfonate (316 mg, 0.734 mmol, 1.2 equiv.) was suspended in dry dichloromethane (6 mL) and cooled to -78 °C. After 90 minutes of enolization, the suspension was cannulated over at -78 °C and the reaction was allowed to slowly warm to r.t. over 16h. Quenched with 2 mL sat NH₄Cl and transferred to a sep. funnel; diluted with sat. NH₄Cl and extracted with 3 x ~ 30 mL EtOAc. Organics were combined, washed with ~ 50 mL sat. NaHCO₃ and brine, dried over MgSO₄, and concentrated. Purified on a silica column with 0-15% EtOAc:hexanes. **S34** (26.7 mg, 10%) obtained as a waxy white solid. ¹H NMR (400 MHz, CDCl₃) δ = 8.26 (br s, 1H), 7.81 (s, 1H), 7.77 - 7.71 (m, 2H), 7.57 (dd, *J* = 7.9, 17.9 Hz, 2H), 7.37 - 7.29 (m, 4H), 7.21 (br t, *J* = 7.1 Hz, 1H), 7.11 (br d, *J* = 6.6 Hz, 2H), 5.03 (br d, *J* = 11.2 Hz, 1H), 3.98 (br s, 1H), 3.77 (s, 3H); ¹³C NMR (100 MHz, CDCl₃) δ = 172.22, 167.10, 142.74 (br s), 141.07, 137.13 (br s), 131.21 (q, *J* = 33.0 Hz, 1C), 130.43 (br s), 129.44 (br s), 129.22, 128.95, 127.87, 127.18 (br s), 126.51, 124.80 (br s), 124.37 (br s), 123.58 (q, *J* = 274.1 Hz), 117.69 (br s), 62.19 (br s), 60.36 (br s), 53.13; ¹⁹F NMR (376 MHz, CDCl₃) δ = -62.78 (s, 3F); LRMS (ESI) calculated for C₂₄H₁₉F₃NO₃ [M + H]⁺ m/z 426.13, found 425.97.

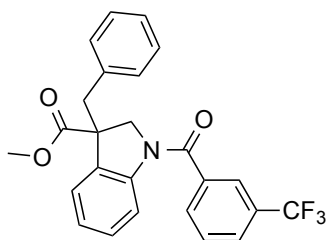


3-phenyl-1-(3-(trifluoromethyl)benzoyl)indoline-3-carboxylic acid (S35). **S34** (26.7 mg, 0.063 mmol, 1.0 equiv.) was reacted in methanol (4 mL) with 1M lithium hydroxide (3 mL, 3 mmol, 48 equiv.) according to general procedure B. Semi-crude **S35** (25.3 mg,

98%) obtained as a white solid. ^1H NMR (400 MHz, CD_3OD) δ = 8.18 (br s, 1H), 7.82 (br d, J = 5.6 Hz, 2H), 7.78 (br d, J = 7.8 Hz, 1H), 7.71 - 7.63 (m, 1H), 7.57 (dd, J = 0.7, 7.8 Hz, 1H), 7.37 - 7.20 (m, 5H), 7.16 (br d, J = 7.1 Hz, 2H), 4.99 - 4.91 (m, 1H), 4.03 - 3.93 (m, 1H); ^{13}C NMR (100 MHz, CD_3OD) δ = 173.30, 167.58, 142.40 (br s), 141.32, 137.20 (br s), 132.88, 130.82 (br q, J = 32.7 Hz), 130.48 (br s), 129.46, 129.25, 128.76 (br s), 128.51, 128.11, 127.41, 127.01 (br s), 126.42, 126.37, 124.94 - 124.60 (m), 123.83 (br d, J = 5.1 Hz), 123.78 (q, J = 271.7 Hz), 117.51 (br s), 62.28 (br s), 60.45 (br s); ^{19}F NMR (376 MHz, CD_3OD) δ = -64.23 (s, 3F); LRMS (ESI) calculated for $\text{C}_{23}\text{H}_{17}\text{F}_3\text{NO}_3$ [$\text{M} + \text{H}$] $^+$ m/z 412.12, found 411.99.

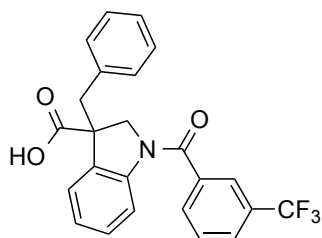


3-phenyl-*N*-(1*H*-tetrazol-5-yl)-1-(3-(trifluoromethyl)benzoyl)indoline-3-carboxamide (14). Semi-crude **S35** (25.3 mg, 0.062 mmol, 1.0 equiv.) was reacted with 5-aminotetrazole monohydrate (1.1 equiv.) in 3 mL DMF according to general procedure D (10m activation). **14** (6.9 mg, 24%) obtained as a white solid. ^1H NMR (400 MHz, CD_3OD) δ = 7.96 - 7.85 (m, 3H), 7.81 (br d, J = 7.5 Hz, 1H), 7.76 - 7.68 (m, 1H), 7.56 - 7.16 (m, 8H), 5.12 (br d, J = 9.5 Hz, 1H), 4.08 (br d, J = 10.2 Hz, 1H); ^{19}F NMR (376 MHz, CD_3OD) δ = -64.25 (br s, 3F); LRMS (ESI) calculated for $\text{C}_{24}\text{H}_{16}\text{F}_3\text{N}_6\text{O}_2$ [$\text{M} - \text{H}$] $^-$ m/z 477.13, found 477.05.

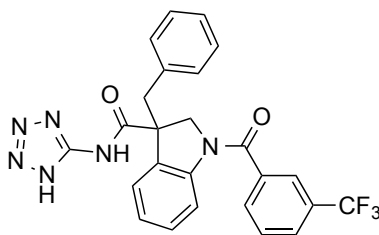


methyl 3-benzyl-1-(3-(trifluoromethyl)benzoyl)indoline-3-carboxylate (S36). S33

(49.1 mg, 0.141 mmol, 1.0 equiv.) was dissolved in dry tetrahydrofuran (3.3 mL) and cooled to $-78\text{ }^{\circ}\text{C}$. LHMDS (134 μL , 0.134 mmol, 0.95 equiv.) (1M in tetrahydrofuran) was then added dropwise to the solution -- stirred at $-78\text{ }^{\circ}\text{C}$ for 45m. Benzyl bromide (20 μL , 0.169 mmol, 1.2 equiv.) was then added dropwise, and the reaction was allowed to slowly warm to r.t. over 16h. Quenched with 2 mL sat NH_4Cl and transferred to a sep. funnel; diluted with sat. NH_4Cl and extracted with 3 x ~ 30 mL EtOAc. Organics were combined, washed with ~ 50 mL sat. NaHCO_3 and brine, dried over MgSO_4 , and concentrated. Purified on a silica column with 0-20% EtOAc:hexanes. **S36** (60.0 mg, 97%) obtained as a colorless oil. ^1H NMR (400 MHz, CDCl_3) δ = 8.47 - 7.84 (m, 1H), 7.73 (br d, J = 7.3 Hz, 1H), 7.66 - 7.48 (m, 4H), 7.26 - 7.09 (m, 5H), 6.84 (br s, 2H), 4.51 (br d, J = 4.6 Hz, 1H), 3.96 (br s, 1H), 3.81 (s, 3H), 3.35 (br d, J = 13.6 Hz, 1H), 3.18 (br d, J = 12.7 Hz, 1H); ^{19}F NMR (376 MHz, CDCl_3) δ = -62.70 (s, 3F); LRMS (ESI) calculated for $\text{C}_{25}\text{H}_{21}\text{F}_3\text{NO}_3$ $[\text{M} + \text{H}]^+$ m/z 440.15, found 440.11.

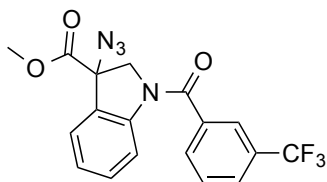


3-benzyl-1-(3-(trifluoromethyl)benzoyl)indoline-3-carboxylic acid (S37). **S36** (60.0 mg, 0.137 mmol, 1.0 equiv.) was reacted in methanol (6 mL) with 1M lithium hydroxide (5 mL, 5 mmol, 37 equiv.) according to general procedure B. Semi-crude **S37** (64.6 mg, 111%) obtained as a white solid. ^1H NMR (400 MHz, CD_3OD , drops CDCl_3) δ = 8.01 (br s, 1H), 7.84 - 7.75 (m, 1H), 7.74 - 7.50 (m, 3H), 7.46 - 7.04 (m, 6H), 6.86 (br s, 2H), 4.56 - 4.37 (m, 1H), 3.90 (br s, 1H), 3.36 (d, J = 13.4 Hz, 1H), 3.14 (br s, 1H); ^{19}F NMR (376 MHz, CD_3OD , drops CDCl_3) δ = -64.04 (br s, 3F); LRMS (ESI) calculated for $\text{C}_{24}\text{H}_{17}\text{F}_3\text{NO}_3$ $[\text{M} - \text{H}]^-$ m/z 424.12, found 424.15.

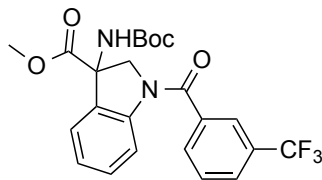


3-benzyl-N-(1H-tetrazol-5-yl)-1-(3-(trifluoromethyl)benzoyl)indoline-3-carboxamide (15). Semi-crude **S37** (64.6 mg, 0.152 mmol, 1.0 equiv.) was reacted with 5-aminotetrazole monohydrate (1.1 equiv.) in 3 mL DMF according to general procedure D (10m activation). **15** (18.6 mg, 25%) obtained as a white solid. ^1H NMR (400 MHz, DMSO-d_6) δ = 7.99 (br s, 1H), 7.90 (br d, J = 7.3 Hz, 1H), 7.85 - 7.66 (m, 3H), 7.35 (br s, 1H), 7.30 - 7.00 (m, 5H), 6.91 (br s, 2H), 4.41 (br d, J = 9.5 Hz, 1H), 4.21 (br s, 1H), 3.66 (br d, J = 13.6 Hz, 1H), 3.27 - 3.13 (m, 1H); ^{13}C NMR (100 MHz, DMSO-d_6) δ = 170.71 (br s), 165.81 (br s), 152.19 (br s), 142.28 (br s), 137.50 (br s), 135.90 (br s),

133.53 (br s), 130.90 (br s), 129.86, 129.50 (br s), 129.24 (d, $J = 31.8$ Hz), 128.93 - 128.55 (m), 128.00, 126.84 (br s), 125.73 - 125.28 (m), 124.64 - 124.11 (m), 123.76 - 123.48 (m), 123.84 (d, $J = 272.4$ Hz), 116.89 (br s), 56.91 (br s), 56.28 (br s), 41.72; ^{19}F NMR (376 MHz, DMSO- d_6) $\delta = -61.18$ (s, 3F); LRMS (ESI) calculated for $\text{C}_{25}\text{H}_{18}\text{F}_3\text{N}_6\text{O}_2$ $[\text{M} - \text{H}]^-$ m/z 491.15, found 491.15.

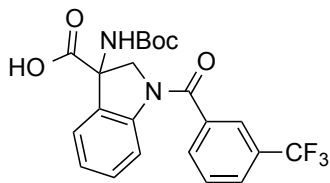


methyl 3-azido-1-(3-(trifluoromethyl)benzoyl)indoline-3-carboxylate (S38). **S33** (255.6 mg, 0.732 mmol, 1.0 equiv.) was reacted in 15 mL tetrahydrofuran according to general procedure F. **S38** (210.4 mg, 74%) obtained as a white solid. ^1H NMR (400 MHz, CDCl_3) $\delta = 8.22$ (br s, 1H), 7.88 (s, 1H), 7.78 (br dd, $J = 3.7, 6.8$ Hz, 2H), 7.65 - 7.59 (m, 1H), 7.50 (d, $J = 7.5$ Hz, 1H), 7.43 (br s, 1H), 7.20 (br t, $J = 7.2$ Hz, 1H), 4.67 (d, $J = 12.2$ Hz, 1H), 3.97 (br s, 1H), 3.90 (s, 3H); ^{13}C NMR (100 MHz, CDCl_3) $\delta = 168.86, 167.01, 142.30$ (br s), 136.50, 131.41 (br s), 131.32 (q, $J = 33.0$ Hz), 130.47 (br s), 129.36, 127.53 (br d, $J = 2.9$ Hz), 124.73 (br s), 124.35 (br s), 123.93 (br s), 123.47 (q, $J = 272.9$ Hz), 117.84 (br s), 69.68 (br s), 59.16 (br s), 53.71; ^{19}F NMR (376 MHz, CDCl_3) $\delta = -62.79$ (s, 3F); LRMS (ESI) calculated for $\text{C}_{18}\text{H}_{14}\text{F}_3\text{N}_4\text{O}_3$ $[\text{M} + \text{H}]^+$ m/z 391.10, found 390.81.

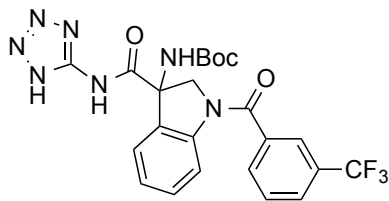


methyl 3-((tert-butoxycarbonyl)amino)-1-(3-(trifluoromethyl)benzoyl)indoline-3-carboxylate (S39). A round bottom flask was charged with **S38** (150.8 mg, 0.386 mmol, 1.0 equiv.) and dry methanol (3.5 mL), then cooled to 0 °C. Anhydrous tin(II) chloride (147 mg, 0.773 mmol, 2.0 equiv.) was then added; stirred at 0 °C for 5m, then r.t. for 2h. The methanol was then removed under reduced pressure. 1,4-dioxane (3 mL) was then added, followed by di-tert-butyl dicarbonate (126 mg, 0.580 mmol, 1.5 equiv.) in 700 uL 1,4-dioxane. Finally, a slurry of sodium bicarbonate (130 mg, 1.55 mmol, 4.0 equiv.) in water (700 uL) was added, and the resulting slurry was allowed to stir for 22h. The reaction mixture was then transferred to a sep. funnel with excess EtOAc and water and adjusted to pH 1 with 2N NaHSO₄. The layers were separated, and the aqueous layer was further extracted with ~ 50 mL EtOAc. The organic layers were combined, washed with sat. NaHCO₃, dried over MgSO₄, and concentrated under reduced pressure. Purified on a silica column with 15% EtOAc:hexanes. **S39** (157.0 mg, 88%) obtained as a colorless oil. ¹H NMR (400 MHz, CDCl₃) δ = 8.24 (br s, 1H), 7.84 (br s, 1H), 7.75 (br t, *J* = 6.5 Hz, 2H), 7.63 - 7.54 (m, 1H), 7.36 (d, *J* = 7.5 Hz, 1H), 7.27 (br s, 1H), 7.10 (br t, *J* = 6.7 Hz, 1H), 4.91 (br d, *J* = 11.2 Hz, 1H), 4.09 (br s, 1H), 3.75 (s, 3H), 1.39 (br s, 9H); ¹³C NMR (100 MHz, CDCl₃) δ = 171.02, 167.31 (br s), 154.72 (br s), 142.51 (br s), 136.96, 131.32, 130.83 (d, *J* = 33.0 Hz), 130.76 (br s), 130.28 (br s), 129.45 (br s), 127.18 (br d, *J* = 2.9 Hz), 125.09 - 124.66 (m), 124.20 (br s), 123.35 (br s), 123.51 (q, *J* = 272.2 Hz), 117.86 (br s), 80.89 (br s), 64.55 (br s), 60.64 (br s), 53.25, 28.00 (br s);

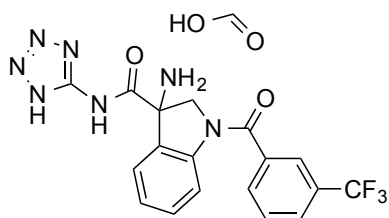
^{19}F NMR (376 MHz, CDCl_3) $\delta = -62.83$ (s, 3F); LRMS (ESI) calculated for $\text{C}_{23}\text{H}_{24}\text{F}_3\text{N}_2\text{O}_5$ $[\text{M} + \text{H}]^+$ m/z 465.16, found 465.04.



3-((tert-butoxycarbonyl)amino)-1-(3-(trifluoromethyl)benzoyl)indoline-3-carboxylic acid (S40). **S39** (157.0 mg, 0.338 mmol, 1.0 equiv.) was reacted in methanol (7 mL) with 1M lithium hydroxide (700 μL , 0.700 mmol, 2.1 equiv.) according to general procedure B, except the reaction was cooled to 0 $^\circ\text{C}$ prior to hydroxide addition, and allowed to slowly warm to r.t. for 3h. Semi-crude **S40** (134.6 mg, 88%) obtained as a white solid. ^1H NMR (400 MHz, CD_3OD , drops CDCl_3) $\delta = 8.20$ (br s, 1H), 7.85 (br s, 1H), 7.80 (br s, 2H), 7.72 - 7.62 (m, 1H), 7.47 (d, $J = 8.0$ Hz, 1H), 7.38 (br s, 1H), 7.16 (br s, 1H), 4.88 (br s, 1H), 4.10 (br s, 1H), 1.40 (br s, 9H); ^{13}C NMR (100 MHz, CD_3OD , drops CDCl_3) $\delta = 173.34$ (br s), 169.04 (br s), 156.90 (br s), 143.33 (br s), 138.24 (br s), 132.24 (br d, $J = 33.0$ Hz), 131.39, 130.66, 128.31 (br s), 126.75 - 125.88 (m), 125.12 (br s), 124.78 (q, $J = 271.9$ Hz), 119.10 (br s), 82.70 (br s), 65.61 (br s), 62.31 (br s), 28.86 (br s); ^{19}F NMR (376 MHz, CD_3OD , drops CDCl_3) $\delta = -63.58$ (s, 3F); LRMS (ESI) calculated for $\text{C}_{22}\text{H}_{20}\text{F}_3\text{N}_2\text{O}_5$ $[\text{M} - \text{H}]^-$ m/z 449.13, found 449.08.

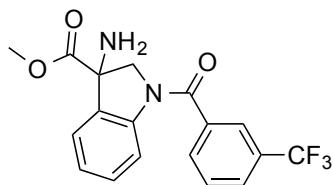


tert-butyl (3-((1*H*-tetrazol-5-yl)carbamoyl)-1-(3-(trifluoromethyl)benzoyl)indolin-3-yl)carbamate (16). Semi-crude **S40** (68.0 mg, 0.151 mmol, 1.0 equiv.) was reacted with 5-aminotetrazole monohydrate (1.1 equiv.) in 4 mL DMF according to general procedure D (10m activation). **16** (36.0 mg, 46%) obtained as a white solid. ^1H NMR (400 MHz, CD_3OD , drops CDCl_3) δ = 8.20 (br s, 1H), 7.92 (br s, 2H), 7.84 (br d, J = 7.8 Hz, 1H), 7.75 - 7.67 (m, 1H), 7.62 (d, J = 7.5 Hz, 1H), 7.39 (br s, 1H), 7.18 (br s, 1H), 5.16 (br s, 1H), 4.06 (br d, J = 9.7 Hz, 1H), 1.37 (br s, 9H); ^{19}F NMR (376 MHz, CD_3OD , drops CDCl_3) δ = -63.82 (s, 3F); LRMS (ESI) calculated for $\text{C}_{23}\text{H}_{21}\text{F}_3\text{N}_7\text{O}_4$ [$\text{M} - \text{H}$] $^-$ m/z 516.16, found 516.27.

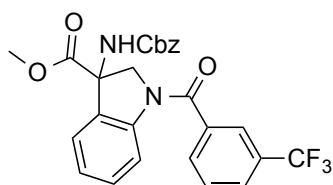


3-amino-*N*-(1*H*-tetrazol-5-yl)-1-(3-(trifluoromethyl)benzoyl)indoline-3-carboxamide formate (17). **16** (22.0 mg, 0.043 mmol, 1.0 equiv.) was reacted with 4M HCl in dioxanes (4 mL) according to general procedure E (42h), except the resulting residue was taken up in DMF and purified by reverse phase HPLC (water/MeOH/0.05% formic acid) to afford **17** (19.0 mg, 96%) as a white solid. ^1H NMR (400 MHz, $\text{DMSO}-d_6$) δ = 8.27 (br s, 1H), 8.01 - 7.89 (m, 3H), 7.86 - 7.77 (m, 1H), 7.58 (br s, 1H), 7.43 (d, J = 7.8 Hz, 1H), 7.23 (br s, 1H), 4.74 (d, J = 13.1 Hz, 1H), 4.17 (br s, 1H); ^{19}F NMR (376 MHz,

DMSO-d₆) δ = -61.26 (s, 3F); LRMS (ESI) calculated for C₁₈H₁₅F₃N₇O₂ [M + H]⁺ m/z 418.12, found 417.77.

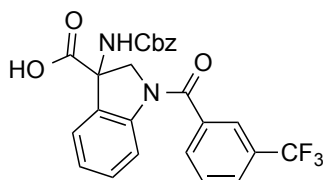


methyl 3-amino-1-(3-(trifluoromethyl)benzoyl)indoline-3-carboxylate (S41). **S38** (946.9 mg, 2.43 mmol, 1.0 equiv.) was suspended in dry methanol (44 mL) and cooled to 0 °C. Anhydrous tin(II) chloride (920 mg, 4.85 mmol, 2.0 equiv.) was then added, and the reaction was stirred at 0 °C for 10m, then allowed to warm to r.t. for an additional 3h. The methanol was removed under reduced pressure; the resulting foam was transferred to a sep. funnel with ~ 75 mL EtOAc and partitioned with ~ 75 mL sat. NaHCO₃. The aqueous layer was further extracted with 2 x 50 mL EtOAc; the organics were combined, dried over MgSO₄, and concentrated to give semi-crude **S41** (913.5 mg, 103%) as a light yellow oil. LRMS (ESI) calculated for C₁₈H₁₆F₃N₂O₃ [M + H]⁺ m/z 365.11, found 364.95.



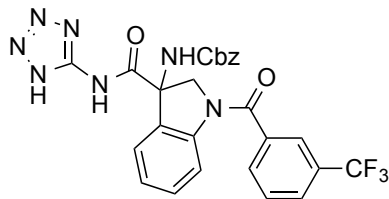
methyl 3-(((benzyloxy)carbonyl)amino)-1-(3-(trifluoromethyl)benzoyl)indoline-3-carboxylate (S42). Semi-crude **S41** (295.4 mg, 0.811 mmol, 1.0 equiv.) was reacted with commercially available benzyl chloroformate in dry dichloromethane (7.5 mL) according to general procedure A, with slight modification: prior to base addition, the

reaction vessel was cooled to 0 °C; 2.5 equiv. of *N,N*-diisopropylethylamine was used, and allowed to stir at 0 °C for 5m; after chloroformate addition, the reaction mixture was allowed to slowly warm to r.t. **S42** (314.0 mg, 78%) obtained as a colorless oil. ¹H NMR (400 MHz, CDCl₃) δ = 8.27 (br s, 1H), 7.87 (br s, 1H), 7.77 (br d, *J* = 7.8 Hz, 2H), 7.66 - 7.55 (m, 1H), 7.39 - 7.29 (m, 7H), 7.14 (br t, *J* = 6.7 Hz, 1H), 5.15 - 5.02 (m, 2H), 4.93 (br d, *J* = 11.9 Hz, 1H), 4.21 (br s, 1H), 3.77 (s, 3H); ¹³C NMR (100 MHz, CDCl₃) δ = 171.10, 167.28 (br s), 155.07, 142.66 (br s), 136.89, 135.68, 131.29 (d, *J* = 32.3 Hz), 131.30 - 130.59 (m), 130.34 (br s), 129.32, 128.52, 128.35, 128.11, 127.33 (br d, *J* = 3.7 Hz), 124.97 (br d, *J* = 3.7 Hz), 124.35 (br s), 123.20 (br s), 123.56 (d, *J* = 272.0 Hz), 116.27 (br s), 67.31, 64.77 (br s), 60.36 (br s), 53.57; ¹⁹F NMR (376 MHz, CDCl₃) δ = -62.76 (s, 3F).

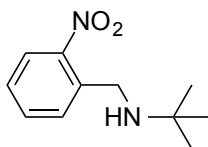


3-(((benzyloxy)carbonyl)amino)-1-(3-(trifluoromethyl)benzoyl)indoline-3-

carboxylic acid (S43). **S42** (37.4 mg, 0.075 mmol, 1.0 equiv.) was reacted in methanol (3 mL) with 1M lithium hydroxide (3 mL, 3 mmol, 40 equiv.) according to general procedure B. Semi-crude **S43** (33.1 mg, 91%) obtained as a white solid. LRMS (ESI) calculated for C₂₅H₁₈F₃N₂O₅ [M - H]⁻ m/z 483.12, found 483.05.

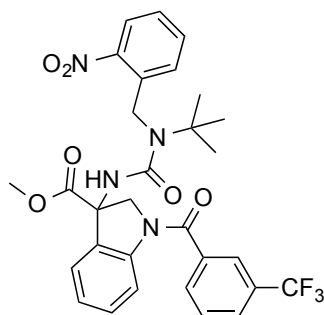


benzyl 3-((1*H*-tetrazol-5-yl)carbamoyl)-1-(3-(trifluoromethyl)benzoyl)indolin-3-yl)carbamate (18). Semi-crude **S43** (33.1 mg, 0.068 mmol, 1.0 equiv.) was reacted with 5-aminotetrazole monohydrate (1.1 equiv.) in 2 mL DMF according to general procedure D (10m activation). **18** (8.7 mg, 23%) obtained as a white solid. ^1H NMR (400 MHz, DMSO- d_6) δ = 8.13 (br s, 1H), 8.06 - 7.87 (m, 3H), 7.79 (br d, J = 6.8 Hz, 2H), 7.31 (br s, 6H), 7.16 (br s, 1H), 5.04 (br s, 2H), 4.90 (br d, J = 6.6 Hz, 1H), 4.11 (br d, J = 10.7 Hz, 1H); ^{13}C NMR (100 MHz, DMSO- d_6) δ = 168.26, 166.36 (br s), 156.82 (br s), 155.50 (br s), 142.09 (br s), 137.65, 136.46 (br s), 131.05 (br s), 129.87 (br s), 129.40 (br d, J = 32.2 Hz), 128.29, 127.76, 127.52 (br s), 127.01 (br s), 125.56 - 125.08 (m), 124.29 (br s), 123.88 (br s), 123.85 (d, J = 272.5 Hz), 117.04 (br s), 65.84 (br s), 60.41 (br s); ^{19}F NMR (376 MHz, DMSO- d_6) δ = -61.13 (br s, 3F); LRMS (ESI) calculated for $\text{C}_{26}\text{H}_{19}\text{F}_3\text{N}_7\text{O}_4$ $[\text{M} - \text{H}]^-$ m/z 550.15, found 550.39.



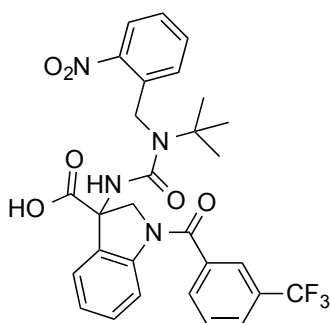
2-methyl-*N*-(2-nitrobenzyl)propan-2-amine (S44). A 20 mL vial was charged with 2-nitrobenzaldehyde (108 mg, 0.714 mmol, 1.0 equiv.), fitted with a septa, and purged with Ar. tert-butylamine (75 μL , 0.714 mmol, 1.0 equiv.) was then added, followed by dry methanol (3 mL). The vial was foiled; stirred overnight. Sodium borohydride (30 mg, 0.785 mmol, 1.1 equiv.) was then added in one portion. After 2h of stirring, the reaction

mixture was quenched with ~ 30 mL water and transferred to a sep. funnel with additional water, then extracted with 3 x 40 mL DCM. The organic layers were combined, dried over MgSO₄, and concentrated. Purified on a silica column with 0-100% EtOAc:hexanes. **S44** (136.3 mg, 92%) obtained as a yellow oil. **Note:** Fairly photo stable, but avoid direct sunlight. ¹H NMR (400 MHz, CDCl₃) δ = 7.88 (dd, *J* = 1.1, 8.2 Hz, 1H), 7.65 (d, *J* = 7.5 Hz, 1H), 7.55 (dt, *J* = 1.2, 7.5 Hz, 1H), 7.40 - 7.32 (m, 1H), 3.93 (s, 2H), 1.16 (s, 9H); ¹³C NMR (100 MHz, CDCl₃) δ = 149.22, 136.63, 133.09, 131.65, 127.60, 124.35, 50.79, 44.13, 28.95; LRMS (ESI) calculated for C₁₁H₁₇N₂O₂ [M + H]⁺ m/z 209.13, found 209.06.

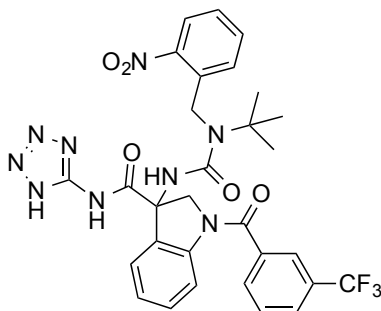


methy **3-(3-(tert-butyl)-3-(2-nitrobenzyl)ureido)-1-(3-(trifluoromethyl)benzoyl)indoline-3-carboxylate (S45)**. Semi-crude **S41** (53.1 mg, 0.146 mmol, 1.0 equiv.) was reacted with partner amine **S44** (1.1 equiv.) according to general procedure G. The reaction vessel was foiled. **S45** (83.6 mg, 96%) obtained as a white solid. ¹H NMR (400 MHz, CDCl₃) δ = 8.11 (d, *J* = 8.3 Hz, 1H), 8.19 (br s, 1H), 7.84 - 7.77 (m, 3H), 7.77 - 7.71 (m, 2H), 7.63 - 7.56 (m, 1H), 7.54 - 7.48 (m, 1H), 7.29 (br s, 1H), 6.99 - 6.88 (m, 2H), 5.06 - 4.94 (m, 3H), 4.76 (d, *J* = 19.7 Hz, 1H), 3.75 (s, 3H), 1.40 (s, 9H); ¹³C NMR (100 MHz, CDCl₃) δ = 171.05, 167.43 (br s), 158.09, 147.18, 142.72 (br s), 137.01, 134.84, 134.14, 131.20 (q, *J* = 32.9 Hz), 130.74 (br s), 130.26 (br

s), 129.57 - 129.35 (m), 129.30, 128.43, 127.95, 127.20 (br d, $J = 2.9$ Hz), 125.73, 125.07 - 124.63 (m), 124.25 (br d, $J = 3.9$ Hz), 122.57 (br s), 123.56 (q, $J = 272.6$ Hz), 118.33 (br s), 65.28 (br s), 61.46 (br s), 57.17, 53.15, 46.87, 28.80; ^{19}F NMR (376 MHz, CDCl_3) $\delta = -62.75$ (s, 3F); LRMS (ESI) calculated for $\text{C}_{30}\text{H}_{30}\text{F}_3\text{N}_4\text{O}_6$ $[\text{M} + \text{H}]^+$ m/z 599.21, found 599.16.

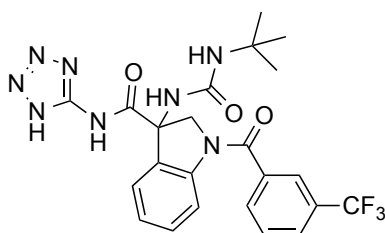


3-(3-(tert-butyl)-3-(2-nitrobenzyl)ureido)-1-(3-(trifluoromethyl)benzoyl)indoline-3-carboxylic acid (S46). **S45** (83.6 mg, 0.140 mmol, 1.0 equiv.) was reacted in methanol (5 mL) with 1M lithium hydroxide (196 μL , 0.196 mmol, 1.4 equiv.) according to general procedure B, except a second addition of 1M lithium hydroxide (75 μL) was required. The reaction vessel was foiled. Semi-crude **S46** (70.5 mg, 86%) obtained as a white solid. LRMS (ESI) calculated for $\text{C}_{29}\text{H}_{26}\text{F}_3\text{N}_4\text{O}_6$ $[\text{M} - \text{H}]^-$ m/z 583.18, found 583.20.

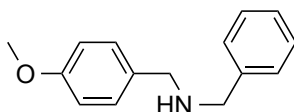


3-(3-(tert-butyl)-3-(2-nitrobenzyl)ureido)-N-(1H-tetrazol-5-yl)-1-(3-(trifluoromethyl)benzoyl)indoline-3-carboxamide (S47). Semi-crude **S46** (70.5 mg,

0.121 mmol, 1.0 equiv.) was reacted with 5-aminotetrazole monohydrate (1.1 equiv.) in 3.5 mL DMF according to general procedure D (1h activation; 48h), except the product was unstable to purification/concentration. Crude **S47** (13.0 mg, 17%) obtained as a white solid (~ 70% pure). LRMS (ESI) calculated for C₃₀H₂₇F₃N₉O₅ [M - H]⁻ m/z 650.21, found 650.33.

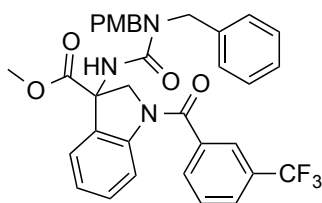


3-(3-(tert-butyl)ureido)-N-(1H-tetrazol-5-yl)-1-(3-(trifluoromethyl)benzoyl)indoline-3-carboxamide (19). Crude **S47** (13.0 mg, 0.020 mmol, 1.0 equiv.) was taken up in methanol (2.5 mL) and irradiated with 365 nm hv (TLC lamp, 4 watt) for 90m. The reaction mixture was concentrated and purified by reverse phase HPLC (water/MeOH/0.05% formic acid) to afford **19** (3.3 mg, 4% over 3 steps) as a white solid. ¹H NMR (400 MHz, DMSO-d₆) δ = 12.10 (br s, 1H), 8.13 (br s, 1H), 8.06 - 7.91 (m, 3H), 7.87 - 7.77 (m, 2H), 7.44 (br s, 1H), 7.22 (br t, J = 6.8 Hz, 1H), 6.93 (s, 1H), 6.52 (s, 0.5H), 6.13 (s, 1H), 4.97 - 4.83 (m, 1H), 4.14 (br dd, J = 3.4, 5.6 Hz, 1H), 1.17 (s, 9H); ¹⁹F NMR (376 MHz, DMSO-d₆) δ = -61.17 (s, 3F); LRMS (ESI) calculated for C₂₃H₂₂F₃N₈O₃ [M - H]⁻ m/z 515.18, found 515.24.



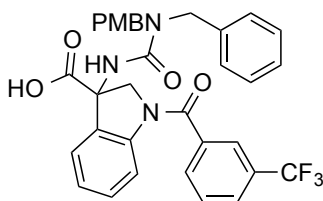
N-benzyl-1-(4-methoxyphenyl)methanamine (S48). A 20 mL vial was charged with 4-anisaldehyde (111 uL, 0.916 mmol, 1.0 equiv.), fitted with a septa, and purged with Ar.

Benzylamine (100 μ L, 0.916 mmol, 1.0 equiv.) was then added, followed by dry methanol (3 mL); stirred overnight. Sodium borohydride (38.1 mg, 1.01 mmol, 1.1 equiv.) was then added in one portion. After 2h of stirring, the reaction mixture was quenched with \sim 30 mL water and transferred to a sep. funnel with additional water, then extracted with 3 x 40 mL DCM. The organic layers were combined, dried over MgSO_4 , and concentrated. Purified on a silica column with 0-55% EtOAc:hexanes. **S48** (183.9 mg, 88%) obtained as a yellow oil. ^1H NMR (400 MHz, CDCl_3) δ = 7.43 - 7.37 (m, 4H), 7.35 - 7.30 (m, 3H), 6.96 - 6.95 (m, 1H), 6.94 - 6.92 (m, 1H), 3.86 (s, 2H), 3.84 (s, 3H), 3.81 (s, 2H); ^{13}C NMR (100 MHz, CDCl_3) δ = 158.46, 140.13, 132.17, 129.17, 128.21, 127.99, 126.75, 113.60, 55.02, 52.83, 52.33; LRMS (ESI) calculated for $\text{C}_{15}\text{H}_{18}\text{NO}$ $[\text{M} + \text{H}]^+$ m/z 228.14, found 228.02.

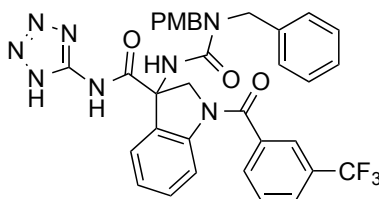


methy **3-(3-benzyl-3-(4-methoxybenzyl)ureido)-1-(3-(trifluoromethyl)benzoyl)indoline-3-carboxylate (S49)**. Semi-crude **S41** (72.8 mg, 0.200 mmol, 1.0 equiv.) was reacted with partner amine **S48** (1.1 equiv.) according to general procedure G. **S49** (108.0 mg, 88%) obtained as a white solid. ^1H NMR (400 MHz, CDCl_3) δ = 8.22 (br s, 1H), 7.85 (s, 1H), 7.76 (br d, J = 7.1 Hz, 2H), 7.63 - 7.56 (m, 1H), 7.38 - 7.28 (m, 4H), 7.21 (br d, J = 6.8 Hz, 2H), 7.13 (d, J = 8.5 Hz, 2H), 7.00 (br t, J = 7.4 Hz, 1H), 6.90 - 6.83 (m, 3H), 5.28 (s, 1H), 5.07 (br d, J = 11.9 Hz, 1H), 4.44 (br s, 2H), 4.40 (br s, 2H), 3.80 (s, 3H), 3.74 (s, 3H); ^{13}C NMR (100 MHz, CDCl_3) δ = 170.69, 167.41 (br s), 159.16, 157.47, 142.57 (br s), 137.04, 136.86 (br s), 131.13 (q, J

= 33.0 Hz), 130.65 (br s), 130.20 (br s), 129.52 (br s), 129.26, 128.73, 128.63 (br s), 127.65, 127.25 (br s), 127.17 - 127.02 (m), 124.69 (br s), 124.16 (br d, $J = 2.2$ Hz), 122.84 (br s), 123.55 (q, $J = 272.2$ Hz), 118.14 (br s), 114.10, 65.05 (br s), 61.33 (br s), 55.15, 53.03, 50.35, 50.00; ^{19}F NMR (376 MHz, CDCl_3) $\delta = -62.68$ (s, 3F); LRMS (ESI) calculated for $\text{C}_{34}\text{H}_{31}\text{F}_3\text{N}_3\text{O}_5$ $[\text{M} + \text{H}]^+$ m/z 618.22, found 618.10.

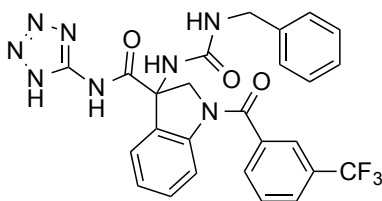


3-(3-benzyl-3-(4-methoxybenzyl)ureido)-1-(3-(trifluoromethyl)benzoyl)indoline-3-carboxylic acid (S50). **S49** (108.0 mg, 0.175 mmol, 1.0 equiv.) was reacted in methanol (5.5 mL) with 1M lithium hydroxide (245 μL , 0.245 mmol, 1.4 equiv.) according to general procedure B, except a second addition of 1M lithium hydroxide (50 μL) was required. Semi-crude **S50** (99.5 mg, 94%) obtained as a white solid. LRMS (ESI) calculated for $\text{C}_{33}\text{H}_{27}\text{F}_3\text{N}_3\text{O}_5$ $[\text{M} - \text{H}]^-$ m/z 602.19, found 602.13.



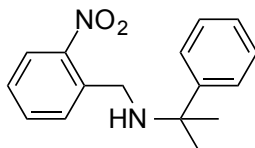
3-(3-benzyl-3-(4-methoxybenzyl)ureido)-N-(1H-tetrazol-5-yl)-1-(3-(trifluoromethyl)benzoyl)indoline-3-carboxamide (S51). Semi-crude **S50** (99.5 mg, 0.165 mmol, 1.0 equiv.) was reacted with 5-aminotetrazole monohydrate (1.1 equiv.) in 2.5 mL DMF according to general procedure D (1h activation). **S51** (52.3 mg, 45% over 2 steps) obtained as a white solid. ^1H NMR (400 MHz, DMSO-d_6) $\delta = 12.33$ (br s, 1H),

8.13 (br s, 1H), 8.09 - 7.88 (m, 4H), 7.89 - 7.74 (m, 2H), 7.44 (br s, 1H), 7.33 - 7.00 (m, 8H), 6.82 (br s, 2H), 5.07 (br s, 1H), 4.77 (br s, 2H), 4.10 (br d, $J = 9.0$ Hz, 1H), 3.95 (br s, 2H), 3.71 (br s, 3H); ^{19}F NMR (376 MHz, DMSO- d_6) $\delta = -61.13$ (br s, 3F); LRMS (ESI) calculated for $\text{C}_{34}\text{H}_{28}\text{F}_3\text{N}_8\text{O}_4$ $[\text{M} - \text{H}]^-$ m/z 669.22, found 670.11.

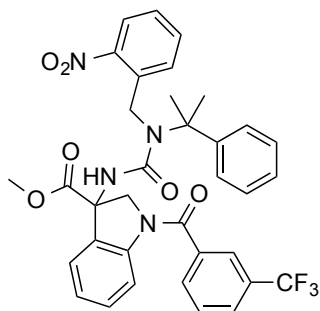


3-(3-benzylureido)-N-(1H-tetrazol-5-yl)-1-(3-(trifluoromethyl)benzoyl)indoline-3-carboxamide (20). **S51** (44.9 mg, 0.067 mmol, 1.0 equiv.) was suspended in acetonitrile (2.4 mL) and water (600 μL). Ammonium cerium(IV) nitrate (165 mg, 0.301 mmol, 4.5 equiv.) was then added in 0.5 equiv. portions over 3h. The crude reaction mixture was transferred to a sep. funnel with EtOAc and water; the layers were separated, and the aqueous layer was further extracted with 3 x 50 mL EtOAc. The organics were combined, dried over MgSO_4 , and concentrated. Purified by reverse phase HPLC (water/MeOH/0.05% formic acid) to afford **20** (10.7 mg, 29%) as a white solid. ^1H NMR (400 MHz, DMSO- d_6) $\delta = 12.25$ (br s, 1H), 8.15 (br s, 1H), 8.01 (br s, 2H), 7.95 (br d, $J = 7.8$ Hz, 1H), 7.88 (br d, $J = 7.8$ Hz, 1H), 7.84 - 7.77 (m, 1H), 7.53 - 7.39 (m, 1H), 7.32 - 7.18 (m, 6H), 6.75 (t, $J = 5.8$ Hz, 0.5H), 4.94 (br d, $J = 9.5$ Hz, 1H), 4.28 - 4.13 (m, 2H), 4.09 (d, $J = 11.2$ Hz, 1H); ^{13}C NMR (100 MHz, DMSO- d_6) $\delta = 170.69, 166.31, 157.25, 157.20, 150.16$ (br s), 142.02 (br s), 139.93, 137.37, 131.06, 130.45 (br s), 130.33 - 130.09 (m), 130.00, 129.48 (d, $J = 32.0$ Hz), 128.19, 127.34 - 127.12 (m), 126.84, 126.66, 124.89 - 124.65 (m), 124.61 - 124.42 (m), 123.81 (br d, $J = 3.3$ Hz), 123.83 (q, $J = 272.0$ Hz), 117.68 (br s), 65.32 (br s), 61.41 (br s), 42.79; ^{19}F

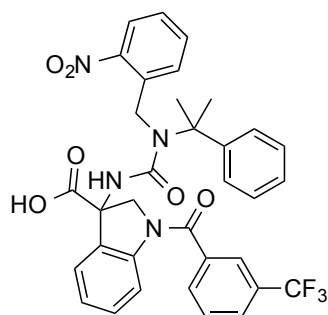
NMR (376 MHz, DMSO- d_6) δ = -61.11 (s, 3F); LRMS (ESI) calculated for $C_{26}H_{20}F_3N_8O_3$ [M - H]⁻ m/z 549.16, found 549.14.



***N*-(2-nitrobenzyl)-2-phenylpropan-2-amine (S52).** A 20 mL vial was charged with 2-nitrobenzaldehyde (105 mg, 0.695 mmol, 1.0 equiv.), fitted with a septa, and purged with Ar. cumylamine (100 μ L, 0.695 mmol, 1.0 equiv.) was then added, followed by dry methanol (3 mL). The vial was foiled; stirred overnight. Sodium borohydride (29 mg, 0.765 mmol, 1.1 equiv.) was then added in one portion. After 2h of stirring, the reaction mixture was quenched with ~ 30 mL water and transferred to a sep. funnel with additional water, then extracted with 3 x 40 mL DCM. The organic layers were combined, dried over $MgSO_4$, and concentrated. Purified on a silica column with 0-25% EtOAc:hexanes. **S52** (150.0 mg, 80%) obtained as a yellow oil. **Note:** Fairly photo-stable, but avoid direct sunlight. 1H NMR (400 MHz, $CDCl_3$) δ = 7.93 - 7.88 (m, 1H), 7.62 - 7.53 (m, 4H), 7.42 - 7.36 (m, 3H), 7.30 - 7.24 (m, 1H), 3.72 (s, 2H), 1.57 (s, 6H); ^{13}C NMR (100 MHz, $CDCl_3$) δ = 149.20, 147.30, 136.53, 133.15, 131.67, 128.22, 127.65, 126.41, 125.91, 124.39, 56.29, 44.71, 29.61; LRMS (ESI) calculated for $C_{16}H_{19}N_2O_2$ [M + H]⁺ m/z 271.14, found 271.04.

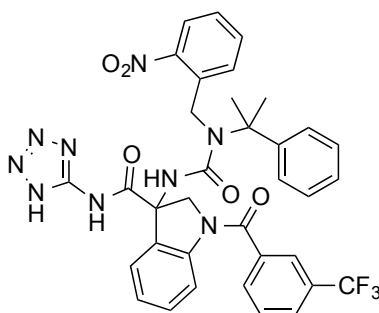


methy **3-(3-(2-nitrobenzyl)-3-(2-phenylpropan-2-yl)ureido)-1-(3-(trifluoromethyl)benzoyl)indoline-3-carboxylate (S53)**. Semi-crude **S41** (80.2 mg, 0.220 mmol, 1.0 equiv.) was reacted with partner amine **S52** (1.1 equiv.) according to general procedure G. The reaction vessel was foiled. **S53** (126.0 mg, 87%) obtained as a white solid. ^1H NMR (400 MHz, CDCl_3) δ = 8.16 (br s, 1H), 7.98 (dd, J = 1.1, 8.2 Hz, 1H), 7.80 (s, 1H), 7.75 - 7.64 (m, 4H), 7.59 - 7.52 (m, 1H), 7.46 - 7.34 (m, 6H), 7.28 (br s, 1H), 6.92 (br t, J = 7.3 Hz, 1H), 6.31 (d, J = 7.5 Hz, 1H), 5.31 - 5.21 (m, 1H), 5.18 (s, 1H), 5.14 - 5.06 (m, 1H), 4.93 (br d, J = 11.7 Hz, 1H), 3.66 (s, 3H), 1.66 (s, 3H), 1.50 (s, 3H); ^{13}C NMR (100 MHz, CDCl_3) δ = 170.48, 167.26 (br s), 158.19, 147.49, 146.34, 142.25 (br s), 137.01, 135.83, 133.32, 131.06 (q, J = 32.8 Hz), 130.70 - 130.40 (m), 130.13 (br s), 129.41, 129.23, 128.96, 127.92, 127.50, 127.18 - 126.95 (m), 125.22, 124.72, 124.46 (br s), 124.19 - 123.92 (m), 122.56 (br s), 123.51 (q, J = 272.6 Hz), 118.08 (br s), 65.07 (br s), 61.68 (br s), 61.06, 52.85, 45.16, 30.89, 26.52 (br s); ^{19}F NMR (376 MHz, CDCl_3) δ = -62.74 (s, 3F); LRMS (ESI) calculated for $\text{C}_{35}\text{H}_{32}\text{F}_3\text{N}_4\text{O}_6$ [$\text{M} + \text{H}$] $^+$ m/z 661.23, found 661.13.



3-(3-(2-nitrobenzyl)-3-(2-phenylpropan-2-yl)ureido)-1-(3-

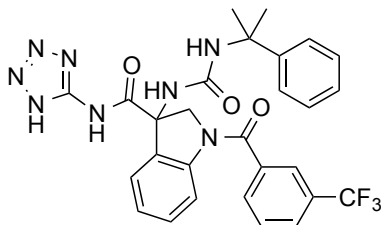
(trifluoromethyl)benzoyl)indoline-3-carboxylic acid (S54). **S53** (126.0 mg, 0.191 mmol, 1.0 equiv.) was reacted in methanol (6 mL) with 1M lithium hydroxide (267 uL, 0.267 mmol, 1.4 equiv.) according to general procedure B, except a second addition of 1M lithium hydroxide (50 uL) was required. The reaction vessel was foiled. Semi-crude **S54** (124.2 mg, 101%) obtained as a white solid. LRMS (ESI) calculated for $C_{34}H_{28}F_3N_4O_6$ $[M - H]^-$ m/z 645.20, found 645.09.



3-(3-(2-nitrobenzyl)-3-(2-phenylpropan-2-yl)ureido)-N-(1H-tetrazol-5-yl)-1-(3-

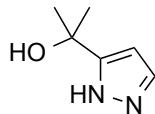
(trifluoromethyl)benzoyl)indoline-3-carboxamide (S55). Semi-crude **S54** (124.2 mg, 0.192 mmol, 1.0 equiv.) was reacted with 5-aminotetrazole monohydrate (1.1 equiv.) in 3 mL DMF according to general procedure D (1h activation), except the product was unstable to purification/concentration. Crude **S55** (31.2 mg, 23%) obtained as a white

solid (~ 56% pure). LRMS (ESI) calculated for C₃₅H₂₉F₃N₉O₅ [M - H]⁻ m/z 712.22, found 712.31.

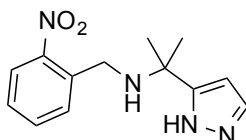


3-(3-(2-phenylpropan-2-yl)ureido)-N-(1H-tetrazol-5-yl)-1-(3-

(trifluoromethyl)benzoyl)indoline-3-carboxamide (21). Crude **S55** (31.2 mg, 0.044 mmol, 1.0 equiv.) was taken up in methanol (3 mL) and irradiated with 365 nm hv (TLC lamp, 4 watt) for 3h. The reaction mixture was concentrated and purified by reverse phase HPLC (water/MeOH/0.05% formic acid) to afford **21** (7.5 mg, 7% over 3 steps) as a white solid. ¹H NMR (400 MHz, DMSO-d₆) δ = 12.27 (br s, 1H), 8.15 (br s, 1H), 7.99 (br s, 2H), 7.92 (br t, *J* = 7.2 Hz, 2H), 7.81 - 7.74 (m, 1H), 7.46 (br s, 1H), 7.31 (br d, *J* = 7.5 Hz, 2H), 7.28 - 7.21 (m, 1H), 7.19 - 7.11 (m, 2H), 7.10 - 7.04 (m, 1H), 6.74 (d, *J* = 1.5 Hz, 0.6H), 4.88 - 4.78 (m, 1H), 3.99 (d, *J* = 11.2 Hz, 1H), 1.48 (br s, 6H); ¹³C NMR (100 MHz, DMSO-d₆) δ = 171.20, 166.80 (br s), 156.60, 156.56, 150.42 (br s), 148.56, 142.48 (br s), 137.85, 131.48, 130.96 (br s), 130.79 - 130.54 (m), 130.44, 129.94 (br d, *J* = 32.3 Hz), 128.21, 127.79 - 127.49 (m), 126.12, 125.25 (br s), 124.87 (br s), 124.38 - 124.05 (m), 124.28 (d, *J* = 272.9 Hz), 118.10 (br s), 65.49 (br s), 61.98 (br s), 55.14, 30.57 (br s), 30.46; ¹⁹F NMR (376 MHz, DMSO-d₆) δ = -61.15 (s, 3F); LRMS (ESI) calculated for C₂₈H₂₄F₃N₈O₃ [M - H]⁻ m/z 577.19, found 577.27.



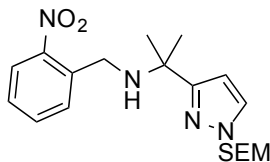
2-(1H-pyrazol-5-yl)propan-2-ol (S56). A round bottom was charged with tetrahydrofuran (5 mL) and methylmagnesium bromide (1.427 mL, 4.28 mmol, 3.0 equiv.) (3.0M in diethyl ether), then cooled to 0 °C. Ethyl 2H-pyrazole-3-carboxylate (200 mg, 1.43 mmol, 1.0 equiv.) was then added, followed by a 1.5 mL tetrahydrofuran rinse. After the addition was complete, the vessel was immediately warmed to r.t. and allowed to stir for 3h. The reaction mixture was quenched with 0.1N HCl until bubbling ceased, and transferred to a sep. funnel with EtOAc and brine. The aqueous pH was adjusted to 6 with 12M HCl; extracted with 3 x 50 mL 20% isopropanol:chloroform. The organics were combined, dried over MgSO₄, and concentrated to give **S56** (161.8 mg, 90%) as a white solid. ¹H NMR (400 MHz, CDCl₃, CD₃OD) δ = 7.35 (br d, *J* = 7.8 Hz, 1H), 6.07 (br d, *J* = 7.8 Hz, 1H), 1.51 (s, 3H), 1.48 (d, *J* = 1.2 Hz, 3H); ¹³C NMR (100 MHz, CDCl₃, CD₃OD) δ = 154.83, 134.32, 100.91, 68.56, 30.20; LRMS (ESI) calculated for C₆H₁₁N₂O [M + H]⁺ m/z 127.09, found 127.27.



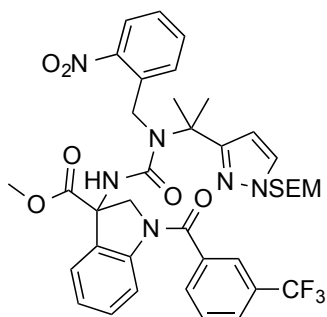
N-(2-nitrobenzyl)-2-(1H-pyrazol-5-yl)propan-2-amine (S57). A flask was charged with **S56** (161.8 mg, 1.28 mmol, 1.0 equiv.), sodium azide (183 mg, 2.82 mmol, 2.2 equiv.), and dry dichloromethane (3 mL), then cooled to 0 °C. A solution of trifluoroacetic acid (491 uL, 6.41 mmol, 5.0 equiv.) in dichloromethane (1 mL) was then added; the reaction mixture was allowed to warm to r.t. overnight. The reaction was then pushed to

completion by the addition of 4.4 equiv. sodium azide and 25 equiv. trifluoroacetic acid over 3d (r.t.), and heating at 40 °C for 5h (behind a blast shield). After complete SM consumption by LCMS, the crude reaction mixture was transferred to a sep. funnel with dichloromethane and sat. NaHCO₃. The layers were separated, and the aqueous layer was further extracted with 3 x 50 mL 20% isopropanol:chloroform. The organics were combined, dried over MgSO₄, and concentrated; dried under hivaac for 5m. The resulting oil was taken up in dry methanol (13 mL) and cooled to 0 °C. Anhydrous tin(II) chloride (486 mg, 2.67 mmol, 2.0 equiv.) was then added, and after 10m the reaction was immediately warmed to r.t. and stirred for 14h. The methanol was then removed under reduced pressure, and the residue transferred to a sep. funnel with 20% isopropanol:chloroform. 1M NaHCO₃ was added, the layers separated, and the aqueous layer further extracted with 3 x 50 mL 20% isopropanol:chloroform. The combined organic layers were dried over MgSO₄ and concentrated to dryness in a 20 mL vial. The vial was purged with Ar, foiled, and charged with 2-nitrobenzaldehyde (426 mg, 2.82 mmol, 2.20 equiv.) and dry tetrahydrofuran (12 mL). After stirring for 12h, sodium borohydride (107 mg, 2.82 mmol, 2.20 equiv.) was added, and the reaction was stirred for an additional 12h. The crude reaction mixture was transferred to a sep. funnel with EtOAc and sat. NaHCO₃; the layers were separated, and the aqueous layer was further extracted with 2 x 50 mL EtOAc. The organics were combined, dried over MgSO₄, and concentrated; the resulting residue was purified on a silica column with 40-100% EtOAc:hexanes to yield **S57** (24.7 mg, 7%) as a yellow film. ¹H NMR (400 MHz, CDCl₃) δ = 7.90 - 7.86 (m, 1H), 7.55 - 7.46 (m, 3H), 7.37 (ddd, *J* = 2.2, 6.4, 8.2 Hz, 1H), 6.21 (d, *J* = 1.9 Hz, 1H), 3.77 (s, 2H), 1.55 (s, 6H); ¹³C NMR (100 MHz, CDCl₃) δ =

152.99 (br), 149.16, 135.81, 135.23 (br), 133.25, 131.82, 127.90, 124.47, 102.62, 53.23, 44.96, 28.52; LRMS (ESI) calculated for C₁₃H₁₇N₄O₂ [M + H]⁺ m/z 261.13, found 261.10.

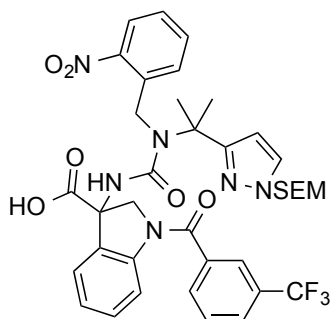


***N*-(2-nitrobenzyl)-2-(1-((2-(trimethylsilyl)ethoxy)methyl)-1*H*-pyrazol-3-yl)propan-2-amine (S58)**. A 20 mL vial was charged with **S57** (24.7 mg, 0.095 mmol, 1.0 equiv.), *N,N*-diisopropylethylamine (33 μ L, 0.190 mmol, 2.0 equiv.), and dry dichloromethane (1.5 mL); 2-(trimethylsilyl)ethoxymethyl chloride (17 μ L, 0.095 mmol, 1.0 equiv.) was then added dropwise. The reaction vial was foiled as stirred for 14h, at which point additional 2-(trimethylsilyl)ethoxymethyl chloride (8 μ L) and dichloromethane (500 μ L) were added. After an additional 5h, the reaction mixture was directly loaded onto a silica column and purified with 0-50% EtOAc:hexanes. **S58** (28.2 mg, 76%) was obtained as a yellow oil. ¹H NMR (400 MHz, CDCl₃) δ = 7.86 (dd, *J* = 1.2, 8.0 Hz, 1H), 7.64 - 7.59 (m, 1H), 7.53 (dt, *J* = 1.3, 7.5 Hz, 1H), 7.49 (d, *J* = 2.4 Hz, 1H), 7.38 - 7.32 (m, 1H), 6.29 (d, *J* = 2.4 Hz, 1H), 5.39 (s, 2H), 3.79 (s, 2H), 3.56 (dd, *J* = 7.7, 8.6 Hz, 2H), 1.52 (s, 6H), 0.92 - 0.87 (m, 2H), -0.05 (s, 9H); ¹³C NMR (100 MHz, CDCl₃) δ = 159.15, 149.20, 136.65, 132.99, 131.57, 130.22, 127.52, 124.31, 104.13, 79.87, 66.37, 53.68, 44.79, 28.34, 17.64, -1.53; LRMS (ESI) calculated for C₁₉H₃₁N₄O₃Si [M + H]⁺ m/z 391.22, found 391.15.

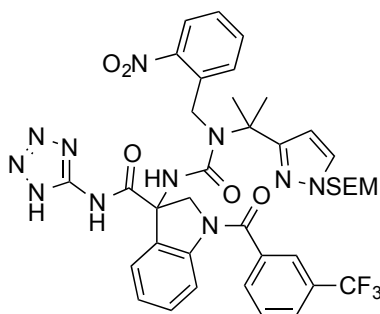


methyl 3-(3-(2-nitrobenzyl)-3-(2-(1-((2-(trimethylsilyl)ethoxy)methyl)-1H-pyrazol-3-yl)propan-2-yl)ureido)-1-(3-(trifluoromethyl)benzoyl)indoline-3-carboxylate (S59).

Semi-crude **S41** (27.6 mg, 0.076 mmol, 1.0 equiv.) was reacted with partner amine **S58** (0.95 equiv.) according to general procedure G. The reaction vessel was foiled. **S59** (47.2 mg, 80%) obtained as a white solid. ^1H NMR (400 MHz, CDCl_3) δ = 8.23 (br s, 1H), 8.03 - 7.99 (m, 1H), 7.81 (s, 1H), 7.73 (d, J = 7.8 Hz, 2H), 7.64 - 7.52 (m, 4H), 7.39 (dt, J = 2.1, 7.4 Hz, 1H), 7.40 (br s, 1H), 7.24 - 7.19 (m, 1H), 7.19 - 7.13 (m, 1H), 6.39 (s, 1H), 6.23 (d, J = 2.2 Hz, 1H), 5.12 - 5.06 (m, 3H), 4.98 (d, J = 11.0 Hz, 1H), 4.94 (br d, J = 11.9 Hz, 1H), 3.71 (s, 3H), 3.42 (dd, J = 7.5, 8.5 Hz, 2H), 1.76 (s, 3H), 1.58 (s, 3H), 0.82 (dt, J = 1.8, 8.1 Hz, 2H), -0.05 (s, 9H); ^{13}C NMR (100 MHz, CDCl_3) δ = 170.58, 167.45 (br s), 158.39, 157.82, 147.32, 142.57 (br s), 137.01, 136.38, 133.31, 131.83, 131.23 (d, J = 33.0 Hz), 130.85 - 130.53 (m), 130.31 - 130.10 (m), 129.69, 129.33, 128.79, 127.41, 127.23 (br d, J = 3.3 Hz), 124.82, 124.70 (br s), 124.35 - 124.06 (m), 123.44 (br s), 123.58 (d, J = 272.5 Hz), 118.45 (br s), 104.40, 79.79, 66.66, 65.09 (br s), 61.68 (br s), 56.66, 53.08, 45.45, 28.13, 27.21 (br s), 17.49, -1.53; ^{19}F NMR (376 MHz, CDCl_3) δ = -62.73 (s, 3F); LRMS (ESI) calculated for $\text{C}_{38}\text{H}_{44}\text{F}_3\text{N}_6\text{O}_7\text{Si}$ $[\text{M} + \text{H}]^+$ m/z 781.30, found 781.28.

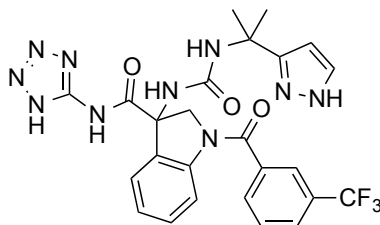


3-(3-(2-nitrobenzyl)-3-(2-(1-((2-(trimethylsilyl)ethoxy)methyl)-1H-pyrazol-3-yl)propan-2-yl)ureido)-1-(3-(trifluoromethyl)benzoyl)indoline-3-carboxylic acid (S60). **S59** (47.2 mg, 0.060 mmol, 1.0 equiv.) was reacted in methanol (2.5 mL) with 1M lithium hydroxide (85 uL, 0.085 mmol, 1.4 equiv.) according to general procedure B (48h), except a second addition of 1M lithium hydroxide (20 uL) was required for completion. The reaction vessel was foiled. Semi-crude **S60** (45.1 mg, 97%) obtained as a brown oil. LRMS (ESI) calculated for $C_{37}H_{40}F_3N_6O_7Si$ $[M - H]^-$ m/z 765.29, found 765.39.



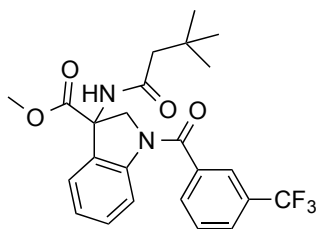
3-(3-(2-nitrobenzyl)-3-(2-(1-((2-(trimethylsilyl)ethoxy)methyl)-1H-pyrazol-3-yl)propan-2-yl)ureido)-N-(1H-tetrazol-5-yl)-1-(3-(trifluoromethyl)benzoyl)indoline-3-carboxamide (S61). Semi-crude **S60** (45.1 mg, 0.059 mmol, 1.0 equiv.) was reacted with 5-aminotetrazole monohydrate (1.1 equiv.) in 2.5 mL DMF according to general procedure D (1h activation), except the product was unstable to

purification/concentration. Crude **S61** (15.3 mg, 31%) obtained as a white solid (~ 26% pure). LRMS (ESI) calculated for C₃₈H₄₁F₃N₁₁O₆Si [M - H]⁻ m/z 832.30, found 832.54.

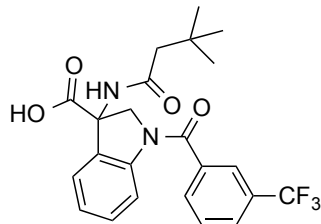


3-(3-(2-(1H-pyrazol-3-yl)propan-2-yl)ureido)-N-(1H-tetrazol-5-yl)-1-(3-

(trifluoromethyl)benzoyl)indoline-3-carboxamide (22). Crude **S61** (15.3 mg, 0.018 mmol, 1.0 equiv.) was taken up in methanol (5 mL) and irradiated with 365 nm hv (TLC lamp, 4 watt) for 2h. The methanol was then removed under reduced pressure; the residue was dissolved in dry tetrahydrofuran (3 mL). Tetrabutylammonium fluoride (3 mL, 3.0 mmol, 163 equiv.) (1M solution in tetrahydrofuran) was then added, and the reaction was heated at 40 °C for 26h. The crude reaction mixture was transferred to a sep. funnel with EtOAc and water, and the aqueous layer was adjusted to pH 2.5 with 0.1N HCl. The layers were separated, and the aqueous layer was further extracted with 2 x 50 mL EtOAc. The organics were combined, dried over MgSO₄, and concentrated. The resulting residue was purified by reverse phase HPLC (water/MeOH/0.05% formic acid) to afford **22** (1.6 mg, 5% over 3 steps) as a white solid. ¹H NMR (400 MHz, DMSO-d₆) δ = 12.70 (br s, 1H), 12.23 (br s, 1H), 8.21 (br s, 1H), 8.05 - 7.91 (m, 3H), 7.87 - 7.74 (m, 2H), 7.44 (br s, 2H), 7.34 (br s, 1H), 7.28 - 7.16 (m, 1H), 6.60 (s, 1H), 6.52 (s, 0.5H), 6.11 (s, 1H), 5.01 - 4.74 (m, 1H), 4.01 (d, J = 11.2 Hz, 1H), 1.51 (br s, 3H), 1.50 (br s, 3H); ¹⁹F NMR (376 MHz, DMSO-d₆) δ = -61.14 (br s, 3F); LRMS (ESI) calculated for C₂₅H₂₂F₃N₁₀O₃ [M - H]⁻ m/z 567.18, found 567.16.

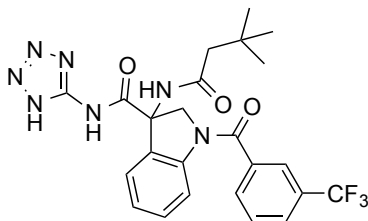


methyl 3-(3,3-dimethylbutanamido)-1-(3-(trifluoromethyl)benzoyl)indoline-3-carboxylate (S62). Semi-crude **S41** (41.9 mg, 0.115 mmol, 1.0 equiv.) was reacted with commercially available 3,3-dimethylbutyryl chloride in dry dichloromethane (2 mL) according to general procedure A, with slight modification: prior to base addition, the reaction vessel was cooled to 0 °C; 2.2 equiv. of *N,N*-diisopropylethylamine was used; after acyl chloride addition, the reaction mixture was allowed to slowly warm to r.t. **S62** (32.1 mg, 60%) obtained as a white solid. ^1H NMR (400 MHz, CDCl_3) δ = 8.22 (br s, 1H), 7.83 (s, 1H), 7.79 - 7.71 (m, 2H), 7.64 - 7.56 (m, 1H), 7.39 (d, J = 7.5 Hz, 1H), 7.40 (br s, 1H), 7.16 (br t, J = 7.4 Hz, 1H), 6.26 (s, 1H), 5.04 (d, J = 11.9 Hz, 1H), 4.04 (br d, J = 9.3 Hz, 1H), 3.77 (s, 3H), 2.04 (s, 2H), 1.01 (s, 9H); ^{13}C NMR (100 MHz, CDCl_3) δ = 171.74, 169.74, 167.49 (br s), 142.76, 136.85, 131.06 (br s), 131.34 (q, J = 33.0 Hz), 130.22 (br s), 129.36, 127.53 - 127.14 (m), 125.22 - 124.95 (m), 124.41 - 124.06 (m), 123.42 (br s), 123.54 (q, J = 272.6 Hz), 118.50 (br s), 64.27 (br s), 60.51 (br s), 53.30, 49.35, 31.14, 29.59; ^{19}F NMR (376 MHz, CDCl_3) δ = -62.81 (s, 3F); LRMS (ESI) calculated for $\text{C}_{24}\text{H}_{26}\text{F}_3\text{N}_2\text{O}_4$ $[\text{M} + \text{H}]^+$ m/z 463.18, found 463.03.



3-(3,3-dimethylbutanamido)-1-(3-(trifluoromethyl)benzoyl)indoline-3-carboxylic acid (S63).

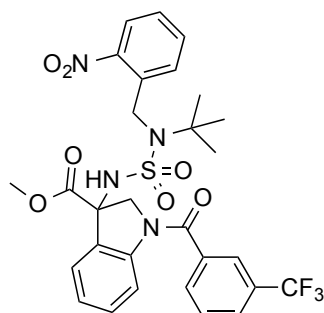
S62 (32.1 mg, 0.069 mmol, 1.0 equiv.) was reacted in methanol (3 mL) with 1M lithium hydroxide (416 μ L, 0.416 mmol, 6.0 equiv.) according to general procedure B. Semi-crude **S63** (32.0 mg, 103%) obtained as a white solid. ^1H NMR (400 MHz, CDCl_3 , CD_3OD) δ = 8.11 (br s, 1H), 7.73 (br s, 1H), 7.67 (br d, J = 7.5 Hz, 2H), 7.56 - 7.49 (m, 1H), 7.38 (br d, J = 7.3 Hz, 1H), 7.29 (br s, 1H), 7.06 (br s, 1H), 4.89 (br d, J = 11.9 Hz, 1H), 3.92 (br s, 1H), 1.95 (br s, 2H), 0.88 (s, 9H); ^{13}C NMR (100 MHz, CDCl_3 , CD_3OD) δ = 172.62, 171.13, 167.65 (br s), 142.25 (br s), 136.67 (br s), 131.05 (q, J = 33.3 Hz), 130.50 - 130.23 (m), 130.21 - 129.95 (m), 129.24, 127.32 - 126.99 (m), 125.22 - 124.80 (m), 123.88 (br s), 123.36 (q, J = 272.5 Hz), 117.97 (br s), 63.95 (br s), 60.41 (br s), 48.70 (br s), 30.87, 29.28; ^{19}F NMR (376 MHz, CHLOROFORM- d) δ = -59.14 (s, 3F); LRMS (ESI) calculated for $\text{C}_{23}\text{H}_{22}\text{F}_3\text{N}_2\text{O}_4$ $[\text{M} - \text{H}]^-$ m/z 447.15, found 447.22.



3-(3,3-dimethylbutanamido)-N-(1H-tetrazol-5-yl)-1-(3-

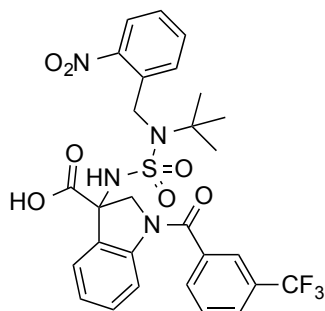
(trifluoromethyl)benzoyl)indoline-3-carboxamide (23). Semi-crude **S63** (32.0 mg, 0.071 mmol, 1.0 equiv.) was reacted with 5-aminotetrazole monohydrate (1.1 equiv.) in

1.5 mL DMF according to general procedure D (20m activation). **23** (5.2 mg, 14% over 2 steps) obtained as a white solid. ^1H NMR (400 MHz, DMSO- d_6) δ = 10.69 (br s, 1H), 8.82 (br s, 1H), 8.39 (br s, 1H), 8.13 (br s, 1H), 8.05 - 7.96 (m, 1H), 7.96 - 7.90 (m, 2H), 7.83 - 7.72 (m, 2H), 7.41 (br s, 1H), 7.24 - 7.09 (m, 1H), 5.00 (br d, J = 11.4 Hz, 1H), 4.02 - 3.92 (m, 1H), 2.12 (br d, J = 13.4 Hz, 1H), 1.97 - 1.90 (m, 1H), 0.85 (s, 9H); ^{19}F NMR (376 MHz, DMSO- d_6) δ = -61.23 (s, 3F); LRMS (ESI) calculated for $\text{C}_{24}\text{H}_{23}\text{F}_3\text{N}_7\text{O}_3$ $[\text{M} - \text{H}]^-$ m/z 514.18, found 514.33.



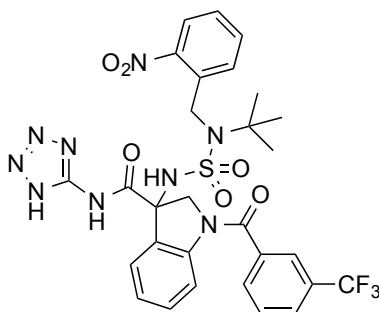
methyl 3-((N-(tert-butyl)-N-(2-nitrobenzyl)sulfamoyl)amino)-1-(3-(trifluoromethyl)benzoyl)indoline-3-carboxylate (S64). Semi-crude **S41** (50.2 mg, 0.138 mmol, 1.0 equiv.) was reacted with partner amine **S44** (1.1 equiv.) according to general procedure G, except sulfuryl chloride (1.1 equiv.) was used instead of p-nitrophenyl chloroformate. The reaction vessel was foiled. **S64** (17.9 mg, 21%) obtained as a light yellow oil. ^1H NMR (400 MHz, CDCl_3) δ = 8.24 (br s, 1H), 8.04 (dd, J = 1.2, 8.3 Hz, 1H), 7.88 - 7.81 (m, 2H), 7.76 (br d, J = 7.8 Hz, 2H), 7.66 - 7.56 (m, 2H), 7.45 - 7.31 (m, 3H), 7.19 - 7.10 (m, 1H), 5.06 (br s, 1H), 4.90 - 4.71 (m, 3H), 4.50 (br d, J = 10.5 Hz, 1H), 3.78 (s, 3H), 1.42 (s, 9H); ^{13}C NMR (100 MHz, CDCl_3) δ = 169.96, 167.40 (br s), 147.15, 142.47, 136.75, 135.72, 133.66, 131.25 (br s), 131.32 (d, J = 32.7 Hz), 130.31 (br s), 129.32, 129.12, 127.75, 127.56 - 127.29 (m), 125.13 - 124.93 (m), 124.87,

124.45 (br s), 124.25 - 123.92 (m), 123.55 (d, $J = 272.3$ Hz), 118.19 (br s), 67.36 (br s), 60.65, 59.11 (br s), 53.79, 47.77, 29.54; ^{19}F NMR (376 MHz, CDCl_3) $\delta = -62.82$ (s, 3F); LRMS (ESI) calculated for $\text{C}_{29}\text{H}_{29}\text{F}_3\text{N}_4\text{NaO}_7\text{S}$ [$\text{M} + \text{H}$] $^+$ m/z 657.16, found 657.18.



3-((*N*-(tert-butyl)-*N*-(2-nitrobenzyl)sulfamoyl)amino)-1-(3-

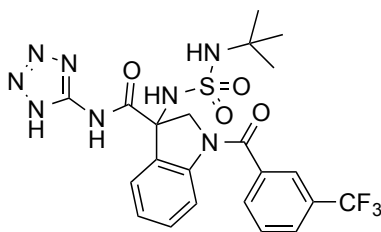
(trifluoromethyl)benzoyl)indoline-3-carboxylic acid (S65). **S64** (17.9 mg, 0.028 mmol, 1.0 equiv.) was reacted in methanol (2 mL) with 1M lithium hydroxide (40 μL , 0.040 mmol, 1.4 equiv.) according to general procedure B, except a second addition of 1M lithium hydroxide (15 μL) was required. The reaction vessel was foiled. Semi-crude **S65** (18.8 mg, 107%) obtained as a brown oil. LRMS (ESI) calculated for $\text{C}_{28}\text{H}_{28}\text{F}_3\text{N}_4\text{O}_7\text{S}$ [$\text{M} + \text{H}$] $^+$ m/z 621.16, found 621.14.



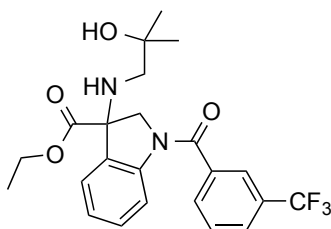
3-((*N*-(tert-butyl)-*N*-(2-nitrobenzyl)sulfamoyl)amino)-*N*-(1*H*-tetrazol-5-yl)-1-(3-

(trifluoromethyl)benzoyl)indoline-3-carboxamide (S66). Semi-crude **S65** (17.5 mg, 0.028 mmol, 1.0 equiv.) was reacted with 5-aminotetrazole monohydrate (1.1 equiv.) in

2 mL DMF according to general procedure D (1h activation; 72h), except the product was unstable to purification/concentration. Crude **S66** (3.7 mg, 19%) obtained as a white solid (~ 80% pure). LRMS (ESI) calculated for $C_{29}H_{28}F_3N_9NaO_6S$ $[M + Na]^+$ m/z 710.17, found 710.18.

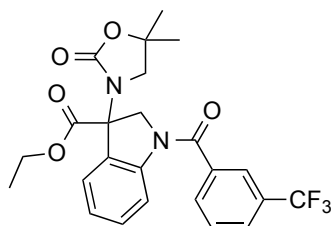


3-((N-(tert-butyl)sulfamoyl)amino)-N-(1H-tetrazol-5-yl)-1-(3-(trifluoromethyl)benzoyl)indoline-3-carboxamide (24). Crude **S66** (3.7 mg, 0.005 mmol, 1.0 equiv.) was taken up in methanol (3 mL) and irradiated with 365 nm hv (TLC lamp, 4 watt) for 3h. The reaction mixture was concentrated and purified by reverse phase HPLC (water/MeOH/0.05% formic acid) to afford **24** (1.1 mg, 7% over 3 steps) as a white solid. 1H NMR (400 MHz, DMSO- d_6) δ = 12.01 (br s, 1H), 8.02 - 7.93 (m, 3H), 8.06 (br s, 1H), 7.85 - 7.76 (m, 2H), 7.43 (br s, 1H), 7.19 (br s, 1H), 6.88 (br s, 1H), 6.52 (s, 1H), 4.77 (br d, J = 11.2 Hz, 1H), 4.59 (br d, J = 11.2 Hz, 1H), 1.13 (s, 9H); ^{19}F NMR (376 MHz, DMSO- d_6) δ = -61.14 (br s, 3F); LRMS (ESI) calculated for $C_{22}H_{22}F_3N_8O_4S$ $[M - H]^-$ m/z 551.14, found 551.19.



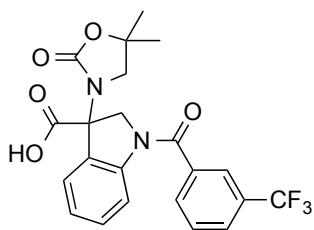
ethyl 3-((2-hydroxy-2-methylpropyl)amino)-1-(3-(trifluoromethyl)benzoyl)indoline-3-carboxylate (S67). Semi-crude **S41** (53.8 mg, 0.148 mmol, 1.05 equiv.) was dissolved in absolute ethanol (2 mL); isobutylene oxide (12.5 uL, 0.141 mmol, 1.0 equiv.) was then added, followed by *N,N*-diisopropylethylamine (25.8 uL, 0.148 mmol, 1.05 equiv.). The reaction vial was sealed and heated at 80 °C overnight. The reaction was pushed to completion by adding 3 equiv. isobutylene oxide every day for an additional 5d (80 °C). The crude reaction mixture was transferred to a sep funnel with ~ 75 mL EtOAc and partitioned with ~ 75 mL sat. NaHCO₃. The aqueous layer was washed with an additional 2 x 50 mL EtOAc; the organics were combined, dried over MgSO₄, and concentrated. Purified on a silica column with 0-50% EtOAc:hexanes. **S67** (50.1 mg, 79%) obtained as a colorless oil. **Note:** Atropisomers of the secondary amide observable by NMR; split peaks reported by integration values in 1H. ¹H NMR (400 MHz, CDCl₃) δ = 8.24 (br s, 1H), 7.90 - 7.83 (m, 1H), 7.77 (br d, *J* = 7.5 Hz, 2H), 7.66 - 7.58 (m, 1H), 7.44 - 7.24 (m, 2H), 7.13 (br s, 1H), 4.69 (d, *J* = 11.2 Hz, 0.2H), 4.59 (br d, *J* = 10.0 Hz, 0.8H), 4.28 - 4.17 (m, 2H), 3.97 (br s, 0.8H), 3.12 (d, *J* = 13.4 Hz, 0.2H), 2.47 - 2.26 (m, 2H), 1.59 (s, 0.6H), 1.48 (s, 0.6H), 1.26 (t, *J* = 7.1 Hz, 3H), 1.14 (s, 4.8H); ¹³C NMR (100 MHz, CDCl₃) δ = 171.54, 169.92, 167.32 (br s), 167.04, 142.45 (br s), 141.74, 137.14 (br s), 131.75 (br s), 131.27 (q, *J* = 33.0 Hz), 130.48 - 130.20 (m), 130.17 - 129.80 (m), 129.35, 129.28, 127.53 - 127.35 (m), 127.32 - 127.09 (m), 124.85 - 124.43 (m), 124.39 - 124.01 (m), 123.99 - 123.34 (m), 123.55 (q, *J* = 272.2 Hz), 118.19

(br s), 83.69, 69.28, 68.64 (br s), 62.26, 58.07 (br s), 54.33, 27.20, 27.07, 26.67, 26.46, 14.00; ^{19}F NMR (376 MHz, CDCl_3) δ = -62.75 (s, 0.9F), -62.79 (s, 3F); LRMS (ESI) calculated for $\text{C}_{23}\text{H}_{26}\text{F}_3\text{N}_2\text{O}_4$ $[\text{M} + \text{H}]^+$ m/z 451.18, found 451.21.

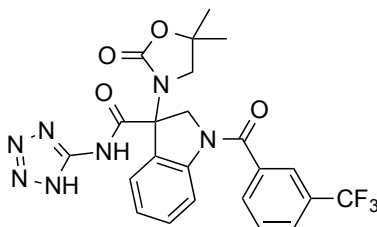


ethyl 3-(5,5-dimethyl-2-oxooxazolidin-3-yl)-1-(3-(trifluoromethyl)benzoyl)indoline-3-carboxylate (S68). **S67** (50.1 mg, 0.111 mmol, 1.0 equiv.) was dissolved in dry dichloromethane (4.44 mL). *N,N*-diisopropylethylamine (39 μL , 0.222 mmol, 2.0 equiv.), 1,1'-carbonyldiimidazole (19 mg, 0.117 mmol, 1.05 equiv.), and 4-dimethylaminopyridine (14 mg, 0.111 mmol, 1.0 equiv.) were then added, and the reaction vial was firmly sealed and heated at 50 $^\circ\text{C}$ overnight. The reaction was pushed to completion by adding 1.05 equiv. 1,1'-carbonyldiimidazole every day for an additional 4d (70 $^\circ\text{C}$). The crude reaction mixture was transferred to a sep. funnel with \sim 80 mL dichloromethane; the organic layer was washed with \sim 50 mL sat. NaHCO_3 , 0.1N HCl, and brine. Dried over MgSO_4 , concentrated, and purified on a silica column with 0-40% EtOAc:hexanes. **S68** (36.9 mg, 70%) obtained as a colorless oil. ^1H NMR (400 MHz, CDCl_3) δ = 8.19 (br s, 1H), 7.86 (s, 1H), 7.77 (d, J = 8.0 Hz, 2H), 7.66 - 7.58 (m, 1H), 7.51 - 7.41 (m, 1H), 7.38 (d, J = 7.1 Hz, 1H), 7.21 - 7.15 (m, 1H), 5.01 (d, J = 12.2 Hz, 1H), 4.35 (br d, J = 11.0 Hz, 1H), 4.30 (q, J = 7.1 Hz, 2H), 3.45 (d, J = 8.3 Hz, 1H), 2.86 (d, J = 8.0 Hz, 1H), 1.48 (s, 3H), 1.35 (s, 3H), 1.31 (t, J = 7.1 Hz, 3H); ^{13}C NMR (100 MHz, CDCl_3) δ = 168.90, 167.39, 157.02, 143.22, 136.48, 131.33, 131.43 (q, J = 33.0

Hz), 130.23, 129.41, 127.63 (d, $J = 3.7$ Hz), 127.28, 125.04, 124.70, 124.42 (q, $J = 4.2$ Hz), 123.49 (br q, $J = 272.2$ Hz), 118.55 (br s), 79.11, 66.92 (br s), 62.86, 59.52 (br s), 56.35, 27.13, 26.65, 14.01; ^{19}F NMR (376 MHz, CDCl_3) $\delta = -62.81$ (s, 3F); LRMS (ESI) calculated for $\text{C}_{24}\text{H}_{24}\text{F}_3\text{N}_2\text{O}_5$ $[\text{M} + \text{H}]^+$ m/z 477.16, found 477.12.

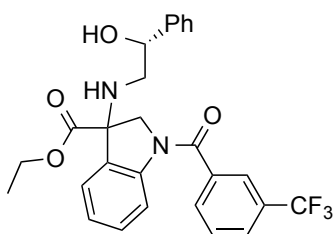


3-(5,5-dimethyl-2-oxooxazolidin-3-yl)-1-(3-(trifluoromethyl)benzoyl)indoline-3-carboxylic acid (S69). **S68** (36.9 mg, 0.077 mmol, 1.0 equiv.) was reacted in methanol (3 mL) with 1M lithium hydroxide (93 μL , 0.093 mmol, 1.2 equiv.) according to general procedure B, except three additions of 1M lithium hydroxide (155 μL , 0.155 mmol, 2.0 equiv.) were required (2d). The resulting residue was purified on a silica column with 0-15% dichloromethane:methanol. Semi-crude **S69** (17.0 mg, 49%) obtained as a white solid. LRMS (ESI) calculated for $\text{C}_{22}\text{H}_{18}\text{F}_3\text{N}_2\text{O}_5$ $[\text{M} - \text{H}]^-$ m/z 447.12, found 447.21.



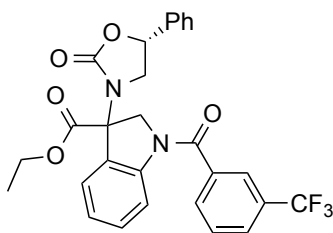
3-(5,5-dimethyl-2-oxooxazolidin-3-yl)-N-(1H-tetrazol-5-yl)-1-(3-(trifluoromethyl)benzoyl)indoline-3-carboxamide (25). Semi-crude **S69** (17.0 mg, 0.038 mmol, 1.0 equiv.) was reacted with 5-aminotetrazole monohydrate (1.1 equiv.) in 1 mL DMF according to general procedure D (20m activation). **25** (10.4 mg, 53%)

obtained as a white solid. ^1H NMR (400 MHz, CD_3OD , drops CDCl_3) δ = 8.18 - 7.91 (m, 3H), 7.88 (br d, J = 8.0 Hz, 1H), 7.79 - 7.71 (m, 1H), 7.57 (br d, J = 7.5 Hz, 1H), 7.46 (br s, 1H), 7.25 (br t, J = 7.3 Hz, 1H), 5.03 (br d, J = 12.2 Hz, 1H), 4.37 (br d, J = 11.7 Hz, 1H), 3.57 (br d, J = 8.5 Hz, 1H), 3.10 (br d, J = 8.5 Hz, 1H), 1.57 (s, 3H), 1.40 (s, 3H); ^{19}F NMR (376 MHz, CD_3OD , drops CDCl_3) δ = -64.16 (s, 3F); LRMS (ESI) calculated for $\text{C}_{23}\text{H}_{19}\text{F}_3\text{N}_7\text{O}_4$ $[\text{M} - \text{H}]^-$ m/z 514.15, found 514.33.



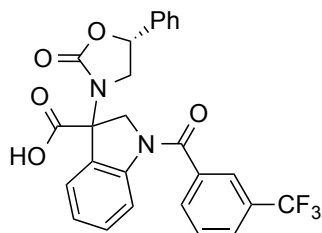
ethyl 3-(((R)-2-hydroxy-2-phenylethyl)amino)-1-(3-(trifluoromethyl)benzoyl)indoline-3-carboxylate (S70). Semi-crude **S41** (53.3 mg, 0.146 mmol, 1.0 equiv.) was dissolved in absolute ethanol (2 mL); (R)-styrene oxide (17 μL , 0.146 mmol, 1.0 equiv.) was then added, followed by *N,N*-diisopropylethylamine (27 μL , 0.154 mmol, 1.05 equiv.). The reaction vial was sealed and heated at 80 $^\circ\text{C}$ overnight. The reaction was pushed to completion by adding 5.0 equiv. (R)-styrene oxide over 7d (80 $^\circ\text{C}$). The crude reaction mixture was transferred to a sep funnel with ~ 75 mL EtOAc and partitioned with ~ 75 mL sat. NaHCO_3 . The aqueous layer was washed with an additional 2 x 50 mL EtOAc; the organics were combined, dried over MgSO_4 , and concentrated. Purified on a silica column with 0-50% EtOAc:hexanes. **S70** (45.5 mg, 62%) (mixture of diastereomers) obtained as an orange oil. **Note:** Diastereomers combined with the atropisomers of the secondary amide resulted in a multitude of split peaks. ^1H NMR (400 MHz, CDCl_3) δ = 8.25 (br s, 0.5H), 7.86 (br s,

0.5H), 7.82 - 7.74 (m, 1H), 7.73 - 7.59 (m, 1H), 7.48 - 7.40 (m, 1H), 7.40 - 7.25 (m, 7H), 7.23 - 7.04 (m, 2H), 4.79 (dd, $J = 3.4, 8.3$ Hz, 0.5H), 4.73 - 4.52 (m, 1H), 4.31 - 4.18 (m, 1H), 4.17 - 3.93 (m, 1H), 3.77 - 3.70 (m, 0.5H), 3.70 - 3.55 (m, 1H), 3.53 - 3.43 (m, 0.5H), 2.87 - 2.67 (m, 1H), 2.68 - 2.43 (m, 1H), 1.31 - 1.15 (m, 3H); ^{13}C NMR (100 MHz, CDCl_3) $\delta = 171.45$ (br s), 167.27 (br s), 167.03 (br s), 141.98 (br s), 141.70, 141.64, 140.94, 140.90, 140.56, 131.40 (br s), 131.01 (br s), 130.76 (br s), 130.56 - 130.21 (m), 130.20 - 129.82 (m), 129.63, 129.36, 128.97 - 128.75 (m), 128.63, 128.62, 128.44, 128.42, 127.85, 127.95 - 127.75 (m), 127.26 (br s), 126.84, 125.99, 125.71, 125.65, 124.79 (br s), 124.22 (br s), 123.55 (q, $J = 272.9$ Hz), 118.04 (br s), 74.57, 72.75, 72.54, 68.02, 67.09, 62.47, 62.37, 62.33, 62.28, 59.41 (br s), 58.31 (br s), 51.49, 51.38, 13.98, 13.79; ^{19}F NMR (376 MHz, CDCl_3) $\delta = -62.62$ (br s, 1F), -62.68 (br s, 1F), -62.75 (br s, 3F); LRMS (ESI) calculated for $\text{C}_{27}\text{H}_{26}\text{F}_3\text{N}_2\text{O}_4$ $[\text{M} + \text{H}]^+$ m/z 499.18, found 499.08.

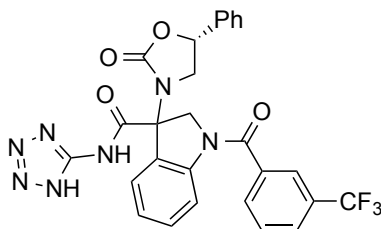


ethyl 3-((*R*)-2-oxo-5-phenyloxazolidin-3-yl)-1-(3-(trifluoromethyl)benzoyl)indoline-3-carboxylate (S71). **S70** (45.5 mg, 0.091 mmol, 1.0 equiv.) was dissolved in dry dichloromethane (3.5 mL). *N,N*-diisopropylethylamine (32 μL , 0.183 mmol, 2.0 equiv.), 1,1'-carbonyldiimidazole (16 mg, 0.096 mmol, 1.05 equiv.), and 4-dimethylaminopyridine (11 mg, 0.091 mmol, 1.0 equiv.) were then added, and the reaction vial was firmly sealed and heated at 70 $^\circ\text{C}$ overnight. Additional 1,1'-carbonyldiimidazole (7.4 mg, 0.046 mmol, 0.5 equiv.) was then added; heated at 70 $^\circ\text{C}$

for two days. 1.0 equiv. 4-dimethylaminopyridine was then added every day for an additional 3d (80 °C). The crude reaction mixture was transferred to a sep. funnel with ~ 80 mL dichloromethane; the organic layer was washed with ~ 50 mL sat. NaHCO₃, 0.5M KHSO₄, and brine. Dried over MgSO₄, concentrated, and purified on a silica column with 0-40% EtOAc:hexanes. **S71** (18.7 mg, 39%) (mixture of diastereomers) obtained as a colorless oil. ¹H NMR (400 MHz, CDCl₃) δ = 8.28 (br s, 0.6H), 7.92 (s, 0.4H), 7.84 - 7.76 (m, 2H), 7.72 - 7.59 (m, 2H), 7.51 - 7.33 (m, 5H), 7.32 - 7.10 (m, 3H), 5.57 (dd, *J* = 5.8, 8.5 Hz, 0.6H), 5.39 (dd, *J* = 8.2, 9.4 Hz, 0.4H), 5.03 (dd, *J* = 2.6, 12.3 Hz, 0.9H), 4.90 (d, *J* = 12.2 Hz, 0.1H), 4.55 - 4.47 (m, 0.5H), 4.41 - 4.23 (m, 2.5H), 4.02 (t, *J* = 8.5 Hz, 0.6H), 3.80 - 3.75 (m, 0.1H), 3.70 (dd, *J* = 8.5, 9.5 Hz, 0.4H), 3.66 - 3.61 (m, 0.1H), 3.41 (t, *J* = 8.2 Hz, 0.4H), 3.05 (dd, *J* = 5.8, 8.5 Hz, 0.6H), 1.41 - 1.23 (m, 3H); ¹³C NMR (100 MHz, CDCl₃) δ = 169.02, 168.50, 167.42, 167.32, 157.59, 157.19, 143.38 (br s), 143.04 (br s), 137.90, 137.20, 136.49, 136.43, 131.66, 131.49 (br s), 131.42 (br s), 131.32, 130.35, 130.17 (br s), 129.44, 129.39, 129.26, 129.10, 128.98, 128.93, 128.68, 127.83 - 127.57 (m), 127.18, 126.72, 126.12, 125.16, 125.05 (br s), 124.98 - 124.80 (m), 124.75 - 124.55 (m), 124.48 - 124.25 (m), 123.54 (d, *J* = 272.4 Hz), 123.51 (d, *J* = 272.3 Hz), 118.54 (br s), 76.47, 75.41, 67.16 (br s), 63.07, 63.02, 59.65 (br s), 59.05 (br s), 53.00, 51.54, 14.14, 14.07; ¹⁹F NMR (376 MHz, CDCl₃) δ = -62.77 (br s, 3F), -62.78 (s, 2.5F); LRMS (ESI) calculated for C₂₈H₂₄F₃N₂O₅ [M + H]⁺ m/z 525.16, found 525.08.

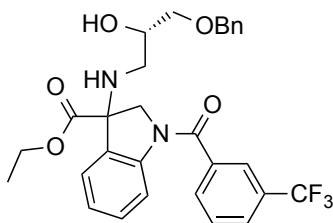


3-((*R*)-2-oxo-5-phenyloxazolidin-3-yl)-1-(3-(trifluoromethyl)benzoyl)indoline-3-carboxylic acid (S72**).** **S71** (18.7 mg, 0.036 mmol, 1.0 equiv.) was reacted in methanol (3 mL) with 1M lithium hydroxide (43 μ L, 0.043 mmol, 1.2 equiv.) according to general procedure B, except three additions of 1M lithium hydroxide (71 μ L, 0.071 mmol, 2.0 equiv.) were required (**2d**). The resulting residue was purified on a silica column with 0-10% dichloromethane:methanol with 0.1% formic acid. Semi-crude **S72** (7.6 mg, 43%) (mixture of diastereomers) obtained as a white solid. LRMS (ESI) calculated for $C_{26}H_{18}F_3N_2O_5$ $[M - H]^-$ m/z 495.12, found 495.02.



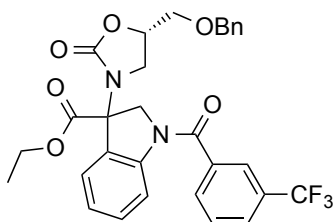
3-((*R*)-2-oxo-5-phenyloxazolidin-3-yl)-*N*-(1*H*-tetrazol-5-yl)-1-(3-(trifluoromethyl)benzoyl)indoline-3-carboxamide (26**).** Semi-crude **S72** (7.6 mg, 0.015 mmol, 1.0 equiv.) was reacted with 5-aminotetrazole monohydrate (1.1 equiv.) in 1 mL DMF according to general procedure D (20m activation). **26** (2.3 mg, 27%) (mixture of diastereomers) obtained as a white solid. 1H NMR (400 MHz, CD_3OD) δ = 7.98 - 7.88 (m, 3H), 7.76 (t, J = 7.7 Hz, 1H), 7.66 (d, J = 7.8 Hz, 1H), 7.52 - 7.34 (m, 7H), 7.32 - 7.20 (m, 2H), 5.79 (t, J = 8.6 Hz, 1H), 5.12 (br d, J = 11.9 Hz, 1H), 4.33 (br d, J = 11.7 Hz, 1H), 4.07 (t, J = 8.3 Hz, 1H); ^{19}F NMR (376 MHz, CD_3OD) δ = -64.19 (s,

1F), -64.22 (s, 3F); LRMS (ESI) calculated for C₂₇H₂₁F₃N₇O₄ [M + H]⁺ m/z 564.16, found 564.12.



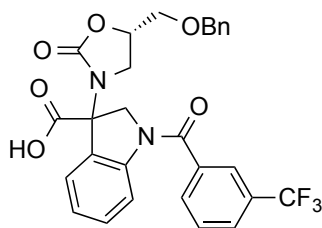
ethyl 3-(((S)-3-(benzyloxy)-2-hydroxypropyl)amino)-1-(3-(trifluoromethyl)benzoyl)indoline-3-carboxylate (S73). Semi-crude **S41** (156.8 mg, 0.430 mmol, 1.0 equiv.) was dissolved in absolute ethanol (6 mL); benzyl (s)-(+)-glycidyl ether (66 μ L, 0.430 mmol, 1.0 equiv.) was then added, followed by *N,N*-diisopropylethylamine (79 μ L, 0.452 mmol, 1.05 equiv.). The reaction vial was sealed and heated at 80 °C overnight. The reaction was pushed to completion by adding 2.0 equiv. benzyl (s)-(+)-glycidyl ether over 3d (80 °C). The crude reaction mixture was transferred to a sep funnel with ~ 75 mL EtOAc and partitioned with ~ 75 mL sat. NaHCO₃. The aqueous layer was washed with an additional 2 x 50 mL EtOAc; the organics were combined, dried over MgSO₄, and concentrated. Purified on a silica column with 0-50% EtOAc:hexanes. **S73** (143.8 mg, 62%) (mixture of diastereomers) obtained as a light yellow oil. **Note:** Diastereomers combined with the atropisomers of the secondary amide resulted in a multitude of split peaks. ¹H NMR (400 MHz, CDCl₃) δ = 8.26 (br s, 1H), 7.91 - 7.83 (m, 1H), 7.76 (m, 2H), 7.63 - 7.50 (m, 1H), 7.42 - 7.25 (m, 6.5H), 7.24 - 7.19 (m, 0.5H), 7.12 (br s, 1H), 4.69 - 4.54 (m, 1H), 4.50 (s, 1.6H), 4.42 (br d, *J* = 1.5 Hz, 0.4H), 4.27 - 4.16 (m, 2H), 3.98 (br s, 1H), 3.87 - 3.77 (m, 1H), 3.52 - 3.31 (m, 2H), 2.65 - 2.41 (m, 2H), 1.30 - 1.21 (m, 3H); ¹³C NMR (100 MHz, CDCl₃) δ =

171.38, 171.32, 170.02, 169.84, 167.09 (br s), 142.30 (br s), 137.70, 137.46, 137.16, 137.08 (br s), 131.09 (q, $J = 33.0$ Hz), 130.28 (br s), 129.83 (br s), 129.23, 128.42, 128.34, 128.28, 127.92, 127.71, 127.69, 127.63, 127.58, 127.56, 127.55, 127.29 - 126.94 (m), 124.60 (br s), 124.30 - 123.58 (m), 123.49 (q, $J = 272.4$ Hz), 123.44 (d, $J = 272.9$ Hz), 118.00 (br s), 73.83, 73.68, 73.28, 73.25, 72.45, 72.34, 69.71, 69.64, 69.24, 69.21, 68.43 (br s), 62.09, 62.06, 57.98 (br s), 46.41, 46.17, 13.88, 13.86; ^{19}F NMR (376 MHz, CDCl_3) $\delta = -62.67$ (br s, 0.7F), -62.71 (s, 3F), -62.74 (br s, 0.3F); LRMS (ESI) calculated for $\text{C}_{29}\text{H}_{30}\text{F}_3\text{N}_2\text{O}_5$ $[\text{M} + \text{H}]^+$ m/z 543.21, found 543.09.



ethyl **3-((S)-5-((benzyloxy)methyl)-2-oxooxazolidin-3-yl)-1-(3-(trifluoromethyl)benzoyl)indoline-3-carboxylate (S74)**. **S73** (143.8 mg, 0.265 mmol, 1.0 equiv.) was dissolved in dry dichloromethane (10.5 mL). *N,N*-diisopropylethylamine (92 μL , 0.530 mmol, 2.0 equiv.), 1,1'-carbonyldiimidazole (45 mg, 0.278 mmol, 1.05 equiv.), and 4-dimethylaminopyridine (32 mg, 0.265 mmol, 1.0 equiv.) were then added, and the reaction vial was firmly sealed and heated at 70 $^{\circ}\text{C}$ overnight. Additional 1,1'-carbonyldiimidazole (21.5 mg, 0.133 mmol, 0.5 equiv.) was then added; heated at 70 $^{\circ}\text{C}$ for 4d. 1.0 equiv. 4-dimethylaminopyridine was then added every day for an additional 2d (80 $^{\circ}\text{C}$). The crude reaction mixture was transferred to a sep. funnel with ~ 80 mL dichloromethane; the organic layer was washed with ~ 50 mL sat. NaHCO_3 , 0.5M KHSO_4 , and brine. Dried over MgSO_4 , concentrated, and purified on a silica column with

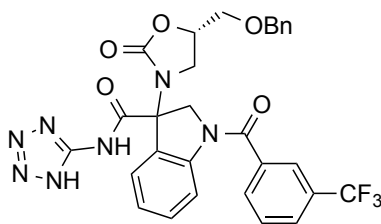
0-30% EtOAc:hexanes. **S74** (110.9 mg, 74%) (mixture of diastereomers) obtained as a colorless oil. ^1H NMR (400 MHz, CDCl_3) δ = 8.25 (br s, 0.5H), 7.88 (s, 0.5H), 7.82 - 7.71 (m, 2H), 7.67 - 7.57 (m, 1H), 7.56 - 7.50 (m, 0.6H), 7.43 (br d, J = 7.5 Hz, 1.4H), 7.39 - 7.24 (m, 5H), 7.22 - 7.13 (m, 2H), 4.98 (dd, J = 10.1, 12.1 Hz, 1H), 4.67 (qd, J = 4.2, 8.7 Hz, 0.5H), 4.62 - 4.54 (m, 1.5H), 4.53 - 4.43 (m, 1H), 4.39 (br d, J = 11.4 Hz, 0.5H), 4.33 - 4.21 (m, 2.5H), 3.73 (t, J = 8.6 Hz, 0.5H), 3.70 - 3.59 (m, 1.5H), 3.56 (dd, J = 4.1, 10.7 Hz, 0.5H), 3.45 (dd, J = 3.8, 10.6 Hz, 0.5H), 3.16 - 3.03 (m, 1H), 1.31 - 1.20 (m, 3H); ^{13}C NMR (100 MHz, CDCl_3) δ = 168.73, 168.59, 167.22 (br s), 157.17, 157.06, 143.16 (br s), 137.32, 137.03, 136.50, 136.40, 131.29 (br d, J = 3.7 Hz), 131.28 (q, J = 33.0 Hz), 131.23 (q, J = 33.0 Hz), 130.25 (br s), 130.12 (br s), 129.28, 129.25, 128.42, 128.37, 127.88, 127.85, 127.67, 127.55 (br s), 127.51, 127.40 (br s), 127.36 (br s), 127.03 (br s), 125.08 (br s), 124.61 (br), 124.49 (br s), 124.45 (br s), 124.31 (br s), 124.27 (br s), 123.46 (d, J = 272.9 Hz), 123.44 (d, J = 272.9 Hz), 118.39 (br s), 73.54, 73.47, 73.39, 72.88, 69.67, 69.45, 66.96 (br s), 62.79, 59.33 (br s), 58.94 (br s), 46.68, 45.94, 13.91; ^{19}F NMR (376 MHz, CHLOROFORM- d) δ = -62.73 (s, 2.8F), -62.74 (br s, 3F); LRMS (ESI) calculated for $\text{C}_{30}\text{H}_{28}\text{F}_3\text{N}_2\text{O}_6$ [$\text{M} + \text{H}$] $^+$ m/z 569.19, found 569.09.



3-((S)-5-((benzyloxy)methyl)-2-oxooxazolidin-3-yl)-1-(3-

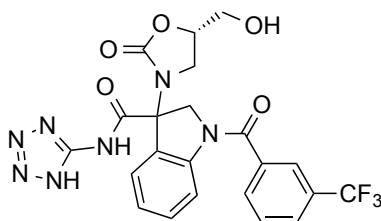
(trifluoromethyl)benzoyl)indoline-3-carboxylic acid (S75). S74 (49.5 mg, 0.087 mmol, 1.0 equiv.) was reacted in methanol (3.5 mL) with 1M lithium hydroxide (218 μL ,

0.218 mmol, 2.5 equiv.) according to general procedure B. The resulting residue was purified on a silica column with 0-15% dichloromethane:methanol. Semi-crude **S75** (25.2 mg, 54%) (mixture of diastereomers) obtained as a white solid. LRMS (ESI) calculated for C₂₈H₂₂F₃N₂O₆ [M - H]⁻ m/z 539.14, found 539.29.



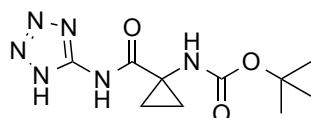
3-((S)-5-((benzyloxy)methyl)-2-oxooxazolidin-3-yl)-N-(1H-tetrazol-5-yl)-1-(3-(trifluoromethyl)benzoyl)indoline-3-carboxamide (28). Semi-crude **S75** (25.2 mg, 0.047 mmol, 1.0 equiv.) was reacted with 5-aminotetrazole monohydrate (1.1 equiv.) in 2 mL DMF according to general procedure D (20m activation). **28** (21.6 mg, 76%) (mixture of diastereomers) obtained as a white solid. ¹H NMR (400 MHz, CD₃OD, drops CDCl₃) δ = 8.24 (br s, 0.5H), 7.97 - 7.88 (m, 1H), 7.87 - 7.79 (m, 2H), 7.73 - 7.68 (m, 1H), 7.66 - 7.56 (m, 1.5H), 7.52 - 7.40 (m, 1.3H), 7.40 - 7.18 (m, 5.7H), 5.05 (br dd, *J* = 11.9, 17.8 Hz, 1H), 4.79 - 4.71 (m, 1H), 4.56 - 4.41 (m, 2H), 4.17 (br d, *J* = 11.4 Hz, 0.6H), 3.85 (t, *J* = 8.6 Hz, 0.6H), 3.79 - 3.66 (m, 2H), 3.58 - 3.51 (m, 1H), 3.51 - 3.36 (m, 0.6H), 3.26 (dd, *J* = 7.1, 8.0 Hz, 0.7H); ¹³C NMR (100 MHz, CD₃OD, drops CDCl₃) δ = 169.78, 169.48, 169.04 (br s), 160.08, 159.58, 151.63 (br s), 151.45 (br s), 144.26 (br s), 144.09 (br s), 139.24, 139.21 (br s), 138.79, 138.44, 138.18 (br s), 138.05, 132.54 (br s), 132.50 (br s), 132.21 (br s), 132.17, 131.84 (br s), 131.71 (br s), 130.85 (br s), 130.82 (br s), 129.63, 129.58, 129.46, 129.37, 129.33, 129.24, 129.04, 128.83 (br s), 128.82 (br s), 128.79, 128.68 (br s), 126.57 (br s), 126.47 - 126.22 (m), 125.53 - 125.18

(m), 123.69 (br s), 123.65, 119.49 (br s), 75.87, 75.48, 74.69, 74.50, 73.48, 73.11, 71.66, 70.87, 62.25, 61.59, 59.16 (br s), 58.84 (br s), 46.67, 46.29; ^{19}F NMR (376 MHz, CD_3OD , drops CDCl_3) δ = -63.89 (br s, 0.5F), -63.91 (br s, 0.5F), -63.94 (s, 3F), -63.98 (s, 1.6F); LRMS (ESI) calculated for $\text{C}_{29}\text{H}_{23}\text{F}_3\text{N}_7\text{O}_5$ $[\text{M} - \text{H}]^-$ m/z 606.17, found 606.31.



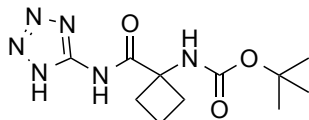
3-((S)-5-(hydroxymethyl)-2-oxooxazolidin-3-yl)-N-(1H-tetrazol-5-yl)-1-(3-(trifluoromethyl)benzoyl)indoline-3-carboxamide (27). **28** (18.3 mg, 0.030 mmol, 1.0 equiv.) was dissolved in ethanol (10 mL) and hydrogenated for 3h using an “H-Cube” flow hydrogenator with a 10% Pd/C cartridge; 1 mL/min, 10 bar H_2 , 25 °C, loop configuration. The reaction mixture was concentrated and purified by reverse phase HPLC (water/MeOH/0.05% formic acid) to afford **27** (7.2 mg, 46%) (mixture of diastereomers) as a white solid. **Note:** Diastereomers combined with the atropisomers of the secondary amide resulted in a multitude of split peaks. ^1H NMR (400 MHz, CD_3OD , drops CDCl_3) δ = 8.23 (br s, 1H), 8.03 - 7.92 (m, 2H), 7.91 - 7.84 (m, 1H), 7.78 - 7.69 (m, 1H), 7.61 (m, 0.5H), 7.55 - 7.40 (m, 1.5H), 7.26 (b q, J = 7.1 Hz, 1H), 5.14 - 5.03 (m, 0.4H), 4.95 - 4.87 (m, 1H), 4.81 - 4.68 (m, 0.8H), 4.56 (d, J = 12.7 Hz, 0.25H), 4.51 (br d, J = 12.4 Hz, 0.25H), 4.44 (br d, J = 11.4 Hz, 0.05H), 4.26 (br d, J = 11.7 Hz, 0.3H), 4.22 (br dd, J = 2.1, 5.7 Hz, 0.1H), 3.98 - 3.84 (m, 0.4H), 3.81 (dd, J = 2.4, 12.7 Hz, 0.3H), 3.75 (t, J = 8.5 Hz, 0.4H), 3.72 - 3.39 (m, 2.5H), 3.23 (t, J = 7.7 Hz, 0.3H); ^{13}C NMR (100 MHz, CD_3OD , drops CDCl_3) δ = 170.24, 169.59 (br s), 160.60, 160.22,

154.80 (br s), 152.08 (br s), 145.58 (br s), 144.64 (br s), 138.77 (br s), 138.69 (br s), 133.05 - 132.90 (m), 132.90 - 132.76 (m), 132.62 - 132.38 (m), 132.28 - 132.08 (m), 131.26, 131.23, 131.16 (br s), 130.20, 129.59, 129.31 - 129.05 (m), 129.03 - 128.85 (m), 127.37 - 127.07 (m), 126.78 - 126.55 (m), 125.98 - 125.73 (m), 125.72 - 125.52 (m), 125.53 (q, $J = 271.9$ Hz), 119.77 (br s), 77.64, 77.09, 73.09 (br s), 71.19, 70.64, 69.46, 65.66, 64.79, 64.49, 63.03, 61.88, 59.11 (br s), 47.12, 46.09, 45.99; ^{19}F NMR (376 MHz, CD_3OD , drops CDCl_3) $\delta = -64.15$ (s, 3F), -64.19 (s, 2.2F); LRMS (ESI) calculated for $\text{C}_{22}\text{H}_{17}\text{F}_3\text{N}_7\text{O}_5$ $[\text{M} - \text{H}]^-$ m/z 516.12, found 516.07.



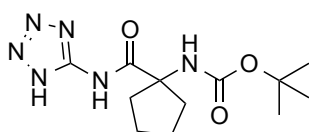
tert-butyl (1-((1H-tetrazol-5-yl)carbamoyl)cyclopropyl)carbamate (29).

Commercially available 1-((tert-Butoxycarbonyl)amino)cyclopropanecarboxylic acid (100 mg, 0.497 mmol, 1.0 equiv.) was reacted with 5-aminotetrazole monohydrate (1.5 equiv.) in 4 mL DMF according to general procedure D (10m activation), except 3.0 equiv. *N,N*-diisopropylethylamine was added initially, with no second addition. **29** (106.5 mg, 80%) obtained as a white solid. **Note:** Atropisomers resulted in some split peaks. ^1H NMR (400 MHz, DMSO-d_6) $\delta = 11.88$ (br s, 0.2H), 11.73 (br s, 0.8H), 7.41 (br s, 0.8H), 7.11 (br s, 0.2H), 1.54 - 1.23 (m, 11H), 1.10 (br s, 2H); ^{13}C NMR (100 MHz, DMSO-d_6) $\delta = 172.45$, 155.84 (br), 150.20 (br), 78.67, 35.40 (br), 28.21, 17.87; LRMS (ESI) calculated for $\text{C}_{10}\text{H}_{15}\text{N}_6\text{O}_3$ $[\text{M} - \text{H}]^-$ m/z 267.12, found 267.10.



tert-butyl (1-((1*H*-tetrazol-5-yl)carbamoyl)cyclobutyl)carbamate (30). Commercially available boc-1-amino-1-cyclobutanecarboxylic acid (100 mg, 0.465 mmol, 1.0 equiv.) was reacted with 5-aminotetrazole monohydrate (1.5 equiv.) in 4 mL DMF according to general procedure D (10m activation), except 3.0 equiv. *N,N*-diisopropylethylamine was added initially, with no second addition. **30** (101.1 mg, 77%) obtained as a white solid.

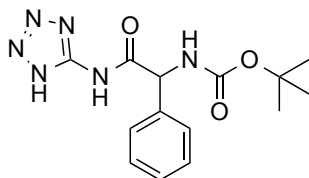
Note: Atropisomers gave many split peaks in ¹H and ¹³C. ¹H NMR (400 MHz, DMSO-*d*₆) δ = 11.71 (br s, 0.3H), 11.59 (br s, 0.7H), 7.46 (br s, 0.7H), 7.10 (br s, 0.3H), 2.62 - 2.46 (m, 2H), 2.12 (q, *J* = 9.3 Hz, 2H), 1.88 (br s, 1H), 1.81 - 1.67 (m, 1H), 1.33 (br s, 6H), 1.18 (br s, 3H); ¹³C NMR (100 MHz, DMSO-*d*₆) δ = 173.37 (br), 173.01, 154.57, 153.53 (br), 150.35 (br), 78.77, 58.69 (br), 30.92 (br), 30.32, 28.16 (br), 14.65, 14.32 (br); LRMS (ESI) calculated for C₁₁H₁₇N₆O₃ [M - H]⁻ *m/z* 281.14, found 281.06.



tert-butyl (1-((1*H*-tetrazol-5-yl)carbamoyl)cyclopentyl)carbamate (31). Commercially available 1-*N*-Boc-Aminocyclopentanecarboxylic acid (100 mg, 0.436 mmol, 1.0 equiv.) was reacted with 5-aminotetrazole monohydrate (1.5 equiv.) in 4 mL DMF according to general procedure D (10m activation), except 3.0 equiv. *N,N*-diisopropylethylamine was added initially, with no second addition. **31** (99.2 mg, 77%) obtained as a white solid.

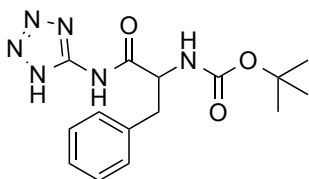
Note: Atropisomers resulted in some split peaks. ¹H NMR (400 MHz, DMSO-*d*₆) δ = 11.83 (br s, 0.3H), 11.69 (br s, 0.7H), 7.08 (br s, 0.7H), 6.79 (br s, 0.3H), 2.20 - 2.04 (m,

2H), 1.86 (br s, 2H), 1.75 - 1.51 (m, 4H), 1.32 (br s, 9H); ^{13}C NMR (100 MHz, DMSO- d_6) δ = 173.95 (br), 154.93 (br), 150.34 (br), 78.61 (br), 66.47 (br), 35.91 (br), 28.14 (br), 23.91; LRMS (ESI) calculated for $\text{C}_{12}\text{H}_{19}\text{N}_6\text{O}_3$ $[\text{M} - \text{H}]^-$ m/z 295.15, found 295.10.



tert-butyl (2-((1H-tetrazol-5-yl)amino)-2-oxo-1-phenylethyl)carbamate (32).

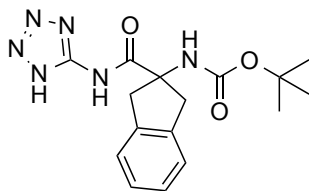
Commercially available tert-butoxycarbonylamino-phenyl-acetic acid (100 mg, 0.398 mmol, 1.0 equiv.) was reacted with 5-aminotetrazole monohydrate (1.5 equiv.) in 4 mL DMF according to general procedure D (10m activation), except 3.0 equiv. *N,N*-diisopropylethylamine was added initially, with no second addition. **32** (50.3 mg, 40%) obtained as a white solid. **Note:** Slight atropisomerism observed by ^1H NMR. ^1H NMR (400 MHz, DMSO- d_6) δ = 12.34 (br s, 1H), 7.78 (br d, J = 7.3 Hz, 0.85H), 7.49 (br d, J = 7.1 Hz, 2.15H), 7.42 - 7.22 (m, 3H), 5.41 (br d, J = 7.3 Hz, 0.85H), 5.27 (br s, 0.15H), 1.39 (s, 7.6H), 1.30 (br s, 1.4H); ^{13}C NMR (100 MHz, DMSO- d_6) δ = 170.08, 155.25, 149.53 (br), 136.13, 128.54, 128.30, 127.90, 78.67, 58.13, 28.17; LRMS (ESI) calculated for $\text{C}_{14}\text{H}_{17}\text{N}_6\text{O}_3$ $[\text{M} - \text{H}]^-$ m/z 317.14, found 317.16.



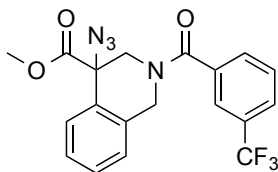
tert-butyl (1-((1H-tetrazol-5-yl)amino)-1-oxo-3-phenylpropan-2-yl)carbamate (33).

Commercially available boc-DL-Phe-OH (100 mg, 0.377 mmol, 1.0 equiv.) was reacted with 5-aminotetrazole monohydrate (1.5 equiv.) in 4 mL DMF according to general

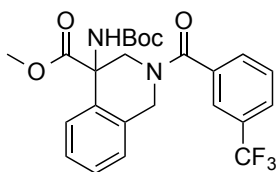
procedure D (10m activation), except 3.0 equiv. *N,N*-diisopropylethylamine was added initially, with no second addition. **33** (33.3 mg, 27%) obtained as a white solid. **Note:** Slight atropisomerism observed by ¹H NMR. ¹H NMR (400 MHz, DMSO-d₆) δ = 12.27 (br s, 1H), 7.42 - 7.24 (m, 5H), 7.24 - 7.15 (m, 1H), 6.96 (br s, 0.2H), 4.41 (br s, 1H), 3.10 - 2.93 (m, 1H), 2.91 - 2.74 (m, 1H), 1.31 (s, 7.6H), 1.20 (br s, 1.4H); ¹³C NMR (100 MHz, DMSO-d₆) δ = 171.73, 155.46, 149.53 (br), 137.52, 129.27, 128.11, 126.46, 78.36, 56.20, 36.58, 28.12; LRMS (ESI) calculated for C₁₅H₁₉N₆O₃ [M - H]⁻ m/z 331.15, found 331.14.



tert-butyl (2-((1*H*-tetrazol-5-yl)carbamoyl)-2,3-dihydro-1*H*-inden-2-yl)carbamate (34). Commercially available boc-2-aminoindane-2-carboxylic acid (100 mg, 0.361 mmol, 1.0 equiv.) was reacted with 5-aminotetrazole monohydrate (1.5 equiv.) in 3 mL DMF according to general procedure D (10m activation), except 3.0 equiv. *N,N*-diisopropylethylamine was added initially, with no second addition. **34** (84.6 mg, 68%) obtained as a white solid. ¹H NMR (400 MHz, DMSO-d₆) δ = 12.14 (br s, 0.25H), 12.00 (br s, 0.75H), 7.50 (br s, 0.7H), 7.25 - 7.18 (m, 2H), 7.18 - 7.12 (m, 2H), 3.60 (br d, *J* = 16.6 Hz, 2H), 3.22 (br d, *J* = 16.6 Hz, 2H), 1.35 (br s, 9H); ¹³C NMR (100 MHz, DMSO-d₆) δ = 173.45 (br), 155.45 (br), 150.80, 140.42, 127.08, 124.89, 79.29 (br), 66.87 (br), 42.78 (br), 28.55 (br); LRMS (ESI) calculated for C₁₆H₁₉N₆O₃ [M - H]⁻ m/z 343.15, found 343.16.

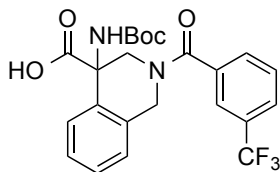


methyl 4-azido-2-(3-(trifluoromethyl)benzoyl)-1,2,3,4-tetrahydroisoquinoline-4-carboxylate (S76). **S23** (87.1 mg, 0.240 mmol, 1.0 equiv.) was reacted in 8 mL tetrahydrofuran according to general procedure F. **S76** (90.8 mg, 94%) obtained as a colorless oil. **Note:** Atropisomerism observed by NMR. ^1H NMR (400 MHz, CDCl_3) δ = 7.93 - 7.68 (m, 3H), 7.67 - 7.53 (m, 1.5H), 7.48 - 7.20 (m, 3.5H), 5.54 (br s, 0.5H), 4.55 (br s, 2H), 3.95 (br s, 1H), 3.80 (br s, 3H), 3.70 (br s, 0.5H); ^{13}C NMR (100 MHz, CDCl_3) δ = 170.07 (br s), 169.71 (br s), 135.74, 132.42 (br s), 131.14 (br s), 130.99 - 130.64 (m), 130.49 (br s), 130.31, 130.30, 129.80 (br s), 129.09, 129.01, 128.99, 127.83 (br s), 127.75 - 127.20 (m), 127.01 (br s), 126.86 - 126.57 (m), 126.57 - 125.99 (m), 124.79 - 124.18 (m), 124.03, 124.00, 123.59 (q, J = 272.7 Hz), 123.55 (q, J = 272.4 Hz), 66.59 (br s), 53.36, 50.84 (br s), 44.12 (br s); ^{19}F NMR (376 MHz, CDCl_3) δ = -62.75 (s, 3F); LRMS (ESI) calculated for $\text{C}_{19}\text{H}_{16}\text{F}_3\text{N}_4\text{O}_3$ $[\text{M} + \text{H}]^+$ m/z 405.12, found 405.07.



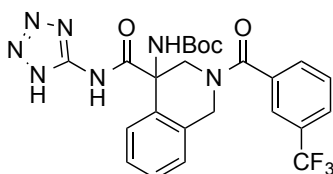
methyl 4-((tert-butoxycarbonyl)amino)-2-(3-(trifluoromethyl)benzoyl)-1,2,3,4-tetrahydroisoquinoline-4-carboxylate (S77). A round bottom flask was charged with **S76** (90.8 mg, 0.225 mmol, 1.0 equiv.) and dry methanol (4 mL), then cooled to 0 °C. Anhydrous tin(II) chloride (85.2 mg, 0.449 mmol, 2.0 equiv.) was then added; stirred at 0 °C for 5m, then r.t. for 3.5h. The methanol was then removed under reduced pressure.

1,4-dioxane (3 mL) was then added, followed by di-tert-butyl dicarbonate (74 mg, 0.337 mmol, 1.5 equiv.) in 500 μ L 1,4-dioxane. Finally, a slurry of sodium bicarbonate (75 mg, 0.898 mmol, 4.0 equiv.) in water (1 mL) was added, and the resulting slurry was allowed to stir for 22h. 2.0 equiv. di-tert-butyl dicarbonate and 1 mL water were then added; stirred for 24h. Additional 2.0 equiv. di-tert-butyl dicarbonate and 1 mL water were added; stirred for 32h. The reaction mixture was then transferred to a sep. funnel with excess EtOAc and water and adjusted to pH 1 with 2N NaHSO₄. The layers were separated, and the aqueous layer was further extracted with ~ 50 mL EtOAc. The organic layers were combined, washed with sat. NaHCO₃, dried over MgSO₄, and concentrated under reduced pressure. Purified on a silica column with 15-30% EtOAc:hexanes. **S77** (70.6 mg, 66%) obtained as a colorless oil. **Note:** Atropisomerism observed by NMR. ¹H NMR (400 MHz, CDCl₃) δ = 7.80 - 7.64 (m, 2H), 7.64 - 7.48 (m, 2H), 7.41 (br d, *J* = 6.8 Hz, 1H), 7.37 - 7.18 (m, 2.6H), 6.97 (br s, 0.4H), 5.27 (br s, 0.5H), 5.15 (br s, 0.6H), 5.01 (br s, 0.4H), 4.84 - 4.53 (m, 2H), 4.41 (br s, 0.5H), 3.70 (s, 3H), 1.32 (br s, 7.5H), 1.06 (br s, 1.5H); ¹³C NMR (100 MHz, CDCl₃) δ = 170.86 (br s), 169.89 (br s), 154.08 (br s), 153.39 (br s), 136.44 - 135.89 (m), 133.59 (br s), 131.78 (br s), 131.15 (br s), 130.85 (br s), 130.73 - 129.80 (m), 129.37 - 128.70 (m), 128.64 - 128.11 (m), 127.70 (br s), 127.36 - 126.82 (m), 126.58 (br s), 126.04 (br s), 124.86 - 124.33 (m), 124.25 - 123.67 (m), 123.60 (q, *J* = 272.2 Hz), 80.29 (br s), 59.86 (br s), 53.48 (br s), 52.99 (br s), 49.61 (br s), 45.27 (br s), 44.32 (br s), 28.08 (br s); ¹⁹F NMR (376 MHz, CDCl₃) δ = -62.71 (br s, 3F), -62.82 (br s, 1.6F); LRMS (ESI) calculated for C₂₄H₂₆F₃N₂O₅ [M + H]⁺ *m/z* 479.18, found 479.10.



4-((tert-butoxycarbonyl)amino)-2-(3-(trifluoromethyl)benzoyl)-1,2,3,4-

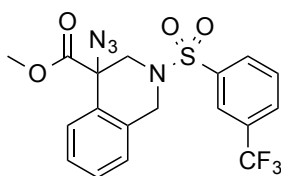
tetrahydroisoquinoline-4-carboxylic acid (S77). **S77** (70.6 mg, 0.148 mmol, 1.0 equiv.) was reacted in methanol (3.5 mL) with 1M lithium hydroxide (370 μ L, 0.370 mmol, 2.5 equiv.) according to general procedure B, except the reaction was cooled to 0 °C prior to hydroxide addition, and allowed to slowly warm to r.t.; three additions of 1M lithium hydroxide (370 μ L, 0.370 mmol, 2.5 equiv.) were added over the following 8h. Semi-crude **S78** (64.7 mg, 94%) obtained as a colorless oil. LRMS (ESI) calculated for $C_{23}H_{22}F_3N_2O_5$ $[M - H]^-$ m/z 463.15, found 463.14.



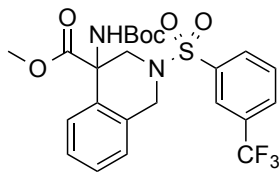
tert-butyl (4-((1H-tetrazol-5-yl)carbamoyl)-2-(3-(trifluoromethyl)benzoyl)-1,2,3,4-

tetrahydroisoquinolin-4-yl)carbamate (35). Semi-crude **S78** (64.7 mg, 0.139 mmol, 1.0 equiv.) was reacted with 5-aminotetrazole monohydrate (1.1 equiv.) in 3.5 mL DMF according to general procedure D (10m activation). **35** (30.0 mg, 41%) obtained as a white solid. **Note:** Atropisomerism observed by NMR. 1H NMR (400 MHz, DMSO- d_6) δ = 12.30 (br s, 0.25H), 12.18 (br s, 0.25H), 12.02 (br s, 0.25H), 7.94 - 7.45 (m, 5.5H), 7.38 (br s, 1.5H), 7.33 - 7.22 (m, 1.5H), 7.12 (br s, 0.5H), 5.15 - 5.01 (m, 0.25H), 4.98 - 4.43 (m, 2.25H), 4.34 (br d, J = 12.4 Hz, 1H), 4.25 - 4.09 (m, 0.25H), 3.86 - 3.70 (m, 0.25H), 1.51 - 1.20 (m, 7H), 0.85 (br s, 2H); ^{13}C NMR (100 MHz, DMSO- d_6) δ = 170.30 (br s),

168.79 (br s), 155.30 (br s), 150.44 (br s), 137.34 (br s), 134.22, 132.55 - 131.03 (m), 130.24 - 129.64 (m), 129.43, 128.94 (br s), 127.91 - 127.47 (m), 127.44 - 127.01 (m), 126.88 - 126.49 (m), 124.59 - 124.20 (m), 124.38 (d, $J = 272.2$ Hz), 80.17 (br s), 79.42 (br s), 61.14 (br s), 50.15 (br s), 49.41 (br s), 44.94 (br s), 28.54 (br s), 27.64 (br s); ^{19}F NMR (376 MHz, DMSO- d_6) $\delta = -61.17$ (br s, 1.5F), -61.24 (br s, 3F); LRMS (ESI) calculated for $\text{C}_{24}\text{H}_{23}\text{F}_3\text{N}_7\text{O}_4$ $[\text{M} - \text{H}]^-$ m/z 530.18, found 530.17.

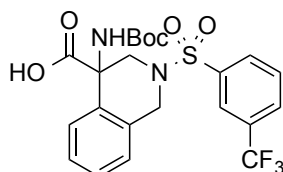


methyl 4-azido-2-((3-(trifluoromethyl)phenyl)sulfonyl)-1,2,3,4-tetrahydroisoquinoline-4-carboxylate (S79). **S25** (96.3 mg, 0.241 mmol, 1.0 equiv.) was reacted in 8 mL tetrahydrofuran according to general procedure F. **S79** (105.0 mg, 99%) obtained as a colorless oil. ^1H NMR (400 MHz, CDCl_3) $\delta = 8.16$ (s, 1H), 8.13 - 8.04 (m, 1H), 7.88 (d, $J = 7.8$ Hz, 1H), 7.73 (t, $J = 7.9$ Hz, 1H), 7.41 - 7.33 (m, 1H), 7.33 - 7.27 (m, 2H), 7.24 - 7.18 (m, 1H), 4.67 (d, $J = 15.6$ Hz, 1H), 4.23 (d, $J = 15.3$ Hz, 1H), 3.97 (dd, $J = 1.2, 12.7$ Hz, 1H), 3.82 (s, 3H), 3.70 (d, $J = 15.8$ Hz, 1H); ^{13}C NMR (100 MHz, CDCl_3) $\delta = 169.43, 138.37, 131.43, 131.79$ (q, $J = 33.5$ Hz), 130.71 (br s), 130.07, 129.96, 129.72 (q, $J = 3.7$ Hz), 129.61, 129.36, 129.26, 127.80, 127.65, 127.09, 127.01 (d, $J = 1.5$ Hz), 126.41, 124.47 (q, $J = 3.9$ Hz), 123.02 (q, $J = 272.9$ Hz), 66.45, 53.44, 50.31, 46.98; ^{19}F NMR (376 MHz, CDCl_3) $\delta = -62.79$ (s, 3F); LRMS (ESI) calculated for $\text{C}_{18}\text{H}_{15}\text{F}_3\text{N}_4\text{NaO}_4\text{S}$ $[\text{M} + \text{Na}]^+$ m/z 463.07, found 462.99.

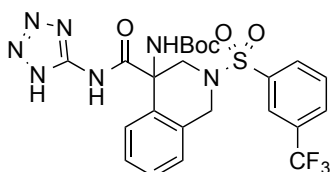


methyl 4-((*tert*-butoxycarbonyl)amino)-2-((3-(trifluoromethyl)phenyl)sulfonyl)-1,2,3,4-tetrahydroisoquinoline-4-carboxylate (S80). A round bottom flask was charged with **S79** (105.0 mg, 0.238 mmol, 1.0 equiv.) and dry methanol (4.4 mL), then cooled to 0 °C. Anhydrous tin(II) chloride (90.4 mg, 0.477 mmol, 2.0 equiv.) was added; stirred at 0 °C for 5m, then r.t. for 4.5h. The methanol was then removed under reduced pressure. 1,4-dioxane (3.2 mL) was added, followed by di-*tert*-butyl dicarbonate (78 mg, 0.358 mmol, 1.5 equiv.) in 500 μ L 1,4-dioxane. Finally, a slurry of sodium bicarbonate (80 mg, 0.954 mmol, 4.0 equiv.) in water (1 mL) was added, and the resulting slurry was allowed to stir for 14h. 2.0 equiv. di-*tert*-butyl dicarbonate and 1 mL water were then added; stirred for 24h. Additional 2.0 equiv. di-*tert*-butyl dicarbonate and 1 mL water were added; stirred for 28h. The reaction mixture was then transferred to a sep. funnel with excess EtOAc and water and adjusted to pH 1 with 2N NaHSO₄. The layers were separated, and the aqueous layer was further extracted with ~ 50 mL EtOAc. The organic layers were combined, washed with sat. NaHCO₃, dried over MgSO₄, and concentrated under reduced pressure. Purified on a silica column with 10-25% EtOAc:hexanes. **S80** (84.5 mg, 69%) obtained as a colorless oil. ¹H NMR (400 MHz, CDCl₃) δ = 8.11 (s, 1H), 8.06 (br d, *J* = 7.8 Hz, 1H), 7.87 (d, *J* = 7.8 Hz, 1H), 7.75 - 7.69 (m, 1H), 7.53 (br d, *J* = 7.5 Hz, 1H), 7.33 - 7.23 (m, 2H), 7.13 (dd, *J* = 0.7, 7.3 Hz, 1H), 4.61 (br d, *J* = 14.9 Hz, 1H), 4.51 (br d, *J* = 12.7 Hz, 1H), 4.10 (br d, *J* = 14.3 Hz, 1H), 3.77 (s, 3H), 3.53 (br d, *J* = 12.7 Hz, 1H), 1.45 (s, 9H); ¹³C NMR (100 MHz, CDCl₃) δ = 170.70, 153.87, 138.60, 132.32, 131.89 (q, *J* = 33.8 Hz), 131.63, 130.66, 130.09,

129.53 (q, $J = 3.7$ Hz), 129.03, 127.99, 126.98, 126.80, 124.29 (q, $J = 3.9$ Hz), 123.11 (q, $J = 273.6$ Hz), 80.53, 59.85, 53.03, 48.19, 47.60, 28.18; ^{19}F NMR (376 MHz, CDCl_3) $\delta = -62.73$ (s, 3F); LRMS (ESI) calculated for $\text{C}_{23}\text{H}_{26}\text{F}_3\text{N}_2\text{O}_6\text{S}$ [$\text{M} + \text{H}$] $^+$ m/z 515.15, found 515.05.

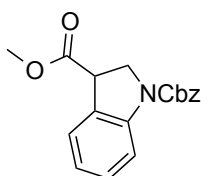


4-((tert-butoxycarbonyl)amino)-2-((3-(trifluoromethyl)phenyl)sulfonyl)-1,2,3,4-tetrahydroisoquinoline-4-carboxylic acid (S81). **S80** (84.5 mg, 0.164 mmol, 1.0 equiv.) was reacted in 1,4-dioxane (3 mL) with 1M lithium hydroxide (3 mL, 3.0 mmol, 18.3 equiv.) according to general procedure B. Semi-crude **S81** (88.2 mg, 107%) obtained as a white solid. LRMS (ESI) calculated for $\text{C}_{22}\text{H}_{22}\text{F}_3\text{N}_2\text{O}_6\text{S}$ [$\text{M} - \text{H}$] $^-$ m/z 499.12, found 499.09.

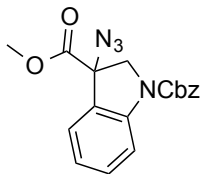


tert-butyl (4-((1H-tetrazol-5-yl)carbamoyl)-2-((3-(trifluoromethyl)phenyl)sulfonyl)-1,2,3,4-tetrahydroisoquinolin-4-yl)carbamate (36). Semi-crude **S81** (88.2 mg, 0.176 mmol, 1.0 equiv.) was reacted with 5-aminotetrazole monohydrate (1.1 equiv.) in 4.4 mL DMF according to general procedure D (10m activation). **36** (26.6 mg, 27%) obtained as a white solid. ^1H NMR (400 MHz, DMSO-d_6) $\delta = 12.01$ (br s, 1H), 8.14 (d, $J = 7.3$ Hz, 2H), 8.04 (s, 1H), 7.97 - 7.89 (m, 1H), 7.69 (br s, 1H), 7.44 (br d, $J = 7.1$ Hz, 1H), 7.36 - 7.22 (m, 3H), 6.54 (br s, 0.1H), 4.44 (br d, $J = 15.3$ Hz, 1H), 4.23 (br d, $J = 15.3$ Hz, 1H),

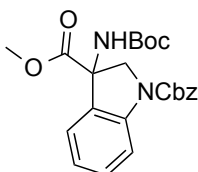
4.09 (br d, $J = 11.9$ Hz, 1H), 3.84 (br d, $J = 12.2$ Hz, 1H), 1.40 (br s, 9H); ^{13}C NMR (100 MHz, DMSO- d_6) $\delta = 169.89, 155.11$ (br s), 150.81, 137.68, 133.12, 132.92, 131.90 (br d, $J = 3.8$ Hz), 130.70 (br d, $J = 4.5$ Hz), 130.64 (br d, $J = 32.9$ Hz), 128.90, 127.81, 127.66, 127.05, 124.11 (d, $J = 4.0$ Hz), 123.81 (d, $J = 273.0$ Hz), 79.48, 61.61, 48.21 (br s), 48.02, 28.64 (br s); ^{19}F NMR (376 MHz, DMSO- d_6) $\delta = -61.33$ (br s, 3F); LRMS (ESI) calculated for $\text{C}_{23}\text{H}_{23}\text{F}_3\text{N}_7\text{O}_5\text{S}$ $[\text{M} - \text{H}]^-$ m/z 566.14, found 566.21.



1-benzyl 3-methyl indoline-1,3-dicarboxylate (S82). Semi-crude **S32** (149.8 mg, 0.701 mmol, 1.0 equiv.) was reacted with commercially available benzyl chloroformate in dry dichloromethane (6.2 mL) according to general procedure A, with slight modification: prior to base addition, the reaction vessel was cooled to 0 °C; 2.5 equiv. of *N,N*-diisopropylethylamine was used, and allowed to stir at 0 °C for 5m; after acyl chloride addition, the reaction mixture was allowed to slowly warm to r.t. **S82** (178.3 mg, 82%) obtained as a colorless oil. ^1H NMR (400 MHz, CDCl_3) $\delta = 7.96$ (br s, 1H), 7.51 - 7.33 (m, 6H), 7.32 - 7.19 (m, 1H), 7.02 (br t, $J = 7.3$ Hz, 1H), 5.40 - 5.21 (m, 2H), 4.51 (dd, $J = 5.0, 10.6$ Hz, 1H), 4.28 - 4.13 (m, 2H), 3.78 (s, 3H); ^{13}C NMR (100 MHz, CDCl_3) $\delta = 171.49, 152.31$ (br), 142.16 (br), 136.06 (br), 128.95, 128.45, 128.09, 127.91 (br), 127.41 (br), 124.98 (br), 122.66, 114.91 (br), 66.97 (br), 52.47, 49.44 (br), 44.72 (br); LRMS (ESI) calculated for $\text{C}_{18}\text{H}_{17}\text{NNaO}_4$ $[\text{M} + \text{Na}]^+$ m/z 334.11, found 333.97.

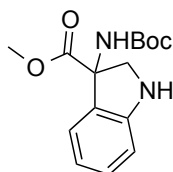


1-benzyl 3-methyl 3-azidoindoline-1,3-dicarboxylate (S83). **S82** (178.3 mg, 0.573 mmol, 1.0 equiv.) was reacted in 12 mL tetrahydrofuran according to general procedure F. **S83** (103.3 mg, 51%) obtained as a colorless oil. ^1H NMR (400 MHz, CDCl_3) δ = 8.05 (br s, 1H), 7.53 - 7.33 (m, 7H), 7.11 (br t, J = 7.4 Hz, 1H), 5.30 (br s, 2H), 4.60 (d, J = 12.4 Hz, 1H), 4.09 (br d, J = 11.7 Hz, 1H), 3.89 (s, 3H); ^{13}C NMR (100 MHz, CDCl_3) δ = 169.17, 152.02 (br), 142.57 (br), 135.67 (br), 131.59, 128.57, 128.34, 128.13 (br), 126.06 (br), 123.84 (br), 122.97, 115.70, 69.64 (br), 67.45 (br), 56.78 (br), 53.57; LRMS (ESI) calculated for $\text{C}_{18}\text{H}_{16}\text{N}_4\text{NaO}_4$ $[\text{M} + \text{Na}]^+$ m/z 375.10, found 375.00.

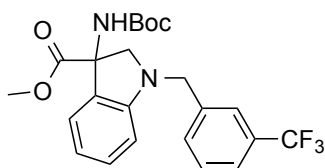


methoxy 4-((tert-butoxycarbonyl)amino)-2-((3-(trifluoromethyl)phenyl)sulfonyl)-1,2,3,4-tetrahydroisoquinoline-4-carboxylate (S84). A round bottom flask was charged with **S83** (103.3 mg, 0.293 mmol, 1.0 equiv.) and dry methanol (6 mL), then cooled to 0 °C. Anhydrous tin(II) chloride (111 mg, 0.586 mmol, 2.0 equiv.) was added; stirred at 0 °C for 5m, then r.t. for 4 h. The methanol was then removed under reduced pressure. 1,4-dioxane (5.5 mL) was added, followed by di-tert-butyl dicarbonate (96 mg, 0.440 mmol, 1.5 equiv.) in 700 μL 1,4-dioxane. Finally, a slurry of sodium bicarbonate (99 mg, 1.17 mmol, 4.0 equiv.) in water (1.4 mL) was added, and the resulting slurry was allowed to stir for 14h. The reaction mixture was then transferred to a sep. funnel

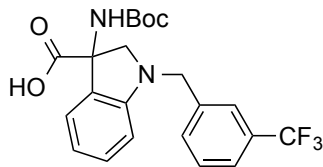
with excess EtOAc and water and adjusted to pH 1 with 1M KHSO₄. The layers were separated, and the aqueous layer was further extracted with ~ 50 mL EtOAc. The organic layers were combined, washed with sat. NaHCO₃, dried over MgSO₄, and concentrated under reduced pressure. Purified on a silica column with 0-15% EtOAc:hexanes. **S84** (88.9 mg, 71%) obtained as a colorless oil. ¹H NMR (400 MHz, CDCl₃) δ = 7.96 (br d, *J* = 6.6 Hz, 1H), 7.48 - 7.28 (m, 7H), 7.01 (br t, *J* = 7.4 Hz, 1H), 5.28 (br s, 2H), 4.95 (br d, *J* = 10.7 Hz, 1H), 4.22 (br d, *J* = 10.2 Hz, 1H), 3.76 (s, 3H), 1.45 (br s, 9H); ¹³C NMR (100 MHz, CDCl₃) δ = 170.74 (br), 154.76 (br), 152.39 (br), 142.81 (br), 135.95 (br), 130.98 (br), 128.52, 128.19 (br), 128.07 (br), 123.25 (br), 123.03 (br), 115.48 (br), 80.70 (br), 67.16 (br), 64.28 (br), 58.26 (br), 53.23; LRMS (ESI) calculated for C₂₃H₂₆N₂NaO₆ [M + Na]⁺ *m/z* 449.17, found 449.00.



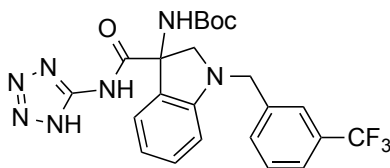
methyl 3-((tert-butoxycarbonyl)amino)indoline-3-carboxylate (S85). **S84** (810.9 mg, 1.90 mmol, 1.0 equiv.) was dissolved in methanol (100 mL) and hydrogenated for 6h using an “H-Cube” flow hydrogenator with a 10% Pd/C cartridge; 2 mL/min, 1 atm H₂, 40 °C, loop configuration. The reaction mixture was concentrated and transferred to a sep. funnel with ~ 75 mL EtOAc and partitioned with ~ 75 mL sat. NaHCO₃. The organic layer was separated, and the aqueous layer was further extracted with 2 x 50 mL EtOAc. The organic layers were combined, dried over MgSO₄, and concentrated. **S85** (548.4 mg, 99%) obtained as a waxy white solid; used without further purification. LRMS (ESI) calculated for C₁₅H₂₁N₂O₄ [M + H]⁺ *m/z* 293.15, found 293.03.



methyl 3-((tert-butoxycarbonyl)amino)-1-(3-(trifluoromethyl)benzyl)indoline-3-carboxylate (S86). In a 20 mL vial, **S85** (40.0 mg, 0.137 mmol, 1.0 equiv.) was reacted with commercially available 3-(trifluoromethyl)benzyl bromide in dry dichloromethane (2 mL) according to general procedure A, with slight modification: prior to base addition, the reaction vessel was cooled to 0 °C; 2.0 equiv. of *N,N*-diisopropylethylamine was used; after halide addition, the reaction mixture was allowed to slowly warm to r.t. overnight. Since reaction progress was slow, the vial was firmly sealed and heated at 80 °C for 48h. **S86** (38.8 mg, 63%) obtained as a colorless oil. ¹H NMR (400 MHz, CDCl₃) δ = 7.63 (s, 1H), 7.58 - 7.52 (m, 2H), 7.51 - 7.43 (m, 1H), 7.26 (dd, *J* = 1.0, 7.8 Hz, 1H), 7.20 (dt, *J* = 1.2, 7.8 Hz, 1H), 6.75 - 6.68 (m, 1H), 6.51 (br d, *J* = 7.8 Hz, 1H), 4.52 - 4.38 (m, 2H), 4.34 (d, *J* = 10.5 Hz, 1H), 3.79 (s, 3H), 3.66 (br d, *J* = 10.2 Hz, 1H), 1.43 (br s, 9H); ¹³C NMR (100 MHz, CDCl₃) δ = 171.19 (br s), 154.86 (br s), 151.43 (br s), 138.87, 130.98, 130.71 (br s), 130.96 (br q, *J* = 32.3 Hz), 129.08, 126.21, 124.27 - 123.97 (m), 123.83, 124.08 (q, *J* = 272.2 Hz), 117.92, 107.42, 80.42 (br s), 65.09 (br s), 62.52 (br s), 52.96, 51.65, 28.17; ¹⁹F NMR (376 MHz, CDCl₃) δ = -62.56 (s, 3F); LRMS (ESI) calculated for C₂₃H₂₆F₃N₂O₄ [M + H]⁺ *m/z* 451.18, found 451.06.

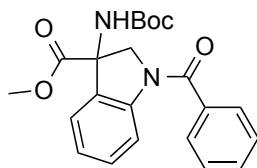


3-((tert-butoxycarbonyl)amino)-1-(3-(trifluoromethyl)benzyl)indoline-3-carboxylic acid (S87). **S86** (38.8 mg, 0.086 mmol, 1.0 equiv.) was reacted in methanol (3.5 mL) with 1M lithium hydroxide (172 uL, 0.172 mmol, 2.0 equiv.) according to general procedure B, except the reaction was cooled to 0 °C prior to hydroxide addition, and allowed to slowly warm to r.t. overnight. Since conversion was slow, an additional 2.0 equiv. 1M lithium hydroxide and methanol (500 uL) were added; stirred at 35 °C for 22h. An additional aliquot of 2.0 equiv. 1M lithium hydroxide was subsequently added; heated at 50 °C for 23h. Semi-crude **S87** (38.8 mg, 103%) obtained as a white solid. LRMS (ESI) calculated for C₂₂H₂₂F₃N₂O₄ [M - H]⁻ m/z 435.15, found 435.17.

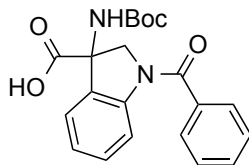


tert-butyl (3-((1H-tetrazol-5-yl)carbamoyl)-1-(3-(trifluoromethyl)benzyl)indolin-3-yl)carbamate (37). Semi-crude **S87** (38.8 mg, 0.089 mmol, 1.0 equiv.) was reacted with 5-aminotetrazole monohydrate (1.1 equiv.) in 3 mL DMF according to general procedure D (20m activation, 48h). **37** (20.1 mg, 45%) obtained as a tan solid. **Note:** Atropisomerism observed by NMR. ¹H NMR (400 MHz, DMSO-d₆) δ = 12.29 (br s, 0.3H), 12.15 (br s, 0.7H), 7.82 (br s, 1H), 7.74 (s, 1H), 7.72 - 7.42 (m, 4H), 7.19 - 7.10 (m, 1H), 6.73 - 6.58 (m, 2H), 4.65 - 4.53 (m, 1H), 4.52 - 4.33 (m, 2H), 3.41 - 3.35 (m, 1H), 1.36 (br s, 6H), 1.21 (br s, 3H); ¹³C NMR (100 MHz, DMSO-d₆) δ = 170.34, 155.25,

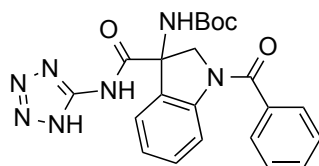
151.18, 150.30 (br s), 139.65, 131.67 (br s), 130.43, 129.53, 129.21 (q, $J = 31.5$ Hz), 125.54 (br s), 125.30, 124.24 (q, $J = 3.9$ Hz), 123.96 - 123.77 (m), 124.28 (q, $J = 272.4$ Hz), 117.25, 107.40, 79.23 (br s), 65.96, 62.18 (br s), 50.81, 28.04 (br s); ^{19}F NMR (376 MHz, DMSO- d_6) $\delta = -60.96$ (s, 3F); LRMS (ESI) calculated for $\text{C}_{23}\text{H}_{23}\text{F}_3\text{N}_7\text{O}_3$ $[\text{M} - \text{H}]^-$ m/z 502.18, found 502.09.



methyl 1-benzoyl-3-((tert-butoxycarbonyl)amino)indoline-3-carboxylate (S88). **S85** (40.0 mg, 0.137 mmol, 1.0 equiv.) was reacted with commercially available benzoyl chloride in dry dichloromethane (2 mL) according to general procedure A, with slight modification: prior to base addition, the reaction vessel was cooled to 0 °C; 2.0 equiv. of *N,N*-diisopropylethylamine was used; after acyl chloride addition, the reaction mixture was allowed to slowly warm to r.t. **S88** (50.1 mg, 92%) obtained as a colorless oil. ^1H NMR (400 MHz, CDCl_3) $\delta = 8.19$ (br s, 1H), 7.61 - 7.53 (m, 2H), 7.52 - 7.41 (m, 3H), 7.39 - 7.21 (m, 2H), 7.08 (br t, $J = 6.8$ Hz, 1H), 5.46 (br s, 1H), 4.97 (br d, $J = 11.4$ Hz, 1H), 4.18 (br s, 1H), 3.76 (s, 3H), 1.40 (br s, 9H); ^{13}C NMR (100 MHz, CDCl_3) $\delta = 170.58$ (br), 169.03 (br), 154.66 (br), 142.94 (br), 136.18, 130.71 (br), 130.58, 129.43 (br), 128.61, 127.11, 124.40 (br), 123.25 (br), 118.17 (br s), 80.81 (br), 64.52 (br), 60.73 (br), 53.25, 28.09 (br); LRMS (ESI) calculated for $\text{C}_{22}\text{H}_{25}\text{N}_2\text{O}_5$ $[\text{M} + \text{H}]^+$ m/z 397.18, found 397.03.

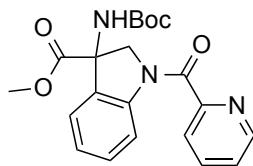


1-benzoyl-3-((tert-butoxycarbonyl)amino)indoline-3-carboxylic acid (S89). S88 (50.1 mg, 0.126 mmol, 1.0 equiv.) was reacted in methanol (3 mL) with 1M lithium hydroxide (379 μ L, 0.379 mmol, 3.0 equiv.) according to general procedure B, except the reaction was cooled to 0 °C prior to hydroxide addition, and allowed to slowly warm to r.t. Semi-crude **S89** (50.1 mg, 104%) obtained as a white solid. LRMS (ESI) calculated for $C_{21}H_{21}N_2O_5$ $[M - H]^-$ m/z 381.15, found 381.23.



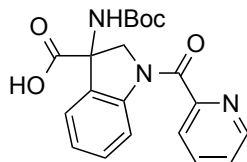
tert-butyl (3-((1H-tetrazol-5-yl)carbamoyl)-1-benzoylindolin-3-yl)carbamate (38). Semi-crude **S89** (50.1 mg, 0.131 mmol, 1.0 equiv.) was reacted with 5-aminotetrazole monohydrate (1.1 equiv.) in 3 mL DMF according to general procedure D (20m activation, 48h). **38** (26.6 mg, 45%) obtained as a white solid. **Note:** Atropisomerism observed by NMR. 1H NMR (400 MHz, DMSO- d_6) δ = 12.47 (br s, 0.3H), 12.32 (br s, 0.7H), 8.25 (br s, 1H), 8.08 (br s, 1H), 7.83 (br d, J = 6.8 Hz, 1H), 7.65 (br s, 2H), 7.61 - 7.48 (m, 3H), 7.37 (br s, 1H), 7.15 (br s, 1H), 4.90 (br d, J = 10.5 Hz, 1H), 4.15 - 3.95 (m, 1H), 1.36 (br s, 6H), 1.15 (br s, 3H); ^{13}C NMR (100 MHz, DMSO- d_6) δ = 170.10 (br), 167.86 (br), 155.50, 150.03 (br), 142.21 (br), 136.39 (br), 130.60, 130.14 (br), 129.46 (br), 128.63 (br), 127.10, 125.53 (br), 124.17 (br), 117.06 (br), 79.69 (br), 65.61 (br),

60.66 (br), 28.05 (br); LRMS (ESI) calculated for $C_{22}H_{22}N_7O_4$ $[M - H]^-$ m/z 448.17, found 448.06.

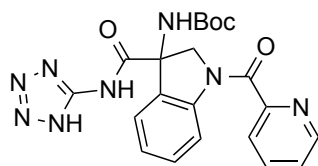


methyl 3-((tert-butoxycarbonyl)amino)-1-picolinoylindoline-3-carboxylate (S90).

S85 (40.0 mg, 0.137 mmol, 1.0 equiv.) was reacted with commercially available pyridine-2-carbonyl chloride hydrochloride in dry dichloromethane (2 mL) according to general procedure A, with slight modification: prior to base addition, the reaction vessel was cooled to 0 °C; 3.0 equiv. of *N,N*-diisopropylethylamine was used; after acyl chloride addition, the reaction mixture was allowed to slowly warm to r.t. **S90** (42.8 mg, 79%) obtained as a colorless oil. 1H NMR (400 MHz, $CDCl_3$) δ = 8.64 (d, J = 4.9 Hz, 1H), 8.35 (br d, J = 6.6 Hz, 1H), 7.89 (br s, 1H), 7.88 - 7.80 (m, 1H), 7.47 - 7.32 (m, 3H), 7.13 (br t, J = 7.4 Hz, 1H), 5.42 (br s, 1H), 5.21 (br d, J = 11.4 Hz, 1H), 4.57 (br d, J = 11.9 Hz, 1H), 3.74 (s, 3H), 1.41 (br s, 9H); ^{13}C NMR (100 MHz, $CDCl_3$) δ = 170.66 (br), 166.11 (br), 154.78 (br), 153.58, 148.28 (br), 143.50 (br), 137.04, 130.84 (br), 129.25 (br), 125.29, 124.72, 124.22 (br), 123.14 (br), 118.56 (br), 80.71 (br), 64.97 (br), 60.93 (br), 53.21, 28.11 (br); LRMS (ESI) calculated for $C_{21}H_{24}N_3O_5$ $[M + H]^+$ m/z 398.17, found 398.09.

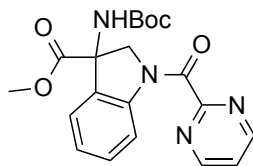


3-((tert-butoxycarbonyl)amino)-1-picolinoylindoline-3-carboxylic acid (S91). S90 (42.8 mg, 0.108 mmol, 1.0 equiv.) was reacted in methanol (3.5 mL) with 1M lithium hydroxide (323 μ L, 0.323 mmol, 3.0 equiv.) according to general procedure B, except the reaction was cooled to 0 °C prior to hydroxide addition, and allowed to slowly warm to r.t. Semi-crude **S91** (41.3 mg, 100%) obtained as a white solid. LRMS (ESI) calculated for $C_{20}H_{20}N_3O_5$ $[M - H]^-$ m/z 382.14, found 382.44.

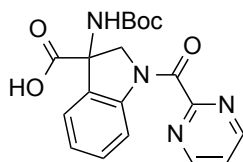


tert-butyl (3-((1H-tetrazol-5-yl)carbamoyl)-1-picolinoylindolin-3-yl)carbamate (39). Semi-crude **S91** (41.3 mg, 0.108 mmol, 1.0 equiv.) was reacted with 5-aminotetrazole monohydrate (1.1 equiv.) in 3 mL DMF according to general procedure D (20m activation, 48h). **39** (23.3 mg, 48%) obtained as a white solid. **Note:** Slight atropisomerism observed by NMR. 1H NMR (400 MHz, DMSO- d_6) δ = 12.31 (br s, 1H), 8.70 (br d, J = 4.4 Hz, 1H), 8.29 - 8.12 (m, 2H), 8.05 (dt, J = 1.6, 7.7 Hz, 1H), 7.95 - 7.75 (m, 2H), 7.61 (dd, J = 5.1, 7.1 Hz, 1H), 7.44 (br t, J = 7.7 Hz, 1H), 7.19 (br t, J = 7.4 Hz, 1H), 5.11 (br d, J = 11.7 Hz, 1H), 4.22 (br d, J = 10.5 Hz, 1H), 1.36 (br s, 6H), 1.18 (br s, 3H); ^{13}C NMR (100 MHz, DMSO- d_6) δ = 170.11 (br), 165.41 (br), 155.45 (br), 153.34, 150.28 (br), 148.35 (br), 142.51, 137.78, 130.32 (br), 129.34 (br), 125.87, 125.47 (br),

124.54 (br), 123.96 (br), 117.26, 79.66 (br), 65.78 (br), 60.56 (br), 28.03 (br); LRMS (ESI) calculated for C₂₁H₂₁N₃O₄ [M - H]⁻ m/z 449.17, found 449.05.

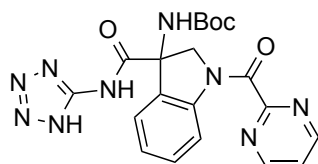


methyl 3-((tert-butoxycarbonyl)amino)-1-(pyrimidine-2-carbonyl)indoline-3-carboxylate (S92). Pyrimidine-2-carboxylic acid (17 mg, 0.137 mmol, 1.0 equiv.) was reacted with **S85** (40.0 mg, 0.137 mmol, 1.0 equiv.) in 2 mL DMF according to general procedure D (10m activation), except the resulting mixture was transferred to a sep. funnel with ~ 75 mL EtOAc. The organic layer was washed with ~ 50 mL sat. NaHCO₃, water, and 0.1N HCl; dried over MgSO₄ and concentrated. Purified on a silica column with 0-40% EtOAc:hexanes. **S92** (29.7 mg, 55%) obtained as a colorless oil. ¹H NMR (400 MHz, CDCl₃) δ = 8.88 (d, *J* = 4.9 Hz, 2H), 8.41 (br d, *J* = 8.3 Hz, 1H), 7.47 - 7.34 (m, 3H), 7.19 - 7.11 (m, 1H), 5.36 (br s, 1H), 5.10 (br d, *J* = 11.9 Hz, 1H), 4.34 (br d, *J* = 12.2 Hz, 1H), 3.75 (s, 3H), 1.40 (br s, 9H); ¹³C NMR (100 MHz, CDCl₃) δ = 170.36 (br), 163.31 (br), 161.12, 157.43, 154.79 (br), 142.88, 131.11 (br), 129.06 (br), 125.07, 123.18 (br), 121.79, 118.58 (br), 80.83 (br), 64.85 (br), 59.96 (br), 53.28 (br), 28.11 (br); LRMS (ESI) calculated for C₂₀H₂₃N₄O₅ [M + H]⁺ m/z 399.17, found 399.01.

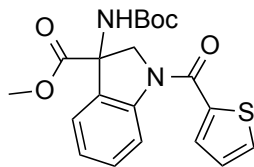


3-((tert-butoxycarbonyl)amino)-1-(pyrimidine-2-carbonyl)indoline-3-carboxylic acid (S93). **S92** (29.7 mg, 0.075 mmol, 1.0 equiv.) was reacted in methanol (3 mL) with

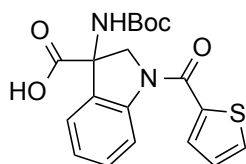
1M lithium hydroxide (224 μ L, 0.224 mmol, 3.0 equiv.) according to general procedure B, except the reaction was cooled to 0 $^{\circ}$ C prior to hydroxide addition, and allowed to slowly warm to r.t. Semi-crude **S93** (25.1 mg, 88%) obtained as a white solid. LRMS (ESI) calculated for $C_{19}H_{19}N_4O_5$ $[M - H]^{-}$ m/z 383.14, found 383.35.



tert-butyl (3-((1*H*-tetrazol-5-yl)carbamoyl)-1-(pyrimidine-2-carbonyl)indolin-3-yl)carbamate (40). Semi-crude **S93** (25.1 mg, 0.065 mmol, 1.0 equiv.) was reacted with 5-aminotetrazole monohydrate (1.1 equiv.) in 2 mL DMF according to general procedure D (20m activation). **40** (16.2 mg, 55%) obtained as a white solid. **Note:** Slight atropisomerism observed by NMR. 1H NMR (400 MHz, $DMSO-d_6$) δ = 12.36 (br s, 1H), 9.03 (d, J = 4.9 Hz, 2H), 8.25 (br s, 1H), 8.20 (d, J = 8.0 Hz, 1H), 7.85 (br d, J = 7.5 Hz, 1H), 7.72 (t, J = 4.9 Hz, 1H), 7.51 - 7.42 (m, 1H), 7.22 (t, J = 7.5 Hz, 1H), 4.90 (br d, J = 11.0 Hz, 1H), 3.95 (br d, J = 11.4 Hz, 1H), 1.35 (br s, 6H), 1.12 (br s, 3H); ^{13}C NMR (100 MHz, $DMSO-d_6$) δ = 169.99 (br), 162.89, 160.75, 157.97, 155.55 (br), 150.21 (br), 141.71, 130.62, 129.09 (br), 125.56 (br), 124.94, 122.65, 116.91, 79.75 (br), 65.74 (br), 59.55 (br), 27.98 (br); LRMS (ESI) calculated for $C_{20}H_{20}N_9O_4$ $[M - H]^{-}$ m/z 450.16, found 450.11.

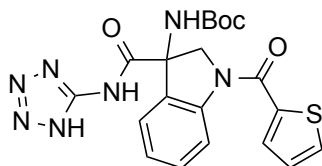


methyl 3-((tert-butoxycarbonyl)amino)-1-(thiophene-2-carbonyl)indoline-3-carboxylate (S94). **S85** (40.0 mg, 0.137 mmol, 1.0 equiv.) was reacted with commercially available 2-thiophenecarbonyl chloride in dry dichloromethane (2 mL) according to general procedure A, with slight modification: prior to base addition, the reaction vessel was cooled to 0 °C; 2.0 equiv. of *N,N*-diisopropylethylamine was used; after acyl chloride addition, the reaction mixture was allowed to slowly warm to r.t. **S94** (53.0 mg, 96%) obtained as a colorless oil. ^1H NMR (400 MHz, CDCl_3) δ = 8.20 (br d, J = 7.1 Hz, 1H), 7.64 (d, J = 3.4 Hz, 1H), 7.57 (br d, J = 4.9 Hz, 1H), 7.42 - 7.31 (m, 2H), 7.16 - 7.05 (m, 2H), 5.45 (br s, 1H), 5.30 (br d, J = 11.2 Hz, 1H), 4.52 (br d, J = 11.4 Hz, 1H), 3.78 (s, 3H), 1.43 (br s, 9H); ^{13}C NMR (100 MHz, CDCl_3) δ = 170.53 (br), 161.47 (br), 154.81 (br), 143.40, 138.80 (br), 130.96, 130.77, 130.28 (br), 128.81 (br), 127.49 (br), 124.60, 123.13, 118.50 (br), 80.94 (br), 65.02 (br), 60.64 (br), 53.36, 28.13; LRMS (ESI) calculated for $\text{C}_{20}\text{H}_{23}\text{N}_2\text{O}_5\text{S}$ $[\text{M} + \text{H}]^+$ m/z 403.13, found 403.03.

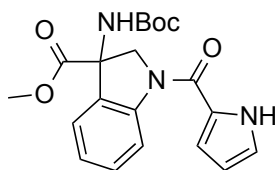


3-((tert-butoxycarbonyl)amino)-1-(thiophene-2-carbonyl)indoline-3-carboxylic acid (S95). **S94** (53.0 mg, 0.132 mmol, 1.0 equiv.) was reacted in methanol (3 mL) with 1M lithium hydroxide (395 μL , 0.395 mmol, 3.0 equiv.) according to general procedure B, except the reaction was cooled to 0 °C prior to hydroxide addition, and allowed to slowly

warm to r.t. Semi-crude **S95** (52.5 mg, 103%) obtained as a white solid. LRMS (ESI) calculated for $C_{19}H_{19}N_2O_5S$ $[M - H]^-$ m/z 387.10, found 387.08.

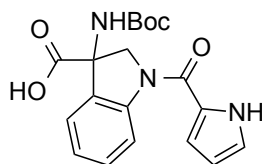


tert-butyl 3-((1H-tetrazol-5-yl)carbamoyl)-1-(thiophene-2-carbonyl)indolin-3-yl)carbamate (41). Semi-crude **S95** (52.5 mg, 0.135 mmol, 1.0 equiv.) was reacted with 5-aminotetrazole monohydrate (1.1 equiv.) in 3 mL DMF according to general procedure D (20m activation, 48h). **41** (24.4 mg, 40%) obtained as a white solid. **Note:** Slight atropisomerism observed by NMR. 1H NMR (400 MHz, $DMSO-d_6$) δ = 12.52 (br s, 0.4H), 12.36 (br s, 0.6H), 8.31 (br s, 1H), 8.01 (br d, J = 7.3 Hz, 1H), 7.92 (d, J = 4.9 Hz, 1H), 7.88 - 7.75 (m, 2H), 7.39 (t, J = 7.4 Hz, 1H), 7.30 - 7.23 (m, 1H), 7.21 - 7.12 (m, 1H), 5.28 (br d, J = 10.5 Hz, 1H), 4.40 (br d, J = 10.2 Hz, 1H), 1.39 (br s, 6H), 1.25 (br s, 3H); ^{13}C NMR (100 MHz, $DMSO-d_6$) δ = 172.04, 160.73 (br), 155.53 (br), 150.16 (br), 142.48, 138.64, 131.64 (br), 130.57 (br), 130.21 (br), 129.35 (br), 127.92, 125.52 (br), 124.35 (br), 117.42, 79.67 (br), 65.95 (br), 60.75 (br), 28.09 (br); LRMS (ESI) calculated for $C_{20}H_{20}N_7O_4S$ $[M - H]^-$ m/z 454.13, found 454.06.

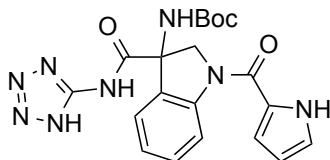


methyl 3-((tert-butoxycarbonyl)amino)-1-(1H-pyrrole-2-carbonyl)indoline-3-carboxylate (S96). Pyrrole-2-carboxylic acid (15.2 mg, 0.137 mmol, 1.0 equiv.) was reacted with **S85** (40.0 mg, 0.137 mmol, 1.0 equiv.) in 2 mL DMF according to general

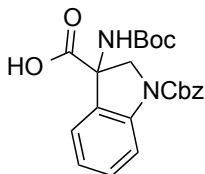
procedure D (10m activation). After 24h, the reaction was heated at 80 °C; 1.0 equiv. acid and 1.0 equiv HATU were added every day for 4d. The resulting mixture was transferred to a sep. funnel with ~ 75 mL EtOAc. The organic layer was washed with ~ 50 mL sat. NaHCO₃, water, and 0.1N HCl; dried over MgSO₄ and concentrated. Purified on a silica column with 0-50% EtOAc:hexanes. **S96** (11.1 mg, 21%) obtained as a colorless oil. ¹H NMR (400 MHz, CDCl₃) δ = 8.33 (d, *J* = 7.8 Hz, 1H), 7.43 - 7.35 (m, 2H), 7.09 (dt, *J* = 1.0, 7.5 Hz, 1H), 7.05 (br s, 1H), 6.86 (br s, 1H), 6.35 (br d, *J* = 2.9 Hz, 1H), 5.63 (br s, 0.2H), 5.43 (br s, 0.8H), 5.32 (br d, *J* = 10.7 Hz, 1H), 4.60 (br d, *J* = 11.2 Hz, 1H), 3.79 (s, 3H), 1.45 (br s, 9H); LRMS (ESI) calculated for C₂₀H₂₄N₃O₅ [M + H]⁺ m/z 386.17, found 386.09.



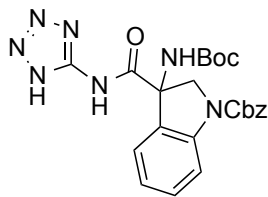
3-((tert-butoxycarbonyl)amino)-1-(1H-pyrrole-2-carbonyl)indoline-3-carboxylic acid (S97). **S96** (11.1 mg, 0.029 mmol, 1.0 equiv.) was reacted in methanol (3 mL) with 1M lithium hydroxide (58 uL, 0.058 mmol, 2.0 equiv.) according to general procedure B, except the reaction was cooled to 0 °C prior to hydroxide addition, and allowed to slowly warm to r.t. After 18h, additional 1M lithium hydroxide (2.0 equiv) and methanol (500 uL) were added; allowed to stir for 30h. Semi-crude **S96** (10.7 mg, 100%) obtained as a white solid. LRMS (ESI) calculated for C₁₉H₂₀N₃O₅ [M - H]⁻ m/z 370.14, found 370.14.



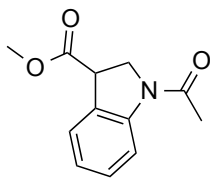
tert-butyl 3-((1*H*-tetrazol-5-yl)carbamoyl)-1-(1*H*-pyrrole-2-carbonyl)indolin-3-yl)carbamate (42). Semi-crude **S97** (10.7 mg, 0.029 mmol, 1.0 equiv.) was reacted with 5-aminotetrazole monohydrate (1.1 equiv.) in 2 mL DMF according to general procedure D (20m activation, 48h). **42** (2.7 mg, 21%) obtained as a tan solid. ^1H NMR (400 MHz, CD_3OD , CDCl_3) δ = 8.19 (br d, J = 8.0 Hz, 1H), 7.58 (br d, J = 7.5 Hz, 1H), 7.37 (br t, J = 7.8 Hz, 1H), 7.11 (br t, J = 7.4 Hz, 1H), 7.06 (br s, 1H), 6.84 (br s, 1H), 6.33 - 6.29 (m, 1H), 5.56 (br d, J = 11.2 Hz, 1H), 4.39 (br d, J = 11.2 Hz, 1H), 3.70 - 3.66 (m, 1H), 3.58 - 3.54 (m, 1H), 1.43 (br s, 9H); LRMS (ESI) calculated for $\text{C}_{20}\text{H}_{21}\text{N}_8\text{O}_4$ $[\text{M} - \text{H}]^-$ m/z 437.17, found 436.92.



1-((benzyloxy)carbonyl)-3-((tert-butoxycarbonyl)amino)indoline-3-carboxylic acid (S98). **S84** (88.9 mg, 0.208 mmol, 1.0 equiv.) was reacted in methanol (4 mL) with 1M lithium hydroxide (625 μL , 0.625 mmol, 3.0 equiv.) according to general procedure B, except the reaction was cooled to 0 $^\circ\text{C}$ prior to hydroxide addition, and allowed to slowly warm to r.t. Semi-crude **S98** (89.3 mg, 104%) obtained as a colorless oil. LRMS (ESI) calculated for $\text{C}_{22}\text{H}_{23}\text{N}_2\text{O}_6$ $[\text{M} - \text{H}]^-$ m/z 411.16, found 411.16.

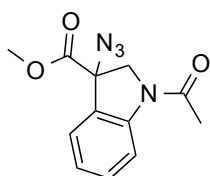


benzyl 3-((1*H*-tetrazol-5-yl)carbamoyl)-3-((tert-butoxycarbonyl)amino)indoline-1-carboxylate (43). Semi-crude **S98** (89.3 mg, 0.217 mmol, 1.0 equiv.) was reacted with 5-aminotetrazole monohydrate (1.1 equiv.) in 4 mL DMF according to general procedure D (10m activation). **43** (53.0 mg, 51%) obtained as a white solid. **Note:** Extreme peak broadening in the ¹H NMR; presumably atropisomerism. ¹H NMR (400 MHz, CD₃OD, drops CDCl₃) δ = 7.89 (br s, 1H), 7.58 - 7.17 (m, 7H), 6.95 (br s, 1H), 5.25 (br s, 3H), 4.12 - 3.87 (m, 2H), 1.26 (br s, 9H); ¹³C NMR (100 MHz, CD₃OD, drops CDCl₃) δ = 170.11, 155.08 (br), 152.41 (br), 150.16, 142.18 (br), 135.42 (br), 131.07, 128.30 (br), 128.07 (br), 127.83 (br), 126.74 (br), 123.58 (br), 123.11 (br), 115.29 (br), 80.98, 67.20 (br), 65.12 (br), 57.74, 27.64; LRMS (ESI) calculated for C₂₃H₂₄N₇O₅ [M - H]⁻ m/z 478.18, found 478.19.

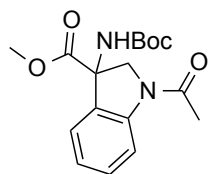


methyl 1-acetylimidazole-3-carboxylate (S99). Semi-crude **S32** (145.0 mg, 0.679 mmol, 1.0 equiv.) was reacted with commercially available acetyl chloride in dry dichloromethane (6 mL) according to general procedure A, with slight modification: prior to base addition, the reaction vessel was cooled to 0 °C; 2.5 equiv. of *N,N*-diisopropylethylamine was used, and allowed to stir at 0 °C for 5m; after acyl chloride addition, the reaction mixture was allowed to slowly warm to r.t. **S99** (119.2 mg, 80%)

obtained as a colorless oil. ^1H NMR (400 MHz, CDCl_3) δ = 8.19 (d, J = 8.0 Hz, 1H), 7.37 (br d, J = 7.3 Hz, 1H), 7.23 (t, J = 7.7 Hz, 1H), 7.01 (t, J = 7.4 Hz, 1H), 4.46 (dd, J = 5.6, 10.5 Hz, 1H), 4.25 (br dd, J = 5.5, 9.9 Hz, 1H), 4.14 - 4.07 (m, 1H), 3.76 (s, 3H), 2.41 (br s, 0.3H), 2.22 (s, 2.6H); ^{13}C NMR (100 MHz, CDCl_3) δ = 171.29, 168.34, 142.40, 128.90, 127.62, 124.82, 123.53, 116.90, 52.58, 50.57, 45.05, 24.02; LRMS (ESI) calculated for $\text{C}_{12}\text{H}_{14}\text{NO}_3$ $[\text{M} + \text{H}]^+$ m/z 220.10, found 219.91.

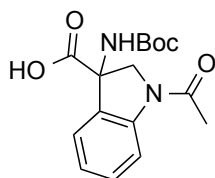


methyl 1-acetyl-3-azidoindoline-3-carboxylate (S100). **S99** (119.2 mg, 0.554 mmol, 1.0 equiv.) was reacted in 11.3 mL tetrahydrofuran according to general procedure F. **S100** (77.7 mg, 55%) obtained as a colorless oil. ^1H NMR (400 MHz, CDCl_3) δ = 8.29 (d, J = 8.3 Hz, 1H), 7.48 - 7.39 (m, 2H), 7.12 (dt, J = 1.0, 7.5 Hz, 1H), 4.64 (d, J = 11.4 Hz, 1H), 3.95 (d, J = 11.4 Hz, 1H), 3.89 (s, 3H), 2.46 (br s, 0.4H), 2.25 (s, 2.6H); ^{13}C NMR (100 MHz, CDCl_3) δ = 169.01, 168.27, 142.79, 131.65, 126.12, 123.80, 123.58, 117.69, 69.87, 57.80, 53.67, 24.00; LRMS (ESI) calculated for $\text{C}_{12}\text{H}_{13}\text{N}_4\text{O}_3$ $[\text{M} + \text{H}]^+$ m/z 261.10, found 261.06.



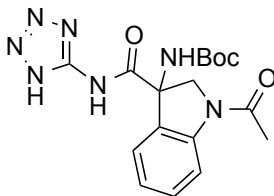
methyl 1-acetyl-3-((tert-butoxycarbonyl)amino)indoline-3-carboxylate (S101). A round bottom flask was charged with **S100** (77.7 mg, 0.299 mmol, 1.0 equiv.) and dry methanol (6 mL), then cooled to 0 °C. Anhydrous tin(II) chloride (113 mg, 0.597 mmol,

2.0 equiv.) was added; stirred at 0 °C for 5m, then r.t. for 4 h. The methanol was then removed under reduced pressure. 1,4-dioxane (5.5 mL) was added, followed by di-tert-butyl dicarbonate (97 mg, 0.448 mmol, 1.5 equiv.) in 700 uL 1,4-dioxane. Finally, a slurry of sodium bicarbonate (100 mg, 1.19 mmol, 4.0 equiv.) in water (1.4 mL) was added, and the resulting slurry was allowed to stir for 18h. The reaction mixture was then transferred to a sep. funnel with excess EtOAc and water and adjusted to pH 1 with 1M KHSO₄. The layers were separated, and the aqueous layer was further extracted with ~ 50 mL EtOAc. The organic layers were combined, washed with sat. NaHCO₃, dried over MgSO₄, and concentrated under reduced pressure. Purified on a silica column with 0-45% EtOAc:hexanes. **S101** (70.7 mg, 71%) obtained as a colorless oil. ¹H NMR (400 MHz, CDCl₃) δ = 8.21 (d, *J* = 8.3 Hz, 1H), 7.36 - 7.29 (m, 2H), 7.03 (t, *J* = 7.5 Hz, 1H), 5.57 (s, 1H), 4.97 (br d, *J* = 11.2 Hz, 1H), 4.14 (br d, *J* = 11.4 Hz, 1H), 3.76 (s, 3H), 2.21 (s, 3H), 1.44 (br s, 9H); ¹³C NMR (100 MHz, CDCl₃) δ = 170.56 (br), 168.66 (br), 154.96 (br), 142.92, 130.98, 128.07 (br), 123.89, 123.16, 117.50, 80.86 (br), 64.56 (br), 59.42 (br), 53.26, 28.13, 24.09; LRMS (ESI) calculated for C₁₇H₂₃N₂O₅ [M + H]⁺ m/z 335.16, found 335.04.



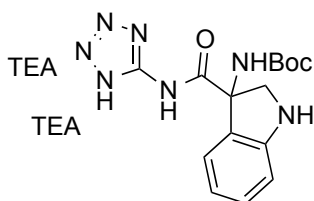
1-acetyl-3-((tert-butoxycarbonyl)amino)indoline-3-carboxylic acid (S102). **S101** (70.7 mg, 0.211 mmol, 1.0 equiv.) was reacted in methanol (4 mL) with 1M lithium hydroxide (634 uL, 0.634 mmol, 3.0 equiv.) according to general procedure B, except the reaction was cooled to 0 °C prior to hydroxide addition, and allowed to slowly warm

to r.t. Semi-crude **S102** (65.2 mg, 96%) obtained as a white solid. LRMS (ESI) calculated for $C_{16}H_{19}N_2O_5$ $[M - H]^-$ m/z 319.13, found 319.16.



tert-butyl (3-((1*H*-tetrazol-5-yl)carbamoyl)-1-acetylimidolin-3-yl)carbamate (44).

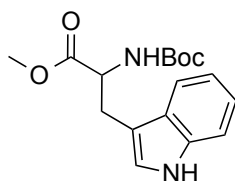
Semi-crude **S102** (65.2 mg, 0.204 mmol, 1.0 equiv.) was reacted with 5-aminotetrazole monohydrate (1.1 equiv.) in 4 mL DMF according to general procedure D (10m activation). **44** (58.3 mg, 74%) obtained as a white solid. **Note:** Slight atropisomerism observed by NMR. 1H NMR (400 MHz, DMSO- d_6) δ = 12.49 (br s, 0.3H), 12.35 (br s, 0.7H), 8.19 (br s, 1H), 8.09 (br d, J = 7.8 Hz, 1H), 7.77 (br s, 1H), 7.33 (br t, J = 6.9 Hz, 1H), 7.08 (br s, 1H), 5.01 (br d, J = 10.7 Hz, 1H), 4.06 (br d, J = 11.2 Hz, 1H), 2.24 (br s, 3H), 1.40 (br s, 6H), 1.29 (br s, 3H); ^{13}C NMR (100 MHz, DMSO- d_6) δ = 170.28 (br), 168.35, 155.49 (br), 150.22 (br), 142.46, 130.36 (br), 128.41 (br), 125.42 (br), 123.43 (br), 116.17, 79.64 (br), 65.52 (br), 58.94 (br), 28.13 (br), 24.09 (br); LRMS (ESI) calculated for $C_{17}H_{20}N_7O_4$ $[M - H]^-$ m/z 386.16, found 386.07.



tert-butyl (3-((1*H*-tetrazol-5-yl)carbamoyl)imidolin-3-yl)carbamate, bis-

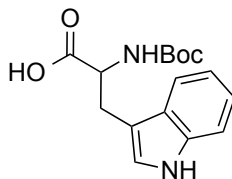
triethylammonium salt (45). **43** (23.0 mg, 0.048 mmol, 1.0 equiv.) was dissolved in ethanol (40 mL) and DMF (300 μ L) and hydrogenated for 5h using an “H-Cube” flow

hydrogenator with a 10% Pd/C cartridge; 1 mL/min, 1 atm H₂, 40 °C, loop configuration. The crude reaction mixture was concentrated and directly purified by reverse phase HPLC (water/MeOH/0.1% TEA:AcOH) to afford the desired product as a triethylammonium salt. **Note:** Crude reaction mixture unstable; store cold or purify immediately. **45** (3.9 mg, 18%) obtained as a tan film. ¹H NMR (400 MHz, CD₃OD) δ = 7.41 (br d, *J* = 7.5 Hz, 1H), 7.14 (t, *J* = 7.5 Hz, 1H), 6.77 - 6.70 (m, 2H), 4.52 (br d, *J* = 10.5 Hz, 1H), 3.67 - 3.62 (m, 1H), 3.13 (q, *J* = 7.3 Hz, 12H), 1.44 (br s, 9H), 1.26 (t, *J* = 7.2 Hz, 18H); LRMS (ESI) calculated for C₁₅H₁₈N₇O₃ [M - H]⁻ *m/z* 344.15, found 344.14.

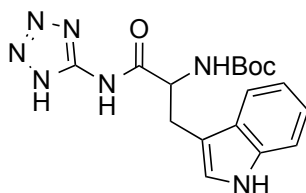


methyl (tert-butoxycarbonyl)tryptophanate (S103). Commercially available DL-tryptophan methyl ester hydrochloride (100 mg, 0.393 mmol, 1.0 equiv.) was reacted with di-tert-butyl dicarbonate in dry dichloromethane (4 mL) according to general procedure A, except 1.1 equiv. of *N,N*-diisopropylethylamine was used, and the reaction mixture was concentrated and directly purified, sans workup. **S103** (125.2 mg, 100%) obtained as a white solid. **Note:** Atropisomerism observed by NMR. ¹H NMR (400 MHz, DMSO-d₆) δ = 10.85 (br s, 0.3H), 7.49 (d, *J* = 7.8 Hz, 1H), 7.34 (d, *J* = 8.3 Hz, 1H), 7.20 (br d, *J* = 8.0 Hz, 0.4H), 7.16 (s, 1H), 7.11 - 7.04 (m, 1H), 7.03 - 6.94 (m, 1H), 4.25 - 4.16 (m, 0.84H), 4.12 (br s, 0.16H), 3.60 (s, 3H), 3.16 - 3.06 (m, 1H), 3.05 - 2.94 (m, 1H), 1.33 (s, 7.5H), 1.22 (br s, 1.5H); ¹³C NMR (100 MHz, DMSO-d₆) δ = 172.93, 155.31, 136.09, 135.93, 127.02, 123.73, 123.57, 120.94, 118.39, 117.99, 111.38,

109.70, 78.23, 54.67, 54.58, 51.73, 28.13, 27.75 (br), 26.76; LRMS (ESI) calculated for $C_{17}H_{22}N_2NaO_4$ $[M + Na]^+$ m/z 341.15, found 341.03.

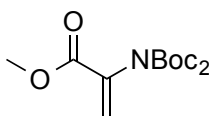


(tert-butoxycarbonyl)tryptophan (S104). **S103** (105.2 mg, 0.330 mmol, 1.0 equiv.) was reacted in methanol (5 mL) with 1M lithium hydroxide (661 μ L, 0.661 mmol, 2.0 equiv.) according to general procedure B, except after 7h additional 1M lithium hydroxide (2.0 equiv.) and methanol (2 mL) were added. Semi-crude **S104** (99.1 mg, 99%) obtained as a white solid. LRMS (ESI) calculated for $C_{16}H_{19}N_2O_4$ $[M - H]^-$ m/z 303.14, found 303.3.

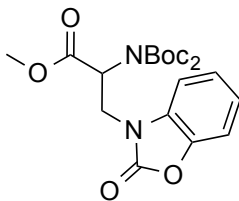


tert-butyl (1-((1H-tetrazol-5-yl)amino)-3-(1H-indol-3-yl)-1-oxopropan-2-yl)carbamate (46). Semi-crude **S104** (99.1 mg, 0.326 mmol, 1.0 equiv.) was reacted with 5-aminotetrazole monohydrate (1.1 equiv.) in 2 mL DMF according to general procedure H. **46** (32.2 mg, 28%) obtained as a light tan solid. **Note:** Product is prone to oxidation (N-oxide) on the benchtop; store cold under Ar. **Note:** Slight atropisomerism observed by 1H NMR. 1H NMR (400 MHz, DMSO- d_6) δ = 12.28 (br s, 1H), 10.84 (br s, 1H), 7.71 (br d, J = 7.8 Hz, 1H), 7.32 (d, J = 8.0 Hz, 1H), 7.21 (br s, 1H), 7.17 (br d, J = 7.3 Hz, 1H), 7.05 (t, J = 7.4 Hz, 1H), 7.00 - 6.91 (m, 1H), 4.52 - 4.36 (m, 1H), 3.21 - 3.09

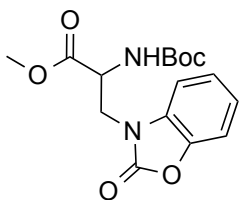
(m, 1H), 3.01 (br dd, $J = 9.4, 14.2$ Hz, 1H), 1.32 (s, 7.4H), 1.17 (br d, $J = 2.9$ Hz, 1.6H); ^{13}C NMR (100 MHz, DMSO- d_6) $\delta = 172.19, 155.36, 149.64$ (br), 136.03, 127.11, 124.25, 120.91, 118.64, 118.20, 111.29, 109.30, 78.35, 55.33, 28.14, 27.21; LRMS (ESI) calculated for $\text{C}_{17}\text{H}_{20}\text{N}_7\text{O}_3$ $[\text{M} - \text{H}]^-$ m/z 370.16, found 370.19.



2-(bis((tert-butoxy)carbonyl)amino)prop-2-enoate (S105). A dried 50 mL RB was charged with commercially available methyl (tert-butoxycarbonyl)serinate (1.500 ml, 7.40 mmol, 1.0 equiv.) and dry acetonitrile (14.8 mL). Di-tert-butyl dicarbonate (4.039 g, 18.5 mmol, 2.5 equiv.) was then added, followed by dropwise addition of *N,N*-diisopropylethylamine (2.579 ml, 14.8 mmol, 2.0 equiv.). After 3h, 4-dimethylaminopyridine (452 mg, 3.70 mmol, 0.5 equiv.) was added. Another 0.5 equiv. 4-dimethylaminopyridine was added at 5h, followed by 1.0 equiv. 4-dimethylaminopyridine at 7h. After 24h, 0.5 equiv. 4-dimethylaminopyridine was added, and the reaction was heated at 45 °C for 4h. The crude reaction mixture was transferred to a sep. funnel with ~ 125 mL EtOAc and washed with sat. NH_4Cl , sat. NaHCO_3 , and brine. The organic layer was further washed with 3 x 50 mL sat. NH_4Cl , dried over MgSO_4 , and concentrated. The resulting oil was dried under hovac overnight. **S105** (2.440 g, 109%, wet with EtOAc) obtained as a yellow solid. ^1H NMR (400 MHz, CDCl_3) $\delta = 6.33$ (s, 1H), 5.63 (s, 1H), 3.78 (s, 3H), 1.45 (s, 18H); ^{13}C NMR (100 MHz, CDCl_3) $\delta = 163.93, 150.58, 136.02, 124.61, 83.10, 52.32, 27.81$; LRMS (ESI) calculated for $\text{C}_{14}\text{H}_{23}\text{NNaO}_6$ $[\text{M} + \text{Na}]^+$ m/z 324.14, found 324.10.

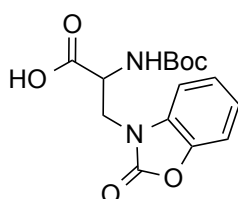


methyl 2-(bis((tert-butoxy)carbonyl)amino)-3-(2-oxo-2,3-dihydro-1,3-benzoxazol-3-yl)propanoate (S106). A 3 mL vial was charged with **S105** (200.0 mg, 0.664, 1.0 equiv.), benzo[d]oxazol-2(3*H*)-one (92 mg, 0.682 mmol, 1.0 equiv.), and dry acetonitrile (2 mL). Cesium carbonate (22 mg, 0.066 mmol, 0.1 equiv.) was then added, and the vial was sealed and heated at 80 °C overnight. The crude reaction mixture was transferred to a sep. funnel with ~ 100 mL EtOAc and washed with ~ 50 mL water and brine; the organic layer was dried over MgSO₄, concentrated, and purified on a silica column with 0-40% EtOAc:hexanes. **S106** (256.9 mg, 89%) obtained as a colorless oil. ¹H NMR (400 MHz, CDCl₃) δ = 7.10 - 7.02 (m, 2H), 7.02 - 6.95 (m, 1H), 6.87 (d, *J* = 7.8 Hz, 1H), 5.31 (dd, *J* = 5.4, 8.8 Hz, 1H), 4.45 - 4.32 (m, 2H), 3.68 (s, 3H), 1.27 (s, 18H); ¹³C NMR (100 MHz, CDCl₃) δ = 168.40, 153.88, 151.27, 142.35, 130.99, 123.53, 122.13, 109.62, 107.91, 83.46, 55.82, 52.19, 41.56, 27.36; LRMS (ESI) calculated for C₂₁H₂₈N₂NaO₈ [M + Na]⁺ *m/z* 459.17, found 459.08.

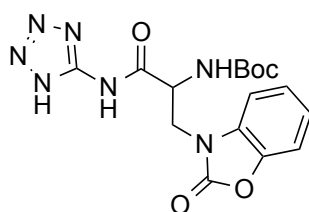


methyl 2-((tert-butoxycarbonyl)amino)-3-(2-oxobenzo[d]oxazol-3(2*H*)-yl)propanoate (S107). A 20 mL vial was charged with **S106** (257 mg, 0.589, 1.0 equiv.) and dry acetonitrile (5.9 mL). Lithium bromide (153 mg, 1.77 mmol, 3.0 equiv.) was then

added, and the vial was sealed and heated at 65 °C overnight. The crude reaction mixture was transferred to a sep. funnel with EtOAc and partitioned with water; the layers were separated, and the aqueous layer was further extracted with 2 x 50 mL EtOAc. The organics were combined, dried over MgSO₄, and concentrated. Crude **S107** (211.0 mg, 107%) obtained as a colorless oil. LRMS (ESI) calculated for C₁₆H₂₀N₂NaO₆ [M + Na]⁺ m/z 359.12, found 359.03.

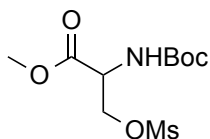


2-((tert-butoxycarbonyl)amino)-3-(2-oxobenzo[d]oxazol-3(2H)-yl)propanoic acid (S108). Crude **S107** (198.0 mg, 0.589 mmol, 1.0 equiv.) was reacted in methanol (10 mL) with 1M lithium hydroxide (1.177 mL, 1.18 mmol, 2.0 equiv.) according to general procedure B. Semi-crude **S108** (165.0 mg, 87%) obtained as a tan solid. LRMS (ESI) calculated for C₁₅H₁₇N₂O₆ [M - H]⁻ m/z 321.11, found 321.21.

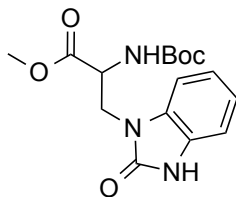


tert-butyl (1-((1H-tetrazol-5-yl)amino)-1-oxo-3-(2-oxobenzo[d]oxazol-3(2H)-yl)propan-2-yl)carbamate (47). Semi-crude **S108** (165.0 mg, 0.512 mmol, 1.0 equiv.) was reacted with 5-aminotetrazole monohydrate (1.1 equiv.) in 3.5 mL DMF according to general procedure D (20m activation). **47** (64.9 mg, 28% over 3 steps) obtained as an off-white solid. ¹H NMR (400 MHz, DMSO-d₆) δ = 12.34 (br s, 0.25H), 7.42 - 7.21 (m,

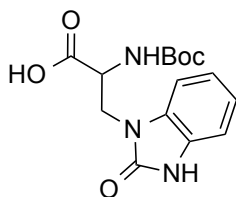
2.5H), 7.21 - 7.04 (m, 2H), 4.64 (br s, 1H), 4.28 - 4.13 (m, 1H), 4.14 - 4.00 (m, 1H), 1.23 (s, 9H); ^{13}C NMR (100 MHz, DMSO- d_6) δ = 169.20 (br), 154.99, 154.94, 153.75, 149.40 (br), 142.00, 131.25, 123.67, 122.19, 109.53, 109.19, 78.72, 52.24 (br), 52.16, 43.02 (br), 27.86; LRMS (ESI) calculated for $\text{C}_{16}\text{H}_{18}\text{N}_7\text{O}_5$ $[\text{M} - \text{H}]^-$ m/z 388.14, found 388.12.



methyl *N*-(tert-butoxycarbonyl)-*O*-(methylsulfonyl)serinate (S109). A dried 100 mL RB was charged with commercially available methyl (tert-butoxycarbonyl)serinate (1.200 ml, 5.92 mmol, 1.0 equiv.) and dry dichloromethane (36 mL), then cooled to 0 °C. Methanesulfonyl chloride (550 μL , 7.11 mmol, 1.2 equiv.) was then added, followed by dropwise addition of *N,N*-diisopropylethylamine (1.238 mL, 7.11 mmol, 1.2 equiv.). After addition was complete, the reaction mixture was immediately warmed to r.t. and allowed to stir for 1h. The crude reaction mixture was then transferred to a sep. funnel with dichloromethane and water, the layers separated, and the organic layer was washed with 2 x ~ 60 mL brine. Dried over MgSO_4 and concentrated; dried under hivaac for 2h. **Note:** This product is unstable at r.t., and rapidly begins to decompose. Crude **S109** (1.760 g, 100%) obtained as a yellow oil. ^1H NMR (400 MHz, CDCl_3) δ = 5.48 (br d, J = 7.3 Hz, 1H), 4.59 - 4.49 (m, 1H), 4.48 - 4.41 (m, 1H), 3.77 - 3.72 (m, 3H), 2.98 (s, 3H), 1.40 (s, 9H); ^{13}C NMR (100 MHz, CDCl_3) δ = 168.98, 154.91, 80.38, 68.87, 52.83, 52.39, 37.14, 28.03; LRMS (ESI) calculated for $\text{C}_{10}\text{H}_{19}\text{NNaO}_7\text{S}$ $[\text{M} + \text{Na}]^+$ m/z 320.08, found 320.07.

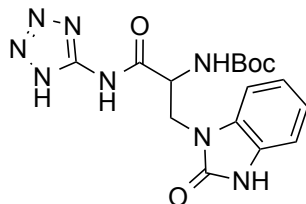


methyl 2-((tert-butoxycarbonyl)amino)-3-(2-oxo-2,3-dihydro-1H-benzo[d]imidazol-1-yl)propanoate (S110). A 3 mL vial was charged with crude **S109** (326.4 mg, 1.10 mmol, 1.0 equiv.), 2-hydroxybenzimidazole (147 mg, 1.10 mmol, 1.0 equiv.), cesium carbonate (715 mg, 2.20 mmol, 2.0 equiv.), and dry DMF (2 mL). The vial was sealed and heated at 60 °C overnight. The crude reaction mixture was transferred to a sep. funnel with ~ 100 mL EtOAc and sat. NH₄Cl, the layers separated, and the organic layer further extracted with brine. Dried over MgSO₄, concentrated, and purified on a silica column with 30-60% EtOAc:hexanes. **S110** (74.4 mg, 20%) obtained as a white solid. ¹H NMR (400 MHz, CD₃OD, drops CDCl₃) δ = 7.08 - 6.89 (m, 5H), 4.54 (br t, *J* = 5.5 Hz, 1H), 4.20 (br d, *J* = 5.8 Hz, 2H), 3.65 (s, 3H), 1.32 (s, 9H); ¹³C NMR (100 MHz, CD₃OD, drops CDCl₃) δ = 171.05, 156.02, 155.79, 130.43, 128.30, 122.19, 121.72, 109.90, 108.22, 80.48, 53.31, 52.90, 42.42, 28.30; LRMS (ESI) calculated for C₁₆H₂₂N₃O₅ [M + H]⁺ m/z 336.16, found 336.09.

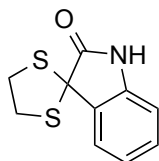


2-((tert-butoxycarbonyl)amino)-3-(2-oxo-2,3-dihydro-1H-benzo[d]imidazol-1-yl)propanoic acid (S111). **S110** (74.4 mg, 0.222 mmol, 1.0 equiv.) was reacted in methanol (5 mL) with 1M lithium hydroxide (444 uL, 0.444 mmol, 2.0 equiv.) according

to general procedure B. Semi-crude **S111** (70.2 mg, 99%) obtained as a white solid. LRMS (ESI) calculated for C₁₅H₁₈N₃O₅ [M - H]⁻ m/z 320.13, found 320.15.

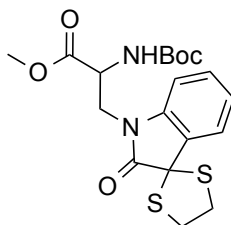


tert-butyl (1-((1H-tetrazol-5-yl)amino)-1-oxo-3-(2-oxo-2,3-dihydro-1H-benzo[d]imidazol-1-yl)propan-2-yl)carbamate (48). Semi-crude **S111** (70.2 mg, 0.218 mmol, 1.0 equiv.) was reacted with 5-aminotetrazole monohydrate (1.1 equiv.) in 2.5 mL DMF according to general procedure D (10m activation). **48** (8.4 mg, 10% over two steps) obtained as a white solid. ¹H NMR (400 MHz, DMSO-d₆) δ = 12.27 (br s, 1H), 10.91 (br s, 1H), 7.23 - 7.04 (m, 2H), 6.94 (br s, 3H), 4.54 (br d, J = 6.1 Hz, 1H), 4.25 - 4.03 (m, 2H), 1.28 (s, 9H); ¹³C NMR (100 MHz, DMSO-d₆) δ = 169.68 (br), 154.88, 154.57, 149.60 (br), 130.30, 128.27, 120.99, 120.40 (br), 108.77, 107.72, 78.74, 53.68 (br), 41.47, 27.94; LRMS (ESI) calculated for C₁₆H₁₉N₈O₄ [M - H]⁻ m/z 387.15, found 387.13.



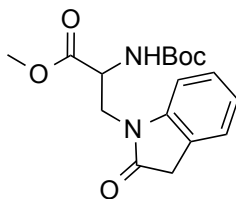
spiro[indoline-3,2'-[1,3]dithiolan]-2-one (S112). A dried 25 mL RB was charged with indoline-2,3-dione (200 mg, 1.36 mmol, 1.0 equiv.), then purged with Ar. Dry dichloromethane (6.5 mL) was then added, followed by 1,2-ethanedithiol (125 ul, 1.50 mmol, 1.1 equiv.). Boron trifluoride diethyl etherate (218 uL, 1.77 mmol, 1.3 equiv.) was

then added dropwise. The reaction mixture was allowed to stir at r.t. overnight. The crude reaction mixture was then directly purified on a silica column with 0-35% EtOAc:hexanes. **S112** (288.2 mg, 95%) obtained as a white solid. ^1H NMR (400 MHz, DMSO- d_6) δ = 10.62 (br s, 1H), 7.41 (dd, J = 0.7, 7.5 Hz, 1H), 7.25 (dt, J = 1.3, 7.7 Hz, 1H), 7.02 (dt, J = 1.0, 7.5 Hz, 1H), 6.85 (d, J = 7.8 Hz, 1H), 3.80 - 3.65 (m, 4H); ^{13}C NMR (100 MHz, DMSO- d_6) δ = 178.32, 141.57, 129.98, 126.62, 125.17, 122.37, 110.00, 61.98, 40.10; LRMS (ESI) calculated for $\text{C}_{10}\text{H}_{10}\text{NOS}_2$ $[\text{M} - \text{H}]^-$ m/z 224.02, found 224.00.



methyl 2-((tert-butoxycarbonyl)amino)-3-(2-oxospiro[indoline-3,2'-[1,3]dithiolan]-1-yl)propanoate (S113). A 20 mL vial was charged with crude **S109** (361.4 mg, 1.22 mmol, 1.0 equiv.), **S112** (271.4 mg, 1.22 mmol, 1.0 equiv.), cesium carbonate (792 mg, 2.43 mmol, 2.0 equiv.), and dry DMF (6 mL). The vial was sealed and stirred overnight. The crude reaction mixture was transferred to a sep. funnel with ~ 100 mL EtOAc and water, the layers separated, and the organic layer further extracted with 2 x 60 mL brine, dried over MgSO_4 , concentrated, and purified on a silica column with 0-35% EtOAc:hexanes. Semi-crude **S113** (335.8 mg, 65%) obtained as a yellow oil; contaminated with ~ 15% **S112** (^1H NMR). ^1H NMR (400 MHz, CDCl_3) δ = 7.49 (d, J = 7.3 Hz, 1H), 7.31 - 7.25 (m, 1H), 7.10 - 7.05 (m, 1H), 7.06 - 7.00 (m, 1H), 5.51 (br d, J = 7.3 Hz, 1H), 4.55 (q, J = 6.7 Hz, 1H), 4.08 - 4.03 (m, 1H), 4.02 - 3.94 (m, 1H), 3.88 -

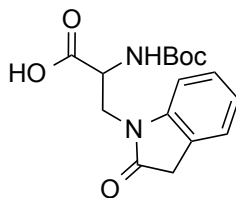
3.81 (m, 2H), 3.70 (s, 3H), 3.65 - 3.59 (m, 2H), 1.39 (s, 9H); ^{13}C NMR (100 MHz, CDCl_3) δ = 178.13, 170.43, 154.82, 142.06, 129.90, 125.91, 125.33, 123.22, 108.74, 79.97, 61.87, 52.87, 51.23, 41.69, 40.29, 40.18, 28.05; LRMS (ESI) calculated for $\text{C}_{19}\text{H}_{25}\text{N}_2\text{O}_5\text{S}_2$ $[\text{M} + \text{H}]^+$ m/z 425.12, found 425.04.



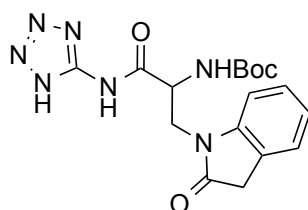
methyl 2-((tert-butoxycarbonyl)amino)-3-(2-oxoindolin-1-yl)propanoate (S114).

Semi-crude **S113** (335.8 mg, 0.791 mmol, 1.0 equiv.) was taken up in dry methanol (20 mL). Nickel(II) bromide ethylene glycol dimethyl ether complex (488 mg, 1.58 mmol, 2.0 equiv.) was then added; sodium borohydride (126 mg, 3.32 mmol, 4.2 equiv.) was then added portionwise (12 mg per) over 2h30m. **NOTE:** Sodium borohydride addition is very exothermic – do not add in bulk without sufficient thermal control. Once addition was complete, the crude reaction mixture was diluted with EtOAc and filtered through Celite. The organic washings were transferred to a sep. funnel and diluted with water; adjusted to pH 1 with 0.1N HCl. The layers were separated, and the organic layer was further washed with 2 x 60 mL brine. Dried over MgSO_4 , concentrated, and purified on a silica column with 0-15% acetone:dichloromethane. **S114** (116.4 mg, 29% over two steps) obtained as a white solid. ^1H NMR (400 MHz, CDCl_3) δ = 7.26 - 7.17 (m, 2H), 7.05 - 6.98 (m, 1H), 6.95 (br d, J = 7.8 Hz, 1H), 5.53 (br d, J = 6.8 Hz, 1H), 4.54 (q, J = 5.8 Hz, 1H), 4.05 (br d, J = 5.6 Hz, 2H), 3.71 (s, 3H), 3.48 (s, 2H), 1.37 (s, 9H); ^{13}C NMR (100 MHz, CDCl_3) δ = 175.67, 170.55, 155.01, 144.11, 127.81, 124.32, 124.18, 122.40,

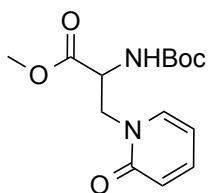
108.33, 79.96, 52.69, 52.22, 41.58, 35.32; LRMS (ESI) calculated for C₁₇H₂₃N₂O₅ [M + H]⁺ m/z 335.16, found 335.03.



2-((tert-butoxycarbonyl)amino)-3-(2-oxoindolin-1-yl)propanoic acid (S115). **S114** (116.4 mg, 0.348 mmol, 1.0 equiv.) was reacted in methanol (5 mL) with 1M lithium hydroxide (696 μ L, 0.696 mmol, 2.0 equiv.) according to general procedure B. Semi-crude **S115** (107.6 mg, 97%) obtained as a tan solid. LRMS (ESI) calculated for C₁₆H₁₉N₂O₅ [M - H]⁻ m/z 319.13, found 319.39.

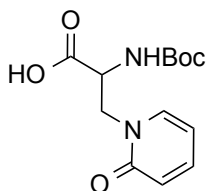


tert-butyl (1-((1H-tetrazol-5-yl)amino)-1-oxo-3-(2-oxoindolin-1-yl)propan-2-yl)carbamate (49). Semi-crude **S115** (50.0 mg, 0.156 mmol, 1.0 equiv.) was reacted with 5-aminotetrazole monohydrate (1.1 equiv.) in 2 mL DMF according to general procedure D (10m activation). **49** (16.9 mg, 13% over two steps) obtained as a light tan solid. ¹H NMR (400 MHz, DMSO-d₆) δ = 12.25 (br s, 0.5H), 7.30 - 7.11 (m, 2H), 7.06 - 6.90 (m, 2H), 4.50 (br s, 1H), 4.11 - 3.88 (m, 2H), 3.49 (br s, 2H), 1.28 (br s, 9H); ¹³C NMR (100 MHz, DMSO-d₆) δ = 175.01, 169.79 (br), 154.94 (br), 149.51 (br), 144.22, 127.30, 124.61, 124.21, 121.82, 108.35, 78.75, 52.58 (br), 40.80 (br), 34.98, 27.95; LRMS (ESI) calculated for C₁₇H₂₀N₇O₄ [M - H]⁻ m/z 386.16, found 386.29.



methyl 2-((tert-butoxycarbonyl)amino)-3-(2-oxopyridin-1(2H)-yl)propanoate (S116).

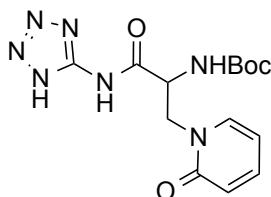
A 3 mL vial was charged with crude **S109** (328.3 mg, 1.10 mmol, 1.0 equiv.), 2-hydroxypyridine (105 mg, 1.10 mmol, 1.0 equiv.), cesium carbonate (720 mg, 2.21 mmol, 2.0 equiv.), and dry DMF (2 mL). The vial was sealed and heated at 100 °C overnight. The crude reaction mixture was transferred to a sep. funnel with ~ 100 mL EtOAc and water, and the aqueous pH was adjusted to 7 with 0.1N HCl. The layers were separated, and the organic layer was further washed with 2 x 50 mL brine, dried over MgSO₄, concentrated, and purified on a silica column with 0-70% EtOAc:hexanes. **S116** (24.6 mg, 8%) obtained as a gray film. ¹H NMR (400 MHz, CDCl₃) δ = 7.33 (br t, *J* = 7.3 Hz, 1H), 7.22 (br d, *J* = 6.6 Hz, 1H), 6.54 (br d, *J* = 9.0 Hz, 1H), 6.15 (t, *J* = 6.6 Hz, 1H), 5.77 (br d, *J* = 5.8 Hz, 1H), 4.64 - 4.48 (m, 1H), 4.34 (br d, *J* = 2.4 Hz, 2H), 3.76 (s, 3H), 1.39 (s, 9H); ¹³C NMR (100 MHz, CDCl₃) δ = 170.38, 163.14, 155.30, 139.98, 138.26, 120.83, 106.11, 80.13, 53.33, 52.73, 50.33, 28.17; LRMS (ESI) calculated for C₁₄H₂₁N₂O₅ [M + H]⁺ m/z 297.14, found 297.15.



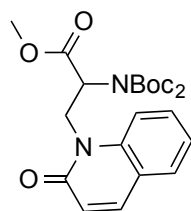
2-((tert-butoxycarbonyl)amino)-3-(2-oxopyridin-1(2H)-yl)propanoic acid (S117).

S116 (42.6 mg, 0.144 mmol, 1.0 equiv.) was reacted in methanol (3 mL) with 1M lithium

hydroxide (288 μL , 0.288 mmol, 2.0 equiv.) according to general procedure B (5h). Semi-crude **S117** (29.7 mg, 73%) obtained as a brown film. LRMS (ESI) calculated for $\text{C}_{13}\text{H}_{17}\text{N}_2\text{O}_5$ $[\text{M} - \text{H}]^-$ m/z 281.11, found 281.29.

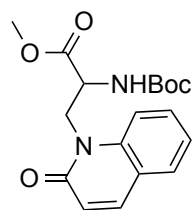


tert-butyl (1-((1H-tetrazol-5-yl)amino)-1-oxo-3-(2-oxopyridin-1(2H)-yl)propan-2-yl)carbamate (50). Semi-crude **S117** (29.7 mg, 0.105 mmol, 1.0 equiv.) was reacted with 5-aminotetrazole monohydrate (1.1 equiv.) in 2 mL DMF according to general procedure D (20m activation). **50** (12.9 mg, 26% over two steps) obtained as a tan solid. ^1H NMR (400 MHz, CD_3OD) δ = 7.53 (br s, 2H), 6.56 (br d, J = 8.5 Hz, 1H), 6.38 (br d, J = 5.6 Hz, 1H), 4.83 (br s, 1H), 4.71 - 4.56 (m, 1H), 4.19 - 3.96 (m, 1H), 1.37 (s, 9H); ^{13}C NMR (100 MHz, CDCl_3) δ = 170.77 (br), 165.27 (br), 157.54 (br), 151.49 (br), 142.68, 140.75 (br), 120.97 (br), 108.75, 81.40, 54.47 (br), 52.18 (br), 28.72; LRMS (ESI) calculated for $\text{C}_{14}\text{H}_{18}\text{N}_7\text{O}_4$ $[\text{M} - \text{H}]^-$ m/z 348.14, found 348.24.

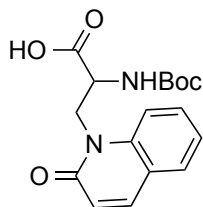


methyl 2-(bis((tert-butoxy)carbonyl)amino)-3-(2-oxo-1,2-dihydroquinolin-1-yl)propanoate (S118). A 3 mL vial was charged with **S105** (200.0 mg, 0.664, 1.0 equiv.), 2-hydroxyquinolone (99 mg, 0.684 mmol, 1.03 equiv.), and dry acetonitrile (2 mL). Cesium carbonate (22 mg, 0.066 mmol, 0.1 equiv.) was then added, and the vial

was sealed and heated at 80 °C overnight. The crude reaction mixture was transferred to a sep. funnel with ~ 100 mL EtOAc and washed with ~ 50 mL water and brine; the organic layer was dried over MgSO₄, concentrated, and purified on a silica column with 30-80% EtOAc:hexanes. **S118** (108.9 mg, 3789%) obtained as a colorless oil. ¹H NMR (400 MHz, CDCl₃) δ = 7.64 - 7.58 (m, 1H), 7.52 - 7.47 (m, 1H), 7.46 - 7.37 (m, 2H), 7.19 - 7.12 (m, 1H), 6.64 - 6.58 (m, 1H), 5.53 - 5.46 (m, 1H), 5.11 - 4.99 (m, 1H), 4.83 (br dd, *J* = 3.0, 14.5 Hz, 1H), 3.75 (br s, 3H), 1.27 (s, 18H); ¹³C NMR (100 MHz, CDCl₃) δ = 169.24, 162.17, 151.36, 139.74, 139.24, 130.47, 128.89, 121.97, 121.35, 120.70, 113.58, 83.07, 56.00, 52.24, 42.06, 27.51; LRMS (ESI) calculated for C₂₃H₃₁N₂O₇ [M + H]⁺ m/z 447.21, found 447.07.

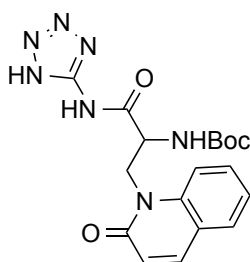


methyl 2-((tert-butoxycarbonyl)amino)-3-(2-oxoquinolin-1(2H)-yl)propanoate (S119). A 20 mL vial was charged with **S118** (108.9 mg, 0.244, 1.0 equiv.) and dry acetonitrile (2.45 mL). Lithium bromide (64 mg, 0.732 mmol, 3.0 equiv.) was then added, and the vial was sealed and heated at 65 °C overnight. The crude reaction mixture was transferred to a sep. funnel with EtOAc and partitioned with water; the layers were separated, and the aqueous layer was further extracted with 2 x 50 mL EtOAc. The organics were combined, dried over MgSO₄, and concentrated. Crude **S119** (82.8 mg, 98%) obtained as a colorless oil. LRMS (ESI) calculated for C₁₈H₂₃N₂O₅ [M + H]⁺ m/z 347.16, found 347.10.



2-((tert-butoxycarbonyl)amino)-3-(2-oxoquinolin-1(2H)-yl)propanoic acid (S120).

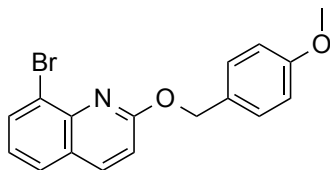
Crude **S119** (82.8 mg, 0.239 mmol, 1.0 equiv.) was reacted in methanol (5 mL) with 1M lithium hydroxide (478 μ L, 0.478 mmol, 2.0 equiv.) according to general procedure B. Semi-crude **S120** (69.9 mg, 88%) obtained as a tan solid. LRMS (ESI) calculated for $C_{17}H_{19}N_2O_5$ $[M - H]^-$ m/z 331.13, found 331.01.



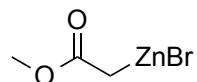
tert-butyl (1-((1H-tetrazol-5-yl)amino)-1-oxo-3-(2-oxoquinolin-1(2H)-yl)propan-2-yl)carbamate (51). Semi-crude **S120** (69.9 mg, 0.210 mmol, 1.0 equiv.) was reacted with 5-aminotetrazole monohydrate (1.1 equiv.) in 2.5 mL DMF according to general procedure D (20m activation). **51** (29.0 mg, 30% over 3 steps) obtained as a white solid.

Note: Slight atropisomerism observed by NMR. 1H NMR (400 MHz, $DMSO-d_6$) δ = 12.32 (br s, 0.3H), 12.22 (br s, 0.7H), 7.92 (d, J = 9.5 Hz, 1H), 7.71 (br d, J = 7.5 Hz, 1H), 7.64 - 7.54 (m, 2H), 7.25 (br t, J = 6.8 Hz, 1H), 7.16 (br d, J = 6.6 Hz, 0.7H), 6.60 (d, J = 9.5 Hz, 1H), 4.68 - 4.48 (m, 3H), 1.25 (s, 7.5H), 1.09 (br s, 1.5H); ^{13}C NMR (100 MHz, $DMSO-d_6$) δ = 169.94, 161.84, 154.96, 149.61 (br), 140.05, 139.36, 130.69,

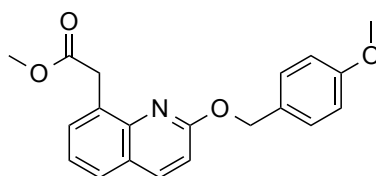
129.05, 122.08, 120.78, 120.48, 114.36, 78.76, 52.78, 42.75, 27.93; LRMS (ESI) calculated for C₁₈H₂₀N₇O₄ [M - H]⁻ m/z 398.16, found 398.14.



8-bromo-2-((4-methoxybenzyl)oxy)quinolone (S121). A dried 25 mL RB was charged with commercially available 8-bromoquinolin-2(1*H*)-one (200 mg, 0.893 mmol, 1.0 equiv.) and dry DMF (8 mL). The reaction mixture was cooled to 0 °C, and 60.0% sodium hydride (43 mg, 1.07 mmol, 1.2 equiv.) was added, followed by a 1 mL rinse of dry DMF. The bubbling suspension was immediately warmed to r.t. and allowed to stir for 30m, at which point 4-methoxybenzylchloride (157 μ L, 1.16 mmol, 1.3 equiv.) was added dropwise. The reaction mixture was stirred at 60 °C overnight. **Note:** Heating NaH/DMF is unsafe, especially at larger scales – take appropriate care. The crude reaction mixture was transferred to a sep. funnel with ~ 100 mL EtOAc and diluted with sat. NH₄Cl. The layers were separated, and the organic layer was washed with additional 2 x 50 mL brine, dried over MgSO₄, and concentrated. Purified on a silica column with 0-25% EtOAc:hexanes. **S121** (241.6 mg, 79%) obtained as a light pink solid. ¹H NMR (400 MHz, CDCl₃) δ = 8.00 - 7.90 (m, 2H), 7.67 - 7.60 (m, 3H), 7.22 (t, *J* = 7.8 Hz, 1H), 6.96 (d, *J* = 8.5 Hz, 3H), 5.63 (s, 2H), 3.83 (s, 3H); ¹³C NMR (100 MHz, CDCl₃) δ = 162.15, 159.40, 143.49, 139.10, 132.95, 130.63, 129.12, 127.01, 126.12, 124.28, 122.40, 113.99, 113.70, 67.69, 55.13; LRMS (ESI) calculated for C₁₇H₁₄BrNNaO₂ [M + Na]⁺ m/z 366.01, found 365.94.

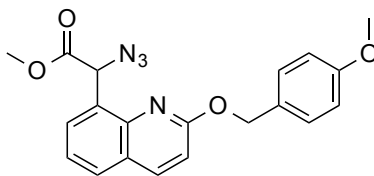


(2-methoxy-2-oxoethyl)zinc(II) bromide (S122). A dried 25 mL pear-shaped RB was charged with zinc powder (415 mg, 6.35 mmol, 2.0 equiv.), then purged with Ar. Dry tetrahydrofuran (12.7 mL) was then added, followed by dropwise addition of chlorotrimethylsilane (40 μ l, 0.318 mmol, 0.1 equiv.). The suspension was allowed to stir at r.t. for 20m, then heated to 45 °C. Methyl bromoacetate (300 μ l, 3.17 mmol, 1.0 equiv.) was then added dropwise, and the reaction was allowed to stir at 45 °C for 45 minutes, then cooled to r.t. The remaining Zn was allowed to settle. The resulting yellow solution was used as a 250 mM stock for couplings. **Note:** The solution was made fresh for couplings; begins to lose coloration ~ 12h at r.t./Ar.

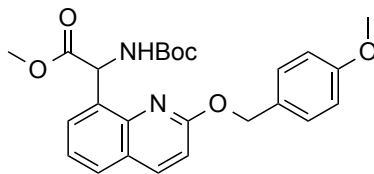


methyl 2-(2-((4-methoxybenzyl)oxy)quinolin-8-yl)acetate (S123). A 20 mL vial was charged with **S121** (266 mg, 0.773 mmol, 1.0 equiv.), tris(dibenzylideneacetone)dipalladium (35.4 mg, 0.039 mmol, 0.05 equiv.), and QPhos (27.5 mg, 0.039 mmol, 0.05 equiv.). The vial was fitted with a septa, purged with Ar, and dry tetrahydrofuran (3 mL) was added, followed by a 0.25M solution of **S122** (3.712 mL, 0.928 mmol, 1.2 equiv.) in THF. The septa was replaced with a teflon cap and the vial was heated at 70 °C overnight. The crude reaction mixture was transferred to a sep. funnel with ~ 100 mL EtOAc and washed with sat. NaHCO₃ and brine, dried over MgSO₄, and concentrated. Purified on a silica column with 0-25% EtOAc:hexanes.

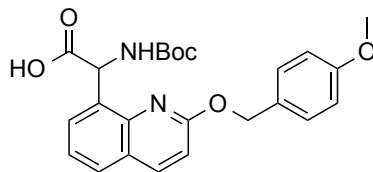
S123 (247.4 mg, 95%) obtained as a light pink solid. ^1H NMR (400 MHz, CDCl_3) δ = 7.96 (d, J = 9.0 Hz, 1H), 7.66 (dd, J = 1.2, 8.0 Hz, 1H), 7.60 (d, J = 7.1 Hz, 1H), 7.57 - 7.52 (m, 2H), 7.37 (dd, J = 7.3, 8.0 Hz, 1H), 7.02 - 6.95 (m, 3H), 5.53 (s, 2H), 4.22 (s, 2H), 3.82 (s, 3H), 3.75 (s, 3H); ^{13}C NMR (100 MHz, CDCl_3) δ = 172.42, 160.92, 159.16, 144.48, 138.83, 131.23, 130.25, 129.70, 129.25, 126.68, 124.74, 123.40, 113.61, 112.90, 67.13, 54.90, 51.48, 37.33; LRMS (ESI) calculated for $\text{C}_{20}\text{H}_{19}\text{NNaO}_4$ [$\text{M} + \text{Na}$] $^+$ m/z 360.12, found 360.01.



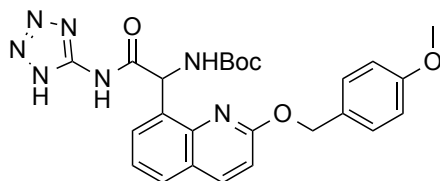
methyl 2-azido-2-(2-((4-methoxybenzyl)oxy)quinolin-8-yl)acetate (S124). **S123** (180.1 mg, 0.534 mmol, 1.0 equiv.) was reacted in 15 mL tetrahydrofuran according to general procedure F. **Note:** The generated enolate was not soluble in THF; rapid stirring of a thick suspension required. **S124** (66.5 mg, 33%) obtained as a white solid. ^1H NMR (400 MHz, CDCl_3) δ = 8.03 (d, J = 9.0 Hz, 1H), 7.78 (dd, J = 1.2, 8.0 Hz, 1H), 7.68 (dd, J = 1.2, 7.3 Hz, 1H), 7.47 (d, J = 8.5 Hz, 2H), 7.45 - 7.40 (m, 1H), 7.00 (d, J = 8.8 Hz, 1H), 6.97 - 6.92 (m, 2H), 5.98 (s, 1H), 5.53 - 5.40 (m, 2H), 3.83 (s, 3H), 3.76 (s, 3H); ^{13}C NMR (100 MHz, CDCl_3) δ = 170.25, 161.74, 159.46, 143.71, 139.16, 130.82, 129.90, 129.09, 129.04, 128.85, 125.30, 123.73, 113.96, 113.90, 68.00, 61.47, 55.26, 52.68; LRMS (ESI) calculated for $\text{C}_{20}\text{H}_{18}\text{N}_4\text{NaO}_4$ [$\text{M} + \text{Na}$] $^+$ m/z 401.12, found 400.95.



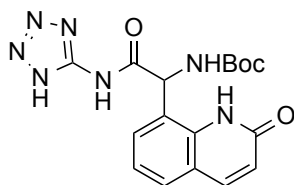
methyl 2-((tert-butoxycarbonyl)amino)-2-(2-((4-methoxybenzyl)oxy)quinolin-8-yl)acetate (S125). A round bottom flask was charged with **S124** (66.5 mg, 0.176 mmol, 1.0 equiv.) and dry methanol (6 mL). Anhydrous tin(II) chloride (67 mg, 0.351 mmol, 2.0 equiv.) was then added; stirred at r.t. for 68h. The crude reaction mixture was transferred to a sep. funnel with ~ 75 mL EtOAc and partitioned with 75 mL sat. NaHCO₃. The aqueous layer was extracted with an additional 2 x 50 mL EtOAc; the organics were combined, dried over MgSO₄, and concentrated. The resulting residue was taken up tetrahydrofuran (2.5 mL); solid di-tert-butyl dicarbonate (46 mg, 0.211 mmol, 1.2 equiv.) was then added, followed by dropwise addition of *N,N*-diisopropylethylamine (37 ul, 0.211 mmol, 1.2 equiv.). The reaction mixture was stirred for 14h, at which point it was transferred to a sep. funnel with ~75 mL EtOAc and washed with ~50 mL sat. NaHCO₃ and brine. The EtOAc layer was dried over MgSO₄ and concentrated -- purified on a silica column with 0-30% EtOAc:hexanes. **S125** (47.2 mg, 59%) obtained as a white solid. ¹H NMR (400 MHz, CDCl₃) δ = 8.01 (d, *J* = 8.8 Hz, 1H), 7.76 - 7.61 (m, 2H), 7.48 (d, *J* = 8.5 Hz, 2H), 7.38 (dd, *J* = 7.3, 8.0 Hz, 1H), 7.01 - 6.91 (m, 3H), 6.20 (br d, *J* = 9.3 Hz, 1H), 5.81 (d, *J* = 9.5 Hz, 1H), 5.49 (d, *J* = 12.4 Hz, 1H), 5.34 (d, *J* = 12.4 Hz, 1H), 3.82 (s, 3H), 3.65 (s, 3H), 1.45 (s, 9H); ¹³C NMR (100 MHz, CDCl₃) δ = 172.07, 161.47, 159.35, 155.49, 143.64, 139.37, 133.66, 130.80, 129.47, 129.14, 127.86, 125.29, 123.96, 113.95, 113.44, 79.72, 67.80, 56.39, 55.20, 52.44, 28.34; LRMS (ESI) calculated for C₂₅H₂₉N₂O₆ [M + H]⁺ m/z 453.20, found 453.15.



2-((tert-butoxycarbonyl)amino)-2-(2-((4-methoxybenzyl)oxy)quinolin-8-yl)acetic acid (S126). **S125** (47.2 mg, 0.104 mmol, 1.0 equiv.) was reacted in methanol (4 mL) with 1M sodium hydroxide (146 μ L, 0.146 mmol, 1.4 equiv.) according to general procedure B, except three additional aliquots of 1M sodium hydroxide (146 μ L, 0.146 mmol, 1.4 equiv.) were added over 3d. Semi-crude **S126** (47.2 mg, 103%) obtained as a white solid. LRMS (ESI) calculated for $C_{24}H_{25}N_2O_6$ $[M - H]^-$ m/z 437.17, found 437.04.



tert-butyl (2-((1H-tetrazol-5-yl)amino)-1-(2-((4-methoxybenzyl)oxy)quinolin-8-yl)-2-oxoethyl)carbamate (S127). Semi-crude **S126** (45.7 mg, 0.104 mmol, 1.0 equiv.) was reacted with 5-aminotetrazole monohydrate (1.1 equiv.) in 3 mL DMF according to general procedure D (1h activation). **S127** (23.0 mg, 43% over two steps) obtained as a white solid. 1H NMR (400 MHz, $DMF-d_7$) δ = 12.46 (br s, 1H), 8.35 (d, J = 9.0 Hz, 1H), 7.95 (d, J = 7.8 Hz, 1H), 7.85 (d, J = 7.1 Hz, 1H), 7.61 (br d, J = 8.5 Hz, 1H), 7.55 - 7.42 (m, 3H), 7.10 (d, J = 8.8 Hz, 1H), 6.98 (d, J = 8.5 Hz, 2H), 6.53 (d, J = 8.5 Hz, 1H), 5.55 - 5.38 (m, 2H), 3.83 (s, 3H), 1.44 (s, 9H); ^{13}C NMR (100 MHz, $DMF-d_7$) δ = 172.01, 162.59, 160.65, 156.75, 151.74, 144.94, 141.09, 134.51, 131.14, 130.66, 130.31, 129.26, 126.38, 124.95, 114.87, 114.35, 79.79, 68.77, 56.89, 55.98, 28.87; LRMS (ESI) calculated for $C_{25}H_{26}N_7O_5$ $[M - H]^-$ m/z 504.20, found 504.22.



tert-butyl (2-((1*H*-tetrazol-5-yl)amino)-2-oxo-1-(2-oxo-1,2-dihydroquinolin-8-yl)ethyl)carbamate (**52**). **S127** (23.0 mg, 0.045 mmol, 1.0 equiv.) was suspended in acetonitrile (4 mL) and water (1 mL). Ammonium cerium(IV) nitrate (224 mg, 0.409 mmol, 9.0 equiv.) was then added in 1.0 equiv. aliquots (25 mg) over 5h. After complete conversion, the crude reaction mixture was transferred to a sep. funnel with EtOAc and water. The layers were separated, and the aqueous layer was further extracted with 2 x 50 mL EtOAc. The organics were combined, dried over MgSO₄, and concentrated. Purified by reverse phase HPLC (water/MeOH/0.05% formic acid) to afford **52** (11.3 mg, 64%) as a white solid. ¹H NMR (400 MHz, DMSO-d₆) δ = 12.42 (br s, 1H), 10.79 (br s, 1H), 8.04 (br s, 1H), 7.96 (d, *J* = 9.5 Hz, 1H), 7.68 (d, *J* = 7.3 Hz, 1H), 7.55 (br d, *J* = 6.8 Hz, 1H), 7.21 (t, *J* = 7.7 Hz, 1H), 6.57 (d, *J* = 9.5 Hz, 1H), 5.83 (br s, 1H), 1.39 (br s, 9H); ¹³C NMR (100 MHz, DMSO-d₆) δ = 169.41 (br), 161.75, 155.55 (br), 149.72 (br), 141.01, 136.96 (br), 130.84 (br), 128.90 (br), 121.98 (br), 121.74, 121.62 (br), 119.93 (br), 79.16, 54.55 (br), 28.10 (br); LRMS (ESI) calculated for C₁₇H₁₈N₇O₄ [M - H]⁻ *m/z* 384.14, found 384.09.

Chapter 5

Fragment Discovery for Diverse β -lactamases

Fragment Screening:

Our previous synthetic efforts to inhibit new β -lactamases were primarily structure-guided migrations from the original CTX-M series, as discussed in **Chapters 1** and **4**. Despite the homology between KPC-2 and CTX-M, these efforts failed to generate an inhibitor scaffold that could target both enzymes. While the resulting scaffold from **Chapter 4** could likely be modified to do so, inhibiting more diverse β -lactamases, such as the metallo-lactamase NDM-1 or the Class D OXA-48, proves to be quite challenging due to the lack of tractable knowledge around non-covalent affinity with these enzymes. Computational screening against CTX-M resulted in chemotypes with cross-class activity (**Chapter 2**), but these molecules were already quite large with poor ligand efficiency (LE), representing a suboptimal approach to gain insight into molecular recognition. To this end, we felt comparative fragment screening offered the best approach, as fragment hits would have higher LE, representing discrete molecular interactions, and cross-class hits would likely bind within a shared substrate envelope, making further optimization tractable. Importantly, these efforts are also backed by robust crystallography, allowing us to view the binding orientation for hits and any subsequent fragment enumeration.

We opted to use surface plasmon resonance (SPR) as our primary screen due to the throughput and material requirements; SPR also allows for subsequent “pair-wise” binding and competition experiments for confirmed hits. In order to validate the approach, various N-terminal tagged His-Avi(Biotin) proteins were immobilized onto a Neutravidin conjugated GE CM5 chip and tested with putative positive controls, which are necessary to adjust for surface degradation throughout the screening run. CTX-M-

14 immobilized well; the positive control was our previously reported compound **1**,¹ which displayed a K_d of 160 nM, in line with our observed K_i of 90 nM (**Figure 5-1**). Importantly, compound **1** binding could be ablated by preincubation with avibactam prior to immobilization, combined with 5 μ M avibactam in the running buffer (CTX-M $t_{1/2}$: ~ 40 m),² suggesting the binding of **1** accurately represents the state of the active site. While carbapenemase KPC-2 immobilized well, we could not bind inhibitor **1**, which has a weaker affinity for KPC-2,³ as well as β -lactam substrates meropenem or nitrocefin. Attempts to alter the buffer composition or temperature did not restore substrate binding; non-specific immobilization with EDC/NHS also failed to produce substrate-active KPC-2. Given these results, we decided that any fragment hit would be assessed for KPC-2 activity at the biochemical validation stage. Metallo-lactamase NDM-1 has been previously used in SPR experiments,⁴ and we confirmed that when immobilized, it recognizes substrate meropenem (not shown). Meropenem has aqueous stability issues making it ill suited for a screening control,⁵ so captopril was tested. Notably, purchased captopril required TCEP in the running buffer, and displayed a two-site binding curve, consistent with the presence of an L and D form (**Figure 5-2**). The observed K_d values were close to the previously reported IC_{50} values,⁶ suggesting captopril would be a reasonable proxy for protein state. OXA-48 has also been used in SPR experiments,⁷ and when immobilized, recognized substrate meropenem (not shown). Substrate binding could be ablated by preincubation with avibactam prior to immobilization (OXA-48 $t_{1/2}$: 17h),² suggesting functional enzyme (not shown). Given the stability of meropenem, we sought to use compound **2** as a control, which was discovered from a previously reported fragment screen.⁷ In our hands compound **2** showed a two-site

binding curve, with a K_{d1} : 28 μM / Stoichiometry: 1 for “site one”, in line with the reported K_d ; “site two” was a weaker, non-specific binding element with some reference channel binding (**Figure 5-3**). Like other positive controls, “site-one” binding could be ablated by preincubation with avibactam prior to immobilization, leaving only the nonspecific binding elements. While imperfect as a control, we felt that sufficiently low concentrations of **2** should approximate active site availability in OXA-48.

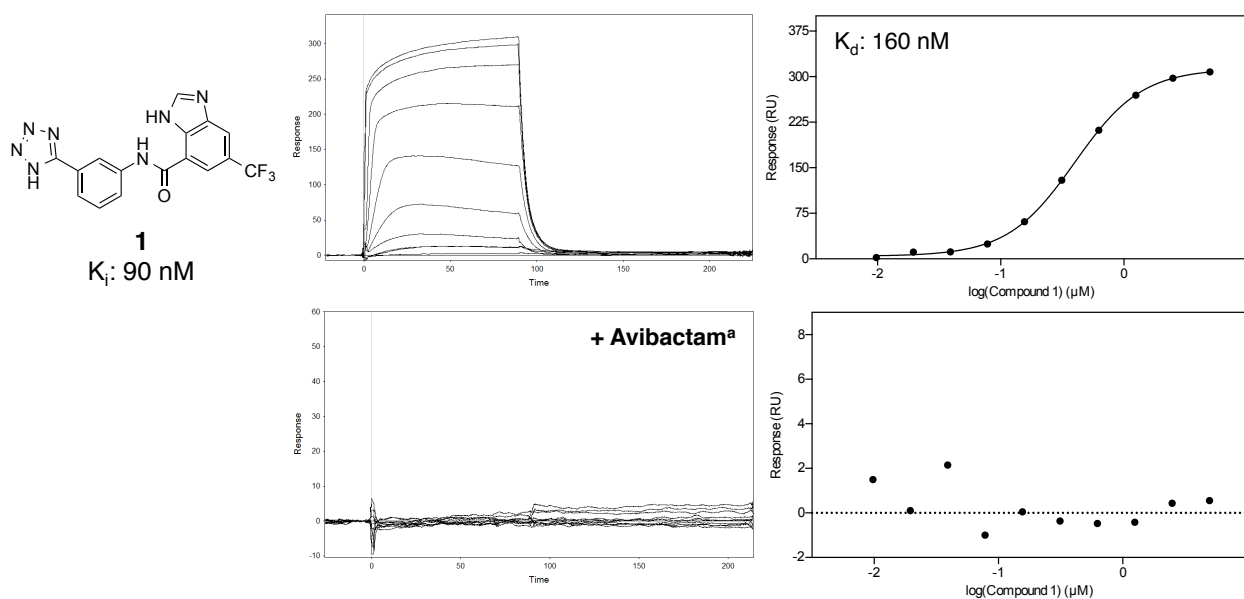
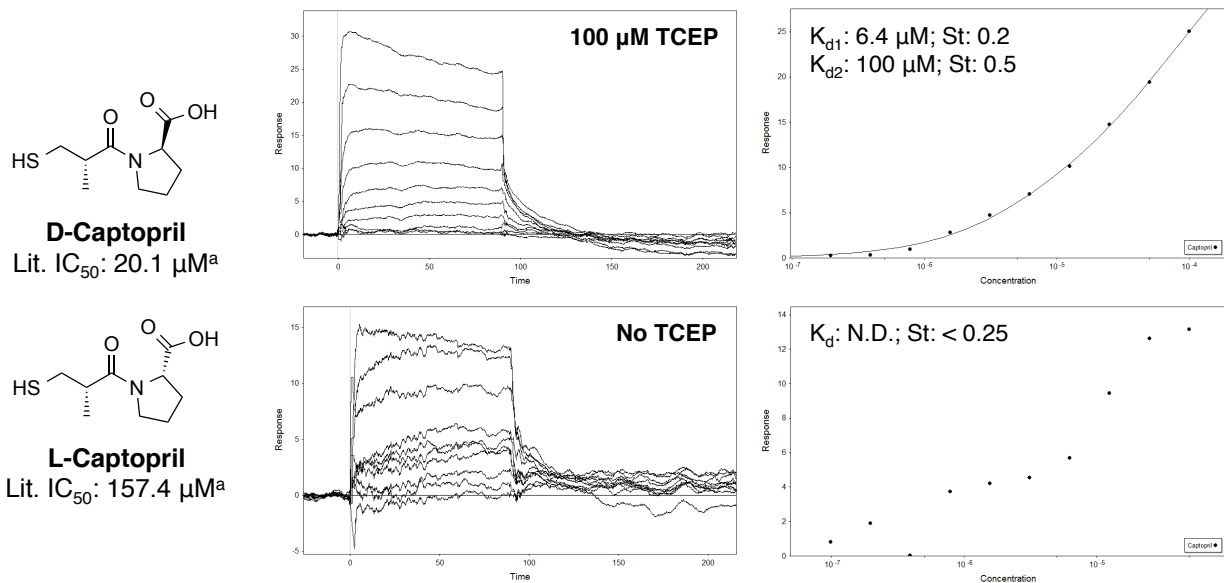


Figure 5-1. Compound 1 binding to CTX-M-14. ^a Compound **1** binding could be ablated by preincubation with avibactam prior to immobilization, combined with 5 μM avibactam in the running buffer.



With controls in hand, we screened CTX-M, NDM-1, and OXA-48 against two fragment libraries totaling ~ 4300 fragments. Our internal library was assembled from commercial fragments available from Maybridge, Life Chemicals, and Asinex; the Drug Discovery Unit (DDU) at University of Dundee also provided a bespoke library, which is structurally distinct and complementary to ours, and in particular possesses a higher proportion of fragments with saturated (sp^3) hybridized carbon atoms (**Figure 5-4**). We anticipate that this second library will help reveal distinct consensus binding interactions, especially when considering the types of scaffolds preferred in **Chapter 4**. Once complete, the primary screening data was loess normalized for surface degradation and inter-assay variability using RALPH.⁸ The resulting scatterplots are shown below with initial hits denoted in red, as defined per boxplot cutoff (75^{th} percentile + $3 \times \text{IQR}$) (**Figure 5-5**).

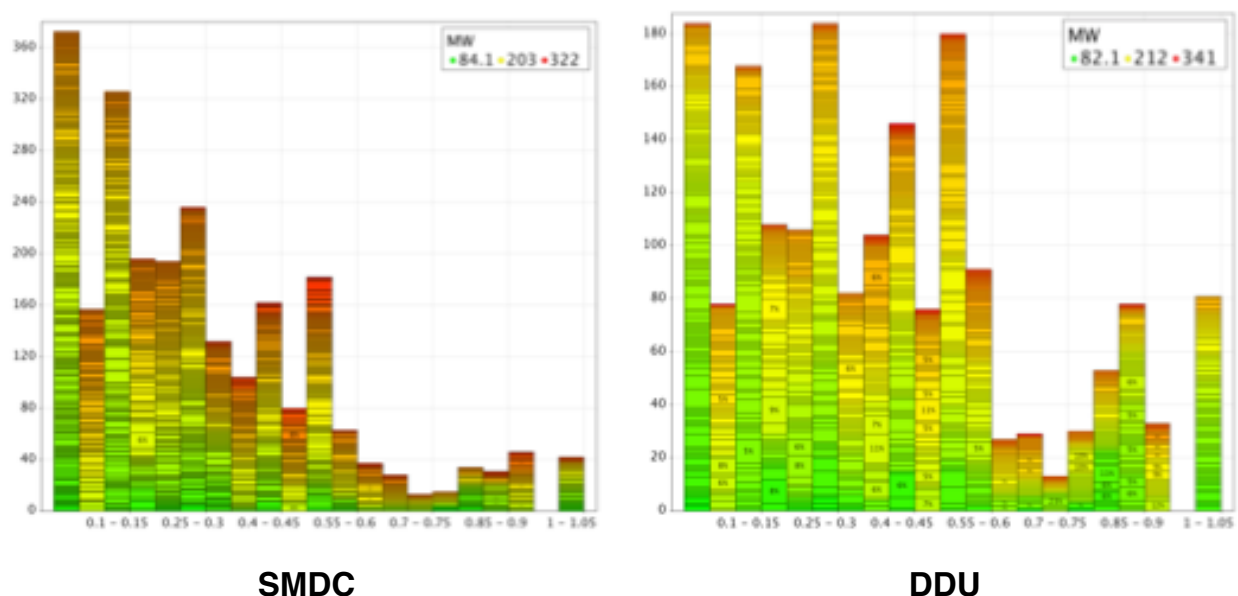
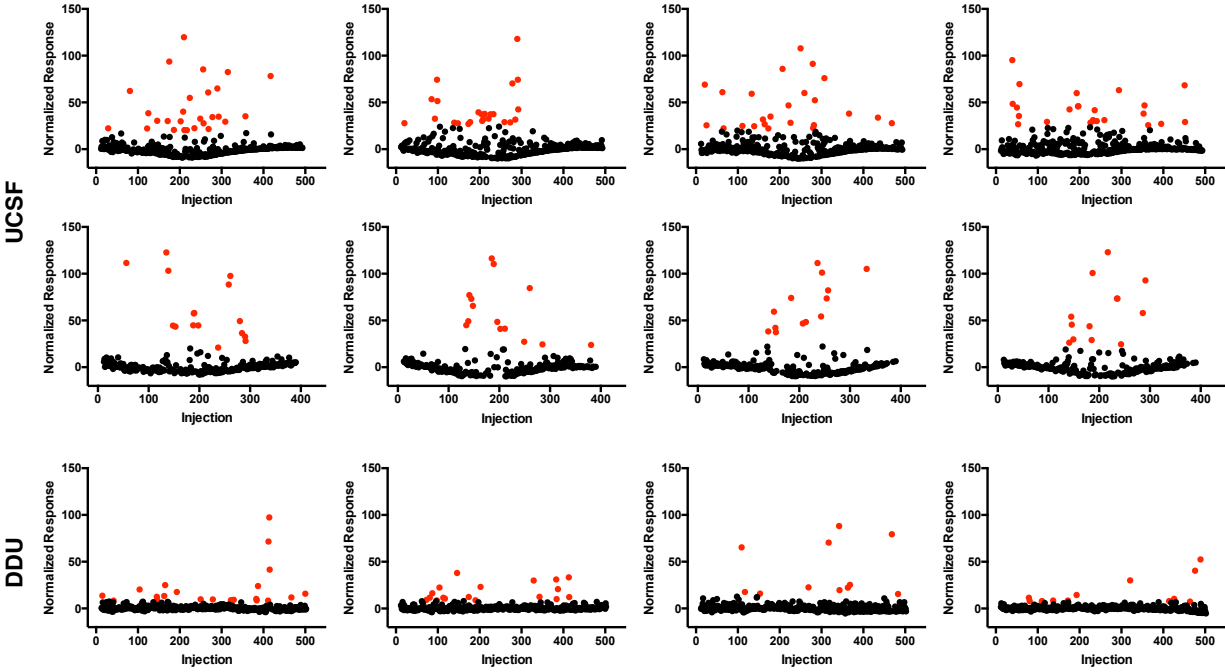
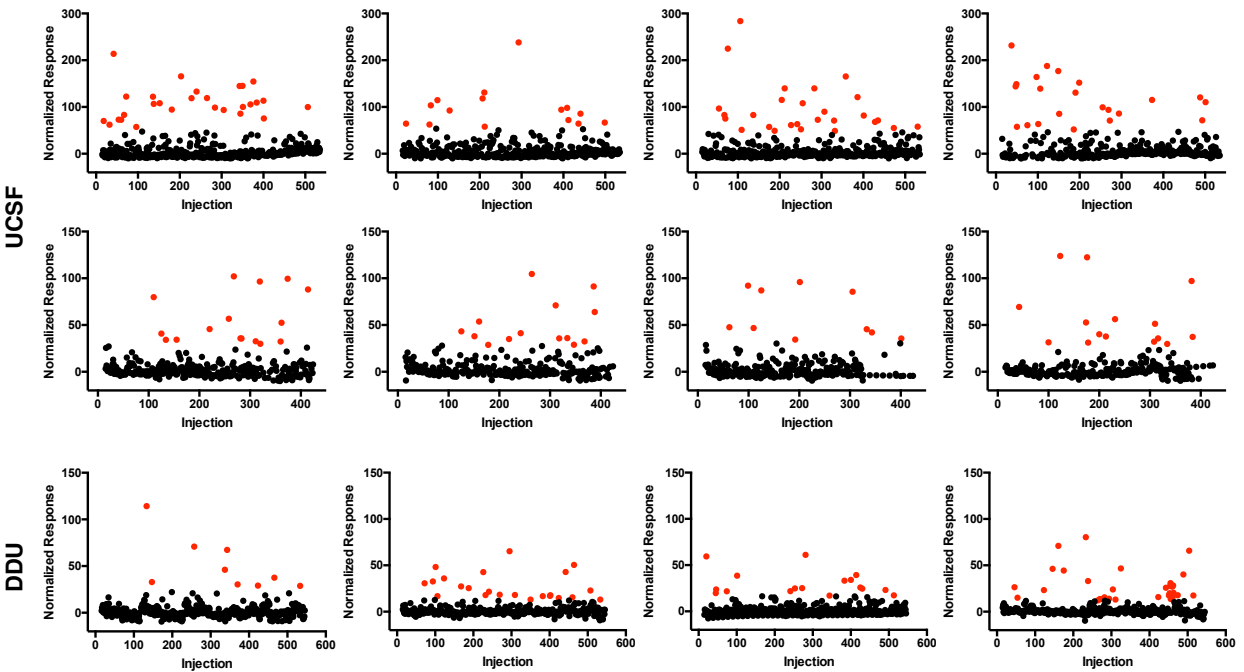


Figure 5-4. Histogram analysis of both fragment libraries. Fraction of sp^3 atoms (0.1-1; x-axis) and molecular weight (color) distribution of fragments in the SMDC and DDU libraries.

CTX-M-14



NDM-1



OXA-48

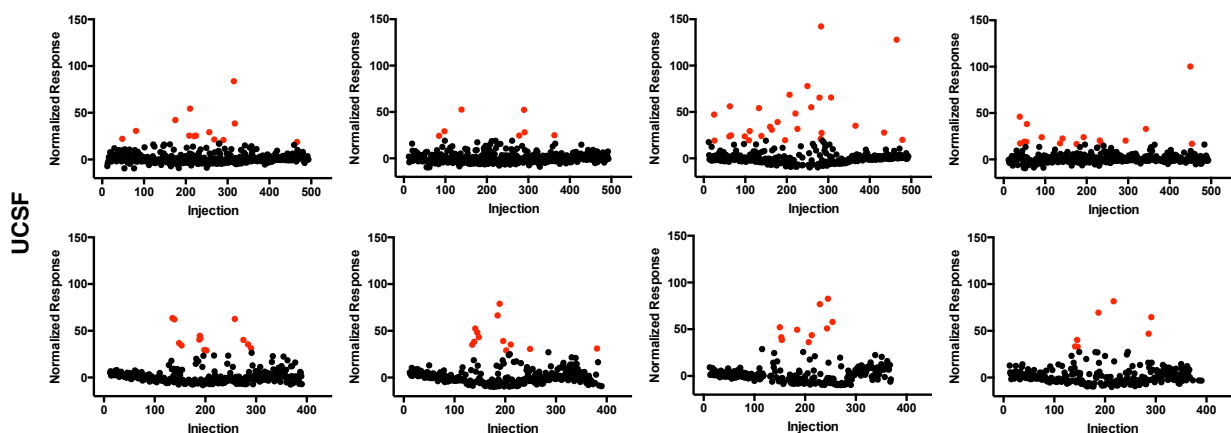


Figure 5-5. Primary screening scatterplots for CTX-M-14, NDM-1, and OXA-48. Solvent corrected data was less normalized for surface degradation and variability per flow cell. Initial hits denoted in red, as defined per boxplot cutoff (75^{th} percentile + $3 \times \text{IQR}$). The DDU fragment collection still needs to be screened against OXA-48.

Fragment Validation:

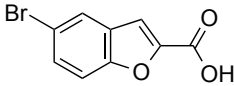
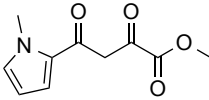
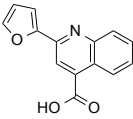
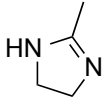
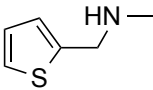
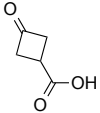
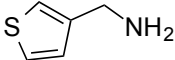
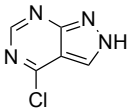
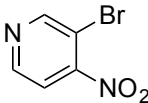
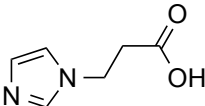
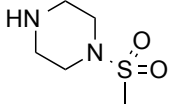
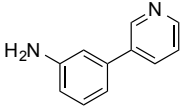
Screening hit rates were roughly equivalent between libraries and enzymes, averaging to about 5% (**Table 5-1**). One of the drawbacks of an unbiased SPR screen is false-positives; fragments are more promiscuous binders by virtue, and can bind allosterically or non-specifically elsewhere in the protein, incorrectly reporting as a hit. In order to weed out non-functional molecules, hits were pooled and tested for biochemical activity in single point response against all enzymes. While this work is still in progress, early results from our internal library are encouraging (**Table 5-2**). Though few of the tested compounds possess tri-class activity, many inhibit two classes, suggesting conserved binding hotspots. Some of the fragments even possess mid- μM activity, especially against OXA-48, which has been challenging to link with Class A active scaffolds. Perhaps unsurprisingly, many of the biochemically active hits are carboxylic acids, which are recognized by the acid-binding motif. The DDU library should nicely compliment these flatter and more rigid fragments, especially during later growing and

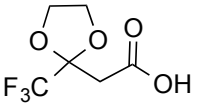
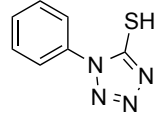
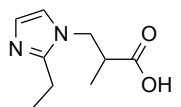
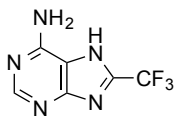
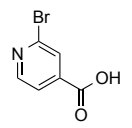
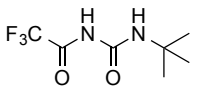
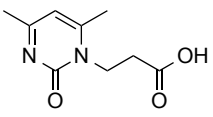
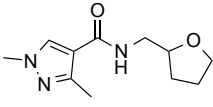
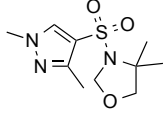
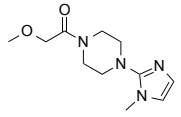
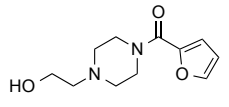
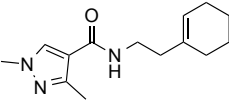
merging efforts. Once the initial hits have been profiled for single point biochemical activity, select fragments will be characterized in dose response for biochemical and SPR activity, and subsequently crystallized with the appropriate proteins. We anticipate that this fragment-based approach will nicely compliment our previous structure-based efforts, helping to create a more discrete rule set for building non-covalent affinity across diverse β -lactamases.

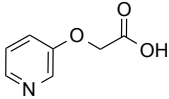
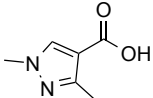
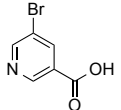
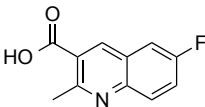
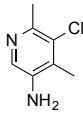
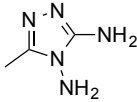
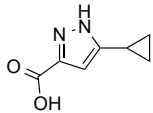
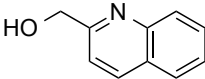
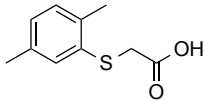
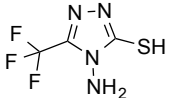
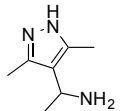
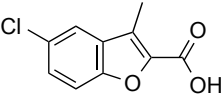
Table 5-1. Hit rate by enzyme and library.

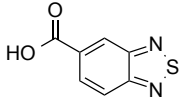
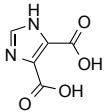
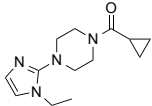
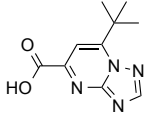
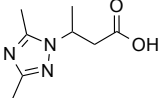
	CTX-M-14	NDM-1	OXA-48
UCSF	158 (5.9%)	148 (5.5%)	108 (4.0%)
DDU	63 (4.0%)	82 (5.2%)	

Table 5-2. Single point inhibition for selected hits (2.4 mM).

	CTX-M-14 Initial Hit	NDM-1 Initial Hit	OXA-48 Initial Hit	Total Hits	CTX-M-14	NDM-1	OXA-48
	Y	Y	Y	3	No Inhibition	No Inhibition	51% Inhib
	Y	Y	Y	3	No Inhibition	Insoluble	17% Inhib
	Y	Y	Y	3	No Inhibition	52% Inhib (Ki: 568 μM)	74% Inhib (Ki = 650 μM)
	Y	N	Y	2	38% Inhib	No Inhibition	No Inhibition
	Y	N	Y	2	24% Inhib	No Inhibition	12% Inhib
	Y	N	Y	2	21% Inhib	No Inhibition	No Inhibition
	Y	N	Y	2	No Inhibition	No Inhibition	21% Inhib
	Y	N	Y	2	No Inhibition	No Inhibition	15% Inhib
	Y	N	Y	2	No Inhibition	No Inhibition	18% Inhib
	Y	N	Y	2	14% Inhib	No Inhibition	No Inhibition
	Y	N	Y	2	Insoluble	No Inhibition	No Inhibition
	Y	N	Y	2	24% Inhib	25% Inhib	16% Inhib

	CTX-M-14 Initial Hit	NDM-1 Initial Hit	OXA-48 Initial Hit	Total Hits	CTX-M-14	NDM-1	OXA-48
	Y	N	Y	2	19% Inhib	No Inhibition	No Inhibition
	Y	N	Y	2	19% Inhib	No Inhibition	32% Inhib
	Y	N	Y	2	17% Inhib	No Inhibition	No Inhibition
	Y	N	Y	2	41% Inhib	No Inhibition	25% Inhib
	Y	N	Y	2	16% Inhib	No Inhibition	25% Inhib
	Y	N	Y	2	21% Inhib	No Inhibition	No Inhibition
	Y	N	Y	2	12% Inhib	No Inhibition	No Inhibition
	Y	N	Y	2	16% Inhib	No Inhibition	No Inhibition
	Y	N	Y	2	14% Inhib	No Inhibition	
	Y	N	Y	2	16% Inhib	No Inhibition	No Inhibition
	Y	N	Y	2	18% Inhib	No Inhibition	No Inhibition
	Y	N	Y	2	28% Inhib	No Inhibition	12% Inhib

	CTX-M-14 Initial Hit	NDM-1 Initial Hit	OXA-48 Initial Hit	Total Hits	CTX-M-14	NDM-1	OXA-48
	Y	N	Y	2	16% Inhib	No Inhibition	No Inhibition
	Y	N	Y	2	14% Inhib	No Inhibition	No Inhibition
	Y	N	Y	2	25% Inhib	No Inhibition	22% Inhib
	Y	N	Y	2	18% Inhib	No Inhibition	64% Inhib
	Y	N	Y	2	12% Inhib	No Inhibition	15% Inhib
	Y	N	N	1	No Inhibition	No Inhibition	No Inhibition
	Y	N	N	1	17% Inhib	No Inhibition	No Inhibition
	N	Y	N	1	12% Inhib	No Inhibition	No Inhibition
	Y	N	N	1	No Inhibition	No Inhibition	37% Inhib
	Y	N	N	1	16% Inhib	No Inhibition	No Inhibition
	Y	N	N	1	No Inhibition	32% Inhib	No Inhibition
	Y	N	N	1	30% Inhib	No Inhibition	90% Inhib ($K_i = 178 \mu\text{M}$)

	CTX-M-14 Initial Hit	NDM-1 Initial Hit	OXA-48 Initial Hit	Total Hits	CTX-M-14	NDM-1	OXA-48
	Y	N	N	1	No Inhibition	No Inhibition	57% Inhib
	Y	N	N	1	No Inhibition	No Inhibition	20% Inhib
	Y	N	N	1	No Inhibition	No Inhibition	No Inhibition
	Y	N	N	1	No Inhibition	19% Inhib	27% Inhib
	Y	N	N	1	No Inhibition	No Inhibition	No Inhibition

Methods:

Fragment Screens

Screening experiments were run on a GE Biacore 4000, which has four flow cells with five hydrodynamically addressable spots per flow cell. N-terminal His-Avi(Biotin) proteins were captured on a Neutravidin conjugated CM5 chip, where the Neutravidin was first conjugated using EDC/NHS and quenched with 1M ethanolamine. Proteins were immobilized to 7-10000 RU using an immobilization buffer consisting of 10 mM HEPES pH 7.5, 150 mM NaCl, 0.05% Tween 20, and 250 μ M TCEP. Unbound Neutravidin was blocked with NH₂-PEG₂-Biotin, including the reference spot, which was also Neutravidin conjugated. Running buffer varied per enzyme, and consisted of the following: CTX-M-14: 10 mM HEPES pH 7.5, 150 mM NaCl, 0.05% Tween 20, 250 μ M TCEP, and 5% DMSO; NDM-1: 100 mM HEPES pH 7.5, 150 mM NaCl, 200 μ M ZnCl₂, 100 μ M TCEP, 0.05% Tween 20, and 5% DMSO; OXA-48: 100 mM Tris-H₂SO₄ pH 7.0, 50 mM NaHCO₃, 0.01% Triton X-100, 250 μ M TCEP, and 5% DMSO. The fragment libraries were split between flow cells and run in parallel. Positive and negative (DMSO blank) controls were run every 10 cycles, and consisted of the following: CTX-M-14: **1** at 150 nM; NDM-1: captopril at 100 μ M; OXA-48: **2⁷** at 50 μ M. All data was reference and blank subtracted per flow cell, and solvent corrected for bulk refractive index shift using a correction curve from 3.75-6.25% DMSO. The corrected data was subsequently normalized per flow cell using RALPH,⁸ which loess normalizes the positive control regression and baseline drift throughout the run. Each scatterplot shown is from a single flow cell. Hits were defined per boxplot cutoff (75th percentile + 3xIQR).

References:


1. D. A. Nichols, P. Jaishankar, W. Larson, E. Smith, G. Liu, R. Beyrouthy, R. Bonnet, A. R. Renslo, and Y. Chen. *J. Med. Chem.*, 2012, 55, 2163-2172.
2. D. E. Ehmman, H. Jahic, P. L. Ross, R. Gu, J. Hu, T. F. Durand-Reville, S. Lahiri, J. Thresher, S. Livchak, N. Gao, T. Palmer, G. K. Walkup, and S. L. Fisher. *J. Biol. Chem.* 2013, 288 (39), 27960-27971.
3. O. A. Pemberton, X. Zhang, D. A. Nichols, K. DeFrees, P. Jaishankar, R. Bonnet, J. Adams, L. N. Shaw, A. R. Renslo, and Y. Chen. *Antimicrob. Agents Chemother.*, 2018, 62 (8), e02563-17.
4. T. Christopeit, H. S. Leiros. *Bioorg. Med. Chem. Lett.* 2016, 26, 1973-1977.
5. C. Jamieson, M. C. Allwood, D. Stonkute, A. Wallace, A. Wilkinson, T. Hills. *Eur. J. Hosp. Pharm.* DOI: 10.1136/ejhpharm-2018-001699.
6. J. Brem, S. S. van Berkel, D. Zollman, S. Y. Lee, O. Gileadi, P. J. McHugh, T. R. Walsh, M. A. McDonough, C. J. Schofield. *Antimicrob. Agents Chemother.* 2016, 60 (1), 142-150.
7. B. A. Lund, T. Christopeit, Y. Guttormsen, A. Bayer, H. S. Leiros. *J. Med. Chem.* 2016, 59 (11), 5542-5554.
8. A. M. Giannetti, H. N. Gilbert, K. E. Pitts, B. J. Bravo, D. P. Huddler, *Royal Society of Chemistry Drug Discovery Series: Fragment-Based Drug Discovery.* 2014, Chapter 2.

Publishing Agreement

It is the policy of the University to encourage the distribution of all theses, dissertations, and manuscripts. Copies of all UCSF theses, dissertations, and manuscripts will be routed to the library via the Graduate Division. The library will make all theses, dissertations, and manuscripts accessible to the public and will preserve these to the best of their abilities, in perpetuity.

Please sign the following statement:

I hereby grant permission to the Graduate Division of the University of California, San Francisco to release copies of my thesis, dissertation, or manuscript to the Campus Library to provide access and preservation, in whole or in part, in perpetuity.

DocuSigned by:

A98BB870580049F...

Author Signature

12/12/2019
Date